ACTA TECHNICA

ACADEMIAE SCIENTIARUM HUNGARICAE

REDIGIT: M. MAJOR

TOMUS 93
FASCICULI 1–2

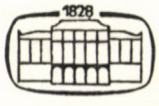

AKADÉMIAI KIADÓ, BUDAPEST 1981

ACTA TECHNICA

Az *Acta Technica* angol, francia, német és orosz nyelven közöl értekezéseket a műszaki tudományok köréből.

Az *Acta Technica* változó terjedelmű füzetekben jelenik meg, több füzet alkot egy kötetet.

A közlésre szánt kéziratok a következő címre küldendők:

Acta Technica
1051 Budapest, Münnich Ferenc u. 7.

Ugyanerre a címre küldendő minden szerkesztőségi és kiadóhivatali levelezés.

Megrendelhető a belföld számára az „Akadémiai Kiadó"-nál (1363 Budapest Pf. 24. Bankszámla 215 11448), a külföld számára pedig a „Kultura" Külkereskedelmi Vállalatnál (1389 Budapest 62, P. O. B. 149 Bankszámla: 218-10990) vagy annak külföldi képviseleteinél és bizományosainál.

Die *Acta Technica* veröffentlichen Abhandlungen aus dem Bereiche der technischen Wissenschaften in deutscher, englischer, französischer und russischer Sprache.

Die *Acta Technica* erscheinen in Heften wechselnden Umfanges. Vier Hefte bilden einen Band.

Die zur Veröffentlichung bestimmten Manuskripte sind an folgende Adresse zu senden.

Acta Technica
H 1051 Budapest,
Münnich Ferenc u. 7.
Ungarn

An die gleiche Anschrift ist auch jede für die Schriftleitung und den Verlag bestimmte Korrespondenz zu richten.

Abonnementpreis pro Band: $ 36.00.

Bestellbar bei »Kultura« Außenhandelsuntelsunternehmen (H-1389 Budapest 62, P. O. B. 149 Bankkonto Nr. 218-10990) oder seinen Auslandsvertretungen.

ACTA TECHNICA

ACADEMIAE SCIENTIARUM HUNGARICAE

REDIGIT: M. MAJOR

TOMUS 93

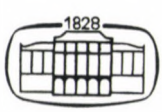

AKADÉMIAI KIADÓ, BUDAPEST 1981

ACTA TECHNICA

TOMUS 93, FASC. 1—4

INDEX

BOOK REVIEWS
BUCHBESPRECHUNG

ACTA TECHNICA

ACADEMIAE SCIENTIARUM HUNGARICAE

REDIGIT: M. MAJOR

TOMUS 93

FASCICULI 1–2

AKADÉMIAI KIADÓ, BUDAPEST 1981

Acta Technica Academiae Scientiarum Hungaricae, 93 (1—2), pp. 3—24 (1981)

GEMEINSAMKEITEN UND GEGENSÄTZLICHKEITEN DER ENERGIETRÄGER*

A. LÉVAI**

ORD. MITGLIED DER UNG. AKAD. DER WISSENSCHAFTEN

[Eingegangen am 18. Juni 1981]

Zum Zwecke, bei den heute überall so häufig diskutierten Problemen der Energetik eine möglichst einheitliche und vorurteilslose Betrachtungsweise zu erhalten, untersucht vorliegende Arbeit die Gemeinsamkeiten und Gegensätzlichkeiten der natürlichen und der umgewandelten Energieträger sowohl aus der Sicht der Naturwissenschaften, als auch der Wirtschaft. Es werden auch gewisse Vergleiche unter ihnen angestellt. Außer den fossilen und den nuklearen Energieträger werden auch die erneuerbaren Energien und die Kernverschmelzung, letztere als die meistversprechende Möglichkeit der Zukunft, gestreift.

1. Naturwissenschaftliche Fragen

1.1. *Nuklearer Ursprung*

Als Ausgangpunkt und gleichzeitig als erstes gemeinsames Merkmal soll hervorgehoben werden, daß praktisch alle Rohenergieformen, die uns zur Verfügung stehen, letzendlich nuklearen Ursprunges sind. So ist, von ihrem Ursprung aus gesehen, die Sonnenenergie, die seit Milliarden Jahren in ungeheurer Menge uns zuströmt, nukleare Energie. Dieser, aus den Kernfusionsprozessen entstandenen Wärme haben wir nicht nur alle, durch die Photosynthese entstandenen fossilen Brennstoffe, sondern auch den Wasserkreislauf auf unserer Erde, die Luftbewegung, die horizontalen und vertikalen Meeresströmungen, usw. zu verdanken. Daß die bekannten irdischen Kernbrennstoffe, wie Uran, Thorium, Wasserstoff und seine Isotopen, ferner Lithium durch Freisetzung der Kernkräfte in ihren gewissen Isotopen, d. h. durch Kernprozesse, zu nützlichen Energiequellen verwandelt werden können, muß nicht besonders betont werden. Die geothermische Energie stammt von der Wärme, die ebenfalls durch Kernspaltungsprozesse in der Erdkruste freigesetzt wird. Allein die Gezeitenenergie bildet als Resultante der Massenanziehungskräfte des Mondes, der Sonne und der Zentrifugalkräfte der Erdrotation eine Ausnahme hievon. (Auch die Luft- und Meeresströmungen der Erde werden von letzterem im geringen Ausmaß beeinflußt).

* Erweiterte Fassung eines Vortrages, gehalten am Energiewirtschaftlichen Seminar der Universität Stuttgart, am 4. 6. 1981.

** Prof. A. Lévai, Fillér u. 56, H-1022 Budapest, Ungarn

Es ist somit gewiß keine Übertreibung, wenn man aus dem beinahe lückenlos gemeinsamen nuklearen Ursprung aller Rohenergieträger ausgehend zur Schlußfolgerung kommt, daß die Nuklearenergie eigentlich die Grundlage eines jeden kosmischen Seins bildet. Sie erlaubt und ermöglicht erst das irdische Leben.

1.2. *Rolle der Massendefekte*

Mit dem gemeinsamen nuklearen Ursprung hängt zusammen, daß bei der Freisetzung der naturgebundenen Energie — soweit es sich nicht um die als Umwandlungsstufe erscheinende kinetische Energie des Wassers, des Windes, oder des thermischen Potentials der geothermischen Energie, der Temperaturunterschiede im Meerwasser, usw. handelt — diese Freisetzung durch Änderung der internuklearen Bindungskräfte geschieht. Das wäre eine zweite Gemeinsamkeit der Energieträger, die sich auch auf die Freisetzung der chemischen Energie erweitern läßt, wobei es sich sinngemäß um die interatomaren, resp. um die intermolekularen Bindungskräfte handelt. In allen Fällen ist die gewonnene Energiemenge aus den Massendefekten der Ursprungs-, resp. der resultierenden Materialien zu errechnen. Als Folge des, im Zuge der feldtheoretischen Forschungen entdeckten Zusammenhangs zwischen Masse und Energie wird nämlich die Energie heute als eine, durch die Zustandsparameter der Materie eindeutig bestimmte, zeitlich konstante Menge angesehen, für welche im Sinne der Relativitätstheorie einerseits das Transformationsgesetz, anderseits das Äquivalenzgesetz ($E=mc^2$) gilt. Masse und Energie, als Eigenschaften der materiellen Systeme, sind voneinander untrennbar und können sich nur im Verhältnis zueinander ändern. Ohne auf die Natur der erwähnten, derzeit noch nicht genügend geklärten Bindungskräfte näher einzugehen, steht fest, daß bei der Freisetzung der nuklearen, resp. der chemischen Energie, die eine Erscheinungsform der Materie, nämlich die Masse, in die immer anwesende andere, in Energie übergeht. Bei der Nuklearenergie im gebräuchlichen Sinne, d. h. bei der Spaltungs- resp. bei der Fusionsenergie ist die Masse der Spaltungsrückstände, resp. des neuen Fusionsproduktes gerade um die gewonnene Energie geringer, als die des Ursprungsmaterials, oder Materialien. Bei der Uranspaltung erscheint rund 1/1000 der ursprünglichen Masse des Atomkerns als Energie: bei der Fusion zu He der leichten Atomkerne H, D oder T läßt sich aus der Differenz der Massendefekte der Ausgangskerne resp. des Fusionsproduktes die als Energie erscheinende Menge errechnen. Sie ist — je nach Ausgangsmaterial — etwa gleich, höchstens 5-mal so groß, als bei der Kernspaltung.

Bei der Freisetzung der chemisch gebundenen Energie z. B. durch Verbrennung oder Vergasung der Kohle können die Bindungskräfte zwischen den Atomen oder Molekülen ebenfalls aus den Differenzen der Massendefekte errechnet werden. Nur sind diese Massendefektsdifferenzen um viele zehner Größenordnungen geringer, als bei den nuklearen Vorgängen. So wird bei der Verbrennung des Kohlenstoffs zu Kohlendioxyd die ursprüngliche Masse des Kohlenstoffs und des Sauerstoffs zusammen nur um rund ein Zehnmilliardstel kleiner. (Die, in Wärmeeinheiten

ausgedrückte frei gewordene Energiemenge beträgt für je 1 g des Ausgangsmaterials bei der Uranspaltung rund 80 GJ, bei der Fusion von je 50% D und T zu He rund 400 GJ, bei der Verbrennung von C zu CO_2 dagegen nur rund 9 kJ. Kernbrennstoffe sind auf die Masseneinheit bezogen 10–40 millionenmal „energiereicher" als die fossilen.)

1.3. *Beeinflussung der Umwelt*

Auf eine dritte Gemeinsamkeit fast aller Energieträger stößt man, wenn man die, in den letzten 10–15 Jahren so wichtig gewordene und oft leidenschaftlich diskutierte Frage der Umweltverschmutzung analysiert. In den kommenden Jahrzehnten wird nämlich m. E. n. sicherlich nicht die mengenmäßige Begrenztheit der Energieträger eine der Hauptsorgen der Menschheit sein — natürlich vorausgesetzt, daß politische oder wirtschaftliche Faktoren dies nicht künstlich bewirken —, sondern die Frage: wie kann der Mensch die ihm reichlich zur Verfügung stehenden Energieträger der Natur so benutzen, daß dadurch die normalen Lebensbedingungen auf der Erde nicht zunichte gemacht werden?

1.3.1. Erwärmung

Eine Folge der bereits erwähnten zweiten Gemeinsamkeit beinahe aller Rohenergieträger ist es, daß bei der Befreigung dieser Energie und bei ihrer Überführung in arbeitsfähige Energieformen — die ja für unser Leben von größter praktischer Bedeutung sind — nach dem II. Hauptsatz, dem Erfahrungsgesetz der Thermodynamik, die Entropie ständig zunimmt. Diese Zunahme soll schließlich zu einem Zustand führen, welcher der maximalen Wahrscheinlichkeit entspricht und von Clausius, dem Schöpfer des Entropiebegriffes, als Wärmetod bezeichnet wurde.

Es stellen sich in diesem Zusammenhang die Fragen: nähert sich das Weltall tatsächlich dem Wärmetod? Warum wurde dieser Zustand nicht schon lange erreicht? Wieso sind in unserer Welt Arbeitsleistungen und Lebenserscheinungen noch überhaupt möglich?

Ohne auf die philosophische Deutung dieser Fragen näher einzugehen, sei nur erwähnt, daß im Universum — dessen räumliche und zeitliche Ausmaße uns heute noch vollkommen unbekannt sind — ständig neue Sterne mit riesigem Gehalt an arbeitsfähiger Energie enstehen und darin physikalische Prozesse größten Ausmaßes ablaufen, die nach den, uns bekannten Gesetzen der Physik gar nicht zu erklären sind. Vielleicht hatte der kühne Physiker und Philosoph Ludwig Boltzmann Recht, als er um die Jahrhundertwende annahm, daß der, vom Wärmetod so stark abweichende Zustand unseres Planeten einer riesenhaften Schwankungserscheinung zu verdanken sein könnte, ähnlich, wie im Mikrokosmos trotz Brown'scher Bewegung mit berechenbarer Wahrscheinlichkeit innerhalb kurzer Zeiträume Unregelmäßigkeiten auftreten. Das sind dort nachweisbare Schwankungserscheinungen. So sagte Boltz-

MANN in seinen Vorlesungen über Gastheorie im Jahre 1898*: „Man kann sich die Welt als ein mechanisches System von einer enorm großen Anzahl von Bestandteilen und von enorm langer Dauer denken, so daß die Dimensionen unseres Fixsternhimmels (Prof. Engelbert BRODA bemerkt hiezu: jedenfalls mit Einschluß aller Spiralnebel unseres Beobachtungsraumes) winzig gegen die Ausdehnung des Universums, und Zeiten, die wir Aeonen nennen, winzig gegen dessen Dauer sind. Es müssen dann im Universum, das sonst überall im Wärmegleichgewicht, also tot is, hier und da solche verhältnismäßig kleine Bezirke von der Ausdehnung unseres Sternenraumes (nennen wir sie Einzelwelten) vorkommen, die während der verhältnismäßig kurzen Zeit von Aeonen erheblich vom Wärmegleichgewicht abweichen, und zwar ebenso häufig solche, in denen die Zustandswahrscheinlichkeit gerade zu- als abnimmt... Diese Methode scheint mir (Boltzmann) die einzige, wonach man den zweiten Hauptsatz, den Wärmetod jeder Einzelwelt, ohne eine einseitige Änderung des gesamten Universums von einem bestimmten Anfangs- gegen einen schließlichen Endzustand denken kann... Im ganzen Universum, dem Inbegriff aller Einzelwelten, aber kommen in der Tat Vorgänge in der umgekehrten Reihenfolge vor. Nur zählen die sie etwa beobachtenden Wesen die Zeit wieder von den unwahrscheinlicheren zu den wahrscheinlicheren Zuständen fortschreitend, und es kann nie entdeckt werden, ob sie die Zeit entgegengesetzt wie wir zählen, da sie in der Zeit durch Aeonen, im Raume durch $10^{10^{10}}$ Siriusfernen von uns getrennt sind, und obendrein ihre Sprache keine Beziehung zu der unserigen hat."

In dieser Boltzmann'schen Welt müßten, als System betrachtet, zeitliche Veränderungen durch Gleichungen beschreibbar sein, „in denen die positive und negative Zeitrichtung gleichberechtigt sind", wobei der Schein der Irreversibilität durch eine besondere spezielle Annahme in langen Zeiträumen erklärbar ist. Dies trifft laut BOLTZMANN gerade bei der atomistischen Weltanschauung zu. Wir sollen nicht vergessen, daß es gerade BOLTZMANN jener Denker war, der durch seine scharfsinnige Analyse die Behauptungen der Gegner der molekularkinetischen Wärmetheorie, wonach die grundsätzliche Nichtumkehrbarkeit auf dem Gebiete der Wärme (z. B. bei dem Wärmeübergang) mit der grundsätzlichen Umkehrbarkeit der Mechanik (z. B. Umkehrungen der Bewegungen und der Kräfte) sich nicht vereinen lassen, entkräftete. Er war es, der durch seine Überlegungen, z. B. durch die Einführung des Wirkungsquerschnittes, — das ist die Wahrscheinlichkeit für das Zustandekommen eines nuklearen (oder chemischen) Ereignisses —, die Bahn für die weitere theoretische Entwicklung der Atomphysik frei machte. Und derselbe BOLTZMANN hat durch seine Entropiegleichung: $S = k \log W$ den Wahrscheinlichkeitszustand des Makrokosmos mit der Wahrscheinlichkeit von unzähligen Trillionen von Elementarteilchen im Mikrokosmos in genialer Weise zu verbinden gewußt.

* Die nachfolgenden Zitate und ein Teil der Gedankengänge sind dem Werk „Ludwig BOLTZMANN: Mensch, Physiker, Philosoph" von Prof. Engelbert Broda, Wien, Fr. Deuticke, 1955 entnommen.

Kehren wir nun aber vom Makrokosmos, das ist das Universum, resp. vom Mikrokosmos, das ist die Welt der Atome und der Atomkerne, auf unsere Erde zurück. Hier stehen wir vor der Tatsache, und das ist eben die dritte erwähnte Gemeinsamkeit aller Energieträger und Energieumwandlungen, daß sämtliche freigelegten Energien unsere Umgebung schließlich als Wärme belasten. (Selbst die Wasser- oder Windkraft wird – soweit sie durch Reibung oder Wirbel nicht sowieso in Wärme übergeht –, nach der Umwandlung über mechanische und elektrische Energie schließlich Wärme).

Um die zwangsweise eintretende Wärmebelastung unserer Umgebung nicht noch stärker zu erhöhen, als unumgängig notwendig, bleibt nichts anderes übrig, als die Energie so rationell, als es technologisch und wirtschaftlich noch vertretbar ist, zu verwenden. Die Möglichkeiten der rationellen Energieverwertung sind außerordentlich mannigfaltig und noch bei weitem nicht erschöpft. Vom Gesichtspunkte der Abwärmenutzung bloß zwei Beispiele: die Koppelung von Kraft und Wärme bei der Stromerzeugung und die Nutzung der Abfallwärme durch Wärmepumpen. Ähnliche Beispiele sind zahllos und jedem Energetiker genügend bekannt.

Ist die Wärmebelastung der Umgebung eine, für alle Rohenergiearten gemeinsame, unliebsame Begleiterscheinung, so ist bei einer weiteren Analyse der Umweltverseuchungen durch die Energieträger doch so manches und nicht unwesentliches als Verschiedenheit festzustellen.

1.3.2. Schadstoffe

Die Schadstoffemissionen der Energieträger lassen sich bekanntlich in zwei große Gruppen einteilen: in die der chemischen und in die der physikalischen Verunreinigungen. In die erste Gruppe gehören im allgemeinen die Verbrennungs- oder Vergasungsprodukte der fossilen Energieträger, das sind also: Kohlendioxyd, Kohlenmonoxyd, Schwefeldioxyd, Kohlenwasserstoffe, Stickstoffoxyde, usw. Die Gruppe der physikalischen Verunreinigungen wird neben der bereits behandelten Abwärme, oder gemeinhin eher Wärme, von den Festkörpern Asche, Staub, Ruß usw. und von den radioaktiven Abfällen gebildet.

Maßgebend für das irdische Leben sind bekanntlich die Immissionswerte der einzelnen Verunreinigungen, das sind also die, auf die Raumenheit entfallenden Schadstoffe, gemeinhin an der Erdoberfläche gemessen. Bei der globalen Umrechnung der Emission auf die Immissionen kann man von der Annahme ausgehen, daß der größte Teil der Energieträger heute noch auf der nördlichen Hemisphäre, etwa zwisschen dem 30 und 60 Breitegrad verbraucht wird. Die freigelegten Schadstoffe kommen in die etwa 10 km dicke Troposphäre, deren Rauminhalt etwa 16% der gesamten Troposphäre der Erde ausmacht. (Ungefähr $800 \cdot 10^6$ km^3.) In diesem Raum sind etwa $150 \cdot 10^{12}$ T Sauerstoff, $520 \cdot 10^{12}$ T Stickstoff und $320 \cdot 10^9$ T Kohlendioxyd vorhanden. Bei der Immissionsrechnung wird vorausgesetzt, daß die kurzlebigen Schadstoffe sich in dem erwähnten Kugelschalenschnitt gleichmäßig

verteilen, während die langlebigen (u. a. das Kohlendioxyd und die Radionuklide mit langer Halbwertszeit) in die gesamte Troposphäre kommen.

Die mengenmäßig bedeutendste Verunreinigung ist das Kohlendioxyd, deren Menge heute jährlich etwa 35 Milliarden T ausmacht und bis zum Jahre 2000 auf etwa 60 Milliarden T zunehmen wird. Es ist eindeutig festgestellt, daß der Kohlendioxydgehalt der Atmosphäre zu folge der menschlichen Tätigkeit langsam, aber ständig zunimmt (seit 1900 um etwa 15—20%).* Der frühere Zustand, in dem die natürlichen Auswürfe aus den Vulkanen, Fäulnisprodukten usw. und der Verbrauch hauptsächlich durch die Photosynthese sich das Gleichgewicht hielten, ist nicht mehr vorhanden. Die maßlose Ausrottung der Urwälder trägt neben dem zunehmenden Energieverbrauch sicherlich zur Verschlechterung der Situation bei. Die Folgen der Zunahme des Kohlendioxydgehaltes sind noch nicht genügend geklärt. Allgemein rechnet man mit einer Zunahme der durchschnittlichen Lufttemperatur, die man dem sog. „Treibhauseffekt" zuschreibt. Gegenteilige Meinungen sind aber ebenfalls zu hören und diese stützen sich auf die Tatsache, daß die mittlere Temperatur an der Erdoberfläche seit den 40-er Jahren trotz Erhöhung der CO_2-Konzentration ständig abnimmt. Mit Gewißheit kann man aber damit rechnen, daß durch den CO_2-Ausstoß ernste Folgen zu erwarten sind. (Nebenbei bemerkt: die umweltgefährdenden Ausstöße der chemischen Industrie, so u. a. des die Ozonschicht zerstörenden Fluors, oder Quecksilber, Arsen u. s. w. in den Gewässern, sind bestimmt viel gefährlicher, als die Beiprodukte der Energiegewinnung).

Der jährliche Auswurf an Kohlenmonoxyd (derzeit jährlich etwa 200 Millionen Tonnen) liegt nahe dem natürlichen Gehalt der Luft. (Cca 600 Millionen Tonnen). Der Umstand, daß trotz des gewaltigen Ausstosses — in erster Linie aus den Fahrzeugmotoren — keine globale oder auch regionale Anreicherung der Luft mit diesem sehr giftigen Gas festzustellen ist, wird gewissen, kohlenmonoxyd-verbrauchenden Mikroorganismen des Bodens zugeschrieben.

Von den Verbrennungsprodukten der fossilen Energieträger verursacht heute das Schwefeldioxyd die meisten Sorgen. Seine jährliche Menge ist allein aus den Kraftwerken (cca 50 Millionen Tonnen) etwa 100-mal so groß, als der natürliche Gehalt der Luft an diesem Schadstoff. Die Zunahme des Auswurfes bis zur Jahrhundertwende wird gewaltig sein, besonders dann, wenn die heutigen Technologien zur Freisetzung der chemischen Energie unverändert bleiben. Es ist aber anzunehmen, daß bis zu diesem Zeitpunkt solch' neue Technologien breite Anwendung finden werden, die die schwefeligen Abgase nicht in ihrer starken Verdünnung zu reinigen versuchen werden, sondern den Schwefel, — wenigstens zum großen Teil — schon während der Verbrennung zu binden trachten, wie die Schwebefeuerung (fuel bed combustion). Die Entschwefelung der Energieträger wird heute bei der Rohölraffinerie zu gewissen Zwecken durchgeführt, bei der Kohle noch im Versuchs-

* W. W. KELLOGG, R. SCHWARE: „Climate Change and Society", Westview Press, Boulder, 1981.

stadium. Bei der Kohlevergasung wird das Gas von der weitaus höheren Konzentration an Schwefeloxyden gereinigt.

Einstweilen kommt aber die vorher erwähnte große Menge an Schwefeldioxyd in die Atmosphäre und würde, — selbst bei der günstigsten Verteilung darin —, in unserem, der Berechnung zu Grunde gelegten Kugelschalenschnitt einen Immissionswert erreichen, der weit über den heute zugelassenen Wert liegt. Zum Glück- oder Unglück- gelangt aber das SO_2 durch Diffusion oder als Aerosol zum Boden und übt dort seine Wirkung lokal oder regional aus. Eindeutige Beweise dafür liegen vielfältig vor.

Die bei der Verbrennung, besonders bei hoher Temperatur entstehenden Stickstoffoxyde sind ebenfalls eine lästige Begleiterscheinung der Verwendung der fossilen Energieträger, die ihre schädliche Wirkung größtenteils lokal ausüben.

Auf die umweltgefährdenden Schadstoffauswürfe bei der Nutzung der Kernenergie übergehend, sollte nicht näher auf die heute, vielerorts so leidenschaftlich diskutierte Frage der Gefährlichkeit des Reaktors, des Brennstoffzyklus, der Entsorgung, usw. eingegangen werden. Fest steht jedenfalls, daß aus einem Kernreaktor mit einer gewissen, wenn auch sehr geringen Wahrscheinlichkeit betriebsmäßig Radionuklide (so u. a. Co^{60}, Kr^{85}, Sr^{90}, C^{14}, Xe^{133} u. a. m.) entweichen können, die aber mit den, heute mit genügender Sicherheit zur Verfügung stehenden Mitteln von der Biosphäre ferngehalten, resp. dorthin stark verdünnt emittiert werden können.

1.3.3. Vergleich der Risikofaktoren: Kohle-Spaltungsenergie

Es ist hier vielleicht von Interesse die fossilen und die nuklearen Energieträger vom Standpunkte ihrer Auswirkung an die Umweltverunreinigung zu vergleichen. Bei dieser Gegenüberstellung ist natürlich nicht nur die absolute Menge der Schadstoffe und deren Verteilung in der Atmosphäre (oder im Wasser) von Bedeutung, sondern in erster Linie der sog. Risikofaktor, d. h. der Einfluß der Verunreinigungen auf die lebenden Organismen, zuletzt auf den Menschen.

Dem Risikofaktor wird beim Vergleich von Energiesystemen untereinander, also z. B. Kohle gegenüber Uran, besondere Bedeutung beigemessen. Dabei spielt der objektive, also tatsächlich vorhandene oder realistisch geschätzte Risikofaktor bei der Entscheidung, aber auch bei der Beeinflussung der öffentlichen Meinung eine eher untergeordnete Rolle gegenüber dem subjektiven, also durch die persönliche Einstellung beeinflußten Risikofaktor. Die Gründe hiefür liegen teilweise in dem sehr weitgespannten Bogen der Forschungstätigkeit, die sich beginnend vom Auswurf der Schadstoffe in den verschiedenen Phasen der Technologie, über die Verteilung in der Biosphäre und die darin inzwischen stattfindenden physikalischen und chemischen Umwandlungen bis zur Aufnahme durch den Letztverbraucher erstreckt. Dabei stellt der, in den lebenden Organismen entstandene Schaden allein ein heute noch mit sehr wesentlichen Unsicherheiten behaftetes Forschungsgebiet dar. Die Forschungen sind noch relativ jung, sie begannen etwa vor 10 – 15 Jahren: wegen der ungenügenden Tiefe

Tabelle 1

Wahrscheinliche jährliche Todesfälle im kompletten Zyklus (1000 MWe, 65%)

	Kohlezyklus	Uranzyklus
Bergbau		
Betriebsunfälle und Krankheiten	0,62—1,0	0,44
Bevölkerung	—	0,08
	0,62—1,0	0,52
Aufbereitung		
Werksbeschäftigte	0,05	0,038
Bevölkerung	—	0,002
	0,05	0,04
Transport		
Beschäftigte	0,3—1,3	0,01
Bevölkerung	—	$6{,}1 \cdot 10^{-4}$
	0,3—1,3	0,01
Kraftwerk		
Werksbeschäftigte	0,1	0,183
Bevölkerung (innerhalb 50 Meilen)	0,6	0,017
Ganze Bevölkerung (in USA)	6	—
	6,7	0,20
Aufarbeitung der Rückstände		
Beschäftigte	—	$5{,}1 \cdot 10^{-5}$
Bevölkerung	—	$7{,}45 \cdot 10^{-4}$
		$8 \cdot 10^{-4}$
Kraftwerksabbau		
Beschäftigte	—	0,005
Gesamtsumme	7,7—9,1	0,77

Nb.: Die Daten dieser Tabelle sind einer Arbeit von L. D. HAMILTON: „Comparative Risks from Different Energy Systems: Evolution of the Methods of Studies", erschienen im *IAEA-Bulletin*, Vol. **22.**, $N^0 = 5/6$, October 1980, entnommen.

der Kenntnisse ist die Signifikanz der Resultate verhältnismäßig schwach (etwa unter 60% gegenüber über 95% bei erfolgreichen Forschungen). Dieser Umstand wird z. B. im Falle der Kernenergie zur Irreführung der öffentlichen Meinung zur Genüge ausgenutzt.

Die vorstehende Tabelle 1 über die jährlich zu erwartenden Todesfälle beim Vergleich eines Kohlezyklus mit einem Uranzyklus für ein 1000 MWe Kraftwerk bei einem Ausnutzungsgrad von 65% ist also in diesem Sinne zu verstehen. Die erwarteten Todesfälle in der Tabelle sind meistens getrennt für die, im Werk, Transport usw.

beschäftigten und für die allgemeine Bevölkerung angeführt. Die Zusammenstellung wurde für Verhältnisse aus den Vereinigten Staaten von den dortigen staatlichen Organen errechnet und sollte somit prinzipiell als objektiv angesehen werden.

Wenn auch viele der in der Tabelle 1 angeführten Zahlen durch reiches Tatsachenmaterial belegt oder gründlich erforscht worden sind, so sind andere bestimmt bloß geschätzt. So ist z. B. die, beim Kohlezyklus auffallend hoch erscheinende Zahl von 6 Todesfällen in der Bevölkerung durch den Schwefeldioxyd einfach durch Multiplikation mit der Zahl 10 des gründlicher erforschten Zahlenwertes im Umkreis von 50 Meilen entstanden. (Bezeichnend für diese Unsicherheit ist, daß z. B. vom Internationalen Atomenergiebehörde in Wien für die durch Schwefeloxyde verursachten Todesfälle je 100 000 Einwohner, Jahr und $\mu g/m^3$ Sulfatgehalt nach dem sozialem Stand, Rasse, Geschlecht, usw. Zahlen zwischen 0 und 12 genannt werden. Die fixe Zahl von 6 in der angeführten Tabelle erscheint also zumindest stark fragwürdig.) Die Tabelle weist zumindest aber deutlich auf die Gegensätzlichkeiten bei der Beurteilung im Umweltverhalten von Kohle und Kernenergie hin.

Im Zusammenhang mit dem Vergleich von Kohle- resp. Kernkraftwerk sollte auf einen Punkt noch besonders hingewiesen werden. Das ist der Ausstoß von radioaktiven Gasen resp. Dämpfen. Bekanntlich stoßen auch die Kohlekraftwerke eine nicht zu vernachlässigende Menge von solchen Gasen resp. Dämpfen in die Luft; diese stammen aus den Bestandteilen der Kohlenasche. So kommt das radioaktive Gas Ra^{226} in den durchschnittlichen Kohlenaschen in einer Konzentration von etwa $1 - 10$ Bq/kg vor, was bei einem 1000 MWe Kraftwerk einem jährlichen durchschnittlichen Ausstoß von 1,8 GBq entspricht. (Es sei bemerkt, daß z. B. die Donietzer Kohle einen $10 - 20$ mal so hohen Radiumgehalt hat, als eine Durchschnittskohle. Unter Berücksichtigung der anderen radioaktiven Bestandteile der Kohlenasche erreicht der Ausstoß an radioaktiven Ra-, Th-, Po- und U-Dämpfen und Gasen bei Verwendung dieser Kohlensorte pro 1000 MWe und Jahr einen Gesamtwert von 380—420 GBq, also etwa 200mal so viel, wie beim Durchschnittskohlekraftwerk.)* Selbst der letztgenannte Wert erscheint aber beim Vergleich mit dem Auswurf an radioaktiven Gasen von $100 - 1000$ TBq/a eines gleich großen Kernkraftwerkes der Druckwassertype als sehr gering. Was die Beeinflussung der Umgebung anbelangt, muß aber hierbei berücksichtigt werden, daß es beim Kernkraftwerk hauptsächlich Edelgase (darunter maßgeblich A, Kr^{85} und Xe^{133}) sind, die aus dem Schlot entweichen, deren Wirkung auf die lebendigen Organismen um einige Zehnerpotenzen geringer ist, als die der Aerosole und Dämpfe. (Letztere machen nur einen Bestandteil von $0{,}5 - 5$ GBq/a, 1000 MWe aus). Die Ganzkörperbestrahlung in der Umgebung eines Kohlekraftwerkes wird zu etwa 4mal so hoch errechnet, als beim Kernkraftwerk. Auf einige Organe spezifiziert (z. B. Lunge oder Knochenmark) steigt dieser vierfache Faktor bis auf einige 100 an.

* Gács Iván: Erőművi levegőszennyezés megítélésének módszerei. (Methoden zur Bewertung der Luftverseuchung aus Kraftwerken) Dr.-Dissertation, Technische Universität, Budapest 1978.

Aus dem Standpunkte der Umweltbeeinträchtigung kann zusammenfassend die Schlußfolgerung gezogen werden, daß praktisch alle Energieumformungen mit Schadstoffemission verbunden sind, die die Lebensbedingungen im verschiedenen Ausmaß beeinflussen. Sieht man von der landschaftbeeinträchtigenden Wirkung der Wasserkraftwerke, oder der durch die Hohlspiegel bedeckten Fläche der Sonnenkraftwerke ab, und betrachtet bloß die im Betrieb kontinuierlich ausgestoßenen Schadstoffe, so können bei den fossilen Brennstoffen das Kohlendioxyd und der Schwefel im größeren Umfang Schäden anrichten, als die Radionuklide der Kernkraftwerke. Unvorhergesehene größere Betriebsunfälle der letzteren könnten aber einmal diesen, bis dato durch die Tatsachen nicht in Frage gestellten, Vorteil der Kernkraftwerke im negativen Sinne wettmachen.

2. Wirtschaftliche Fragen

Wenn bei der bisherigen Betrachtung des Energiehorizonts unser Augenmerk in erster Linie auf die Gemeinsamkeiten und Gegensätzlichkeiten gerichtet wurde, die mit naturwissenschaftlichen Grundlagen und mit den, daraus folgenden Erscheinungen zusammenhängen, so sollen im Weiteren eher Fragen wirtschaftlicher Natur behandelt werden. Selbstretend sind letztere für die praktische Beurteilung entscheidend.

2.1. *Vorräte*

An erster Stelle stehen natürlich die Vorräte und deren Ausnutzung, resp. die zu erwartende Lebensdauer der Reserven. Wie bekannt, bestehen zwischen den einzelnen Rohenergieträgern in dieser Hinsicht erhebliche Unterschiede. Tabelle 2 gibt darüber hauptsächlich nach den Angaben der XI. Weltenergiekonferenz Aufschluß; darin sind für die fossilen Energieträger die ausbauwürdigen gesicherten Reserven, die geologisch wahrscheinlichen Vorräte und der Verbrauch des Jahres 1979. angeführt. Die Aufteilung der gesicherten, ausbauwürdigen Reserven beträgt danach: Kohle 70,7%, Öl 20,6% (darunter rund ein Drittel in Schiefern und Sand), Erdgas 8,7%. Bei Berücksichtigung der geologisch wahrscheinlichen Vorräte verschieben sich die Verhältnisse zugunsten der Kohle zu 84,5%, während Öl mit 12,7% (darunter rund 75% in Schiefer und Sand) und Erdgas nur mit 2,8% figuriert. Wir glauben, auf die bekannten Unsicherheiten dieser Daten nicht besonders hinweisen zu müssen, einstweilen muß man gewiß mit den nachgewiesenen, ausbauwürdigen Reserven rechnen.

Vergleicht man die Verbrauchsstruktur z. B. des Jahres 1979 mit der Struktur dieser Reserven, so ergibt sich etwa, daß das Rohöl sechsmal, Erdgas fünfmal so rasch verbraucht wird, als die Kohle. (Bei Betrachtung der geologisch wahrscheinlichen Reserven sind die auf die Kohle bezogenen Verhältniszahlen bei Öl 12, bei Erdgas

Tabelle 2

Fossile Energieträger Reserven (10^3 EJ), *Jahresverbrauch* (1979, EJ), *Strukturen in* %

	Ausbauwürdig		Geol. wahrscheinlich		Verbrauch	
	10^3 EJ	%	10^3 EJ	%	EJ/a	%
Steinkohle und Lignit	18,7	70,7	296,0	84,5	85,0	32,0
Erdöl	5,4	20,6	42,1	12,7	125,0	47,2
		(100)		(100)		(100)
(davon in Schiefer und Sand)	(1,7)	(31,5)	(31,6)	(74,5)	(4,5)	(3,6)
Erdgas	2,3	8,7	8,1	2,8	55,0	20,8
Insgesamt	26,4	100	346,2	100	265,0	100

Vorratsdaten: = Ausbauwürdig: XI. World Energy Conference, München, 1980. Survey of Energy Resources. Part. B. Appendixes

= geol. wahrscheinlich: XI. World Energy Conference, München, 1980. Generalbericht Gl, p. 260

Verbrauchsdaten (1979): = Peter ENGELMANN: Resource Requirements ANS-Transactions, Vol. 37, p. 15

sogar 23). Die allgemein bekannte Ausbeutung der Vorräte an Kohlenwasserstofen ist evident.

Es ist in dieser Hinsicht vielleicht nicht uninteressant an Hand der Abbildung 1 einen Blick auf die zeitliche Entwicklung der gesicherten Reserven der fossilen Energieträger zu werfen. Es wurden hierbei immer die Zahlen derselben Quelle, in diesem Falle der offiziellen Ausgaben der Weltenergiekonferenz zu Grunde gelegt, da es auf dieser Weise noch am ehesten eine Vergleichbarkeit der Angaben angenommen werden kenn. (Bei den Kohlenwasserstoffen fehlen die Angaben bis 1962).

Aus den exponentiell berechneten jährlichen Zuwachsraten der gesicherten Reserven lassen sich einige interessante Folgerungen ziehen: während die gesicherten Reserven der fossilen Energieträger in der Periode 1962—74 jährlich um 2,7% zunahmen, sank diese Zahl in der Zeit zwischen 1975—80 auf 2%. Schuld daran ist das Öl, mit einer jährlichen Zunahme der gemeldeten Reserven von rund 10% zwischen 1962—74 (darunter Ölschiefer und Sand sogar 12,2%). Für die Periode 1974 ÷ 80, also nach dem grossen Ölpreisanstieg, wurden überhaupt keine neuen Ölreserven mehr gemeldet. Es steht außer Zweifel, daß letztere Zahlen aus wirtschaftspolitischen Gründen manipuliert sind. Bei Erdgas sank die jährliche Zuwachsrate von 10% der ersten Periode auf 6,7 in der zweiten. Die Steinkohlenreserven weisen schon seit 1950 überhaupt keine Zunahme auf, bei der Braunkohle stieg die Zuwachsrate von 0,4% der Periode 1962 ÷ 74 nach dieser Zeit auf 2,4%, ein Zeichen für das zunehmende Interesse der Kohlengruben am Energiemarkt.

Bei der Kohle kann man außerdem ein leichtes Ansteigen des Verhältnisses der gesicherten Reserven zu den geologisch wahrscheinlichen Vorräten feststellen. In

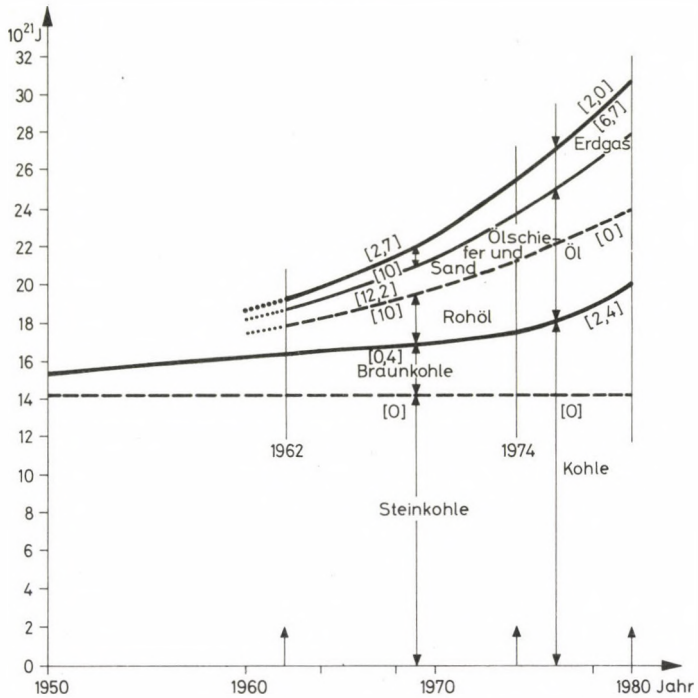

Abb. 1. Änderung der gesicherten Reserven der fossilen Energieträger 1950—1980 [jährliche exp. Zuwachsraten %/a]

Prozenten ausgedrückt waren es: 1974 5,5%, 1976 6,2%, 1977 6,3%. Hierbei dürften auch die verbesserten Abbaumethoden der Kohlenförderung, so der Übergang auf Frontabbau, Tagebau usw. mit eine Rolle spielen, diese ermöglichen eine bedeutende Verringerung der Abbauverluste. Bei der Ölförderung soll das heutige, mit primären Methoden erreichte Ausbringen von bloß 25 – 30% durch die Einführung von sekundären und tertiären Methoden vielleicht sogar verdoppelt werden, was aber von vielen Fachleuten der Ölwirtschaft bezweifelt wird. Immerhin macht eine neueste Studie der Europäischen Wirtschaftsgemeinschaft (EWG) bekannt, daß der Wirkungsgrad des Energieausbringens im Raume der EWG von 46% im Jahre 1970 für den Beginn der 90er Jahre um 28 bis 54% erhöht werden kann.*

2.2. *Energiestruktur*

Zurückkommend auf die Angaben der Tabelle 1 sei bemerkt, daß neben den absoluten, resp. prozentuellen Vorratsmengen der einzelnen Energieträger und neben deren Vergleich mit dem Jahresverbrauch, die zeitliche Änderung, d. h. die Dynamik

* The Economic Commission for Europe and Energy Conservation. Recent Experience and Prospects. UN/ECE/985 New York 1980.

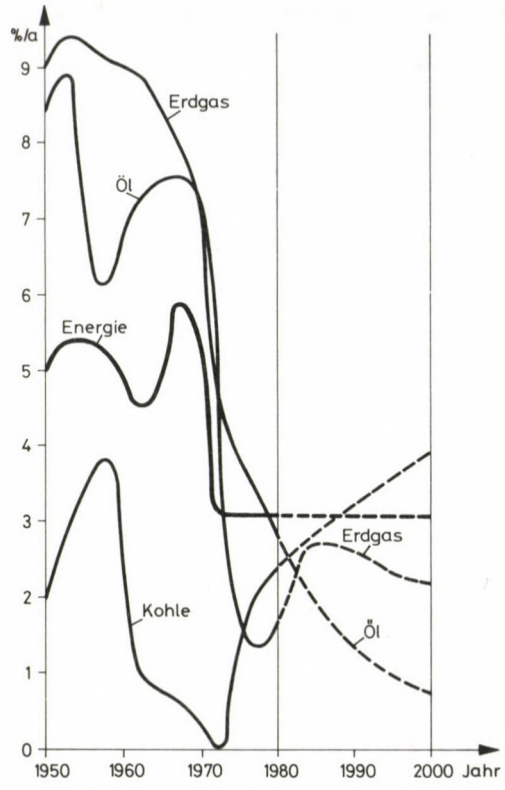

Abb. 2. Jährliche Zuwachsraten der fossilen Energieträger und des Gesamtenergieverbrauches %/a

der Energiestruktur interessante Unterschiede aufweist. Diese können an Hand der Abbildung 2 verfolgt werden. In dieser Abbildung ist auf Grund von Daten resp. für die Zeit nach 1980 auf Grund von Schätzungen der XI. Weltenergiekonferenz der zeitliche Ablauf der jährlichen Verbrauchszuwachsraten der Gesamtenergie und der fossilen Energieträger dargestellt.

Bis zum Beginn der 50er Jahre, als die Kohle als der wichtigste Energieträger noch vorherrschend war, wußte man: ohne Kohle wäre unsere gesamte Zivilisation lahm. Das dauerte so lange, bis die Technik der westlichen Welt sich dem billigen Öl zugewandt hat.

Die Zuwachsrate der Kohlenförderung sank von der II. Hälfte der 50er Jahre beginnend kontinuierlich, bis zum Tiefpunkt Null in den Jahren 1970 – 75. Kohlengruben wurden geschlossen, Millionen von Bergarbeiter arbeitslos. Rohöl und Erdgas erreichten vor 1970 jährliche Zuwachsraten von 6 – 8% und darüber. Dies dauerte bis zur sog. Ölkrise, die eigentlich nie eine Ölkrise, sondern nur eine Krise der Rohölpreise war und ist es auch heute noch. Damit begann ein Come-back der Kohle, die neben der Kernenergie wieder der Energieträger der Gegenwart geworden ist. Nach Schätzungen

werden die jährlichen Zuwachsraten der Kohlenförderung bis zur Jahrhundertende bei etwa 2–3% liegen, Erdgas dürfte auf die 2% Grenze kommen, Rohöl bleibt wahrscheinlich erheblich darunter. Die Wasserkraft behauptet praktisch seit 1920 ihren Anteil an der Weltenergieerzeugung mit ungefähr 6% — oder zeitweilig leicht darüber — und dürfte bis zum Jahre 2000 etwas unter dieser Zahl liegen.

2.3. *Ausnutzbarkeit der Uranvorräte*

Die Frage der Kernenergie benötigt besondere Überlegungen. Da ihre praktische, d. h. friedliche Nutzung erst mit den 60er Jahren beginnt, lagen die jährlichen Zuwachsraten anfänglich sehr hoch und betrugen in der Periode 1976–80 noch immer 26,6%/a. (Sie sind in der Abb. 2 gar nicht eingetragen). Der Gesamtanteil der Kernenergie am Weltenergieverbrauch im Jahre 1980 war 3,1% und wird bis zur Jahrhundertwende etwa bis 13—17% ansteigen. Bei dieser Schätzung bestehen aber bekanntlich sehr große Unsicherheiten. Diese liegen einerseits in den nur sehr angenähert bekannten — oder bekannt gegebenen — Ressourcen, andererseits in dem sog. Materialausnutzungsgrad der Uran- resp. Thoriumerze. Darunter soll das Verhältnis der effektiv gewonnenen Nutzenergie zum potentiellen Energieinhalt der Erze verstanden werden. Dieser Ausnutzungsgrad ist bei den heute meistverbreiteten Leichtwasserreaktoren sehr niedrig. Er liegt größenordnungsmäßig nur bei etwa 0,5–0,6%, d. h. nicht höher, als vor 250 Jahren bei der Newcomenschen atmosphärischen Dampfmaschine (dort natürlich auf die Förderkohle bezogen). Unter Berücksichtigung der heutzutage nur in sehr geringem Umfang durchgeführten Plutoniumrezirkulation würde sich dieser Wert auf etwa 0,8% erhöhen, bleibt also auch weiterhin sehr niedrig. Zu einer, mit den fossilen Brennstoffen auch nur vergleichbar guten Ausnutzung der Naturenergiequellen, — im Falle von Wärmekraftwerken also bis zu einem Wert von über 30% —, wäre bekanntlich die weit ausgedehnte Einführung des Brütersystems notwendig. Durch das Brüterprinzip lassen sich theoretisch Materialausnutzungsgrade von 70–75% erreichen. Praktisch werden aber die Brüter immer mit den, bis zum Zeitpunkt ihrer kommerziellen Einführung vorhandenen thermischen Reaktoren zusammenarbeiten müssen, d. h. sie werden mit letzteren immer ein Kernkraftwerkssystem bilden. — Der Materialausnutzungsgrad eines solchen Systems hängt hauptsächlich von zwei Gruppen von Faktoren ab. Diese sind: einerseits die Breederparameter, das sind sowohl der ursprüngliche Bedarf des Reaktors an spaltbarem Material (U^{235} und Pu^{239}) als auch die Erzeugungsgeschwindigkeit des neuen Brutstoffes (Verdoppelungszeit des Spaltstoffes). Anderseits sind die Zusammensetzung des Kernkraftwerkssystems und dessen Ausbautempo, die auf den Materialausnutzungsgrad des Systems schwerwiegend einwirken.

Vorausgesetzt, daß Brüterreaktoren in absehbarer Zeit zur Verfügung stehen, die den technischen Anforderungen genüge leisten und auch wirtschaftlich konkurrenzfähig sind — wohlbemerkt, keine dieser Bedingungen wird heute noch

selbst von den fortschrittlichsten Brütern erfüllt — kann im System nach dem Jahre 2000 mit einem Materialausnutzungsgrad von höchstens 3–4% gerechnet werden. Selbst diese niedrigen Werte sind aus den erwähnten Gründen heute noch äußerst fraglich.

Sich auf die Nutzung der Spaltungsenergie zu verlassen, ist also — neben allen anderen Problemen —, gleichbedeutend mit einer starken Verschwendung der uns zur Verfügung stehenden Rohenergiequellen. Allein aus diesem Grunde kann daher die Kernenergie aus Spaltungsreaktoren immer nur eine, neben den anderen Energiequellen ergänzende, kompetitive, Energieform bleiben.

2.4. *Preise*

Nach dem II. Weltkrieg, als Energie und Rohstoffe verhältnismäßig reichlich und billig zur Verfügung standen, bildete dies einen der grundlegenden Faktoren der raschen wirtschaftlichen Entwicklung. Demgegenüber muß die, nach dem Jahre 1973 entstandene neue Situation selbst auf lange Sicht nicht nur als ein vorübergehender, sondern als ein permanenter Faktor der Wirtschaftsentwicklung betrachtet werden. Die Energetik wird heute im allgemeinen mit gutem Grund als ein Erreger der Inflation betrachtet, hauptsächlich in Ländern mit vorwiegend starkem Import an Energieträgern. In diesen wird ein immer größer werdender Anteil der Zahlungsbilanz zum Ausgleich der Energieimporte benutzt, wobei die, in vielen Ländern beobachtete Verschlechterung der Austauschverhältnisse mit zur Gravierung der Lage beiträgt. Schwere Gleichgewichtsstörungen im Außenhandel dieser Staaten sind die Folge. Bekannte und betrübliche Beispiele liefern die meisten, Agrarprodukte oder Rohstoffe erzeugenden Entwicklungsländer. Das mehr oder weniger ständige Ansteigen der Energiepreise wird bis zur Entdeckung und wirtschaftlichen Nutzbarmachung neuer, ungemein reichlichen Energiequellen kaum aufzuhalten sein. Die heute vielerorts untersuchte Frage ist die, wie es sich in dieser Hinsicht mit den verschiedenen Energieträgern verhält? Es sollen hier die Resultate des bekannten Wirtschaftsforschers, LEONTIEFF zitiert werden. Er hat einen sog. kostenbedingten Preis der Energieträger durch gleichzeitige Berücksichtigung der geologischen Verhältnisse und des technischen Fortschrittes errechnet unter Zugrundelegung der finanziellen Aufwände der Basisperiode 1970. Nach LEONTIEFF war im Jahre 1980 der relative Preisindex der Kohle cca. 0,95, des Rohöls 1,7, des Erdgases 1,5. Im Jahre 1990 wären der Reihe nach kostenbedingte Preise 0,9, 5,2 resp. 2,7 und im Jahre 2000 sogar 0,7, 7,3 resp. 3,7 zu erwarten. Die Kohle käme danach zufolge der noch zahlreichen günstigen geologischen Lagerstätten mit bewährten Fördertechnologien zum Vorteil gegenüber den Kohlenwasserstoffen. Bei letzteren müßten auch die in großer Tiefe, am kontinentalen Schelf und in großen Entfernungen gelegenen Vorräte mit in die Produktion genommen werden.

Die Erfahrung bestätigt aber, daß ziffermäßig so bedeutende Prioritäten derjenigen der Rohölverarbeitung beträgt. Immerhin sind solche Anstrengungen

Verbraucher meistgesuchten, am leichtesten transportierbaren, lagerbaren und benutzbaren Energieträgers zieht nämlich den Preis des billiger produzierbaren Energieträgers nach. Hinreichendes Beispiel liefert hierfür die Entwicklung des Weltmarktpreises des Urans.

2.5. *Gebrauchswert*

Vom Standpunkte des Verbrauchers ist aber niemals der Preis allein wirtschaftlich ausschlaggebend, sondern der Gebrauchswert des Energieträgers. Der Gebrauchswert ist der, auf die Einheit der Erzeugung (Lieferung, Transportleistung, etc.) bezogene und in Währungseinheiten ausgedrückte Verbrauch der verschiedenen Energieträger. In diesem spiegelt sich der wirtschaftliche Vor- resp. Nachteil wieder, wobei außer den energietechnischen Faktoren, wie Wirkungsgrade, Ausnutzungsgrade, Leistungsziffer, usw. die zur Erreichung dieser Faktoren notwendigen Investitionen, ferner die, auf die gleiche Basis gebrachten Aufwendungen für den Umweltschutz und alle anderen Begleitumstände mitberücksichtigt werden müssen. Die Bestimmung der jeweiligen, sich mit der Zeit dynamisch ändernden Gebrauchswertes ist eine vordringliche Aufgabe eines jeden Energiewirtschafters.

In Ungarn wurde seit längerer Zeit für den wirtschaftlich-technischen Vergleich der verschiedenen Energieträger untereinander der Begriff des sog. Schattenpreises eingeführt. Dieser gibt eigentlich ebenfalls den Gebrauchswert des Energieträgers wieder, nur ist er prinzipiell jeweils nur für geringe zusätzliche Verbrauchsmengen der einzelnen Sektoren zu verstehen. Er ist also ein Zuwachspreis, der sich aus dem Durchrechnen des totalen Landesenergieprogrammes für einen gewissen Energieträger bei gegebenem Gesamtenergieverbrauch ergibt. Als Bezugsgröße dient jeweils der Preis des Rohöls aus dem nahen Orient. Diesen zu 100% angenommen ergibt sich nach derzeitigen Rechnungen für das Jahr 1990 z. B. für die einheimische Kraftwerksbraunkohle ein Schattenpreis von rund 40% des Rohölpreises, für das importierte Erdgas in der Landwirtschaft ein solcher von rund 75%.*

2.6. *Welthandel*

Im Rahmen der wirtschaftlichen Fragen liegt zwischen den Energieträgern ein großer Unterschied bestimmt im deren Anteil am Welthandelsumsatz. Dieser beträgt heute bei der Kohle weniger als 6% der Produktion, bei Rohöl über 50%. Um zu dem, von Sachverständigen für die Jahrhundertwende erwarteten Anteil der Kohle im Weltenergieverbrauch von rund 27% zu kommen, wäre es notwendig, daß das Volumen des Kohlenhandels am Weltmarkt sich etwa vervier-bis fünffacht, und einen Jahresbetrag von rund 1 Milliarde T erreicht. Die hiezu notwendige Infrastruktur an

* OMFB 1-7103 Et. Az energiagazdálkodás komplex vizsgálata (Komplexe Untersuchung der Energiebewirtschaftung). Budapest, 1981, V.

Verladeeinrichtungen, Transportmitteln am Land und See, Hafenanlagen erfordert lange Zeit und große Investitionen. (Allein die Kosten für die Anschaffung der benötigten cca 1000 Frachtschiffe mit je 100 000 T Wasserverdrängung wurden zu 40 Milliarden $ ermittelt, die Gesamtkosten der Umstellung der Energiestruktur von Öl auf Kohle und Kernbrennstoff sollen in der Größenornung von 10 Billionen $ liegen). Es ist nur natürlich, daß das Rohöl unter solchen Umständen den Welthandel am Energiemarkt beherrscht und noch lange beherrschen wird.

Das Erdgas — mit ungefähr 6% Beteiligung im Außenhandel — nimmt dabei eine spezielle Rolle ein, da es an allen Transportwegen besondere Einrichtungen verlangt. Unabhängig davon, ob der Transport via Pipe-line oder Tanker mit flüssigem Erdgas erfolgt, müssen zwischen dem exportierendem und dem importierenden Land ganz enge Verbindungen bestehen, die aber leicht störungsanfällig werden können. Von den politischen Implikationen abgesehen, hat die Atomenergie gegenüber den anderen Energieträgern in dieser Hinsicht ganz besondere Vorteile aufzuweisen.

3. Allgemeine energiepolitische Fragen

Anschließend zu den wirtschaftlichen Faktoren sollen kurz einige allgemeine energiepolitische Fragen berührt werden, die heutzutage sozusagen in jedem Landesprogramm enthalten sind und die für alle Energieträger allgemeine Gültigkeit haben sollten.

3.1. *Energiebewirtschaftung*

An erster Stelle steht, — oder sollte zumindest überall stehen — der möglichst sparsame, rationelle Verbrauch der Rohenergien. (Hierfür gebraucht man heute oft den Ausdruck: Energiekonservierung, da darunter nicht nur die Einsparungen im gebräulichen Sinne, sondern auch die bereits erwähnten technologischen Änderungen des Ausbringens verstanden werden sollen.) Es gehört auch die energiepolitisch zweckmässige Auswahl der Produktionstruktur unter Berücksichtigung der energietechnischen Investitionen hierzu.

Als eines der Endziele der industriellen und landwirtschatlichen Produktion sollte stets des Streben nach einer möglichst niedrigen, auf die Einheit des Bruttonationalproduktes bezogenen Energiebedarfs sein. (Nach Berechnungen, die in Ungarn durchgeführt worden sind, können sich bei verschiedenen Varianten der prognostisierten Landesproduktion, — die alle den gleichen Wirtschaftswachstum voraussetzen, voneinander aber in der Zusammensetzung der Produktionsstruktur unterscheiden —, im Landesenergiebedarf Unterschiede bis zu 100%, in den notwendigen Investitionen des Energiesektors und im Energieimport bis zu 400% ergeben.) Die richtige Lenkung des Energiebedarfs wird sicherlich allmählich einer der wichtigsten Faktoren bei den staatlichen und privatwirtschaftlichen Entscheidungen über die zukünftige Entwicklung sein.

3.2. Neuerungen im Energiesektor

Die notwendige Senkung des Energiebedarfs im allgemeinen und auf die Landesproduktion bezogen im besonderen, ferner eine vernünftige Energiebewirtschaftung sind Forderungen, die ohne Unterschied für alle Energieträger Gültigkeit haben sollten. Wenn man aber die Möglichkeiten betrachtet, die in der aus Produktion, Umwandlung, Transport und Verbrauch bestehenden Kette der einzelnen Energieträger als Neuerungen, Innovationen, in Frage kommen, so findet man wieder gewaltige Verschiedenheiten. Einige davon sollen kurz erwähnt werden.

3.2.1. Kohle

Die allgemeinverbreitete direkte Verbrennung der Kohle wird — wenigstens bei kleineren Einheiten — wahrscheinlich durch die Wirbelschichtfeuerung verdrängt, die in erster Linie bezüglich Umweltbelastung günstigere Bedingungen zu bieten verspricht. (Es sei nur nebenbei erwähnt, daß das, durch die ungarischen Ingenieure SZIKLA und ROZINEK weit vor dem II. Weltkrieg entwickelte Verfahren der zweistufigen Verbrennung praktisch auf demselben Prinzip ruhte. Nur kam man damals noch nicht auf den Gedanken, die schädlichen Bestandteile der Asche durch chemische Beimengungen in die flüßige Schlacke einzuführen.)

Weltweit werden große Anstrengungen gemacht um aus der Kohle durch Vergasung oder durch Verflüssigung günstigere Zweitenergieträger zu erzeugen. Für kleine und mittlere Verbraucher wird kurzzeitig wahrscheinlich die Ausbreitung der Gasdarbietung in der Form von umweltfreundlichen Generatorgas verhältnismäßig niedrigen Heizwertes (5—15 MJ/m^3) die zweckmäßige Lösung sein. Auf lange Sicht gesehen dürfte das synthetische Erdgas (SNG-Gas) mit einem Mindestheizwert von 34 MJ/m^3, zum großen Teil durch die bestehenden Erdgasleitungen zum Verbraucher geführt, die rasch zunehmende Diskrepanz zwischen Erdgasangebot und Nachfrage ausgleichen. Die technologische Entwicklung bei der Vergasung wird durch das Streben nach größeren Einheitsleistungen, besseren Wirkungsgrad, effektivere Gasreiningung gekennzeichnet. Es wird die Bereitstellung der nötigen Reaktionswärme aus äußerer Quelle, so z. B. von Hochtemperaturreaktoren in Erwägung gezogen. Da eine wirtschaftlich ausgereifte Entwicklung solcher Hochleistungs- und Hochtemperaturreaktoren noch mindentens 10 Jahre in Anspruch nehmen wird, ist eine grundlegende Beeinflussung der Energiestruktur auf diesem Wege in diesem Jahrhundert kaum zu erwarten.

Dies dürfte für die verschiedenen Kohleverflüssigungsverfahren in erhöhtem Ausmaße zutreffen, da die diesbezüglichen Forschungen derzeit noch weit hinter denen der Kohlevergasung stehen. Das synthetische Öl wird wahrscheinlich eher als Rohstoff der Chemie und in viel geringerem Ausmaß als Energieträger zur Verfügung stehen, da z. B. der Umwandlungswirkungsgrad bei der Kohleverflüssigung nur etwa 60 – 70% derjenigen der Rohölverarbeitung beträgt. Immerhin sind solche Anstrengungen

bezeichnend für alle Anwendungsgebiete, wo man nicht mit der Konkurrenz der Atomenergie rechnen muß. Das ist also in erster Linie im Verkehrswesen, in der Industrie, im kommunalen Bereich.

Da die Atomenergie selbst zur Jahrhundertwende in erster Linie in Kernkraftwerken benutzt werden kann und solche dann etwa 20–25% der Kraftwerkskapazität ausmachen dürften mit einem Anteil der Kernenergie — wie bereits erwähnt — von 13 bis 17%, bleibt für die Kohlevergasung resp. Verflüssigung ein hinreichend großes Anwendungsgebiet. (Die verflüssigte Kohle kann z. B. von den riesigen Kohlengruben der mittelasiatischen und fernöstlichen Sowietrepubliken durch Rohrleitungen bestimmt wirtschaftlicher und betriebssicherer ferntransportiert werden, als die elektrische Energie durch Höchstspannungsleitungen).

3.2.2. Kernenergie

Über die hauptsächlichste Entwicklungsrichtung der Kernspaltungsreaktoren ist bereits im Zusammenhang mit der Ausnutzung der Uran- und Thoriumvorräte gesprochen worden. Das Ziel ist die Erreichung eines 20–40-mal größeren Materialausnutzungsgrades durch des Brüterverfahren, ein Ziel, das aber die Gesamtheit der Kernkraftwerke betrachtet, noch in der fernen Zukunft zu liegen scheint. Es besteht die große Frage, ob es überhaupt noch zu dieser Entwicklung kommen wird.

Denn die andere Möglichkeit der Kernenergienutzung, die durch Fusion der leichten Atomkerne, steht — wenn auch nicht unmittelbar — vor der Tür, schickt ihre Boten aber bereits in die wissenschaftlichen Laboratorien voraus und — wird wahrscheinlich noch in diesem oder im nächsten Jahrzehnt — in den Versuchsbetrieben erscheinen. Nach neuesten Berichten ist es in Princeton (USA) gelungen die stattgefundene Fusion zwischen He^3 und D-Kernen mit einer Leistung von 60 W zu beweisen. Mit ihren tatsächlich unerschöpflichen Rohstoffen aus dem Meerwasser (Anteil des D_2 rund 1/6000-stel) und mit dem weit umweltfreundlicheren Verhalten gegenüber der Spaltungsenergie wird die Fusion gewiß die wichtigste Energiequelle der Zukunft sein. Selbst dann, wenn heute noch der physikalische Beweis der Durchführbarkeit des Verfahrens nicht erbracht ist und die technischen und technologischen Schwierigkeiten ungeheuer groß sind, von der erwarteten Wirtschaftlichkeit ganz zu schweigen.

3.2.3. Erneuerbare Energien

Diese sind sehr wichtig obwohl sie heute und in den kommenden 1–2 Jahrzehnten keinen wesentlichen Beitrag zur Lösung des Weltenergieproblems liefern können.

Wie bereits bemerkt, trägt die Wasserkraft heute mit ungefähr 6% zum Gesamtenergieaufwand der Welt bei, wobei aber erst cca. 17% der technisch möglichen

Kapazität ausgebaut sind. Weit die größere Hälfte der nicht erschöpften Möglichkeiten liegt in den Entwicklungsländern, wo akuter Kapitalmangel herrscht. Dies und in den meisten Fällen die unzugängliche Gegend des zukünftigen Wasserkraftwerkes, daher kostspielige Energiefortleitung, das Fehlen des technisch geschulten Personals usw., sind die wesentlichsten Motive der bisher so schwachen Ausnutzung der Wasserkraft.

Für die übrigen wichtigeren erneuerbaren Energiequellen, wie Sonne, geothermale Energie, Biomasse, Wind usw. kann man als gemeinsames Merkmal die äußerst geringe Leistungsdichte hervorheben, wozu sich in den meisten fällen — wie auch bei der Wasserkraft — geographische Gebundenheiten dazukommen. Um nur einige Vergleichsdaten zu nennen: die Leistungsdichte der Sonnenbestrahlung an der Erdoberfläche in der besten Position — Mittagstunden im Sommer, am Äquator, wolkenloser Himmel — beträgt rund 160 W/m^2. Demgegenüber finden wir im Automobilzylinder einen 500-fachen, im Brennkammer eines Hochleistungsdampferzeugers einen 5000-fachen, im Druckgefäß eines Druckwasserreaktors einen 2 millionenfachen Wert. Andererseits ist die durchschnittliche Leistungsdichte der geothermischen Energie an der Erdoberfläche nur rund 1/3000 der Sonnenenergie, natürlich mit großen lokalen Abweichungen.

Die geringe Leistungsdichte verlangt beträchtliche Investitionen, die durch die, mit dem Verbrauch zeitlich nicht in Einklang stehende Bereitschaft (z. B. bei der Sonne), resp. zu deren Ausgleich notwendigen Speicheranlagen noch weiter erhöht werden. Das Fehlen der Wirtschaftlichkeit ist heute noch das gemeinsame Merkmal der weit ausgedehnten Nutzung der Sonnenenergie sowohl als direkte Wärmequelle (bei niedrigen und noch mehr bei höheren Temperaturen), als auch am Wege der Biokonversion. Bei letzterer kommen noch Schwierigkeiten organisatorischer Art dazu. Als Beispiel für die mögliche Nutzung der Biomasse sei Ungarn genannt, wobei jährlich eine lufttrockene pflanzliche Fitomasse von etwa 93 Millionen T entsteht, die von der Luft rund 35 Millionen T elementaren Kohlenstoff bindet. Der Karbongehalt der, von der Landwirtschaft primär nicht benutzten Nebenprodukte ist rund 14 Millionen T jährlich, dies entspricht dem Karbongehalt der gesamten ungarischen Produktion von fossilen Brennstoffen.* Durch Erzeugung von Biogas mit einem Methangehalt von 55 – 70% und einem Heizwert von 22 – 26 MJ/m^3, oder durch Fermentation zu Alkohol, usw. könnte die ungarische Landwirtschaft energetisch selbsterhaltend werden, also eine vielversprechende Möglichkeit der Zukunft. Weltweit gesehen bedeutet die Biomasse ebenfalls die günstigste Verwendung der erneuerbaren Energierohstoffe.

Ebenso lokal oder regional bedingt ist die Nutzung mehrerer anderen erneuerbaren Energiequellen, wie Wind, Gezeiten, Wellen usw. Man rechnet — nicht ganz sinngemäß — auch die geothermische Energie zu dieser Kategorie.

* LÁNG István: „A magyar mezőgazdaság és a természeti erőforrások, lehetőségek és korlátok". (Die ungarische Landwirtschaft und die natürlichen Kraftquellen, Möglichkeiten und Grenzen.). Gazdálkodás **24** (1980), 5

4. Zusammenfassung

Hinreichende Energie ist eine, wenn auch nicht die einzige Voraussetzung des Wohlstandes, dabei soll das Wort „hinreichend" keinesfalls im Sinne der Verschwendung verstanden werden. Im Gegenteil: äußerste Sparsamkeit, vorausblickende Planung, Ausarbeitung von verschiedenen Optionen sind zur Erreichung einer ausreichenden Sicherheit der Darbietung unumgänglich notwendig. Dabei müssen die Gesichtspunkte des Umweltschutzes und der Bereitstellung der notwendigen Investitionen ebenfalls in den Vordergrund treten.

Der Kampf um den Rohstoff Energie dehnt sich zusehendst vom technisch-wirtschaftlichem Bereich auch in das politisch-militärische aus. Es ist bestimmt überflüssig in diesem Zusammenhang auf die offenen oder halboffenen kriegerischen Auseinandersetzungen dieses Jahrhunderts um den Besitz der Ölfelder, Kohlen- oder Urangruben hinzuweisen. Solche Kriege wurden in der Vergangenheit oft geführt und werden leider auch in der Zukunft noch geführt. Dies dürfte in unserer Betrachtungsweise die letzte, aber weitaus gefährlichste Gemeinsamkeit der heute benutzten Energieträger sein.

Dieses düstere Gebiet absichtlich ausklammernd sollen abschließend die gemeinsamen friedlicheren Aspekte hervorgehoben werden. Diese sind:

— der beinahe lückenlos gemeinsame nukleare Ursprung,
— das bei der Umwandlung ebenfalls fast lückenlos anwendbare Äquivalenzgesetz,
— die bei allen Energieumsetzungen frei gewordene Wärme als Umweltbelastung.
— die gemeinsame Bewertbarkeit der Energieträger,
— die zwingende Bewirtschaftung.

Gleichzeitig liegen tiefgreifende Gegensätzlichkeiten vor:

— in der Verschiedenheit der chemischen, physikalischen und biologischen Risikofaktoren,
— in den Vorräten und deren Änderungsraten,
— in der Dynamik der Verbrauchsstruktur,
— in der Preisentwicklung,
— im Welthandelsumsatz,
— in den Innovationsmöglichkeiten.

Eine sorgfältige Abwägung der Gemeinsamkeiten und der Gegensätzlichkeiten mit Hilfe der Wissenschaft ist unerläßlich um gepaart mit dem menschlichen Erfindergeist die Bedingungen schaffen zu können, die notwendig sind um die zunehmenden, aber auf das erforderliche Mindestmass reduzierten Energiebedarfsmengen technisch und wirtschaftlich sicher, unter Vermeidung der Umweltbelästigungen zur Verfügung zu stellen.

Identities and Contrasts between Energy Carriers. — The purpose of the paper is to promote the correct discrimination among the energy problems, discussed so often and at so many forums by analysing the identities and contrasts between the natural and processed energy carriers from the point of view of natural science and economy, and to make comparison between them. Besides the classic fossile and nuclear energy carriers and also the renewable sources of energy and fusion are treated, as promising potentialities for the future.

Acta Technica Academiae Scientiarum Hungaricae, 93 (1—2), pp. 25—29 (1981)

К ВОПРОСУ РАСЧЕТА КОНЦЕНТРАЦИЙ ВРЕДНЫХ ГАЗООБРАЗНЫХ ПРИМЕСЕЙ ОТ ПРОМЫШЛЕННЫХ ИСТОЧНИКОВ

ВОЛКОВ Э. П.

Для расчета концентраций вредных примесей от промышленных источников в приземном слое атмосферы широко используются выражения, получаемые при решении параболического уравнения турбулентной диффузии. Проведенные нами в аэродинамической трубе исследования гидродинамической и тепловой составляющих подъема факела и натурные эксперименты на действующих станциях, позволили получить расчетные выражения для определения подъема факела при различных метеорологических и режимных параметрах. Используя расчетную схему для определения подъема факела, можно предложить математическую модель расчета концентраций вредных примесей на уровне дыхания людей при различных технологических и метеорологических условиях.

Для расчета концентраций вредных примесей от промышленных источников в приземном слое атмосферы широко используются выражения, получаемые при решении параболического уравнения турбулентной диффузии [1, 2, 3]. В этом случае реальный источник выброса примесей заменяется условным, точечным, приподнятым на высоту подьема факела над устьем газоотводящей трубы. Высота подьема факела, обусловленная наличием начальных импульсов движения и тепла, определяется по весьма разнообразным формулам, которые не всегда коррелируют между собой [4]. Проведенные нами в аэродинамической трубе исследования гидродинамической и тепловой составляющих подъема факела и натурные эксперименты на действующих станциях, позволили получить расчетные выражения для определения подъема факела при различных метеорологических и режимных параметрах [5, 6]. Используя расчетную схему для определения подъема факела, можно предложить математическую модель расчета концентраций вредных примесей на уровне дыхания людей при различных технологических и метеорологических условиях, которая сводится к следующему. При конечной скорости распространения примеси угол раскрытия факела определяется интенсивностью турбулентности, возникающей при взаимодействии факела со сносящим потоком на начальном участке подъема факела (гидродинамический подьем) и интенсивностью турбулентности атмосферы в конечной стадии подъема факела (тепловой подъем). Если при упрощенном подходе принять, что интенсивность турбулености в вертикальной плоскости вдоль всей траектории движения факела постоянна и определяется вертикальной составляющей интенсивности турбулентности атмосферы ε_z, то границы факела при его расширении определяются достаточно просто.

Из рассмотрения средней траектории движения можно записать уравнение средней линии подъема факела [5].

$$z = kx^n$$

где (1)

$$K = \sqrt{0{,}42\frac{W_0 D_0}{U} + 0{,}3\frac{gW_0 D_0^2 \Delta T}{T_r U^3 \varepsilon_y}}$$

Здесь W_0, U — соответственно, скорость выхода газов из устья трубы и скорость ветра; D_0 — диаметр устья трубы; ΔT — перепад температур между выбрасываемыми газами и окружающей средой на уровне устья трубы; T_r — температура газов на выходе из трубы; ε_y — поперечная составляющая интенсивности турбулентности атмосферы в зоне подъема факела; n — показатель степени (в случае $\frac{x_3}{D_0} \leq 120$ $n = 0{,}5$, при $\frac{x_3}{D_0} > 120$ $n = 0{,}35$). Тогда выражение для нижней границы факела, обусловленной конечной скоростью распространения примесей запишется в виде

$$z = h + kx^n - \varepsilon_z \cdot x \tag{2}$$

где h = геометрическая высота газоотводящей трубы. При условии $z = 0$ получаем точку касания земли нижней границей факела $-x_3$. В случае $n = 0{,}5$

$$x_3 = \frac{k^2 + 2h\varepsilon_z + K\sqrt{k^2 + 4h\varepsilon_z}}{2\varepsilon_z^2} \tag{3}$$

Подъем факела над устьем трубы определяется как разница между точкой средней траектории движения факела А и верхним обрезом газоотводящей трубы по вертикали в месте касания нижней границей факела земли. Поместив на этой высоте точечный источник, при условии изотропной в вертикальной плоскости атмосферы ($\varepsilon_z = \text{const}$), мы будем иметь поля концентраций пассивных примесей примерно одинаковые от точечного и реального источников.

Заменив реальный источник точечным, поля концентраций просто рассчитать, воспользовавшись для этого данными [7]. Математическая модель для расчета концентраций газообразных выбросов при различных состояниях атмосферы и технологических параметрах представлена на рис. 1.

Для проверки предложенной модели на тепловой электростанции общей мощностью 3600 МВт с трубами высотой 320 м были проведены комплексные натурные эксперименты. Одновременно фиксировались характеристики выбросов через дымовые трубы ГРЭС, метеорологические параметры, положение дымового факела и концентрации газообразных ингредиентов на уровне

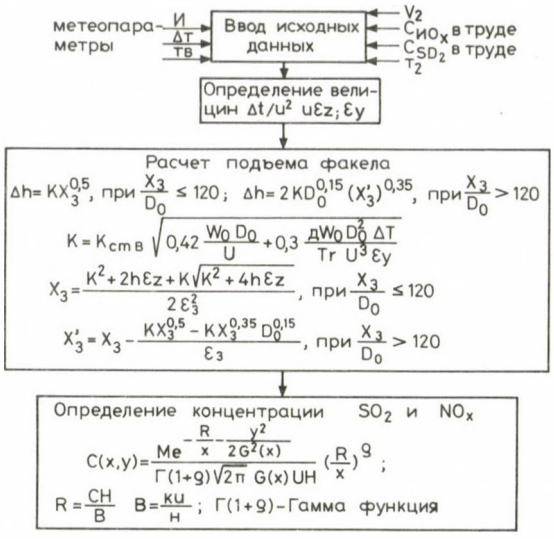

Рис. 1. Математическая модель расчета концентрации вредных примесей с учетом технологических и метеорологических параметров

дыхания людей. Как видно из рис. 2 результаты расчетов концентраций пассивных примесей по предлагаемой математической модели удовлетворительно соотносятся с экспериментальными данными, полученными в условиях развитого турбулентного обмена в атмосфере и в случае нейтральной стратификации. Предлагаемая модель может быть использована при разработке актуальных в настоящее время задач по созданию автоматизированных систем контроля загазованности атмосферы от вредных выбросов промышленных предприятий [8]. Она позволяет установить функциональные связи между исходными и результирующими характеристиками и может быть использована, как научная основа для организации постоянного контроля за выбросами промпредприятий. Более того, зная годовое изменение метеорологических и технологических параметров, возможно прогнозирование уровня концентраций в районе расположения мощного промышленного источника, что, в совокупности с набором мероприятий по кратковременному снижению выбросов, позволяет установить их предельно-допустимые значения. Модель позволяет также подойти к новой сангигиенической оценке воздействия выбросов на окружающую среду. Если в настоящее время критерием воздействия на биосферу является предельно-допустимые разовые и суточные концентрации вредных выбросов, то, используя модель, мы можем рассчитывать дозу воздействия, вредных выбросов на биосферу, под которой понимается воздействие определенной концентрации примесей в течение времени её действия на данный сектор местности. Безусловно, определение дозы возможно только при

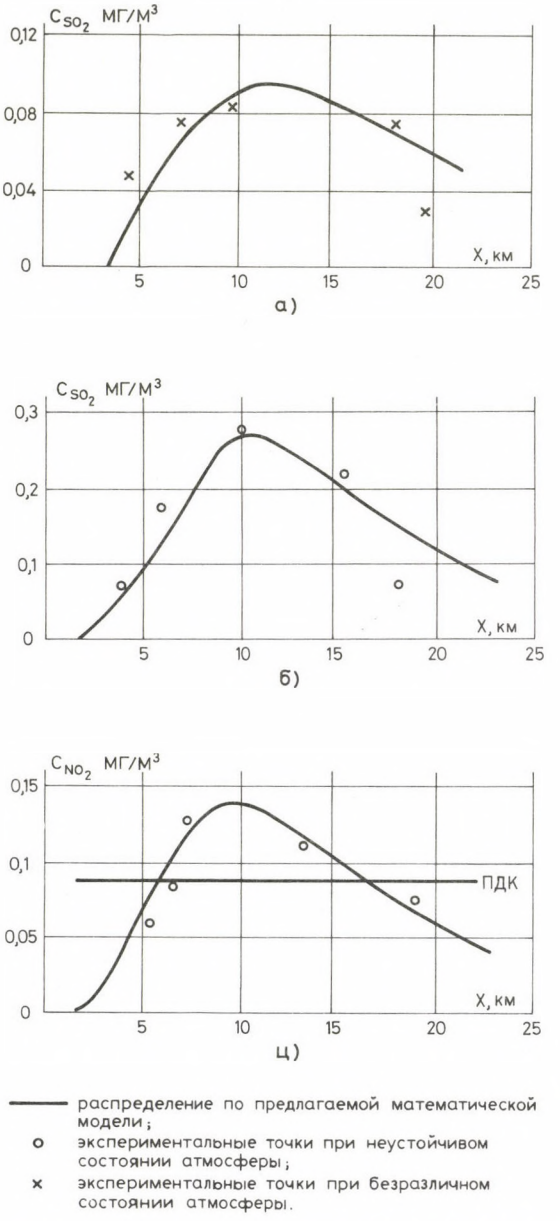

Рис. 2. Распределение концентраций SO_2 и NO_x в зависимости от расстояния до дымовой трубы: — — — распределение по предлагаемой математической модели; ∘ — экспериментальные точки при неустойчивом состоянии атмосферы; X — экспериментальные точки при безразличном состоянии атмосферы

наличии системы контроля загазованности атмосферы, когда фиксируются метеопараметры (скорость и направление ветра и градиент температуры воздуха) и величины выбросов в атмосферу. Данный подход, как нам представляется, позволит более обоснованно определять ущерб, наносимый вредными выбросами окружающей среде, и концентрировать вложения в охрану среды на наиболее опасных источниках.

ЛИТЕРАТУРА

1. Берлянд, М. Е.: Современные проблемы атмосферной диффузии и загрязнения атмосферы. Гидрометеоиздат, Л.: 1975, 448с
2. Монин, А. С.—Яглом, А. М.: Статическая гидромеханика. М. Наука (1965). ч II, 647с
3. Бызова, Н. Л.: Рассеивание примесей в пограничном слое атмосферы. М.: Гидрометеоиздат (1974) г. 189с
4. Рихтер, Л. А.—Волков, Э. П.—Кормилицин, В. И.: Тепловой подъем газов из дымовых труб ТЭС. Теплоэнергетика (1973) № 2, с. 52—57
5. Волков, Э. П. Исследование подъема факела над устьем газоотводящих труб. Инж-физ. журнал т. XXXVI (1979), с. 700—707
6. Волков, Э. П.—Грибков, А. М.—Санаров, М. И.: Распространение дымового факела в процессе эксплуатации тепловой электростанции. Теплоэнергетика (1979) № 3, с. 33—37
7. Бызова, Н. Л.: Методическое пособие по расчету рассеяния примесей в пограничном слое атмосферы, Гидрометеоиздат, М.: (1973), 44с
8. Волков, Э. П.—Жабо, В. В.—Сапаров, М. И.: Особенности разработки системы контроля загрязнения атмосферы выбросами ТЭС. Теплоэнергетика (1980) № 11, с. 9—13

Problems in the Calculation of the Concentration of the Injurious Gaseous Impurities of Industrial Pollution Sources. — For the calculation of the concentration of the impurities produced by the industrial pollution sources on the atmospheric ground level, the expressions obtained in solving the parabolic equation of the turbulent diffusion are widely used. On the basis of wind-tunnel tests and measurements performed by the author in working power plants calculation relationships have been obtained for the estimation of the hydrodynamic and thermic lift of the column of smoke for different meteorologic and operation parameters. By making use of the calculation method of lift, a mathematical model may be proposed to the calculation of the concentration of the injurious impurities.

Fragen der Konzentrationsberechnung der aus industriellen Quellen entstehenden schädlichen gasartigen Verunreinigungen. — Zur Berechnung der Konzentration der durch die Industrie auf der Grundfläche der Atmosphäre hervorgerufenen Verunreinigungen werden die bei der Lösung der parabolischen Gleichung der turbulenten Diffusion erhaltenen Ausdrücke in weiten Kreisen angewandt. Die vom Autor durchgeführten Windtunnelversuche und in einigen im Betrieb befindlichen Kraftwerken vollgezogenen Messungen ergaben Beziehungen zur Berechnung der hydraulischen und thermischen Hebehöhe der Rauchfahne für verschiedene meteorologische und Betriebsparameter. Mit Hilfe der Berechnungsmethode der Hebehöhe kann man ein mathematisches Modell zur Konzentrationsberechnung der schädlichen Verunreinigungen vorschlagen.

Acta Technica Academiae Scientiarum Hungaricae, 93 (1—3), pp. 31—37 (1981)

ELLIPTIC PLATE WITH CLAMPED EDGE

P. CSONKA

DR. OF TECHN. SCI.

[Manuscript received January 2, 1981]

Applying the usual assumptions of the technical theory of elasticity, an elliptic plate with clamped edge is analysed. The plate in question is subject to normal loads of polynomial distribution. It is demonstrated that exceptionally in the present case the deflection and stress pattern of the plate can be expressed by very simple closed formulae.

1. Introduction

Solution of problems in technical theory of elasticity yields complex relationships as a rule, and but seldom can solution of the arisen problems be expressed by closed formulae. The problem to be considered below, i.e., problem of an elliptic plane plate with clamped edge, subject to normal loads of polynomial distribution, is an exception. Namely in this case, formulae describing deformation and internal forces of the plate are of closed form. Formulae for uniformly distributed normal loads and for linearly varying normal pressure are known from publications [3 to 11]. These solutions will be completed below by a procedure for loads distributed according to an arbitrary polynomial, and formulae directly applicable will be given for certain simple loading cases.

The method to be presented involves the assumption that the plate is made of an orthotropic linear-elastic material, it is of constant thickness, thin compared to other dimensions of the plate. Again, the plate is assumed to undergo slight deformation under load.

2. Basic concepts, notations

Discussions will refer to an orthogonal coordinate system $0(x, y, z)$ with origin 0 at the centre of the elliptic plate, axes x and y coincident with principal axes of the middle plane. Principal radii of the edge line along x and y will be denoted by a and b, resp. (Fig. 1) and simplifying notations

$$\frac{x}{a} \equiv \xi \qquad \frac{y}{b} \equiv \eta \tag{1}$$

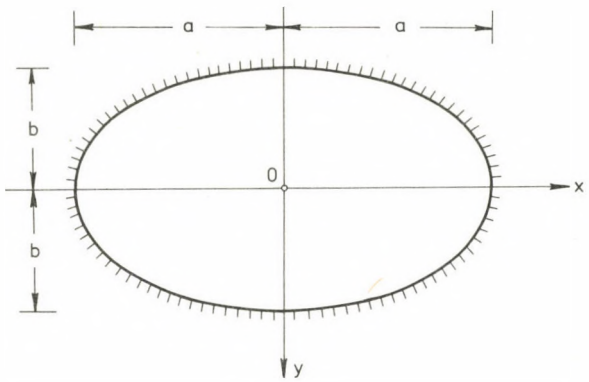

Fig. 1

and

$$\frac{a}{b} = \gamma \tag{2}$$

will be introduced.

In coordinate system $0(x, y, z)$, equation of the middle plane edge line becomes

$$\frac{x_0^2}{a^2} + \frac{y_0^2}{b^2} - 1 = 0 \tag{3}$$

where x_0, y_0 are coordinates x, y of edge line points.

Forces of polynomial distribution will be reckoned with as plate loads, considered as positive if acting in the positive direction z. Their specific value is expressed by polynomial

$$p = p_{00} + p_{10}\xi + p_{01}\eta + p_{20}\xi^2 + p_{11}\xi\eta + p_{02}\eta^2 + \dots \tag{4}$$

where values $p_{00}, p_{10}, p_{01}, p_{20}, p_{11}, p_{02}, \dots$ are given constants.

Plate deformation under loads p is described by displacement function

$$w = w(\xi, \eta) \tag{5}$$

expressing displacement of middle plane points in direction z. In compliance with the technical theory of elasticity [1 to 5] this function corresponds to differential equation

$$\frac{1}{a^4} \cdot \frac{\partial^4 w}{\partial \xi^4} + \frac{2}{a^2 b^2} \cdot \frac{\partial^4 w}{\partial \xi^2 \cdot \partial \eta^2} + \frac{1}{b^4} \cdot \frac{\partial^4 w}{\partial \eta^4} = \frac{p}{K} \tag{6}$$

where K is the so-called plate constant expressing the bending stiffness of the plate, i.e.:

$$K = \frac{Et_0^3}{12(1-\mu^2)}. \tag{7}$$

Here E is the Young's modulus, and μ the Poisson's ratio of the material, and t_0 the plate thickness.

The plate being clamped at its edge, displacement function w has to meet boundary conditions

$$w = 0 \tag{8}$$

and

$$\frac{\partial w}{\partial \xi} = 0; \qquad \frac{\partial w}{\partial \eta} = 0. \tag{9}$$

3. Solution of the problem

The unknown displacement function w is attempted to be assumed in the form

$$w = \frac{a^4}{K}(\xi^2 + \eta^2 - 1)^2 G(\xi, \eta) \tag{10}$$

where $G(\xi, \eta)$ is a polynomial of unknown coefficients of the same number of degrees as that of the load function:

$$G = G_{00} + G_{10}\xi + G_{01}\eta + G_{20}\xi^2 + G_{11}\xi\eta + G_{02}\eta^2 + \ldots . \tag{11}$$

By its very builtup, function w of the construction above *a priori* meets boundary condition (8), and at the same time boundary conditions (9). Thereby solution of the problem is reduced to the determination of unknown coefficients $G_{00}, G_{10}, G_{01}, G_{20}, G_{11}, G_{02}, \ldots$ having values such that function w exactly meets differential equation (6).

Polynomial G is advisably composed of parts corresponding to terms in the load polynomial. Coefficients of each part — in lack of relevant, tabulated, complete formulae — have to be determined from differential equation (6). This operation requires to solve a set of more or less linear equations depending on the order of magnitude and structure of the load polynomial. The calculation itself is advisably performed step by step, conveniently grouping the terms.

For instance, if the load polynomial is a function even both in x and in y, of pure order m, then polynomial G is a function of order m with $m!$ terms. Now, solution of the problem requires to determine $m!$ unknowns, thus, to solve a set of $m!$ linear equations. Calculation starts by determining coefficients of terms of order m, requiring to solve a set of $(m/2+1)$ linear equations. Thereafter coefficients of terms of order $(m-2)$ are to

Table 1

p	Coefficients of polynomial G
1	$G_{00}=\dfrac{1}{8(3+2\gamma^2+3\gamma^4)}$
ξ	$G_{10}=\dfrac{1}{24(5+2\gamma^2+\gamma^4)}$
η	$G_{01}=\dfrac{1}{24(1+2\gamma^2+5\gamma^4)}$
ξ^2	$G_{00}=\dfrac{2(3+11\gamma^2+41\gamma^4+9\gamma^6)}{3(3+2\gamma^2+3\gamma^4)(5+20\gamma^2+78\gamma^4+20\gamma^6+5\gamma^8)}$ $G_{20}=\dfrac{1+4\gamma^2+15\gamma^4}{3(5+20\gamma^2+78\gamma^4+20\gamma^6+5\gamma^8)}$ $G_{02}=\dfrac{-(2+2\gamma^2)}{3(5+20\gamma^2+78\gamma^4+20\gamma^6+5\gamma^8)}$
$\xi\eta$	$G_{11}=\dfrac{1}{24(5+6\gamma^2+5\gamma^4)}$
η^2	$G_{00}=\dfrac{2(9\gamma^2+41\gamma^4+11\gamma^6+3\gamma^8)}{3(3+2\gamma^2+3\gamma^4)(5+20\gamma^2+78\gamma^4+20\gamma^6+5\gamma^8)}$ $G_{20}=\dfrac{-(2\gamma^2+2\gamma^4)}{3(5+20\gamma^2+78\gamma^4+20\gamma^6+5\gamma^8)}$ $G_{02}=\dfrac{15+4\gamma^2+\gamma^4}{3(5+20\gamma^2+78\gamma^4+20\gamma^6+5\gamma^8)}$

be determined, requiring to solve a set of $(m/2-1)$ equations. Proceeding step by step, at last, coefficient of the absolute term will be determined, involving to solve a single equation.

Unknown coefficients of polynomial G are advisably determined in similar steps in other load cases, too.

For certain simple cases, coefficients of polynomial G may be read off Table 1, directly yielding solution of the problem in any load case described by a second-order polynomial.

From among possible load cases, special mention is due to the case of a plate loaded along ellipses similar to the edge line by forces of uniform intensity, outwards

quadratically increasing. In this particular case

$$p_{20}=p_{02}\equiv A$$

and the load function is

$$p=A(\xi^2+\eta^2)\,.$$

Displacement function

$$w=\frac{a^4}{K}(\xi^2+\eta^2-1)^2\,(G_{20}\xi^2+G_{02}\eta^2+G_{00})$$

where G_{00}, G_{20} and G_{02} are composed of two parts, each corresponding to both load terms:

$$G_{00}=\frac{2A}{3}\cdot\frac{(3+11\gamma^2+41\gamma^4+9\gamma^6)+(9\gamma^2+41\gamma^4+11\gamma^6+3\gamma^8)}{(3+2\gamma^2+3\gamma^4)\,(5+20\gamma^2+78\gamma^4+20\gamma^6+5\gamma^8)}$$

$$G_{20}=\frac{A}{3}\cdot\frac{(1+4\gamma^2+15\gamma^4)-(2\gamma^2+2\gamma^4)}{5+20\gamma^2+78\gamma^4+20\gamma^6+5\gamma^8}$$

$$G_{02}=\frac{A}{3}\cdot\frac{(15+4\gamma^2+\gamma^4)-(2+2\gamma^2)}{5+20\gamma^2+78\gamma^4+20\gamma^6+5\gamma^8}\,.$$

4. Plate stresses

In possession of displacement function w, moments due to load p are obtained from known formulae of the theory of plates [1 to 5]:

$$m_x=-K\left(\frac{\partial^2 w}{\partial x^2}+\frac{\partial^2 w}{\partial y^2}\right),$$

$$m_{xy}=-K(1-\mu)\frac{\partial^2 w}{\partial x\cdot\partial y}\,,$$

$$m_y=-K\left(\frac{\partial^2 w}{\partial y^2}+\frac{\partial^2 w}{\partial x^2}\right).$$

At a point $x=x_0$, $y=y_0$ of the plate edge line (Fig. 2) it is:

$$\tan\varphi=-\frac{1}{\partial y/\partial x}=\frac{a}{b}\cdot\frac{\sqrt{a^2-x_0^2}}{x_0}=\frac{a^2y_0}{b^2x_0}\,,$$

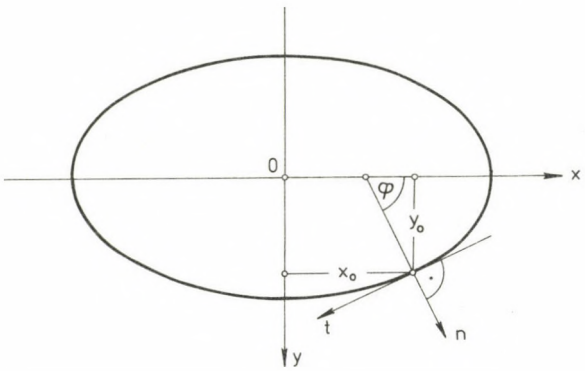

Fig. 2

hence:

$$\sin^2 \varphi = \frac{a^4 y_0^2}{b^4 x_0^2 + a^4 y_0^2},$$

$$\cos^2 \varphi = \frac{b^4 x_0^2}{b^4 x_0^2 + a^4 y_0^2},$$

$$\sin \varphi \cdot \cos \varphi = \frac{a^2 b^2 x_0 y_0}{b^4 x_0^2 + a^4 y_0^2}.$$

Accordingly, known transformation formulae lead to moments acting at boundary point x_0, y_0 in directions n, t [1]:

$$m_n = m_x \cos^2 \varphi + m_y \sin^2 \varphi + 2m_{xy} \sin \varphi \cdot \cos \varphi,$$

$$m_{nt} = (m_y - m_x) \sin \varphi \cdot \cos \varphi + m_{xy}(\cos^2 \varphi - \sin^2 \varphi),$$

$$m_t = m_x \sin^2 \varphi + m_y \cos^2 \varphi - m_{xy} \sin \varphi \cdot \cos \varphi.$$

All these formulae yield closed relationships for the moments.

REFERENCES

1. GIRKMANN, K.: Flächentragwerke. Einführung in die Elastostatik der Scheiben, Platten, Schalen und Faltwerke. Springer-Verlag, Wien 1959, 5. Aufl. pp. 159—165
2. TIMOSHENKO, S.—WOINOWSKY-KRIEGER, S.: Theory of Plates and Shells. McGraw-Hill Book Company, Inc., New York—Toronto—London 1959, 2nd Ed., pp. 310—313
3. L'HERMITE, R.: Résistance des matériaux. Théorique et expérimentale. Tome I, Dunod Paris, pp. 554—555

4. SZILARD, R.: Theory and Analysis of Plates. Classical and Numerical Methods. Prentice Hall, Inc. Englewood Cliffs, New Jersey 1974, pp. 124—125
5. LOVE, A. E. H.: A Treatise on the Mathematical Theory of Elasticity. At the University Press, Cambridge 1944, 1952, p. 484
6. SENGUPTA, H. M.: The Bending of an Elliptic Plate under Certain Distribution of Load. *Bulletin Calcutta Math. Soc*, **40** (March and June 1948, December 1949), 17—35, 55—63
7. PERRY, C. L.: The Bending of Thin Elliptical Plates. *Proc. III. Symp. Appl. Math.* McGraw Hill **3** (1950), 131—139
8. SETH B. R.: Bending of an Elliptic Plate with a Confocal Hole. *The Quarterly Journal of Mechanics and Applied Mathematics* **2** (1949), 177—181
9. HAPPEL, H.: Über das Gleichgewicht von elliptischen Platten. *Mathematische Zeitschrift* **11** (1921), 194—223
10. NICOLAS, M.M.: Plaques minces de contour elliptique *Annales des Ponts et Chaussées* **107** (1937). — VII (Juillet), 161—166
11. OLSSON, R. G.: Biegung elliptischer und kreisförmiger Platten veränderlicher Dicke bei hydrostatischer Belastung. *Ingenieur Archiv* **9** (1938), 108—115

Eliptische Platte mit Randeinspannung. — Im Rahmen der technischen Elastizitätslehre wird eine ringsherum fest eingespannte elliptische Platte unter polynomartig verteilter Normallast behandelt. Es wird nachgewiesen, daß in diesem speziellen Ausnahmsfall die Formänderung und das Kräftespiel der Platte durch einfache geschlossene Formeln ausgedrückt werden können.

Acta Technica Academiae Scientiarum Hungaricae, 93 (1—2), pp. 39–65 (1981)

STATIC AND STABILITY INVESTIGATION OF BENT FOLDED PLATES

A. KEREK*

(Manuscript received 2 January 1980)

Static and Stability Analysis of Bent Folded Plates. — The lateral deformations of bent (shell-) beams of straight centre-line and of open cross section, put side by side, assuming their coaction in load bearing, will be hindered. The detained deformation reacts to the stress pattern of the structure (folded plate) which requires a new formulation of the criterion of stability. The paper is concerned with the determination of the vertical deformation, critical moment, longitudinal stresses induced in the cross section and transverse moment of some typical cross sections.

1. Introduction, setting of objective

The strength and stability behaviour of bent folded plates will be deduced below by the use of the theory of shell beams. By the term *shell beam* a thin walled bearing member of open cross section and straight centre line is meant. The cross section of such a beam has commonly, in practice, only one single axis of symmetry (Fig. 1).

The value of the flexural rigidity (EI_y) of such beams is rather high, however, the deformation of the cross section of the beam under the load greatly influences the deformation and stress pattern of the beam. The flexural stresses, that is, the forces originating from the tensile and compressive parts of the flexural stresses applied on both sides of the deformed element of dz length (Fig. 2) yield resultant forces which are perpendicular to the curved centre line of the beam and cause transverse bending of the beam cross section. In consequence of this effect the thin cross section undergoes a strong deformation which causes flattening and bulging.

In case of a low value of the bending moment this deformation may be neglected, but in case of higher moment-values, the change in stiffness becomes ever more noticeable: the bulging cross section causes the stiffness of the cross section to grow more and more and, in turn, the flattening gradually reduces the stiffness while, at a certain value of the bending moment (M_{cr}), the beam loses its stability and the so-called *Durchschlag* phenomenon takes place (Fig. 3).

In consequence of the deformation described above, also the distribution of the longitudinal stresses caused by bending deviate from Navier's straight-line distribution (Fig. 4).

* Dr. r. A. KEREK, Apáczai Csere J. u. 19. II. 3. H-2400 — Dunaújváros, Hungary

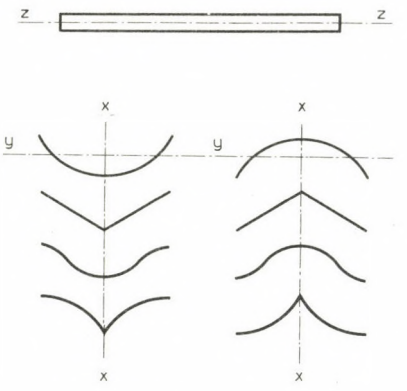

Fig. 1

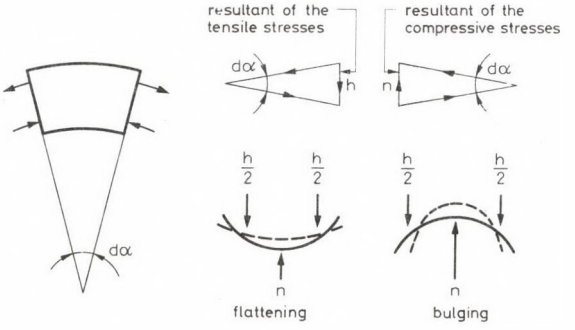

Fig. 2

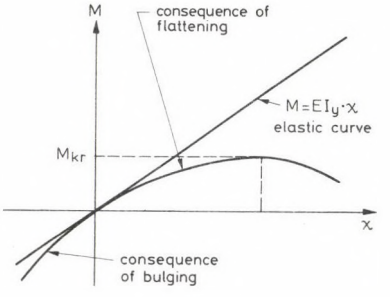

Fig. 3

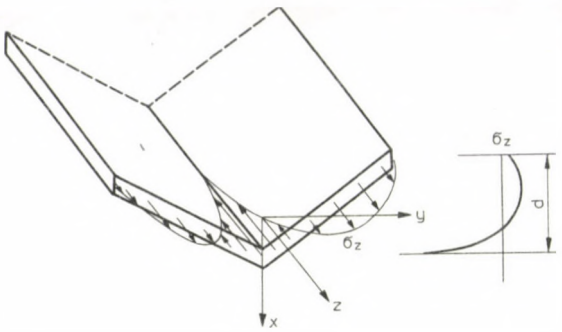

Fig. 4

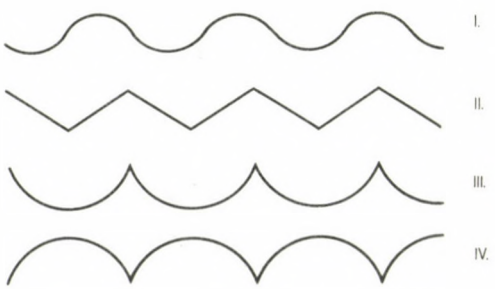

Fig. 5

The static and stability problems of the shell beams have been treated in details by KOLLÁR [1]. However, the literature published up till now is restricted to dealing with separate, independent shell beams only.

Placing several shell beams side-by-side, their coaction being assured, the transverse deformations, except the extreme ones, will be impeded. This deformation reciprocally impeded hinders, at the same time, also the flattening or bulging of the cross section. Further, such structures do not involve the risk of lateral buckling. These structures are called *folded plates*. Their application in the field of metallic structures (trapezoidal or corrugated plates) and of the monolithic reinforced concrete constructions (for covering large spaces) is in current use (Fig. 5). To this group of structures also belong the surfaces assembled from shell beams, wherein, to assure the above mentioned advantages, the individual beams, after placing them into position are attached to each other by welding, site-concreting etc. which realizes their interaction.

The purpose of this paper is to determine the vertical deformation, critical bending moment, the longitudinal stresses and transverse bending moments induced in the cross sections, for the case of the folded plates represented in Fig. 5, by keeping the principle of treatment and by using the notation of study [1] mentioned above.

For the calculation it will be assumed that

— the material is homogeneous, isotropic and elastic,
— the transverse displacements, parallel to the axis $y-y$, may freely take place,
— the radius of curvature of the deformation (R) is much greater than the thickness (d) of the folded plate,
— the width of the folded plate is infinite,
— the external loads are applied at the median plane of the shell beams constituting the folded plate,
— the dead weight, is acting in the same way as the external forces,
— the value of the bending moment may be considered to be constant, along the whole length,
— the transverse contraction (the Poisson's ratio) may be neglected.

Thus, the elements of the structure to be investigated are stiffening each other only by preventing the twist at the edges of the shell beam sections, but they do not impede their lateral displacements. This condition requires the application of flexible columns at the supports but excludes the application of horizontal tie rods at the plane of the end cross-sections.

2. Pure flexural deformation of the cross sections

The cross sections of the folded plates depicted in Fig. 5 may be divided into unit-components (Fig. 6). These unit-components are curves described by the function $x_0(y)$.

After the deformation the elongation of the cross sections associated with the radius of curvature R is

$$\varepsilon_z = \frac{\frac{R-x}{R} - l}{l} = -\frac{x}{R} \tag{1}$$

The transverse curvature of the cross sections is expressed by formula

$$\chi_z = -\frac{d^2u}{dy^2} \tag{2}$$

wherein u denotes the dislocation in the x-direction at the points of the cross section caused by the deformation of the cross section (Fig. 7):

$$u = x - x_0 \,. \tag{3}$$

Introducing the parameter

$$\beta = \frac{\sqrt[4]{3}}{\sqrt{h \cdot R}} = \frac{1.316}{\sqrt{h \cdot R}}, \tag{4}$$

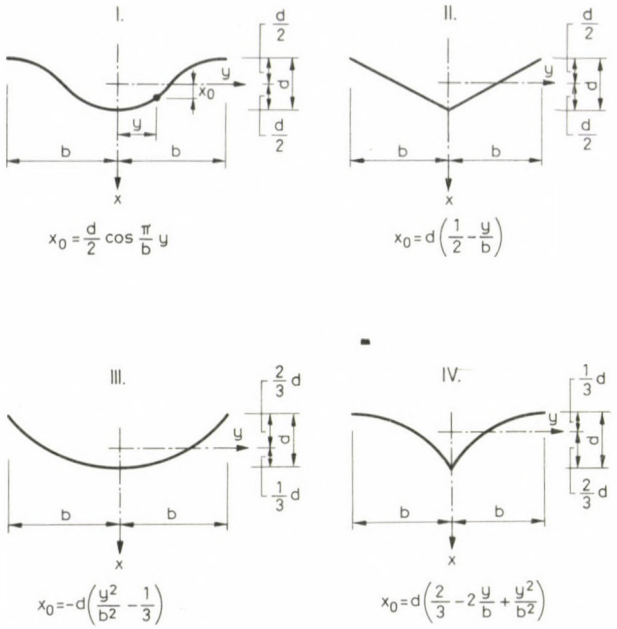

Fig. 6

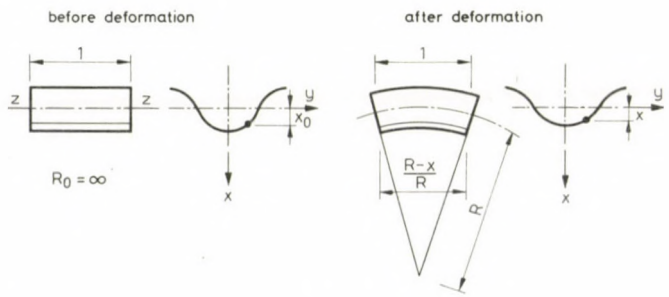

Fig. 7

which describes the geometry of the shell, the deformation of the folded plate can be described with the linear inhomogeneous differential equation

$$\frac{d^4u}{dy^4} + 4\beta^4 \cdot u = -4\beta^4 \cdot x_0 \tag{5}$$

wherein to a given (fixed) M, $\beta = \text{const.}$ is coordinated.

The solution to this equation consists of two parts, that is, of the solution u_0 to the homogeneous equation and the particular solution u_1 to the inhomogeneous equation:

$$u = u_0 + u_1 \,. \tag{6}$$

The solution to the homogeneous equation is the same for any form of the cross sections represented in Fig. 6:

$$\begin{aligned} u_0 = {} & A \cosh \beta y \cdot \cos \beta y + B \sinh \beta y \cdot \sin \beta y \\ & + C \cosh \beta y \cdot \sin \beta y + D \sinh \beta y \cdot \cos \beta y \,, \end{aligned} \tag{7}$$

wherein A, B, C, D are constants of integration which are to be determined from the boundary conditions.

The solution u_1 varies according to the different cross-section forms, wherefore, it has to be individually determined for each particular case.

Returning to the boundary conditions, let us assume that the components of the structure having the cross sections represented in Fig. 6, continuously join to the contiguous units. Thus, one obtains the following boundary conditions with respect to u:

1) at the centre of the cross section, due to the symmetry, the tangent remains horizontal. Therefore:

$$\frac{du}{dy}(0) = 0 \,; \tag{8}$$

2) At the centre of the cross section, due to the symmetry, the value of the shear force in the transverse direction is equal to zero, that is,

$$\frac{d^3u}{dy^3}(0) = 0 \,; \tag{9}$$

3) due to the coaction and the symmetry, the tangent remains horizontal at the edge of the cross section,

$$\frac{du}{dy}(\pm b) = 0 \,; \tag{10}$$

4) at the edge of the cross section the shear force is equal to zero

$$\frac{d^3u}{dy^3}(\pm b) = 0 \,. \tag{11}$$

The constants of integration $A-D$ will be determined from the above boundary conditions.

At the edge-value $y=b$ the following notation will be introduced:

$$\sin \beta b = s,$$

$$\cos \beta b = c,$$

$$\sinh (\beta b) = S,$$

$$\cosh (\beta b) = C. \tag{12}$$

In the following, the cross-sectional forms to be seen in Figs 5 and 6 will be analysed separately.

Cross section type I

The equation of this cross section is

$$x_0 = \frac{d}{2} \cos \frac{\pi}{b} y . \tag{13}$$

The particular solution to Eq. (5) is

$$u_1 = -\delta x_0 , \tag{14}$$

wherein

$$\delta = \frac{1}{1 + \frac{\pi^4}{4(\beta b)^4}} .$$

Consideration of Eqs (6), (7), (14) and the boundary conditions (8) – (14) as well as performing the derivations, yields

$$A = B = C = D = 0, \tag{15}$$

which means that the value of the deflection u is identical with that obtained according to formula (14):

$$u = u_1 .$$

Cross section type II

The equation at the right-hand side of the cross section (Fig. 6) is

$$x_0 = d\left(\frac{1}{2} - \frac{y}{b}\right). \tag{16}$$

The particular solution to Eq. (5) is

$$u_1 = -x_0 = -d\left(\frac{1}{2} - \frac{y}{b}\right). \tag{17}$$

After carrying out the derivations and considering the boundary conditions (8)–(11), by omitting the presentation of the calculation, one obtains the following expressions to the constants of integration:

$$A = d\left[\frac{1}{2\beta b}\frac{(SC - sc) - (Sc - Cs)}{Sc \cdot Sc + Cs \cdot Cs}\right] = d \cdot Z_A,$$

$$B = d\left[\frac{1}{2\beta b}\frac{(SC + sc) - (Sc + Cs)}{Sc \cdot Sc + Cs \cdot Cs}\right] = d \cdot z_B,$$

$$C = d\left(-\frac{1}{2\beta b}\right) = d \cdot Z_C,$$

$$Dd\left(-\frac{1}{2\beta b}\right) = d \cdot Z_D. \tag{18}$$

Cross section type III

The equation at the right-hand side of the cross section is

$$x_0 = d\left(\frac{1}{3} - \frac{y^2}{b^2}\right), \tag{19}$$

and the particular solution to the deformation equation:

$$u_1 = -x_0 = -d\left(\frac{1}{3} - \frac{y^2}{b^2}\right). \tag{20}$$

Table I

βb	Type II			Type III		Type IV		
	Z_A	Z_B	$Z_C=Z_D$	Z_A	Z_B	Z	Z_B	$Z_C=Z_D$
0.5	+0.4989	+0.0207	−1.00	+0.3323	−3.9806	+0.6656	+4.0221	−2.000
1.0	+0.4839	+0.0800	−0.500	+0.3175	−0.9254	+0.6503	+1.0856	−1.000
1.5	+0.4301	+0.1556	−0.333	+0.2647	−0.3011	+0.5954	+0.6124	−0.666
2.0	+0.3389	+0.2030	−0.250	+0.1763	−0.0683	+0.5015	+0.4744	−0.500
2.5	+0.2494	+0.2045	−0.200	+0.0921	−0.0127	+0.4066	+0.3963	−0.400
3.0	+0.1865	+0.1813	−0.166	+0.0376	+0.0282	+0.3353	+0.3344	−0.333
3.5	+0.1479	+0.1543	−0.143	+0.0101	+0.0222	+0.2857	+0.2864	−0.285
4,0	+0.1244	+0.1315	−0.125	$-9.489\cdot10^{-4}$	+0.0129	+0.2498	+0.2501	−0.250
4.5	+0.1091	+0.1140	−0.111	$-3.785\cdot10^{-3}$	+0.00586	+0.2221	+0.2221	−0.222
5.0	+0.0983	+0.1008	−0.100	$-3.348\cdot10^{-3}$	+0.00181	+0.1999	+0.1999	−0.200
6.0	+0.0828	+0.0830	−0.083	$-1.024\cdot10^{-3}$	$-0.5624\cdot10^{-3}$	+0.1666	+0.1666	−0.166
7.0	+0.0714	+0.0712	−0.071	$-2.524\cdot10^{-5}$	$-0.3675\cdot10^{-3}$	+0.1428	+0.1428	−0.142
80	+0.0625	+0.0824	−0.062	$+9.517\cdot10^{-5}$	$-0.7077\cdot10^{-4}$	+0.1250	+0.1250	−0.125
9.0	+0,0555	+0,0555	−0,055	$+3.628\cdot10^{-5}$	$+0.1368\cdot10^{-4}$	+0,1111	0.1111	−0.111
10.0	+0.0500	+0.0500	−0.050	$+0.2679\cdot10^{-5}$	$+0.1255\cdot10^{-4}$	+0.1000	+0.1000	−0.100
				$Z_C=Z_D=0$				

The constants of integration are:

$$A=d\left(-\frac{1}{\beta b}\,\frac{Sc-Cs}{Sc\cdot Sc+Cs\cdot Cs}\right)=d\cdot Z_A,$$

$$B=d\left(-\frac{1}{\beta b}\,\frac{Sc+Cs}{Sc\cdot Sc+Cs\cdot Cs}\right)=d\cdot Z_B, \tag{21}$$

$$C=d\cdot Z_C=0,$$

$$D=d\cdot Z_D=0.$$

Cross section type IV

Equation at the right-hand side of the cross section and the particular solution are

$$x_0=d\left(\frac{2}{3}-2\frac{y}{b}+\frac{y^2}{b^2}\right), \tag{22}$$

$$u_1 = -x_0 = -d\left(\frac{2}{3} - 2\frac{y}{b} + \frac{y^2}{b^2}\right), \tag{23}$$

and for the constants of integration one obtains the following relationships:

$$\begin{aligned} A &= d\left(\frac{1}{\beta b}\,\frac{SC - sc}{Sc \cdot Sc + Cs \cdot Cs}\right) = d \cdot Z_A, \\ B &= d\left(\frac{1}{\beta b}\,\frac{SC + sc}{Sc \cdot Sc + Cs \cdot Cs}\right) = d \cdot Z_B, \\ C &= d\left(-\frac{1}{\beta b}\right) = d \cdot Z_C, \\ D &= d\left(-\frac{1}{\beta b}\right) = d \cdot Z_D. \end{aligned} \tag{24}$$

In the formulae (18), (21), (24) the symbols Z_A, Z_B, Z_C, Z_D have been introduced. With the aid of these auxiliary terms, the constants of integration can be rendered independent of the thickness d of the folded plate. For different values of βb which occur in the practice, the numerical values of Z_A, Z_B, Z_C, Z_D are indicated to the cross-section types II, III and IV.

3. Relationships between the bending moment and curvature

In the preceding paragraph the longitudinal change in curvature χ has been determined, assuming that the translation u of an arbitrary point of the folded plate was known. Now, it should be investigated, what relationship exists between χ and the external bending moment M applied on the folded plate.

By neglecting the moment induced by the longitudinal bending of the plate element it may be written:

$$m_y = \frac{Eh^3}{12}\chi = 0.$$

Since $h \ll d$, the equilibrium of the external and internal moments may be written as follows:

$$M = -\int_{-b}^{+b} n_z x dy \tag{25}$$

In this formula n_z is a membrane force perpendicular to the cross section which, according to Hooke's law may be expressed by ε_z:

$$n_z = Eh\varepsilon_z . \tag{26}$$

Taking into consideration the relationships (26), (1), (3), (2) and carrying out the replacements Eq. (25) reads:

$$M = E\chi[h \cdot \int_{-b}^{+b} x_0^2 dy + 2h \int_{-b}^{+b} x_0 u \cdot dy + h \int_{-b}^{+b} u^2 \cdot dy] \tag{27}$$

Since χ is implied in the dislocation u entering the second and third term, the relationship between the external moment M and change in curvature χ is not linear (Fig. 3). Otherwise, the first term within the bracket is

$$h \int_{-b}^{+b} x_0^2 dy = I_y , \tag{28}$$

that is, the so-called elementary moment of inertia of the cross section.

The exact determination of the curve, that is, the description of the function will be carried out in different ways for the four different cross sections.

Cross section type I

Since according to (14) and (15)

$$u_0 = 0,$$

$$u = u_1 = -\delta x_0 ,$$

therefore, the relationship (27) in the modified form reads as:

$$M = E\chi[h \int_{-b}^{+b} x_0^2 \cdot dy - 2h \int_{-b}^{+b} x_0(\delta x_0) dy + h \int_{-b}^{+b} (-\delta x_0)^2 \cdot dy] .$$

By introducing the notation

$$\gamma = 1 - \delta(2 - \delta) , \tag{29}$$

on the basis of (28) the relationship between the moment and curvature can be written in the following form:

$$M = (EI_y)\gamma)\chi \tag{30}$$

Table II

βb	γ		
	I.	II.	III.—IV.
0	1,0	1.0	1.0
0.5	0.994 886 70	0.994 761	0.995 132
1.0	0.922 667 45	0.923 589	0.928 125
1.5	0.685 406 16	0.689 756	0.707 709
2.0	0.364 202 56	0.373 127	0.407 841
2.5	0.147 468 11	0.159 292	0.201 750
3.0	0.053 430 74	0.066 151	0.100 254
3.5	0.019 494 52	0.031 979	0.064 655
4.0	0.007 545 20	0.019 207	0.043 498
4.5	0.003 142 46	0.013 644	0.030 800
5.0	0.001 406 43	0.010 566	0.022 516
6.0	0.000 340 17	0.006 805	0.013 021
7.0	0.000 100 82	0.004 434	0.008 298
8.0	0.000 034 93	0.002 958	0.005 492
9.0	0.000 013 68	0.002 061	0.003 857
10.0	0.000 005 90	0.001 498	0.002 812

Table III

βb	$(\beta b)^2$	$\frac{M}{EI_y}\frac{\sqrt{3}\,b^2}{h}$		
		I.	II.	III—IV.
0.0	0.00	0.000	0.000	0.000
0.1	0.01	0.009	0.009	0.009
0.2	0.04	0.039	0.033	0.039
0.3	0.09	0.089	0.089	0.089
0.4	0.16	0.159	0.159	0.159
0.5	0.25	0.247	0.248	0.248
0.6	0.36	0.354	0.356	0.356
0.7	0.49	0.480	0.480	0.481
0.8	0.64	0.618	0.619	0.620
0.9	0.81	0.808	0.797	0.770
1.0	1.00	0.922	0.923	0.928
1.1	1.21	1.076	1.078	1.086
1.2	1.44	1.222	1.225	1.238
1.3	1.69	1.355	1.358	1.377
1.4	1.96	1.462	1.469	1.497
1.5	2.25	1.541	1.551	1.592
1.6	2.56	1.587	1.602	1.657
1.7	2.89	*1.603*	*1.620*	1.692
1.8	3.24	1.581	1.605	*1.697*
1.9	3.61	1.534	1.56	1.675
2.0	4.00	1.451	1.492	1.631

In lieu of the curvature, taking (2) and (4) into account, the dimensionless variable βb should be introduced:

$$\frac{M}{EI_y} \cdot \frac{\sqrt{3} \cdot b^2}{h} = (\beta b)^2 \gamma \,. \tag{31}$$

In Tables II and III the factor γ and the value of the product $\gamma(\beta b)^2$ can be found for the different values of βb. It is to be noted that for the value 1.7 of βb, the moment function has a maximum which corresponds to the critical moment M_{cr}.

Cross section type II

On the basis of formulae (6), (17), (7), Eq. (27) reads

$$M = Eh\chi[\int_{-b}^{+b} x_0^2 \cdot dy + 2\int_{-b}^{+b} x_0(u_0 - x_0)dy +$$

$$+ \int_{-b}^{+b} (u_0 - x_0)^2 \cdot dy] = E\chi h \int_{-b}^{+b} u_0^2 \cdot dy =$$

$$= E\chi h d^2 \int_{-b}^{+b} [Z_A \cosh \beta y \cdot \cos \beta y +$$

$$+ Z_B \sinh \beta y \cdot \sin \beta y + Z_C \cosh \beta y \cdot \sin \beta y +$$

$$+ Z_D \sinh \beta y \cdot \cos \beta y]^2 \cdot dy \,.$$

Considering that

$$I_y = hd^2 2 \int_0^b \left(\frac{1}{2} - \frac{y}{b}\right)^2 dy = \frac{1}{6} hd^2 b \,,$$

and performing the integrations one obtains

$$\frac{M}{E\chi} = I_y \cdot 6 \cdot \frac{1}{4\beta b} [Z_A^2(0.5 \cdot \sinh 2\beta b \cdot \cos 2\beta b +$$

$$+ 0{,}5 \cdot \cosh 2\beta b \cdot \sin 2\beta b + \sinh 2\beta b + \sin 2\beta b +$$

$$+ 2\beta b(+Z_B^2) - 0{,}5 \cdot \sinh 2\beta b \cdot \cos 2\beta b - 0{,}5 \cdot \cosh 2\beta b \cdot \sin 2\beta b +$$

$$+\sinh 2\beta b+\sin 2\beta b-2\beta b)+$$

$$+2Z_C^2(\sinh 2\beta b-\sin 2\beta b)+(Z_A Z_B+Z_C^2)$$

$$(\cosh 2\beta b\cdot\sin 2\beta b-\sinh 2\beta b\cdot\cos 2\beta b)+$$

$$+2Z_A Z_C(\sinh 2\beta b\cdot\sin 2\beta b+\cosh 2\beta b-\cos 2\beta b)+$$

$$+2Z_B Z_C(-\cosh 2\beta b\cdot\cos 2\beta b+\cosh 2\beta b+$$

$$+\cos 2\beta b-1)]=I_y\gamma\,. \tag{33}$$

Similarly to the procedure applied in the case of the cross section type I, I_y has been factored out and the other terms depending only on βb have been denoted by γ. In evolving Eq. (33) the equality $Z_C=Z_D$ was taken into account.

Thus formulae (30) and (31) determined above here also hold true. The numerical values are given in Tables II and III. The critical moment also here occurs at the value $\beta b=1{,}7$.

Cross sections of types III and IV

By virtue of formulae (20), (21), (23), (24), the relationship (32) also here is valid.

By factoring out the elementary moments of inertia

$$I_y\,(\text{type III})=hd^2\int_{-b}^{+b}\left(\frac{1}{3}-\frac{y^2}{b^2}\right)^2\cdot dy=\frac{8}{45}\cdot hd^2\cdot b\,,$$

and

$$I_y\,(\text{type IV})=hd^2\cdot 2\int_0^b\left(\frac{2}{3}-\frac{2y}{b}+\frac{y^2}{b^2}\right)^2\cdot dy=\frac{8}{45}hd^2\cdot b$$

are obtained whence, the integration results in the relationship (33) with the difference that instead of the number 6 standing after I_y which follows the first equal sign, the fraction 45/8 should be taken into account.

The relationships (30) and (31) are invariably valid. The values of γ calculated for the different βb values, were the same for both types which means that, disregarding signs, curve $M(\chi)$ and the associated critical moment (for the value $\beta b=1{,}8$) of these two types are quite similar. In Tables II and III the numerical values are indicated in the same column.

4. The longitudinal stresses

The longitudinal stresses σ_z induced by the flexural moment in the cross section of the folded plate are not distributed linearly through the depth of the cross section due to the deformation of this latter. (See Fig. 4.)

The exact pattern of stress distribution pertaining to the treated types of cross sections will be determined below, assuming that the moment M or the associated curvature as well as, on the basis of paragraph 2, the displacement u are known.

Considering the formulae (26), (1), (3), (6) the following can be written

$$\sigma_z = E\varepsilon_z = -E\frac{x}{R} = -E\chi(x_0+u),$$

$$\sigma_z = -E\chi(x_0+u_0+u_1), \tag{34a}$$

or, according to (30):

$$\sigma_z = -\frac{M}{I_y\gamma}(x_0+u_0+u_1). \tag{34b}$$

In case of the cross section type I, Eq. (34b), by using Eqs (14), (15), (13),takes the form

$$\sigma_z = -\frac{M}{I_y} d \frac{1}{\gamma}\cdot\frac{1}{2}(1-\delta)\cos\frac{\pi}{b}y.$$

By making use of the notation

$$\xi = \frac{1}{\gamma}\cdot\frac{1}{2}(1-\delta)\cos\frac{\pi}{b}y,$$

Eq. (34b) may be transposed into the form:

$$\sigma_z = -\frac{M}{I_y} d\cdot\xi, \tag{35a}$$

or

$$\sigma_z = -E\chi d\cdot\gamma\cdot\xi. \tag{35b}$$

Since, M, I_y and d are, within the cross section, constant, therefore, the change in stress is expressed by ξ. Table IV gives the values of ξ to the different βb-values at a few characteristic points determined by y/b and x/d.

Table IV

Value of ξ for cross-section of type I

y/b	0	0.2677	0.3918	0.500	0.6089	0.7323	1.000
x/d	+0.5	+0.333	+0.167	0	−0.167	−0.333	−0.500
$\beta b=$ 0	+ 0.5	+ 0.333	+ 0.167	0	− 0.167	− 0.333	− 0.500
0.5	+ 0.501	+ 0.334	+ 0.167	0	− 0.167	− 0.333	0.500
1.0	+ 0.520	+0.347	+ 0.174	0	− 0.174	− 0.347	− 0.174
1.5	+ 0.604	+0.402	+ 0.202	0	− 0.202	− 0.402	− 0.202
2.0	+ 0.828	+ 0.552	+ 0.277	0	− 0.277	− 0.552	− 0.277
2.5	+ 1.302	+ 0.868	+ 0.435	0	− 0.435	− 0.868	− 0.435
3.0	+ 2.163	+ 1.441	+ 0.722	0	− 0.722	− 1.441	− 0.722
3.5	+ 3.581	+ 2.386	+ 1.195	0	− 1.195	− 2.386	− 1.195
4.0	+ 5.748	+ 3.828	+ 1.920	0	− 1.920	− 3.828	− 5.748
6.0	+ 27.109	+ 18.073	+ 9.036	0	− 9.036	− 18.073	− 27.109
8.0	+ 84.598	+ 56.399	+18.199	0	−28.199	− 56.399	− 84.598
10.0	+205.82	+137.21	+68.61	0	−68.61	−137.21	−205.82

Table V

Value of ξ for cross-section of type II

y/b	0	0.125	0.250	0.375	0.500	0.625	0.750	0.375	1.0
x/d	+0.5	+0.375	+0.250	+0.125	0	−0.125	−0.250	−0.375	−0.5
$\beta b=0$	+ 0.500	+0.375	+0.250	+0.125	0	−0.125	−0.250	−0.375	− 0.500
0.5	+ 0.501	+0.376	+0.251	+0.125	0	−0.125	−0.251	−0.376	− 0.501
1.0	+ 0.524	+0.390	+0.258	+0.129	0	−0.129	−0.258	−0.390	− 0.524
1.5	+ 0.624	+0.450	+0.291	+0.143	0	−0.143	−0.291	−0.450	− 0.624
2.0	+ 0.908	+0.607	+0.366	+0.171	0	−0.171	−0.366	−0.607	− 0.908
2.5	+ 1.566	40.904	+0.465	+0.189	0	−0.189	−0.465	−0.904	− 1.566
3.0	+ 2.819	+1.306	+0.467	+0.110	0	−0.110	−0.467	−1.306	− 2.819
3.5	+ 4.625	+1.617	+0.181	−0.175	0	+0.175	−0.181	−1.617	− 4.625
4.0	+ 6.477	+1.624	−0.406	−0.623	0	+0.623	+0.406	−1.624	− 6.477
6.0	+12.167	+0.191	−2.630	−1.734	0	+1.734	+2.630	−0.191	−12.167
8.0	+21.129	−0.333	−3.854	−1.352	0	+1.352	+3.854	+0.333	−21.129
10.0	+33.378	−6.075	−3.805	−0.267	0	+0.267	+3.805	+6.075	−33.378

Table VI

Value of ξ for cross-section of type III

y/b	0	0.408	0.577	0.707	0.896	0.913	1.000
x/d	+0.333	+0.167	0	−0.167	−0.333	−0.500	−0.667
$\beta b =$ 0.0	+0.333	+0.167	0	−0.167	−0.333	−0.500	− 0.667
0.5	+0.339	+0.167	+0.001	−0.168	−0.334	−0.501	− 0.669
1.0	+0.342	+0.174	+0.004	−0.169	−0.344	−0.522	− 0.701
1.5	+0.374	+0.206	+0.219	−0.176	−0.388	−0.610	− 0.841
2.0	+0.432	+0.289	+0.085	−0.173	−0.483	−0.838	− 1.229
2.5	+0.456	+0.439	+0.255	−0.093	−0.597	−1.245	− 2.016
3.0	+0.124	+0.214	+0.194	+0.051	−0.217	−0.608	− 1.110
3.5	+0.156	+0.718	+0.886	+0.519	−0.475	−2.131	− 4.108
4.0	−0.021	+0.731	+1.168	+0.947	−0.198	−2.423	− 5.742
6.0	−0.077	+0.192	+1.408	+2.577	1.869	−2.792	−12.823
8.0	+0.018	−0.200	+0.564	+3.036	+4.673	−1.418	−22.727
10.0	+0.036	−0.107	−0.214	+2.250	+7.0	−1.786	−35.714

Table VII

Value of ξ for cross-section of type IV

y/b	0.0	0.087	0.183	0.293	0.422	0.592	1.000
x/d	0.667	0.500	0.333	0.167	0	−0.167	−0.333
$\beta b =$ 0	+ 0.667	+0.500	+0.333	+0.167	0	−0.167	−0.333
0.5	+ 0.669	+0.501	+0.334	+0.168	−0.001	−0.167	−0.339
1.0	+ 0.701	+0.522	+0.344	+0.169	−0.004	−0.174	−0.342
1.5	+ 0.841	+0.610	+0.388	+0.176	−0.219	−0.206	−0.374
2.0	+ 1.229	+0.838	+0.483	+0.173	−0.085	−0.289	−0.432
2.5	+ 2.016	+1.245	+0.597	+0.093	−0.255	−0.439	−0.456
3.0	+ 1.110	+0.608	+0.217	−0.051	−0.194	−0.214	−0.124
3.5	+ 4.108	+2.131	+0.475	−0.519	−0.886	−0.718	−0.156
4.0	+ 5.742	+2.423	+0.198	−0.947	−1.168	−0.731	+0.021
6.0	+12.823	+2.792	−1.869	−2.577	−1.408	−0.192	+0.077
8.0	+22.727	+1.418	−4.673	−3.036	−0.564	+0.200	−0.018
10.0	+35.714	+1.786	−7.0	−2.250	+0.214	+0.107	−0.036

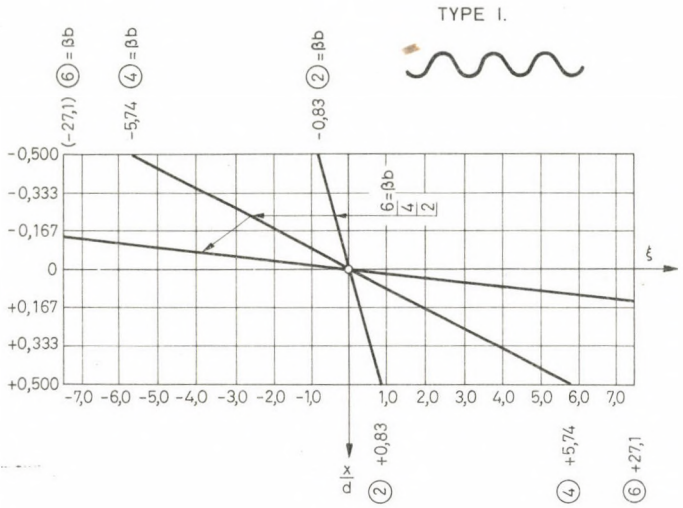

Fig. 8

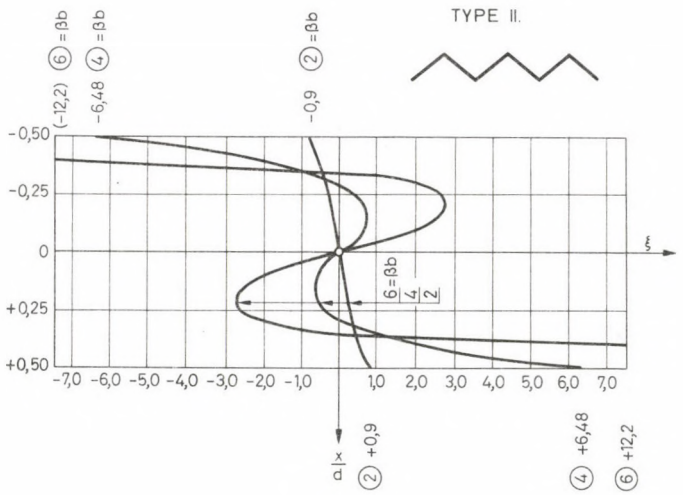

Fig. 9

In case of cross section type II, the stress pattern can be determined with the same logic. By making use of Eqs (17), (18), (34) one obtains

$$\sigma_z = -\frac{M}{I_y \gamma} u_0 \,, \tag{36a}$$

$$\sigma_z = -E\chi u_0 \,. \tag{36b}$$

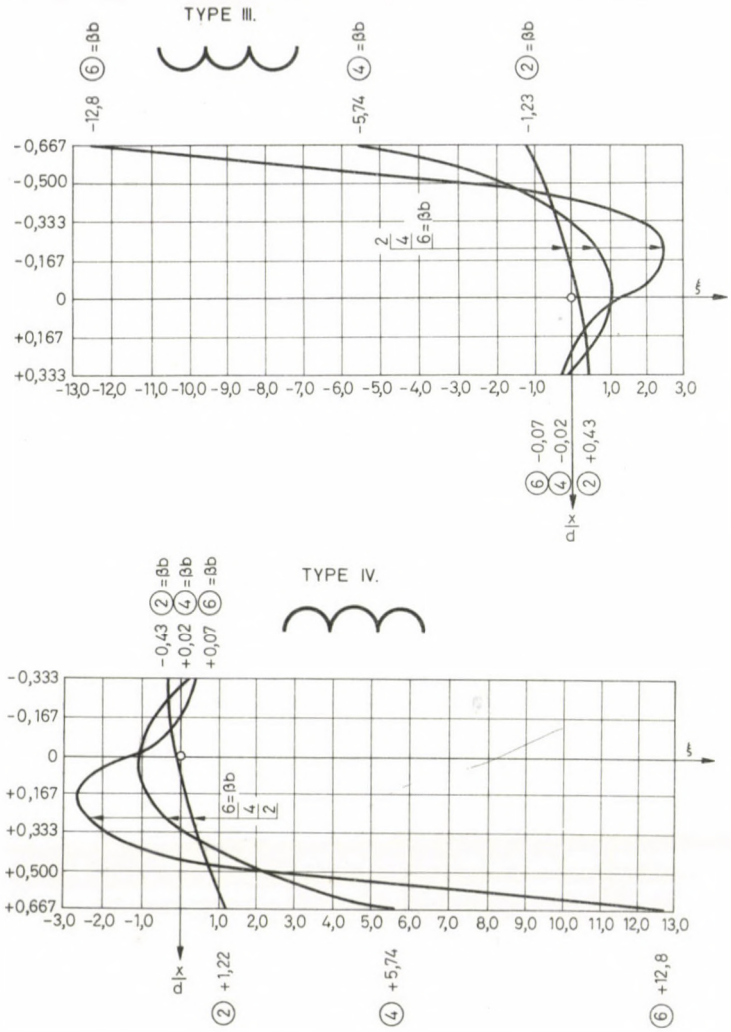

Fig. 10

By introducing the notation

$$\xi = \frac{1}{\gamma}(Z_A \cosh \beta y \cdot \cos \beta y + Z_B \sinh \beta y \cdot \sin \beta y + \\ + Z_C \cosh \beta y \cdot \sin \beta y + Z_D \sinh \beta y \cdot \cos \beta y), \tag{37}$$

and by making use of Eqs (7) and (18), one obtains the relationships (35a) and (35b). The numerical values for the cross section in question are contained in Table V.

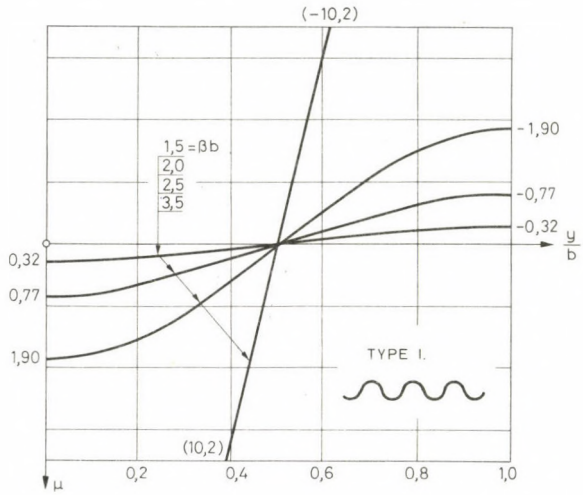

Fig. 11

Also in case of cross sections types III and IV the Eqs (35), (36), (37) hold true. In Eq. (37), as a matter of course, the respective values $Z_A \cdot Z_B, Z_C, Z_D$ belonging to the cross section are to be taken into account. The actual numerical values are listed in Tables VI and VII. From the two tables it is evident that the absolute values ξ of the points of both cross sections identified with each other, are the same. This means that the stress distributions taking place in these cross sections, under bending, with an opposite sign are the same. Consequently, a similar result is also obtained for the function $M(\chi)$.

The functions ξ associated with the cross-section types I, II and III, IV have also been plotted in diagram form for the curvature values $\beta b = 2$, $\beta b = 4$ and $\beta b = 6$ (Figs 8, 9, 10).

5. The transverse bending moments

The deformation u, is, in the folded plate, associated with a bending moment m_z in the transverse direction. Using the known relationship

$$m_z = \frac{Eh^3}{12} \chi_z ,$$

and Eq. (2) yields

$$m_z = -\frac{Eh^3}{12} \cdot \frac{d^2u}{dy^2} , \tag{38}$$

wherein m_z is positive in the case where it induces tensile stress in the lower fibre.

Table VIII

Value of μ for cross-section of type I

y/b	0.0	0.2	0.4	0.6	0.8	1.0
$\beta b=$ 0.5	+ 0.029 32	+ 0.023 72	+ 0.009 06	− 0.009 06	− 0.023 72	− 0.029 32
1.0	+ 0.121 79	+ 0.098 53	+ 0.037 63	− 0.037 63	− 0.098 53	− 0.121 79
1.5	+ 0.317 96	+ 0.257 23	+ 0.098 25	− 0.098 25	− 0.257 23	− 0.317 96
2.0	+ 0.775 45	+ 0.627 35	+ 0.239 62	− 0.239 62	− 0.627 35	− 0.775 45
2.5	+ 1.904 15	+ 1.540 48	+ 0.588 41	− 0.588 41	− 1.540 48	− 1.904 15
3.0	+ 4.555 31	+ 3.685 31	+ 1.407 66	− 1.407 66	− 3.685 31	− 4.555 31
3.5	+ 10.264 7	+ 8.304 37	+ 3.171 99	− 3.171 99	− 8.304 37	− 10.264 7
4.0	+ 21.550 03	+ 17.434 5	+ 6.659 42	− 6.659 42	− 17.434 5	− 21.550 3
6.0	+ 228.361	+ 184.748	+ 70.567 4	− 70.567 4	− 184.748	− 228.361
8.0	+ 1266.90	+ 1024.94	+ 391.493	− 391.493	− 1024.94	− 1266.90
10.0	+ 4816.12	+ 3896.32	+ 1488.26	− 1488.26	− 3896.32	− 4816.12

Table IX

Value of μ cross-section of type II

y/b	0.0	0.2	0.4	0.6	0.8	1.0
$\beta b=$ 0.5	+ 0.006 02	+ 0.004 77	+ 0.001 78	− 0.001 78	− 0.004 77	− 0.006 02
1.0	+ 0.025 03	+ 0.020 89	+ 0.007 39	− 0.007 39	− 0.020 89	− 0.025 03
1.5	+ 0.065 18	+ 0.051 38	+ 0.001 91	− 0.001 91	− 0.051 39	− 0.065 18
2.0	+ 0.157 07	+ 0.122 72	+ 0.045 21	− 0.045 21	− 0.122 72	− 0.157 07
2.5	+ 0.370 62	+ 0.284 05	+ 0.102 51	− 0.102 51	− 0.284 05	− 0.370 62
3.0	+ 0.791 38	+ 0.586 39	+ 0.203 63	− 0.203 63	− 0.586 39	− 0.791 38
3.5	+ 1.393 06	+ 0.979 36	+ 0.318 95	− 0.318 95	− 0.979 36	− 1.393 06
4.0	+ 1.976 88	+ 1.290 67	+ 0.381 11	− 0.381 11	− 1.290 67	− 1.976 88
6.0	+ 3.523 88	+ 1.406 32	+ 0.108 74	− 0.108 74	− 1.406 32	− 3.523 88
8.0	+ 6.095 33	+ 1.183 23	− 0.216 39	+ 0.216 39	− 1.183 23	− 6.095 33
10.0	+ 9.639 51	+ 0.640 85	− 0.267 02	− 0.267 02	− 0.640 85	− 9.639 51

Taking into consideration Eqs (4), (6), (7), (14) yields the general formula of m_z

$$m_z = -\frac{E\chi h^2 \cdot d}{2\sqrt{3}}\left[\frac{g(y)}{(\beta b)^2} - Z_A \sinh \beta y, \sin \beta y + \right.$$

$$+ Z_B \cosh \beta y \cdot \cos \beta y + Z_C \sinh \beta h \cdot \cos \beta y -$$

$$\left. - Z_D \cosh \beta y \cdot \sin \beta y \right], \qquad (39)$$

Table X

Value of μ cross-section of type III

y/b	0.0	0.2	0.4	0.6	0.8	1.0
$\beta b=$ 0.5	+0.005 63	+0.004 68	+0.002 08	−0.001 48	−0.004 86	−0.006 43
1.0	+0.023 19	+0.019 32	+0.008 62	−0.006 11	−0.020 12	−0.026 63
1.5	+0.058 47	+0.048 92	+0.022 29	−0.014 90	−0.051 25	−0.068 55
2.0	+0.128 57	+0.108 83	+0.052 35	−0.030 38	−0.115 77	−0.158 88
2.5	+0.247 19	+0.214 03	+0.113 71	−0.048 13	−0.234 55	−0.338 14
3.0	+0.401 40	+0.360 68	+0.220 86	−0.048 10	−0.413 48	−0.643 51
3.5	+0.463 69	+0.437 71	+0.316 14	+0.000 15	−0.531 13	−0.914 08
4.0	+0.500 48	+0.498 64	+0.423 24	+0.086 90	−0.641 18	−1.245 34
6.0	+0.603 64	+0.639 73	+0.751 09	+0.636 66	−0.824 82	−3.078 87
8.0	+0.817 55	+0.810 27	+0.870 36	+1.103 42	−0.466 13	−5.748 36
10.0	+1.027 74	+1.024 18	+1.009 86	+1.290 89	+0.341 39	−9.238 97

Table XI

Value of μ cross-section of type IV

y/b	0.0	0.2	0.4	0.6	0.8	1.0
$\beta b=$ 0.5	+0.006 43	+0.004 86	+0.001 48	−0.002 08	−0.004 68	−0.005 63
1.0	+0.026 63	+0.020 12	+0.006 11	−0.008 62	−0.019 32	−0.023 19
1.5	+0.068 55	+0.051 25	+0.014 90	−0.022 29	−0.048 92	−0.058 47
2.0	+0.158 88	+0.115 77	+0.030 38	−0.052 35	−0.108 83	−0.128 57
2.5	+0.338 14	+0.234 55	+0.048 13	−0.113 71	−0.214 03	−0.247 19
3.0	+0.643 51	+0.413 48	+0.048 10	−0.220 86	−0.360 68	−0.401 40
3.5	+0.914 08	+0.531 13	−0.000 15	−0.316 14	−0.437 71	−0.463 69
4.0	+1.245 34	+0.641 18	−0.086 90	−0.423 24	−0.498 64	−0.500 48
6.0	+3.078 87	+0.824 82	−0.636 66	−0.751 09	−0.639 73	−0.603 64
0.8	+5.748 36	+0.466 13	−1.103 42	−0.870 36	−0.810 27	−0.817 55
10.0	+9.238 97	−0.341 39	−1.290 89	−1.009 96	−1.024 18	−1.027 74

wherein

$$g(y) = \frac{d^2 u_1}{dy^2} \cdot \frac{b^2}{2d}.$$

For the four types of cross sections the expressions of $g(y)$ are as follows:

Type I: $$g(y) = \delta \frac{\pi^2}{4} \cos \frac{\pi}{b} y,$$

Type II: $$g(y) = 0,$$

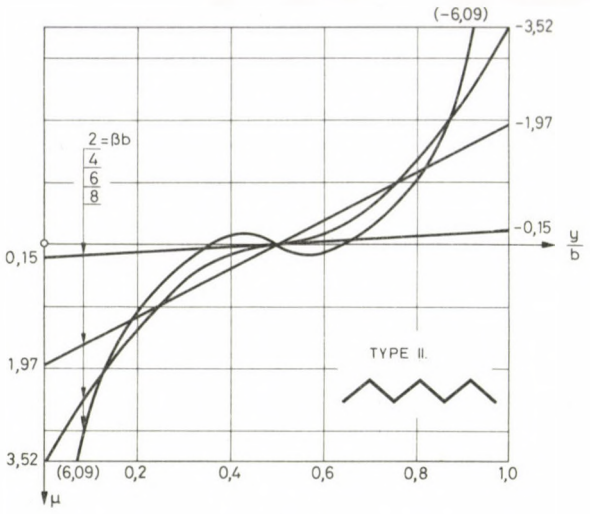
(-6,09)
-3,52
-1,97
-0,15
2=βb
4
6
8
0,15
1,97
3,52
(6,09)
0,2
0,4
0,6
0,8
1,0
μ
TYPE II.

Fig. 12

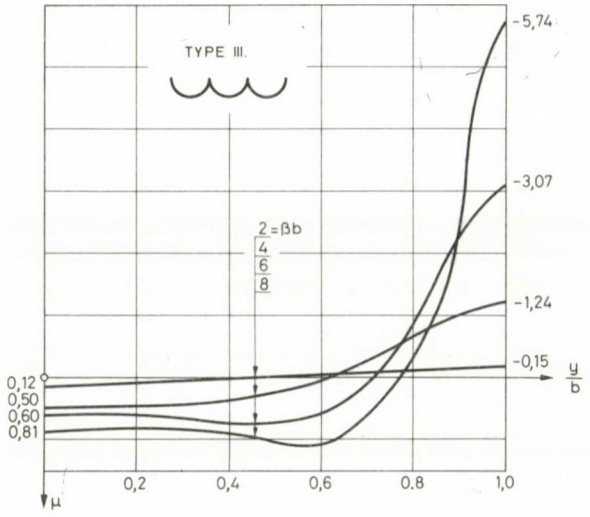
TYPE III.
-5,74
-3,07
-1,24
-0,15
2=βb
4
6
8
0,12
0,50
0,60
0,81
0,2
0,4
0,6
0.8
1,0
μ

Fig. 13

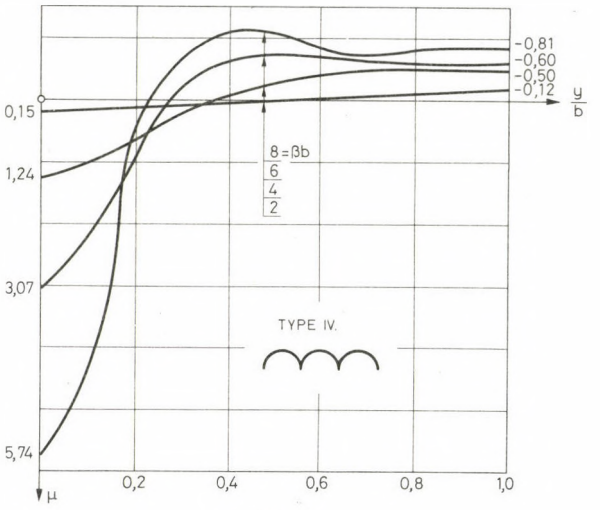

Fig. 14

Type III: $g(y)=1$ and

Type IV: $g(y)=-1$.

The expression of the transverse bending moment (39), considering Eq. (30) will be modified as

$$m_z=-\frac{M}{b}\cdot\frac{h}{d}\left[\frac{hd^2\cdot b}{I_y\gamma}\cdot\frac{1}{2\sqrt{3}}\left(\frac{g(y)}{(\beta b)^2}-Z_A\sinh\beta y\cdot\right.\right.$$

$$\sin\beta y+Z_B\cosh\beta y\cdot\cos\beta y+Z_C\sinh\beta y\cdot\cos\beta y-$$

$$\left.\left.-Z_D\cosh\beta y\cdot\sin\beta y\right)\right]=-\frac{M}{b}\cdot\frac{h}{d}\mu(y). \tag{40}$$

The function $\mu(y)$ which describes the change of the bending moment with respect to y is given in Tables VIII, IX, X, XI as well as in Figs 12, 13, 14 for the different values of βb to the four types of cross sections treated above.

6. Numerical example

Let us consider the cross section represented in Fig. 15a. The folded plate, hinge-supported at its two edges, at a distance 24,0 m is submitted to a critical load, the value of which is $g=8{,}0$ kN/m^2. The material of the structure is r.c., with B-200 concrete quality, the Young's modulus of which is $E_n=8{,}0\cdot 10^6$ kN/m^2.

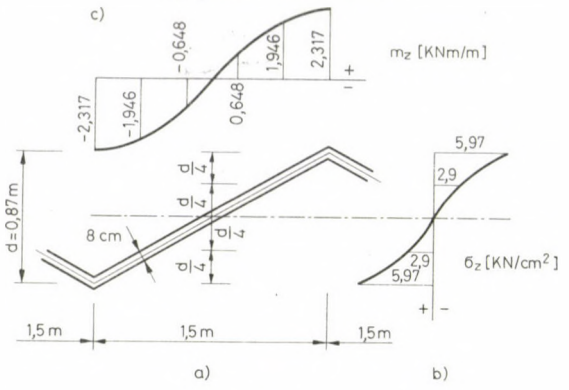

Fig. 15

Let us determine the longitudinal stresses induced in the cross section.

(The calculation is carried out on a section of 3 m width assuming, on the safe side, that the value of the moment is constant along the whole length.)

The critical moment is:

$$M = \frac{q \cdot l^2 \cdot 3}{8} = \frac{80 \cdot 24^2 \cdot 3}{8} = 1728 \text{ kNm}.$$

The elementary moment of inertia of the cross section is, taking into account that according to the specifications concerning r.c. only structures with a reduced depth $h = 8 - 2 \cdot 0{,}5$ cm should be calculated,

$$I_y = \frac{1}{6} h \cdot d^2 \cdot b = \frac{1}{6} \cdot 0{,}07 \cdot 0{,}87^2 \cdot 1{,}5 = 0{,}0132 \text{ m}^4.$$

The left-hand side of Eq. (31) reads

$$\frac{M}{EI_y} \cdot \frac{\sqrt{3} \cdot b^2}{h} = \frac{1728}{8 \cdot 10^6 \cdot 1{,}32 \cdot 10^{-2}} \cdot \frac{1{,}73 \cdot 2{,}25}{7 \cdot 10^{-2}} = 0{,}91.$$

By identifying the value obtained with those contained by Table III one finds that $\beta b = 1{,}0$. This value is lower than $\beta b = 1{,}7$ associated with the M_{cr}. From Eq. (31) and from Table III one obtains:

$$M_{cr} = 1{,}624 \frac{E \cdot I_y}{\sqrt{3} \cdot b^2} h = 1{,}62 \frac{8 \cdot 10^6 \cdot 1{,}32 \cdot 10^{-2}}{3 \cdot 1{,}5^2} \cdot$$

$$\cdot 7 \cdot 10^{-2} = 3076 \text{ kNm}.$$

The value of the safety factor calculated to M_{cr} is:

$$c = \frac{M_{cr}}{M} = \frac{3076}{1728} = 1{,}78.)$$

The values of ξ are to be found in Table VI. Multiplying these values with the "cross-sectional" constant Md/I_y (see formula 35a), one obtains the following values for the desired longitudinal stresses:

x/d	ξ	$\sigma_z = 1139\xi$ [daN/cm^2]
+0,5	+0,5240	+596,84
+0,375	+0,3900	+444,21
+0,250	+0,2584	+294,32
+0,125	+0,1287	+146,59
0	0	0
−0,125	−0,1287	−146,59
−0,250	−0,2584	−294,32
−0,375	−0,3900	−444,21
−0,5	−0,5240	−596,84

The stress pattern is shown in Fig. 15b.

The values of the bending moment of transverse direction can be calculated by making use of the formula (40) and Table IX:

$$m_z = -\frac{M}{b} \cdot \frac{h}{d} \mu(y) = -\frac{1728}{1{,}5} \cdot \frac{7 \cdot 10^{-2}}{0{,}87} \mu(y) =$$

$$= -92{,}69\mu(y) \text{ [kNm/m]}.$$

y/b	$\mu(y)$	m_z [kNm]
0,0	0,025	−2,317
0,2	0,021	−1,946
0,4	0,007	−0,648
0,6	−0,007	+0,648
0,8	−0,021	+1,946
1,0	−0,025	+2,317

The stress pattern is represented in Fig. 15c.

REFERENCES

1. KOLLÁR, L.: Statik und Stabilität der Schalenbogen und Schalenbalken. Akadémiai Kiadó, Budapest 1973
2. TIMOSHENKO, S.—GERE, J.: Theory of Elastic Stability, 2nd ed. McGraw-Hill, New York, 1961

Statische und Stabilitätsuntersuchung der gebogenen Faltwerke. — Behandelt werden einige Festigkeits- und Stabilitätsprobleme der in einer Richtung gebogenen Faltwerke aufgrund der Analogie der Schalenträgertheorie. Der Querschnitt erleidet durch die Biegung eine starke Verformung (Verflachung oder Wölbung), die die Spannungs- und Stabilitätsverhältnisse der Konstruktion entschiedend beeinflußt. Nach der genauen Berechnung dieser Verformung ermittelt der Autor mit Hilfe der Krümmungsfunktionen für die, in der Praxis gebrauchten Querschnittstype den kritischen Stabilitätszustand hervorrufende Momentwerte, und erörtert schließlich die längsgerichteten Normalspannungen. Der Aufsatz enthält auch die, bei der praktischen Planung anwendbaren Diagramme und Tabellen.

Acta Technica Academiae Scientiarum Hungaricae, 93 (1—2), pp. 67—75 (1981)

THE EFFECT OF AIR OR CO_2 IMPURITY ON THE CHARACTERISTICS OF MERCURY-ARGON DISCHARGE AT LOW PRESSURE

SABAH TAUFIK, A*

[Manuscript received May 8, 1981]

Based on the results of earlier research investigations performed by the TUNGSRAM Research Institute a quick-working, semi-automatic diagnosis system has been worked out with the aid of which, at the low-pressure Hg/Ar-discharge used for light source, under the usual circumstances the effect on the utilization of light of the two impurities, air and CO_2 occurring the most frequently in the course of bulk manufacture, has been investigated.

1. Introduction

A lot of experimental and theoretical studies have been carried out on the electrical discharge of the fluorescent lamps which are used as sources of light.

These studies as far as we know have not dealt with the effects of CO_2 or air introduced into the fluorescent lamp that working at low pressure Hg/Ar discharges.

This paper presents the results of firstly experimental studies on the effect of CO_2 and air introduced into the fluorescent tubes, since air and CO_2 can exist during the manufacturing of fluorescent lamp.

It is very easy to characterize the effect of these impurities if we use the well known formula for the light utilization, since the discharge induced in a mixture of low-pressure mercury vapour and inert gas gives the mercury resonant line of 254 nm wavelength transformed by the luminous powder fitted to the visibility curve generating wide-band radiation [1] so one can state the formula for the light utilization as,

$$\eta = \eta_1 \eta_2 \eta_3 ,$$

where η is the ratio of the light power fitted to the eye sensitivity and received from that part of the tube which is coated with luminous powder, and transferred into visible, to the input power, namely light efficiency of the light source, η_1, η_2 and η_3, characterize the loss arising at the electrodes, where the knowledges connected with the cathode processes is most well summarized by Bitó[2], in the positive column and on the luminous powder, $\eta_1 = \frac{P_{\text{pos. col.}}}{P_{\text{in}}}$ is the relation of electrical power supplied to the

* Sabah Taufik Ahmed, Ahmed, Fő utca 26, II. 4., H-1011 Budapest, Hungary

positive column to the total effective power, $\eta_2 = \frac{P_{254}}{P_{\text{pos. col.}}}$ characterizes the proportion of the power of the 254 nm wavelength ultra violet radiation generated in the positive column and the power supplied into the positive column, $\eta_3 = \frac{P_{\text{visible}}}{P_{254}}$ is the ratio of the visibility curve and of the resonant line of 254,6 nm namely the efficiency of the coverting into visible field.

To get the necessary experimental information about the effects of CO_2 and air in working tubes there was built a diagnostic system that is suitable for deciding not only the microparameters of the plasma but the $\eta_1\eta_2$ or η_3 efficiencies.

2. Experimental method

Few standard tubes were necessary to follow the modifications in the fluorescent lamp, while a similar measuring system that used by ANTAL—GÁTI [3] was built in order to determine the microparameters of the positive column as well as the other parameters that necessary for the control of the light utilization. 1% of CO_2 or air was introduced into the tube by opening small capsule containing the impurity.

After starting the discharge, the stabilization time was measured as the time dependence of burning voltage $U(t)$ for tubes operating at a.c. voltage, also the following parameters are taken as a function of a direct discharge current I_e;

— $U_e(I_e)$ burning voltage.

— $U_{pc}(I_e)$ the voltage of cathode side probe.

— $\Delta U_{pcA}(I_e)$ the voltage drop between the probes.

— $U_{sc}(I_e)$ the voltage across the cathode spiral.

— $U_{sA}(I_e)$ the voltage across the anode spiral.

— $\Phi(I_e)$ the signal which is directly proportional to the light flux originated from unit surface area that is covered by powder. Beside these a set of probe characteristics were recorded.

Results

The alternating burning voltage recorded against time following the start of the tubes, where in the tubes filled by krypton + argon the following phenomena was observed that two minutes after the start an overvoltage peak of 1 – 2 percent could be observed then by end of fourth minute the voltage has stabilized. In tubes filled by argon the burning voltage is decreased from a higher starting value to a stable value, and the stabilizing time of argon tubes are longer by an average of two minutes.

An approximate order can be recognized according to times of stabilizations, these are; krypton + argon, argon, argon + air, argon + CO_2. Instabilities due to long time of stabilization in tubes containing carbon dioxide could be observed visually too.

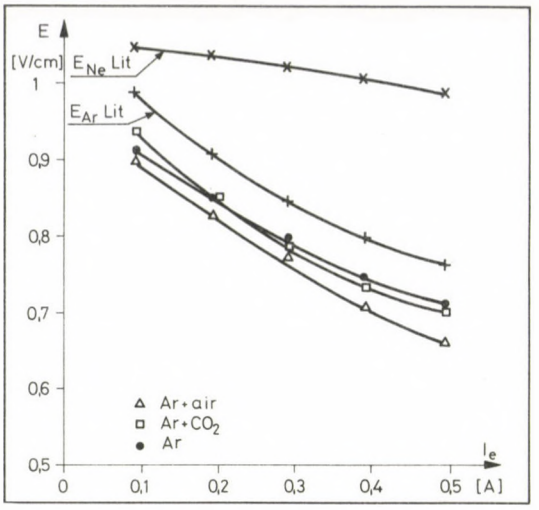

Fig. 1. The averaged electric field intensity as a function of discharge current

At one of the sample the stabilization proceeded during a period of oscillation more than 15 minutes. In the tubes containing air and immediatly after the start a reddish luminous space near the surroundings of the capsule had diffused in 5 – 10 seconds to whole tube, while its intensity decreased gradually, the effect related to nitrogen diffusion. The longitudinal field intensity E plotted against discharging current is shown in Fig. 1. For comparison, experimental neon curve of VERBEEK [4] and argon curve of VERWEIJ [5] for electric field intensity is indicated. Our curve concerning argon is similar to the curve of technical l'erature, the difference is only a constant multiplicator which occurred in consequence of different gas filling pressure.

In argon tubes with 1 percent contamination the variation of electric field in a range of 100 – 500 ma current is much lower than that in the case of argon gas fillings.

From the probe curves that have been recorded two other important plasma characteristics can be obtained; these are the electron temperature and electron concentration plotted against discharge current as shown in the Fig. 2 and Fig. 3.

In both of these figures the curve of VERWEIJ [5] for pure argon and the curve of VERBEEK—DROP [6] for pure neon, are indicated. Air contamination has not modified essentially the function of $T_e(I_e)$ and $n_e(I_e)$, but the contamination of CO_2 had significantly changed both of the microparameters. In order to describe this effect it is necessary to underline that the degree of average electron concentration (and due to quasi-neutral feature of the plasma the ion concentration of Hg^+) $n_e = 10^{11}$ cm^{-3} and carbon dioxide concentration of 1 percent supplied as contamination

$$n_{CO_2} = 10^{18} \text{ cm}^{-3} .$$

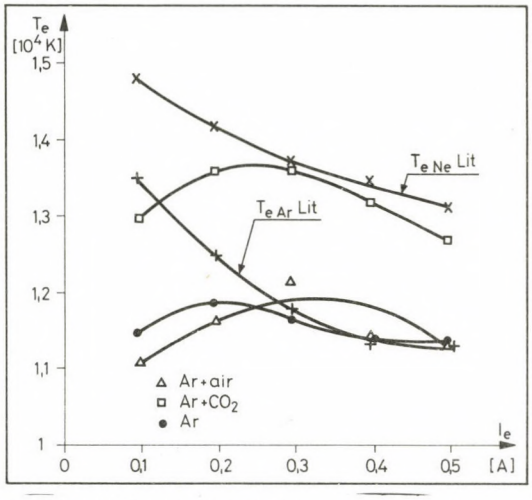

Fig. 2. The averaged electron temperature as a function of discharge current

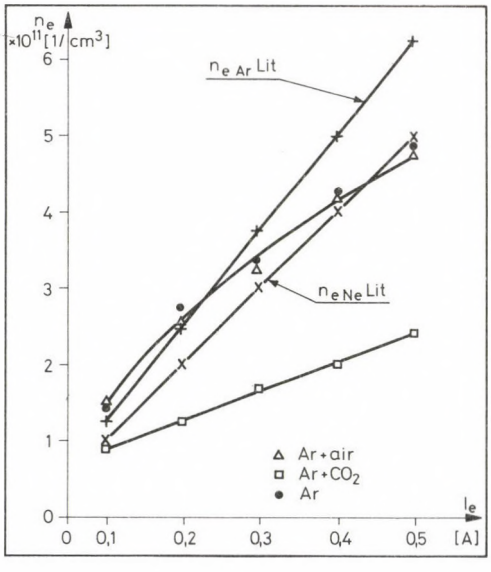

Fig. 3. The averaged electron concentration as a function of discharge current

During long burning periods CO_2 is disintegrating to carbon and oxygen. As a first step of this process the molecule of CO_2 is impacting inelastically to electrons of low energy and at the time by electron capture produces a CO_2^- molecule-ion

$$e^- + CO_2 = CO_2^-$$

and that of course is disintegrating again.

In uncontaminated tubes Maxwell's distribution law can be presumed with about 1 ev average of energy for electron.

To the 4—4,8 ev energy interval, where the manner of action of the above mentioned reaction is high, about 5 per cent of the whole electrons could get in, which is not negligible. In consequence that the CO_2 concentration is seven times higher in order of magnitude than the number of electrons which are continuously decreasing in the chanel of about 4,4 ev energy level, and this is the explanation for the 60 percent lower value of electron concentration. As the field intensity has not changed so one can expect an increase of electron temperature which compensates the drop of electron concentration by the same discharging current intensity. But the increasing of this temperature was only 15 percent, therefore it can be supposed that in addition to the electron concentration the negative ions play an important part too. The mass of one oxygen atom is about 30 000 times havier than the mass of electron and therefore its mobility is much less but the abundance of oxygen a great importance. The less drop of electron concentration and increasing of temperature in air — contaminated tubes can be explained by the above mentioned mechanism too.

Fig. 4 shows the relative powers dissipated on the spirals plotted against discharge current.

The spiral losses come to about 5 percent of the total power even by high discharge current intensities therefore they have only minor importance for qualification of electrodes for determination of duration of life been expected. The effect of CO_2 contamination on the power dissipated on cathode spiral was 25 percent lower.

For the balance of energy of the whole tube, the investigation of cathode and anode fall has a greater importance (Fig. 5) because the amount of them can reach 30 percent of the whole power.

The power consumption of the cathode fall is approximately independent of discharge current at each case of samples but air contamination has a considerable effect.

Air contamination caused a relatively higher cathode fall by 1,5 percent. The effect of CO_2 contamination at 500 ma caused higher relative anode fall by 3,5 percent.

All the losses arising in spirals and in their surroundings are characterized by efficiency η_1 which is indicated in Fig. 6.

Near the working point it was found for the tubes contaminated by CO_2 the value of η_1 was 3 — 5 percent lower. The contamination made no difference concerning this parameter.

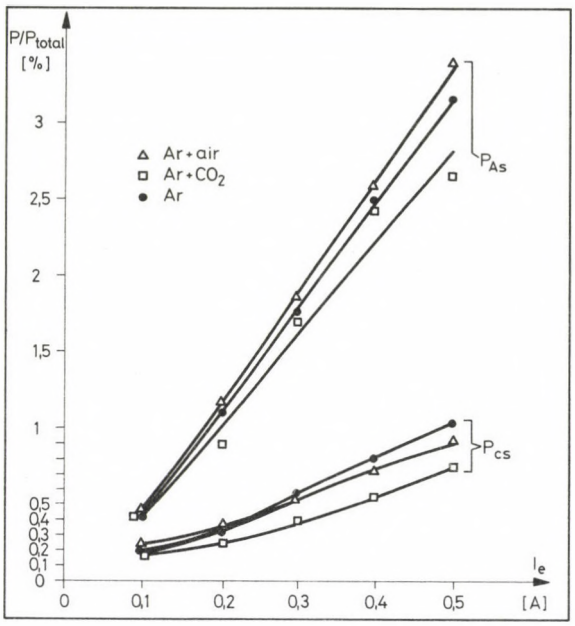

Fig. 4. The averaged losses on cathode and anode spiral relative to the total power as a function of current

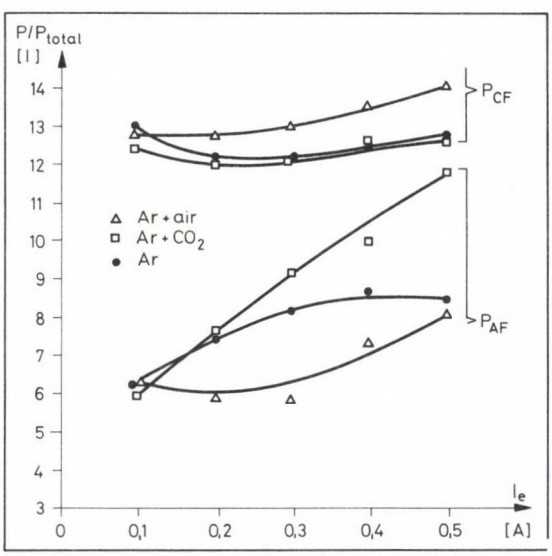

Fig. 5. Current dependence of the cathode and anode fall related to the total energy

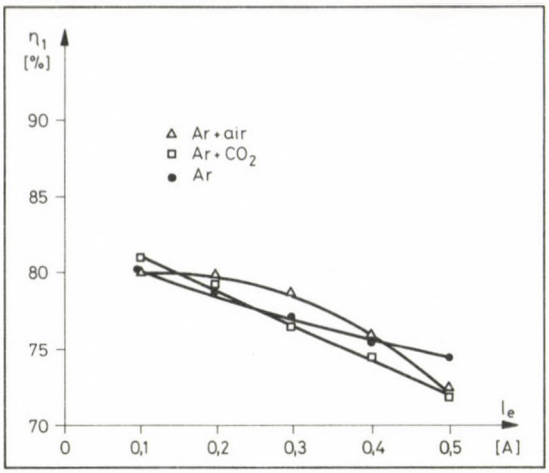

Fig. 6

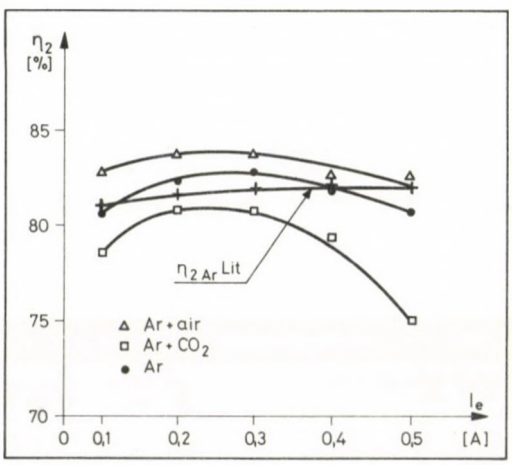

Fig. 7

As a result of optical measurements by determination of light intensity the efficiency η_2 plotted against discharge current (Fig. 7) was not carried out by absolute measurements so one can make equal efficiency η_2 of pure argon tubes by the value given intechnical literature [3] of 82 percent at 400 ma, then it was easy to determine all the other curves. In the above figure the curve of VERWEIJ was used as a reference curve.

At argon tubes contaminated by air η_2 is higher in the whole current interval with an average of 1 percent than at the average of pure argon tubes, at CO_2 tubes this value is $1-3$ percent lower.

In the tubes contaminated by CO_2 the lower light emitting efficiency can be explained above all by the decreased electron concentration.

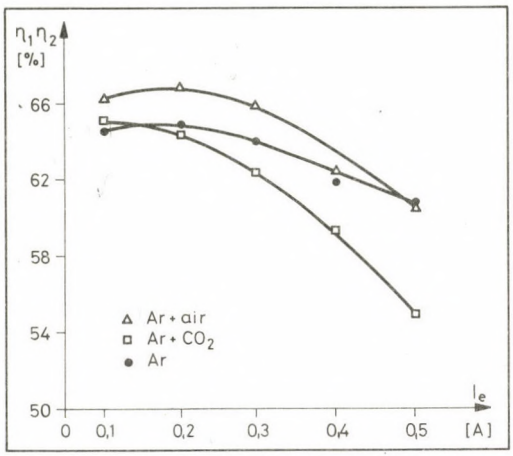

Fig. 8. Current dependence of averaged product of $\eta_1\eta_2$ which is proportional to the light utilization

A considerable part of power charged into the column gets lost due to the fact that CO_2 molecule binds electron by self-ionisation therefore the electron getting lost although it takes part as a negative ion in montaining of discharge current, it is not able to produce further electron-ion pairs nor to excite Hg atoms.

Increasing efficiency to a slight degree by the effect of air can be imputed to nitrogen and probably this effect could be stronger by charging pure nitrogen, (the oxygen which is charged into the tube with air, effects as same as CO_2 contamination, which causes the decrease in the efficiency), but this is not economical therefore tubes contaminated artificially by nitrogen are not manufactured.

Fig. 8 shows the product $\eta_1 \cdot \eta_2$ which is proportional to light utilization applying the same quality of luminous powder. As it could be expected the light utilization has decreased considerably by 5 percent near to working point due to CO_2 contamination while light utilization has increased slightly by the effect of air.

4. Summary

By the help of measurements system it was determined experimentally with zero hour position for 40 W tubes contaminated by CO_2 or air the followings;

— Power dissipated on spirals and also on anode and cathode regions.

— Characteristics of positive column, axial electric field intensity, electron temperature and concentration.

— Light emitting efficiency of the positive column.

— Light utilization in relative units.

In tubes filled by argon and contaminated by CO_2 or air, all the measurements and derived characteristics (with the exception of η_2 and $\eta_1\eta_2$ have caused deviation of

same tendency which can be explained in both cases by existance of electro-negative oxygen.

Under the effect of air the axial electric field intensity of positive column was lower by 8 percent, while the effect of CO_2 has not caused essential deviation.

Introducing of CO_2 into the tubes increases the electron temperature to 15 percent, and drop the electron concentration to 60 percent, while these two parameters in the case of air are lower.

In both cases there were no considerable effect in the value of η_1.

The light emitting efficiency η_2 has the most important role which was smaller in value by 2,5 percent in the case of CO_2 contamination, while the effect of air has increased η_2 by 0,5 percent. And this effect can be proceeded due to result of resonance energy transfer between nitrogen gas and 6^3P triplets of generated Hg atoms and which create a slight increase of light utilization.

One can conclude that by the effect of carbon dioxide contamination by even less than 1 percent in zone hour tubes such characteristic changes are going to be formed which makes possible to detect CO_2 contamination in new tubes too.

Detection of air contamination of small quantity is possible as well, but only by evaluation of measuring series.

Acknowledgements

Author would like to thank his supervisor Dr. János Bitó the technical manager of TUNGSRAM for his valuable propositions and discussions during the course of this work, as well he would like to thank everyone who helped him to carry out this work in the TUNGSRAM Research Institute.

REFERENCES

1. Elenbaas, W.: Fluorescent Lamps; Philips Technical Library, 1971
2. Bitó, J.: Az oxidkatódos ívkisülések katód oldali jelenségeiről — Kandidates Dissertation, 1966
3. Antal, K. G.—Gáti, E.: Entladungsphysikalisches Prüfsystem für die Untersuchung der die Leuchtstofflampen beeinflussenden Faktoren; Tungsram technische Mitteilungen, 1976 Nr. 29
4. Verbeek, T. G.: Probe Measurements in the Positive Column of Low Pressure Mercury-Neon and Mercury-Argon-Neon Discharges; *2nd International Conference on Gas Discharges*, **94** (1972)
5. Verweij, W.: Probe Measurements and Determination of Electron Mobility in the Positive Column of Low Pressure Mercury-Argon Discharges; *Philips Research Report Supplements;* **53** (1961), 2
6. Verbeek, T. G.—Drop, P. C.: The Positive Column of Low Pressure Hg/Ne and Hg/Ar Discharges; *Journal of Physics, D; Applied Physics* **7** (1974)

Die Einwirkung der Schmutzstoffe Luft und Kohlensäure auf die Charakteristiken der Quecksilber—Argon-Entladung bei Niederspannung. — Basierend auf den Ergebnissen der früher durch das Forschungsinstitut TUNGSRAM durchgeführten Forschungsarbeit wurde ein schnellwirkendes halbautomatisches Diagnosesystem entwickelt, mit Hilfe dessen die in den für Lichtquellen gebrauchten Hg/Ar Niederdruckentladungen unter üblichen Umständen auf die Lichtbenutzung ausgeübte Wirkung der im Laufe der Großbetriebsproduktion am häufigsten vorkommenden Schmutzstoffe der Luft und der Kohlensäure untersucht wurde.

Acta Technica Academiae Scientiarum Hungaricae, 93 (1—2), pp. 77—99 (1981)

ANALYTISCHES NÄHERUNGSVERFAHREN ZUR BERECHNUNG VON WIRBELSTRÖMEN IN METALLPLATTEN

D. KERÉNYI*

KANDIDAT DER TECHNISCHEN WISSENSCHAFTEN

Es wird ein analytisches Näherungsverfahren zur Berechnung der Wirbelstromverluste in einer von einem magnetischen Wechselfeld durchsetzten Platte dargestellt. In der Berechnung wird sowohl die endliche Dicke der Platte als auch der Einfluß der neben der Platte liegenden wirbelstromfreien Schichten (Luft, Öl) auf die Verluste berücksichtigt. Ausgehend von den Maxwellschen Gleichungen und nach Einführung mehrerer Näherungen ergibt sich eine einfache Formel zur Berechnung der Wirbelstromverluste. Diese Formel deckt auch die Rolle der einzelnen, die Wirbelstromerscheinungen beeinflussenden Parameter auf. Das Verfahren kann auch für die Berechnung der Wirbelstromverluste von im Magnetfeld konzentrischer Wicklungen liegenden Platten, z. B. Transformatorkesseln benützt werden.

Für die Konstrukteure von elektrischen Hochleistungsmaschinen (besonders von Hochleistungstransformatoren) ist es eine wichtige Aufgabe, die in den Konstruktionsteilen vom magnetischen Streufeld erzeugten Wirbelstromverluste zu bestimmen. Eine exakte rechnerische Behandlung dieses Problems ist nur mit Hilfe von numerischen Verfahren möglich [1, 2]. Bei der Durchführung von praktischen Berechnungen können aber die wirklichen Feldverhältnisse — die Abhängigkeit der Permeabilität von der Feldstärke, die dreidimensionalen Feldprobleme, die Rückwirkung von Wirbelströmen — auch in den numerischen Verfahren mehr oder weniger nur mit Vernachlässigungen abgebildet werden [z. B. 3]. Die Verluste in Metallteilen einfacherer Form (Schiene mit einem rechteckförmigen Querschnitt, Quader, Platten) können auch analytisch berechnet werden. Auf Grund der auf diese Weise erhaltenen Berechnungsformeln können einerseits die Verluste leichter und schneller bestimmt werden, andererseits aber kann auch die Wirkung der einzelnen Parameter besser beurteilt werden [z. B. 4, 5].

In diesem Aufsatz wird ein analytisches Näherungsverfahren zur Berechnung der Wirbelstromverluste in rechteckigen Platten dargestellt. Es wird die normale Komponente der Feldstärke (das heißt die senkrecht zur Platte verlaufende Feldstärke) angegeben. Die Feldverteilung wird aber nicht an der Oberfläche der Platte, sondern in einer zur Platte parallel liegenden Ebene, und zwar innerhalb eines mit der Plattenfläche gleichen Rechteckes vorgeschrieben. Längs der Achse, parallel zu einer Seite des Rechteckes, kann der Verlauf der magnetischen Feldstärke beliebig sein, am Rand der Fläche muß aber die normale Komponente der Feldstärke gleich Null

* Dr. D. Kerényi, Modori u. 12, H-1021 Budapest, Ungarn.

sein. Längs der hierzu senkrechten Richtung ist die Feldstärke konstant (Bild 1). Der Verlauf der Feldstärke ist zeitlich sinusförmig.

In elektrischen Maschinen verwendet man oft Platten als Konstruktionsteile. Die in Platten vom Streufeld erzeugten Verluste wurden schon von mehreren Autoren berechnet [z. B. 1, 6, 7]. Die hier dargestellte Methode unterscheidet sich von den in der Fachliteratur angegebenen Verfahren durch folgende Eigenschaften:

a) Nach unserer Methode wird die Verteilung der Verluste auch im Inneren der Platte berücksichtigt; auf diese Weise können die Verluste auch in Platten endlicher Dicke berechnet werden. (Das in der Abhandlung [1] dargestellte Verfahren ist nur für die Berechnung von dünnen Platten geeignet, die man mit einer einzigen Stromschicht abbilden kann).

b) Man kann das magnetische Feld in einer zur Metallplatte parallel liegenden Ebene vorschreiben, deren Abstand von der Platte angegeben ist. So kann die reelle Feldverteilung besser abgebildet werden. Diese Eigenschaft der Methode ist neu im Vergleich mit den bekannten und in der Praxis verwendeten Methoden. (In den Verfahren nach [6] und [7] wurde die Feldstärke an der Oberfläche der Platte vorgeschrieben.)

Die Verluste in der Platte werden auf Grund der Maxwellschen Gleichungen bestimmt, es müssen aber mehrere Näherungen und Vereinfachungen eingeführt werden. Die Genauigkeit der Methode hängt davon ab, in welchem Maße unsere Voraussetzungen sich der Wirklichkeit nähern. Stimmt das als Grund der Berechnungen angenommene physikalische Bild mit der Wirklichkeit im großen und ganzen überein, so werden auch die berechneten Verluste mit den reellen, das heißt gemessenen Verlusten gut übereinstimmen.

Das hier behandelte analytische Verfahren kann mit Korrektion auch für die Berechnung der Wirbelstromverluste von im Streufeld konzentrischer Wicklungen

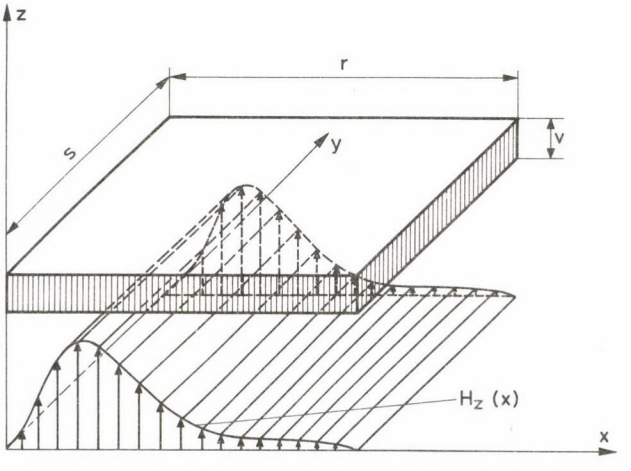

Bild 1. Platte in Magnetfeld

liegenden Platten benutzt werden. Die Verwendbarkeit der Methode für diesen Zweck wird untersucht, indem wir die Ergebnisse der analytischen Berechnungen mit denen eines numerischen Verfahrens vergleichen, welches als genaueres Verfahren berücksichtigt werden kann, da bei diesem wenigere Näherungen durchgeführt werden. Der Vergleich der zwei Methoden kann auch dazu dienen, die Verteilung der Feldstärken, Wirbelstromdichten und Verluste in der Platte zu untersuchen.

1. Darstellung der Methode

Die Berechnung der Wirbelstromverluste, die in der im Bild 1 gezeigten Platte erzeugt werden, wird auf Grund des im Bild 2 dargestellten, dreischichtigen, zweidimensionalen Modells durchgeführt. An der Grenzfläche der ersten Schicht ($z=0$) wird für die normale Komponente der Feldstärke längs der x-Achse ein periodischer Verlauf

$$H_{z0}=H_m \sum_{k=1}^{n} b_k \sin k\alpha x e^{j\omega t} \tag{1}$$

angenommen, wobei $\alpha=\pi/r$ die räumliche Kreisfrequenz der ersten (räumlichen) Harmonischen, $\omega=2\pi f$ die zeitliche Kreisfrequenz, r [m] die Abmessung der Platte in Richtung der x-Achse, und f [1/s] die Zeitfrequenz bedeuten. Die Fourier-Koeffizienten b_k müssen so gewählt werden, daß man über die Strecke r den gewünschten Verlauf der Feldstärkeverteilung erreicht. Die erste und die zweite Schicht haben endliche Dicken v_1 [m] bzw. v_2 [m], die dritte Schicht wird aber unendlich dick angenommen ($v_3\to\infty$). Die drei Schichten sind in Richtung x und y (senkrecht zur Bildebene des Bildes 2) unendlich ausgedehnt, in Richtung y ist die Feldstärke konstant.

Nachfolgend werden die Wirbelstromverluste in einem endlichen Teilgebiet der unendlich ausgedehnten Platte bestimmt. Dieses Teilgebiet ist ein Rechteck, dessen Abmessungen r (in Richtung x) und 1 (in Richtung y) sind. (r ist die Länge einer

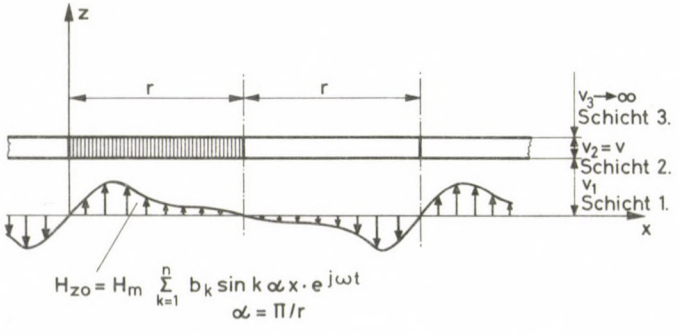

Bild 2. Zweidimensionales, dreischichtiges Modell für die Berechnungen

räumlichen Halbwelle.) Die für dieses Teilgebiet erhaltenen Verluste müssen mit einem früher bestimmten [5] Faktor multipliziert werden, um die Wirbelstromverluste in einem in der y-Richtung s langen Plattengebiet zu erhalten. Die im Teilgebiet $r \times s$ der mittleren Schicht erzeugten Verluste werden als Verluste der im Bild 1 dargestellten endlichen Platte angenommen. Außerdem wird noch folgendes vorausgesetzt:

a) Es wird angenommen daß der an der Begrenzungsfläche der ersten Schicht in Gleichung (1) vorgeschriebene Verlauf der Feldstärke durch die in der Platte erzeugten Wirbelströme nicht beeinflußt wird.

b) Um die Berechnungen zu vereinfachen, wird vorausgesetz, daß nur die Amplituden der einzelnen räumlichen Harmonischen der senkrecht zur Platte (in Richtung z) gerichteten Feldstärkekomponente von z abhängen, ihre Wellenlängen und Phasenlagen aber konstant bleiben. Man kann diese Näherung für alle Werte von $v_1 < 0{,}25r$ geben, wie dies aus Punkt 3.2 hervorgeht.

c) Die Permeabilität von ferromagnetischen Platten wird konstant (unabhängig von der Feldstärke) angenommen.

d) Die Hysterese wird vernachlässigt. Diese Näherung ist bei dicken Platten berechtigt [6]. (Es soll bemerkt werden, daß bei den kaltgewalzten Transformatorblechen bester Qualität die Hysteresisverluste ungefähr 50% der gesamten Verluste betragen. Nimmt aber die Dicke zu, so nimmt dieses Verhältnis rasch ab.)

Für quasistationäre Felder lauten die Maxwellschen Gleichungen:

$$\Delta \mathbf{H} = \mu\gamma \frac{\partial \mathbf{H}}{\partial t}, \tag{2}$$

$$\operatorname{div} \mathbf{H} = 0, \tag{3}$$

$$\operatorname{rot} \mathbf{H} = \gamma E. \tag{4}$$

Dabei bedeuten $\mathbf{H}$ [A/m] den Vektor der magnetischen Feldstärke, $\mathbf{E}$ [V/m] den Vektor der elektrischen Feldstärke, μ [H/m] die magnetische Permeabilität und γ [S/m] die elektrische Leitfähigkeit. In unserem Falle besitzt $\mathbf{H}$ nur die Komponenten x und z ($H_y = 0$), und $\mathbf{H}$ ist von y unabhängig $\left(\frac{\partial \mathbf{H}}{\partial y} = 0\right)$. Daraus folgt, daß die Wirbelstromdichte in einer unendlich langen Platte nur eine y Komponente besitzt ($i_x = i_z = 0$). Es wird vorausgesetzt daß alle drei Schichten endliche elektrische Leitfähigkeit haben.

Es läßt sich leicht zeigen, daß die Lösungen

$$H_{zl} = H_m \sum_{k=1}^{n} f_k(x) \cdot g_{lk}(z) \cdot e^{j\omega t} \tag{5}$$

und

$$H_{xl}=H_m\sum_{k=1}^{n}\frac{1}{(k\alpha)^2}f'_k(x)\cdot g'_{lk}(z)\cdot e^{j\omega t} \tag{6}$$

die Differentialgleichungen (2) und (3) unter den obigen Voraussetzungen für alle drei Schichten genügen, wobei

$$f_k(x)=b_k\sin k\alpha x\,, \tag{7}$$

$$g_{lk}(z)=C_{lk1}e^{p_{lk}z}+C_{lk2}e^{-p_{lk}z}\,, \tag{8}$$

$$p_{lk}^2=(k\alpha)^2+j\omega\mu_l\gamma_l\,, \tag{9}$$

und der Index l die Nummer der betreffenden Schicht anzeigt ($l=1, 2, 3$). Die Stromdichte ergibt sich aus der Differentialgleichung (4) durch Berücksichtigung der Formel (5) und (6)

$$i_{yl}=j\omega\mu_l\gamma_l H_m\sum_{k=1}^{n}\frac{1}{(k\alpha)^2}f'_k(x)\cdot g_{lk}(z)\cdot e^{j\omega t}\,. \tag{10}$$

Man erhält für die Verluste in einem zum Punkt (x, y) gehörigen Elementarquader, dessen Länge in Richtung y gleich 1 ist, die Beziehung

$$dP_l(x,z)=\frac{1}{2}\frac{1}{\gamma_l}|i_{yl}(x,z)|^2\,dx\cdot dz\,. \tag{11}$$

(Die Verluste müssen mit einem Faktor 1/2 multipliziert werden, da $i_{yl}(x, z)$ den Scheitelwert der zeitlich sinusförmigen Stromdichte bedeutet.) Daraus erhalten wir die Verluste in einem Plattengebiet von den Abmessungen r (in Richtung x) und 1 (in Richtung y) durch Integration:

$$P_1=\frac{1}{2}\frac{1}{\gamma_1}\int_0^{v_1}\int_0^{r}|i_{y1}(x,z)|^2\,dx\cdot dz\,, \tag{12}$$

$$P_2=\frac{1}{2}\frac{1}{\gamma_2}\int_{v_1}^{v_1+v_2}\int_0^{r}|i_{y2}(x,z)|^2\,dx\cdot dz\,, \tag{13}$$

$$P_3=\frac{1}{2}\frac{1}{\gamma_3}\int_{v_1+v_2}^{\infty}\int_0^{r}|i_{y3}(x,z)|^2\,dx\cdot dz\,. \tag{14}$$

Die Verluste in einer in der y-Richtung s langen Platte ergeben sich mit guter Näherung [5] durch Multiplikation mit dem Faktor

$$k_s = s \frac{1}{\left(\frac{r}{s}\right)^2 + 1}, \tag{15}$$

also

$$P_{sl} = P_l k_s . \tag{16}$$

Die Integrationskonstante C_{lk1} und C_{lk2} erhält man aus den Randbedingungen:
a) $H_{z1} = H_{z0}$ für $z = 0$, so ergibt sich aus Gl. (1), (5), (7) und (8)

$$C_{1k1} + C_{1k2} = 1 . \tag{17}$$

b) $H_{z3} \to 0$ für $z \to \infty$, so ergibt sich aus Gl. (5), (7) und (8)

$$C_{3k1} = 0 . \tag{18}$$

c) An der Trennfläche der einzelnen Schichten müssen die tangentialen Komponenten von **H** und die Normalkomponenten von **B** stetig sein. So gibt an der Trennfläche der 1. und 2. Schicht ($z = v_1$)

$$\mu_1 H_{z1} = \mu_2 H_{z2} ,$$

und

$$H_{x1} = H_{x2} ,$$

und so bekommt man aus Gl. (5), (6) und (8)

$$\begin{aligned} &\mu_1 (C_{1k1}\, e^{p_{1k} v_1} + C_{1k2}\, e^{-p_{1k} v_1}) = \\ &= \mu_2 (C_{2k1}\, e^{p_{2k} v_1} + C_{2k2}\, e^{-p_{2k} v_1}) , \end{aligned} \tag{19}$$

und

$$\begin{aligned} &p_1 (C_{1k1}\, e^{p_{1k} v_1} - C_{1k2}\, e^{-p_{1k} v_1}) = \\ &= p_2 (C_{2k1}\, e^{p_{2k} v_1} - C_{2k2}\, e^{-p_{2k} v_1}) . \end{aligned} \tag{20}$$

An der Trennfläche der 2. und 3. Schicht ($z = v_1 + v_2$)

$$\mu_2 H_{z2} = \mu_3 H_{z3}$$

und

$$H_{x2} = H_{x3}$$

so erhält man

$$\mu_2(C_{2k1}\, e^{p_{2k}(v_1+v_2)} + C_{2k2}\, e^{-p_{2k}(v_1+v_2)}) = \\ = \mu_3 C_{3k2}\, e^{-p_{3k}(v_1+v_2)} \tag{21}$$

und

$$p_2(C_{2k1}\, e^{p_{2k}(v_1+v_2)} - C_{2k2}\, e^{-p_{2k}(v_1+v_2)}) = \\ = -p_3 C_{3k2}\, e^{-p_{3k}(v_1+v_2)}. \tag{22}$$

Nach der Lösung des Gleichungssystems (17) und (19)–(22) in 5 Unbekannten ergeben sich die Konstanten C_{1k1}, C_{1k2}, C_{2k1}, C_{2k2} und C_{3k2}.

Die bisher angegebenen Formeln gelten für eine allgemeine Anordnung mit drei Schichten; jede Schicht kann eine endliche elektrische Leitfähigkeit besitzen. Ist nur die zweite Schicht leitend (also mit nicht leitenden Schichten z. B. mit Luft umgeben), so werden Verluste nur in dieser Schicht erzeugt, die aus der Formel

$$P_{s2} = \frac{1}{2}\frac{1}{\gamma_2} s \frac{1}{\left(\frac{r}{s}\right)^2 + 1} \int_{v_1}^{v_1+v_2} \int_0^r |i_{y2}(x,z)|^2 \, dx \cdot dz \tag{23}$$

berechnet werden können.

Ist der räumliche Verlauf der Feldstärke an der Oberläche der Platte ($v_1 = 0$) einfach sinusförmig, kann man also

$$H_{z0} = H_m \sin \alpha x e^{j\omega t}, \tag{24}$$

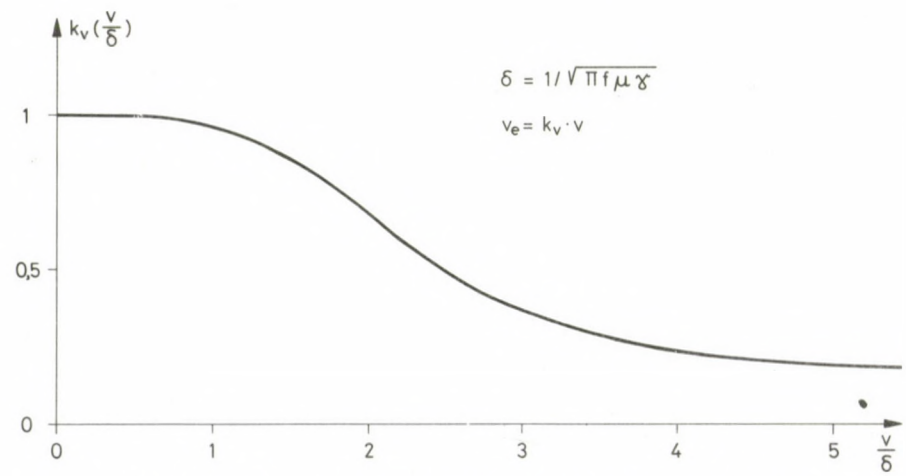

Bild 3. **Der Faktor k_r zur Bestimmung der equivalenten Dicke der Platte**

schreiben, so ergibt sich

$$P_{s2}=\gamma_2 f^2(\mu_2 H_m)^2 r^3 s \frac{1}{\left(\frac{r}{s}\right)^2+1} k_v \cdot v_2 , \tag{25}$$

wobei der Faktor k_v im Bild 3 über dem Verhältnis der Plattendicke (v_2) und der Eindringungstiefe ($\delta=1\sqrt{\pi f \gamma_2 \mu_2}$) dargestellt ist. Das Produkt $k_v v_2$ kann als *die equivalente Dicke der Platte* berücksichtigt werden.

Die Beziehung (23) kann bei beliebiger räumlichen Feldstärkeverteilung in der Form gleich (25) geschrieben werden, man muß nur die Feldstärke H_m in (25) mit einem von der Feldverteilung abhängigen Faktor k_H multiplizieren. So ergibt sich für die Verluste in allen Fällen die Formel

$$P_{s2}=\gamma_2 f^2(\mu_2 k_H H_m)^2 r^3 s \frac{1}{\left(\frac{r}{s}\right)^2+1} k_v \cdot v_2 .$$

Aus dieser Beziehung kann man den Einfluß der Parameter auf die Verluste sofort beurteilen.

2. Vergleich der berechneten Werte mit Meßwerten

Bei früheren Versuchen [8, 9] wurde eine ferromagnetische Platte der Abmessungen $2r=0{,}8$ m, $s=0{,}46$ m und $v_2=0{,}01$ m von einem senkrecht zur Oberfläche gerichteten Wechselfeld ($f=50$ Hz) durchsetzt. Längs der längeren Seite der Platte (in Richtung der x-Achse) wurde an der Oberfläche die im Bild 4 dargestellte Induktionsverteilung gemessen. Längs der kürzeren Seite (in Richtung der y-Achse) war die Induktion praktisch konstant. Die gemessenen Verluste in der Platte betrugen 2825 W.

Die Verluste wurden auch nach der im Punkt 1 beschriebenen Methode berechnet. Die für die Berechnung angenommene Feldstärkeverteilung wurde aus der Induktionsverteilung des Bildes 4 bestimmt ($v_1=0$), und die Berechnung wurde für eine relative magnetische Permeabilität von $\mu_r=50$ und eine elektrische Leitfähigkeit von $\gamma=7\cdot 10^6$ S/m durchgeführt. Die für die Hälfte der Versuchsplatte ($r=0{,}4$ m) berechneten Wirbelstromverluste betrugen 1440 W, daraus ergibt sich für die ganze Platte 2880 W, was man als ein ungewöhnlich gutes Ergebnis beurteilen kann.

Der Wert 50 wurde für μ_r auf Grund von Erfahrungen angenommen. Die Richtigkeit unserer Schätzung kann in Bild 5 kontrolliert werden. In diesem Bild sieht man den Absolutwert der aus Gl. (6) berechneten, senkrecht zur Platte verlaufenden Feldstärke H_x an der Oberfläche über x. (In Aufgaben dieser Art übersteigen die H_x

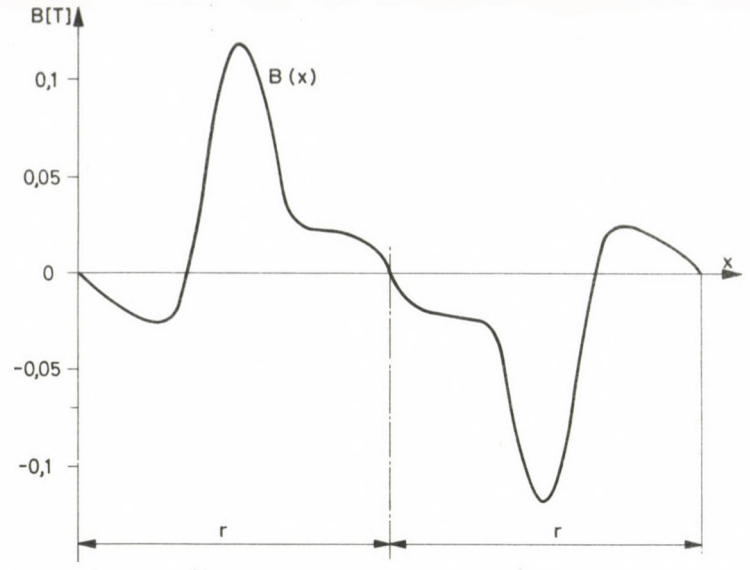

Bild 4. **Verteilung der senkrecht zur Oberfläche gerichteten Induktion an der Versuchsplatte [8]**

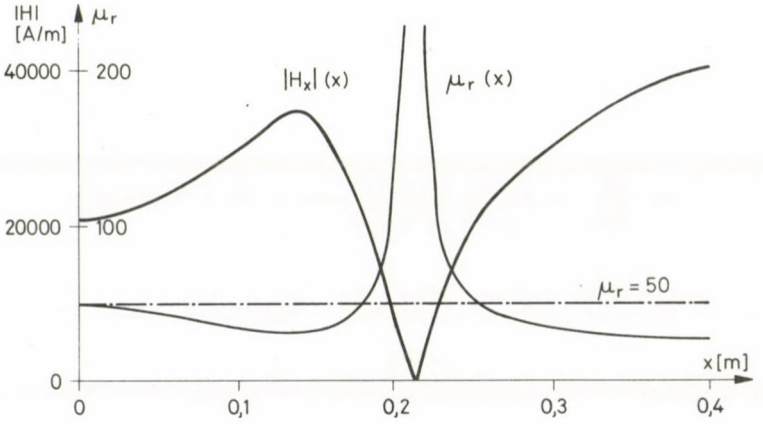

Bild 5. Absolutwert der parallel zur Platte gerichteten Feldstärke und die dazu gehörige Permeabilität an der Plattenoberfläche

Werte im allgemeinen um zwei-drei Größenordnungen die H_z Werte, so können wir die Feldstärkekomponente H_x als maßgebend für μ_r annehmen.)

Die Beziehung zwischen der relativen Permeabilität (μ_r) und der Feldstärke (H_r) kann für die Versuchsplatte folgendermaßen beschrieben werden

$$\mu_r = 2|H| \qquad (H < 450 \text{ A/m})$$

und

$$\mu_r = 955(1{,}0014 - e^{-\frac{1075}{|H|}}). \qquad (H \geqq 450 \text{ A/m})$$

Aus diesen Beziehungen kann man für jede Feldstärke H_x eine relative Permeabilität μ_r bestimmen, so bekommt man die Kurve $\mu_r(x)$. Aus Bild 5 ist ersichtlich, daß man den in den Berechnungen benutzten Wert $\mu_r = 50$ als einen Mittelwert für die ganze Platte betrachten kann, die Schätzung war also richtig. In Berechnungen muß man immer aus einem auf Grund von Erfahrungen geschätzten Wert von μ_r ausgehen, und die Wahl durch den für den gegebenen Fall aufgezeichneten Verlauf von μ_r über x kontrollieren. Nimmt H_x ab, so kann μ_r bedeutend zunehmen; in einer anderen Berechnung erwies sich für $H_{x\,\max} = 6000$ A/m $\mu_r = 500$ als richtiger Wert.

Der Einfluß der Wahl der Größe von μ_r auf die berechneten Verlusten ist beträchtlich. So bekommt man für die Verluste der Platte von der Länge $2r$ für $\mu_r = 100$, $P = 1940\ w$, und für $\mu_r = 500$, $P = 624\ w$. Wird aber die Feldstärke weit von der Platte vorgeschrieben, ist also v_1 groß, so hat die Größe der Permeabilität eine geringe Bedeutung. Die für $\mu_r = 50$ berechneten Verluste bei einem Abstand von $v_1 = 0{,}5$ m unterscheiden sich von den für $\mu_r = 500$ berechneten Verlusten nur um 30%. Es soll bemerkt werden, daß man in exakten Berechnungen auch die Ortsabhängigkeit von μ_r berücksichtigen muß. In unserem Näherungsverfahren wird aber die Permeabilität als konstant angenommen.

3. Platten im Streufeld konzentrischer zylindrischer Spulen

Bild 6 zeigt das Modell des Streufeldes von zwei konzentrischen, zylindrischen Spulen mit Eisenkern. Neben den Spulen, parallel zu deren Achse liegt eine Metallplatte, in der das Streufeld Wirbelströme erzeugt. Ist die Verteilung der Radialkomponenten der Streuinduktion bzw. der Streufeldstärke längs der Oberfläche der äußeren Spule, also die nach Gl. (1) berechnete Feldstärke $H_{z0}(x, t)$ bekannt, so können die Wirbelstromverluste nach unserer Methode bestimmt werden. Es soll untersucht werden, wieweit die auf diese Weise, also auf Grund der an der Oberfläche der äußeren Spule verlaufenden radialen Feldstärkekomponente berechneten magnetischen und elektrischen Größen (Feldstärken, Stromdichten und Verluste) von den auf Grund der reellen Feldverteilung aus den Amperewindungen der Spulen berechneten Werten abweichen. Im weiteren werden die Ergebnisse der numerischen Berechnung als Referenzwerte berücksichtigt.

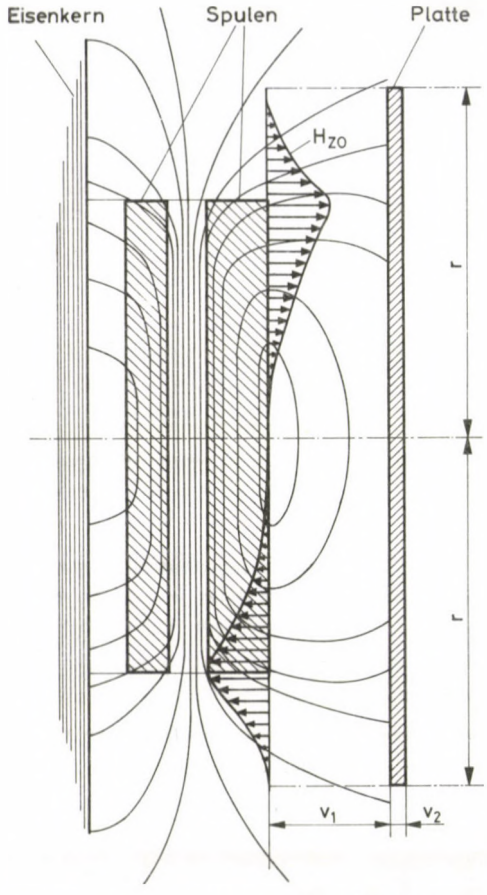

Bild 6. Platte im Magnetfeld von konzentrischen Wicklungen mit Eisenkern

Es ist zu erwarten, daß sich die berechneten Feldbilder sowohl an der Oberfläche als auch im Inneren der Platte wegen den verschiedenen Anfangsbedingungen der zwei Methoden unterscheiden werden. Gibt aber die analytische Methode ein richtiges qualitatives Bild, so können die auf diese Weise berechneten Verluste durch einen richtig gewählten Korrektionsfaktor einfach korrigiert werden.

Die Berechnung wurde für Aluminiumplatten ($\gamma = 33 \cdot 10^6$ S/m, $\mu = 1{,}256 \cdot 10^{-6}$ H/m) der Dicken 10 mm und 16 mm, und für eine ferromagnetische Platte ($= 7 \cdot 10^6$ S/m, $\mu = 100 \cdot 1{,}256 \cdot 10^{-6}$ H/m) der Dicke 10 mm nach der Anordnung des Bildes 6 mit beiden Methoden durchgeführt. Die Länge der Platten betrug 4,4 m ($2r = 4{,}4$ m). Der Abstand zwischen der Oberfläche der äußeren Wicklung und der Platte wurde von 0,1 m bis 0,5 m zu je 0,1 m verändert. Die numerische Berechnung wurde mit Hilfe eines früher ausgearbeiteten zweidimensionalen quasistationären Feldberechnungsverfahrens [10] durchgeführt.

Für das Programm wurden folgende Annahmen berücksichtigt:

a) Sowohl die magnetische Permeabilität als auch die spezifische Leitfähigkeit wurden als isotrope Materialeigenschaften (also von der Richtung unabhängig) angenommen. Diese Werte sind auch von den magnetischen und elektrischen Feldstärken unabhängig.

b) Der Verlauf aller elektrischen und magnetischen Größen ist zeitlich sinusförmig.

c) Da das Programm zweidimensionale Feldprobleme behandelt, besitzt der Strom in einem kartesischen Koordinatensystem nur eine Komponente. Die Ströme, die geometrische Anordnung und die Materialeigenschaften sind von dieser Koordinate unabhängig.

3.1. Die Rückwirkung der Wirbelströme auf die radiale Induktionsverteilung an der Spulenoberfläche

Werden keine Wirbelströme erzeugt (in einer Spulenanordnung ohne Platte), so verläuft die Radialkomponente der Feldstärke an der Oberfläche der Spule nach der Kurve a) des Bildes 7. Diese Verteilung wird durch die neben der Spule liegende ferromagnetische Platte im untersuchten Bereich (Plattenabstand von 0,1 m bis 0,5 m) praktisch nicht beeinflußt. Die Form des Verlaufes wird auch durch die Aluminiumplatte nur wenig verzerrt, seine Amplitude kann aber bedeutend reduziert werden. (Siehe die Kurve b) im Bild 7). (Unter Aluminiumplatte versteht man hier und im weiteren die Platte der Dicke 10 mm. Die für die Platte der Dicke 16 mm berechneten Größen unterscheiden sich qualitativ kaum von den für die Platte der Dicke 10 mm berechneten Werten.) Die Reduktion der Amplituden ist im Bild 8 sichtbar, wo das Verhältnis der an der Oberfläche der Spule verlaufenden maximalen Feldstärke (H_{max}) zur idealen (das ist ohne die Rückwirkung der in der Platte erzeugten Wirbelströme berechneten) maximalen Feldstärke ($H_{max\,i}$) über den Plattenabstand dargestellt wird. Aus den Verläufen der Feldstärkeverhältnisse ist zu erkennen, in welchem Maße die für die Konstanz der Ausgangsfeldstärke (H_z) im Punkt 2 aufgestellte Annahme erfüllt wird.

Das abweichende Verhalten der Aluminiumplatte und der ferromagnetischen Platte läßt sich durch den bedeutenden Unterschied der Permeabilitäten erklären. Die Wirbelströme wirken nämlich in beiden Fällen dem sie erzeugenden magnetischen Fluß entgegen, somit reduzieren sie die an der Oberfläche der Spule verlaufende radiale Feldstärke. Im Falle von ferromagnetischen Platten wird aber dieser Effekt dadurch kompensiert, daß das Material großer Permeabilität und kleines magnetischen Widerstandes den Fluß einsaugt.

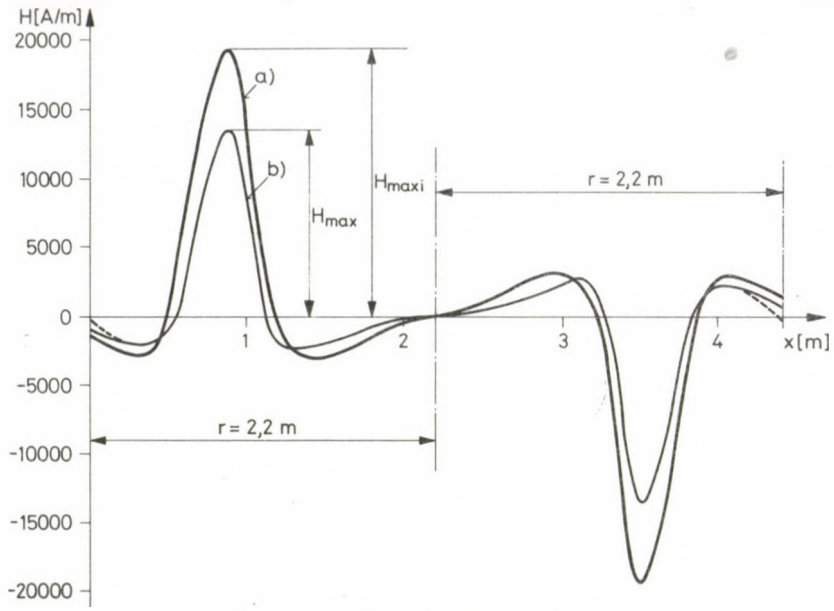

***Bild* 7.** Verlauf der Radialkomponente der Feldstärke an der Oberfläche der Spule a) ohne Platte (wirbelstromfrei) b) bei einer Aluminiumplatte (Abstand Spule-Platte 0,1 m)

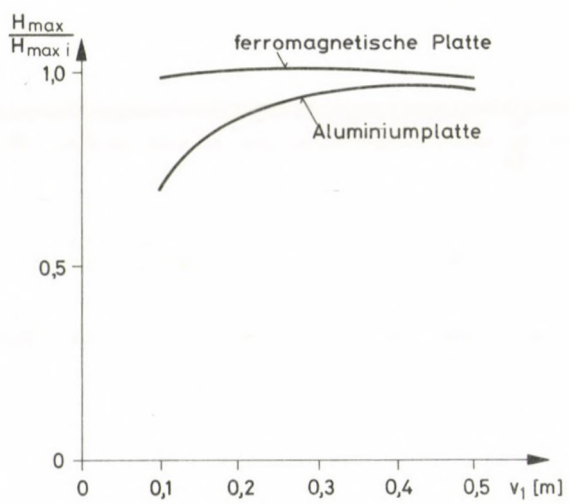

Bild 8. Verhältnis der maximalen Radialfeldstärke (H_{max}) zum Maximum der idealen (ohne Rückwirkung der Wirbelströme berechneten) Feldstärke ($H_{max\,i}$)

3.2. Senkrecht zur Platte gerichtete Feldstärken

Wird an der Oberfläche der Spule in beiden Berechnungen dieselbe radiale Feldstärkeverteilung angenommen, so gibt das analytische Verfahren an der Oberfläche der Platte größere Feldstärken, als die numerische Methode, die Verläufe sind aber fast gleichförmig. Dies wird in Bild 9 veranschaulicht, wo die Realteile (die mit der Ausgangsfeldstärke H_{z0} gleichphasigen Komponenten H_{zra} und H_{zrn}) und die Imaginärteile (die zur Ausgangsfeldstärke H_{z0} um 90° phasenverschobene Komponenten H_{zia} und H_{zin}) der an der Oberfläche der von der Spule 0,3 m weit liegenden Platte verlaufenden Feldstärken dargestellt sind. Hier und im weiteren werden die analytisch berechneten Größen mit Index *a*, die numerisch berechneten Größen mit Index *n* bezeichnet. In der Mitte der Platte ergeben beide Verfahren ganz gleiche Ergebnisse, ein bedeutender Unterschied zwischen den Verläufen kann nur an den Rändern der Platte beobachtet werden. In Bild 10 wurde die Verteilung der Feldstärkekomponenten im Innern der Platte an der Stelle $x = 0{,}9$ m, wo die Feldstärken nach Bild 9 am größten sind, dargestellt. Man kann sehen, daß die entsprechenden Verläufe voneinander kaum abweichen.

Bild 11 zeigt das Verhältnis der Realteile der analytisch und numerisch berechneten maximalen Feldstärken über dem Abstand Spule — Platte.

Als eine Zusammenfassung der Vorgeführten kann man feststellen, daß die Annahme für die Formtreue der Feldstärkeharmonischen (Annahme *b*) in Punkt 1) qualitativ richtige Feldstärkeverläufe ergibt, aber auch die Größen der analytisch berechneten Feldstärken unterscheiden sich nur wenig von den nach dem richtigen Feldbild numerisch berechneten Werten.

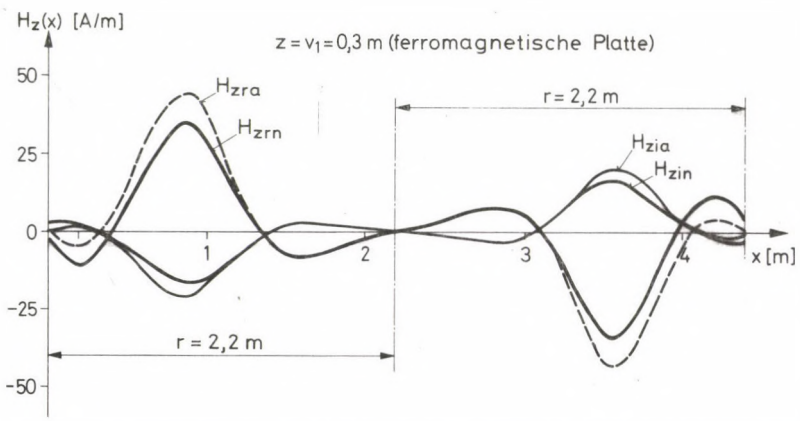

Bild 9. Die analytisch (Index a) und numerisch (Index n) berechneten Realteile (Index r) und Imaginärteile (Index i) der senkrecht zur Platte gerichteten Feldstärke an der Oberfläche der ferromagnetischen Platte ($v_1 = 0{,}3$ m)

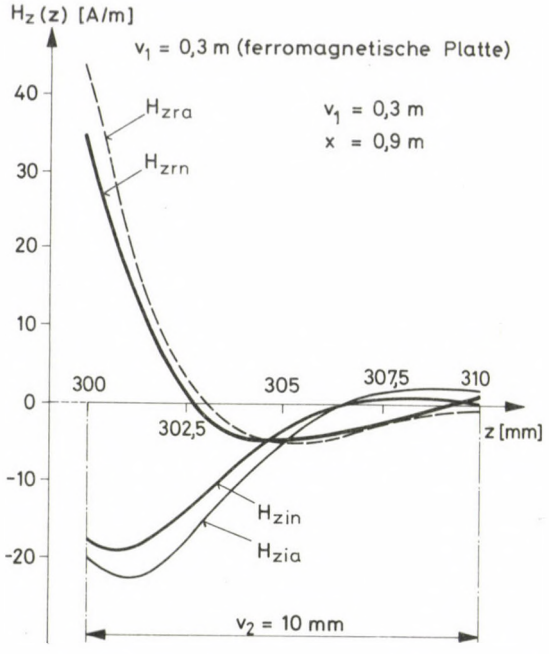

Bild 10. Verlauf der senkrecht zur Platte gerichteten Feldstärkekomponenten im Inneren der Platte längs der z-Achse. (Die Bezeichnung der Indexe siehe im Bild 9)

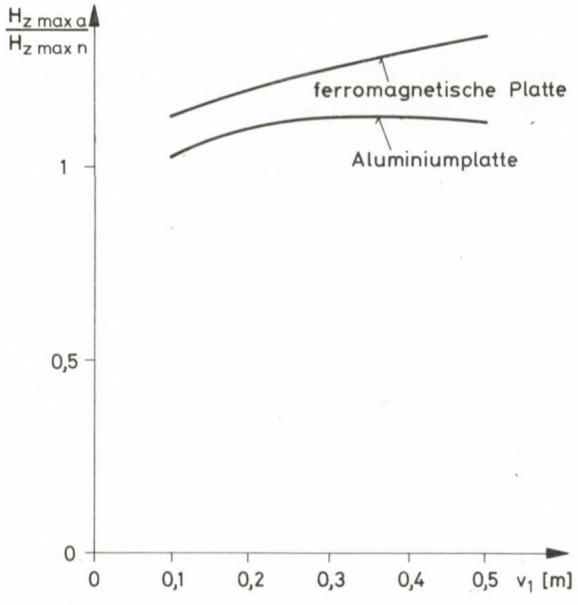

Bild 11. Verhältnis der analytisch und numerisch berechneten maximalen Radialfeldstärken an der Oberfläche der Platte

3.3. Parallel zur Platte gerichtete Feldstärken

Die Verläufe der parallel zur Platte gerichteten Feldstärken H_x an der Plattenoberfläche werden beispielsweise für den Fall einer im Abstand von 0,5 m liegenden ferromagnetischen Platte dargestellt. Man kann sehen, daß sowohl die Realteile (H_{xra}, H_{xrn}) als auch die Imaginärteile der Feldstärken bei dem Maximum von H_z das Vorzeichen umkehren. Die nach den zwei verschiedenen Verfahren berechneten Feldstärkeverteilungen sind im Mittelteil der Platte ähnlichen Verlaufes, der Charakter der Verläufe ist nur an den Rändern verschieden. Das analytisch berechnete Maximum des Realteiles ist in dem untersuchten Bereich, also zwischen den Plattenabständen 0,1 m und 0,5 m, im Mittelteil für die Aluminiumplatte 1,04—1,26-mal größer, und für die ferromagnetische Platte 1,34—1,48-mal größer als die numerisch für dieselbe Stelle bestimmten Maxima. Für die Maxima an den Rändern ergab sich im Falle der Aluminiumplatte ein Verhältnis von 1,31—1,64, und im Falle der ferromagnetischen Platte ein solches von 2,06—3,46. Der Unterschied zwischen den nach den verschiedenen Verfahren berechneten Imaginärteilen ist noch größer, die Komponenten sind aber viel kleiner als die realen Komponenten, wie dies in Bild 12 ersichtlich ist.

Die Verläufe der Komponenten H_x im Inneren der Platte (die Funktion $H_x(z)$ längs der z-Achse) werden für die Maximumstelle nach Bild 12 in Bild 13 dargestellt. Man kann sehen, daß der Unterschied zwischen den nach den verschiedenen

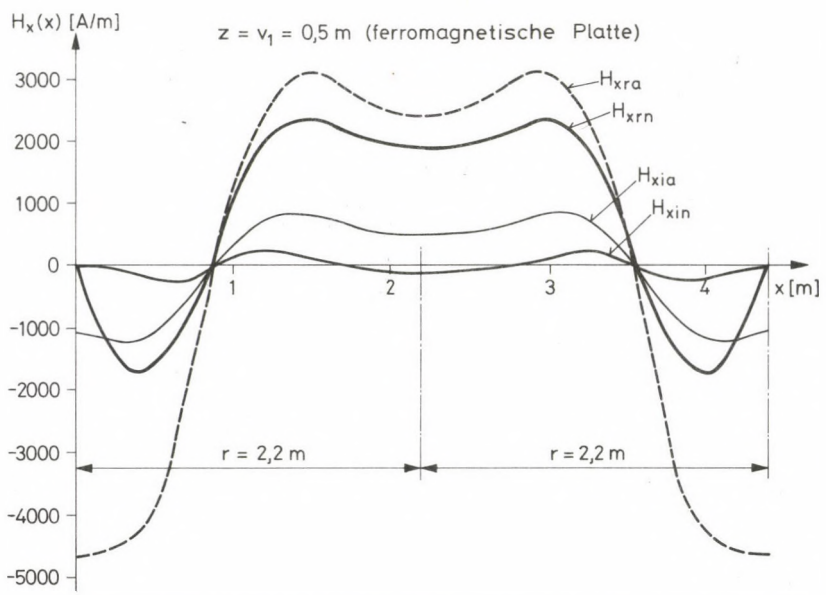

Bild 12. Verlauf der parallel zur Platte gerichteten Feldstärken and der Oberfläche der ferromagnetischen Platte ($v_1 = 0{,}5$ m). (Die Bezeichnung der Indexe siehe in Bild 9.)

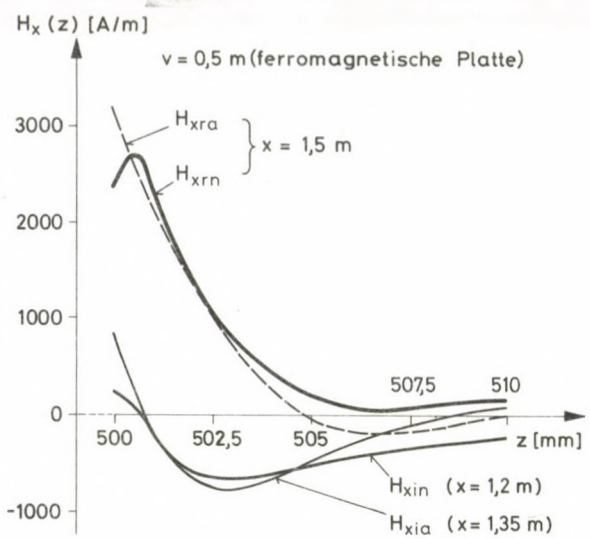

Bild 13. Verlauf der parallel zur Platte gerichteten Feldstärkekomponenten im Inneren der Platte längs der z-Achse. (Die Bezeichnung der Indexe siehe in Bild 9.)

Methoden berechneten Feldstärkekomponenten im Inneren der Platte viel kleiner ist, als an der Oberfläche.

Das analytische Verfahren gibt also ein richtiges qualitatives Bild auch für die Verteilung der Feldstärkekomponenten H_x im Mittelteil der Platte, an den Rändern ist der Unterschied zwischen den analytisch berechneten H_{xra} und H_{xia}, und den numerisch berechneten H_{xrn} und H_{xin} sowohl qualitativ als auch quantitativ groß. Diese Erscheinung kann hauptsächlich dadurch begründet werden, daß die Berechnung nach dem analytischen Verfahren für eine $2r$ lange Strecke einer in der x-Richtung unendlich langen Platte, nach dem numerischen Verfahren aber für eine Platte endlicher Länge von $2r$ durchgeführt wird.

3.4. Stromdichten

Der Verlauf der Stromdichten ist ähnlich dem Verlauf der parallel zur Platte gerichteten Feldstärkekomponenten H_x, die Kurven $i(x)$ und $H_x(x)$ sind also gleichen Charakters. Die nach den beiden Methoden berechneten Realteile und Imaginärteile der Stromdichten sind für den oben betrachteten Fall einer im Abstand 0,5 m liegenden ferromagnetischen Platte in Bild 14 dargestellt. Unter den analytisch und numerisch berechneten Stromdichten kann man einen kleineren Unterschied beobachten als unter den parallel zur Platte verlaufenden Feldstärken. Der Verlauf der im Mittelteil der Platte an der Maximumstelle auftretenden Stromdichten ist längs der z-Achse in Bild 15 dargestellt. Die nach den zwei verschiedenen Methoden berechneten Verläufe unterscheiden sich nur geringfügig.

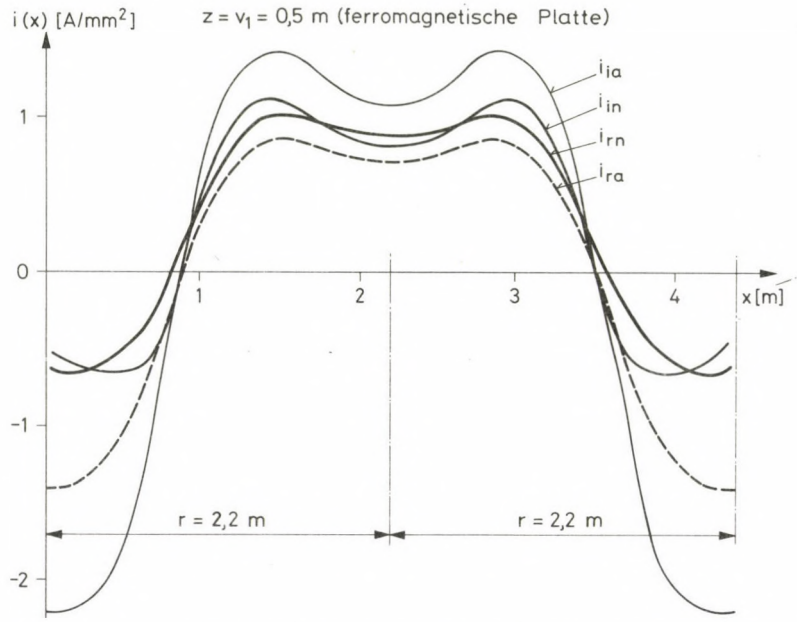

Bild 14. **Verlauf der Komponenten der Wirbelstromdichte an der Oberfläche der ferromagnetischen Platte** ($v_1 = 0{,}5$ m). **(Die Bezeichnung der Indexe siehe in Bild 9.)**

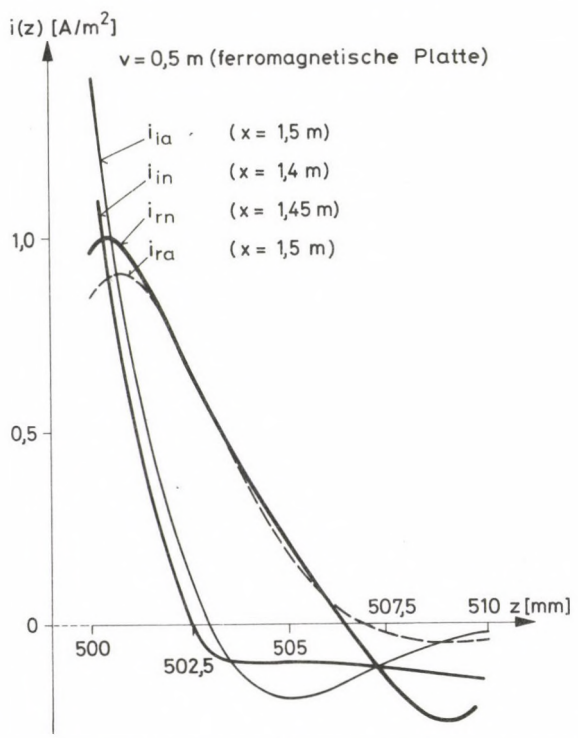

Bild. 15. **Verlauf der Stromdichtekomponenten im Inneren der Platte längs der** z**-Achse. (Die Bezeichnung der Indexe siehe in Bild 9.)**

3.5. Verluste

Die Verluste sind proportional zum Quadrat des Absolutwertes der Stromdichte, so besitzen die Verläufe der Verlustverteilung eine Nullstelle und zwei Maxima längs einer Halbplatte. Die nach den zwei Methoden berechneten Verlustverteilungen sind beispielsweise für eine im Abstand $v_1 = 0{,}3$ m und $v_1 = 0{,}5$ m liegende ferromagnetische Platte in den Bildern 16.a und 16.b dargestellt. Die analytisch berechneten Verluste P_a sind viel größer als die numerisch berechneten Werte, wie dies aus den bisher ausgeführten Feststellungen zu erwarten war. Auf Grund des Bildes können die Verluste abhängig von ihrem Entstehungsort in zwei Teilverluste aufgeteilt werden: die Verluste P_{ba} und P_{bn} werden im Mittelteil der Platte (das heißt im Plattengebiet gegenüber der Spule), die Verluste P_{ka} und P_{kn} in den Randgebieten (das heißt in den sich über die Spulen ausbreitenden Plattenteilen) erzeugt. Das Verhältnis der nach beiden Methoden berechneten Verluste und Verlustteile wird über den Plattenabstand für eine ferromagnetische Platte in Bild 17 dargestellt. (Für eine Aluminiumplatte ergab sich ein viel kleineres Verhältnis.) Man kann sehen, daß das Verhältnis P_{ba}/P_{bn} für die Verluste des Mittelteiles im untersuchten Bereich viel kleiner ist, als das für die Verluste der Randgebiete sich ergebende Verhältnis P_{ka}/P_{kn}. Außerdem nimmt das ersterwähnte Verhältnis in Abhängigkeit der Plattendicke sich aber nur wenig. Diese Beobachtung gibt uns die Möglichkeit, die durch die Randeffekte verursachten

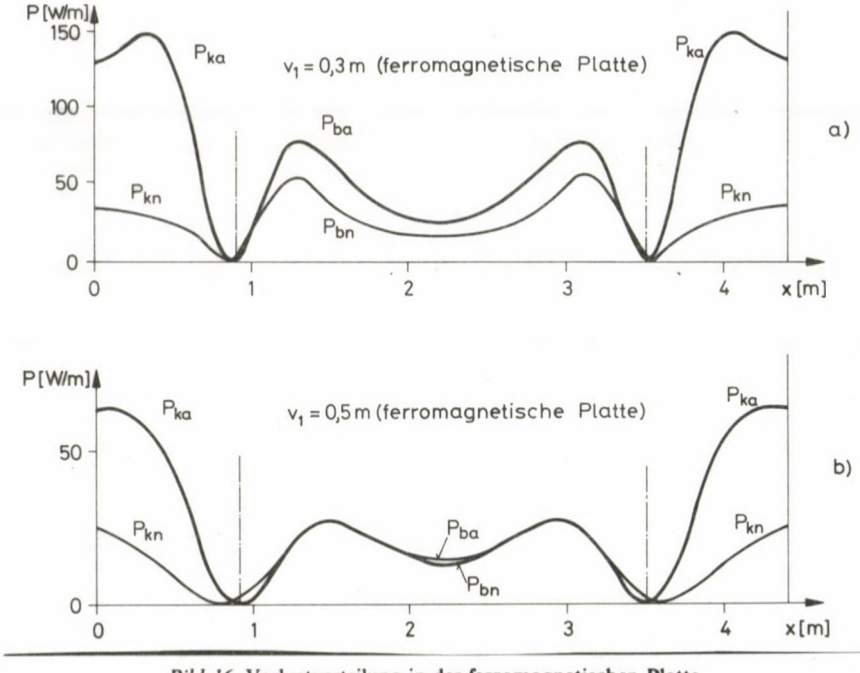

Bild 16. Verlustverteilung in der ferromagnetischen Platte

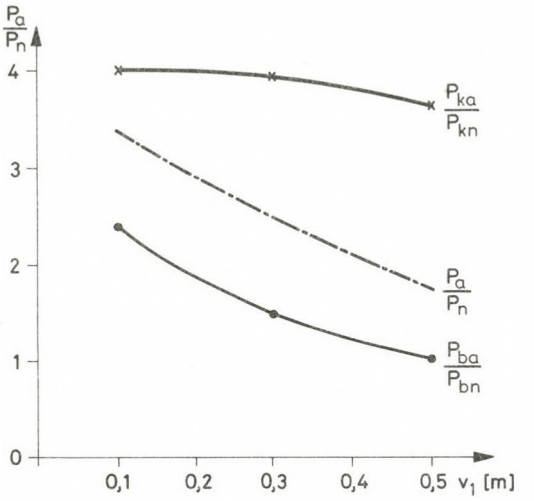

Bild 17. Verhältnis der analytisch und numerisch berechneten Verluste und Verlustteile der ferromagnetischen Platte

Fehler mit Hilfe von zwei Korrektionsfaktoren zu eliminieren, und zwar mit einem für den Mittelteil gültigen Faktor k_b und mit einem für die Randgebiete gültigen Faktor k_k. Auf diese Weise können die Ergebnisse des analytischen Verfahrens auch für solche Platten verwendet werden, deren Abmessungen und Feldverteilung von denselben Daten der behandelten Platte abweichen. Die reellen Verluste können in diesem Falle nach der Beziehung

$$P_v = k_b P_{ba} + k_k P_{ka}$$

berechnet werden. Die Korrektionsfaktoren ergeben sich als Reziprokwerte der in Bild 17 engegebenen Verlustverhältnisse.

Als ein Beispiel für die Verwendung des analytischen Verfahrens soll die Berechnung der *im Kessel von Transformatoren hervorgerufenen Verluste* erwähnt werden (siehe Bild 18). In diesem Falle werden die im parallel zu den Wicklungen liegenden Teil der Kesselwand hervorgerufenen Verluste berechnet. Dieses Wandgebiet wird entsprechend den oben angeführten Feststellungen in zwei Gebiete aufgeteilt in den gegenüber den Wicklungen sich befindlichen Wandteil, und in die sich über die Wicklungen ausbreitenden Wandteile. Die Korrektionsfaktoren ergaben sich aus für die gewöhnlichen Anordnungen von Hochleistungstransformatoren der Spannung 220 kV und 400 kV durchgeführten numerischen Berechnungen. Nach den Ergebnissen dieser Berechnungen müssen die analytisch berechneten Werte des Mittelteiles mit einem vom Abstand Wicklung-Kesselwand abhängigen Faktor k_b multipliziert werden, der für die im Bau von Großtransformatoren üblichen Abstände von 250 mm—350 mm die Werte 0,6—0,7 beträgt. Der Korrektionsfaktor für die äußeren

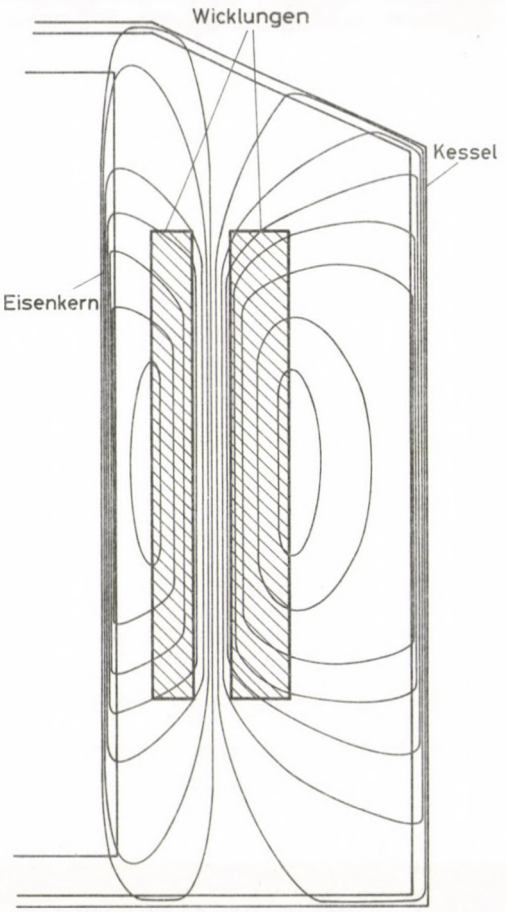

Bild 18. Modell zur Berechnung der Verluste im Kessel von Transformatoren

(nicht gegenüber den Wicklungen liegenden) Kesselwandteile ergab sich zu $k_k = 0{,}65$. (Die in den Randgebieten erzeugten Verluste müssen hier in geringerem Maße korrigiert werden als bei den Platten, da hier die Randeffekte wegen der Kesseldecke und des Kesselbodens kleiner sind.)

Beispiel: Nach dem vorgeführten analytischen Verfahren wurden die Verluste in der Kesselwand eines dreiphasigen Transformators der Spannung 400 kV und der Leistung 270 MVA für $p_b = 18\,250$ W und $P_k = 24\,400$ W berechnet. Mit den oben angegebenen Korrektionsfaktoren ergeben sich die im Kessel durch den Streufluß hervorgerufenen Verluste zu

$$P_{ea} = 0{,}7 \cdot 18\,250 + 0{,}65 \cdot 24\,400 = 28\,635 \text{ W}.$$

Für die Anordnung des Bildes 18 bekommt man nach dem numerischen Verfahren die Verluste

$$P_{en} = 29\,250 \text{ W}.$$

4. Schlußfolgerungen

Eine exakte rechnerische Behandlung der in den Konstruktionsteilen von elektrischen Maschinen durch den Streufluß hervorgerufenen Wirbelstromverluste ist prinzipiell nur mit Hilfe von numerischen Verfahren möglich. Die Verluste in Metallteilen einfacher Form z. B. in Platten können aber *näherungsweise* auch analytisch berechnet werden. Die analytische Berechnung kann leichter und schneller durchgeführt werden, und auf Grund der erhaltenen Formeln kann der Einfluß der einzelnen Parameter beurteilt werden. Die analytischen Verfahren sind besonders in der Konstruktionsarbeit nützlich, wenn man mehrere Varianten miteinander schnell vergleichen muß. Die analytischen Verfahren besitzen aber noch einen Vorteil, den man nicht vernachlässigen darf: die Ergebnisse der Berechnung können leicht kontrolliert werden, auf diese Weise kann man dieses Verfahren auch zur Kontrolle der komplizierten, schwer übersehbaren numerischen Methoden benützen.

Das im Aufsatz dargestellte Berechnungsverfahren geht von den für quasistationäre Felder gültigen Maxwellschen Gleichungen aus, und nach der Einführung mehreren Näherungen gibt es eine einfache Formel zur Berechnung der in rechteckigen Platten erzeugten Verluste. In der Berechnung werden sowohl die endliche Dicke der Platte, als auch der Einfluß der sich neben der Platte befindlichen und parallel zur Platte liegenden wirbelstromfreien Schichten (Luft, Öl) berücksichtigt. Die Wirbelstromverluste sind zu einer im Aufsatz definierten *equivalenten Dicke* der Platte proportional.

Das Verfahren kann auch für die Berechnung der Wirbelstromverluste von im Streufeld konzentrischer Wicklungen liegenden Platten, z. B. von Transformatorkesseln benützt werden. Das analytische Verfahren wurde anhand eines Beispiels mit der numerischen Methode verglichen und es wurden die an der Oberfläche und im Inneren der Platte sich herausbildenden Feldstärke-, Stromdichte- und Verlustverteilungen untersucht.

Danksagung

Der Verfasser dankt hiermit Herrn László Szabó, Forschungsingenieur der Ganz Elektrotechnischen Werke, für die Durchführung der numerischen Berechnungen.

SCHRIFTTUM

1. Carpenter, C. J.—Djurović, M.: Three-dimensional Numerical Solution of Eddy Currents in Thin Plates. *Proc. IEE*, **122** (1975) 681—688
2. Weiland, Th.: Ein Verfahren zur Berechnung von Wirbelströmen in massiven, dreidimensionalen, beliebig geformten Eisenköpern. *ETZ Archiv*, (1979) H. **9**, 263—267
3. Carpenter, C. J.—Sharpless, K. O.—Djurović, M.: Heating in Transformer Cores due to Radial Leakage Flux. Part 2: Computed results. *Proc. IEE*, **124** (1977), 1181—1186
4. Stoll, R. L.: Approximate Formula for the Eddy-Current Loss Induced in a Long Conductor of Rectangular Cross-Section by a Transverse Magnetic Field. *Proc. IEE*, **116** (1969) 1003—1008

5. KERÉNYI D.: Approximate Formula for the Eddy Current Losses Induced in Rectangular Metal Blocks by Magnetic Field. *Ganz Electric Review*, No 16. (1977), 13—22
6. AGARWAL, Paul, D.: Eddy-Current Losses in Solid and Laminated Iron. *Transactions AIEE* **78** (1959), Part II, 169—179
7. DE MEY, G.: A Method for Calculating Eddy Currents in Plates of Arbitrary Geometry. *Archiv für Elektrotechnik* **56** (1974), 137—140
8. KARSAI K.—KERTÉSZ V.: Untersuchung der durch den Streufluß von Transformatoren hervorgerufenen Zusatzverluste. 3. Teil. *VEIKI Bericht*, No. VBF 317. 1975 (ungarisch)
9. KARSAI K.—KERÉNYI D.—KERTÉSZ V.: Verluste und Erwärmungen im radialen Streufeld von Transformatoren. *Elektrotechnika* **70** (1977), 237—246 (ungarisch)
10. MÁRKON S.—SZABÓ L.: Quasi-Stationary Magnetic Field Computing Program and its Application in Special Calculation of Electrical Machines. *Ganz Electric Review*, No **16** (1977), 35—46

Analytic Method for the Approximate Calculation of the Eddy-Current Loss of a Metal Plate Placed into a Magnetic Field. — To the approximate calculation of the eddycurrent loss of a metal plate put into a magnetic field an analytic method is presented which takes into account also the finite thickness of the plate and the effect exerted by the layer which is free of eddy current (air, oil) near the plate. Starting from Maxwell's equations but by using several approximate assumptions a simple formula is yielded to the determination of the eddy-current loss from which the role of the factors affecting the phenomenon may clearly be seen. The method may be used to calculate the loss of a plate, for example, a transformer tank, placed into a magnetic field of concentric coils.

Acta Technica Academiae Scientiarum Hungaricae, 93 (1—2), pp. 101—114 (1981).

ON THE PRIMAL VARIATIONAL PRINCIPLES IN LINEAR ELASTODYNAMICS

I. KUTI*

[Manuscript received June 10, 1981]

A general variational principle is developed for the primal mixed boundary problems of the linear elastodynamics. The employed scalar product is the convolution bilinear form and this circumstance makes a possibility to contain the initial conditions of the mixed boundary problems explicitly by the variational principles.

1. Introduction

It can be easily seen that the classical bilinear forms of the type

$$[u_1, u_2] = \int_{\Omega} \int_{0}^{t_0} u_1(\mathbf{x}, t)\, u_2(\mathbf{x}, t)\, \mathrm{d}\mathbf{x}\mathrm{d}t \tag{1.1}$$

which are widely spread to derive variational principles are not symmetrical for the expression $[\partial u/\partial t, u]$. (Here Ω is a bounded open region in the 3 dimensional Euclidean space and $0 \leq t \leq t_0$ is a closed time interval.) Therefore the operators including the term $\partial/\partial t$ are not directly potential types. Similarly it can be seen that the convolution bilinear form:

$$\langle u_1, u_2 \rangle = \int_{\Omega} \int_{0}^{t_0} u_1(\mathbf{x}, t)\, u_2(\mathbf{x}, t_0 - t)\mathrm{d}\mathbf{x}\mathrm{d}t \tag{1.2}$$

is symmetrical for the expression $\langle \partial u/\partial t, u \rangle$.

Thus the term $\partial \cdot /\partial t$ may be applied to develop operators of potential types. First GURTIN [1, 2, 3] introduced the convolution bilinear form to construct variational principles for linear initial value problems which include the initial conditions in implicit way. TONTI [4] pointed out that the $\langle \partial u/\partial t, u \rangle$ scalar product is symmetrical and presented a variational principle for the heat conduction equation. After this time ODEN and REDDY [5] and REDDY [6, 7] presented variational principles with scalar product (1.2) including the initial conditions in explicit form with respect to linear elastodynamics.

In present paper a general mixed variational principle is developed for the primal mixed boundary value problems in linear elastodynamics. The employed mathemat-

* Dr. I. KUTI, József Attila utca 22, H-1212, Budapest, Hungary

ical procedure corresponds to the abstract mathematical procedure presented in [3] (pp. 82—92).*

Finally we derive some variational functionals from the elaborated functional by different constraints (the Reissner type, the total potential energy and the complementary energy functionals).

2. The canonical equations of the primal problem

Symbols and definitions

$\mathbf{x}=(x_1, x_2, x_3)$	is a point in a rectangular Cartesian frame of the 3 dimensional Euclidean space,
$t \in [0, t_0]$	t is a point of the closed time interval $0 \leqq t \leqq t_0$,
R	is a bounded open region in the 3 dimensional Euclidean space,
$\bar{\mathrm{R}}$	is the closure of R,
B	is the boundary of R and $\bar{\mathrm{R}}$ regions,
$\mathbf{n}(\mathbf{x})=(n_1(\mathbf{x}),$ $n_2(\mathbf{x}),\ n_3(\mathbf{x}))^T$:	is the normal vector of external surface with unit length in any point $\mathbf{x} \in \mathrm{B}$.

An arbitrary point $\mathbf{x} \in \mathrm{B}$(or $[\mathbf{x}, t] \in \mathrm{B} \times [0, t_0]$) is regular if $\mathbf{n}(\mathbf{x})$ is continuous at $\mathbf{x}$ (or $(\mathbf{x}, t)$). Open subregion $\mathrm{B}_\alpha \subset \mathrm{B}$ is regular if every point $\mathbf{x} \in \mathrm{B}_\alpha$ are regular. Subregions $\mathrm{B}_u \subset \mathrm{B}$ and $\mathrm{B}_\sigma \subset \mathrm{B}$ have the next properties: $\mathrm{B}_u \cap \mathrm{B}_\sigma = \Phi$ $\mathrm{B}_u \cup \mathrm{B}_\sigma = \mathrm{B}$ and they are constructed by finite union of regular subregions, where *Φ is the empty set.*

A function $\mathbf{g}(\mathbf{x}, t)=(g_1(\mathbf{x}, t),\ g_2(\mathbf{x}, t),\ g_3(\mathbf{x}, t))^T$ is piecewise regular on the subregion $\mathrm{B}_u \times [0, t_0]$ ($\mathrm{B}_\sigma \times [0, t_0]$) if $\mathbf{g}(\mathbf{x}, t)$ is continuous on all regular subregions of $\mathrm{B}_u \times [0, t_0]$, ($\mathrm{B}_\sigma \times [0, t_0]$) so that every regular points $\mathbf{x}$ in $\mathrm{B}_u(\mathrm{B}_\sigma)$ are continuity points of function $\mathbf{g}(\mathbf{x}, t)$ at the same time.**

Let

$$\mathbf{u}(\mathbf{x}, t)=(u_1(\mathbf{x}, t),\ u_2(\mathbf{x}, t),\ u_3(\mathbf{x}, t))^T \in \mathrm{C}^{1,1}\bar{\mathrm{R}} \times [0, t_0]),$$

$$\mathbf{v}(\mathbf{x}, t)=(v_1(\mathbf{x}, t),\ v_2(\mathbf{x}, t),\ v_3(\mathbf{x}, t))^T \in \mathrm{C}^{0,0}(\bar{\mathrm{R}} \times [0, t_0]),$$

$$\mathbf{p}(\mathbf{x}, t)=(p_1(\mathbf{x}, t),\ p_2(\mathbf{x}, t),\ p_3(\mathbf{x}, t))^T \in \mathrm{C}^{0,1}(\bar{\mathrm{R}} \times [0, t_0]),$$

$$\mathbf{e}(\mathbf{x}, t)=\{e_{ij}(\mathbf{x}, t)\}_{ij=1,2,3} \in \mathrm{C}^{0,0}(\bar{\mathrm{R}} \times [0, t_0]),$$

$$\boldsymbol{\sigma}(\mathbf{x}, t)=\{\sigma_{ij}(\mathbf{x}, t)\}_{ij=1,2,3} \in \mathrm{C}^{1,0}(\bar{\mathrm{R}} \times [0, t_0])$$

* It is important to mention that ODEN and REDDY [5] also presented similar functional with scalar product (1.1), but it didn't contain the initial conditions.

** The prescriptions of the previous conditions follow the prescriptions of paper [2].

be the displacement, velocity, the momentum density vectors and the strain and stress tensors subsequently.

$$\mathbf{e}(\mathbf{x}, t) \quad \text{and} \quad \boldsymbol{\sigma}(\mathbf{x}, t)$$

are symmetrical tensors that is

$$e_{ij}(\mathbf{x}, t) = e_{ji}(\mathbf{x}, t), \quad \sigma_{ij}(\mathbf{x}, t) = \sigma_{ji}(\mathbf{x}, t), \quad i, j = 1, ,2, 3$$

on $\bar{\mathrm{R}} \times [0, t_0]$.

Let

$$\mathbf{E}(\mathbf{x}) = \{E_{ijkl}(\mathbf{x})\} \quad \text{and} \quad \mathbf{C}(\mathbf{x}) = \{C_{ijkl}(\mathbf{x})\}, \qquad i, j, k, l = 1, 2, 3$$

denote the rigidity and inverse rigidity tensors. The $\mathbf{E}(\mathbf{x})$ and $\mathbf{C}(\mathbf{x})$ are symmetrical tensors, that is.

$$E_{ijkl} = E_{jikl} = E_{klij}, \qquad i, j, k, l = 1, 2, 3 \tag{2.1}$$

and

$$C_{ijkl} = C_{jikl} = C_{klij}, \qquad i, j, k, l = 1, 2, 3 \tag{2.2}$$

Let the function $\rho = \rho(\mathbf{x}) \in \mathrm{C}^1(\bar{\mathrm{R}})$ denote the mass density. $\mathrm{C}^{i,j}(\mathrm{R} \times [0, t_0])$ is the space of functions, which are continuously differentiable i-times according to $\mathbf{x}$ and j-times according to t on region $\mathrm{R} \times [0, t_0]$.

The $\mathrm{C}^i(\bar{\mathrm{R}})$ is the space of functions which are continuously differentiable i-times according to $\mathbf{x}$ on region $\bar{\mathrm{R}}$.*

With the previous symbols the canonical equations of the primal mixed boundary value problem has the form:

$$\frac{1}{2}(\nabla \mathbf{u}(\mathbf{x}, t) + (\nabla \mathbf{u}(\mathbf{x}, t))^T) = \mathbf{e}(\mathbf{x}, t), \qquad (\mathbf{x}, t) \in \mathrm{R} \times [0, t_0], \tag{2.3}$$

$$\frac{\partial \mathbf{u}(\mathbf{x}, t)}{\partial t} = \mathbf{v}(\mathbf{x}, t), \qquad (\mathbf{x}, t) \in \mathrm{R} \times [0, t_0], \tag{2.4}$$

$$\mathbf{E}(\mathbf{x}) : \mathbf{e}(\mathbf{x}, t) = \boldsymbol{\sigma}(\mathbf{x}, t),^{**} \qquad (\mathbf{x}, t) \in \bar{\mathrm{R}} \times [0, t_0], \tag{2.5}$$

$$\rho(\mathbf{x})\mathbf{v}(\mathbf{x}, t) = \mathbf{p}(\mathbf{x}, t), \qquad (\mathbf{x}, t) \in \mathrm{R} \times [0, t_0], \tag{2.6}$$

$$\frac{\partial \mathbf{p}(\mathbf{x}, t)}{\partial t} - \operatorname{div} \boldsymbol{\sigma}(\mathbf{x}, t) - f(\mathbf{x}, t) = 0, \qquad (\mathbf{x}, t) \in \mathrm{R} \times [0, t_0], \tag{2.7}$$

$$\mathbf{T}(\mathbf{x}, t) = \hat{\mathbf{T}}(\mathbf{x}, t), \qquad (\mathbf{x}, t) \in \mathrm{B}_\sigma \times [0, t_0], \tag{2.8}$$

* Other symbols employed in this paper are usually employed in mathematics and mechanics.

** The: denotes the double scalar product between two matrix.

$$\mathbf{u}(\mathbf{x}, t) = \hat{\mathbf{u}}(\mathbf{x}, t), \qquad (\mathbf{x}, t) \in B_u \times [0, t_0], \tag{2.9}$$

$$\mathbf{p}(\mathbf{x}, 0) = \mathbf{p}^0(\mathbf{x}), \qquad \mathbf{x} \in \bar{R}, \tag{2.10}$$

$$\mathbf{u}(\mathbf{x}, 0) = \mathbf{u}^0(\mathbf{x}), \qquad \mathbf{x} \in \bar{R}, \tag{2.11}$$

where:

$\nabla \mathbf{u}(\mathbf{x}, t) = \operatorname{grad} \mathbf{u}(\mathbf{x}, t)$,
$\mathbf{T}(\mathbf{x}, t) = \boldsymbol{\sigma}(\mathbf{x}, t)\, \mathbf{n}(\mathbf{x})$ is the surface stress on $B \times [0, t_0]$,
$\hat{\mathbf{T}}(\mathbf{x}, t)$ is the prescribed external surface traction on
$B_\sigma \times [0, t_0]$ and it is regular on subregions of $B_\sigma \times [0, t_0]$,
$\hat{\mathbf{u}}(\mathbf{x}, t)$ is the prescribed displacement on
$B_u \times [0, t_0]$ and it is continuous on $B_u \times [0, t_0]$,
$\mathbf{u}^0(\mathbf{x})$ and $\mathbf{p}^0(\mathbf{x})$ are the prescribed initial displacement and momentum density vectors on $\bar{R}$ at $t = 0$ time point and they are continuous on $\bar{R}$.

3. Construction of the variational principle

We first define some spaces of the square integrable functions and mappings among these spaces of functions in correspondence with mixed boundary value problem (2.3)—(2.11). Let H_u, G_e, G_v, H'_u, G'_e, G'_v moreover H_B, G_B, H'_B, G'_B and H_0, G_0, H'_0, G'_0 denote the Hilbert spaces of functions beeing square-integrable on regions $R \times [0, t_0]$, $B \times [0, t_0]$ and on R at the time points $t = 0$, $t = t_0$. So we can construct the product spaces H, G, H′, G′ with elements **U**, **V**, **U**′, **V**′.

$$H = H_u \times H_B \times H_0, \qquad \mathbf{U} = (\mathbf{u}, \mathbf{u}_B, \mathbf{u}_0) \in H,$$

$$G = G_e \times G_v \times G_B \times G_0, \qquad \mathbf{V} = (\mathbf{e}, \mathbf{v}, \mathbf{g}_B, \mathbf{g}_0) \in G,$$

$$H' = H'_u \times H'_B \times H'_0, \qquad \mathbf{U}' = (\mathbf{h}', \mathbf{h}'_B, \mathbf{h}'_0) \in H',$$

$$G' = G'_e \times G'_v \times G'_B \times G'_0, \qquad \mathbf{V}' = (\boldsymbol{\sigma}, \mathbf{p}, \mathbf{T}, \mathbf{p}_0) \in G'.$$

The concrete forms of the Hilbert spaces are defined by equalities:

$$H_u = \{\mathbf{u}(\mathbf{x}, t) : \mathbf{u}(\mathbf{x}, t) \in C^{1,1}(\bar{R} \times [0, t_0])\}, \tag{3.1a}$$

$$H_B = \{\mathbf{u}_B(\mathbf{x}, t) : \mathbf{u}_B(\mathbf{x}, t) = \gamma_B \mathbf{u}(\mathbf{x}, t), \mathbf{u}(\mathbf{x}, t) \in H_u\}, \tag{3.1b}$$

$$H_0 = \{\mathbf{u}_0(\mathbf{x}, t) : \mathbf{u}_0(\mathbf{x}, t) = \gamma_0 \mathbf{u}(\mathbf{x}, t), \mathbf{u}(\mathbf{x}, t) \in H_u\}, \tag{3.1c}$$

$$G_e = \{\mathbf{e}(\mathbf{x}, t) : \mathbf{e}(\mathbf{x}, t) \in C^{0,0}(\bar{R} \times [0, t_0])\}, \tag{3.1d}$$

$$G_v = \{\mathbf{v}(\mathbf{x}, t) : \mathbf{v}(\mathbf{x}, t) \in C^{0,0}(\bar{R} \times [0, t_0])\}, \tag{3.1e}$$

$$G'_e = \{\boldsymbol{\sigma}(\mathbf{x}, t) : \boldsymbol{\sigma}(\mathbf{x}, t) \in C^{1,0}(\bar{R} \times [0, t_0])\}, \tag{3.1f}$$

$$G'_v = \{\mathbf{p}(\mathbf{x}, t) : \mathbf{p}(\mathbf{x}, t) \in C^{0,1}(\bar{R} \times [0, t_0])\}, \tag{3.1g}$$

$$G'_B = \{\mathbf{T}(\mathbf{x}, t) : \mathbf{T}(\mathbf{x}, t) = \delta_B \boldsymbol{\sigma}(\mathbf{x}, t), \boldsymbol{\sigma}(\mathbf{x}, t) \in G'_e\}, \tag{3.1h}$$

$$G'_0 = \{\mathbf{p}_0(\mathbf{x}, t) : \mathbf{p}_0(\mathbf{x}, t) = \delta_0 \mathbf{p}(\mathbf{x}, t), \mathbf{p}(\mathbf{x}, t) \in G'_v\}, \tag{3.1i}$$

where:

$$\gamma_B \mathbf{u}(\mathbf{x}, t) = \mathbf{u}(\mathbf{x}, t)|_{(\mathbf{x}, t) \in B \times [0, t_0]}, \tag{3.1j}$$

$$\delta_B \boldsymbol{\sigma}(\mathbf{x}, t) = \boldsymbol{\sigma}(\mathbf{x}, t) \cdot \mathbf{n}(\mathbf{x})|_{(\mathbf{x}, t) \in B \times [0, t_0]}, \tag{3.1k}$$

$$\gamma_0 \mathbf{u}(\mathbf{x}, t) = \mathbf{u}(\mathbf{x}, t)|_{\mathbf{x} \in R,\, t = 0 \text{ or } t = t_0}, \tag{3.1l}$$

$$\delta_0 \mathbf{p}(\mathbf{x}, t) = \mathbf{p}(\mathbf{x}, t)|_{\mathbf{x} \in R,\, t = 0 \text{ or } t = t_0}, \tag{3.1m}$$

and $\mathbf{h}'$, $\mathbf{h}'_B$, $\mathbf{h}'_0$ are the elements of the Hilbert spaces H'_u, H'_B, H'_0. With the previous prescription the spaces H, G, H′, G′ are Hilbert spaces indeed.

The γ_B, δ_B, γ_0, δ_0 are continuous linear operators by definition and their names are the boundary operators.

Let's define mappings A, A* between spaces H and G and between G′ and H′ respectively:

$$A = \begin{bmatrix} \frac{1}{2}(\nabla\cdot + (\nabla\cdot)^T) & 0 & 0 \\ \frac{\partial\cdot}{\partial t} & 0 & 0 \\ 0 & I_B & 0 \\ 0 & 0 & I_0 \end{bmatrix}, \tag{3.2}$$

$$A^* = \begin{bmatrix} -\operatorname{div} & \frac{\partial\cdot}{\partial t} & 0 & 0 \\ 0 & 0 & I_B^* & 0 \\ 0 & 0 & 0 & I_0^* \end{bmatrix}, \tag{3.3}$$

where I_B, I_0, I_B^* and I_0^* are continuous linear mappings defined by the equations

$$\mathbf{I}_B \gamma_B \mathbf{u}(\mathbf{x}, t) = -\mathbf{u}(\mathbf{x}, t)|_{(\mathbf{x},t) \in \mathbf{B} \times [0, t_0]} \in \mathbf{G}_B , \tag{3.4}$$

$$\mathbf{I}_0 \gamma_0 \mathbf{u}(\mathbf{x}, t) = \mathbf{u}(\mathbf{x}, 0)|_{\mathbf{x} \in \bar{\mathbf{R}}} \in \mathbf{G}_0 , \tag{3.5}$$

$$\mathbf{I}_B^* \delta_B \boldsymbol{\sigma}(\mathbf{x}, t) = \mathbf{T}(\mathbf{x}, t)|_{(\mathbf{x},t) \in \mathbf{B} \times [0, t_0]} \in \mathbf{H}'_B , \tag{3.6}$$

$$\mathbf{I}_0^* \delta_0 \mathbf{p}(\mathbf{x}, t) = \mathbf{p}(\mathbf{x}, 0)|_{\mathbf{x} \in \bar{\mathbf{R}}} \in \mathbf{H}'_0 . \tag{3.7}$$

According to equations (3.1a)—(3.1c), (3.1f)—(3.1m) and (3.4)—(3.7) it is clear that functions $\mathbf{I}_B \gamma_B \mathbf{u}(\mathbf{x}, t)$, $\mathbf{I}_0 \gamma_0 \mathbf{u}(\mathbf{x}, t)$, $-\operatorname{div} \boldsymbol{\sigma}(\mathbf{x}, t) + \partial \mathbf{p}(\mathbf{x}, t)/\partial t$, $\mathbf{I}_B^* \gamma_B \mathbf{u}(\mathbf{x}, t)$ and $\mathbf{I}_0^* \delta_0 \mathbf{p}(\mathbf{x}, t)$ are the elements of the Hilbert spaces $\mathbf{G}_B$ $\mathbf{G}_0$, $\mathbf{H}'_u$, $\mathbf{H}'_B$ and $\mathbf{H}'_0$. Furthermore $\mathbf{H}'_u$, $\mathbf{H}'_B$, $\mathbf{H}'_0$, $\mathbf{G}'_e$, $\mathbf{G}'_v$, $\mathbf{G}'_B$ and $\mathbf{G}'_0$ are the dual spaces of $\mathbf{H}_u$, $\mathbf{H}_B$, $\mathbf{H}_0$, $\mathbf{G}_e$, $\mathbf{G}_v$, $\mathbf{G}_B$ and $\mathbf{G}_0$ and they are reflexive spaces that is $(\mathbf{H}'_u)' = \mathbf{H}_u, \ldots, (\mathbf{G}'_0)' = \mathbf{G}_0$. The comma in superscripts denotes the dual Hilbert space of a Hilbert space. Moreover according to equations (3.3), (3.6), (3.7) and (3.2), (3.4), (3.5) $\mathbf{H}'$ is the dual space of $\mathbf{H}$ and $\mathbf{G}'$ is the dual space of $\mathbf{G}$ and H and G are reflexive spaces therefore $(\mathbf{H}')' = \mathbf{H}$ and $(\mathbf{G}')' = \mathbf{G}$. So we can define the next scalar products between the subspaces of the product spaces $\mathbf{H}$, $\mathbf{H}'$ and $\mathbf{G}$, $\mathbf{G}'$ respectively:

$$\langle \mathbf{h}', \mathbf{u} \rangle_{\mathbf{H}_u} = \int_{\mathbf{R}} \int_0^{t_0} \mathbf{h}'(\mathbf{x}, t)^T \mathbf{u}(\mathbf{x}, t_0 - t) \mathrm{d}\mathbf{x} \mathrm{d}t , \tag{3.8a}$$

$$\langle \mathbf{h}'_B, \mathbf{u}_B \rangle_{\mathbf{H}_B} = \int_{\mathbf{B}_\sigma} \int_0^{t_0} \mathbf{h}'_B(\mathbf{x}, t)^T \mathbf{u}(\mathbf{x}, t_0 - t) \mathrm{d}\mathbf{x} \mathrm{d}t , \tag{3.8b}$$

$$\langle \mathbf{h}'_0, \mathbf{u}_0 \rangle_{\mathbf{H}_0} = \int_{\mathbf{R}} \mathbf{h}'_0(\mathbf{x}, 0)^T \mathbf{u}(\mathbf{x}, t_0) \mathrm{d}\mathbf{x} , \tag{3.8c}$$

$$\langle \boldsymbol{\sigma}, \mathbf{e} \rangle_{\mathbf{G}_e} = \int_{\mathbf{R}} \int_0^{t_0} \boldsymbol{\sigma}(\mathbf{x}, t) : \mathbf{e}(\mathbf{x}, t_0 - t) \, \mathrm{d}x \, \mathrm{d}t , \tag{3.9a}$$

$$\langle \mathbf{p}, \mathbf{v} \rangle_{\mathbf{G}_v} = \int_{\mathbf{R}} \int_0^{t_0} \mathbf{p}(\mathbf{x}, t) \mathbf{v}(\mathbf{x}, t_0 - t) \, \mathrm{d}\mathbf{x} \, \mathrm{d}t , \tag{3.9b}$$

$$\langle \mathbf{T}, \mathbf{g}_B \rangle_{\mathbf{G}_B} = \int_{\mathbf{B}_u} \int_0^{t_0} \mathbf{T}(\mathbf{x}, t)^T \mathbf{g}_B(\mathbf{x}, t_0 - t) \, \mathrm{d}\mathbf{x} \, \mathrm{d}t , \tag{3.9c}$$

$$\langle \mathbf{p}_0, \mathbf{g}_0 \rangle_{\mathbf{G}_0} = \int_{\mathbf{R}} \mathbf{p}(\mathbf{x}, t_0)^T \mathbf{g}_0(\mathbf{x}, 0) \, \mathrm{d}\mathbf{x} , \tag{3.9d}$$

$$\langle \mathbf{e}, \boldsymbol{\sigma} \rangle_{\mathbf{G}'_e} = \int_{\mathbf{R}} \int_0^{t_0} \mathbf{e}(\mathbf{x}, t) : \boldsymbol{\sigma}(\mathbf{x}, t_0 - t) \, \mathrm{d}\mathbf{x} \, \mathrm{d}t , \tag{3.10a}$$

$$\langle \mathbf{v}, \mathbf{p} \rangle_{G_v'} = \int_R \int_0^{t_0} \mathbf{v}(\mathbf{x}, t)^T \mathbf{p}(\mathbf{x}, t_0 - t)\, d\mathbf{x}\, dt\,, \tag{3.10b}$$

$$\langle \mathbf{g}_B, \mathbf{T} \rangle_{G_B'} = \int_{B_u} \int_0^{t_0} \mathbf{g}_B(\mathbf{x}, t)^T \mathbf{T}(\mathbf{x}, t_0 - t)\, d\mathbf{x}\, dt\,, \tag{3.10c}$$

$$\langle \mathbf{g}_0, \mathbf{p}_0 \rangle_{G_0'} = \int_R \mathbf{g}_0(\mathbf{x}, 0)^T \mathbf{p}(\mathbf{x}, t_0)\, d\mathbf{x}\,. \tag{3.10d}$$

It can be seen with a simple tranformations of the previous integrals that:

$$\langle \boldsymbol{\sigma}, \mathbf{e} \rangle_{G_e} = \langle \mathbf{e}, \boldsymbol{\sigma} \rangle_{G_e'}\,, \langle \mathbf{p}, \mathbf{v} \rangle_{G_v} = \langle \mathbf{v}, \mathbf{p} \rangle_{G_v'}\,, \langle \mathbf{T}, \mathbf{g}_B \rangle_{G_B} = \langle \mathbf{g}_B, \mathbf{T} \rangle_{G_B'}$$

moreover $\langle \mathbf{p}_0, \mathbf{g}_0 \rangle_{G_0} = \langle \mathbf{g}_0, \mathbf{p}_0 \rangle_{G_0}$ by definitions. These facts make possible the simplifications of the symbols for the scalar products:

$$\begin{gathered} \langle \mathbf{h}', \mathbf{u} \rangle_{H_u} = \langle \mathbf{h}', \mathbf{u} \rangle_R\,, \langle \mathbf{h}_B', \mathbf{u}_B \rangle_{H_B} = \langle \mathbf{h}_B', \mathbf{u} \rangle_B\,, \\ \langle \mathbf{h}_0', \mathbf{u}_0 \rangle_{H_0} = \langle \mathbf{h}_0', \mathbf{u} \rangle_0\,, \end{gathered} \tag{3.11}$$

$$\begin{gathered} \langle \boldsymbol{\sigma}, \mathbf{e} \rangle_{G_e} = \langle \boldsymbol{\sigma}, \mathbf{e} \rangle_R\,, \langle \mathbf{T}, \mathbf{g}_B \rangle_{G_B} = \langle \mathbf{T}, \mathbf{g}_B \rangle_{B_u} \\ \langle \mathbf{p}, \mathbf{v} \rangle_{G_v} = \langle \mathbf{p}, \mathbf{v} \rangle_R\,, \langle \mathbf{p}_0, \mathbf{g}_0 \rangle_{G_0} = \langle \mathbf{g}_0, \mathbf{p} \rangle_0\,. \end{gathered} \tag{3.12}$$

Using the mappings A, A^* and the scalar products (3.11) and (3.12), we now construct a generalization of Green formula for the discussed problem (2.3)—(2.11). Let the scalar products between the product spaces $H' - H$ and $G' - G$ defined by equalities:

$$\langle \mathbf{U}', \mathbf{U} \rangle_H = \langle \mathbf{h}', \mathbf{u} \rangle_R + \langle \mathbf{h}_B', \mathbf{u} \rangle_{B_\sigma} + \langle \mathbf{h}_0', \mathbf{u}_0 \rangle_0\,,$$

$$\langle \mathbf{V}', \mathbf{V} \rangle_G = \langle \boldsymbol{\sigma}, \mathbf{e} \rangle_R + \langle \mathbf{p}, \mathbf{v} \rangle_R + \langle \mathbf{T}, \mathbf{g}_B \rangle_{B_u} + \langle \mathbf{g}_0, \mathbf{p} \rangle_0\,.$$

Than it can be seen by partial integration and the divergence theorem that A^* is the adjoint mapping of mapping A, namely

$$\langle \mathbf{V}', A\mathbf{U} \rangle_G = \langle A^* \mathbf{V}', \mathbf{U} \rangle_H\,, \tag{3.13}$$

or in more detailed form

$$\begin{aligned} &\left\langle \boldsymbol{\sigma}, \frac{1}{2}(\nabla \mathbf{u} + (\nabla \mathbf{u})^T) \right\rangle_R + \left\langle \mathbf{p}, \frac{\partial \mathbf{u}}{\partial t} \right\rangle_R - \langle \mathbf{T}, \mathbf{u} \rangle_{B_u} + \langle \mathbf{u}, \mathbf{p} \rangle_0 \\ &= -\langle \operatorname{div} \boldsymbol{\sigma}, \mathbf{u} \rangle_R + \left\langle \frac{\partial \mathbf{p}}{\partial t}, \mathbf{u} \right\rangle_R + \langle \mathbf{T}, \mathbf{u} \rangle_{B_\sigma} + \langle \mathbf{p}, \mathbf{u} \rangle_0\,. \end{aligned} \tag{3.14}$$

This result can be considered as a generalization of the classical Green formula.

To construct the variational functional, which is equivalent to the discussed boundary value problem, we now define the mappings between the subspaces of product spaces G and G′:

$$\mathbf{E}(\mathbf{x}): \mathbf{e}(\mathbf{x}, t) = \boldsymbol{\sigma}(\mathbf{x}, t), \mathbf{e} \in G_e, \qquad \boldsymbol{\sigma} \in G'_e, \tag{3.15}$$

$$\mathbf{p}(\mathbf{x}, t) = \rho(\mathbf{x})\mathbf{v}(\mathbf{x}, t), \mathbf{p} \in G'_v, \quad \mathbf{v} \in G_v, \tag{3.16}$$

where:
$\mathbf{E}(\mathbf{x})$, $\mathbf{x} \in \mathbf{R}$ is a canonical isomorphism from G_e to G'_e, and $\rho = \rho(\mathbf{x}) \in C^1(\bar{\mathbf{R}})$, $(\rho(\mathbf{x}) > 0$, $\mathbf{x} \in \bar{\mathbf{R}})$ is a canonical isomorphism from G_v to G'_v too. Let's write the equations (2.3)—(2.11) in the form:

$$\begin{bmatrix}
0 & 0 & 0 & \frac{\partial .}{\partial t} & -\mathrm{div}. & & & & \\
0 & \rho & 0 & -1 & 0 & & & & \\
0 & 0 & E & 0 & -1 & 0 & & & \\
\frac{\partial .}{\partial t} & -1 & 0 & 0 & 0 & & & & \\
\frac{1}{2}((\nabla .)+(\nabla .)^T) & 0 & -1 & 0 & 0 & & & & \\
 & & & & & 0 & I_B^* & & \\
 & 0 & & & & I_B & 0 & 0 & \\
 & & & & & & 0 & 0 & I_0^* \\
 & & & & & & & I_0 & 0
\end{bmatrix}
\begin{bmatrix} \mathbf{u} \\ \mathbf{v} \\ \mathbf{e} \\ \mathbf{p} \\ \boldsymbol{\sigma} \\ \gamma_B \mathbf{u} \\ \delta_B \boldsymbol{\sigma} \\ \gamma_0 \mathbf{u} \\ \delta_0 \mathbf{p} \end{bmatrix}
-
\begin{bmatrix} \mathbf{f} \\ \mathbf{0} \\ \mathbf{0} \\ \mathbf{0} \\ \mathbf{0} \\ \hat{\mathbf{T}} \\ -\hat{\mathbf{u}} \\ \mathbf{p}^0 \\ \mathbf{u}^0 \end{bmatrix}
= \mathbf{0} \tag{3.17}$$

or in concise form:

$$P\Lambda - \Gamma = \mathbf{0} \tag{3.18}$$

where:
vector $\Lambda = (\mathbf{u}, \mathbf{v}, \mathbf{e}, \mathbf{p}, \boldsymbol{\sigma}, \gamma_B \mathbf{u}, \delta_B \boldsymbol{\sigma}, \gamma_0 \mathbf{u}, \delta_0 \mathbf{0})$ is an element of the product space

$$W = H_u \times G_v \times G_e \times G'_v \times G'_e \times H_B \times G'_B \times H_0 \times G'_0,$$

vector $\Gamma = (\mathbf{f}, \mathbf{0}, \mathbf{0}, \mathbf{0}, \mathbf{0}, \hat{\mathbf{T}}, -\hat{\mathbf{u}}, \mathbf{p}^0, \mathbf{u}^0)$ is an element of the product space

$$W' = H'_u \times G'_v \times G'_e \times G_v \times G_e \times H'_B \times G_B \times H'_0 \times G_0.$$

It is clear that P is a continuous linear mapping from W to W′ and moreover W′ is the dual space of W, therefore the scalar product

$$\langle P\Lambda_1, \Lambda_2 \rangle_W, \Lambda_1, \Lambda_2 \in W \tag{3.19}$$

can be constructed. The scalar product (3.19) is interpreted by the scalar products between the suitable subspaces of the product spaces W and W′ corresponding to the equalities (3.8a) — (3.8c), (3.9a), (3.9b) and (3.10a) — (3.10d). Using the Green's formula (3.14) it can be seen easily that scalar product (3.19) is symmetrical, that is:

$$\langle \mathrm{P}\Lambda_1, \Lambda_2\rangle_{\mathrm{W}} = \langle \mathrm{P}\Lambda_2, \Lambda_1\rangle_{\mathrm{W}}, \quad \Lambda_1, \Lambda_2 \in \mathrm{W}\,. \tag{3.20}$$

The operator P is linear and continuous, W and W′ are Hilbert spaces moreower equality (3.20) is valid, therefore operator P is potential. On the basis of these facts we can use the Theorem 2.17 from [5] (pp. 42), which says that a functional can be construct according to the equality:

$$\Phi(\Lambda) = \int_0^1 \langle \mathrm{P}(s\Lambda) - \Gamma, \Lambda\rangle_{\mathrm{W}}\, \mathrm{d}s\,, \tag{3.21}$$

where s is a real parameter.

If equations (3.17) are replaced into the right hand side of equality (3.21) and the integral is calculated, then we obtain

$$\begin{aligned}
\Phi(\Lambda) = {} & \frac{1}{2}\left\langle \frac{\partial \mathbf{p}}{\partial t}, \mathbf{u}\right\rangle_{\mathrm{R}} - \frac{1}{2}\langle \operatorname{div}\boldsymbol{\sigma}, \mathbf{u}\rangle_{\mathrm{R}} - \langle \mathbf{f}, \mathbf{u}\rangle_{\mathrm{R}} + \frac{1}{2}\langle \rho\mathbf{v}, \mathbf{v}\rangle_{\mathrm{R}} \\
& - \frac{1}{2}\langle \mathbf{p}, \mathbf{v}\rangle_{\mathrm{R}} + \frac{1}{2}\langle \mathbf{E}\colon \mathbf{e}, \mathbf{e}\rangle_{\mathrm{R}} - \frac{1}{2}\langle \boldsymbol{\sigma}, \mathbf{e}\rangle_{\mathrm{R}} + \frac{1}{2}\left\langle \frac{\partial \mathbf{u}}{\partial t}, \mathbf{p}\right\rangle_{\mathrm{R}} - \frac{1}{2}\langle \mathbf{v}, \mathbf{p}\rangle_{\mathrm{R}} \\
& + \frac{1}{2}\left\langle \frac{1}{2}(\nabla\mathbf{u} + (\nabla\mathbf{u})^T), \boldsymbol{\sigma}\right\rangle_{\mathrm{R}} - \frac{1}{2}\langle \mathbf{e}, \boldsymbol{\sigma}\rangle_{\mathrm{R}} + \frac{1}{2}\langle \mathbf{T}, \mathbf{u}\rangle_{\mathrm{B}_\sigma} - \langle \hat{\mathbf{T}}, \mathbf{u}\rangle_{\mathrm{B}_\sigma} \\
& - \frac{1}{2}\langle \mathbf{u}, \mathbf{T}\rangle_{\mathrm{B}_u} + \langle \hat{\mathbf{u}}, \mathbf{T}\rangle_{\mathrm{B}_u} + \frac{1}{2}\langle \mathbf{p}, \mathbf{u}\rangle_0 - \langle \mathbf{p}^0, \mathbf{u}\rangle_0 + \frac{1}{2}\langle \mathbf{u}, \mathbf{p}\rangle_0 \\
& - \langle \mathbf{u}^0, \mathbf{p}\rangle_0\,,
\end{aligned} \tag{3.22}$$

where equations (3.1j)—(3.1m) and (3.4)—(3.7) were used. Now using the Green's formula (3.14) and equality (3.22) we get

$$\begin{aligned}
\Phi(\Lambda) = {} & \frac{1}{2}\langle \rho\mathbf{v}, \mathrm{v}\rangle_{\mathrm{R}} + \left\langle \mathbf{p}, \frac{\partial \mathbf{u}}{\partial t} - \mathbf{v}\right\rangle_{\mathrm{R}} + \left\langle \boldsymbol{\sigma}, \frac{1}{2}(\nabla\mathbf{u} + (\nabla\mathbf{u})^T) - \mathbf{e}\right\rangle_{\mathrm{R}} \\
& + \frac{1}{2}\langle \mathbf{E}\colon \mathbf{e}, \mathbf{e}\rangle_{\mathrm{R}} - \langle \mathbf{f}, \mathbf{u}\rangle_{\mathrm{R}} - \langle \mathbf{T}, \mathbf{u} - \hat{\mathbf{u}}\rangle_{\mathrm{B}_u} - \langle \hat{\mathbf{T}}, \mathbf{u}\rangle_{\mathrm{B}_\sigma} \\
& + \langle \mathbf{u} - \mathbf{u}^0, \mathbf{p}\rangle_0 - \langle \mathbf{p}^0, \mathbf{u}\rangle_0
\end{aligned} \tag{3.23}$$

Using again the Green's formula (3.14), from equality (3.23) we have:

$$\Phi(\Lambda)=\frac{1}{2}\langle\rho\mathbf{v},\mathbf{v}\rangle_R-\langle\mathbf{p},\mathbf{v}\rangle_R+\frac{1}{2}\langle\mathbf{E}:\mathbf{e},\mathbf{e}\rangle_R$$

$$-\langle\boldsymbol{\sigma},\mathbf{e}\rangle_R+\left\langle\frac{\partial\mathbf{p}}{\partial t}-\operatorname{div}\boldsymbol{\sigma}-\mathbf{f},\mathbf{u}\right\rangle_R+\langle\mathbf{T},\hat{\mathbf{u}}\rangle_{B_u}+\langle\mathbf{T}-\hat{\mathbf{T}},\mathbf{u}\rangle_{B_\sigma}$$

$$-\langle\mathbf{u}^0,\mathbf{p}\rangle_0+\langle\mathbf{p}-\mathbf{p}^0,\mathbf{u}\rangle_0 \tag{3.24}$$

Finally we prove that the functional $\Phi(\Lambda)$ assumes a stationary value when Λ satisfies (3.17) and inversely, if Λ satisfies (3.17) than the function $\Phi(\Lambda)$ assumes a stationary value. To this proof we fist define the space $\bar{W}$ of possible variations $\bar{\Lambda}$.

$$\bar{H}_B=\{\gamma_B\mathbf{u}(\mathbf{x},t)\in H_B:\gamma_B\mathbf{u}(\mathbf{x},t)=\mathbf{0},(\mathbf{x},t)\in B_u\times[0,t_0]\} \tag{3.25}$$

$$\bar{H}_0=\{\gamma_0\mathbf{u}(\mathbf{x},t)\in H_0:\gamma_0\mathbf{u}(\mathbf{x},t)=\mathbf{0},\mathbf{x}\in\bar{R},t=0\} \tag{3.26}$$

$$\bar{G}'_B=\{\delta_B\boldsymbol{\sigma}(\mathbf{x},t)\in G'_B:\delta_B\boldsymbol{\sigma}(\mathbf{x},t)=\mathbf{T}(\mathbf{x},t)=\mathbf{0},(\mathbf{x},t)\in B_\sigma\times[0,t_0]\} \tag{3.27}$$

$$\bar{G}'_0=\{\delta_0\mathbf{p}(\mathbf{x},t)\in G'_0:\delta_0\mathbf{p}(\mathbf{x},t)=\mathbf{0},\mathbf{x}\in\bar{R},t=0\} \tag{3.28}$$

$$\bar{W}=\{\Lambda\in W:\gamma_B\mathbf{u}(\mathbf{x},t)\in\bar{H}_B,\gamma_0\mathbf{u}(\mathbf{x},t)\in\bar{H}_0,\delta_B\boldsymbol{\sigma}(\mathbf{x},t)\in\bar{G}'_B,$$

$$\delta_0\mathbf{p}(\mathbf{x},t)\in\bar{G}'_0\} \tag{3.29}$$

Let $\bar{\Lambda}$ be an arbitrary element of $\bar{W}$, and now construct the variation of $\Phi(\Lambda)$.

$$\delta\Phi(\Lambda;\bar{\Lambda})=\frac{\partial}{\partial\varepsilon}\Phi(\Lambda+\varepsilon\bar{\Lambda})|_{\varepsilon=0}$$

$$=\langle\rho\mathbf{v}-\mathbf{p},\bar{\mathbf{v}}\rangle_R+\left\langle\frac{\partial\mathbf{u}}{\partial t}-\mathbf{v},\bar{\mathbf{p}}\right\rangle_R$$

$$+\frac{1}{2}\langle(\nabla\mathbf{u}+(\nabla\mathbf{u})^T)-\mathbf{e},\bar{\boldsymbol{\sigma}}\rangle_R+\langle\mathbf{E}:\mathbf{e}-\boldsymbol{\sigma},\bar{\mathbf{e}}\rangle_R$$

$$+\left\langle\frac{\partial\mathbf{p}}{\partial t}-\operatorname{div}\boldsymbol{\sigma}-\mathbf{f},\bar{\mathbf{u}}\right\rangle_R-\langle\mathbf{u}-\hat{\mathbf{u}},\bar{\mathbf{T}}\rangle_{B_u}$$

$$+\langle\mathbf{T}-\hat{\mathbf{T}},\bar{\mathbf{u}}\rangle_{B_\sigma}+\langle\mathbf{u}-\mathbf{u}^0,\bar{\mathbf{p}}\rangle_0+\langle\mathbf{p}-\mathbf{p}^0,\bar{\mathbf{u}}\rangle_0 \tag{3.30}$$

where the Green's formula (3.14) and the simmetricity of scalar products on R, B_u and B_σ were employed.

Let's suppose that

$$\delta\Phi(\Lambda, \bar{\Lambda}) = 0 . \tag{3.31}$$

In this case, since $\bar{\Lambda}$ is an arbitrary element of $\bar{W}$, if Λ satisfies equation (3.31) then at the same time it's the solution of equations (3.17). Inversely if Λ is the solution of (3.17) then (3.31) is satisfied.*

4. Special variational functionals

Now we derive from the functional $\Phi(\Lambda)$ a Reissner-type functional, the functional of total potential energy and the functional of complementary energy.

a) Reissner type functional: $\Phi_R(\mathbf{u}, \mathbf{p}, \boldsymbol{\sigma})$ Constraints:

(i) $$\mathbf{e}(\mathbf{x}, t) = \mathbf{C}(\mathbf{x}, t) : \boldsymbol{\sigma}(\mathbf{x}, t), (\mathbf{x}, t) \in R \times [0, t_0], \mathbf{x} \in R ,$$

(ii) $$\mathbf{v}(\mathbf{x}, t) = \frac{1}{\rho(\mathbf{x})} \mathbf{p}(\mathbf{x}, t), (\mathbf{x}, t) \in \bar{R} \times [0, t_0], \mathbf{x} \in R .$$

Considering the constraints (i) and (ii), from (3.23) we have:

$$\Phi_R(\mathbf{u}, \mathbf{p}, \boldsymbol{\sigma}) = \left\langle \mathbf{p}, \frac{\partial \mathbf{u}}{\partial t} \right\rangle_R - \frac{1}{2} \left\langle \mathbf{p}, \frac{1}{\rho} \mathbf{p} \right\rangle_R - \langle \mathbf{f}, \mathbf{u} \rangle_R$$

$$+ \left\langle \boldsymbol{\sigma}, \frac{1}{2} (\nabla \mathbf{u} + (\nabla \mathbf{u})^T) \right\rangle_R - \frac{1}{2} \langle \boldsymbol{\sigma}, \mathbf{C} : \boldsymbol{\sigma} \rangle_R - \langle \mathbf{T}, \mathbf{u} - \hat{\mathbf{u}} \rangle_{B_u}$$

$$- \langle \hat{\mathbf{T}}, \mathbf{u} \rangle_{B_\sigma} + \langle \mathbf{u} - \mathbf{u}^0, \mathbf{p} \rangle_0 - \langle \mathbf{p}^0, \mathbf{u} \rangle_0 \tag{4.1}$$

If the constraint $\mathbf{v}(\mathbf{x}, t) = \dfrac{\partial \mathbf{u}(\mathbf{x}, t)}{\partial t}$ is also valid, then we have:

$$\Phi_R(\mathbf{u}, \boldsymbol{\sigma}) = \left\langle \rho \frac{\partial \mathbf{u}}{\partial t}, \frac{\partial \mathbf{u}}{\partial t} \right\rangle_R - \langle \mathbf{f}, \mathbf{u} \rangle_R + \left\langle \boldsymbol{\sigma}, \frac{1}{2} (\nabla \mathbf{u} + (\nabla \mathbf{u})^T) \right\rangle_R$$

* This variational principle can be proved with the analogy of the proofs of variational principles in paper [2].

$$-\frac{1}{2}\langle \boldsymbol{\sigma}, \mathbf{C}:\boldsymbol{\sigma}\rangle_{\mathrm{R}} - \langle \mathbf{T}, \mathbf{u}-\hat{\mathbf{u}}\rangle_{\mathrm{B}_u} - \langle \hat{\mathbf{T}}, \mathbf{u}\rangle_{\mathrm{B}_\sigma} + \left\langle \mathbf{u}-\mathbf{u}^0, \rho\frac{\partial \mathbf{u}}{\partial t}\right\rangle_0$$

$$-\left\langle \rho\left(\frac{\partial \mathbf{u}}{\partial t}\right)^0, \mathbf{u}\right\rangle_0 \tag{4.2}$$

where: $$\left(\frac{\partial \mathbf{u}}{\partial t.}\right)^0 = \frac{1}{\rho}\mathbf{p}^0 .$$

If the constraints are choosen in a suitable manner then the Reissner type functionals $\Phi_{\mathrm{R}}(\mathbf{u}, \mathbf{v}, \mathbf{e})$, and $\Phi_{\mathrm{R}}(\mathbf{u}, \mathbf{e})$ can be derive from $\Phi(\Lambda)$ too.

b) The total potential energy functional: $\Phi_{\mathrm{p}}(\mathbf{u})$

Constraints:

(i) $\mathbf{u}(\mathbf{x}, t) \in \mathrm{C}^{2,2}(\mathrm{R} \times [0, t_0])$

(ii) $\mathbf{u}(\mathbf{x}, t) = \hat{\mathbf{u}}(\mathbf{x}, t), \quad (\mathbf{x}, t) \in \mathrm{B}_u \times [0, t_0]$

(iii) $\mathbf{u}(\mathbf{x}, 0) = \mathbf{u}^0(\mathbf{x}), \quad \mathbf{x} \in \bar{\mathrm{R}}$

(iv) $\mathbf{v}(\mathbf{x}, t) = \dfrac{\partial \mathbf{u}(\mathbf{x}, t)}{\partial t}, \quad (\mathbf{x}, t) \in \bar{\mathrm{R}} \times [0, t_0]$

(v) $\mathbf{p}(\mathbf{x}, t) = \rho(\mathbf{x})\mathbf{v}(\mathbf{x}, t), \quad (\mathbf{x}, t) \in \bar{\mathrm{R}} \times [0, t_0]$

(vi) $\boldsymbol{\sigma}(\mathbf{x}, t) = \mathbf{E}(\mathbf{x}):\mathbf{e}(\mathbf{x}, t), \quad (\mathbf{x}, t) \in \mathrm{R} \times [0, t_0]$

(vii) $\mathbf{e}(\mathbf{x}, t) = \dfrac{1}{2}(\nabla \mathbf{u}(\mathbf{x}, t) + (\nabla \mathbf{u}(\mathbf{x}, t))^T), \quad (\mathbf{x}, t) \in \mathrm{R} \times [0, t_0]$.

Considering the constraints (i)—(vii), from (3.23) we have:

$$\Phi_{\mathrm{p}}(\mathbf{u}) = \frac{1}{2}\left\langle \rho\frac{\partial \mathbf{u}}{\partial t}, \frac{\partial \mathbf{u}}{\partial t}\right\rangle_{\mathrm{R}} + \frac{1}{2}\left\langle \frac{1}{2}\mathbf{E}:(\nabla \mathbf{u} + (\nabla \mathbf{u})^T),\right.$$

$$\left.\frac{1}{2}(\nabla \mathbf{u} + (\nabla \mathbf{u})^T)\right\rangle_{\mathrm{R}} \langle \mathbf{f}, \mathbf{u}\rangle_{\mathrm{R}} - \langle \hat{\mathbf{T}}, \mathbf{u}\rangle_{\mathrm{B}_\sigma} - \left\langle \rho\left(\frac{\partial \mathbf{u}}{\partial t}\right)^0, \mathbf{u}\right\rangle_0 \tag{4.3}$$

c) The complementary energy functional $\Phi_{\mathrm{k}}(\mathbf{p}, \boldsymbol{\sigma})$ Constraints:

(i) $\mathbf{e}(\mathbf{x}, t) = \mathbf{C}(\mathbf{x}):\boldsymbol{\sigma}(\mathbf{x}, t) \quad \mathbf{x} \in \mathrm{R}, \qquad (\mathbf{x}, t) \in \mathrm{R} \times [0, t_0]$

(ii) $\mathbf{T}(\mathbf{x}, t) = \hat{\mathbf{T}}(\mathbf{x}, t), \qquad (\mathbf{x}, t) \in \mathrm{B}_\sigma \times [0, t_0]$

(iii) $$\frac{\partial \mathbf{p}(\mathbf{x}, t)}{\partial t} - \operatorname{div} \boldsymbol{\sigma}(\mathbf{x}, t) - \mathbf{f}(\mathbf{x}, t) = 0 \qquad (\mathbf{x}, t) \in \mathrm{R} \times [0, t_0]$$

(iv) $$\mathbf{p}(\mathbf{x}, 0) = \mathbf{p}^0(\mathbf{x}), \qquad \mathbf{x} \in \bar{\mathrm{R}}$$

Using the constraints (i)—(iv), from (3.24) we have

$$\tilde{\Phi}_k(\mathbf{p}, \boldsymbol{\sigma}) = -\frac{1}{2}\left\langle \mathbf{p}, \frac{1}{\rho}\mathbf{p} \right\rangle_{\mathrm{R}} - \frac{1}{2}\langle \boldsymbol{\sigma}, \mathbf{C}:\boldsymbol{\sigma} \rangle_{\mathrm{R}} + \langle \mathbf{T}, \hat{\mathbf{u}} \rangle_{B_u} - \langle \mathbf{u}^0, \mathbf{p} \rangle_0 , \tag{4.4}$$

and:

$$\Phi_k(\mathbf{p}, \boldsymbol{\sigma}) = -\tilde{\Phi}_k(\mathbf{p}, \boldsymbol{\sigma}) . \tag{4.5}$$

If we choose the contraints in a suitable manner then we can derive further four primal mixed variational functionals from functional $\Phi(\Lambda)$ ([5], Example 4.7, page 115).

Summary

In this paper a variational principle including all the primal mixed variational principles in linear elastodynamics has been elaborated. The special variational principles can be derived from this variational principle by choice of suitable constraints.

REFERENCES

1. Gurtin, M. E.: Variational Principles in the Linear Theory of Viscoelasticity. *Arch. Rational Mech. Anal.* **3** (1963), 179—191.
2. Gurtin, M. E.: Variational Principles for Linear Elastodynamics. *Archive for Rational Mechanics and Analysis* **16**, (1964), 34—50.
3. Gurtin, M. E.: Variational Principles for Linear Initialvalue Problems. *Quart Appl. Math.* **22**, (1964), 252—256
4. Tonti, E.: On the Variational Formulation for Linear Initial Value Problems. *Annali di Matematica pura ed Applicata* **95**, (1973), 331—359
5. Oden, J. T.—Reddy, J. N.: Variational Methods in Theoretical Mechanics. Springer-Verlag, Berlin—Heidelberg—New York 1976
6. Reddy, J. N.: A Note on Mixed Variational Principles for Initial Value Problems. *Q. J. Mech. Appl. Math.* 28, (1975), 123—132
7. Reddy, J. N.: Modified Gurtin's Variational Principles in the Linear Dynamic Theory of Viscoelasticity. *Int. J. Solids and Structures* 12, (1976), 227—235

APPENDIX

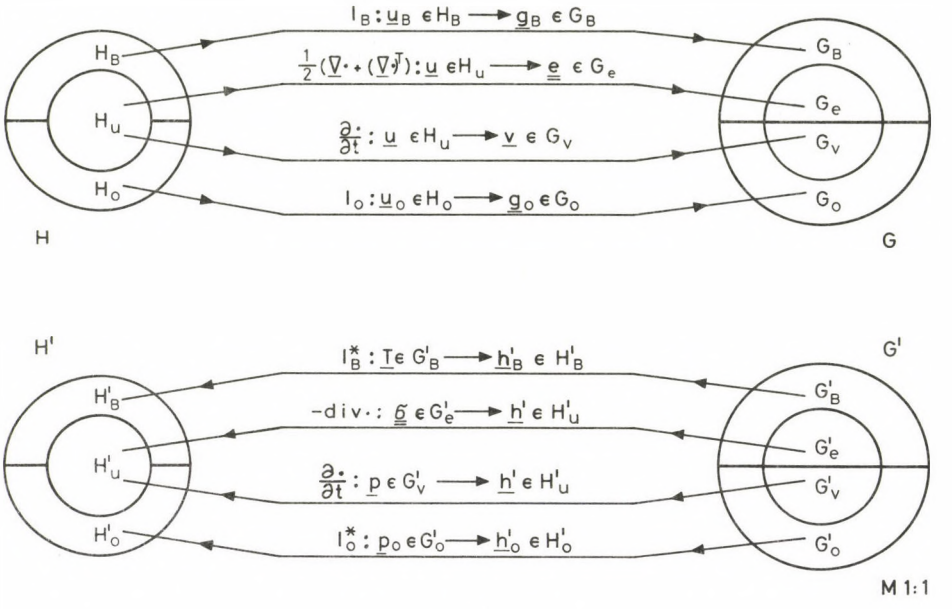

Fig. 1

Fig. 1 illustrates the mappings between subspaces of the product spaces H, G and G′, H′.

The mechanical meanings of the (vector or tensor) subspaces of product spaces H, G, G′ and H′ are followings:

H_u is the space of displacements	in $\bar{R} \times [0, t_0]$,
H_B is the space of displacements	on $B \times [0, t_0]$,
H_0 is the space of displacements	in $\bar{R}$, $t=0$, or $t=t_0$,
G_e is the space of strains	in $\bar{R} \times [0, t_0]$,
G_v is the space of velocities	in $\bar{R} \times [0, t_0]$,
G_B is the space of displacements	on $B \times [0, t_0]$,
G_0 is the space of displacements	in $\bar{R}$, $t=0$,
G'_e is the space of stresses	in $\bar{R} \times [0, t_0]$,
G'_v is the space of momentum densities	in $\bar{R} \times [0, t_0]$,
G'_B is the space of stresses	on $B \times [0, t_0]$,
G'_0 is the space of momentum densities	in $\bar{R}$, $t=0$, or $t=t_0$,
H'_u is the space of volumetric forces	in $\bar{R} \times [0, t_0]$,
H'_B is the space of stresses	on $B \times [0, t_0]$,
H'_0 is the space of momentum densities	in $\bar{R}$, $t=0$.

Variationsgrundsätze in der linearen Elastodynamik. — Entwickelt wird ein allgemeines Variationsprinzipium zu den grundlegenden Randwertbedingungen der linearen Elastodynamik. Das angewandte Skalarprodukt ist die Konvolute bilinearer Form; dieser Umstand bildet eine Möglichkeit für die Variationsprinzipien um die Anfangsbedingungen der gemischten Randwertaufgaben in einer expliziten Form zu umfassen.

Acta Technica Academiae Scientiarum Hungaricae, 93 (1—2), pp. 115—126 (1981)

LA REDUCTION DES OXYDES METALLIQUES DANS UN BAIN DES CARBURES METALLIQUES CHAUFFÉ PAR PLASMA

L. HÉDAI*

[Manuscript recu le]

La réduction des oxydes métalliques dans le bain des carbures métalliques chauffé par plasma est beaucoup plus rapide que lorsqu'on utilise du charbon en grains ou pulverisé. Le rapport rend compte d'essai de réduction de différents oxydes métalliques réalisés dans des fours chauffés par générateur à plasma de 20 KW, de 55 KW et de 100 KW.

1. Introduction

On sait que la plupart des carbures métalliques ont relativement d'élevée teneur en carbone (tableau 1). Cette teneur en carbone on peut utiliser pour la réduction des oxydes métalliques, si nous pouvons fondre des carbures. C'est que la vitesse de réaction est beaucoup plus grande avec du carbone dissous dans le bain qu'avec du charbon en morceaux ou pulvérisé [1, 2]. Avec l'utilisation de la torche à plasma on peut réaliser la fusion et surchauffe tous les carbures métalliques et ainsi nous pouvons créer de nouveaux procédés technologiques pour des oxydes métalliques.

Tableau 1
Les points de fusion des carbures et les teneurs en carbone

Carbure métallique	Le point de fusion, (°)	Teneur en carbone, (%)
TiC	3100	20,05
ZrC	3400	11,64
HfC	3900	6,30
VC	2700	19,08
NbC	3600	11,45
TaC	3800	6,23
Mo_2C	2500	5,89
WC	2800	6,13
Cr_3C_2	1800	13,33
Fe_3C	1450	6,67

* L. HÉDAI, Népköztársaság út 30. H-2800, Tatabánya, Hongrie

La réduction dans le bain des carbures métalliques peut être se jouer selon les réactions suivantes:

$$MeC + (MeO) = Me + CO \ldots \quad (1)$$

$$MeC \rightleftharpoons Me + [C] \ldots \quad (2)$$

$$[C] + (MeO) = Me + CO \ldots \quad (3)$$

L'énergie libre de formation (ΔG_i) des réductions de telle type c'est très supérieure à l'énergie libre de formation du gaz CO (Figure 1).

Ceci signifie que à 2500 K, on se trouve dans des conditions thermodynamiques très favorable pour la réduction des oxydes métalliques dans le bain des carbures chauffé par plasma.

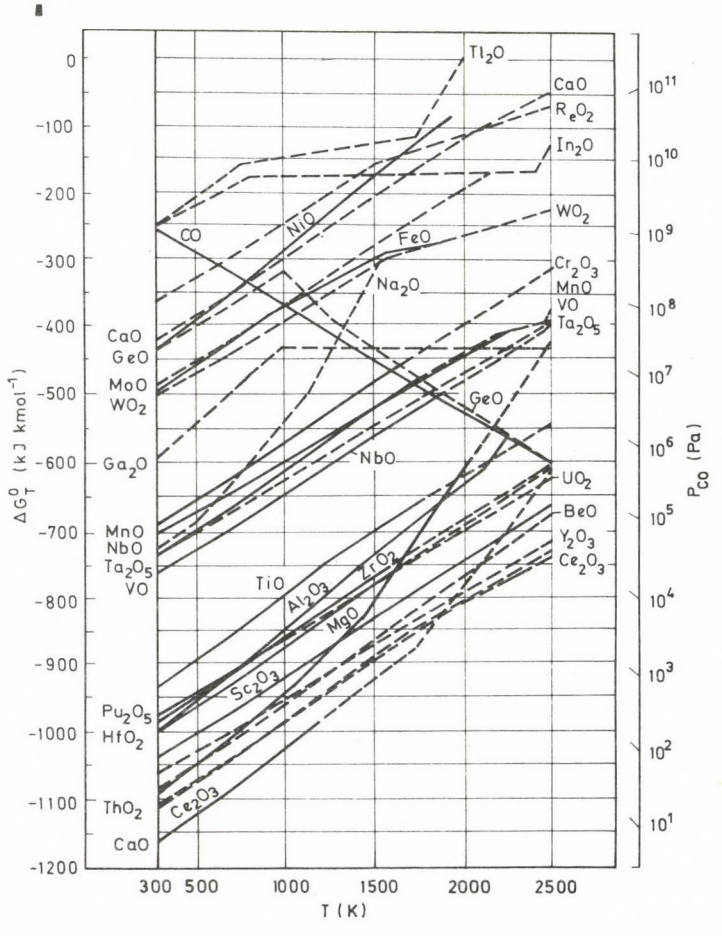

Fig. 1. Les énergies libres de formation (ΔG_T^0) des oxydes métalliques et du gaz CO

Tableau 2

Caractéristiques du générateur à plasma de puissance 20 kW

Puissance nominale maximum	20 kW
Plages d'utilisation voltage-courant:	
100 V	10–140 A
100 V	80–200 A
Gaz plasmagènes: argon et hydrogène	
Débit d'argon:	15–25 l/min
Pression d'argon:	3,5–4,0 bar
Débit d'hydrogène:	4 –6 l/min
Pression d'hydrogène:	3,5–4,0 bar
Matériau de la tuyère:	cuivre
Matériau de la cathode:	tungstène
Pression de l'eau de refroidissement: 1,5 bar	

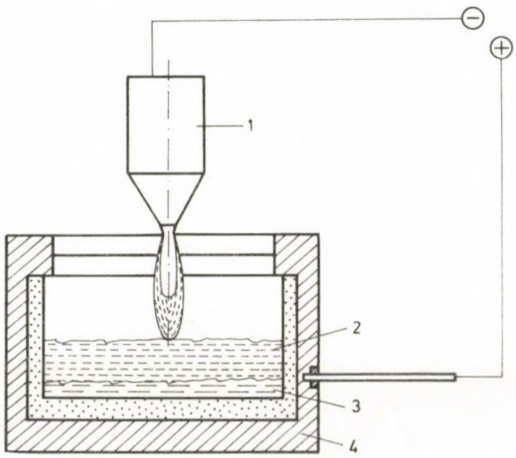

Fig. 2. Four à plasma expérimental

Parallélement le gaz de la torche à plasma provoque un brassage intense du bain des carbures et de l'oxyde fondu; il se forme une émulsion oxydecarbure dans laquelle les distances de diffusion sont considérablement réduites; la vitesse de réduction s'en trouve considérablement augmentée.

A partir de ces considérations, l'auteur a fait différentes expériences de réduction d'oxydes métalliques dans un bain des carbures chauffé par torche à plasma. Pour ces essais, il a utilisé des générateurs à plasma d'une puissance de 20 kW, de 55 kW et de 100 kW. Ses caractéristiques de ces générateurs à plasma sont préseutées dans les tableaux 2. 3 et 4.

Le four à plasma est représenté à la figure 2 [3, 4].

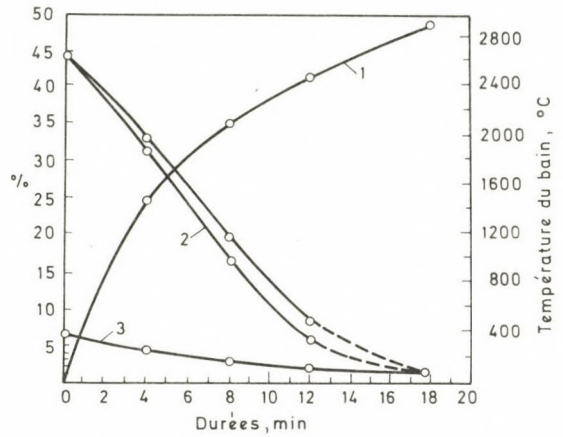

Fig. 3. Variation de la teneur en oxyde, de la teneur en carbone et de la température en fonction du temps de chauffage. 1 — température du bain, 2 — teneur en oxyde du bain, 3 — teneur en carbone du bain

Tableau 3

Les caractéristiques du générateur à plasma de puissance 55 kW

Puissance nominale maximum	55 kW
Courant nominale	250 A
Voltage nominale	220 V
Gaz plazmagène	nitroge'n
Débit de nitrogèn	4,5 – 5,5 Nm^3/heure

Tableau 4

Caractéristiques du générateur à plasma de puissance 100 kW

Puissance nominale maximum:	100 kW
Gaz plasmagènes:	argon et hydrogène
Débit d'argon:	58 l/min
Pression d'argon:	3,0 – 3,5 bar
Débit d'hydrogène:	33 l/min
Pression d'hydrogène:	3,5 – 4,0 bar
Matériau de la tuyère de la torche:	cuivre
Matériau de la cathode:	tungstène
Caractéristiques du transformateur d'alimentation:	
Puissance du réseau:	
Puissance sortant du transformateur:	100 kW
Voltage	200 V
Courant	500 A
Cos	0,85

2. Expériences avec le générateur à plasma de puissance de 20 kW

La composition des produits de base est la suivante:

Porteurs de carbone:

Déchets de métal dur:

$W = 80—85\%$; $C = 6{,}0—6{,}2\%$; $Co = 2—10\%$; $Si = 0{,}05—0{,}06\%$, $Fe = 0{,}3—0{,}4\%$

Ferromanganèse:

$Mn = 81{,}5\%$; $C = 6{,}9\%$; $Si = 1{,}95\%$; $P = 0{,}32\%$; $S = 0{,}03\%$.

Déchets de fonte:

$C = 3{,}5\%$; $Si = 1{,}8\%$; $Mn = 0{,}6\%$; $S = 0{,}10\%$; $P = 0{,}12\%$.

Porteurs des oxydes métalliques:

Concentrés du minerai de tungstène:

$WO_3 = 65{,}5\%$; $MnO = 8{,}48\%$; $FeO = 15{,}5\%$; $SiO_2 = 5{,}21\%$; $As = 0{,}06\%$; $P = 0{,}042\%$; $Cu = 0{,}06\%$.

Battitures:

$Fe_3O_4 = 93—95\%$; $SiO_2 = 3—5\%$; $P = -0{,}1—0{,}3\%$; $S = -0{,}1—0{,}5\%$.

Concentré de minerai de fer:

$Fe_2O_3 = 94{,}2\%$; $SiO_2 = -2{,}8\%$; $Al_2O_3 = 1{,}9\%$; $MgO = -0{,}15\%$; $CaO = 0{,}22\%$.

Minerai de manganèse:

$Fe = 9{,}6\%$; $Mn = 39{,}4\%$; $SiO_2 = 11{,}5\%$; $Al_2O_3 = 7{,}8\%$; $CaO = 2{,}4\%$; $MgO = 1{,}4\%$; $P = 0{,}18\%$.

Quartzite:

$SiO_2 = 95{,}7\%$; $Fe_2O_3 = 1{,}7\%$; $Al_2O_3 = 1{,}2\%$; $CaO = 0{,}3\%$; $MgO—0{,}15\%$.

Les résultats expérimentaux sont présentés dans le tableau 5.

Au cours des essais de réduction de tungstène avec le générateur à plasma de 20 kW, le chauffage a été interrompu à des intervalles donnés (après 4, 8, 12, 18 minutes) de façon à analyser les teneurs en oxydes et en carbone des produits obtenus. On a pu ainsi déterminer la fraction de la teneur en oxyde déjà réduite au moment considéré. Le tableau 6 et la figure 3 montrent ces résultats experimentaux. Pendant ces expériences nous avons aussi mesuré les températures du bain.

3. Expériences avec le générateur à plasma de puissance de 55 kW

La composition des produits de base est la suivante: Déchet de métal dur:

$W = 81{,}0\%$; $C = 5{,}42\%$; $Co = 11{,}0\%$; $Ti < 0{,}1\%$; $Si = 0{,}05\%$; $Fe = 0{,}32\%$.

Acide tungstique:

$H_2WO_4 = 99{,}9\%$.

Les résultats expérimentaux sont présentés dans le tableau 7.

Acta Technica Academiae Scientiarum Hungaricae 93, 1981

Tableau 5

Principaux résultats des essais avec le générateur à plasma de 20 kW

Numéro de l'essai	Déchets de tungstène, g	Concentrés de minerai de tungstène, g	Déchets de fonte, g	Battitures, g	Concentrés de minerai de fer, g	Ferro-manganèse, g	Minerai de manganèse, g	Quartzite, g	Quantité de produit métallique g/charge	Quantité de scorie, g	Durée du chauffage, min.
1	150	—	—	80	—	—	—	—	164	21	18
2	150	—	—	85	—	—	—	—	159	23	18
3	150	45	—	40	—	—	—	—	170	10	18
4	100	80	—	—	—	—	—	—	162	13	18
5	—	—	120	120	—	—	—	—	189	22	14
6	—	—	120	100	—	—	—	20	180	36	15
7	—	—	120	—	120	—	—	—	183	19	14
8	—	—	—	—	—	80	120	20	118	48	12
9	—	—	—	—	—	80	140	—	125	53	12
10	—	—	—	—	—	60	120	—	102	52	12

Tableau 5. (Cont.)

Composition des produits métalliques: %							Caractéristiques de fonctionnement du générateur					Consommation spécifique d'énergie électrique kWh/kg produit
W	Si	C	Mn	S	P	Co	Voltage	Courant	Puissance moyenne, kW	Débit Ar l/min	de gaz H l/min	
76,2	0,60	2,5	0,25	0,003	0,018	5,5	70	200	14,0	22,0	4,5	25,0
74,0	0,20	2,2	0,09	0,006	0,012	4,2	70	190	13,3	20,0	3,8	24,0
78,8	0,76	1,2	0,80	0,002	0,020	3,7	70	195	13,6	21,5	3,0	21,0
86,4	0,50	1,5	0,95	0,004	0,025	2,2	70	200	14,0	22,0	4,0	22,2
—	0,10	0,14	0,11	0,005	0,060	—	70	195	13,6	21,0	4,5	17,0
—	3,85	0,63	0,42	0,008	0,050	—	70	200	14,0	22,0	4,5	19,0
—	0,05	0,17	0,06	0,008	0,070	—	—	195	13,6	22,0	4,0	19,0
—	3,81	4,97	49,9	0,006	0,019	—	70	190	13,3	22,0	3,5	22,2
—	1,8	3,90	55,6	0,005	0,025	—	70	200	14,0	22,0	4,0	22,1
—	2,2	3,40	53,9	0,008	0,050	—	70	195	13,6	21,0	4,0	26,6

Tableau 6

Résultats de la réduction du tungstène en fonction du temps de chauffage

Durée du chauffage; minutes	Température du bain métallique, °C	Teneur en oxyde dans les moments divers; %	Teneur en carbone dans les moments divers; %
0	—	44,5	6,15
4	1520	33,4; 31,9	4,8; 4,9
8	2050	19,8; 15,8	3,0; 3,1
12	2460	5,6; 9,2	2,0; 2,05
18	2890	—	1,3; 1,4

Tableau 7

Principaux résultats des essais avec le générateur à plasma de 55 kW

Numéro de l'essai	Composition de la charge		Quantité de produit métallisé g/charg	Compositions des produits métallisés (%)					
	déchet de métal dur, g	H_2WO_4, g		C	W	Co	Si	Fe	Mn
1.	250	150	285	4,45	88,4	4,2	0,18	0,4	0,15
2.	250	150	290	3,52	90,2	3,0	0,20	0,6	0,20
3.	250	150	291	1,92	92,0	2,6	0,12	0,54	0,10
4.	250	150	276	1,76	92,1	2,45	0,16	0,3	0,18
5.	250	150	273	0,6	95,6	2,01	0,20	0,8	0,12

Tableau 7. (Contin.)

Quantité de scorie, g	Durée du chauffage min.	Caractéristiques de fonctionnement du générateur				Consommation spécifique d'énergie électrique kWh/kg produit
		Voltage, V	Courent A	Puissance moyenne, kW	Débit de gaz N_2 l/min	
88	4	180	250	45,0	5,0	10,5
81	7	190	250	47,5	5,0	19,0
85	10	112	400	45,0	5,5	25,4
73	13	110	380	41,8	5,5	32,4
70	16	105	370	39,0	5,0	38,2

4. Expériences avec le générateur à plasma de puissance de 100 kW

La composition des produits de base est la suivante:

Porteur de carbone:

Déchet de fonte:

$$C = 3{,}6\%;\ Si = 1{,}2\%;\ Mn = 0{,}6\%;$$
$$P = 0{,}10\%;\ S = 0{,}12\%.$$

Porteurs des oxydes métalliques:

Sidérite:

$$Fe = 37{,}18\%;\ FeO = 45{,}36\%;\ MnO = 2{,}6\%;$$
$$CO_2 = 34{,}5\%;\ SiO_2 = 6{,}62\%;\ CaO = 5{,}33\%;$$
$$MgO = 3{,}14\%.$$

Mineral de manganèse:

$$Mn = 19{,}08\%;\ Fe = 10{,}70\%;\ CO_2 = 17{,}06\%;$$
$$SiO_2 = 22{,}57\%;\ Al_2O_3 = 8{,}38\%;\ CaO = 4{,}04\%;$$
$$MgO = 2{,}6\%;\ P = 0{,}42\%.$$

Battiture:

$$Fe_3O_4 = 94{,}8\%;\ MnO = 1{,}75\%;\ SiO_2 = 2{,}21\%;$$
$$S = 0{,}45\%;\ P = 0{,}27\%.$$

Les résultats expérimentaux sont présentés dans tableau 8.

5. Conclusions

De ces résultats experimentaux on peut déduire les conclusions suivantes:

1. La réduction des oxydes dans un bain des carbures métalliques chauffé par plasma peut être réalisée de façon efficace aussi dans un four ouvert, car il n'est pas nécessaire d'avoir une atmosphère réductrice.

Cette condition simplifie beaucoup la construction des fours et diminue les investissements nécessaires pour à établir des fours de telle type.

2. L'énergie nécessaire pour la réduction déterminée par l'énergie nécessaire pour la fusion et surchauffe de la charge et par la teneur définitive en carbone du produit.

3. La réduction dans un bain des carbures métalliques chauffé par plasma rend possible la fabrication d'aciers alliés spéciaux et aussi de métaux divers; à partir d'une charge constituée de déchets et de minerais de faible valeur.

4. La réduction dans un bain des carbures métalliques chauffé par plasma rend possible l'affinage des ferroalliages carburés, c'est à dire la fabrication des ferroalliages affinés à partir de ferroalliages carburés.

Acta Technica Academiae Scientiarum Hungaricae 93, 1981

Tableau 8

Principaux résultats des essais avec le générateur à plasma de 100 kW

Numéro de l'essai	Composition de la charge					Quantité de produit métallisé kg/charge	Compositions des produits métallisés, %				
	minerai de fer kg	déchet de fonte kg	Battitures kg	minerai de manganèse kg	quartzite kg		C	Si	Mn	P	S
1	6,0	6,0	—	—	—	8,2	1,42	0,05	0,05	0,03	0,038
2	6,0	8,0	—	—	—	10,3	2,04	1,00	0,50	0,09	0,05
3	8,0	6,0	—	—	—	9,3	1,32	0,03	0,05	0,06	0,04
4	3,0	6,0	3,0	—	—	9,2	2,05	0,07	0,18	0,08	0,018
5	4,0	5,0	2,0	—	—	8,6	1,60	0,04	0,05	0,05	0,06
6	—	6,0	6,0	—	—	10,0	0,03	0,27	0,54	0,03	0,02
7	—	5,0	7,0	—	—	9,8	0,04	0,32	0,43	0,02	0,03
8	5,0	6,0	—	3,8	—	8,8	1,70	0,48	8,50	0,07	0,08
9	5,0	6,0	—	4,0	—	9,6	1,55	0,37	9,30	0,06	0,07
10	—	6,0	2,0	—	2,0	7,8	1,40	8,90	0,23	0,06	0,05
11	—	6,0	1,0	—	2,0	7.2	1,64	10,20	0,16	0,03	0,04

Tableau 8. (Cont.)

Quantité de scories kg	Durée du chauffage min	Caractéristiques de fonctionnement du générateur					Consommation spécifique d'énergie électrique kWh/kg produit
		Voltage V	Courant A	Puissance moyenne kW	Débit de gaz Ar l/mn	Débit de gaz H l/mn	
1,15	12	200	480	96,0	62	33	2,3
1,05	10	200	490	98,0	61	32	1,6
1,30	12	200	475	95,0	62	32	2,2
1,50	12	200	485	97,0	60	32	2,1
1,70	13	200	490	98,0	62	33	2,4
0,90	14	200	480	96,0	63	32	2,2
1,00	14	200	490	98,0	62	32	2,3
2,10	14	200	470	94,0	61	31	2,5
2,30	14	200	485	97,0	62	31	2,4
1,95	14	200	470	94,0	62	32	2,8
1,80	14	200	480	96,0	63	32	3,1

BIBLIOGRAPHIE

1. ASTIER, J.: Electric Iron Making Furnace. *Journal of Metals* **15** (1963), 619
2. SZIKLAVÁRI, J.: Accelerated Reduction of a Molten Charge of High FeO-Content by Means of Carbon Solved in Iron. *Acta Technica* **69** (1970), 171
3. HÉDAI, L.: Plazmával túlhevített fém-karbid olvadékban végrehajtott reakciók. Dissertation, 1980 Budapest
4. HÉDAI, L.: La réduction des oxydes métalliques dans un bain métallique chauffé par plasma. *9.Congrès International de UIE.* Cannes, 20—24 octobre, 1980

Reduction of Metal Oxides in Metal Carbide Fusion Superheated with Plasma. — It is well known that a significant part of metals are capable of binding a high quantity of carbon in the form of carbide. The carbide fusion produced as a result of smelting and superheating, metal carbides with the use of plasma might be a medium to be utilized for the reduction of different metal oxides, whilst also the original carbide structure of the metal carbides will be reduced to metallic structure. The experiments conducted by taking into account the above mentioned considerations, and by making use of plasma equipments of 20, 55, and 100 kW performances, are described. On the basis of the results of the experiments performed, the following statements are to be made: 1. The oxide reductions taking place in the metal carbide fusion might also be carried out in open-hearth furnaces, because no reducing atmosphere during this procedure is necessitated. 2. The quantity of energy required is basically defined by the energy needed for smelting and superheating the metal carbide. 3. The method for producing the metal described may be mainly applied for the allied production and high-purity steels as well as for that of ferro-alloys.

Reduktion von Metalloxyden in einer mit Plasma überhitzten Hartmetallschmelze. — Wie bekannt, kann ein großer Teil der Metalle eine verhältnismäßig große Menge von Kohlenstoff in Karbidform abbinden. Die als Folge des Schmelzens und der Überhitzung von Hartmetallen mit Plasma hergestellten Karbidschmelze kann als ein geeignetes Mittel zur Reduktion von verschiedenen Metalloxyden dienen, wobei auch die originale Karbidstruktur der Metallkarbide eine metallartige Struktur annimt. In der Abhandlung werden die unter Berücksichtigung der obenerwähnten Erwägungen die mit Plasmaeinrichtungen mit einer Leistung von 20, 55, 100 kW durchgeführten Versuche beschrieben. Aufgrund der Versuche kann folgendes festgestellt werden: 1. Die in der Metallkarbidschmelzen stattfindenden Oxydreduktionen können auch in den Siemens—Martin-Öfen durchgeführt werden, da zu diesem Verfahren keine Reduktionsatmosphäre erforderlich ist. 2. Der erforderliche Energieverbrauch wird grundsätzlich durch die zum Schmelzen und zur Überhitzung des Hartmetalls nötige Energie festgesetzt. 3. Die vorgeführte Metallherstellungsmethode kann, in erster Linie, in der Produktion von hochreinen und legierten Stählen sowie von Eisenlegierungen Rolle spielen.

Acta Technica Academiae Scientiarum Hungaricae, 93 (1—2), pp. 127—143 (1981)

FLEXIBILITY DESIGN OF PIPING SYSTEMS**

PART I. THE TASK AND MEANS OF DESIGNING

F. KOLONITS*

CAND. OF TECHN. SCI.

[Manuscript received 11. May, 1981]

The paper gives a survey — mainly from the viewpoint of the piping of thermal power plants — over the most important methodological problems of piping design, considers the requirements subsequent to the modernization of structures and also the potentialities in the effective application of the computer technique.

1. Introduction

The problems of designing pipe networks as the means of transportation for conveying steam, gas, liquids or any other media to be considered as such, has become more and more complex, parallel to the technical evolution. The field of technologies, mainly that of the thermal generation of energy and chemical industry, requiring the transportation of a great amount of media of high temperature and pressure, has been extended and gained an ever growing significance. Besides the internal material transportation within the area of the works, creating connection between the main units of the plant and realizing the continuity of the working process this way, a steady growth of the significance of the pipings assuring the interconnection between the different works is also experienced. In this latter case, it is the pipeline itself which represents *the* main unit, however, also the pipings within the works might amount to the third or half of the value of the technological part, and 15 to 30 per cent of the total of the invested capital [1] and according to other estimates, even more [8].

As defined by the *technological process*, the design requirements are, in the first line, of dimensional, topological, hydraulic, and thermal character.

The principal production equipments of a given layout are to be connected by a piping through which the actual trace of flow needed at the different phases of working may be realized by making use of shut-off/bypass valves, and wherein the losses of heat and pressure remain within the limits defined by the process. However, these reqirements should be realized in such a way that the conditions of *safety* and *economy* should be satisfied. The safety, i.e., the requirement that neither the piping nor the

* Dr. F. KOLONITS, Cirmos u. 4, H-1112 Budapest, Hungary

** Report at the session of the Commission for Machine Construction of the Hungarian Academy of Sciences, held on 21st April 1980.

environment should be damaged, is a most significant one, all other conditions should be subordinated to the aspect of safety. The risk of damaging may have several potential forms depending on the applied technology, but in every case, the common general requirement of outstanding significance is the adequate strength of the piping elements.

In strength dimensioning, as a matter of course, is, in the first line, the forces acting on the pipes which should be taken into account but, to determine them, different investigations should be performed according to their fields of application. However, within the general problem a "common part" may be circumscribed which is characeterized, in general, by the effects created by the function of transportation of the media having temperatures and pressures which differ from those of the environment. The analysis is not restricted to the simple determination of the effects and their consequences on strength requirements: this is mainly the task of other disciplines, namely, that of the engineering mechanics. The strength dimensioning of the piping, besides the specialization of more general items of the latter and the simple summing up, contains a further element: all these are arranged in an appropriate approach with the view to determine and realize the dimensions and other characteristics of the piping. This is not only a chapter of the engineering mechanics (which even in itself is a part of the mechanics occurring in the engineering application, and accordingly its part which has been developed further to that end), but a "more engineering" mechanics which puts its practical use more into the foreground. The dimensioning beyond the more or less exact scientific fundamentals, is based on experiences and subjective invention to a considerable extent; surely the former does not show the way to be followed in connection with every problem in out days neither.

From among the different fields of application, maybe the pipings of thermal power plants are those, in connection with which these general problems mostly occur: in this aspect it may be considered as a model of "piping engineering" which, in the following, will be taken as a basis.

Hereafter, two aspects of the design problem of piping will be considered: in the present first part, the question, to what changes the increasing demands may lead in applying the current methods of designing, i.e., what tendencies are being in development in the current design practice in connection with the computer aided design (CAD) methods. In the second part which will just be based on these tendencies, a new method will be developed to one of the most intricate design calculation, i.e., the flexibility analysis of pipe networks.

2. The process and means of designing

2.1. General remarks

The initial conditions of design work are the knowledge of the actual functional requirements of the project to be realized, the materials at disposal for the construction, the potentialities in manufacturing/mounting as well as that of the nature of installation to be constructed. These are, as a rule, in actual cases the issues of the earlier projectorial decisions. Thus, to remain within our scope, it is given that certain tasks of transportation should conveniently be solved by as piping system (has been decided on, in that case where also an alternative would have presented itself, for example, an open channel), also the material of the pipes available and the technology of their manufacturing, the temperature and pressure of the medium to be transported are given. The task of the designer is to determine by consecutive decisions all of the parameters needed to the construction and working of the installation: the actual material, dimensions etc. and to integrate those into a system including all details, without inconsistency, i.e. into a project.

In making decisions, the designer has to follow the prescriptions of standard codes and other governmental regulations and it is at least advisable for him to keep the current status of science and technics in sight. It is a question of responsibility and ethics of the designer how and how much of that he uses in his design activities [2].

The "present state of knowledge and technics", beside various theoretical and empirical dependencies/formulae, does appear in form of principles, practical arrangements, etc. which can with difficultly, if at all, be defined in strict, say, numerical terms. The positive or negative experiences made with equipments installed earlier make up an essential part of it.

The design work is not of deterministic character at all, i.e., from the data at disposal at the moment of designing, one cannot draw a definite conclusion to all of the parameters to be prescribed for the equipment in question, for example, by solving a set of equations of several variables or an optimum problem. The knowledge to be used, even if it could be numerically fully formulated or expressed by algorithms, would result in a set of conditions which would be imperfect and contradictory at the same time, and, considering the computer time and hardware being at disposal, in general, also unsuitable for processing.

The traditional approach, due to the fully empirical character of the earlier knowledge as well as to the imperfection of the system of conditions, has obviously offered itself: instead of directly concluding from the given objective, the parameters of the equipment should be assumed and then to be check in a theoretical or experimental way. In case, where checking the conditions of major importance are found not to be fulfilled, the assumptions are to be corrected and checked anew, etc.

This procedure is, strictly speaking, a heuristic iteration or, much rather, a relaxation concentrated to the most dangerous negative possibility which, in the case

where the problem of the convergence, the uniqueness or completeness has been cleared, is quite equivalent to the direct method. Its application may also be motivated by the fact that the basic relationships are mostly of analytic character: from the parameters of the equipment the processes taking place in it may be concluded at.

The constructive, i.e., synthetizing deduction would be just in the reverse direction: which parameters are needed to eliminate or, on the contrary, to bring forth certain situations. In case of a simple relationship where the effect in question might be separated from the others, at least to a certain degree, this might be attained by due rearrangement. The wall thickness of the pipe may be calculated on the basis of the internal overpressure by transformation of the stress formula (the so-called boiler formula): against all other stresses, because of the character of the multiaxial stress pattern, this wall has a significant reserve. However, in general, such an inversion of the whole process of construction and even of each partial steps could only be carried out, if ever, with extraordinary difficulties or at least with very much labour.

In applying an iterative method taken in its accurate sense, the way of correction of the starting values is definitely prescribed depending on the deviation obtained in the course of checking. In the construction, the potentialities of such a prescription are rather restricted; the point in question may be rather that the tendencies of the influences of each factor should be made clear up by a series of investigations. The convergence criterion of the "learning algorithm" is the engineering feeling and the sensible taking risks of by the constructiong engineer. The same has a decisive role in the completeness of the solution. Even with problems of mathematically exact objectives, to which several solutions may be found, by assuming a starting value it has already been decided implicitly which of them will be obtained as a result, and the others may remain accidentally without consideration and, in addition it might occur that in case of a particularly disadvantageous assumption no convergence takes place at all. In case of the construction problem the "solution" is, in the space of parameters, a very intricate region, each point of that being a realizable construction and that may be narrowed down by further optimizing conditions if they have not been included a priori in to the set of conditions (however, as having fixed stiff prescriptions for optimizing in advance it quite often turns out that the result leaves much to be desired from other points of view). But, in the practice, for example, in designing the layout of the piping mostly it is only possible to arrive at a solution which satisfies all the conditions given, accidentally to analyse some variants; in general there is not time enough to do more, and still the risk exists, that much labour results only in a few improvements. Although with minor partial systems the labour requirement is less, nevertheless, it is necessary to adjust oneself to the other parts designed earlier or simultaneously, which reduces the manoeuvrability in designing. Eventually, the solution appearing in the drawings depends on the direction from where one enters into the said region of possible solutions; according to the commonplace of constructing engineers "that which is good enough, is good". And this is mostly decided by the primary assumption and by further ones which play a role in the modifications; but one can only assume what one had

already seen or what is imaginable on this basis. Among the set of the possible solutions one arrives to an element which, in a certain sense, is the nearest to the structures realized earlier; "in constructioning there is no leap" excepting the case of a particularly ingenious constructing engineer.

Making use of latest scientific issues or analytic methods does not necessarily lead to better constructions, only in that case where the designer, seeing his "risk-taking capital" partly relieved this way, reinvests it into a more daring assumption which utilizes better the appearing feasibilities; otherwise he can check a roman aquaduct even on a most up-to-date computer, it will not have another quality, as it was "quite good enough" in those times.

The construction adapting the scientific results will be a scientific construction only in that case where it permits, at least, in some partial stages a reduction of the subjective empirical character of the assumptions for the benefit of reconcluding from the objectives and conditions. This is not an inversion necessarily taken in the mathematical sense: if a calculation can be carried out more simply and more rapidly than a former one, the constructing engineer may survey more thoroughly the possibilities (at a given time and in the framework of given costs), among which also such may be found which for him had been unimaginable in advance.

2.2. The process of designing of the piping and the problem of compensation

Designing of pipe networks takes place in the framework of the general plan of the installation simultaneously with the other parts of the designing work, in continuous interaction with them. Accordingly, the designing work is divided into phases built upon each other as being developed by experiences made in practice. In the outset, in every phase, the decisions of the designers developed in different branches of the preceding phase are summarized and, if needed, coordinated, on the basis of which one proceeds with a new, more detailed assumption, and by new decisions one begins to a more concrete state of the system to be realized. The effects of the parameters to be determined later, should be preestimated. The essential content of each phase, besides the exigencies of the relatively independent investigation is also influenced by the actual organization, professional structure and the different traditions of different countries and firms [3].

The first phase of the actual designing work is the development of the *heat balance* (conceptual diagram of the technology). Here, the decisive factors are determined: the parameters of the boiler, turbine, etc. which means, in most cases, the choice of the type, maybe with some modification of a given type; all these largely define the construction of the diagram. The piping appears more or less as a hollow "black box" which is assumed not to affect parameters of the technology, or this effect is approximately taken into account by pre-estimating the loss of pressure and heat. As a result of the calculation of the diagram the quantities of media to be transported, the

temperatures and pressures are yielded which constitute the "basic initial condition" of the subsequent phase of the actual design procedure of the piping.

In the following, the places of the main equipments are designated and the architectural design begins. Simultaneously, the second phase of the designing, i.e., the development of the *diagram of the piping* (flow diagram) proceeds. In this work, by taking into consideration the assortment in material and dimensions at their disposal, the material, diameter and wall thickness of the pipes (or pairs of pipes in parallel, if necessary) realizing each transport line should be selected. The "conceptual" piping of the heat balance diagram will be drawn in details according to the actual requirements of the equipments and extended by further necessary collecting and change-over conduits. Thus, the topology of the pipe network will be worked out and the points of branchings and locking devices marked.

For the pipes the diameters should selected in such a way that the flow velocity of the medium should not exceed a given empirical value which limits the loss of pressure, and reduces the risk of an accidental occurrence of the phenomena of the water hammer. The dimensioning of the wall thickness takes place according to the standard procedure against the internal overpressure (with consideration to the strength of material at working temperature).

The next phase is the preparation of the *plan for the general arrangement*. Adjusting oneself to the building construction designed meanwhile, the actual layout of the pipe system should be shaped according to the system developed in the piping diagram; the thermal insulation should be prescribed and the positions of the pipe brackets (and anchors) designated. The load applied to the supporting system by weight should be determined (in general, without the calculation of the network, by approximate methods), the supporting structure should be designed or, to a certain extent assumed and the reaction forces/moments generated by the restrained thermal expansion, along with movements and stresses, should be calculated. In case where loads on both the pipes and accessories and the supporting system are acceptable, the drawings of the supporting structure should be considered as final. If needed, a calculation should also be made to check the flow and thermal conditions. Then the detailed construction drawings, the list of materials, etc., are to be prepared. In carrying out the work described above a continuous collaboration with the designing group of achitectures and electro-automatics engineers is needed.

Considering how the technical evolution affected the strength dimensioning, it could be stated that in case of the thermal power plants (and also of other works) both the applied temperature of the media to be transported and pressures as well as the unit performances have been increased. However, the former ones have attained for about two decades the level still acceptable with respect to gains vs. costs and from the region of the supercritical parameters, even a certain backing-down became necessary. The unit outputs and simultaneously the flow rates of the media have greatly increased. The effect of the temperature exerted on the material behaviour, the principles of a detailed stress analysis which became necessary, due to the higher stresses and more expensive

pipe materials, have been elaborated ans standardized [4]—[7]. Besides the necessity of a more detailed stress analysis, the increase in quantities and consequently of the diameters of the pipes has been calling the attention more and more to the flexibility analysis and dimensoning of the system. Although the problem might be solved by inserting special pipe components which may be deformed by applying relatively small effort, for example, using expansion joints which, however, due to the costs and other factors are not always practicable; mostly the trace itself ought to be formed in such a way that under the effect of forces applied to it, no loads damaging the pipes or their accessories might be created.

Let us see, where the stresses approximately do tend in case of pipes being thin-walled with respect to their diameter. In the said process of dimensioning the established *wall thickness*

$$s = \frac{Dp}{2\sigma_m} \tag{2.1}$$

where

p — internal pressure,
D — mean value of diameter,
σ_m — stress permitted in dependence on temperature,

increases with every tendency mentioned above. The bending moment induced by the *dead and live load* on the piping may be estimated as $ql^2/10$ [8], where q is the specific weight per meter and l the mean span (distance between supports). Leaving the pipe insulation out of consideration, the bending stress

$$\sigma_s = \frac{l^2}{D}\left(0{,}4\rho_c + 0{,}2\frac{\sigma_m}{p}\rho_t\right)g \tag{2.2}$$

(ρ_c being the density of the pipe material and ρ_t that of the medium transported), was a decreasing tendency and may be influenced, independently of other factors, by the span.

The order of magnitude of thermal dilations is, in case of a characteristic length L, a coefficient of thermal expansion α and working temperature t (setting for simplification 0 °C for the temperature of assembling), $L\alpha t$; the reacting forces induced deform the system to this extent. A reacting bending moment (or force) causes a deformation $c_a(L^n)/IE$ of the pipe,

where

I — moment of inertia of pipe cross section,
E — Young's modulus of elasticity
c_a and n — values depending on the form of the trace of piping and on meaning of deformation and reaction (rotation or displacement; in case of this latter $n \geqq 1$).

The reaction force/moment induced is:

$$P, M = \frac{\pi}{8} D^3 s \frac{L}{c_a}(E\alpha t) \tag{2.3}$$

provided, as a matter of course, the trace not being a straight line from a fixed point to another fixed point which would result in extremely high stresses in the axial direction, but lateral displacements could take place generating bending moments, the compensation stress (being considered as a bending stress) is

$$\sigma_k = \frac{1}{2} D \frac{L}{c_a} (E\alpha t) . \tag{2.4}$$

The values of E and α decrease or increase with the temperature; the product $E\alpha t$, mainly in case of austenitic materials, increases. It may be stated that the evolution tends to increase both the reactions and the stresses.

The increase in wall thickness which is an efficient solution for resisting the internal pressure, is here ineffective or even disadvantageous, merely the reduction of the value of the quotient L/c_a, i.e., applying a more flexible trace, may be expedient. The latter is commonly known by the construction engineers, while the former might be experienced.

But, from the aforesaid the recognition that the ratio of the reactions and stresses is proportional to $D^3 p/\sigma_m$, may also be concluded which means that it is vigorously increasing. As a consequence of the growth of the parameters and outputs, the main equipments become less "monolithic" and mostly the rotating machines become more and more sensitive to the external loads. Therefore, the manufacturers delimit the load and moment permissible at the attachments, and at this juncture, it is very likely that the limits constitute relatively ever more severe conditions. Consequently, the situation already experienced in practice, took place necessarily: that the reaction forces and moments constitute a keener demand than the strength of the pipe.

According to appearance, both problems are alleviated by prestressing the pipes in cold state (cold spring) by the eth of the thermal expansion (which encounters great difficulties when carrying it out to perfection) and the reaction appearing at the initial hot state, will be reduced to the value $(1-e)R$. In the cold state the reaction eRE_h/E_m will be generated and also the stress pattern will be proportionately developed, provided no plastic deformation takes place. However, the strength of the pipe is evaluated by the most up-to-date prescriptions on the basis of the entire range of changing of the compensation stresses, thus, permitting theoretically the self-prestressing of the piping by a single plastic deformation called in other fields of technics "self-adjustment" [9], [10], which could have been only anticipated by a cold spring. With respect to the reacting forces, the manufacturer mostly limits the cold state also, often with obligatory consideration of 100 p.c. relaxation. The initial hot reactions may indeed be reduced below the limiting value by prestressing until the cold reactions are permissible; however, the increase of the latter is larger in proportion to the moduli of elasticity than the decrease in the former. The entire relaxation means, in connection with the cold state, that RE_h/E_m (E_h and E_m being the moduli of elasticity in the cold and

hot state respectively) takes place regardless of the prestress applied earlier which can only be influenced by the elastic layout of the system.

In the main steam ranges of the thermal power plants built in recent years in Hungary, all these tendencies have obviously appeared. The reaction limits of the turbine has practically excluded the prestressing and the flexibility needed and could be ensured by spatial expansion loop-like layout only by a long trace unexploited in itself from the point of view of stresses, and, considering the possibility of the arrangement, loss of pressure and costs, could only unfavourably be realized. Therefore, the designing engineer (János FEKETE, ERŐTERV) made use for the starting of a trace which has a reserve strength but was not extremely overdimensioned, then, at a convenient point and direction obtained through a series of calculations, fixed the pipes to the supporting structure.

The pipe supports of the type "Daru" with constant and adjustable load support characteristics permitted the independent handling of the loads from weight and of those from the restriction of the expansion of the piping and/or the modification of the loads. Thus, the reduction of the reaction forces/moments initially of high value succeded to the permissible level. All these did not affect the arrangement of the piping; meanwhile the preparation of working drawings and fabrication could be continued which, however, involved some risk, but was also time saving [11], [12], [13].

2.3. Potentialities in applying computers

The engineering design work was based, two decades ago, from the viewpoint of calculation technique on the slide-rule and graphical procedures and by making use of these appliances on the base of "at most one-inch formulae" as it was a commonplace, and, although the said appliances appear to be obsolete in our days, yet the tasks have been often rather ingeniously solved. Theoretical results had to be utilized in such a form and to such a limit that they could be controlled on this basis. The calculation work at large was not separated, a divison of labour appeared at most within the design group. The main instrument, the slide rule, in spite of the different variants appearing from time to time, plays its role in an accomplished type though slightly differing according to each special field of use, its handling and practical tricks were a part of the "basic training" in engineering instruction.

The rapid evolution in the field of computer technique created a new state of affairs and nowadays it has become evident that to utilize the potentialities and to satisfy the ever growing demands, the analysis on the basis of the new aspects of the designing work is necessary [14]. The changes in the instruments involve a change in methods and objectives, besides they require appropriately instructed personnel in a suitable organization. This problem has already a great past in another field, i.e., in the field of military science [15]: it is very interesting that the categories and terminology developed by it how frequently been applied to "civil life". In the designing

organization it was the computer whereby a "general change of armament" took place for the first time. Initially, the new instrument was used as a new, more efficient variant of the old one, for the purpose and in a way pertaining to it (as the "horse" power in the car shaped as a horse-drawn coach). Then, it turns out that it is capable of larger and other performances and will be differentiated by the opening of the potentialities. By production becoming less expensive and by the extension of the expertness needed in its handling, the mass application begins. The most convenient ways for making use of the new instrument and the development of suitable organizations gradually takes place.

The computerization has now got to about the middle way of the above process. It is of basic significance in the differentiation that the economical tendency, known as Grosch's Law, in conformity with which the small tasks should be collected and to be processed on a large computer in a "partial" time", has been altered, in these days, the use of a computer fitted to the size and conditions of the problem is considered to be economical [16], [17]. Earlier, *large computers* were developed requiring special qualification in their handling and operated at separate centres, whose working order assured the most complete possible utilization of the machine. They cannot be adjusted necessarily to the work of a designer, its use involves intermediators, and a rather strict administration. Though the Hungarian experiences with terminals are rather sparse (mainly due to the demands in expenses), they can only assure a partial modification in connection with the relations mentioned above. In contrast with the large ones, due to the more moderate cost and requirements in handling, the *desktop computers* are eligible for the use of certain design groups/units. They should not be estimated by only taking their degree of utilization into account, but in connection with the performance of the unit being associated with it: it is to be deemed, what a surplus may be obtained from its being permanently and immediately at disposal, i.e., from integrating it into the design work according to actual demands. As personal instruments the slide rules have been replaced by the *pocket calculators* some types of them being already in circulation have realized the technical minimum required for this changing (elementary functions; carrying out short operations without reading-off intermediately). Anyway, the bringing of further improvements deserves special attention because in the design work such sections always remain where the heuristic and numerically definable elements enter into working, in making decisions, "in short bursts or as aimed single shots". A rather large part of the mass-production types of the so-called "programmable" computers are only "pseudo-programmable" units [18], at any rate, the manual input of the program is, in each case, necessary which practically excludes the application of the pre-established algorithms without knowing the details. In addition, the up-to-date storages are "volatile", i.e., by switching off they are cleared. The pocket calculator with a magnetic card which "with pre-loaded ammunition may be put immediately into operation" is to-day a rather expensive but at the time they were begun all types of the pocket calculators were rather expensive. The standardization and development of types which, from the point of view of lucidity and ergonomy, are equivalent to the slide-rule [19], gains an ever-growing momentum. All in all, the general use has begun,

although the desk computers being hardly available in Hungary, constitute a bottle-neck for the computerized design work.

As to the personnel, it is specific in our days that the proportion of engineers and technicians has become notable who have adequate practice and had obtained even their basic qualification with the possibilities of the computer technique in mind, they have not got instructions built upon only the traditional way of processing. On the organization level this generation is now standing "before the gates" in the low-level leadership with all the subjective and objective difficulties of that situation. At any rate, also on this side the possiblity has increased that the computer technique, where it seems to be advisable, should be directly connected to the design organization and after "being expulsed from the paradise of the computer room" the direct contact should be re-established in a new way. Otherwise, this new prospects are stimulating to the "enthusiastic amateurism" which may be estimatedly valuable [16].

The paper [14] considers the general machine construction on similar premisses as discussed in paragraph 2.1. of the paper, according to the phases of forming the conception, design and elaboration. In the design phase the computing work proper is specified (within this, checking, dimensioning, thus "partially inverted" algorithms, and the optimizing ones which realize this work on a higher level), the storage of information and the process of shaping the construction. By considering the "*batch*" (automatic, beginning with the information up to the end result) and *interactive form* (permitting to insert the heuristic decisions of the designer into the computing process) of the use of the computer, proposes development trends according to the possibility of algorithmization of the phases. In the more specified field of the present paper a possibility offers itself to an analysis which also considers the details of the problems, organization and availability of the computers. The development of the comprehensive conceptional decisions and heat balance scheme are excluded from the considerations because they are rather more the preliminaries and not parts of the design of piping. From the point of view of our considerations, it is only significant that due to the great amount of information, in the present hardware situation they can be considered almost exclusively as being solved by using large computers, which means, that the group carrying out the designing work is necessarily in close connection with a computer centre. It is recommendable to investigate the form of the use of the computer and the possibility of algorithmization of the design phases by beginning with the character of the interruption of the computing process. A series of calculations which can essentially be considered as a process, exceeding the mechanical calculation using formulae, is only possible in the case where the decisions depending, in a deterministic way, on the results of those calculations, might be carried out within the computer; this is which makes the difference between the computer being programmable and that the pseudo-programmable. In a limited part of the cases some major problems relatively separable in the design can be more or less directly programmed, the computer work is directed to the final objective. Due to the extent of the demand on time and storage, for this purpose, in general, a large computer is needed which, with respect to a man-

machine relation is, at the same time satisfactory because the operation in question, as a whole, has gotten out of the human process of design. Later on, the results will meet in laying foundations for the next phase, those of other parallel design procedures; the general rate is defined mostly by the latter. In such cases, the interruption of the computation is *complete;* the program, data and results will either be put out or cancelled.

If it is possible to interrupt the program partially, i.e., to suspend the run in a given situation, then, non-self-determined decisions i.e. depending on an earlier different calculation or a heuristic one may be carried out, thus lengthening the computation process bounded by the complete interruption. The partiality implies to have degrees which means, what amount from the actual program information should be conveyed to the operator for making a decision and, that his decisions will affect the program to what an extent. The technique demanded may involve a variety of things from the digital output to colour-display or from press-button to light-pencil, and the presence of the designer is needed meaning a desk-computer or a terminal. In case where the cost of these exceeds the amount which might be gained by the more rapid satisfaction of the real demands of design, invariably the batch mode of operation should be preferred. The category of the computer is dictated by the simpler handling of the great amount of data of the repeated computations remaining of "encircling character".

The desk computers from their very nature have both some technical possibilities of interactive use and organizational ones of a direct contact with the designer. Regarding labour organization it is the better, the less they have a character of a "local computer centre". Although the professional program-development and algorithmization require the application of specialized collaborators; their interestedness, however, should be associated with the performance of the organizational unit attended. It is reasonable to draw in the designers to the work of establishing the programs, and mainly, into an intermediate evaluation during the run as closely as possible and, in the first place not in the framework of a "formal" working connection, but in a kind of a mutual consultation [20]. All of these can be realized in case where, using Parkinson-like formulation, the *rank of the lowest common chief of the designers and the computer centre is the lowest possible.*

Thus, after viewing the problems of the design of piping, it might be stated that first, in the phase of collection and classification of the informations and processing of an enormous amount of information is needed; none the less, the assembly of the different lists, call for tenders, estimates on costs, etc., also requires a good deal of manual labour. In the framework of this activity, in the case where the viewpoints of the normative selection are known, also certain problems of strength dimensioning might be solved [21]. With respect to capacity, a large computer is needed, however, the development of the storage capacity of the desk-type computers makes application of these possible in the near future.

The work of piping construction involves, mostly in close connection heuristic and algorithmic problems and the ones which appear and/or are to be solved in drawing, so that neither a theoretical possibility is offered to the complex mechanization, at least, before achieving a significant development of the drawing-digitalization technique. Among the partial problems able to be defined numerically, from the point of view of the demand on capacity and complexity, one could consider the flexibility design of piping as a representative and attainable maximum. The most part of the rutine design analysis is not more than checking the strength and flow conditions which can be carried out by making use of a pocket calculator of higher quality. A wider application of complex algorithms, a more expressed dimensioning character instead of checking might only be expected in a case where a program stored to a magnetic card is given to the designing engineer, which may be utilized by concentrating his attention directly on the objective without his knowing details and without delay. Even in the case where it would be purposeful and possible to organize in large interactive programs such series of calculations, it is not likely that their demand on capacity exceeds those of the flexibility calculation. The same could be stated in connection with other (for example, hydraulic) network analysis problems.

As a matter of course, also such problems might occur which exceed the attainment of this standard. Such is the general structural analysis of piping which is, considering its principles, identical with the flexibility analysis, but taking into account the weight, the accidental wind load and other effects. The growth of mass-flow rates, the less strongly-built and less material-consumptive structures, the reduction of the risks of effects sofar considered as vis-major nature, as for example, earthquakes and others, create more intricate problems of vibration and hydrodynamics. But, these investigations, for the time being, partly due to the objective and subjective limits of designing, partly to the accuracy attainable under the actual conditions of the erection, cannot be considered as the integral part of the to-day's up-to-date design work on such a level. If, considering the circumstances, it were necessary, it is carried out by expert groups, to a certain extent separated from the design apparatus, as a final checking. For the actual construction, these investigations may be carried out in the form of simplified formulae or principles which increase the chances of this final checking (a typical case is, for example, as the dead weight is taken into account in spacing the supports of the piping).

The demand for analysis emerges in two forms in designing. There are lines constituting the greater part of the piping system which, due to their relatively lower temperature and size, do not represent a significant risk from the point of view of compensation; a greater problem is the lack of space in the arrangement of the layout, being an ever troublesome question, in the construction of pipings, to avoid collisions and to permit their easy supervision, to handle their armature—they must accomodate themselves to the actual local conditions. On the other hand, there are pipings to be considered as main equipments with heavy loading and, therefore, requiring a careful construction and manufacture/erection—they reasonably require accommodation

from other elements (in power plants there are the so-called high-pressure lines, the pipes of steam mains, high-pressure preheaters and feeding systems).

The traces of both categories are constructed on the drawing board of the designing engineer of the layout: considering its character it is a heuristic decision or assumption. A more theoretical basis (established by calculation) taking the to-day's technical conditions into account, would hardly be imaginable. Considerations mostly qualitative or proportional of the compensational proprieties of simpler, for example, L, Z and loop-like configurations, but mainly of the size conditions of earlier arrangements and the experiences of the designing engineer motivate these decisions. Skilled designing engineers arranging layouts "feel" in a remarkable way the requirements of compensation. According to the [5] the detailed formal calculation of the pipe section between two fixed points, otherwise not hindered in heat expansion may be omitted if

$$DY/(L-Q)^2 \leqq 2{,}08 \cdot 10^{-4} \tag{2.5}$$

wherein:

D = diameter of pipe,
Y = total heat expansion to be taken into account,
L = developed length of trace,
Q = distance between fixed points.

In a series of existing piping systems, the author has investigated, as an example, although by freely defining the conditions of application, the fulfilment of (2.5), and it seems that it marks, although with a large scattering, by and large the "mean value" of the designer's estimate about adequate flexibility (the formula being otherwise to be defined according to [9] as an envelope of calculations for simple configurations). Into the estimation by experiences, gained in practice, also such details as the material of the pipe applied, stress concentration in curved sections of small radii might be drawn in, however, as a matter of course, in an ever uncertain, subjective way.

In the general category, the flexibility analysis is final checking commonly yielding positive results. The enforced accommodation, keeping distance from main equipments, anyway, increases the built-in length, the material of the pipe does not much expressively demand, from the economical point of view considering the enormous volumes, a tighter design for which no time is at disposal.

Checking might be separated from designing; for "assembly-line" processing of the great quantities of data, the adequate peripherials are available, in general, at large computers.

It is a quite a different case with the high-pressure piping: the necessary rigorous fulfilment of the conditions, particularly in the case of the permissible reaction forces, which in the category above mentioned do not occur at all, in general, goes beyond the "resolving power" of the constructing engineer's rules of thumb. Carrying out the analysis for several variants of trace is possible and reasonable from the point of view of economy. In choosing a primary trace, to begin with, besides the aspects of the material consumption and loss of pressure also the reserve in strength and the possibilities of

intervention should be preliminarily investigated; "braking" with anchorages might be designed on the base of a series of calculations made with systematic changing a relatively few input data. The procedure is, as a whole, heuristic. The ways of correction may be estimated on the basis of the character of the displacements of the branchings: anchorage or displacement limiting stop induces opposite reaction force which also modifies the reaction forces to be restrained. It is probable in the remaining parts of the pipe, in comparison with the unbraked state, a surplus of stress is caused because the supplementary restrains "redistribute" the deformation, sections far from the critical points constitute a set of forces partly equalizing each other; it is here, where part of the entire deformation of the pipe greater than the earlier will be realized, and the reactions at the spots to be protected will have a lighter task; therefore, it is advisable to retain an adequate reserve of strength for the procedure. If, say, the legs of an expansion loop placed into a straight section will be bound to each other by rigid bars and hinges, such a position could be selected near the head of the loop where the loop compensates the heat expansion of the straight pipe, that no axial force will be present at the fixations but on the other hand, at the head-part of the loop the stresses significantly increase. The legs of the loop making a lever-like rotation around the hinges will equalize the heat expansion of the head and base straight lines. A study of simpler configurations may give rise to thoughts for the solution of more intricate, space problems. At any rate, the present state of affairs makes it inevitable for the continuous collaboration between the machine and designing engineer. Therefore, in spite of the fact that many effective piping analysis programs are available, it proved to be recommendable by the revision of the familiar bases to work out such an algorithm which might be realized by a desk computer. This will be discussed in the next part of the paper (to be published later): it succeeded to reduce the space requirement of the calculation; the evolution of the demand on time is not unambiguous, however, neither is it unfavourable.

The process has been realized on the comparatively small desk computer of the type 8kB-EMG and continually applied for the design work of the Design Institute ERŐTERV. In the present days, the computation in connection with designing the construction of the nuclear power station in Paks and, directed by János FEKETE, with the design of the mains of steam for the Finnish power plant of Salmisaari. According to the experiences obtained, the adoption of the type mentioned above is rather more a pilot-scale experiment which has verified the potentialities of the method. The input of the geometrical data of the trace from the keyboard is troublesome and involves possibilities of errors; owing to the low capacity, the segmentation of the program became necessary, the one and single cassette tape unit which might be considered as a background store is too slow and can only be reached circumstantially as compared with the requirements newly arisen and, in addition, the safety of operation at given volumes does not make advisable the application of an automatic overlay theoretically realizable. Nevertheless, it should be taken into account that these are the limits of the desk computer made in Hungary for a decade or so. Using desk computers

systematically for the design of piping is by all means considered as justified is also due to other problems to be solved in the designers' collaboration or under their supervision. In selecting the type, in the first place, the general safety of operation, the reliable background stores of adequate capacity and an input peripherial permitting the non-keyboard-input of at least basic variations should be considered as a decisive factors. From the point of view of data-supervision and interactivity, the graphic output i.e. plotter is favourable and a hard-copy output periphery results presenting in "deliverable quality", saving retyping, is necessary. The demand on operative storage also grows for the very reason of the dead weight investigation recommendable with system analysis in case of high quality pipings. Nevertheless, the tendency is limited by the fact that the large piping systems occurring in practice are fixed at several points, due to construction motives, thus, the system due to be calculated as one unit does not attain an extreme magnitude (that is why one can be satisfied with the desk type). The efficient input peripheries and mass-storage equipments also permit the series calculations and, furthermore, handling of keeping-in-evidence and data-processing work on the spot. The above requirements may be satisfied in our days with the desk computer types available in a large scale.

A further development would be to work out a more favourable and reliable theoretical basis for the assumption of trace of piping. This could be tried but by the transformation of (2.5) to the length L of the pipe to be laid between the fixed points or, on a more exact base, by the investigation of the relationships of the matrix and vector values of flexibility analysis expressed in terms of their scalar norms permitting scalar estimates in this way. In addition to supporting current work this would largely foster the evolution of the automatizable design processes.

REFERENCES

1. PERRY, J. H. (Editor): Manual for chemical engineers, Műszaki Könyvkiadó. Budapest 1969*
2. SVÁB, J.: Ethical Concerns of Engineers' Risk Undertaking, *Gép* **30** (1978), pp. 201—202*
3. HIRSCH, E.: Piping in Power Plants, Műszaki Könyvkiadó, Budapest 1959*
4. GOSGORTEKHNADZOR USSR—Calculation Norms for the Strength Design of Elements of Reactors, Steam Generators, Vessels and Pipes in Nuclear Power Plants, Experimental and Research Reactors and other Installations, *AEEBF*, Budapest 1974*
5. ANSI B31.1 (Power Piping) 1967—73
6. ANSI B31.7 (Nuclear Power Piping) 1969—71
7. TGL 22160/01—07, Rohrleitungen aus Stahl, Festigkeitsberechnung, Nov. 1975
8. KELLOGG Co.—Design of Piping Systems, Wiley, N. Y. 1956
9. MARKL, A. R. C.: Piping-Flexibility Analysis, *Trans. ASME* **77** (1955) 2, 127—149
10. KALISZKY, S.: Theory of Plasticity, Akadémiai Kiadó, Budapest 1975
11. FEKETE, J.: Strength Problems of Steam Mains *Energia és Atomtechnika* **17** (1964), 221—226*
12. FEKETE, J.: Untersuchungen der elastischen Formänderung von Rohrleitungen und Rohrnetzwerken, *Fortschr. Ber. VDI*, R. 7 Nr. **5**, Juli 1967
13. FEKETE, J.: Significance of Designing Steam Mains in Hungary. *Publishings of the ERŐTERV* **12** (1975), 69—73*

* In Hungarian.

14. VARGA, L. and collaborators: Design-theoretical Problems in Machine Designing by Computers. *Gép* **31** (1979), 416—421
15. BAGRAMJAN, I. H. (Editor): History of Wars and War Art, Zrínyi Könyvkiadó, Budapest 1975*
16. MÜNNICH, A.: Microcomputer Revolution, *Számítástechnika* **9** (1978), *11*, p. 14; *12*, p. 7.*
17. BARTHOLD, L. D.: Software Products for Electric Power Systems. Lecture in the Hungarian Electrotechnical Association, Nov. 30, 1977
18. —ÁL—: How to Purchase Pocket Computer? *Számítástechnika* **9** (1978), 12*
19. GERLE, GY.: Funeral Sermon on a Devoted Fellow-Worker, *Műszaki Élet* **34** (1979), 17 (Aug. 24.)*
20. WEINBERG, G. M.: Psychology of Computer Programming. Közg.—Jogi Könyvkiadó, Budapest 1979*
21. VEGYTERV—Computerized Methods of Diping Design, Programdokumentációk (07655 üi. sz.) 1978—79. Budapest*

Elastische Planung von Rohrsystemen. — Die Abhandlung gibt — hauptsächlich aus der Sicht der Kraftwerkrohrleitungen — eine Übersicht über die wichtigsten Probleme der Planungsmethoden von Rohrleitungen und untersucht die sich aus der Modernisierung der Konstruktionen ergebenden Ansprüche und über die wirksame Benutzung der Rechnungstechnik.

* In Hungarian

Acta Technica Academiae Scientiarum Hungaricae, 93 (1—2), pp. 145—152 (1981)

TWO-DIMENSIONAL SUBSONIC FLOW OF A COMPRESSIBLE MEDIUM

J. HIDASI*

[Manuscript received 26. May, 1981]

The nonharmonic potential—and stream functions of the isentropic, subsonic flow of compressible medium are presented as functions of the density of the medium and by means of harmonic potential—and stream functions. By expressing also the density, by making use of a harmonic function, in determining the velocity-components, expressions are obtained, which are formed only by harmonic functions.

Notations

The following symbols are used in this paper

φ, ϕ— potential functions
ψ, Ψ— stream functions
c_x, c_y— absolute velocity-components
c— absolute velocity
ρ— density of medium
ρ_0— density corresponding to static condition
a_0— sound velocity corresponding to static condition
κ— adiabatic exponent
ϑ— harmonic function
f_1, f_2— functions depending on H
c_1, c_2, k_1, k_2— integration constants, arbitrary terms

1. Introduction

The calculation of the two-dimensional subsonic flow of compressible isentropic medium which is one of the significant problem of the gasdynamics, leads to nonlinear partial differential equations. Due to the coefficients of an intricate structure, in solving the equations in all cases difficulties are to be met, wherefore, the approximate solutions are gaining a great significance.

The great majority of the approximate solutions is based on the linearization of the descriptive equations. The results yielded by the linearized assumptions may frequently be applied with satisfying success. Problems may be treated successfully, wherein, for example, the local components of the velocity only slightly differ from the velocity-components of the undisturbed flow.

The problem can be treated without approximation (linearization) in an exact way according to [1]. Some of the characteristic features of the method are as follows:

* János Hidasi, Somogyi Béla út 14, H-8400 Ajka, Hungary

The essential is that starting point from a given incompressible flow, the corresponding compressible flow can be determined in an iterative way directly on the plane of the flow.

The potential—and the stream functions of the flow are expressed as a function of the density of the medium and by the use of harmonic functions and their derivatives selected in conformity with the boundary conditions. By deriving the potential and stream functions, expressions are yielded, which are suitable for the calculation of the velocity-komponents. The first step of the iteration is to take the components of velocity corresponding to the incompressible flow and satisfying the boundary conditions.

In the region of the procedure described in paper [1] a further step may also be that the density is formed by a harmonic function, and the potential—and stream functions are produced by the density and only by harmonic functions (without making use of their derivatives).

2. Governing equations on the plane

The system of the differential equations of the two-dimensional subsonic, irrotational flow of the compressible medium are constituted by the continuity and the equation of the flow free from vortex as well as Bernouilli-equation for isentropic flow:

$$\frac{\partial}{\partial x}(\rho c_x) + \frac{\partial}{\partial y}(\rho c_y) = 0\,, \tag{1}$$

$$\frac{\partial}{\partial x} c_y - \frac{\partial}{\partial y} c_x = 0\,, \tag{2}$$

$$\frac{\rho}{\rho_0} = \left[1 - \frac{\kappa - 1}{2}\left(\frac{c}{a_0}\right)^2\right]^{\frac{1}{\kappa - 1}}. \tag{3}$$

The potential and stream functions may be defined on the basis of Eqs (1) and (2):

$$c_x = \frac{\partial \varphi}{\partial x}\,, \qquad c_y = \frac{\partial \varphi}{\partial y}\,, \tag{4}$$

$$c_x = H\frac{\partial \psi}{\partial y}\,, \qquad c_y = -H\frac{\partial \psi}{\partial x}\,, \tag{5}$$

$$H = \frac{\rho_0}{\rho}\,. \tag{6}$$

Replacement of the expressions (4), (5), (6) into Eqs (1), (2) and carrying out the possible reductions and operations yields the relationships

$$\frac{\partial^2\varphi}{\partial x^2}+\frac{\partial^2\varphi}{\partial y^2}=+\frac{1}{H}\left(\frac{\partial H}{\partial x}\frac{\partial\varphi}{\partial x}+\frac{\partial H}{\partial y}\frac{\partial\varphi}{\partial y}\right) \tag{7}$$

$$\frac{\partial^2\psi}{\partial x^2}+\frac{\partial^2\psi}{\partial y^2}=-\frac{1}{H}\left(\frac{\partial H}{\partial x}\frac{\partial\psi}{\partial x}+\frac{\partial H}{\partial y}\frac{\partial\psi}{\partial y}\right) \tag{8}$$

i.e., the descriptive equations of the potential and stream function of the flow. Herewith, the solution of the system of differential equations consisting of Eqs (1), (2) is reduced to the determination of the functions φ, ψ, defined by (4), (5) and satisfying Eqs (7), (8).

3. Production of functions φ, ψ by means of harmonic functions

Eqs (7), (8) are second-order partial differential equations independent of each other and have such forms that nonlinear additional terms enter into the Laplace-equation. The most frequently applied method for the solution of the partial differential equations is the Fourier-method. Let us try to find the solution of Eq. (7) according to the method mentioned above using the Fourier-form

$$\varphi=f_1(H)\Phi\,, \tag{9}$$

and in this way to reduce the problem to that of the solution of a linear equation. The nonharmonic potential function of the flow should be formed by a harmonic potential function with the aid of the density function.

In order to determine the function $f_1(H)$ let us produce the first and second derivatives of φ:

$$\frac{\partial\varphi}{\partial x}=\frac{df_1}{dH}\frac{\partial H}{\partial x}\Phi+f_1\frac{\partial\Phi}{\partial x}\,,$$

$$\frac{\partial^2\varphi}{\partial x^2}=\left[\frac{d^2f_1}{dH^2}\left(\frac{\partial H}{\partial x}\right)^2+\frac{df_1}{dH}\frac{\partial^2H}{\partial x^2}\right]\Phi+2\frac{df_1}{dH}\frac{\partial H}{\partial x}\frac{\partial\Phi}{\partial x}+f_1\frac{\partial^2\Phi}{\partial x^2}\,,$$

$$\frac{\partial\varphi}{\partial y}=\frac{df_1}{dH}\frac{\partial H}{\partial y}\Phi+f_1\frac{\partial\Phi}{\partial y}\,,$$

$$\frac{\partial^2\varphi}{\partial y^2}=\left[\frac{d^2f_1}{dH^2}\left(\frac{\partial H}{\partial y}\right)^2+\frac{df_1}{dH}\frac{\partial^2H}{\partial y^2}\right]\Phi+2\frac{df_1}{dH}\frac{\partial H}{\partial y}\frac{\partial\Phi}{\partial y}+f_1\frac{\partial^2\Phi}{\partial y^2}\,.$$

By replacing derivatives, presented above, into Eq. (7), after reduction one obtains

$$f_1\left(\frac{\partial^2\Phi}{\partial x^2}+\frac{\partial^2\Phi}{\partial y^2}\right)+\left(2\frac{df_1}{dH}-\frac{1}{H}f_1\right)\left(\frac{\partial H}{\partial x}\frac{\partial\Phi}{\partial x}+\frac{\partial H}{\partial y}\frac{\partial\Phi}{\partial y}\right)+$$
$$+\Phi\left\{\left[\left(\frac{\partial H}{\partial x}\right)^2+\left(\frac{\partial H}{\partial y}\right)^2\right]\left[\frac{d^2f_1}{dH^2}-\frac{1}{H}\frac{df_1}{dH}\right]+\frac{df_1}{dH}\left[\frac{\partial^2 H}{\partial x^2}+\frac{\partial^2 H}{\partial y^2}\right]\right\}=0. \tag{10}$$

Eqs (7) and (10) may be correlated to each other in the case where the problem will be reduced to the solution of the system of differential equations consisting of equations

$$2\frac{df_1}{dH}-\frac{1}{H}f_1=0, \tag{11}$$

$$\frac{\partial^2\Phi}{\partial x^2}+\frac{\partial^2\Phi}{\partial y^2}=0, \tag{12}$$

$$\frac{df_1}{dH}\left(\frac{\partial^2 H}{\partial x^2}+\frac{\partial^2 H}{\partial y^2}\right)+\left(\frac{d^2f_1}{dH^2}-\frac{1}{H}\frac{df_1}{dH}\right)\left[\left(\frac{\partial H}{\partial x}\right)^2+\left(\frac{\partial H}{\partial y}\right)^2\right]=0. \tag{13}$$

The differential equation (10) describing the flow, disintegrates into three independent equations.

The solution of the first order ordinary differential equation (11) may easily be determined, using the relationship

$$f_1=c_1\sqrt{H} \tag{14}$$

and Eq. (9) the potential function of the flow may be established:

$$\varphi=c_1\sqrt{H}\,\Phi. \tag{15}$$

Deriving Eq. (15) results in the expressions serving for the calculation of the components of velocity:

$$c_x=\frac{1}{2\sqrt{H}}\frac{\partial H}{\partial x}\Phi+\sqrt{H}\frac{\partial\Phi}{\partial x}, \tag{16}$$

$$c_y=\frac{1}{2\sqrt{H}}\frac{\partial H}{\partial y}\Phi+\sqrt{H}\frac{\partial\Phi}{\partial y}. \tag{17}$$

The stream function ψ may be written in the form

$$\psi=f_2(H)\Psi \tag{18}$$

which is similar to that of φ. Without detailing the calculations:

$$f_2 = \frac{c_2}{\sqrt{H}}, \tag{19}$$

and the stream function:

$$\psi = \frac{1}{\sqrt{H}} \Psi . \tag{20}$$

4. Production of the inverse function H of density distribution by means of harmonic function

In conformity with Eq. (13) the inverse function of the flow H cannot be arbitrary; only cases characterized by such density distribution may be treated which are solutions of the equation.

Following the order of ideas treated above, also the function of solution of Eq. (13) should be established by means of some harmonic function ϑ; the arbitrary choice of the harmonic function permits the arbitrary approximation of the function H.

Producing the derivatives of the relationship (14) one obtains

$$\frac{df_1}{dH} = \frac{c_1}{2\sqrt{H}}, \qquad \frac{d^2 f_1}{dH^2} = -\frac{c_1}{4H\sqrt{H}},$$

$$\frac{d^2 f_1}{dH^2} - \frac{1}{H}\frac{df_1}{dH} = -\frac{3c_1}{4}\frac{1}{H\sqrt{H}}$$

and by replacing, one has:

$$\frac{\partial^2 H}{\partial x^2} + \frac{\partial^2 H}{\partial y^2} = \frac{3}{2H}\left[\left(\frac{\partial H}{\partial x}\right)^2 + \left(\frac{\partial H}{\partial y}\right)^2\right]. \tag{21}$$

In the form slightly differing from the expressions (9) and (18)

$$H = H(\vartheta) \tag{22}$$

let us try to find the conditions on the basis of which the solution of Eq. (21) may be carried out according to (22)*.

* Other possibility is when: $\vartheta = \vartheta(H)$.

In order to determine the function H let us produce its derivatives

$$\frac{\partial H}{\partial x} = \frac{dH}{d\vartheta}\frac{\partial \vartheta}{\partial x},$$

$$\frac{\partial^2 H}{\partial x^2} = \frac{d^2 H}{d\vartheta^2}\left(\frac{\partial \vartheta}{\partial x}\right)^2 + \frac{dH}{d\vartheta}\frac{\partial^2 \vartheta}{\partial x^2},$$

$$\frac{\partial H}{\partial y} = \frac{dH}{d\vartheta}\frac{\partial \vartheta}{\partial y},$$

$$\frac{\partial^2 H}{\partial y^2} = \frac{d^2 H}{d\vartheta^2}\left(\frac{\partial \vartheta}{\partial y}\right)^2 + \frac{dH}{d\vartheta}\frac{\partial^2 \vartheta}{\partial y^2}.$$

Replacement of the above results into Eq. (21) yields the following relationship

$$\frac{dH}{d\vartheta}\left(\frac{\partial^2 \vartheta}{\partial x^2} + \frac{\partial^2 \vartheta}{\partial y^2}\right) + \frac{d^2 H}{d\vartheta^2}\left[\left(\frac{\partial \vartheta}{\partial x}\right)^2 + \left(\frac{\partial \vartheta}{\partial y}\right)^2\right] = \\ = \frac{3}{2H}\left(\frac{dH}{d\vartheta}\right)^2\left[\left(\frac{\partial \vartheta}{\partial x}\right)^2 + \left(\frac{\partial \vartheta}{\partial y}\right)^2\right] \tag{23}$$

and after rearrangement:

$$\frac{\partial^2 \vartheta}{\partial x^2} + \frac{\partial^2 \vartheta}{\partial y^2} = -\frac{\frac{d^2 H}{d\vartheta^2} - \frac{3}{2H}\left(\frac{dH}{d\vartheta}\right)^2}{\frac{dH}{d\vartheta}} \times \\ \times\left[\left(\frac{\partial \vartheta}{\partial x}\right)^2 + \left(\frac{\partial \vartheta}{\partial y}\right)^2\right].$$

Thus, after reduction by $\Delta\vartheta = 0$, we have

$$\frac{d^2 H}{d\vartheta^2} - \frac{3}{2H}\left(\frac{dH}{d\vartheta}\right)^2 = 0 \tag{24}$$

which is a defective second-order ordinary differential equation which, by means of the replacement $H' = p(H)$, might easily be solved.

$$H = \frac{1}{(k_1 - k_2\vartheta)^2}. \tag{25}$$

By that, the potential function of the flow

$$\varphi = \frac{1}{k_2 - k_1 \vartheta} \Phi \tag{26}$$

has been established only by harmonic functions.

Solution (26) has such a form from which it follows that the usual classic type of solution may be maintained. From the nonharmonic potential function of the flow of compressible medium the solution to the corresponding incompressible flow may be deduced:

$$H \equiv \text{const.}; \qquad \vartheta \equiv \text{const.}$$

$$\varphi \equiv \Phi. \tag{27}$$

5. Determination of the absolute velocity

Another way of determining the absolute velocity is obtained by starting out from the Bernouilli-equation of the isentropic flow:

$$\frac{1}{H} = \left[1 - \frac{\kappa - 1}{2}\left(\frac{c}{a_0}\right)^2\right]^{\frac{1}{\kappa - 1}}. \tag{28}$$

Expressing the velocity from Eq. (28)

$$c = a_0 \left\{\frac{2}{\kappa - 1}\left[1 - \left(\frac{1}{H}\right)^{\kappa - 1}\right]\right\}^{\frac{1}{2}}, \tag{29}$$

and substituting expression (25) we have:

$$c = a_0 \left\{\frac{2}{\kappa - 1}\left[1 - (k_2 - k_1 \vartheta)^{2(\kappa - 1)}\right]\right\}^{\frac{1}{2}}. \tag{30}$$

The absolute velocity in this way is produced only by the harmonic function ϑ.

REFERENCES

1. Czibere T.: Über die Berechnung der Unterschallströmung von kompressiblen Medien. *Acta Techn. Hung.* **79** (1974)

2. Hidasi J.: Investigation of Irrotational Space Flows of Sources Depending on the Square of Velocity. II. *Energia- és Atomtechnika, Hung.* 1981, May.

3. ZIEREP, J.: Vorlesungen über theoretische Gasdynamik. G. Braun, Karlsruhe 1963
4. HIDASI J.: Reduction of the Cascade Flow Problem of a Part-Channel of Varying Width to the Plane Cascade Problem. I, II. *Acta Techn. Hung.* **89** (1979)

Ebene Unterschallströmung von kompressiblen Medien. — Die nichtharmonischen Potential- und Stromfunktionen der isentropischen Unterschallströmung des kompressiblen Mediums werden mit Hilfe der Dichte des Mediums sowie mit Hilfe der harmonischen Potential- und Stromfunktionen hergestellt. Drückt man auch die Dichte des Mediums mit Hilfe der harmonischen Funktion aus, so erhält man bei der Ermittlung der Geschwindigkeitskomponenten derartige Ausdrücke, die nur durch harmonische Funktionen gebildet sind.

Acta Technica Academiae Scientiarum Hungaricae, 93 (1—2), pp. 153—168 (1981)

ECONOMICALLY COMPUTERIZED CALCULATIONS FOR LARGE-SIZE LOOPED PIPE-NETWORKS

B. ALMÁSSY*—S. BUDAVÁRI**—Z. VAJNA***

[Manuscript received 12. April, 1981]

A new method is presented for computation of flow and pressure conditions in large-size looped pipe-networks. The problem is reduced to a linear equation-system written for only as many unknowns ("basic-flows") as there are loops in the network. An algorithm is also presented not only making the simple computerization of the selection of basic-flows possible, but simplifying the solution of the entire problem, as well.

1. Introduction

A large scale of methods have been published for the computation of flow and pressure conditions in pipe-networks—especially since the advent of high-capacity computers. The computation of radial systems causes no difficulties, only that of looped networks because of the great storage capacity requirements and convergency problems. However, significant the Cross method [1] was in 1936, by the time of manual calculations, at present it lost already its popularity. Every actual method avoids the Crossian excessive simplifications—having consequences for the convergency discussed in several publications (e.g. [2])—and attempts some approximate solution of the non-linear equation system written for as many unknowns (flows or pressures) as there are nodes or loops in the network. Some apply directly the Newton or the Newton—Raphson method (e.g. [3], [4], [5]), others have introduced a special variety of that (e.g. [6], [7]), or make use of other possibilities, such as the variational calculus (e.g. [8], [9]), etc. It seems, that in his Doctor's Thesis ALMÁSSY described first in 1966 the idea of the loop-corrections (mentioned above as second possibility), though unpublished save in a university notebook with some complements [11]. Application of his basic idea for large-size networks permitted to develop a fully automated numerical method likely to be superior to the available methods both by running time and storage capacity demand, and by ease of programming. This method will be illustrated first on a simple case of closed loop networks, then possibility and way of generalization of the method will be presented.

* WRECA, Nigeria
** Municipal Water Works, Budapest
*** Department of Fluid Dynamics, Technical University of Budapest

2. Stating the Confined problem

To understand the essentials of the method, let us consider first a pipe-network of given arrangement, where:

a) the pipe-geometries are known;

b) all pipes join by both ends a node joined by at least another pipe end;

c) medium (further on e.g. water) draw-off or feeding is done exclusively through a node (V m^3/s);

d) a reference pressure in one node is known (p_0 N/m^2);

e) there is a steady-state condition and constant density of flowing medium.

The examination aims at determining the flow in each pipe and the nodal pressures for the given spatial arrangement and nodal loads.

These networks are known to meet equality

$$NN-1+NL-NP=0\,, \tag{1}$$

where

NN number of nodes

NL number of independent loops (to be discussed later)

NP number of pipes in the network.

According to Eq. (1):

$$NN-1=NP-NL$$

hence, deducing the number of loops from the number of pipes, results in the number of independent continuity equations to be written for the nodes. Thereby the idea by ALMÁSSY lies at hand: defining somehow in the network NL flows Q_k ($k=1, 2, \ldots, NL$) the other flows Q_i ($i=NL+1, \ldots, NP$) are linear functions of the former and the nodal loads V_n ($n=1, 2, \ldots, NN$). Thus, utilization of these linear relationships permits to reduce the problem of NP unknowns to the solution of equation system of NL unknowns, and the Q_k solutions directly yield the other Q_i values. Of course, neither then is the equation system to be solved a linear one, but it contains only NL, rather than NP, unknowns.

In a network defined accordingly, in addition to the nodal continuity conditions, flow have also to meet condition

$$\sum_{s\in S} \Delta p_s=0 \tag{2}$$

along any closed loop, where Δp_s (N/m^2) is the pressure difference in each pipe between two nodes affected by a sign, and S the set of subscripts of pipes making up the denoted closed trajet. In writing the continuity equations, be

$$Q_m,\quad V_n>0$$

for a flow towards the node, and in equations type (2), be

$$\Delta p_s > 0$$

if Q_s flows in the — still undefined — direction of advancement along the closed trajet.

The NL "basic flows" Q_k may of course be selected in several ways. Obviously, a single condition has to be met: imagining the "basic pipes" (conveying the "basic flows") to be removed from the network, the water supply of every node has to be safeguarded through the remaining pipes. First an algorithm will be presented, not only making the simple computerization of the selection possible, but simplifying the solution of the entire problem, as well.

3. Algorithm for the selection of the basic pipes (basic flows)

Operation of the algorithm will be illustrated on the small network seen in Fig. 1.

Let us fix now the network arrangement by two vectors such that identically numbered elements of the vectors contain (arbitrary) numerals of nodes constituting two end points of a pipe, in an arbitrary order. According to Fig. 1, the vectors $\underline{B}$ (*b*eginning) and $\underline{E}$ (*e*nd) may be, for instance:

$$\underline{B} = (2, 8, 8, 4, 7, 1, 3, 3, 5, 6, 3, 1),$$

$$\underline{E} = (5, 5, 9, 7, 9, 2, 2, 4, 6, 7, 6, 4).$$

Without the detriment of generality, for the sake of simplicity, let us assume now that in any pipe, the pressure difference (e.g. drop) may be expressed by the flow as:

$$\Delta p_s = a_{2s} |Q_s|^{r-1} Q_s . \tag{3}$$

where, Q_s (m^3/s) and according to the practice $1{,}8 < r \leqq 2$. Fig. 2 shows the same network, indicating numerals a_2 at each pipe, and loads in each node. Now let us tour the network in a prescribed way. If at a branching (node) it has to be decided where to go further, then as an organizing principle let us state e.g. that always that pipe will be

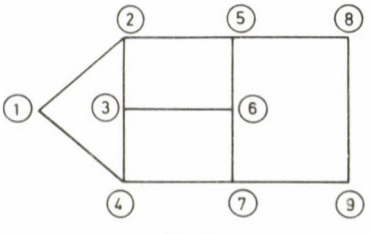

Fig. 1

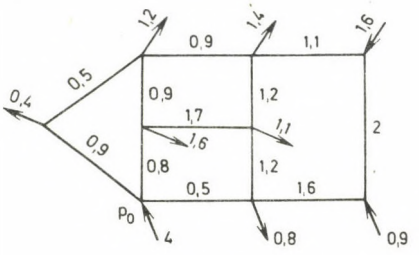

Fig. 2

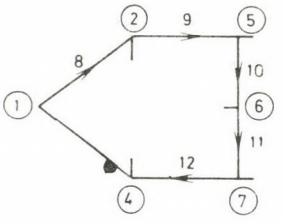

Fig. 3

selected from all the possible ones where the coefficient a_2 is the lowest. It should be stressed that any other organizing strategy may be settled, the mode of selection has no significant consequences. Let us affect each pipe once walked along by an arrow pointing backwards, and a numeral gradually decreasing from NP.

Let us start from node 4. with a given reference pressure $p_0 = 15 \times 10^5$ N/m^2. According to our organizing principle, it is simple to get to node 1. (Fig. 3).

This can be realized numerically by manipulating the elements of vectors $\underline{B}$ and $\underline{E}$: the perambulated pipes will be arranged to the vectors' end, one after the other in a reversed sequence so that the nodal numeral whence the arrow points away gets to vector $\underline{B}$. So, the arrow directions will be fixed, and the vector element numerals identical to the pipe numeral.

Up to node 1., vectors $\underline{B}$, $\underline{E}$ become:

$$\underline{B} = (3, 8, 8, 1, 7, 3, 3, 1, 2, 5, 6, 7),$$

$$\underline{E} = (6, 5, 9, 4, 9, 4, 2, 2, 5, 6, 7, 4).$$

From node 1, one can get only towards node 4. Let us convene: if according to the selection a_2, from a node another node already contacted had to be reached but there are also other possibilities, then one of them is chosen (that with the lowest a_2); else, the found pipe is a basic pipe and gets decreasingly numbered starting from NL. From node 1 only pipe (1, 4) would lead further—but since node 4 has already been contacted, this pipe will be basic pipe 4 ($NL \ldots$ that is, in our case four.) The arrow on basic pipes has to point towards the node whence the basic pipe has been denoted, in our case towards node 1. Let us put subscript pairs of basic pipes to the places

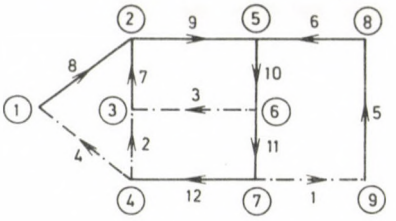

Fig. 4

corresponding to the numerals in vectors $\underline{B}$, $\underline{E}$. (Eventually, they were there only they had to be exchanged because of the direction of the arrow).

$$\underline{B} = (3, 8, 8, 4, 7, 3, 3, 1, 2, 5, 6, 7),$$

$$\underline{E} = (6, 5, 9, 1, 9, 4, 2, 2, 5, 6, 7, 4).$$

If there was no possibility to proceed, then the path laid down has to be ridden back to node 2 where the possibility of going in a direction other than the already perambulated pipe (2, 5) has to be considered. In the positive case, again along the pipe with the lowest a_2 will be ridden, else, the opposite direction will be followed. In our case, pipe (2, 3) is such a possibility. Node 3 being in fact not contacted, hence this pipe may be ridden along, affected by an arrow and numbered 7. In node 3, however, the same happens as in node 1: neither pipe (3, 4) nor that (3, 6) may be taken, since both nodes 4 and 6 have already been visited, and there is no other possibility. So pipes (3, 6) and (3, 4) will be basic pipes 3 and 2, resp. Their succession is only decided that in vectors $\underline{B}$, $\underline{E}$, the subscript pair of pipe (3, 6) came the first. Now, the vectors become:

$$\underline{B} = (8, 4, 6, 4, 7, 8, 3, 1, 2, 5, 6, 7),$$

$$\underline{E} = (9, 3, 3, 1, 9, 5, 2, 2, 5, 6, 7, 4).$$

Thus, there is no where to go from node 3, hence we shall proceed backwards: there being no more possibility in node 2, further back node 5 is arrived at. Here a new possibility exists: node 8 is still intact. Assigning an arrow and a numeral (6) on pipe (5, 8) one can go to node 9. Putting again an arrow and a numeral (5) on pipe (8, 9), one gets to node 9. From here there is no other possibility than to go to node 7 that, however, has already been visited, thus, pipe (7, 9) is again a basic pipe (1). Apparently, all pipes have been numbered and four basic pipes determined. Thereby the organization problem has an end. Our vectors are, in final form (Fig. 4):

$$\underline{B} = (7, 4, 6, 4, 9, 8, 3, 1, 2, 5, 6, 7)$$

$$\underline{E} = (9, 3, 3, 1, 8, 5, 2, 2, 5, 6, 7, 4).$$

Alongside with the arrangement of elements of vectors $\underline{B}$, $\underline{E}$, one or more dimensional arrays containing other pipe parameters (such as diameters, lengths, coefficients a_2)

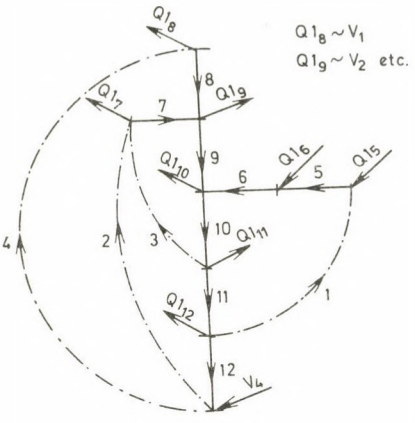

Fig. 5

have to be rearranged, namely thereafter pipes will be referred to according to the developed sequence ("pipe number"). Purely for the sake of illustrativeness, let us make a straightened drawing of the network, indicating pipe numbers and arrows (Fig. 5). On its basis let us define the concept of independents loops quoted at the beginning of Chapter 2: a loop will be the term for a closed path that can be perambulated in a continuous flow so that only a single basic pipe will be proceeded along. Let the loop numeral be the same as the numeral of the contacted basic pipe. Thus, according to Fig. 5, elements of loop

1 are: pipes No. 1, 5, 6, 10, 11,

2 2, 7, 9, 10, 11, 12,

3 3, 7, 9, 10,

4 4, 8, 9, 10, 11, 12.

Let us construct now a vector $\underline{C}$ of NP elements so that its r-th element should be the pipe numeral following the r-th pipe in Fig. 5 according to the continuous flow arrows — as well as a vector $\underline{X}$ of NL elements so that its t-th element should be the last pipe numeral in the t-th loop:

Numeral	Elements of		Numeral	Elements of	
	$\underline{C}$	$\underline{X}$		$\underline{C}$	$\underline{X}$
1	5	11	7	9	
2	7	12	8	9	
3	7	10	9	10	
4	8	12	10	11	
5	6		11	12	
6	10		12	—	

The vectors $\underline{C}$ and $\underline{X}$, and the numbering method will be seen to much simplify the network computation. Further on, nodal loads will be assigned to the numeral of the pipe starting at the given node (according to the arrow) else than a basic pipe. Since there is single such pipe, this reference is inambiguous (e.g. nodal load 2. belongs to pipe numeral 9). No such pipe exists at node 4 but it is irrelevant: there are only $(NN-1)$ independent nodal equations, so node 4 will be that without continuity equation.

Obviously, there are many different ways to construct a convenient program for denoting basic pipes, numbering, producing vectors $\underline{C}$ and $\underline{X}$. In the *Appendix*, a rapid and efficient program will be given, written in ALGOL-60 language. The preceding needs only two complements to suit the program: vector $\underline{K}$ — a global variable containing coefficients a_2 — assumed to be known from the aspect of the procedure "order" just as are vectors $\underline{B}$, $\underline{E}$ and scalars NL, NP; $N3$ being the nodal numeral started from in performing the algorithm (that would be $N3=4$ in our example) hence also given.

4. Network computation—determination of the basic flows

The fundamental idea of the network computation method has been referred to in Chapter 2. After having introduced the concept of basic flows, the non-basic flows may be expressed by means of nodal continuity equations, in terms of nodal loads and basic flows. Having determined the basic flows by means of equations type 2, (merely a problem with NL unknowns), the other flows can be directly computed.

4.1. Non-basic flows in terms of basic flows

As stated by the end of Chapter 3, every nodal load may be assigned to the numeral of the pipe starting from the given node. Obviously, this new vector $\underline{Q1}$ can be derived from nodal loads $\underline{V}$ by using $\underline{B}$ such as:

$$Q1_i := V[B[i]] .$$

(Let us notice here that in what follows, the subscript within a subscript will be denoted as usual in the ALGOL language, and only the simple subscript will be marked a half row lower.)

Considering Fig. 5 it is easy to see, that e.g.

$$Q_9 = Q1_9 + Q1_8 + Q1_7 + Q_2 + Q_3 + Q_4 .$$

In general, every non-basic flow can be produced by summing nodal loads until the preceding end points, then adding basic flows of loops where the given pipe is an element of. Be M_i the set of numerals of loops where the i-th pipe is an element, an

arbitrary non-basic flow becomes:

$$Q_i = \sum_{\text{precedings}} V_m + \sum_{k \in M_i} Q_k \tag{4}$$

From the aspect of programming, the concept of "preceding" and the sets M_i are needless. Our system of subscripts, and vectors $\underline{X}$ and $\underline{C}$ much simplify production of flows Q_i.

a) Let us proceed from the first numeral of non-basic flow (in our case 5) to NP, and be first:

$$Q_i := Q1_i, \quad (i = NL+1, \ldots, NP)$$

b) Let us proceed again along the numerals, and using vector $\underline{C}$, be:

$$Q[C[i]] := Q[C[i]] + Q_i, \quad (i = NL+1, \ldots, NP-1).$$

This operation results in the part of the right-hand side of relationships Q_i independent of the basic flows. Insert this part in vector $Q1$, already utilized for another purpose, denoted here and only now by $Q1^*$. In network computation it will be used again as the invariable part of vector Q_i. Thus, e.g.:

$$Q1_5^* := Q1_9 + Q1_7 + Q1_8$$

A basic flow has to be added to $Q1_1^*$ for producing Q_i if the i-th pipe is element of the given loop. This is made, using the introduced notations such that: starting from the first pipe of loop 1 (C_1, or in our case 5):

$$Q_5 := Q1_5^* + Q_1$$

the fulfilment of the pair of relations

$$C_2 \leqq 5 \leqq X_2$$

has to be checked, and the same has to be done for loops 3 and 4. In the positive case, the pipe is an element of the tested loop, thus, the given basic flow has to be added to the right-hand side. Here e.g.

$$C_2 = 7 > 5; \qquad C_3 = 7 > 5; \qquad C_4 = 8 > 5$$

thus, the quoted relations are missed, the final result being:

$$Q_5 := Q1_5^* + Q_1 .$$

According to vector $\underline{C}$, pipe 5 is followed by pipe 6, to be tested in the same way etc., up to pipe 11, last pipe in loop 1. Loop 2 follows but here only loops 3 and 4 have to be examined, namely loop 1 has already been passed. First pipe in loop 2 is number 7 ($C_2 = 7$), then, according to vector $\underline{C}$, pipe 9 follows (flow examined in our example). Thus

$$Q_9 := Q1_9^* + Q_2 ,$$

then pairs of relations

$$C_3 \leqq 9 \leqq X_3 \quad \text{(true?)}$$

and

$$C_4 \leqq 9 \leqq X_4 \quad \text{(true?)}$$

have to be considered, that is:

$$7 < 9 < 10 \quad \text{(true?)},$$
$$8 < 9 < 12 \quad \text{(true?)},$$

9 being common in both intervals, it is:

$$Q_9 := Q1_9^* + Q_2 + Q_3 + Q_4 = Q1_7 + Q1_8 + Q1_9 + Q_2 + Q_3 + Q_4$$

agreeing with the result of the nodal equation, but appears to be easy to program in possession of $Q1^*$ values (advisably stored in $Q1$) in a single cycle.

4.2. Determination of basic flows — the loop equations

Chapter 2 included Eq. (2)

$$\Sigma \Delta p_s = 0$$

to be met in any closed traget. Obviously, such an equation may be written for every loop, to yield NL equations needed for determining NL basic flows. Writing the equations is facilitated by the continuity of the assumed flow of arrows within one loop, in conformity with our introduced direction system (see Fig. 5). It was assumed to have

$$\Delta p_s = a_{2s} |Q_s|^{r-1} Q_s .$$

Loop equations being of r-th degree, they cannot in general be solved directly, in closed form. It is a well-known procedure in such cases to linearize the equations by introducing Taylor first-order polynomials.

In doing so, however, remind that in our case only the basic flows are considered to be unknown — all non-basic flows being their linear functions according to Eq. (4). Thus, in general:

$$Q_s = f_s(Q_k) \qquad (s = NL+1, \ldots, NP)$$

$$(k = 1, 2, \ldots, NL)$$

hence

$$\Delta p_s = g_s(Q_k) .$$

Let us consider vector $\underline{Q}_0$ to be an approximate, e.g. assessed value of the wanted vector $\underline{Q}$ of basic flows. Substituting the sum of head losses of the n-th loop in the vicinity of this $\underline{Q}_0$ by a first-order polynomial obviously has non-zero result. Be:

$$\sum_{(n)} \Delta p_s|_{Q_0} = S_{n0} ,$$

thus:

$$S_n \simeq S_{n0} + \left.\frac{\partial S_n}{\partial Q_1}\right|_{Q_0} (Q_1 - Q_{10}) + \left.\frac{\partial S_n}{\partial Q_2}\right|_{Q_0} (Q_2 - Q_{20}) +$$

$$+ \ldots + \left.\frac{\partial S_n}{\partial Q_{NL}}\right|_{Q_0} (Q_{NL} - Q_{NL0}) .$$

Determine a better approximation $\underline{Q}_1$ starting from the condition to zero the right-hand side of the equation. Be

$$\underline{Q}_1 - \underline{Q}_0 = \underline{q}_1 ,$$

$$-S_{n0} = \underline{\text{grad}}\, S_n|_{Q_0} \cdot \underline{q}_1 , \tag{5}$$

A total of NL such equations can be written for NL loops, thus:

$$-\underline{S}_0 = \underline{\underline{D}}_0 \cdot \underline{q}_1$$

yielding for the corrections the set of linear equations of NL unknowns

$$\underline{q}_1 = -\underline{\underline{D}}_0^{-1} \underline{S}_0 . \tag{6}$$

Let us consider elements of matrix $\underline{\underline{D}}_0$ and vector $\underline{S}_0$. The m-th element in the n-th row of matrix $\underline{\underline{D}}_0$:

$$d_{n,m} = \left.\frac{\partial S_n}{\partial Q_m}\right|_{Q_0} = \frac{\partial}{\partial Q_m} \sum_{(n)} \Delta p_s \Big|_{Q_0} = \sum_{(n)} \left.\frac{\partial \Delta p_s}{\partial Q_s} \frac{\partial Q_s}{\partial Q_m}\right|_{Q_0} ,$$

where

$$\frac{\partial \Delta p_s}{\partial Q_s} = r a_{2s} |Q_s|^{r-1} ,$$

$$\frac{\partial Q_s}{\partial Q_m} = \begin{cases} 1 & \text{for } m \in M_s \\ 0 & \text{for } m \notin M_s . \end{cases}$$

Thus, denoting by H_t the set of elements in the t-th loop

$$d_{n,m} = \frac{\partial S_n}{\partial Q_m}\bigg|_{Q_0} = \sum_{s \in H_n \cap H_m} r a_{2s} |Q_s|^{r-1} \bigg|_{Q_0}$$

where the sum contains only pipes of the n-th loop that are also parts of the m-th loop. For $n=m$, thus it is an element of the main diagonal, then obviously, all pipes of the loop enter the summing. Therefore, if the pressure difference in all pipes may be expressed by Eq. (3), be

$$U_s = r a_{2s} |Q_s|^{r-1}$$

the matrix will be positive definite having its greatest elements in the main diagonal, hence it is well conditioned. From the formation of the elements it follows that obviously $d_{n,m} = d_{m,n}$, thus the matrix is a symmetrical one.

From the aspect of programming, because of symmetry, it is abvisable to proceed so that in the n-th row, elements are formed only after $d_{n,n}$. The term U_n for the basic pipe n may occur only in element $d_{n,n}$ (one basic pipe can only occur in one loop). Term $U[C[n]]$ of pipe C_n is included in $d_{n,n}$ and in every $d_{n,m}$ $(m>n)$ meeting the pair of relations

$$C_m \leq n \leq X_m$$

hence, elements $d_{n,m}$ can again be produced in one cycle by using vector $\underline{C}$.

In our illustrative example, elements of matrix $\underline{\underline{D}}$ become, e.g.

$d_{1,1} = U_1 + U_5 + U_6 + U_{10} + U_{11}$ (elements in loop 1)

$d_{1,2} = U_{10} + U_{11}$ (elements common in loops $1-2$) etc.

S_n (n-th independent term of the equation system) could be produced by passing through terms n, C_n etc., up to X_n, by summation. Our subscript system leads, however, to an important simplification in programming. Nodal pressures, anyhow needed later, will be simply produced:

$$p_{NP} := p_0 + \Delta p_{NP}$$

then

$$p_i := p[C[i]] + \Delta p_i, \qquad (i = NP-1, \ldots, NL+1).$$

Now:

$$S_n := p[C[n]] - p[C[X[n]]] + \Delta p_n \qquad X_n \neq NP$$

and

$$S_n := p[C[n]] - p_0 + \Delta p_n \qquad X_n = NP$$

Δp_n being the head loss in the basic pipe n due to basic flow Q_n. Distinction between the two cases is directly understood from a glance on Fig. 5.

Thus, according to our example:

$$S_1 = p_5 - p_{12} + \Delta p_1$$

$$S_2 = p_7 - p_0 + \Delta p_2 \quad \text{etc.}$$

Of course, for elements both $d_{n,m}$ and S_n, the Q_i values produced in the way related in connection with Eq. (4) will be made use of.

According to Eq. (6), obviously, the inverted of an NL by NL size matrix has to be produced, advisably by developing a subroutine considering and economically utilizing the symmetry. It is still more economical to place the elements $d_{n,m}$ continuously, in a vector of length $(NL+1) \times NL/2$, and to produce the subroutine of inversion accordingly.

After solving the equation system

$$\underline{Q}_1 = \underline{Q}_0 + \underline{q}_1$$

The iteration (getting better approximations for $\underline{Q}$) have to be continued until e.g.:

$$\sum_{i=1}^{NL} |S_i| < \varepsilon$$

where ε is a bound advisably selected to be rather low.

The convergency of the method was observed to be rather good, monotonous.

It is but slightly sensitive to the initial assumption of $\underline{Q}_0$ that can be ever taken as $\underline{Q}_0 = 0$. Because of the subsequently presented generalization possibilities, it is, however, advisable to assume a slight, though non-zero value, such as:

$$\underline{Q}_0 = 0{,}02\,.$$

Vector Q1* is advisably produced in the preparatory part of the program, and the full value of non-basic flows Q_i to be computed in the iteration cycle by using these ones and the just actual basic flow values.

Obviously, by the end of iteration, all Q flows and nodal pressure values are available computed as partial results — that is, the set problem has been achieved.

5. Generalization of the computation method release of certain restricting conditions

For the sake of comprehensiveness of the essentials some simplifications were introduced that were in fact needless.

At the beginning of Chapter 2, nodes were defined by specifying to permit only constant water draw-off or feed. All results of the presented computation method will

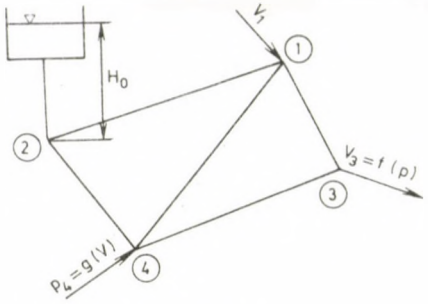

Fig. 6

be valid with a simple complement if nodes are points where pipes are connected or ended and there is

a) constant feed or draw-off, independent of the pressure; or e.g.:

b) a reservoir connected to the system (constant pressure, feed depending on the system);

c) draw-off as a specified function of the local (nodal) pressure;

d) water pumped from a well to the network (at a pressure depending on the suction diagram);

e) water fed by a suction pump from a reservoir, or an outer network, or by a lifting or boosting pump from another point of the system;

f) stabilized pressure is required, etc.

In cases d) and e), obviously, the characteristic curve of the pump $p = f(Q)$ has to be available analytically or numerically.

Cases b) to f) may be reduced to case a) (already considered) on hand of a simple idea. Let us consider e.g. Fig. 6 and assume nodes 1, 2, 3, 4 to be types a), b), c), d), respectively. Assume a fictitious node 5 lacking from the original network, and connect it to all nodes other than type a), by means of equally fictitious pipes (Fig. 7). Assume the pressure difference equations of these fictitious pipes

$$\Delta p_i = f_i(Q_i)$$

to be identical to those for their final nodes (2, 3, 4), and take advisable the (fictitious) node 5 as starting node $N3$ of the algorithm in Chapter 3. Performing computations according to Chapter 4, quantities Q for the fictitious pipes will be the nodal draw-off (feed), pressure differences Δp in the fictitious pipes will be pressure differences created by the pump, the reservoir etc.

To now, also pipes have been considered as "passive" elements, developing head losses according to e.g.

$$\Delta p_s = a_{2s} |Q_s|^{r-1} Q_s .$$

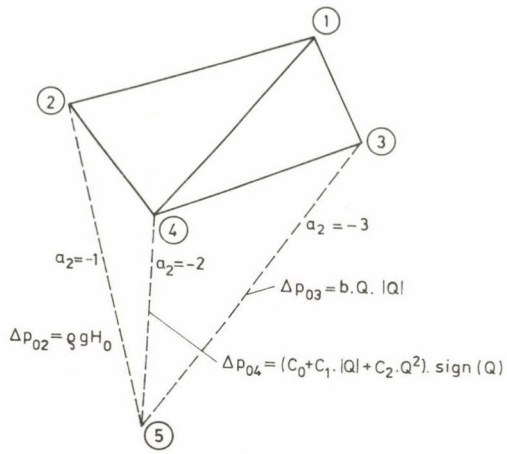

Fig. 7

Fictitious pipes have introduced a different law. There is no objection to generalize it further to have in a pipe e.g. a lifting pump or a pressure control valve. The only change resulting from it will be that such a pipe will not have the above pressure difference function, but expressed by a different $p=f(Q)$ of course, true to sign — but the computation method in Chapter 4 will subsist. Evidently, these functional relationships have to meet a single condition: at least once continuously differentiable with respect to Q for producing the terms

$$U_s=\frac{\partial \Delta p_s}{\partial Q_s}$$

in Chapter 4.

Introducing, however, arbitrary pipe functions $p=f(Q)$, one has to keep in mind that also in this case, a strategy has to be given for the algorithm in Chapter 3, to decide what pipe to select for advancing, if there are several possibilities. Our description suggested to select always the pipe with the lowest a_2. Namely it was observed to contribute to well condition matrix $\underline{\underline{D}}$. For pipes of special equations, e.g. a code number may be given such that $a_2<0$ (integer), permitting operation of the proper subroutine, leaving the existing strategy inaffected.

Obviously, to a node of the looped network, a radial system may be connected with no trouble. Its nodes and end points may be handled as those of the looped network.

Similarly, the restriction of constant medium-density may be lifted by referring our equations to mass flows rather than to volume flows.

APPENDIX

```
begin procedure order;
    begin integer k1, k2, k3, P, A, c1, c2, c3, N5, N6;
        real D;
        procedure change 1;
        begin c3:=E[k2]; E[k2]:=E[k1]; E[k1]:=B[k2];
            B[k2]:=B[k1]; B[k1]:=-c3;
        end;
        procedure change 2(M, s1, s2);
        array M; integer s1, s2;
        begin real C;
            C:=M[s1]; M[s1]:=M[s2]; M[s2]:=C
        end;
    start: for j:=1 step 1 until NP do
            C[j]:=0;
          P:=N3; k1:=NP; k3:=1;
    ind 4: D:=10^40; k2:=0; c1:=0; if k3>k1 then goto out;
        for i:=k3 step 1 until k1 do
          begin if B[i]≠P∩E[i]≠P then goto ind 1;
                if K[i]>D then goto ind 2;
                D:=K[i]; k2:=i;
          ind 2:if B[i]=P then E[i]:=-E[i] else begin c3:=E[i];
                                                      E[i]:=-B[i];
                                                      B[i]:=c3
                                                end
    ind 1: end;
        c2:=k1+1;
    ind 10: if k2=0 then goto ind 3;
        change 1;
        P:=-c3; C[k1]:=c2;
        change 2(K, k2, k1);
        k1:=k1-1; goto ind 4;
    ind 3: for j:=k3 step 1 until k1 do
        if P=-E[j] then begin change 2(E, j, k3);
                              E[k3]:=-E[k3];
                              change 2(B, j, k3);
                              change 2(K, j, k3);
                              C[k3]:=c2; k3:=k3+1
                        end;
        if k3>k1 then goto out;
        if c1=0 then begin c1:=C[k3-1];
                           P:=E[c1]
                     end else begin P:=E[C[c1]]; c1:=C[c1]]
                              end;
        D:=10^40; k2:=0;
        for i:=k3 step 1 until k1 do
          begin if B[i]≠P∨K[i]>D then goto ind 6;
              D:=K[i]; k2:=i
    ind 6: end;
          c2:=C[c1]; goto ind 10;
    out:  E[k3]:=abs(Σ[k3]); C[NP]:=1000;
          N6:=NL÷2; N5=NL+1;
          for i:=1 step 1 until N6 do
```

```
        begin change 2(B, i, N5−1);
              change 2(E, i, N5−i);
              change 2(K, i, N5−i);
              change 2(C, i, N5−i);
        end;
        for i:=1 step 1 until NL do
        begin A:= B[i];
              j:=i;
        ind5: if A=E[C[j]] then goto ind 8;
              j:=C[j]; goto ind 5;
       ind 8: X[i]:=C[j]
        end;
        for i:=N5 step 1 until NP do
          Q1[i]:=V[B[i]];
  end
end order;
```

REFERENCES

1. Cross, H.: Analysis of Flow in Networks of Conduits or Conductors. Bull. No. 286, Urbana Ill. 1936. Univ. of Illinois, Eng. Expl. Stat.
2. Scott, D.—Hinsley, F.: Ventilation Network Theory, *Collesy Engineering*, 1951
3. Martin, D. V.—Peters, G.: The Application of Newton's Method on Network Analysis by Digital Computers. *Jour. Inst. Wat. Eng.* **17** (1963)
4. Rose, D. J.: Foundations of Optimizations, Englewood Cliffs, N. J. Prentice Hall, 1967
5. Chandrashekar, M.—Stewart, K. H.: Sparsity Oriented Analysis of Large Pipe Networks, *Jour. Hydr. Div.—ASCE.* Vol. **101**. No. HY4, Proc. Paper 11260 pp. 341—355, 1975
6. Dodge, E. K.—Hoellein, H. R.—Tetmajer, L.: The Analysis of Large, Complex Water Technologie, *Jour. AWWA.* July, (1978) pp. 366—370
7. Dinic, D.—Blazek, A.: Some Approximations in Analysing the Waternetworks Conditioned by the Computer Capacity, *Automatica* (Yug.), Vol. **12**. No. 1. pp 16—19, 1971
8. Birkhoff, G.: A Variational Principle for Nonlinear Networks. *Quart. Appl. Math.* **21** (1963)
9. Cembrowicz, R. G.: Optimierung von Rohrnetzen. *Das Gas und Wasserfach, Wasser, Abwasser.* **114** (1973) 118—122
10. Almássy B.: Computation of Pipe Networks on Electronic Digital Computers (in Hungarian). Doctor's Thesis, Technical University, Budapest, 1966
11. Vajna, Z.: Selected Chapters of Fluid Mechanics (in Hungarian), Institute of Post-Grad. Engng. Education, Technical University, Budapest G86, 1967

Wirtschaftliche rechenautomatische Berechnungen zur Konstruktion in Schleifen verlegter großer Rohrleitung-systeme. — Es wird ein für Rechenanlagen günstiges Verfahren beschrieben, zur Berechnung eines beliebig großen Rohrleitungs Netzes, das eine beliebige Anzahl von Knotenpunkte enthält. Der Massen-, bzw. Volumenstrom in den einzelnen Leitungen, ferner der Druck in den Knotenpunkten, kann anhand des Verfahrens berechnet werden. Im ersten Teil des Aufsatzes, wird ein Algorithmus geschaffen zur Einordnung der Elemente des Netzes. Dieser ermöglicht das im zweiten Teil beschriebene, verhältnismäßig einfache, gut übersichtliche und gut konvergierende iterative Verfahren. Der Anhang enthält das ALGOL-Program des ordnenden Algorithmus.

Acta Technica Academiae Scientiarum Hungaricae, 93 (1—2), pp. 169—195 (1981)

FLEXIBILITY DESIGN OF PIPING SYSTEMS*

PART II. STORE-ECONOMICAL PIPING ANALYSIS

F. KOLONITS**
CAND. OF TECHN. SCI.

[Manuscript received 11. May 1981]

In the first part of the paper it has been pointed out that both ensuring direct access to the design engineer and operative computing demands of piping design make the application of a desk computer for the use of the design group recommendable. The demand on capacity of the network analysis is rather high; in this part of the paper its reduction will be tried.

Notations

$\bar{f}$ — six-component (three translations, three rotations) movement vector or hypervector produced from them
$\bar{p}$ — six-component (three forces, three moments) load vector (dynam), or hypervector produced from them
$\mathbf{Z}$ — 6×6 flexibility matrix, or hypermatrix produced from them
$\mathbf{F}$ — rotation matrix
$\mathbf{R}$ — matrix representing vectorial multiplication
$\mathbf{B}_{ij}$ — 6×6 matrix transferring motion from point j to point i
REF — point of reference
$\mathbf{S}$ — filter diagonal matrix
$\mathbf{K}$ — filtered flexibility matrix (for constraints)
n — number of nodes or branches
k — number of constraint components (unknown reaction forces)
$\bar{v}$ — direction of pipe vector or of solution-searching
$\bar{r}$ — position vector or vector of remainder of iteration
l — length of straight pipe section
R — radius of pipe bend
Φ — corner angle of pipe bend
I — second-order moment of pipe cross section
E — Young's elasticity modulus of pipe material

3. Structural analysis of the piping

3.1. Contributions of the branch

The constructive elements of the piping are the branches. A branch is formed from a series of flexible straight pipes and pipe bends (elements) as well as of sections to be considered stiff, armatures, for example, adjoining continuously, without any

* Report at the session of the Commission of Mechanical Engineering Structures of the Hungarian Academy of Sciences, held on 21st April 1980.

** Dr. F. KOLONITS, Cand. of Techn. Sci, XI. Cirmos u. 4., H-1112 Budapest, Hungary.

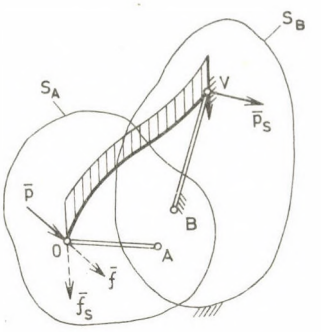

Fig. 1

branching. At the initial and end point of the branches, they can be connected to each other or to the environment: these junction points are the nodes of the piping network. The set of equations of the piping to be described later, establishes relationship between the general load (of six components, forces and moments) applied at the nodes and the motion (translation and rotation) of these points.

This relationship may be established from certain characteristics of the branches connecting the nodal points and because those show how the branch in question contributes to the deformation of the system and to the forces generated within, similarly to the familiar formulae of a cantilever, may be called the contributions of the branch.

The contributions, which give information necessary and sufficient for the purpose described above on the loading and motion relations of the initial and end points of the branch, are the following provided the end of the branch is clamped (Fig. 1):

— The 6×6 spring matrix denoted by $\mathbf{Z}$ in

$$\bar{f} = \mathbf{Z}\bar{p}\,, \tag{3.1}$$

defines the motion $\bar{f}$ of six components (displacement and rotation of the cross section) induced by the load $\bar{p}$ of six components (of forces and moments x, y, z) applied at the initial point, the matrix always being symmetric and positive definite.

— The motion $\bar{f}_{s,o}$ and the load $\bar{p}_{s,v}$ transferred at the fixation, caused by the effect of the load applied on the branch and distributed according to a definite law (the most significant being the uniformly distributed load like weight). They are called together "weight effect".

— At the fixed end also the external load $\bar{p}$ is transferred by static transposition; carrying out this operation will be discussed in a following paragraph. This "contribution" only depends on the relative positions of the initial and end points, not being affected by properties of the branch.

The numerical values representing the contributions depend on the direction of the (orthogonal, right-hand) system of coordinates. Should one turn to such a system I the axis-unit vectors of which in a system K are $\bar{i}, \bar{j}, \bar{k}$, so the matrix of rotation (designating the transposed by an asterisk), (3.2) should be defined;

$$\mathbf{F}_{IK} = \begin{bmatrix} \begin{bmatrix} \bar{i}^* \\ \bar{j}^* \\ \bar{k}^* \end{bmatrix} & \mathbf{0} \\ \mathbf{0} & \begin{bmatrix} \bar{i}^* \\ \bar{j}^* \\ \bar{k}^* \end{bmatrix} \end{bmatrix} \tag{3.2}$$

$\mathbf{FF}^* = \mathbf{F}^*\mathbf{F} = \mathbf{E}$ being an unit matrix. The transformed quantities are

$$\bar{p}_I = \mathbf{F}_{IK}\bar{p}_K\,, \qquad \bar{p}_K = \mathbf{F}^*_{IK}\bar{p}_I \tag{3.3}$$

and in the same way for all load and motion vectors; and for the spring matrix

$$\mathbf{Z}_I = \mathbf{F}_{IK}\mathbf{Z}_K\mathbf{F}^*_{IK}\,, \qquad \mathbf{Z}_K = \mathbf{F}^*_{IK}\mathbf{Z}_I\mathbf{F}_{IK}\,. \tag{3.4}$$

A situation might occur where from the point of view of the analysis it is not the motion of the point O which is significant but that of another point A connected to O by a stiff section. The components of rotation at point O appear at point A invariably, however, the motion changes due to the "mowing" of the connecting stiff section. In case where the rotations are small and the negative of the vector showing the transposition $(\overline{AO})$ is

$$\bar{r}^* = [r_x, r_y, r_z]\,,$$

the increment of the displacement (Fig. 2) will be

$$\Delta\bar{F} = \mathbf{R}_{AO}\bar{\varphi}\,,$$

$$\mathbf{R}_{AO} = \begin{bmatrix} 0 & -r_z & r_y \\ r_z & 0 & -r_x \\ -r_y & r_x & 0 \end{bmatrix}; \tag{3.5}$$

and summed up

$$\bar{f}_A = \mathbf{B}_{AO}\bar{f}_O\,, \quad \mathbf{B}_{AO} = \begin{bmatrix} \mathbf{E} & \mathbf{R}_{AO} \\ \mathbf{0} & \mathbf{E} \end{bmatrix}. \tag{3.6}$$

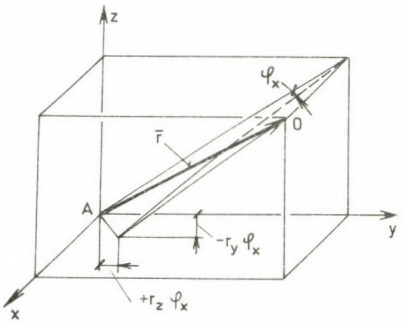

Fig. 2

The above matrix **R** forms the components of a vectorial product with a matrix operation as written in column vector

$$\mathbf{R}\bar{v} = [\bar{r} \times \bar{v}] ,$$

$$\mathbf{R}^* = -\mathbf{R} . \tag{3.7}$$

In case where the load is applied at the end point A of the adjoining stiff section and not at the end of the branch, the forces at point O remain unchanged but, in consequence of the static transposition, the values of the moments are increased. Similarly to those mentioned above it can be pointed out that

$$\bar{p}_O = \mathbf{B}^*_{AO} \bar{p}_A . \tag{3.8}$$

The aforementioned load transferred from the external load at the fixed end (by transposition) is

$$\bar{p}_V = \mathbf{B}^*_{OV} \bar{p}_O .$$

In connection with the transfer matrices **B**, the following formulae are valid:

$$\mathbf{B}_{AO}\mathbf{B}_{OA} = \mathbf{B}^*_{OA}\mathbf{B}^*_{AO} = \mathbf{E} ,$$

$$\mathbf{B}_{AA} = \mathbf{B}^*_{AA} = \mathbf{E} , \tag{3.10}$$

$$\mathbf{B}_{AO} + \mathbf{B}_{OA} = \mathbf{B}^*_{AO} + \mathbf{B}^*_{OA} = 2\mathbf{E} ,$$

and for any point C selected arbitrarily:

$$\mathbf{B}_{AO} = \mathbf{B}_{AC}\mathbf{B}_{CO} , \qquad \mathbf{B}^*_{AO} = \mathbf{B}^*_{CO}\mathbf{B}^*_{AC} . \tag{3.11}$$

Considering the AO stiff bar united with the branch OV as one single branch, the spring matrix of this latter is

$$\mathbf{Z}_A = \mathbf{B}_{AO}\mathbf{Z}_O\mathbf{B}^*_{AO}\,, \tag{3.12}$$

and its own motion caused by its weight is related to the new end point

$$\bar{f}_{s,A} = \mathbf{B}_{AO}\bar{f}_{s,O}\,. \tag{3.13}$$

All these do not change the value of the weight loading transferred at the fixation; in transposing the external load, the change of the initial point should be taken into account.

Neither the spring matrix of the branch, nor the own motion will be affected by assuming the fixation as not being at point V but at point B, by adjoining the stiff section VB to the end of the bar. At the fixation

from the weight loading

$$\bar{p}_{s,B} = \mathbf{B}^*_{VB}\bar{p}_{s,V}\,, \tag{3.14}$$

and from the external loading

$$\bar{p}_B = \mathbf{B}^*_{AB}\bar{p}_A \tag{3.15}$$

will be transferred.

The contributions defined to points A, B and to the original points O, V are in mutually unambiguous interconnection, therefore, they are, as for their necessary and sufficient character, equivalent. It might also be considered that to point V one rigidly attaches the whole space (S_B) and one fixes it; and one also fixes to O the whole space, a "cover space" of the former, (S_A); the external load being applied in this latter. The contributions describe the connection of these two spaces related to an arbitrarily selected point in each (Fig. 1). The motion of a point in S_B is a motion related to its cover point in space S_B. It is possible and convenient to assign both of the reference points in such a way, that in the spaces S_A and S_B, in an unloaded state they are cover points of each other. In other terms, instead of branches extending from a physical node to another node, as network elements such configurations will be used, to the beginning and end points of which stiff bars are connected stretching to the same REF-points. The relationship between the original and REF-contributions results from (3.12—14) while (3.15) yields that the external force applied at the initial point is transferred unchanged (Fig. 3).

Producing the REF-contributions does not require more work than the usual ones, because the branches will be constructed from straight and bent pieces of pipe anyway: it is quite indifferent to which point the summation is carried out, the physical initial or end point or to any other point.

The configuration obtained is functionally similar to the figure of the Javaian puppet-show the limbs of which are agitated by the player using long "wayang" sticks for this purpose, his hand being the reference point.

Fig. 3

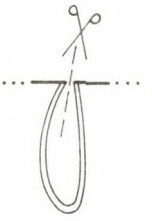

Fig. 4

Into the physical network, the wayang sticks needed for the elements defined in the foregoing may be inserted without any difficulty. Cutting through the pipe at any point, and binding the two ends of the cutting to each other by a stiff section of any desired form (Fig. 4), the resultant configuration is equivalent to the intact pipe in flexibility.

On the branch provided with wayangs, the condition of the static equilibrium is simpler than earlier because of the absence of the transpositions. The acting force, so to say, "runs down" on the branch and creates a matrix-proportional difference in the motions between the initial and end points. A detailed electrical analogy may be established as follows: (3.1) corresponds to Ohm's law, motion to voltage, load to current, spring matrix to impedance and weight effects to voltage and current generators. The methods developed in handling electric networks might be adapted.

Interchanging the initial and end points does not change the values $\mathbf{Z}$ and $\bar{p}_s$.

Introducing *REF* has another advantage, i.e., by the assignment of it as fitted to the piping configuration in question, the contributions are simpler in form. JÜRGENSONN, in analysing an inplane pipe branch forced by heat expansion between two fixed points took, properly speaking, the "elastic centre of gravity" of the trace for *REF* and in this way obtained momentless reaction [2]. This conception cannot be generalized in this respect to space network, however, it will be utilized in the formulation of minimum-extent contributions of the elements constituting the branch. This formulation will be written to conveniently fitted *REF*s, then, having been transformed to the common *REF* of the branch will be summarized (allowing for the fact that the weight load, as transferred, represents an external loading for the other elements).

The transformation formulae between the i(ith) unit *REF* and R common *REF*, also considering the necessary rotation between the K and I, common and fitting systems respectively (3.3,4), are as follows:

$$\begin{aligned} \mathbf{Z}_{R,i} &= \mathbf{B}_{Ri}\mathbf{F}^{*}_{IK}\mathbf{Z}_i\mathbf{F}_{IK}\mathbf{B}^{*}_{Ri}\,, \\ \bar{f}_{s,R,i} &= \mathbf{B}_{Ri}\mathbf{F}^{*}_{IK}\bar{f}_{s,i}\,, \\ \bar{p}_{s,R,i} &= \mathbf{B}^{*}_{iR}\mathbf{F}^{*}_{IK}\bar{p}_{s,i}\,. \end{aligned} \tag{3.16}$$

This means, in comparison to the traditional procedure only so much surplus to the analysing work as the position of the "adequate" unit *REF* should be defined in the space.

It could not be made clear so far whether it is possible or convenient to establish some optimizing constraint in assuming the *REF* of the branch; due to JÜRGENSONN's generalizing problems, this is hardly possible. None the less, it is certain that one must not apply unnecessarily long *wayangs*. The computer represents each quantity by a large but limited number of digits. The errors in rounding appearing in the rotations and forces will be multiplied by the length in consequence of the transposition, the errors of the increments of motion and rotation according to (3.5) may increase, due to "small differences between large numbers". Continuing the analogy with the puppet-show: even with a player having firm hands might slightly tremble which, by transmission will be amassed upon the motion of the puppet to be carried out according to the role that has to be played. The larger the transmission, the more disturbing is the random dancing which, if it becomes excessive, makes the story unrecognizable. On the whole, the transformation (3.16) results in more ill-conditioned contributions.

It is recommendable to try to make the above spoiling as insignificant as possible with respect to the whole of the piping components: the selected *REF* should be "as near to the trace as possible". The pieces of major flexibility do influence the whole arrangement to an extent which exceeds their proportion and also the heavier ones are doing the same. All these considerations lead to some sort of "elastic centre of gravity". However, the accuracy of the machines assures an appropriate reserve, lest an exact optimum should be necessary, it is sufficient to take the *REF* at a rough estimate in the middle of all of the flexible configurations in question. It is certain, however, that the usual definition of the contributions with the reference points taken at the beginning and end of the physical branch is by no means optimal.

According to experiences the spring matrices are inclined to be ill-conditioned which can present difficulties particularly in the trial-and-error method to be applied later. The conditions may be improved by a well-considered programming of the algorithm [6]. It is to be kept in mind that the systems which in certain directions are extraordinarily stiff or their flexibility is unproportionately distributed are, in general, particularly unfavourable in this respect but such situations should be avoided also from merely structural point of view (i.e., because of risk of inaccurate mounting, local overloading). In case of several stiff suspensions on a vertical pipe (which caused local axial tightening) one has met numerical difficulties just as in case of a *REF* erronously assumed at an absurdly placed point.

3.2. Building up contributions from elements

The contributions of the *straight element* are given in the system as shown in Fig. 5. The spring matrix is diagonal, and due to the usual neglect of the axial tension beside bending, singular; $\bar{q}$ is the distributed weight load applied on the unit length of pipe.

$$\mathbf{Z} = \frac{l}{IE}\langle 0, l^2/12, l^2/12, 1+\nu, 1, 1\rangle$$

$$\bar{f}_s = \frac{l^3}{6IE}\begin{bmatrix} 0 & 0 & 0 \\ 0 & 1/4 & 0 \\ 0 & 0 & 1/4 \\ 0 & 0 & 0 \\ 0 & 0 & 1 \\ 0 & -1 & 0 \end{bmatrix}\bar{q}; \qquad \bar{p}_s = l\begin{bmatrix} \mathbf{E} \\ \mathbf{0} \end{bmatrix}\bar{q} \tag{3.17}$$

It is to be noted that the above singularity would cause the singularity of the system matrix only in the case where a straight section would be forced to fulfil the task of absorbing heat expansion. In practice, either the other adjoining elements assure the necessary flexibility of the branch in the direction of the straight axis or for a branch consisting of a single straight line the axial motion is not hindered: otherwise there is a defect in the construction.

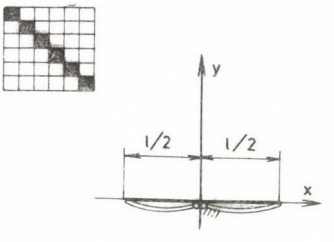

Fig. 5

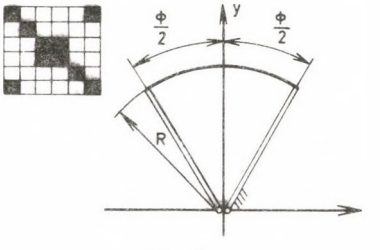

Fig. 6

For the pipe bend shown in Figure 6., the contributions may be calculated by making use of Castigliano's theorem. The factors k_i, k_o, k_t show how many times the deformations caused by a moment loading the pipe bend in its plane, by one acting out-of-plane and by torsional one are larger than in the case of bending a straight pipe. The value of k_i is the reciprocal of the Kármán-number; k_o has the same value or is equal to 1 (this is a less commonly used assumption), $k_t = 1 + \nu$. For designating repeatedly appearing quantities, a shortened notation will be used:

$$
\left.
\begin{aligned}
&P=(\Phi+\sin\Phi)/2\,,\\
&M=(\Phi-\sin\Phi)/2\,,\\
&F=\sin(\Phi/2)\,,\\
&C=2[F-(\Phi/2)\cos(\Phi/2)]\,.
\end{aligned}
\right\}
$$

$$
\mathbf{Z}=\frac{R}{IE}\begin{bmatrix}
k_iR^2P & 0 & 0 & 0 & 0 & 2k_iRF\\
0 & k_iR^2M & 0 & 0 & 0 & 0\\
0 & 0 & k_tR^2\Phi & -2k_tRF & 0 & 0\\
0 & 0 & -2k_tRF & k_tP+k_oM & 0 & 0\\
0 & 0 & 0 & 0 & k_tM+k_oP & 0\\
2k_iRF & 0 & 0 & 0 & 0 & k_i\Phi
\end{bmatrix}
$$

$$
\left.
\begin{aligned}
&\bar{f}_s=\frac{R^3}{IE}\begin{bmatrix}
f_{11} & f_{12} & 0\\
f_{21} & f_{22} & 0\\
0 & 0 & f_{33}\\
0 & 0 & f_{43}\\
0 & 0 & f_{53}\\
0 & f_{62} & 0
\end{bmatrix}\bar{q}, \qquad f_{11}=k_iR(\Phi P/2-2F^2)\,,\\
&\qquad\qquad f_{12}=-k_iR(M+\Phi F^2)/2\,,\\
&\qquad\qquad f_{21}=k_iR(3M-\Phi F^2)/2\,,\\
&\qquad\qquad f_{22}=k_iR\Phi M/2\,,\\
&\qquad\qquad f_{33}=k_tR(\Phi^2/2-2F^2)\,,\\
&\qquad\qquad f_{43}=(k_o-k_t)FM\,,\\
&\qquad\qquad f_{53}=(k_o+k_t)C+(k_o-k_t)M\cos(\Phi/2),\\
&\qquad\qquad f_{62}=-2k_iC\,.
\end{aligned}
\right\} \tag{3.18}
$$

$$
\left.
\begin{aligned}
&\bar{p}_s=R\begin{bmatrix}
p_{11} & 0 & 0\\
0 & p_{12} & 0\\
0 & 0 & p_{33}\\
0 & 0 & p_{43}\\
0 & 0 & 0\\
p_{61} & 0 & 0
\end{bmatrix}\bar{q}, \qquad p_{11}=p_{22}=p_{33}=\Phi\,,\\
&\qquad\qquad p_{43}=-p_{61}=2RF\,.
\end{aligned}
\right\}
$$

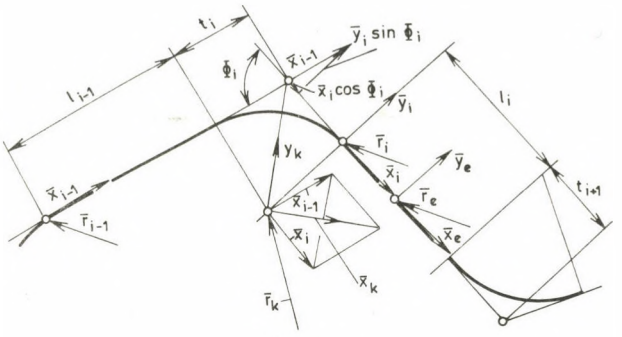

Fig. 7

The formulae of the straight line cannot be made more simple. From the spring matrix of the pipe bend elimination of some elements could be attained by placing the *REF* into the centre of gravity, however, those remaining would be more intricate. In this way, the diagonalization is impossible because the eigenvectors do not separately contain but also together the parts of force and moment of the load.

The contributions will be transposed according to (3.16) into the common system and to *REF*. The summation into the collecting variables $\mathbf{Z}$, $\bar{f}_s$, $\bar{p}_s$ will be carried out as follows (:= is the designation to assign a value)

$$\left.\begin{aligned} &\mathbf{Z} := \mathbf{Z}_1;\ \bar{f}_s := \bar{f}_{s,1};\ \bar{p}_s := \bar{p}_{s,1};\\ &\textbf{for } i := 2, \ldots \textbf{ do}\\ &\quad \textbf{begin } \mathbf{Z} := \mathbf{Z} + \mathbf{Z}_i;\ \bar{f}_s := \bar{f}_s + \bar{f}_{s,1} + \mathbf{Z}_i \bar{p}_s;\ \bar{p}_s := \bar{p}_s + \bar{p}_{s,i}\\ &\quad \textbf{end};\end{aligned}\right\} \tag{3.19}$$

A stiff section only enters with the weight loading being transferred, from the summation of the flexibility constributions is, however, omitted.

The representation of the trace is conveniently possible by the position vector $\bar{r}_0$ of its beginning (o) from the reference point, then by the pipe vectors $\bar{v}_0, \bar{v}_1, \ldots$ directed from corner point to corner point of the trace along with rounding radii $R_1, R_2, \ldots$ valid at their points of starting.

From the input vectors the following may be established (Fig. 7):

$$\begin{aligned} &v_i = \sqrt{\bar{v}_i^* \bar{v}_i}, \qquad \bar{x}_i = \bar{v}_i / v_i, \qquad \Phi_i = \arccos(\bar{x}_{i-1}^* \bar{x}_i),\\ &t_i = R_i \tan(\Phi_i/2), \qquad \bar{y}_i = (\bar{x}_{i-1} - \bar{x}_i \cos \Phi_i)/\sin \Phi_i,\\ &\bar{r}_i = \bar{r}_{i-1} + (l_{i-1} + t_i)\bar{x}_{i-1} + t_i \bar{x}_i, \qquad l_i = v_i - t_i - t_{i+1},\\ &\bar{z}_i = \bar{x}_i \times \bar{y}_i. \end{aligned} \tag{3.20}$$

Since no rounding at the first straight element is applied, from the above said result that $\bar{y}_0$ cannot be formed: the unit vector always being perpendicular to $\bar{x}_0$ and parallel to $x_{0y}-x_{0z}$, $x_{0z}-x_{0x}$, $x_{0x}-x_{0y}$ may be taken.

The fitting coordinate system of the straight element is identic with the one denominated above with i: the REF being

$$r_e=r_i+l_i x_i/2\,. \tag{3.21}$$

The fitting system of the circular arc is

$$\bar{r}_k=\bar{r}_i-R\bar{y}_i\,,$$

$$\bar{x}_k=(\bar{x}_{i-1}+\bar{x}_i)\Big/\left(2\cos\frac{\Phi_i}{2}\right);\quad \bar{y}_k=(\bar{x}_{i-1}-\bar{x}_i)\Big/\left(2\sin\frac{\Phi_i}{2}\right), \tag{3.22}$$

$$\bar{z}_k=\bar{z}_i\,.$$

The distributed load $\bar{q}$ should be rotated into the system of the elements. The formulae are also suitable for the analysis of the wind load, where for the straight section the axial component is omitted, and in the case of a circular arc the load applied on the projection is taken as an approximation, this being uniformly distributed along the trace.

3.3. The system calculated and the constraints

In the general use of terms, an ensemble of, possibly disconnected, pipes constituting a unit system from some technological viewpoint, is called a pipe system (for example, system of steam mains). From the viewpoint of calculation, the system is the ensemble of pipes connected to each other to be calculated as a unit, and it is only, in most cases, a part of the above one. It is a configuration of pipes which is only connected to motionless, fixed points of environment or to ones of known movement, thus, being unaffected by other flexible pipe configurations. The pipe does not end necessarily at its border: a clamping of any kind (fixation) to the environment preventing the motion or a pipe element to be deformed unopposed to any direction (a particular compensator) separates the system in the same way as if it would go no further. The structures in connection with the environment (the constraints) should be investigated together with the piping.

From the formulation of the contributions of the branch made earlier, it is to be seen that an external load may only be taken into account at the nodes of the network, that is, at the terminal points of the section investigated, and motions can only be calculated here. Therefore, the network should be divided by this consideration into branches by assigning the nodes. Thus, the nodes are as follows:

— points where the pipe is connected to the environment by a total (affecting any motion at all of the six directions) or partial link, rigid or of a given flexibility: i.e., by a constraint,
— points where external concentrated forces are applied on the piping,
— points where the pipe branches off or has an end physically (however, if the latter point is not submitted to a loading or constraint, the branch jointed may be omitted from the calculation as an unloaded one),
— points where the motion of the pipe ought to be checked for some reasons (for example, in the case of imminent collision).

To a particular node several of the above conditions might be valid. For the sake of uniformity it could be said that every node is submitted to constraints but, in some cases, to such a one which permits free motion in every direction. The case of external concentrated forces may even be eliminated in two ways from the discussion:

— either incorporating them into the weight effects,
— or a very soft, appropriately stressed spring should be bound to be pipe: its slight displacements do not modify the tension significantly.

The constraint is a particular branch which connects the node and its, in general fixed, cover point in the environment, and

— whose geometrix length is equal to zero,
— which has no weight effects,
— whose spring matrix is, in an appropriate system of coordinates, diagonal and mostly singular.

The actual pipings are commonly fitted to the building structure in such a way that such an orthogonal system of coordinates presents itself to the axes of which the major part of the pipes are fitted. Most of the constraints are suspensions or clampings; the side anchorages and guides are less frequent, and their guiding do not differ in most of cases from that of the main system of coordinates fitted to the piping. Practically, it is sufficient to analyse such constraints which are acting stiffly or flexible in the directions of the axles of coordinates applied to the description of the system as a whole (for more general cases a rotation ought to be inserted).

The spring suspension to be seen in Fig. 8 can be simulated by the configuartion represented beside it where the extremity of the spring is connected by a wayang to the cover point A'. The spring matrix is

$$\mathbf{Z} = \langle \infty, \infty, c, \infty, \infty, \infty \rangle . \tag{3.23}$$

The infinite elements are formal, they do not enter into the calculations. In the analysis it should be investigated how the reaction forces transmitted by the constraints deform the system. As a matter of course, such a reaction force cannot be generated which could cause an infinite motion on the constraint: the constraint automatically filters the possible reaction components. This filtering is realized by the

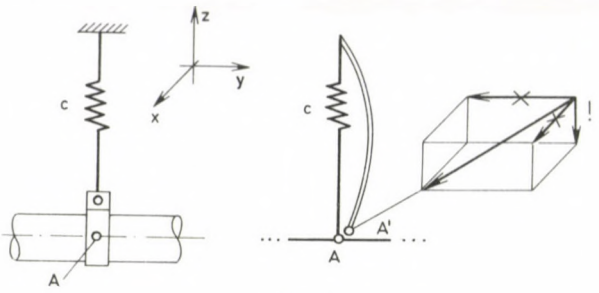

Fig. 8

multiplication with the diagonal matrix

$$\mathbf{S} = \langle 0, 0, 1, 0, 0, 0 \rangle \tag{3.24}$$

consisting of the elements 0 and 1. And in the case where in the calculation merely such compatible reactions are taken into consideration, the filtered spring matrix

$$\mathbf{K} = \mathbf{SZ} = \langle 0, 0, c, 0, 0, 0 \rangle \tag{3.25}$$

can be used.

In the direction of the stiff anchorage the value of the spring constant is equal to zero. The characteristics of the clamping are

$$\mathbf{S} = \mathbf{E}, \qquad \mathbf{K} = \mathbf{Z} = \mathbf{0}. \tag{3.26}$$

The "constraint" of the motion, free in every direction is

$$\mathbf{S} = \mathbf{K} = \mathbf{0}. \tag{3.27}$$

The constraint realized by a spring in every direction will be

$$\mathbf{S} = \mathbf{E}, \qquad \mathbf{K} = \mathbf{Z}. \tag{3.28}$$

The above representation corresponds to the force method where the components of the reaction forces are considered to be unknown. In the case of actual pipings, due to the partial constraints of one or two components (where four or five components of motion are to be dealt with), commonly, one should work with less unknown values in this way, than with the displacement method having as a purpose the determination of the components of the motion. The latter has other advantages in consequence of which, for example, in the case of the method of finite elements, the force method is almost ousted; as is, among others, the fact that the system matrix is rather sparse. For the algorithm of the solution of the equations to be worked out this

difference becomes less interesting, therefore, it does not seem necessary to leave off the traditional force method. This is also supported by the fact that the stiffness matrices **Y** serving as basis for the displacement method cannot directly be established for the pipes, but by inverting the spring matrix. Therefore, the method of motion will not be detailed here, only for good measure, the treatment of the constraints will be outlined.

The stiffness matrix of the constraint investigated

$$\mathbf{Y}=\mathbf{Z}^{-1}=\langle 0, 0, 1/c, 0, 0, 0\rangle \tag{3.29}$$

might be obtained without any difficulties, in a formal way. It contains infinite elements in case where one of the components is stiff. In those directions, as a matter of course, no components of motion might be assigned; according to the above statements, the motion filter $\mathbf{S}_m$ and the filtered stiffness matrix **W** might be defined. (For the instance presented $\mathbf{S}_m=\mathbf{E}$).

In the case of clamping

$$\mathbf{S}_m=\mathbf{0}, \qquad \mathbf{W}=\mathbf{0}; \tag{3.30}$$

in the presence of a "constraint" permitting free motion in every direction

$$\mathbf{S}_m=\mathbf{E}, \qquad \mathbf{W}=\mathbf{Y}=\mathbf{0}; \tag{3.31}$$

and for a constraint flexible in every direction

$$\mathbf{S}_m=\mathbf{E}, \qquad \mathbf{W}=\mathbf{Y}. \tag{3.32}$$

The interdependence between the filtered matrices is

$$\mathbf{KW}=\mathbf{SS}_m=\mathbf{S}+\mathbf{S}_m-\mathbf{E}=\mathbf{E}-(\mathbf{S}-\mathbf{S}_m)^2. \tag{3.33}$$

The spring-filter informations may be stored in a rather concise form by six-digit binary numbers at which regarding the directions taken in order of succession the 0 refers to the lack of constraint whereas 1 refers to its presence, in lack of other complementary information, to a stiff one. In this way 63 is the descriptive symbol of the clamping or that of the constraint flexible in every direction, 8 is the designation of the suspension and $27=011011$ characterizes a guide permitting displacement in x-direction and rotation about x. The information relating to the springed suspension might be implied in this series of description, necessarily consisting of positive numbers as follows. A store vector should be allocated for the spring constants (which, let us denote, say, with A) and all of the constants entering will be written in this, also the repeated ones only once. One of the constraints being springed, after the filter it is indicated by a negative number, which significant component of constraint is in question counted according to the opposed sequence, then the subscript of the spring constant in the store vector will

be written. In processing, the negative sign indicates that no filter-descriptor, but a spring-descriptor follows.

Be the constraint a stiff suspension, and an anchorage springed in the x and y directions, further, the 2nd and 5th element of the vector A should hold the spring constants. The entire description will be

$$\ldots, 56, -3, 2, -2, 5, \ldots$$

Considering that the magnitude of the descriptor elements of the representation is limited, a further densification is possible depending on the feasibilities of the machine used.

In the representation, presented above, no possibility appeared to the general transfer of the constraints along the stiff bar which would permit the making of the whole calculation independent of the spatial position of the nodes. Although a complete constraint, be it flexible, stiff or free for all six components, might be transferred to an arbitrary *REF*, however, in case of a partial constraint, filtering appears in such a way that between the components of the compatible loading, admissible for the *REF*, a linear relation has to be valid; this linear relation is characterized by a section (adjusting itself to the "partiality") of the transfer matrix between the node and the *REF*. Transferring a total flexible constraint, its diagonality will be lost.

3.4. The network equation and its solution

The direct objective of the calculations is to determine what loadings are applied to the system and its nodes where will be displaced on the effect of the acting weight (and concentrated) loads, and owing to the restraining of the thermal expansion. With the results known, the stress analysis of each of the elements may be performed as a separate operation by determining the loads acting on the cross section.

First, the structure should be rendered statically determinate by removing constraints of the required number. In principle, this may be carried out, in several ways. Practically, it is recommendable to have one single fixation left in the system. Such a fixation is always to be found in a pipe network, disregarding some extreme instances. It is advantageous if this fixation does not move itself, for example, in consequence of thermal expansion of an adjoining installation. Should such a fixation not to be found, so the selected fixation ought to be "stopped" by the superposition of an opposite motion on the entire system. Should there be several possibilities, so according to experiences, it is convenient to retain the fixation of the stiffest branch.

The removal of the constraints should be carried out by releasing the cover point in the environment of the node in question. A particular internal constraint is the closed loop. This should be cut through whereby an additional node is created. The opposite of the reaction force or, more correctly, that of the loop force acting here, also appears

on the node being at the other side of the cut, and its magnitude is defined by the requirement of preventing the difference of the motions which might occur between the two nodes: they should follow each other stiffly. With the new node in the representation of the constraints the number 63 is associated.

In the system released in this way, by summarizing the expansion and weight effects of the branches, to be detailed later, it could be determined what displacements the cover points carry out as compared to their original positions in the environment. The difference is increased by the fact that also these places themselves may move (for example, the connection points of the turbine, etc.). At the cover points reactions will be generated which prevent or eliminate, thrust back such differences of motion and the cover point might be connected anew to the environment. At the cross section when cutting through the loop the difference in the motions of the two sides of the cut should be eliminated: the newly created node should be pulled over to the older one.

The traditional method consists in constructing the combined spring matrix $\mathbf{Z}$ of the system from the spring matrices of the branches and constraints by summarizing and ordering in a unified table the threefold products generated with the transfer matrices and by blotting out the inadmissible reaction components (in that direction thrustback could not be prescribed, either, because the motion is of free nature).

Then the equation

$$\mathbf{Z}\bar{p}=\bar{f} \tag{3.34}$$

should be solved.

In this equation

$\bar{p}$—vector of admissible components of reaction force,

$\bar{f}$—ordered vector of needed back-thrust.

They might be generated by the unification of the cover-point loadings and motions and by omitting the free components. Their number of dimension is the number of the components of constraints causing the statical indeterminacy, i.e., the number of the degree of freedom (in the force method) which, in the following will be denoted with k.

By making use of the symmetry, beside the working space needed for the solution, for storing the matrix $(k+1)k/2$ locations are required but the motions taking place in the directions without constraints could not be obtained in this way. To obtain them, from the rows blotted out also the part of an extent $(6n-k)k$ is needed wherein n is the number of the nodes in the network (the remaining fixation being disregarded).

The construction of the matrix is a rather lengthy operation and the spring matrices are highly susceptible to ill-conditioning, thus, the necessitiy of correction by iteration cannot, as a matter of course, be excluded. (Although in practice it could be experienced that in case where the inaccuracy of the solution already attained a disturbing level, the system was so poorly conditioned, mainly due to possible construction errors, that neither was the correction by iteration successful.) By the introduction of the *REF*, the construction of the matrix might significantly be simplified. However, in order to reduce the demand for store one should establish such

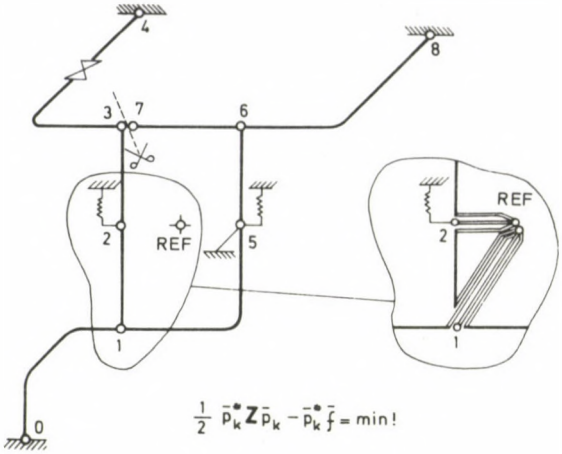

Fig. 9

an algorithm which performs a transformation (3.34) without the explicit knowledge of the matrix and apply an iteration process which, according to that said above, is obviously not a worse approximation than the traditional ones.

Let us number the nodes by proceeding outwards from the retained fixation marked with zero; at the cut of a loop the number of the new node should always be higher than that of the earlier one being on the other side of the cut. The number of the node is, at the same time, that of the branch starting from it toward the fixation. Let us cut down the branches from the node and set out from their end stiff bars to a *REF* which is common with the whole network where the adjoining branches should again be connected to each other. In this way, the branches being wayangized present themselves in the network. The physical nodes and constraints remain in their places and joint to the branch connection formed at the *REF* by a wayang. This could be omitted at the node without constraint, and at fixation as well, because they could also be defined by the *REF*, however, in order to keep uniformity this is disregarded (Fig. 9).

The order of the joining of the branches may succinctly be described by the so-called "tree" and "loop" vectors. The former gives to each node the number of the node to which, towards the fixation, that will be joined with a branch, i.e., it shows the structure of the directed tree-shaped graph. The latter also indicates for each node that if it has been created at the cut of a loop, which node number is situated on the other side; if not, the associated vector element is equal to zero. This is more justified than the mere filling of the space because the cover point of these nodes and the retained fixation considered not being displaced from its position i.e., the node 0, may be connected with a stiff section: the motion may be defined as one being relative with respect to the node 0. Thus, the nodes can be deduced from cutting-through of fictious loops: the one half of the loop is the ensemble of the branches stressed by the node forces to the fixation, the other half of the loop being the stiff, leading back through the environment. Cutting

through the loop, strictly speaking does not take place beside the node but beside its cover point, the constraints connecting to the cover point remain at the node. On the other side, in the original network, the node 0 is not directly situated. Should all these be related to the network transferred to the *REF*, there the constraints do not enter in the picture and the cut might be considered to be between the node in question and the equivalent of the node 0 at the point of reference. The force method, regarding its nature is a loop-method just as the current-method of electric networks; the displacement method similarly to the voltage method investigates the equilibrium of the nodes.

The vector elements for the network of Fig. 9 are indicated in table (3.35).

No.	1	2	3	4	5	6	7	8
Tree	0	1	2	3	1	5	6	6
Loop	0	0	0	0	0	0	3	0

(3.35)

From this, that part of the table enclosed by a heavy line might be considered to be the carrier of relevant information. In an actual piping, loops do not occur frequently. Both vectors might be stored together if the elements of the tree-vectors are given from node 2 consecutively; the elements of the loop-vectors if such exist, should be inserted in the series with negative signs subsequent to the tree-element. The limited magnitude of the descriptors permits also here the densification which depends, however, on the properties of the computer.

Multiplication of a k-extent ordered series of compatible reaction components or, in other terms, of those reduced according to the constraints, by the summarized **Z**, i.e., its transformation into the ordered vector of the components of motion in the directions of the constraints may be carried out in the following steps;

a) An array for the results of k-extent and a working space of $6n$-extent should be assigned. With the aid of the spring-filter descriptors, the compatible reaction components should be "made up" into the working space in order to produce the ordered series of the nodal loads with all their six components, to the places of the components incompatible with the constraints zeros should be written. Simultaneously, the motions of the constraints taking place under the effect of the compatible reaction components should be set into the array of results; if the constraint is stiff, the corresponding component should be zeroed.

b) By multiplying the nodal loads with the transfer matrices in the respective order in the working space the nodal loads transferred to the *REF* will be established.

c) From the load applied to the nodes those applied to the branches should be produced. Backwards from the highest serial number, the descriptors of the linkages ("switch") should be taken one by one and each load should be added to that of the node onto which the tree-vector points and subtracted from that of the node onto which the loop-vector points. (It should be noted that using the displacement method, a calculation of similar nature ought to be carried out but not in such an accumulatory manner.)

d) Multiplying all the loads applied to the branches by the spring matrices, the deformations of the branches should be calculated in the same working space.

e) The deformations of the branches should be summarized into motions of the nodes, to do so, the ladder of the linkage descriptors should be climbed in the opposite direction. The deformation of the branch is the motion of the node bearing the very same number as that of the branch, in case where the other extremity is fixed: this is at 1 the actual motion itself. Further at each node to the motion found there, the motion of the node should be added onto which the tree-vector, while subtracting the motion of the node onto which the loop-vector points. (As for the displacement method, the remark made under point c) remains valid.)

f) The motions of the nodes defined on the *REF* should be transferred with the help of transfer matrices to the physical nodes. In this way, the whole motion of the nodes will immediately to obtained as the by-product which should be calculated separately in the case of ordinarily arranged matrix procedures.

g) With the aid of the filter descriptors, the components of motion of the constraint direction should be selected and added to the constraint deformations to be already found in the store of the results.

Should this final result agree with the back-thrusts prescribed, so the reaction components assigned as starting ones, yield the solution to the problem.

The above algorithm or some parts of it may be used in the summing up to the thermal expansion and the weight effects, i.e., after changing the signs and correcting by the motions of the nozzles of connecting equipment, to the determination of the back-thrusts. The components of number k will be selected with the aid of the filter descriptors from among the six-component back-thrusts which are prescribed for the determination of the reaction forces. Also from the total motion of the node obtained at point f) the whole back-thrust should be subtracted because, in this way, it could be recognized whereto the nodes will be displaced with respect to their environmental cover point (which, possibly, also itself has been displaced); thus, it could be established whether the displacement of the pipe could be permitted on the supports and in break-through of walls, etc. Prestressing may be taken into account by the displacement in the opposite direction of the extremities of the branches being arranged on the side outwards from the fixation retained (namely, it is all the same whether from a branch a section will be cut out and pulled together or drawn asunder at the same rate at the fixations disregarding the problems of retaining the co-axiality of the pipes). At the section between the actual place of the prestressing and the extremities of the branches displaced, the motion calculated for the pipe supports should appropriately be corrected.

The usual methods of iteration will not serve the purpose because they require, besides the transformation, the knowledge of the diagonal elements of the matrix or of other data, for example, being related to the spectrum which, most likely, cannot be simply estimated from the transformation. It is more recommendable to trace back the problem to the minimization of a quadratic form. In case of back-thrusts $\bar{f}$ prescribed,

from among the loadings $\bar{p}_k$ compatible with the constructions, the solution to the problem is the one to which the complementary potential energy

$$Q = \frac{1}{2}\bar{p}_k \mathbf{Z}\bar{p}_k - \bar{p}_k^* \bar{f} = \frac{1}{2}(\bar{p}_k - \mathbf{Z}^{-1}\bar{f})^* \mathbf{Z}(\bar{p}_k - \mathbf{Z}^{-1}\bar{f}) - \frac{1}{2}\bar{f}^* \mathbf{Z}^{-1}\bar{f} \qquad (3.36)$$

is of minimum value. From the transformation it is to be seen that the surface is a dislocated general ellipsoidal paraboloid of vertical axis, whose one single minimum is the solution indeed. The minimum value is the negative value of the potential energy.

The method of reduction along chosen directions may be used conveniently, for the approximation of the minimum. By proceeding from some initial value $\bar{p}_0$ in the direction of the vector $\bar{v}$, the intersection of the surface by a hyper-plane $(\bar{v}, Q)$ should be investigated which is a parabola. The minimum value is obtained at the point $\bar{p}_0 + \alpha\bar{v}$ where

$$\alpha = \bar{v}^*(\bar{f} - \mathbf{Z}\bar{p}_0)/(\bar{v}^* \mathbf{Z}\bar{v}) \qquad (3.37)$$

is valid.

The directions may be assumed as being the simplest that one of the k components should be equal to the unit, the other values being equal to zero. This is only a circumstantial utilization of the Gauss-Seidel-method which is, anyhow, certainly convergent, being $\mathbf{Z}$ positive definite, but only slowly.

The direction of searching might be the negative gradient of Q to be defined as the error of the approximation $\bar{p}$ or as a remainder

$$\bar{r} = \bar{f} - \mathbf{Z}\bar{p}\,. \qquad (3.38)$$

Should, however, the eigenvalues of the matrix $\mathbf{Z}$ strongly differ from each other, i.e., with rough approximation, the flexibilities of the piping to be defined in the different directions would be very different, so the negative gradient points in a long narrow valley almost towards the opposite wall and one may only zigzagging slowly to the deepest point [4]. Such particularities cannot be avoided in practice; all these regarded from another point, are equivalent to an ill-conditioning. Thus, besides the convergence, being slow in itself, also the accumulation of the errors might be expected, with respect to which the processes minimizing along directions suitably calculated, are also particularly sensitive because the direction becomes uncertain.

By selecting more conveniently the direction of the search for the minimum, the convergence may, at the expense of some surplus calculations, be significantly corrected. Let us have such a set of vectors $\bar{v}_1, \ldots, \bar{v}_k$ that

$$\bar{v}_i^* \mathbf{Z} v_j \begin{cases} = 0, & \text{if } i \neq j \\ \neq 0, & \text{if } i = j, \end{cases} \qquad (3.39)$$

Such vectors are called $\mathbf{Z}$-orthogonal or $\mathbf{Z}$-conjugates. Any vector of the space of dimensions k, thus, also the necessary correction of the initial value $\bar{p}_0$ *might be*

produced as the linear combination of these vectors

$$\bar{p} = \sum_{i=1}^{k} \alpha_i \bar{v}_i + \bar{p}_0 \tag{3.40}$$

Making use of (3.39) yields

$$\alpha_i = \bar{v}_i^* \mathbf{Z}(\bar{p} - \bar{p}_0)/(\bar{v}_i^* \mathbf{Z}\bar{v}_i) = \bar{v}_i^*(\bar{f} - \mathbf{Z}\bar{p}_0)/(\bar{v}_i^* \mathbf{Z}\bar{v}_i) \tag{3.41}$$

which is in accordance with (3.37). Should the vectors $\bar{v}_i$ be continuously generated and from the approximation $\bar{p}_0$ should be the terms of (3.40) produced by iterative approximation $\bar{p}_1, \ldots$ so, this iteration (conjugate gradient method) leads to an exact result in k steps, $\bar{p}_k = \bar{p}$. The $\bar{v}$s might be produced from some linearly independent set of vectors consisting of k elements by making use of the Gram-Schmidt procedure. Should there be selected the axis-vectors of the space of k-dimensions, so the procedure would correspond to the Gauss-elimination method. However, it should be pointed out that the remainder vectors (i.e., the negative gradient vectors) which are, anyway, needed for checking the calculation, will be

$$\bar{r}_j = \bar{f} - \mathbf{Z}\bar{p}_{j-1} = \sum_{i=j}^{k} \alpha_i \mathbf{Z}\bar{v}_i \tag{3.42}$$

being also linearly independent, thus, by their use, Gram-Schmidt's calculation scheme will be greatly simplified. The formulae could be established in several ways, however, to reduce the calculation work, it is Fletcher-Reeves's variation which seems to be numerically the most advantageous. Its formulae are [4] [7]:

$$\begin{aligned}
&\bar{v}_1 = \bar{r}_1 = \bar{f} - \mathbf{Z}\bar{p}_0\,, \\
&\vdots \\
&\bar{q}_i = \mathbf{Z}\bar{v}_i\,, \\
&\alpha_i = \bar{r}_i^* \bar{r}_i / \bar{q}_i^* \bar{v}_i\,, \\
&\bar{p}_i = \bar{p}_{i-1} + \alpha_i \bar{v}_i\,, \\
&\bar{r}_{i+1} = \bar{r}_i - \alpha_i \bar{q}_i\,, \\
&\beta_i = \bar{r}_{i+1}^* \bar{r}_{i+1} / \bar{r}_i^* \bar{r}_i\,, \\
&\bar{v}_{i+1} = \bar{r}_{i+1} + \beta_i v_i\,, \\
&\vdots
\end{aligned} \tag{3.43}$$

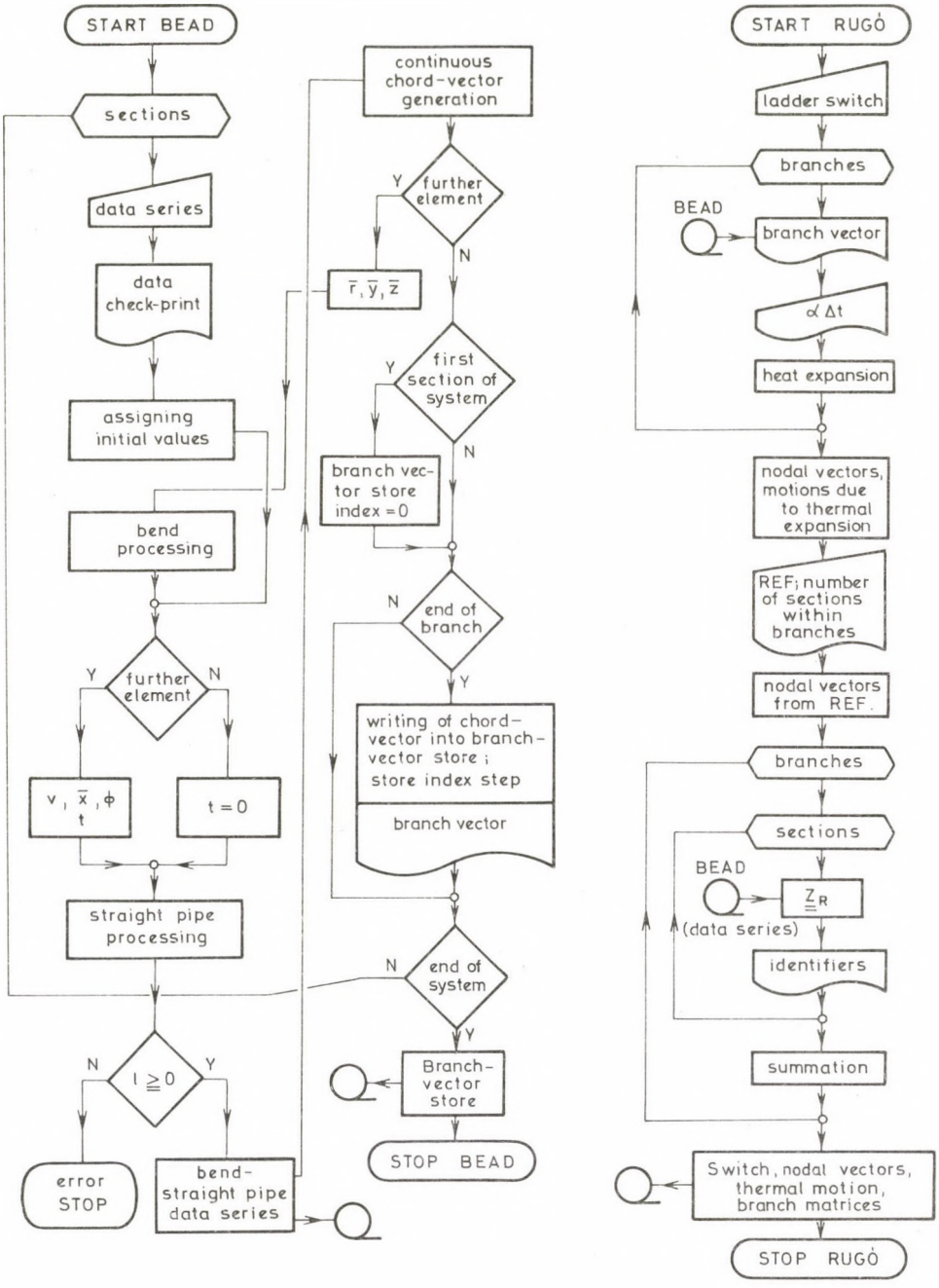
START BEAD
sections
data series
data check-print
assigning initial values
bend processing
further element
Y
N
v, x̄, φ
t
t = 0
straight pipe processing
l ≧ 0
N
Y
error STOP
bend-straight pipe data series
continuous chord-vector generation
further element
Y
N
r̄, ȳ, z̄
first section of system
Y
N
branch vector store index = 0
end of branch
N
Y
writing of chord-vector into branch-vector store; store index step
branch vector
end of system
N
Y
Branch-vector store
STOP BEAD
START RUGÓ
ladder switch
branches
BEAD
branch vector
α Δt
heat expansion
nodal vectors, motions due to thermal expansion
REF; number of sections within branches
nodal vectors from REF.
branches
sections
BEAD
(data series)
identifiers
summation
Switch, nodal vectors, thermal motion, branch matrices
STOP RUGÓ

Fig.

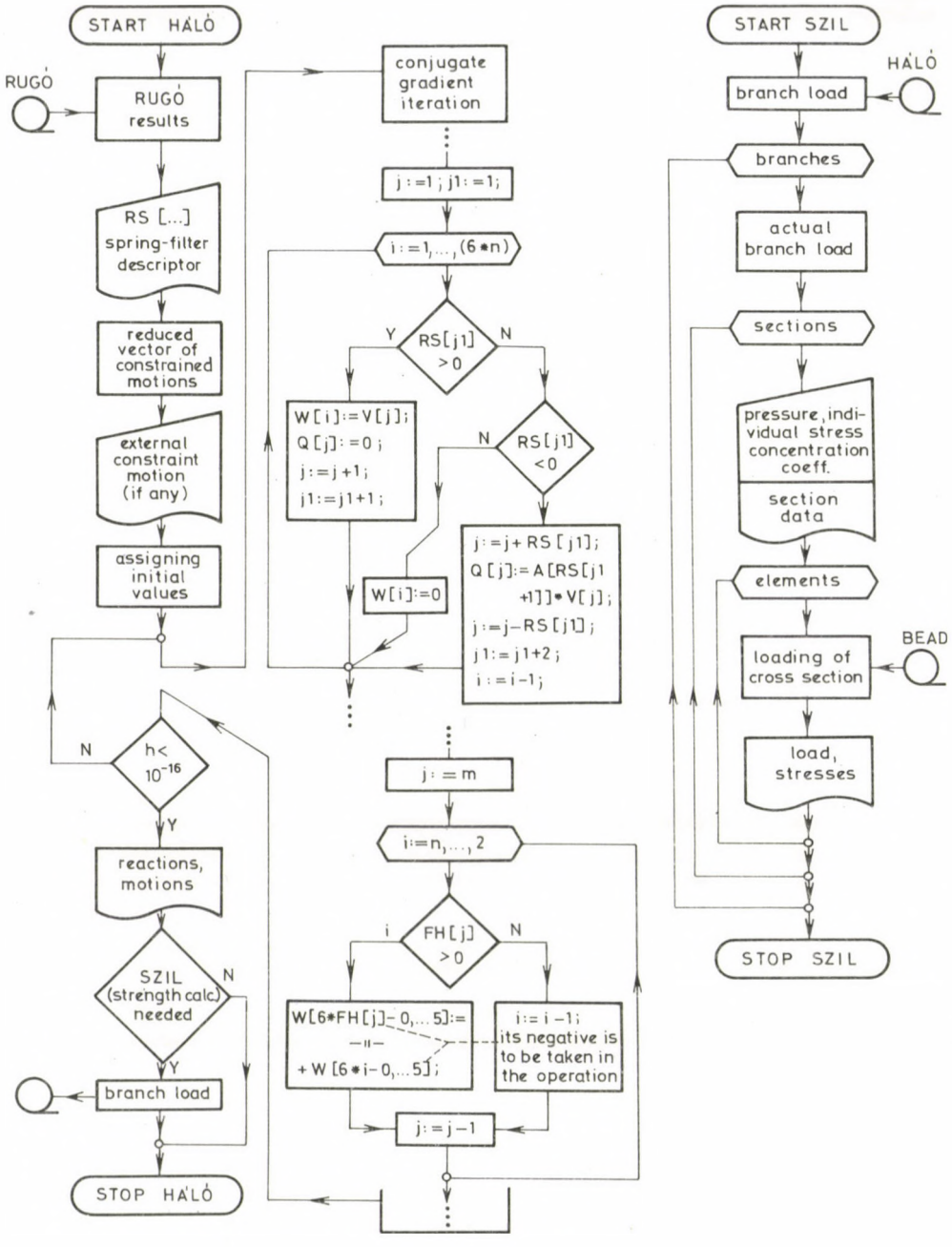
START HÁLÓ
RUGÓ
RUGÓ results
RS [...] spring-filter descriptor
reduced vector of constrained motions
external constraint motion (if any)
assigning initial values
conjugate gradient iteration
j:=1; j1:=1;
i:=1,...,(6*n)
RS[j1] >0
Y
N
W[i]:=V[j]; Q[j]:=0; j:=j+1; j1:=j1+1;
RS[j1] <0
W[i]:=0
j:=j+RS[j1]; Q[j]:=A[RS[j1+1]]*V[j]; j:=j-RS[j1]; j1:=j1+2; i:=i-1;
h< 10^-16
reactions, motions
SZIL (strength calc.) needed
branch load
STOP HÁLÓ
j:=m
i:=n,...,2
FH[j] >0
W[6*FH[j]-0,...5]:= -"- + W[6*i-0,...5];
i:=i-1; its negative is to be taken in the operation
j:=j-1
START SZIL
HÁLÓ
branch load
branches
actual branch load
sections
pressure, individual stress concentration coeff.
section data
elements
BEAD
loading of cross section
load, stresses
STOP SZIL

This method, due to the inevitable accumulation of the errors, does not give, in general, an exact result by k steps, however, by further steps, the remainder could be diminished as far as the accumulation of the errors makes any further correction impossible. Under favourable conditions it may happen that (which, in practice, has been experienced) after some steps, less than k, a very exact result would be obtained.

The space requirement of the method is much less than of one using explicitly the assembled matrix of the system : in both of them the $6n$ work field and a vector of extent k are required for data and results; as a particular space requirement, that of $2k$ of the vectors $\bar{v}$ and $\bar{q}$ can be compared to the extent of the matrix increasing by square proportion with k, and regarding the whole problem of an extent also depending on n. The comparison of the calculation times is quite difficult, because, on the one hand, also the time requirement of the construction of the matrix and the accidental iterative correction after the elimination should also be accounted for and it has to be compared, an the other hand, with requirements also allowing for the time-surplus of necessary steps above k due to error accumulation, only raw guesses being possible for. This problem could only be answered by the statistics of a "comparative shooting" carried out on the very same computer through a great number of networks and for that the procedure in question could not of course be considered as a fact having no chance.

The above procedure has been realized on a small desktop computer EMG-666, together with the strength calculation in the form of four programs joining each other; the data transmission is carried out by tape. Each of the 1008 locations of the computer can hold a floating-point number of an accuracy of 12 decimal digits or eight computer instructions. The bottle-neck is the calculation of the piping network, which restricts the size of the system for 20 branches at $k=42$. Allocation of the store is performed dynamically, for lower values of k, the number of the branches might be augmentes gradually to 24 and vice versa. This span, extreme cases disregarded, is sufficient for the practice. The maximum time requirement remains, by and large, in the range tolerable in connection with the desktop machine (the largest system $n=19$, $k=43$ ran 66 minutes). The danger of accumulating errors depends at the same time both on the number of branches and constraints, from empirical data the necessary number of steps may be estimated in comparison with the theoretical one to

$$K \approx 0{,}1(k+n)k \tag{3.44}$$

whereform, in case of small systems, deviations sooner occur upwards and in the case of large systems, rather downwards. The time-demand of each of the steps depends both on n and k, however, due to the decisive weight of the branch-matrix multiplications, more strongly on the former:

$$t \approx 0{,}792n + 0{,}0543k \quad [\mathrm{s}] \tag{3.45}$$

In the systems serving for basis, two components of constraint fell to one branch, the number of branches being more than sevenfold weight. By eliminating k in the above proportion, and by reducing the two estimates, the time demand summarized is

$$Kt \approx 0{,}09(k+n)kn\,. \tag{3.46}$$

The block diagrams of the partial programs called *BEAD*, *RUGÓ*, *HÁLÓ*, *SZIL* are shown in Fig. 10. The series of operations detailed in the conjugate gradient-iteration are as follows:

— placing the vector $V[1:k]$ reduced according to the constraints to the working space $W[1:6n]$ (i.e., transforming it into a series of complete six-component quantities) and filling up the part of the transformed vector $Q[1:k]$ depending on the spring constants $A[\ldots]$ which is controlled by the spring-filter descriptor $RS[\ldots]$;

— summation of the loads at the *REF*-nodes stored in W into branch loads according to the tree-loop vector $FH[1:m]$.

Although at the expense of some increasing of storage demands remaining, however, still linearly proportional to k, further developments may be carried out by making use of some stabilized variation of the conjugate gradient method (for example, by applying the Lánczos-method [5]). The improvement might be possible by taking into consideration that to the series of the $\bar{v}$s and $\bar{r}$s also certain other relationships are valid, further, if some of the critical partial operations are carried out with the aid of double-precision arithmetics. In the field of the conjugate gradient methods there are further research investigations going on, an improvement in their efficiency might be expected.

3.5. Complementary notes

Two basic elements of the method of solution described above are wayangizing the network and applying the conjugate gradient method without writing down the network matrix. Its advantage lies in the significant reduction of the storage capacity needed for the calculation. It is likely that minor changes in the network might be handled more advantageously this way; but it is unquestionable that for analyzing of several sets of constrained movements of the very same piping the method of explicit matrix is quicker (although it is another question that this possibility is not incorporated in many programs, and its practical significance is not too great, either).

The preliminaries of the application of the wayangs in a special and ad hoc way may be found in the method of JÜRGENSONN and HAMPEL [3] who, however, did not developed it to a comprehensive method of treatment.

In the general analysis of frame structures, HALL and WOODHEAD [9] apply stiff members of arbitrary forms joined to the extremities of the beam section, also in an alternative leading to the very same point but by this latter they suggest only the equilibrium of the forces applied on both extremities and the independence of the

flexibility of the direction of representation. They refer also to the role of elastic centre and of (approximate) principal axes assumed on the basis of the symmetry, if any, and/or by estimation, in the construction of a matrix being at least nearly diagonal and, thus, advantageous from the point of view of the calculation work and definiteness. Besides qualitative references they deal only with inplane configurations similarly to the formulation of JÜRGENSONN. In the framework of another generalization LIVESLEY [10] introduces the reference-point loading and motion as a form of appearance of the general quantities ("stress resultant", "element deformation vector") characterizing the stress and deformation state of a flexible section.

Presumably, the model applied in the present paper may also be useful in solving other structural problems because the change in loading and motion caused by their transposition in space is eliminated from the network analysis.

RALSTON comments the application of the conjugate gradient method to linear algebraic equations in such a way, although appreciating its elegance and efficiency, that one may always find classical direct and/or iterative procedures being more favourable for any kinds of matrix properties. It is probable that in the case of the chosen approximation (considering a direct minimum-search problem instead of system of equations), however, the conjugate gradient method is the most suitable way among those he described and the approximation itself will be the more competitive, the more efficient the method will be made by further investigations (besides the undisputable store economy). Its significance is emphasized by the fact that a very wide field of the technical-physical problems may be formulated in the form of extreme value problems; in a certain conception this may be a general alternative of the classic description of nature by differential equations [8]. The author's proposal is, after all, not associated with the conjugate gradientmethod but to any which may be applied without the explicit knowledge of the matrix.

Acknowledgements

The writer is deeply indebted to the correferents of the paper, prof. Á. BOSZNAY and Dr. J. FEKETE for their valuable advice and comments.

REFERENCES

1. FEKETE J.: Untersuchungen der elastischen Formänderung von Rohrleitungen und Rohrnetzwerken, *Fortschr. Ber. VDI*, R. 7. Nr. 5. Juli 1967
2. JÜRGENSONN, H. v.: Elastizität und Festigkeit im Rohrleitungsbau, Springer, Berlin, 1953
3. HAMPEL, H.: Rohrleitungsstatik, Springer, Berlin, 1972
4. RALSTON, A.: Introduction into the Numerical Analysis, Műszaki Könyvkiadó, Budapest 1977*
5. BAHVALOV, B. Sz.: Numerical Methods of the Computer Mathematics, Műszaki Könyvkiadó, Budapest 1977*

* In Hungarian

6. FORSYTHE, G. E.—MOLER, C. B.: Solutions to Linear Algebraic Problems with the Aid of Computer, Műszaki Könyvkiadó, Budapest 1976*
7. MANGASTRIAN, O. L.: Techniques of Optimization, *Trans. ASME* (Ind.), May 1972. pp. 365—372
8. GYARMATI I.: Non-equilibrium Thermodynamics, Műszaki Könyvkiadó, Budapest 1967*
9. HALL, A. S.—WOODHEAD, R. W.: Frame Analysis (2. ed.). Wiley, N. Y. 1967
10. LIVESLEY, R. K.: Matrix Methods of Structural Analysis (2. ed.), Pergamon, Oxford, 1975

Entwurf von Rohrleitungssystemen aufgrund der elastischen Formänderungen — Im ersten Teil der Abhandlung wurde festgesetzt, daß sowohl die unmittelbare Einbeziehung des Projektingenieurs, als auch die operative Berechnungsansprüche die Zweckmäßigkeit der Anwendung des Tischenrechners neben der Planungsgruppe gleicherweise bekräftigen. Das Kapazitätsbedürfnis der Netzberechnungsprogramme ist erheblich; in diesem zweiten Teil der Abhandlung wird die Reduktion desselben versucht.

Acta Technica Academiae Scientiarum Hungaricae, 93 (1—2), pp. 197—208 (1981)

HYDRODYNAMIC MODELLING OF POWDER INJECTION INTO MELTS

GY. KÁROLY C. SC.* and EL-GHAZALLY SAID A. M. SC.**

[Manuscript received: 12 June 1981]

The authors investigated the hydrodynamics of different densities and grain sizes particulate/nitrogen jets into a water bath. The flow patterns as well as the velocities at chosen sites in the water bath were also investigated. The turbulency amplitude at bath surface, during powder injection was observed. The values of the derived similarity criteria of both the model and the actual powder injection into steel melts, were approximately similar.

Introduction

Powder injection into steel melts is one of the recently known secondary steelmaking processes. A combination of deep addition of fines, stirring, heating and reduced partial pressure, which are favoured in metallurgical reactions, can be accomplished by applying the powder injection technique.

The previous work about the powder injection process, indicates that, severe investigations of both the technological and the theoretical studies have to be made. The important role of that process was stated by a special report on economical — technical analysis of powder injection application in steelmaking processes [1]. Refining, alloying and homogenization of steel melts can easily be obtained by applying the powder/gas deep injection process [2—4]. Few models about that process are published. Predictions of flow, velocity and turbulence energy in a low temperature model were presented [5]. Theoretical as well as experimental explanation of the importance of the emulsion metallurgy in steelmaking was stated [6]. Using a low temperature model, predictions were made for the distance of the gas borne particulate and gas penetration into a liquid when projected from a lance [7]. About the role of stirring steel bath a fluid-mechanical model for removing the non-metallic inclusions was also suggested [8]. The immersion times as well as the penetrations of dropped wood spheres into water were illustrated by R. GUTHRIE [9]. On the other hand, gas/ /particulate jets trajectory as well as jet penetration and liquid splashes during gas or powder/gas injections were presented [10—13].

The purpose of our work was to examine the hydrodynamics of particulates which were deeply carried into a low temperature bath (water) with the aid of an inert

* Dr. GY. KÁROLY, Nehézipari Műszaki Egyetem, Miskolc, Hungary
** Dr. EL-GHAZALLY SAID A. Nehézipari Műszaki Egyetem, Miskolc, Hungary

gas (nitrogen). The obtained results were simulated to that of the prototype using the theories of dimensionless analysis. The low temperature model's results will help in our following research on powder injection into steel melts.

The experimental arrangements

A research was carried out on the injection of individual small particles and train of particles, using an inert gas (nitrogen) as a carrier gas, into a low temperature bath (water). The experimental arrangements are shown in Figs 1 and 2.

In Fig. 1 individual small particles were carried into, or accelerated down to the water bath, using simple-reduced diameter vertical glass tube. The container was made

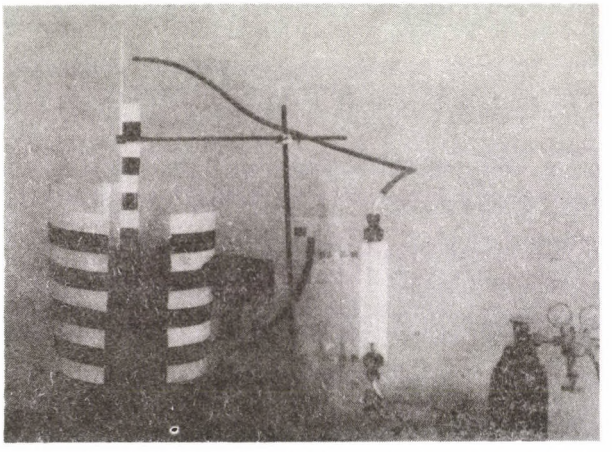

Fig. 1. Experimental arrangement for injecting individual particles into water, using nitrogen as a carrier gas

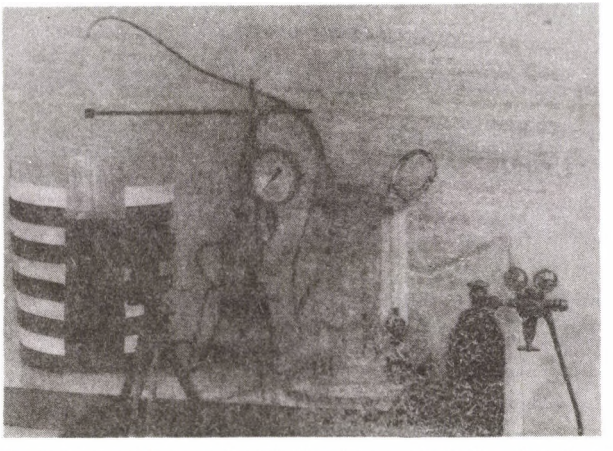

Fig. 2. Experimental arrangement for powder injection into water bath, using nitrogen as a carrier gas

of 5 mm thickness plexiglass plates. The container was ladle shaped and its capacity was 1/8 of 175 tons standard ladle, which dimensions are $3{,}8 \times 3{,}26 \times 4{,}18$ m. The velocity of the injected particles was computed by measuring its falling lengths and the corresponding times near the bath surface. The particles penetration as well as their immersion times in the water bath were also measured. In this respect a high speed camera was used. A specific particle was followed from frame to frame and the displacement as well as the exposure time between those frames were measured by slowly replaying the film. In Fig. 2 train of particulates was injected, using nitrogen as carrier gas, into the same water bath. Experimental powder dispenser of about 0,26 m^3 volume was used. The dispenser was constructed from 3 mm thickness steel sheets, in order to stand at the expected high pressures that can be encountered during operation.

The water bath was chosen, because the kinematic viscosity of both water and steel melts are similar (about 1×10^{-6} m^2/s).

The penetration as well as jet-cone angle were measured with the same photographic method.

The gas flowrates as well as the gas line pressure were measured using standard rotameter and mercury manometer respectively, as shown in the figure.

Experimental results and conclusions

The velocity of injected particles

The velocity of the individually injected particles using nitrogen as carrier gas was measured. Wood particles of different size and density were used. Their velocities were measured just near the water surface and those became the particles entry velocities. Fig. 3 shows a plot between the measured particle velocity and the carrier gas flowrate. It also shows the exit gas velocity, on the basis that, the exit diameter of the accelerating tube was 10 mm. It was clear that the particle velocity near the bath surface was smaller than that of the carrier gas, especially at high flowrates. Many authors [11, 14] postulated that the gas and the particle velocities are similar during the powder injection process. This may be true at very low gas flowrates, but the case is different in the injection process where high flowrates are required to transport the powder into the melt. It was also clear that the particle velocity was proportional to the gas flowrate or the gas velocity. In other words, the particle entry depth was proportional to the gas velocity.

Particles and jet penetrations

The penetrations of individual different particles such as wood, polystyrene and carbon spheres, when injected vertically down into the water bath, versus the modified Froude number are shown in Fig. 4 occasionally, the modified Froude number (N'_{Fr}),

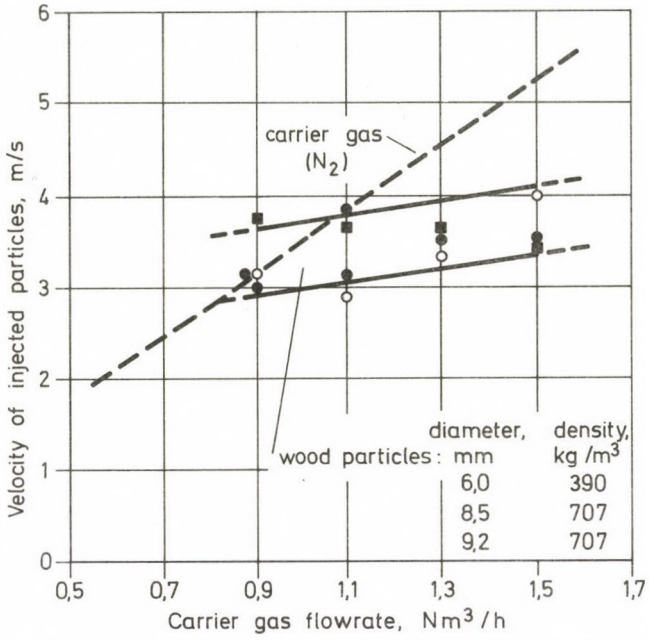

Fig. 3. The measured velocities of different particles as well as of the carrier gas near the bath surface versus the carrier gas flowrates

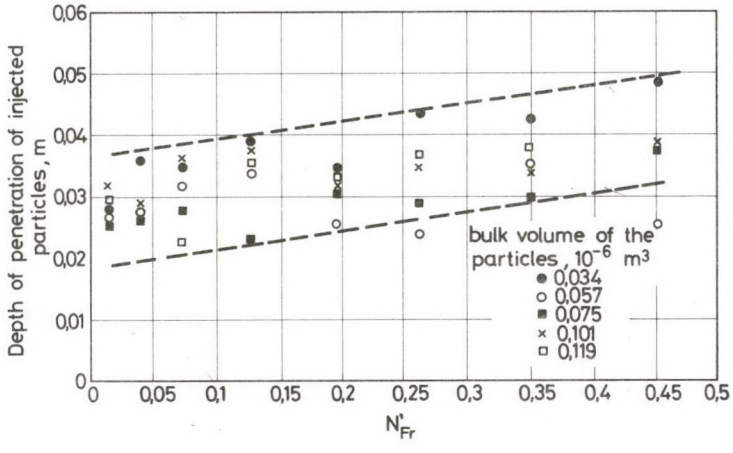

Fig. 4. Dependance of the depth of penetration of the injected particles on the modified Froude number of the jet

which will be deduced, is

$$N'_{\mathrm{Fr}} = \frac{\rho_i \cdot v_j^2}{g \cdot (\rho_b - \rho_j) \cdot d}, \tag{1}$$

where

d: the lance inside diameter, m
g: gravitational acceleration, m/s^2
ρ_j: the jet density, kg/m^3
v_j: the jet velocity, m/s
ρ_b: the bath (water) density, kg/m^3

It was difficult to measure the jet velocity and was approximately taken as that of the carrier gas. It may be clear from Fig. 4 that the different particles penetrations are a function of the modified Froude number, i.e. as the Froude number of the jet increases, the particles penetrations also increase. The penetrations of the individually injected particles were small (<0,05 m, at 1,7 N m^3/h gas flowrate), that was due to the instability of the jet and the action of buoncy force.

The effect of the injected particles grain size or bulk volume (V_p) on their penetrations is shown in Fig. 5. It may be concluded that, the general trend of penetration was proportional to gas velocity.

On the other hand, at a given gas flowrate, as the particle grain size increased (>0,004 m), its penetration hardly increased and in some cases decreased. Meanwhile, the penetration of 0,004 m size particles considerably increased by increasing the jet Froude number. The dependency of particles penetrations on their grain sizes or their bulk volumes may be related to buoncy force as well as the drag force along their immersion depths.

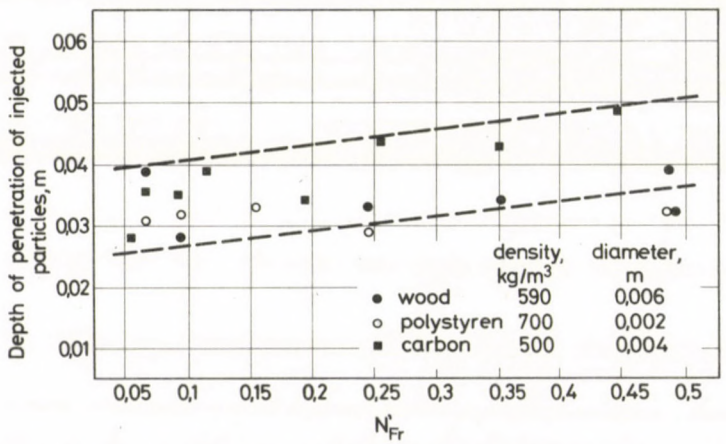

Fig. 5. **Dependance** of the depth of penetration of 500 kg/m^3 density carbon particles on the modified Froude number of the jet

Table 1

Physical parameters of used powders and gas, as well as the jet penetration and immersion times

Injected powders				Carrier gas (N_2)		immersion times, s	Penetration, m	
Particles type	grain size, mm	density, kg/m^3	Flowrate, kg/h	Flowrate, Nm^3/h	Jet velocity, m/s		measured	calculated
Carbon	3	500	288	2,3	12,6	2–3	0,10	0,16
Polystyrene	2	700	324	3	16,4	3–4	0,14	0,2
Sugar	<0,1	1150	342	3,2	17,5	—	0,12	0,18
Sand	<0,63	1300	360	3,5	19,2	—	0,13	0,16

When a continuous particulates/gas jet was practised, the jet penetrated deeper into the water bath than that for individually injected particles. Table 1. shows, the measured penetration for different grains of particles. The continuously injected grains of particles had considerable penetration depths due to their increasing inertia and the stability of their jet cone in the bath.

The theoretical penetration depths of vertically injected particulates using an inert carrier gas (nitrogen), can be approximately determined by making a balance between the inertial and buoncy forces of the jet cone:

$$V_j \cdot \rho_b \cdot g = (m_p \cdot v_p + m_g \cdot v_g), \tag{2}$$

where

m_p, and m_g: are the mass flowrates of both particulates and carrier gas, kg/h
v_p, and v_g: are the velocities of both particulates and carrier gas, m/s.
and V_j: is the jet cone volume, m^3.

According to the geometry of the jet cone Fig. 6

$$V_j = \frac{\pi}{3} \cdot H^3 \cdot \tan^2\left(\frac{\Theta}{2}\right), \tag{3}$$

where

H: is the jet penetration depth, m.
Θ: is the jet cone angle, deg.

From equations (2), and (3) we can obtain

$$H = 0{,}985 \left[\frac{m_p \cdot v_p + m_g \cdot v_g}{\rho_b \cdot g \cdot \tan^2\left(\frac{\Theta}{2}\right)}\right]^{\frac{1}{3}}. \tag{4}$$

The effect of drag and gravitational forces was neglected.

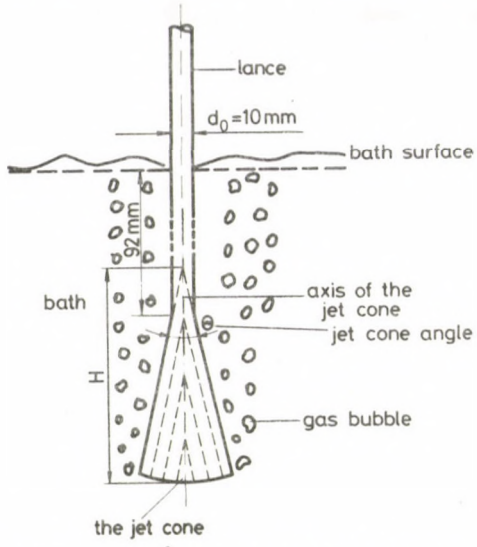

Fig. 6. Schematic representation of the powder/gas jet of the low-temperature model

It was observed that the jet cone angle during injecting polystyrene, carbon, sugar and sand particulates using nitrogen as carrier gas was 15 – 20 °C. The measured angles were similar to those calculated from Donald's approximation [15], that is:

$$\tan\left(\frac{\Theta}{2}\right) = 0{,}238 \cdot \nu^{0{,}133} \tag{5}$$

where ν: is the kinematic viscosity of the bath, m^2/s.

The measured penetrations of the injected particulates/gas grains, and those calculated from equation (4) were approximately similar as shown in Table 1.

Flow pattern and velocity of the bath

The flow pattern and velocity of the bath at chosen sites are measured with the aid of dispersed synthetic particles in a low temperature bath. The length and direction of motion of every chosen site were measured by slowly replaying the photographed film-tape. The turbulency and the flow-pattern of the bath were measured at nine lance positions, Fig. 7. In those positions, and at given powder and gas flowrates, the flow-pattern and velocity of the bath are shown in Fig. 8, a—c. It was clear that the intensity of flow as well as the recirculation, when the lance was situated very near to the ladle-shaped container (position C), were very poor. On the other hand, the optimum movement and turbulency of the bath were obtained with a deep central injection (position a).

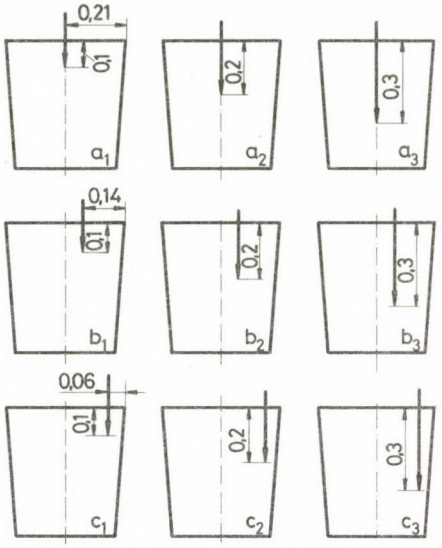

Fig. 7. The different positions of the lance used in the low-temperature model (dimensions in meter)

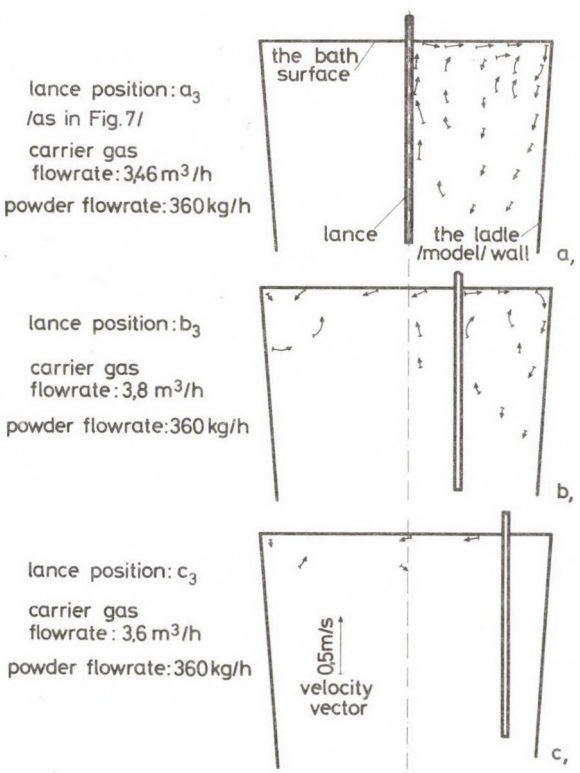

Fig. 8a—c. The measured velocities of the bath (water) at chosen sites at different positions of the lance

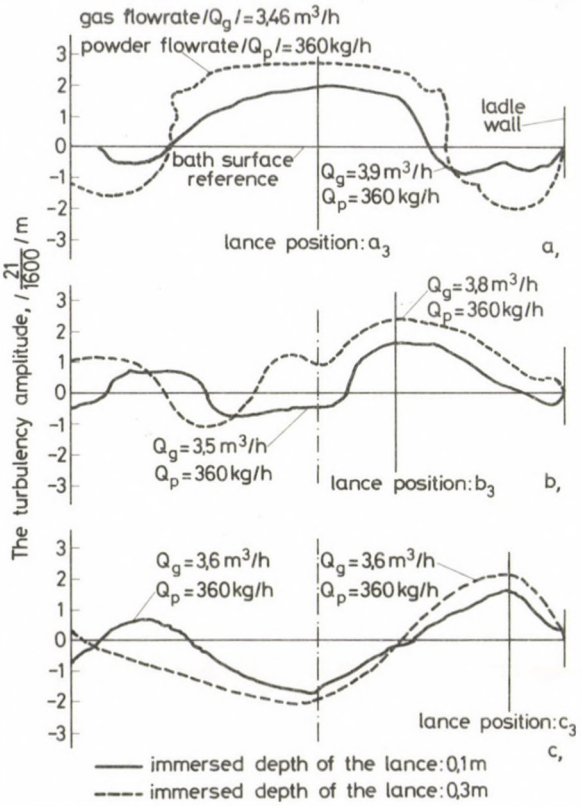

Fig. 9a—c. The measured turbulence amplitude of the low-temperature bath surface at different positions of injection

The turbulency amplitudes along the bath surface, at the previously mentioned lance positions, were also measured. Fig. 9, a—c presents, the maximum measured amplitudes in the first and the third lance position. It became clear that the maximum turbulency amplitude at maximum powder and gas flowrates (360 kg/h and 3,5 N m³/h respectively) was 7,4—11,2% of the bath depth.

Simulation of the model results to the powder Injection process in steel melts

The effective criteriums that were required to extend the low temperature investigation to the powder injection process, were deduced by using the Buckingham dimensionless analysis theorems [16]. The effective parameters that played an important part in the hydrodynamics of the injection process, were gathered together,

using those theorems, to give the following dimensionless groups (π_i):

$$\pi_1 = \frac{H \cdot \mu}{\Theta_j}, \tag{7}$$

$$\pi_2 = \frac{d \cdot \mu}{\Theta_j}, \tag{8}$$

$$\pi_3 = \frac{\rho_b \cdot \Theta_j \cdot v_j}{\mu^2}, \tag{9}$$

$$\pi_4 = \frac{\rho_j \cdot \Theta_j \cdot v_j}{\mu^2}, \tag{10}$$

$$\pi_5 = \frac{g \cdot \Theta_j}{\mu \cdot v_j^2}, \tag{11}$$

$$\pi_6 = \frac{\sigma}{\mu \cdot v_j}, \tag{12}$$

$$\pi_7 = \frac{S \cdot \mu^2}{\Theta_j^2}, \tag{13}$$

$$\pi_8 = \frac{u}{v_j}, \tag{14}$$

where

d: is the lance inside diameter, m
H: the penetration, or the bath depth, m
S: the surface area of the bath, m^2
Θ_j: the jet flowrate, kg/h
v_j: the jet velocity, m/s
ρ_j: the jet density, kg/m^3
ρ_b: the bath density, kg/m^3
u: the velocity of bath motion, m/s
μ: the dynamic viscosity of the bath, kPa · s
g: the gravitational acceleration, m/s^2
σ: the bath jet surface tension, J/m^2

By combining the suitable groups from equations (7—14), we obtained the effective well-known criteria that may help in transferring our results to the actual process. The values of both low temperature model and the actual powder injection process were presented in Table 2. For successful transfer from model data to the actual powder injection process, the following condition must be satisfied:

$$N_i^{\text{model}} = N_i^{\text{actual}}$$

where N_i: one of the effective criteria.

Table 2

Conditions for injection in model and full scale process

Parameters	Values	
	model	full scale
Weight of bath treated, t	0,06	150
Density of bath, kg/m^3	1000	7200
Viscosity of bath, Kpa · s	0,001	0,0064
Surface area of bath, m^2	0,2304	11,341
Depth of bath, m	0,35	~4,5
Injected powder flowrate, kg/h	max. 360	3000
Carrier gas flowrate, Nm^3/h	max. 0,04	0,9
Gas velocity, m/s	max. 19,2	min. 80
Jet density, kg/m^3	~0,1	~0,083
Bath/N_2 surface tension,* J/m^2	0,0738	1,5
Dispenser volume, m^3	0,26	2,0
Dispenser pressure, KPa	120 – 130	700 – 800
Lance inside diameter, m	0,01	0,018
Lance immersed length, m	0,095	3,4 – 3,5
Velocity of bath motion, m/s	~0,35	~1,6

* References [12, 17, 18].

Table 3

The deduced similarity criteria, and their values in both model and full scale

Criterium name	Criterium deduction	deduced formula	Criterium value	
			model	full scale
Reynold, N_{Re}	$\pi_2 \cdot \pi_4$	$\frac{\rho_j \cdot v_j \cdot d}{\mu}$	19,20	18,65
Froude, N_{Fr}	$\frac{1}{\pi_3 - \pi_4} \pi_4 \frac{1}{\pi_2 \cdot \pi_5}$	$\frac{\rho_j \cdot v_j^2}{(\rho_b - \rho_j) \cdot g \cdot d}$	0,418	0,391
Geometry, N_{Geo}	$\frac{\pi_1^2}{\pi_7}$	$\frac{H^2}{s}$	1,55	1,541
Galileo, N_{Ga}	$\pi_1^3 \cdot \pi_4^2 \cdot \pi_5$	$\frac{g \cdot \rho_j \cdot H^3}{\mu^2}$	2153,0	2150,0
Weber, N_{We}	$\frac{1}{\pi_6} \cdot \pi_4 \cdot \pi_2$	$\frac{\rho_j \cdot d \cdot v_j^2}{g \cdot \sigma}$	5,3	6,5
Velocity, N_v	π_8	$\frac{u}{v_j}$	0,018	0,019

Table 3 shows the derivation of the effective criteria and the values of those criteria in both the model and the actual process. It may be clear that there is a similarity between those values, which indicate the reliability of our results to simulate the actual process.

REFERENCES

1. "A porbefúvásos acélkezelési eljárás acélgyártásban betöltött szerepének műszaki-gazdasági elemzése". Tanulmány a KGM részére, Scientific report, Technical University for Heavy Industries, Metallurgical Depart. Miskolc-Hungary 1980, p. 62
2. OREHOSKI, M. A.: Secondary Steelmaking — Refining Processes in the USA". Secondary steelmaking, London 1977
3. LEHNER, T.: Reactor Models for Powder Injection. *Scaninject* 1, Sweden (1977), p. 11
4. WADA, K. et al: Investigation of Desulfurization and Deoxidation in Injection Metallurgy. *Scaninject* II. Sweden (1980), p. 21
5. SZÉKELY, J.—WANG, H.: Flow pattern, Velocity and Turbulence Energy Measurements and Predictions in a Water Model of an Argon Stirred Ladle. *Met. Trans.* V. 7 B. June (1976) p. 287—295
6. GOTO, K. S.—EKETORP, S.: Emulsion Metallurgy and Hydrodynamic Analysis in Bottom Blown Converters. *Scandinavian J. Metall.* **3** (1974), p. 1—10
7. ENGH, T. A.—LARSEN, K.: Penetration of Particle-Gas Jets into Liquids. *Ironmaking Steelmaking* (1979), p. 268—73
8. ENGH, T. A.—LINDSKOG, N.: A fluid Mechanical Model of Inclusion Removal. *Scandinavian J. Metall.* **4** (1975), p. 49—58
9. GUTHRIE, R.—GLIFT, R.: Contacting problems Associated with Aluminium and Ferro-Alloy Additions in Steelmaking. *Metall. Trans.* V.6 B, June 1975, p. 321—29
10. IGWE, PASIL—FULTON, J. C.: Jet Penetration and Liquid Splashes in Submerged Gas Injection. *Metall. Trans.* V.4 B (1973), p. 1887—1894
11. ENGH, T. A.—BERTHEUSSEN, H: Trajectory of a Gas/Particulate-Solid Jet in a Melt. *Scandinavian J. Metall.* **4** (1975), p. 241—49
12. LINDER, S.: Hydrodynamics and Collisions of Small Particles in a Turbulent Metallic Melt. *Scandinavian J. Metall.* **3** (1974), p. 135—150
13. ROBERTSON, D. et al: Model Studies on Gas and Solid Injection and Related Phenomena in Liquid Metal Baths. *Scaninject* II. Sweden (1980) p. 4
14. ENGH, T.: Penetration of Particles through a Gas-Liquid Interface. *Scaninject* 1. p. 6
15. DONALD, M. B.—SINGER: Entrainment in Turbulent Fluid Jets. *Trans. Inst. Chem. Engineers*, **37** (1969), p. 1256—67
16. BUCKINGHAM: Physically Similar Systems; Illustration of the Use of Dimensional Analysis. *Physical Review* **4** (1914), p. 345
17. GREVILLIUS, N. F.: Removal of Inclusions Resulting from Silicon and Manganese Complex Deoxidation. *Jern-Kont. Ann.* **153** (1963), p. 547—572
18. PERRY, R. H. et al: Chemical Engineers Handbook. McGraw-Hill Book Company, 1963

Hydrodynamische Modellierung der Pulverinjektion in Schmelzen. — Die Autoren untersuchten die Hydrodynamik der Teilchen/Stickstrahlen in einem Wasserbad von verschiedenen Dichten und Korngrößen. Auch das Strömungsbild und die Geschwindigkeiten wurden in den beliebig ausgewählten Punkten des Wasserbads untersucht. Die Wirbelamplitude an der Badoberfläche wurde während der Pulverinjektion beobachtet. Die Werte der abgeleiteten Ähnlichkeitskriterien des Modells und der tatsächlichen Pulverinjektion in Stahlschmelzen sind annähernd ähnlich gewesen.

INDEX

PRINTED IN HUNGARY
Akadémiai Nyomda, Budapest

The *Acta Technica* publish papers on technical subjects in English, French, German and Russian.

The *Acta Technica* appear in parts of varying size, making up one volume.

Manuscripts should be addressed to

Acta Technica
H-1051 Budapest
Münnich Ferenc u. 7
Hungary

Correspondence with the editors and publishers should be sent to the same address.

Subscription rate: $ 36.00 a volume.

Orders may be placed with "Kultura" Foreign Trading Company (H-1389 Budapest 62. P. O. B. 149. Account No. 218-10990) or its representatives abroad.

Les *Acta Technica* paraissent en français, allemand, anglais et russe et publient des travaux du domaine des sciences techniques.

Les *Acta Technica* sont publiés sous forme de fascicules qui seront réunis en volumes.

On est prié d'envoyer les manuscrits destinés à la rédaction à l'adresse suivante:

Acta Technica
H-1051 Budapest
Münnich Ferenc u. 7.
Hongrie

Toute correspondance doit être envoyée à cette même adresse.

Le prix de l'abonnement: $ 36.00 par volume.

On peut s'abonner à l'Entreprise du Commerce Extérieur «Kultura» (H-1389) Budapest 62, P. O. B. 149. Compte courant No. 218-10990) ou chez représentants à l'étranger.

«*Acta Technica*» публикуют трактаты из области технических наук на русском немецном, английском и французском языках.

«*Acta Technica*» выходят отдельными выпусками разного объема. Несколько выпусков составляют один том.

Предназначенные для публикации рускописи следует направлять по адресу:

Acta Technica
H-1051 Budapest,
Münnich Ferenc u. 7.
Венгрия

По этому же адресу направлять всякую корреспонденцию для редакции и администрации.

Подписная цена — $ 36.00 за том. Заказы принимает предприятие по внешней торговле «Kultura» (H-1389 Budapest 62, P. O. B. 149 Текущий счет № 218-10990) или его заграничные представительства и уполномоченные.

Periodicals of the Hungarian Academy of Sciences are obtainable at the following addresses:

AUSTRALIA
C.B.D. LIBRARY AND SUBSCRIPTION SERVICE
Box 4886, G.P.O., *Sydney N.S.W. 2001*
COSMOS BOOKSHOP, 145 Ackland Street
St. Kilda (Melbourne), Victoria 3182

AUSTRIA
GLOBUS, Höchstädtplatz 3, *1206 Wien XX*

BELGIUM
OFFICE INTERNATIONAL DE LIBRAIRIE
30 Avenue Marnix, *1050 Bruxelles*
LIBRAIRIE DU MONDE ENTIER
162 rue du Midi, *1000 Bruxelles*

BULGARIA
HEMUS, Bulvar Ruszki 6, *Sofia*

CANADA
PANNONIA BOOKS, P.O. Box 1017
Postal Station "B", *Toronto, Ontario M5T 2T8*

CHINA
CNPICOR, Periodical Department, P.O. Box 50
Peking

CZECHOSLOVAKIA
MAD'ARSKÁ KULTURA, Národní třida 22
115 66 Praha
PNS DOVOZ TISKU, Vinohradská 46, *Praha 2*
PNS DOVOZ TLAČE, *Bratislava 2*

DENMARK
EJNAR MUNKSGAARD, Norregade 6
1165 Copenhagen K

FEDERAL REPUBLIC OF GERMANY
KUNST UND WISSEN ERICH BIEBER
Postfach 46, *7000 Stuttgart 1*

FINLAND
AKATEEMINEN KIRJAKAUPPA, P.O. Box 128
SF-00101 Helsinki 10

FRANCE
DAWSON-FRANCE S. A., B. P. 40, *91121 Palaiseau*
EUROPÉRIODIQUES S. A., 31 Avenue de Versailles, *78170 La Celle St. Cloud*
OFFICE INTERNATIONAL DE DOCUMENTATION ET LIBRAIRIE, 48 rue Gay-Lussac
75240 Paris Cedex 05

GERMAN DEMOCRATIC REPUBLIC
HAUS DER UNGARISCHEN KULTUR
Karl Liebknecht-Straße 9, *DDR-102 Berlin*
DEUTSCHE POST ZEITUNGSVERTRIEBSAMT
Sraße der Pariser Kommüne 3–4, *DDR-104 Berlin*

GREAT BRITAIN
BLACKWELL'S PERIODICALS DIVISION
Hythe Bridge Street, *Oxford OX1 2ET*
BUMPUS, HALDANE AND MAXWELL LTD
Cowper Works, *Olney, Bucks MK46 4BN*
COLLET'S HOLDINGS LTD., Denington Estate
Wellingborough, Northants NN8 2QT
WM. DAWSON AND SONS LTD., Cannon House
Folkstone, Kent CT19 5EE
H. K. LEWIS AND CO., 136 Gower Street
London WC1E 6BS

GREECE
KOSTARAKIS BROTHERS INTERNATIONAL BOOKSELLERS, 2 Hippokratous Street, *Athens-143*

HOLLAND
MEULENHOFF-BRUNA B.V., Beulingstraat 2,
Amsterdam
MARTINUS NIJHOFF B.V
Lange Voorhout 9–11, *Den Haag*
SWETS SUBSCRIPTION SERVICE
347b Heereweg, *Lisse*

INDIA
ALLIED PUBLISHING PRIVATE LTD., 13/14 Asaf Ali Road, *New Delhi 110001*
150 B-6 Mount Road, *Madras 600002*
INTERNATIONAL BOOK HOUSE PVT. LTD.
Madame Cama Road, *Bombay 400039*
THE STATE TRADING CORPORATION OF INDIA LTD., Books Import Division, Chandralok
36 Janpath, *New Delhi 110001*

ITALY
INTERSCIENTIA, Via Mazzé 28, *10149 Torino*
LIBRERIA COMMISSIONARIA SANSONI, Via Lamarmora 45, *50121 Firenze*
SANTO VANASIA, Via M. Macchi 58
20124 Milano
D. E. A., Via Lima 28, *00198 Roma*

JAPAN
KINOKUNIYA BOOK-STORE CO. LTD.
17-7 Shinjuku 3 chome, Shinjuku-ku, *Tokyo 160-91*
MARUZEN COMPANY LTD., Book Department, P.O. Box 5050 Tokyo International, *Tokyo 100-31*
NAUKA LTD. IMPORT DEPARTMENT
2-30-19 Minami Ikebukuro, Toshima-ku, *Tokyo 171*

KOREA
CHULPANMUL, *Phenjan*

NORWAY
TANUM-TIDSKRIFT-SENTRALEN A.S., Karl Johansgatan 41–43, *1000 Oslo*

POLAND
WĘGIERSKI INSTYTUT KULTURY, Marszałkowska 80, *00-517 Warszawa*
CKP I W, ul. Towarowa 28, *00-958 Warszawa*

ROUMANIA
D. E. P., *Bucureşti*
ILEXIM, Calea Grivitei 64–66, *Bucureşti*

SOVIET UNION
SOJUZPECHAT – IMPORT, *Moscow*
and the post offices in each town
MEZHDUNARODNAYA KNIGA, *Moscow G-200*

SPAIN
DIAZ DE SANTOS, Lagasca 95, *Madrid 6*

SWEDEN
ALMQVIST AND WIKSELL, Gamla Brogatan 26
101 20 Stockholm
GUMPERTS UNIVERSITETSBOKHANDEL AB
Box 346, *401 25 Göteborg 1*

SWITZERLAND
KARGER LIBRI AG, Petersgraben 31, *4011 Basel*

USA
EBSCO SUBSCRIPTION SERVICES
P.O. Box 1943, *Birmingham, Alabama 35201*
F. W. FAXON COMPANY, INC
15 Southwest Park, *Westwood Mass. 02090*
THE MOORE-COTTRELL SUBSCRIPTION AGENCIES, *North Cohocton, N. Y. 14868*
READ-MORE PUBLICATIONS, INC
140 Cedar Street, *New York, N. Y. 10006*
STECHERT-MACMILLAN, INC
7250 Westfield Avenue, *Pennsauken N J 08110*

YUGOSLAVIA
JUGOSLOVENSKA KNJIGA, Terazije 27, *Beograd*
FORUM, Vojvode Mišića 1, *21000 Novi Sad*

HU ISSN 0001—7035

Index: 26.025

ACTA TECHNICA

ACADEMIAE SCIENTIARUM HUNGARICAE

REDIGIT: M. MAJOR

TOMUS 93
FASCICULI 3—4

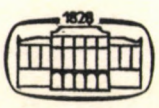

AKADÉMIAI KIADÓ, BUDAPEST 1981

ACTA TECHNICA

Az *Acta Technica* angol, francia, német és orosz nyelven közöl értekezéseket a műszaki tudományok köréből.

Az *Acta Technica* változó terjedelmű füzetekben jelenik meg, több füzet alkot egy kötetet.

A közlésre szánt kéziratok a következő címre küldendők:

Acta Technica
1051 Budapest, Münnich Ferenc u. 7.

Ugyanerre a címre küldendő minden szerkesztőségi és kiadóhivatali levelezés.

Megrendelhető a belföld számára az „Akadémiai Kiadó"-nál (1363 Budapest Pf. 24. Bankszámla 215 11448), a külföld számára pedig a „Kultura" Külkereskedelmi Vállalatnál (1389 Budapest 62, P. O. B. 149 Bankszámla: 218-10990) vagy annak külföldi képviseleteinél és bizományosainál.

Die *Acta Technica* veröffentlichen Abhandlungen aus dem Bereiche der technischen Wissenschaften in deutscher, englischer, französischer und russischer Sprache.

Die *Acta Technica* erscheinen in Heften wechselnden Umfanges. Vier Hefte bilden einen Band.

Die zur Veröffentlichung bestimmten Manuskripte sind an folgende Adresse zu senden.

Acta Technica
H 1051 Budapest,
Münnich Ferenc u. 7.
Ungarn

An die gleiche Anschrift ist auch jede für die Schriftleitung und den Verlag bestimmte Korrespondenz zu richten.

Abonnementpreis pro Band: $ 36.00.

Bestellbar bei »Kultura« Außenhandelsuntelsunternehmen (H-1389 Budapest 62, P. O. B. 149 Bankkonto Nr. 218-10990) oder seinen Auslandsvertretungen.

CONTENTS

BOOK REVIEWS

Acta Technica Academiae Scientiarum Hungaricae, 93 (3—4), pp. 209—213 (1981)

L. GÁBOR

(1910—1981)

Die ungarische Architektur, die Bautechnik und Bauwissenschaft, sowie die Heranbildung von Architekten erlitt einen unersetzbaren Verlust. Am 28. Oktober 1981 verschied der Architekt László Gábor, Träger des Staats- und Ybl-Preises, Gründer und Direktor des Institutes für Baukonstruktionen und -einrichtungen, während nahezu dreier Jahrzehnte leitender Professor des Lehrstuhls für Baukonstruktionen der Budapester Technischen Universität, seit 1973 korrespondierendes, seit 1979 ordentliches Mitglied der Ungarischen Akademie der Wissenschaften. Er war ein Mann von seltenem Format, ein später Nachkomme der Enzyklopädisten, der die Vergangenheit zusammenzufassen und zugleich Neues in die Wege zu leiten vermochte. Er verließ die herkömmliche Welt der Architektur und setzte sich entschieden für die moderne Industrialisierung der Architektur und der Bauwissenschaften ein. Er war einer der Größten, die in der Ausbildung von Architekten das Gleichmaß von Kunst, Wissenschaft und Technik vor Augen hielten und dieses anstrebten.

Sein Lebenswerk bedeutet in der Entwicklung der ungarischen, die Baukonstruktion betreffenden Denkweise einen Meilenstein — und wenn wir seinen reichen Nachlaß fortsetzen — wird seine Bedeutung selbst unsere Landesgrenzen weit überschreiten.

In einem Zeitalter, wo das Detail früher oder später das Gesamtwerk an Bedeutung zu überflügeln scheint, blieb er das lebendige Gewissen jener Architekten, die in der Baukunst von der Industrie auch einen gewerblichen Zug erwarteten. Er verfolgte als Wissenschaftler und Pädagoge seine eigenen Wege und schuf mit seiner Art der Behandlung des Themas und seiner Vortragsweise das Verständnis für die Welt der Baukonstruktionen. Seinem Wirken ist es zuzuschreiben, wenn bei völliger Bejahung der Industrialisierung des Bauwesens, diese in einer Weise zur Geltung

kommt, wo unsere Fähigkeit der Systemschaffung und Konstruktion bereits jene Harmonie erreicht, in welcher die Form nicht — wie heute — der Industrie, sondern umgekehrt die Industrie der Architektur untergeordnet ist, d. h. die Industrie der Form folgt.

László Gábor entstammt einer Intellektuellenfamilie und wurde am 22. November 1910 in Debrecen geboren. Daher seine Vorliebe für das geschriebene und gesprochene Wort, die Achtung des Intellekts, des klaren Gedankens und das Mitteilungsbedürfnis in Wort und Schrift. Er wollte Maler werden und wurde Architekt. Seine Studien beendigte er im Jahre 1933 an der József Nádor Technischen und Wirtschaftswissenschaftlichen Universität in Budapest. Unter dem Zwang der Verhältnisse schuf er unter fremden Namen selbstständige architektonische Werke. Das erste große Mietshaus in Debrecen ist zugleich das erste Werk, das unter seinem Namen erbaut wurde. Nach der Befreiung Ungarns entwarf er mit Mitarbeitern das heutige Parteihaus.

Seine schöpferische architektonische Tätigkeit vertauschte er 1949 mit der pädagogisch-wissenschaftlichen. Bald erwies er sich in der praktischen Forschung als ein, die Probleme zur rechten Zeit richtig erkennender Wissenschaftler, der sich in diese vertiefte, sie analytisch erfaßte und auf Grund seiner humanen Bildung als Architekt bei der Lösung seiner wissenschaftlichen Aufgaben eine Synthese anstrebte. Die ungarische Baukonstruktionslehre — die vor der Befreiung, den damaligen Verhältnissen entsprechend — kaum mehr war, als eine Beschreibung der gebräuchlichen Baukonstruktionen, entwickelte er zu einer, auf objektiven Kriterien beruhenden Wissenschaft. Mit systematischer Arbeit baut er die Beziehungen aus, die jene Anhaltspunkte der naturwissenschaftlichen und bauphysikalischen Kenntnisse enthalten, die für Entwurf und Fortentwicklung von Baukonstruktionen erforderlich sind. Mit Hilfe der zur Verfügung stehenden materiellen Kräfte schafft er eine Versuchsbasis für die pragmatische Untersuchung von Baukonstruktionen. Mit der gleichzeitigen Behandlung der bauphysikalischen, installationstechnischen und baukonstruktiven Probleme eröffnet er tatsächlich eine neue Forschungsrichtung.

Seine Erfahrungen als Architekt, seine Betrachtungsweise und schöpferische Vene bewahren ihn davon, die unter seiner Leitung in seinem Institut vorgenommenen, noch so wichtigen Forschungsarbeiten ausschließlich vom technisch-technologischen Gesichtspunkt zu werten. Mit den Baukonstruktionen befaßt er sich den Gebäuden zuliebe, mit den Gebäuden und der architektonischen Umgebung befaßt er sich im Interesse der Schöpfung eines schöneren menschlichen Lebens. Er erachtet und betreibt die Baukonstruktionslehre als ein Mittel der Konstruktions- und Gebäudeplanung.

Für seinen anspruchsvollen schöpferischen Geist, für seine Sachlichkeit und für seine systemschaffende Logik zeugen seine Fachbücher, vor allem sein vierbändiges Werk „Baukonstruktionslehre", dessen letzter, vierter Band 1979 erschien. Dieses Werk erregte — auch im Ausland — wohlverdient das Interesse der Fachkreise und der praktisch tätigen Architekten. Die Zusammenfassung der vielseitigen und vielfältigen

Fachgebiete zu einem einzigen organischen und logisch aufgebauten System ist eine beispiellose Leistung auf dem Gebiet der Fachliteratur. Eine ähnlich vollständige Konstruktionslehre ist selbst in der bekanntermaßen hervorragend systematisierten deutschen Fachliteratur nicht anzutreffen.

In den letzten Jahren widmete Prof. Gábor mit seinen Mitarbeitern seine Aufmerksamkeit den wissenschaftlichen Problemen der großindustriellen Bauweise zu, um mit dieser, eine Theorie schaffenden Arbeit seine nahezu fünf Jahrzehnte umfassende Tätigkeit als Konstrukteur, Pädagoge und Wissenschaftler gewissermaßen zu vollenden. Er befaßt sich eingehend mit den theoretischen Problemen der Massenbauten, mit den offenen Fragen der Konstruktionssysteme und Bautechnologien, mit den grundlegenden Fragen der Variationen von Planung, Fabrikation und Bauausführung, mit den Zusammenhängen von Koordinierung und Variabilität und den Gesetzmäßigkeiten ihrer Anwendung, mit der Energiewirtschaft im Bauwesen, mit der zeichnungsfreien Darstellung, mit der Theorie der sog. Blindplanung, ferner mit der Theorie der Leichtkonstruktionssysteme auf Silikatbasis und schließlich mit den grundlegenden konstruktionstechnischen Fragen der sog. nichttektonischen Bauweise. Über diese neuen Forschungen konnte er aber nur im Rahmen der, an der Ungarischen Akademie der Wissenschaften gehaltenen, Vorträge berichten. Seine in den Jahren 1973 und 1979 an der Ungarischen Akademie der Wissenschaften gehaltenen Inauguralvorlesungen bilden bedeutende Werte der ungarischen architektonisch-theoretischen Literatur.

Ein besonderes — in der ungarischen Architekturwissenschaft alleinstehendes — Merkmal seiner schöpferischen und auf dem Gebiet der Forschung ausgeübten Tätigkeit bildet der Umstand, daß er sein Lebenswerk nicht aus Einzelteilen aufgebaut, sondern dieses von vornherein als zusammenhängendes Ganzes antizipiert hat. Er erfaßte nie willkürlich einen Teil des Fachgebietes, sondern bearbeitete jeden Einzelteil als einen Bestandteil des Ganzen u. zw. in einer Weise, deren Komponenten im Endresultat nach der Gänze einer unteilbaren „zeitlosen" Architektur weisen. Sein unerwarteter, dramatischer Tod war deshalb so erschütternd, weil er — immer nur Unvollendetheit empfindend — sich mit immer neuen Plänen befaßte und — obzwar er das Erscheinen von mehreren seiner Arbeiten nicht mehr erlebte — uns eine reiche Nachlassenschaft, aber auch zahllose Verpflichtungen hinterließ.

Seine vielseitige wissenschaftspolitische Tätigkeit war durch große Aktivität und Zielbewußtheit gekennzeichnet. Er war Präsident des Bauwissenschaftlichen Ausschusses der Ungarischen Akademie der Wissenschaften, erst Präsident, dann Mitglied der wissenschaftlichen Qualifizierungskommission für Bau- und Verkehrswesen, Vorstandsmitglied des Verbandes der Ungarischen Wissenschaftlichen Vereine, Mitglied des Rates für technische Fortentwicklung des Ministeriums für Bauwesen und Städtebau, Redaktionsmitglied der Zeitschrift *Építés-Építészettudomány* (Bau und Bauwissenschaft), Gründer und während dreier Jahre Präsidialmitglied des Verbandes Ungarischer Baukünstler. Auch beteiligte er sich regelmäßig an den Arbeiten des Landesausschusses für technische Fortentwicklung und des Instituts für die

Verbreitung der Naturwissenschaften, an den Planungsarbeiten des Projektierungsinstituts für Wohnbauten bzw. des Entwurfsbüros für Industriebauten. Im Jahre 1948 verlieh ihm das Ministerium für Bauwesen die Auszeichnung „für hervorragende Arbeit", 1952 erhielt er den Titel „Hervorragender Arbeiter des Unterrichtswesens", 1955 wurde ihm der „Orden für Arbeit" verliehen. 1953 wurde ihm der Ybl Miklós-Preis I. Klasse, 1965 der Staatspreis III. Klasse zuerkannt. Im Jahre 1970 erhielt er die Befreiungsmedaille und den „Goldenen Orden der Arbeit". Als Anerkennung seiner Tätigkeit erhielt er die Erinnerungsmedaillen der Budapester Technischen Universität und des Ungarischen Architektenverbandes. 1981 trat Prof. Gábor in den Ruhestand und wurde bei dieser Gelegenheit mit dem „Verdienstorden für das Sozialistische Ungarn" ausgezeichnet.

László Gábor wurde am 10. November 1981 in Budapest, am Friedhof Farkasrét beigesetzt. Doch wurde nur sein Körper beerdigt, sein Geist und seine Schöpfungen leben fort in der Erinnerung seiner Schüler, Mitarbeiter, Verehrer und Nachfolger zum Besten der ungarischen, sowie der gesamten Architektur.

*M. Párkányi**

Literarische Tätigkeit von Prof. L. GÁBOR

Fachartikel:

1. Wissenschaftliche Methode der Abwägung der Kosten in der Bauindustrie*
2. Konstruktive und wirtschaftliche Untersuchung von Wohnhäusern unterschiedlicher Geschoßzahl, Bestimmung der optimalen Höhe*
3. Technischer und wirtschaftlicher Vergleich verschiedener Wohnhaustypen*
4. Quelques problèmes relatifs à la protection des toits contre l'action thermique et la condensation des vapeurs. *ÉMKE Tudományos Közlemények*, Budapest, 1963
5. Zeitgemäße Wasser- und Feuchtigkeitsisolierung. (mit Mitverfasser), OMFB 1963*
6. Geschichte der 100jährigen Architektenbildung. *Periodica Polytechnica* (1972)
7. Centennial History of the Faculty of Architecture. *Periodica Polytechnica. Architecture.* (1972), No. 3—4.
8. Aufgaben, Bedeutung und Sorgen der Architektur und der Bauwissenschaft. *Magyar Tudomány* (1971) Seiten 434—440*
9. Vorwort zum Katalog der ständigen Ausstellung von M. Kovács (1974)*
10. Begrüßung Máté Majors. *Periodica Polytechnica. Architecture*, Vol. **18.** (1974), No. 1—2
11. Rezension des Werkes Bautechnologie I. von L. Széll. *Műszaki Tudomány* **49** (1974)*
12. Sun Shields. *Periodica Polytechnica. Architecture* **22** (1978), 1—10
13. Rolle der architektonischen Planung und der Bautechnologie und ihr Zusammenhang mit dem Werk. *Építés-Építészettudomány* (1974), 203—214, (Inauguralvorlesung)*
14. „Ich möchte einige sehr zeitgemäße planungstheoretische Fragen des Wohnungsbaues untersuchen" *Magyar Tudomány* (1974), 82—84*

* Mihály Párkányi war László Gábors engster Mitarbeiter, einige wissenschaftliche Arbeiten verfaßten sie gemeinsam. Es scheint daher angebracht zu sein, seiner mit einigen Worten seitens der Redaktion zu gedenken.

M. Major
verantwortlicher Redakteur

15. Architektur, Konstruktion, Fabrikation. *Építés-Építészettudomány* **7** (1975), 275—283*
16. Architecture, structure, manifacture. *Periodica Polytechnica. Architecture* **19** No. 1—2
17. Die architektonischen Probleme der industrialisierten Bauweise. Eröffnungsvortrag gehalten gelegentlich der Enquete 20—21 Mai 1976 der Ungarischen Akademie der Wissenschaften. *Építés-Építészettudomány* (1977), 3—8*
18. Lage und hauptsächlichste Aufgaben der Architektur-Architekturwissenschaft im Bauwesen, in der Industrialisierung des Bauwesens. *Magyar Tudomány* (1978), 815—822*
19. *László Széll*, 1903—1976. *Műszaki Tudomány* **53** (1977), 9—11*
20. The Theory of Blind Design (Mitverfasser M. Párkányi) *Periodica Polytechnica. Architecture* **23** (1979), 1—34
21. Architektur und Energiewirtschaft. Gedanken und Bericht über eine, nach einer eigenartigen Lösung strebenden komplexen Forschung auf Grund der Versuchsergebnisse (Mitverfasser A. Zöld). *Magyar Tudomány* **11** (1979), 842—848*
22. Wochentage und Wunder. Die Welt der Architektur und ihre wissenschaftliche Eigenart. Inauguralvortrag, gehalten an der öffentlichen Sitzung der Sektion der Technischen Wissenschaften der Ungarischen Akademie der Wissenschaften im Februar 1980. *Magyar Tudomány* (1979), 283—293*
23. Technologie, Industrialisierung, architektonische Umgebung. Referat, gehalten an der Generalversammlung 1981 der Ungarischen Akademie der Wissenschaften im Anschluß an das Thema „Wechselwirkung der gebauten Umgebung und der gesellschaftlich-wirtschaftlichen Entwicklung im Urbanisationsvorgang". Veröffentlichungen der Sektion für technische Wissenschaften der Ungarischen Akademie der Wissenschaften, Seiten 1—11, Budapest am 16. April 1981*

Fachbücher

1. Dachdeckungen und Metallplattenarbeiten I—III. Építőipari Könyv- és Lapkiadó, Budapest 1952*
2. Baukonstruktionslehre I. Band. Tankönyvkiadó, Budapest 1960. (sechs Auflagen)*
3. Baukonstruktionslehre II. Band. Tankönyvkiadó, Budapest 1964. (vier Auflagen)*
4. Baukonstruktionslehre III. Band. Tankönyvkiadó, Budapest 1972 (zwei Auflagen)*
5. Baukonstruktionslehre IV. Band. Tankönyvkiadó, Budapest 1979
6. Kunstschlosserarbeit (Manuskript)*
7. Weiterleitung und Empfang von Informationen im industrialisierten Bauwesen. Einleitung in die Theorie der Blindplanung. (Mitverfasser M. Párkányi). Akadémiai Kiadó, Budapest 1979, 141 Seiten*
8. Energiewirtschaft in der Bauindustrie (Mitverfasser A. Zöld). Akadémiai Kiadó, Budapest. Ausgabe im Gange*
9. Die grundlegenden konstruktionstheoretischen Fragen der nichktektonischen Bauweise. (Mitverfasser M. Párkányi) Manuskript. Erscheint in der Monographienserie der Ungarischen Akademie der Wissenschaften*

Bemerkung

In der obigen Aufzählung sind die an verschiedenen Institutionen, Fortbildungskursen, wissenschaftlichen Sitzungen und im Laufe von ausländischen Studienreisen usw. gehaltenen Vorträge nicht enthalten.

* In ungarischer Sprache.

Acta Technica Academiae Scientiarum Hungaricae, 93 (3—4), pp. 215—236 (1981)

GRUBENTURBOLUFTKÜHLER— IHRE THEORIE UND PRAKTISCHE AUSFÜHRUNG

E. PÁSZTOR*

Dr. der techn. Wissenschaften

(Eingegangen am 24. Mai 1982)

The study is summarizing (air-cycle cooling machines) the theory of turbo-air coolers, then dealing with the theoretical and practical problems of mine-turbo-air coolers driven by compressed air. The study analyses the high compressed air driven turbo-air cooler constructions and determines the optimal value of specific cooling output. The study analyses the practical results of two different type of mine-turbo-air coolers and makes comparison between these results and the result to be reached theoretically.

1. Einführung

Die Luftkonditionierung von Tiefbaugruben mittels gekühlter Luft ist in unseren Tagen eine dauernd aktuelle Aufgabe. Da die Abbausohle immer tiefer verlegt wird, so nimmt auch die Gesteintemperatur in nicht vernachläßigbarem Maße zu. Dadurch ist aber das Klima von Tiefbaugruben für den menschlichen Aufenthalt, in erster Linie aber für eine menschliche Tätigkeit nicht geeignet. Die Abbaugränztiefe, für die schon eine Belüftung mittels unkonditionierten Luft nicht ausreicht, liegt in Ungarn in Abhängigkeit von den Gesteinverhältnissen zwischen 800—1000 m. In dieser Tiefe konditioniert die von der Erdoberfläche durch Ventilatoren nach unten geförderte Luft beliebiger Menge nicht in dem gewünschten Maße, da während der Förderung im Rohrsystem mehrerer km-Länge (in der Schacht) die Lufttemperatur praktisch die Grubentemperatur (Gesteintemperatur) annimmt. Diese Erwärmung erfolgt auch unter Verwendung wärmeisolierter Leitungen. Die auf der Erdoberfläche durchgeführte Luftabkühlung entspricht keinem Lösungsproblem, da sich die Luft in diesem Fall während ihres Transportes zum Verbraucherort trotzdem erwärmt.

Um eine Temperaturerhöhung der transportieren Luftmenge fast vollständig zu verhindern, werden möglicherweise die Kältemaschinen in der nächsten Umgebung der Verbraucherorte untergebracht. Somit werden die zum Lufttransport erforderlichen Rohrlängen auch kürzer. Der Kühlleistungsbedarf der Grubenlufträume von Tiefbaugruben beträgt max. 200—500 kW. Die Kältemaschinen dieser Leistungsgröße werden mit dampfartigen Arbeitssubstanzen (Freon, Ammoniak) als Kompressionskältemaschinen betrieben. Sie haben großes Gewicht und Volumen, ihre Disposition ist zeitaufwendig, ihr Transport zwischen den Grubenanlagen, bzw. ihre

* Dr. E. Pásztor, Honfoglalás út 48/B, H-1221 Budapest, Ungarn

zeitlich sich verändernde Inbetriebnahme recht umständlich, wozu noch ein zeitlich verzogener Anlauf zukommt. Bei einer Disposition mit dauerhaftem oder mit wenig veränderlichem Charakter arbeiten die erwähnten Kältemaschinen vorzüglich, wodurch bei großem Kühlleistungsbedarf nur die Anwendung von Kältemaschinen dieses Typs in Frage kommen können.

Bei zeitlich sich verändernden, oder bei nicht ständig besetzten Arbeitsstellen (in Schurfbauen, Schurfstrecken, bzw. auf Arbeitsstellen, die keine ständige Personalabsetzung haben, z. B. in Magazinen) besteht der Bedarf an schnell mobilisierbare und anlegbare Kältemaschinen kleinerer Kühlleistung, die aber relativ kleines Volumen und Gewicht haben. In solchen Fällen können die mit Luft als Arbeitsmedium (Arbeitssubstanz) betriebenen sog. „Turboluftkühler" vorteilhaft eingesetzt werden.

Der Lehrstuhl für Aero- und Thermotechnik des Fahrzeugtechnischen Instituts der TU Budapest führt seit mehreren Jahren eine Forschungsarbeit am Themengebiet der Entwicklung von Turboluftkühlern durch [1]; [2]; [3]. Um den einheimischen Bedarf decken zu können, wurde unter Leitung des Lehrstuhles, basierend auf die am genannten Gebiet erreichten theoretischen und praktischen Ergebnisse, mit Unterstützung der ungarischen Bergindustrie zwei Grubenturboluftkühler unterschiedlichen Typs entwickelt. Der vorliegende Beitrag möchte über die auf diesem Gebiet erreichten theoretischen und praktischen Ergebnisse berichten.

2. Der Kreisprozeß, die grundlegenden Kenngrößen und die Verlustanalyse von Turboluftkühlern

Die mit gasartigen Arbeitsmedien betriebenen Kältemaschinen sind praktisch gleichaltrig mit denen, die mit dampfartigen Arbeitssubstanzen betrieben werden. Ihr Kreisprozeß ist einfach, haben einen schnellen Anlauf, ihr spezifisches Gewicht und Volumen sind wesentlich kleiner als die der mit dampfartiger Arbeitssubstanz betriebenen. Sie haben eine größere spezifische Leistungsaufnahme, aber ihre spezifische Kühlleistung ist kleiner als die der mit dampfartiger Arbeitssubstanz betriebenen Kältemaschinen.

Dieser Nachteil, der infolge den unterschiedlichen Kreisprozessen zweier verschiedenen Kältemaschinentype entsteht, verhinderte, bzw. noch in unseren Zeiten verhindert eine Verbreitung der mit gasartiger Arbeitssubstanz (Luft) betriebenen Kältemaschinen (Turboluftkühler). Infolge ihrer höheren spezifischen Leistungsaufnahme sind sie für einen Dauerbetrieb unwirtschaftlich. Ihre Vorteile kommen erst dort zum Vorschein, wo infolge der durchschnittlich kurzer Betriebszeit, bzw. aussetzenden Betriebes die obengenannten Vorteile der Turboluftkühler in den Vordergrund rücken, und der höhere Energieverbrauch keinesfalls als grundlegender Nachteil bewertet wird. Typisch für dieses Gebiet sind die zeitweilig besetzten und örtlich sich schnell verändernden Schurfstrecken von Tiefbaugruben, wo neben den — infolge der zügigen Disposition, der leichten Inbetriebnahmemöglichkeit und der

praktisch unendlich kleinen Anlaufzeit — entstehenden Vorteilen den, durch den größeren Energieverbrauch verkörperten Nachteilen keine allzugroße Bedeutung beigemessen werden darf.

In dieser Arbeit wird die allgemeine Theorie der Turboluftkühler in dem zu der Behandlung der Grubenturboluftkühler erforderlichen Maße behandelt, die zitierten Arbeiten behandeln diese Fragen ausführlich. [1]; [2]; [3]; [5]; [6].

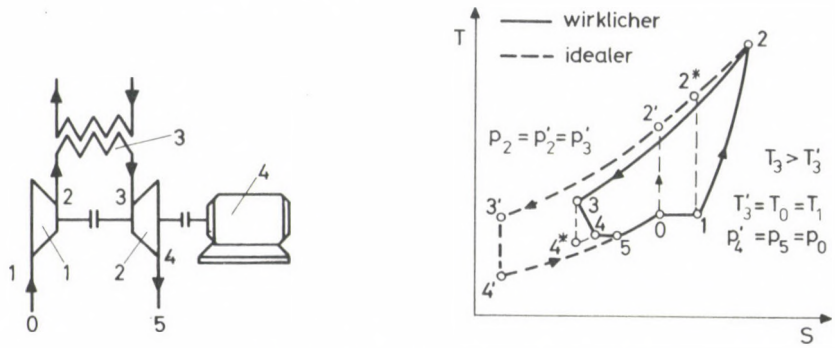

Abb. 1. Skizze und T-s Diagramm des Turboluftkühlers

Abb. 1. stellt den grundlegenden Kreisprozeß der Turboluftkühler und die Skizze der den Kreisprozeß realisierenden Maschineneinheit dar. Der reale Kreisprozeß besteht aus einer adiabatischen (im idealen Fall aus einer isentropischen) Kompression (1—2), der eine isobare Rückkühlung (2—3) und anschließend eine adiabatische Expansion (3—4) folgt. Das Gas (Luft) als Arbeitssubstanz, hat beim Verlassen der Expansionmaschine (Luftturbine) (2) eine niedrigere Temperatur, als es am Eintritt des Luftkompressors (1) hatte. Die aus den beiden Temperaturen entstehende Enthalpiedifferenz liefert, bezogen auf eine Arbeitssubstanz der Masse von 1 kg die Kühlleistung von

$$q_0 = c_p(T_0 - T_4)\,. \tag{1a}$$

Die zum Aufrechterhalten des Kreisprozesses benötigte Arbeit (W) entspricht dem Arbeitsunterschied des Kompressors und der Turbine, sie liefert der Antriebsmotor (4). Ihr Ausdruck lautet:

$$W = W_k - W_t = c_p[(T_2 - T_1) - (T_3 - T_4)] \tag{1b}$$

Die spezifische Kühlleistung (ε) kennzeichnet die energetische Wirtschaftlichkeit des Turboluftkühlers, wobei

$$\varepsilon = \frac{q_0}{W} = \frac{T_0 - T_4}{(T_2 - T_1) - (T_3 - T_4)} \tag{2}$$

gilt.

In den ausgeführten Turboluftkühlern entstehen die mit den nachstehenden Formeln berechenbaren wichtigsten Verluste: (Die Reihenfolge der Aufzählung entspricht der Arbeitssubstanz-Strömungsrichtung.)

— Druckverlust im Saugrohr

$$\sigma_{01} = p_1/p_0$$

— Strömungs- und Wirbelverluste im Kompressor

$$\eta_{\text{isk}} = \frac{T_2^* - T_1}{T_2 - T_1}$$

— Druckverlust im Rückkühler

$$\sigma_{23} = p_3/p_2$$

— Wirbel- und Strömungsverluste in der Turbine

$$\eta_{\text{ist}} = \frac{T_3 - T_4}{T_3 - T_4^*}$$

— Druckverlust in der Rohrleitung nach der Turbine

$$\sigma_{45} = p_5/p_4$$

— Gesamt-Druckverlustfaktor

$$\sigma = \sigma_{01}\sigma_{23}\sigma_{45}$$

— im Rückkühler kann das Arbeitsmedium nicht auf die Temperatur des Kühlmittels abgekühlt werden (Temperaturdifferenz)

$$\varphi = \frac{T_2 - T_3}{T_2 - T_{3'}}$$

Die spezifische Kühlleistung (ε_{id}) des idealen Turboluftkühlers ist nur eine Funktion des Druckverhältnisses [2]; [3]; [8], wobei mit $\varkappa = c_p/c_v$

$$\varepsilon_{\text{id}} = \frac{1}{\left(\frac{p_2}{p_0}\right)^{\frac{\varkappa - 1}{\varkappa}} - 1} \tag{3}$$

gilt.

Die spezifische Kühlleistung des idealen Turboluftkühlers nimmt mit abnehmenden Druckverlust eindeutig zu, und ε_{id} nimmt bei $p_2/p_0 = 1$ einen unendlich großen Wert an.

Die spezifische Kühlleistung des verlustbehafteten Turboluftkühlers ist wesentlich kleiner als die der idealen. Infolge der relativ geringfügigen Rückkühlung

unterscheiden sich die Kompressor- und Turbinearbeiten voneinander nicht allzusehr. In diesem Fall ist ihr Unterschied ($W = W_k - W_t$), also die zum Aufrecherhalten des Kreisprozesses erforderliche Arbeit im realen (verlustbehafteten) Fall ein Mehrfaches der idealen Arbeit, da die Kompressionsarbeit zugenommen, die Turbinenarbeit aber wegen den Verlusten abgenommen hat. Wie aus Abb. 1 ersichtlich ist, nimmt auch die Kühlleistung des Turboluftkühlers ab ($T_4 > T_4^* > T_4'$), wodurch die bedeutende Reduzierung der realen spezifischen Kühlleistung (ε_{wirk}) verständlich wird. Es gilt also:

$$\varepsilon_{id} \gg \varepsilon_{wirk} .$$

Abb. 2 stellt die spezifische Kühlleistung des idealen und des realen Turboluftkühlers in Abhängigkeit von dem Kompressionsdruckverhältnis bei verschiedenen Verlusten dar [3]. Die zunehmenden Zahlen der einzelnen Kurven bedeuten entsprechend den Tabellendaten ständig abnehmende Verluste. Die Daten der Kurve ③ entsprechen dem heutigen optimalen Entwicklungsniveau von Schaufelradmaschinen, somit beträgt der Spitzenwert der realen spezifischen Kühlleistung eines Turbokühlers mit dem einfachsten Kreisprozeß gemäß Abb. 1 $\varepsilon_{wirk} \approx 1$. Die Kompressions-Kältemaschinen mit Dampfzyklus haben eine spezifische Kühlleistung von $\varepsilon_{wirk} = 3 \div 4$, somit beträgt der Energieverbrauch des

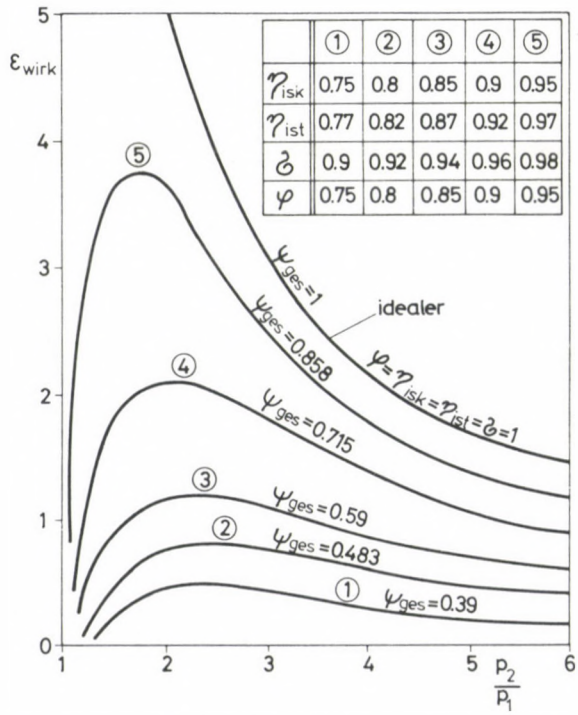

Abb. 2. Verlauf der effektiven spezifischen Kühlleistung (ε_{wirk}) in Abhängigkeit vom Kompressor-Druckverhältnis bei verschiedenen Gesamtverlustfaktoren (ψ_{ges})

Turboluftkühlers ein Vielfaches desjenigen der Kompressions-Kältemaschine mit Dampfzyklus.

Es existiert ein Druckverhältnis p_2/p_1, bei dem der Turboluftkühler einen bestimmten maximalen Wert der spezifischen Kühlleistung (ε_{wirk}) besitzt. Der Druckverlust im Kreisprozeß ruft dieses optimale Druckverhältnis hervor, sein Wert hängt aber auch von den übrigen Verlusten ab [3].

Im Zusammenhang mit Abb. 2 wurde der sog. „Gesamtverlustfaktor" (ψ_{ges}) eingeführt, der als Produkt der einzelnen Verlustfaktoren, also gemäß

$$\psi_{ges} = \eta_{isk}\, \eta_{ist}\, \sigma\varphi \tag{4}$$

definiert wurde. Die Abb. 2 beinhaltet als Parameter auch die Werte von ψ_{ges}. Der optimale Wert von ψ_{ges} liegt unter Berücksichtigung des heutigen und des in der Zukunft zu erwartenden technischen Niveaus zwischen $0{,}5 \div 0{,}55$.

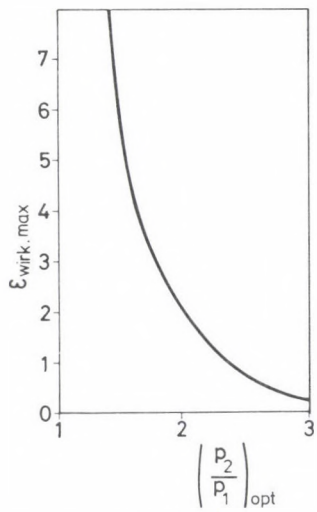

Abb. 3. Verlauf des maximalen ε_{wirk} in Abhängigkeit von dem optimalen Druckverhältnis $(p_2/p_1)_{opt}$

Abb. 3 stellt die zusammenhängenden Werte des optimalen Druckverhältnisses $(p_2/p_1)_{opt}$ und der maximalen spezifischen Kühlleistung ($\varepsilon_{wirk\,max}$) dar. Abnehmende Kreisprozeßverluste verursachen die Reduzierung des optimalen Druckverhältnisses. Diese Tatsache ermöglicht eine konstruktiv günstige Ausbildung, da mit Schaufelradkompressoren kein allzu großer Druckunterschied erzeugt werden kann.

Abb. 4 zeigt in Abhängigkeit von der Funktion ψ_{ges} die Änderung des optimalen Wertes ($\varepsilon_{wirk\,max}$) der spezifischen Kühlleistung bei gegebenem Druckverhältnis. Die Verlustfaktoren der einzelnen Maschineneinheiten beeinflussen die spezifische Kühlleistung des Turboluftkühlers — im Grunde genommen seine Wirtschaftlichkeit

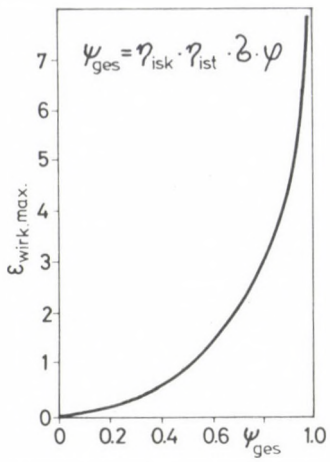

Abb. 4. Verlauf des maximalen ε_{wirk} in Abhängigkeit von dem Gesamtverlustfaktor (ψ_{ges}) des Kreisprozesses

—, wie es vorher durch thermische Überlegungen gezeigt wurde. Auf sie übt der hier definierte Gesamtverlustfaktor ψ_{ges} einen grundlegenden Einfluß aus.

Eine Steigerung der spezifischen Kühlleistung von Turboluftkühlern kann ausschließlich durch eine Verlustreduzierung der einzelnen Maschineneinheiten erreicht werden.

3. Funktionsweise, Antriebsmöglichkeiten und grundlegende konstruktive Ausbildungsmöglichkeiten von Grubenturboluftkühlern

Das Arbeitsprinzip der Grubenturboluftkühler stimmt mit dem des im Abschnitt 2 und in der Abb. 1 gezeigten allgemeinen Turboluftkühlers überein, ein Unterschied besteht lediglich in der Antriebsart. Die Schaufelradmaschinen (Kompressoren und Turbinen) sind bekanntlich hochtourige Maschinen, ihre Drehzahlen nehmen mit abnehmender Strömungssubstanz bedeutend zu. Die Kühlleistung der von der Bergindustrie verlangten und während der Forschungsarbeit entwickelten Turboluftkühler beträgt $\dot{Q} \approx 20 - 30$ kW, die zu dieser Kühlleistung, bzw Maschinengröße gehörige Drehzahl beträgt $n \approx 900 \div 1100\ s^{-1}$.

Das Erreichen solcher Drehzahlen mittels Elektromotoren und Übersetzungsgetrieben bedeutet ein äußerst schwieriges Problem. Das Gewicht und Volumen des Übersetzungsgetriebes wären größer als die Maße des realisierbaren Turboluftkühlers, weshalb dieser Lösungsweg verlassen wurde.

In dem Bergwerken steht aber immer Druckluft zur Verfügung, die zum Antrieb von Turboluftkühlern vorteilhaft verwendet werden kann. Das erforderliche Druckverhältnis des Turboluftkühlerkompressors beträgt $p_2/p_1 \approx 2$, ein höcherliegen-

der Wert als dieser wird im Allgemeinen nicht verlangt (Abb. 2). Das Druckverhältnis der mit den auf Erdoberfläche betriebenen Kompressoren erzeugten Druckluft liegt zwischen $5 \div 6$. Dieser Wert ist aber zu hoch, um ein unmittelbares Einströmen der Luft in die aus dem Turboauflader von Dieselmotoren ausgebildete Turboluftkühlerturbine zuzulassen, und dort nach erfolgter Expansion das Leistungsgleichgewicht der Kompressor- und Turbineneinheit hervorzurufen.

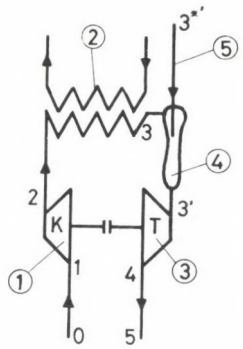

Abb. 5. Schaltungsskizze des Grubenturboluftkühlers mit Injektor

Zu einer wirtschaftlichen Verwendung der Druckluft bieten sich zwei Möglichkeiten an. Gemäß der ersten Lösung (Abb. 5) wird ein Teil Überschußenergie der aus der Netzrohrleitung ⑤ strömenden Druckluft im Injektor ④ ausgenutzt. Die Netzdruckluft entspannt sich im Injektor auf den Wert, der durch die in den Injektor einströmende Luftmenge des Druckwertes p_3 bestimmt wird. Diese Luftmenge mit dem Enddruck p_3 hat den folgenden Strömungsweg: Kompressor ①— Rückkühler ② — Injektor ④. Die sich somit entspannte Leitungsluft großer Menge beschleunigt die aus dem Rückkühler ausströmende und durch den Kompressor komprimierte Luftmenge. Nach einer Vermischung erfolgt im Diffusor des Injektors eine Verzögerung der gesamten Luftmenge, wobei der Druck bis zum Turbineneintritt auf einen Wert von $p'_3 > p_3$ zunimmt. In der Turbine dehnen sich die beiden Luftströme gemeinsam aus, treiben den Kompressor an, und verlassen die Turbine auf einer Temperatur von $T_5 < T_0$. Somit nützt der Injektor in bestimmtem Maße — da bekanntlich die Injektorwirkungsgradwerte niedrig sind — einen Teil der sich aus der Druckrelation $p_3^* > p_3$ ergebenden Druckdifferenz $(p_3^{*\prime} - p_3)$ aus.

Die zweite Lösungsmöglichkeit zeigt die Abb. 6, wo die Netzdruckluft ⑤ des Zustandes 3*' und die vom Kompressor gelieferte Druckluft des Zustandes 3 in das aus zwei Teilen zusammengesetzte Leitrad getrennt einströmt. Danach entspannen sich die Luftmengen in den Turbinenlaufrädern getrennt, aber die Arbeitsmedien verlassen die Turbine schon vermischt. Die Abbildung zeigt auch die Konstruktionsskizze des in zwei Teile aufgespaltenen Spiralgehäuses (Schneckengehäuses) der Zentrifugalturbine.

Energetisch kann diese Lösung günstiger sein, als die mit dem Injektor, aber ihr Nachteil besteht darin, daß die drehenden Schaufelkränze unter Zusammenspiel ungünstiger Umstände bedeutenden, aus Schwingungsbeanspruchungen herrührenden Ermüdungsbeanspruchungen ausgesetzt werden können. Aus den Leiträdern, in die die Netzdrucktluft des Zustandes 3* eintritt, strömt das Medium mit einer wesentlich zugenommenen Geschwindigkeit aus ($p_3^* > p_3$), wodurch auf die Laufräder eine sich periodisch verändernde Impulskraft ihre Wirkung ausübt, die die Schaufelkränze ermüdet. Um eine Verminderung dieser Ermüdungsbeanspruchung erreichen zu können, empfielt es sich nicht die Zuleitung der gesamten Netzdruckluftmenge in das Schneckengehäuse. Eine Reduzierung des Luftdruckes ($p_3^* < p_3^{*\prime}$) kann praktisch mit Drosselung erreicht werden, die aber bedeutende Verluste verursacht. Somit nimmt aber der energetische Vorteil infolge der getrennten Expansion zweier Medien unterschiedlichen Druckes in der Turbine mit Zunahme der Drosselung ab. Nach unseren theoretischen und praktischen Untersuchungen (Messungen) können unter Anwendung günstig ausgebildeter Injektoren nahezu die gleichen energetischen Verhältnisse erreicht werden, wenn der Druck des Netzmediums mit Drosselung ($p_3^* < p_3^{*\prime}$) in dem Maße vermindert wird, damit es für die Turbinenschaufelkränze keine zu berücksichtigende Ermüdungsbeanspruchung hervorruft.

Der Lehrstuhl für Aero- und Thermotechnik des Fahrzeugtechnischen Instituts der TU Budapest entwickelte mit Hilfe von ungarischen Bergindustrieunternehmen Türboluftkühler der beiden erwähnten Type. (Mecseker Bergbauunternehmen, Bergbautechnisches Zentralunternehmen).

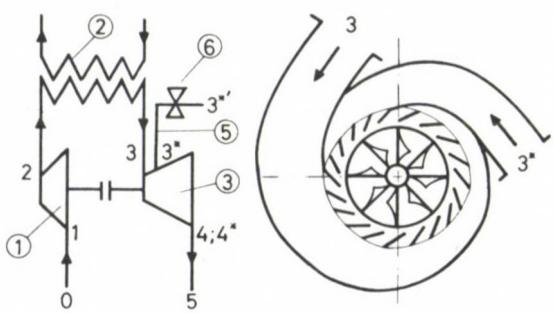

Abb. 6. Schaltungsskizze des injektorlosen Grubenturboluftkühlers mit geteiltem Schneckengehäuse

Diese Turboluftkühler wiesen die Konstruktionseigenschaften von Gasturbinen auf, sie hatten kleines Gewicht und Volumen, ihre Disposition war neben guter Transportfähigkeit einfach. Dazu kam noch eine Anlaufzeit von $1 \div 2s$. Die angefertigten Turboluftkühler trugen und tragen erfolgreich der Beförderung der Mikroklimatisierung von Tiefbaugruben bei.

4. Die Bestimmung der strömungs- und thermotechnischen, sowie der energetischen Kenngrößen von Grubenturboluftkühlern

4.1. Die energetische Analyse des Grubenturboluftkühlers mit Injektor

Das Schaltbild des Grubenturboluftkühlers mit Injektor zeigt Abb. 5, das auf den Injektor bezogene Bezeichnungssystem beinhaltet Abb. 7. Die Bezeichnungen der in den Injektor einströmenden, bzw. diesen verlassenden Medien sind in den beiden Abbildungen die gleichen.

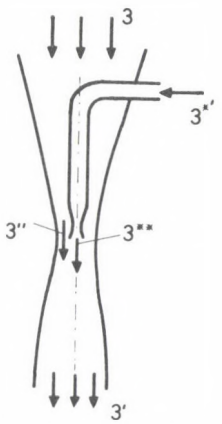

Abb. 7. Bezeichnungssystem des Injektors

Um die thermischen Größen des den Injektor verlassenden Mediums (Luft) bestimmen zu können, sollen die Förderströme (Gewichtsströme) des primären und sekundären Arbeitsmediums bekannt sein. Die Massen und die Massenverhältnisse der primären und sekundären Arbeitssubstanzen können aber aus der Energiegleichgewichtsgleichung der Turbine und des Kompressors bestimmt werden, zu der jedoch das Kenntnis der Zustandsgröße 3′ der den Injektor verlassenden und in die Turbine eintretenden Arbeitssubstanz erforderlich ist. Auf Grund dieser Überlegung soll dieses Problem mit Hilfe einer Iteration gelöst werden. Für die Berechnung des Injektors soll das Verhältnis beider Medien angenommen werden, deren richtige Größe nach der Aufstellung der Energiegleichgewichtsgleichungen der Turbine und des Kompressors kontrolliert werden kann, da aus diesen das Mediumsverhältnis berechenbar ist. Bei einer Abweichung kann die Genauigkeit durch eine Iteration gesteigert werden.

Die (dynamischen) Kenngrößen (p_3; T_3) der den Rückkühler verlassenden abgebremsten (secundären) Arbeitssubstanz (Luft) — Gesamtdruck und Gesamttemperatur — sind bekannt. Wird im Mischhalsrohr des Injektors die Geschwindigkeit der secundären Arbeitssubstanz mit c_3'' angenommen, so können die statischen

Kenngrößen der (ungebremsten) Arbeitssubstanz bei einer Geschwindkeit von c_3'' berechnet werden. (Die „statischen" Kenngrößen werden weiterhin mit dem Index „*st*" bezeichnet.)

Die gesuchten Kenngrößen ergeben sich zu

$$T_{3\,st}'' = T_3 - \frac{c_{3''}^2}{2c_p}, \tag{5}$$

und

$$p_{3\,st}'' = \frac{p_3}{\left(\frac{T_3}{T_{3\,st}''}\right)^{\frac{\varkappa}{\varkappa-1}}}. \tag{6}$$

Die Geschwindigkeit der die Düse (in unserem Fall eine Laval-Düse) der primären Substanz verlassenden Arbeitssubstanz kann auf Grund derjenigen Bedingung bestimmt werden, wonach das Medium in der Düse der primären Arbeitssubstanz auf einen Druck von $p_{3\,st}''$ — bestimmt durch die secundäre Arbeitssubstanz — expandiert. Für diese Geschwindigkeit c_3^{**} gilt:

$$\frac{c_3^{2**}}{2} = \beta^2 c_p T_3^{*'}\left[1 - \frac{1}{\left(\frac{p_3^{*'}}{p_{3\,st}''}\right)^{\frac{\varkappa-1}{\varkappa}}}\right], \tag{7}$$

wobei β den Geschwindigkeitsverlustfaktor der Düse bezeichnet.

Am Ende des Vermischungsraumes hat die gemeinsame Geschwindigkeit beider Arbeitssubstanzen einen Wert von

$$c_3' = \left(\frac{c_3'' + \alpha c_3^{**}}{1+\alpha}\right)\psi, \tag{8}$$

wobei ψ — den Geschwindigkeitsfaktor des Vermischungsabschnittes,

α — das Verhältnis der primären und secundären Förderströme, also

$$\alpha = \frac{\dot{m}_{\mathrm{pr}}}{\dot{m}_{\mathrm{sec}}}$$

bedeuten.

Die Temperatur T_3' des abgebremsten Arbeitssubstanzgemisches kann aus den Temperaturen der abgebremsten primären und secundären Arbeitssubstanzen und dem Förderströmverhältnis α bei denjenigen Bedingungen (Prinzip der Erhaltung der Energie) bestimmt werden, wonach die Gesamtenergie des Arbeitssubstanzgemisches gleich der Summe der Gesamtenergien der primären und secundären Arbeitssubstanz sein soll. Somit ergibt sich für T_3':

$$T'_3 = \frac{T_3 + \alpha T_3^{*'}}{1+\alpha}. \tag{9}$$

Der Druck (Gesamtdruck) des abgebremsten Arbeitssubstanzgemisches kann auf Grund derjenigen gut annähernden Annahme ermittelt werden, wonach der Impulsaustausch der strömenden Substanzen untereinander, bzw. das Entstehen der gemeinsamen Geschwindigkeiten bei dem untereinander gleich großen und konstanten statischen Druck der sich vermischen den Arbeitssubstanzen erfolgt. Es gilt also:

$$p''_{3\,st} = p^{**}_{3\,st} = p'_{3\,st}.$$

Der Gesamtdruck des Arbeitssubstanzgemisches ergibt sich unter Annahme einer isentropischen Verzögerung — wobei die Verluste des Vermischungsabschnittes mit einem Geschwindigkeitsverlustfaktor berücksichtigt wurde — zu

$$p'_3 = p'_{3\,st}\left(\frac{T'_3}{T'_{3\,st}}\right)^{\frac{\varkappa}{\varkappa-1}}, \tag{10}$$

wobei $T'_{3\,st}$ die (statische) Temperatur der strömenden Arbeitssubstanz nach der Vermischung bezeichnet. Für $T'_{3\,st}$ gilt:

$$T'_{3\,st} = T'_3 - \frac{c'^2_3}{2c_p}. \tag{11}$$

Nachdem die Zustandsgrößen der sich vermischenden Arbeitssubstanzen bestimmt wurden, kann aus der Energiegleichgewichtsgleichung des Turboluftkühlers — bezogen auf Kompressor und Turbine — diejenige primäre Substanzmenge berechnet werden, die zum Aufrecherhalten des Gleichgewichtszustandes benötigt wird.

Mit den Bezeichungen der Abb. 5 lautet die für α mit Hilfe der realen (tatsächlichen) Temperaturen aufgeschriebene Energiegleichgewichtsgleichung:

$$\alpha = \frac{(T_2 - T_1) - (T'_3 - T_4)}{(T'_3 - T_4)}. \tag{12}$$

Die spezifische Kühlleistung ε_{inj} der Maschine mit Injektor wird mit Hilfe der Gleichung (2) ausgedrückt:

$$\varepsilon_{\text{inj}} = \frac{(1+\alpha)(T_0 - T_4)}{\alpha T_0\left[\left(\frac{p_3^{*'}}{p_0}\right)^{\frac{\varkappa-1}{\varkappa}} - 1\right]\cdot\frac{1}{\eta_{\text{keff}}}}, \tag{13}$$

wobei η_{keff} den effektiven Wirkungsgrad des die Netzdruckluft erzeugenden Kompressors bezeichnet.

Nach einer Analyse der Injektorbetriebsverhältnisse vergrößern sich die Werte von p'_3, da eine Zunahme der Geschwindigkeit c''_3 die Abnahme des Impulsverlustes hervorruft. Dadurch erhält man günstigere Verhältnisse, weshalb unsere Untersuchungen bei verschiedenen Geschwindigkeiten c''_3 durchgeführt wurde.

Für unsere Berechnungen haben wir für die einzelnen Kenngrößen bzw. Faktoren die nachstehenden realen Werte eingesetzt: $\eta_{isk}=0{,}76$; $\eta_{ist}=0{,}78$; $\sigma=0{,}93$; $\varphi=0{,}87$; $p_0=0{,}11$ MPa; $T_0=308$ K; $\psi=0{,}9$; $\beta=0{,}92$; $p_3^{*\prime}=0{,}6$ MPa.

Der Druck $p_3^{*\prime}$ der Netzdruckluft war während der Untersuchung konstant.

Die Berechnungsergebnisse sind in Abb. 8 aufgetragen. Um eine bequeme Vergleichsmöglichkeit erreichen zu können, wurden in die Abbildung auch die Ergebnisse der Berechnung eines Turboluftkühlers mit geteiltem Schneckengehäuse eingetragen. Diese Turboluftkühlerausführung — die Pkt. *4.2.* behandelt wird — hat die Eigenschaft, daß sich hier die Netzdruckluft ohne Dazwischenschalten eines Injektors unmittelbar in der Turbine expandiert. Die Kurven ② und ③ zeigen die

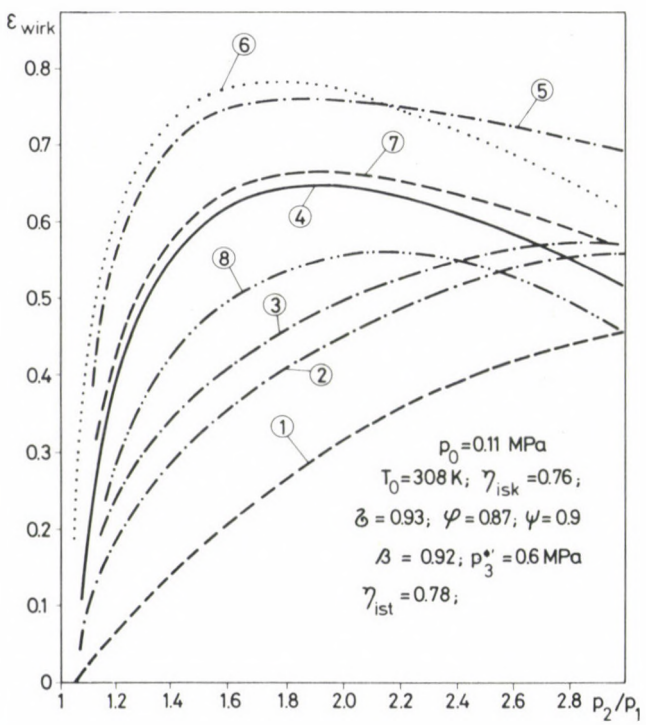

Abb. 8. Änderung der effektiven spezifischen Kühlleistung der Grubenturboluftkühler verschiedener Ausführungsformen in Abhängigkeit von dem Kompressordruckverhältnis

1 — Netzdruckluft-Druck mit Drosselung vermindert $p_3^*=p_3$, $p_3^{*\prime}=0{,}6$ MPa; 2 — Ausführung mit Injektor $c''_3=80$ ms^{-1}; 3 — Ausführung mit Injektor $c''_3=200$ ms^{-1}; 4 — Achsangetriebener Turboluftkühler; 5 — ohne Drosselung $p_3^*=p_3^{*\prime}=0{,}6$ MPa, $\eta_{ist\,3}=\eta_{ist\,3^*}=0.78$; 6 — ohne Drosselung $p_3=p_3^*=p_3^{*\prime}$; 7 — ohne Drosselung $p_3^*=p_3^{*\prime}=0{,}6$ MPa, $\eta_{ist\,3}>\eta_{ist\,3^*}$; 8 — teilweise Drosselung $p_3^*=0{,}6$ MPa; $p_3^*=0{,}4$ MPa, $\eta_{ist\,3}=0{,}78$; $\eta_{ist\,3^*}=0{,}7$

Ergebnisse bei einem Turboluftkühler mit Injektor. Bei Kurve ② beträgt die Geschwindigkeit im kleinsten Injektorquerschnitt $c_3'' = 80\ \mathrm{ms}^{-1}$, sie hat aber bei Kurve ③ einen Wert von $c_3'' = 200\ \mathrm{ms}^{-1}$. Die übrigen Daten sind die gleichen, also die günstigeren Werte der Kurve ③ sind dadurch entstanden, daß infolge einer Geschwindigkeitszunahme von c_3'' die im Injektor durch den Impulsaustausch hervorgerufenen Verluste abnehmen. Wegen der ausgeprägten Verluständerung des Injektors liegt der optimale Wert des Kompressordruckverhältnisses p_2/p_1 des Turboluftkühlers zwischen $3 \div 3{,}5$. Dieses Ergebnis stimmt mit denen in den Abb. 2 und 3 gezeigten überein, wobei erkannt werden kann, daß mit zunehmendem Gesamtverlust (Abnahme von ψ_{ges}) der optimale Wert des Druckverhältnisses p_2/p_1 abnimmt. Aus Abb. 8 kann noch abgelesen werden, daß beim mit Netzdruckluft erfolgten Antrieb unter Verwendung eines Injektors, bei einem realen, im Bereich von $p_2/p_1 = 1{,}8 \div 2$ liegenden Druckverhältnis der maximale Wert von $\varepsilon_{\mathrm{inj}}$ um einen Wert von 0,5 zu erwarten ist.

4.2. Die energetische Analyse des injektorlosen Grubenturboluftkühlers mit geteiltem Schneckengehäuse

Den Ausgangspunkt für eine energetische Analyse des Turboluftkühlers bildet auch in diesem Fall die auf die rotierenden Teile des Turboluftkühlers (Kompressor, Turbine) aufgestellte Energiegleichgewichtsgleichung, wonach die Gesamt-Turbinenarbeit gleich der Arbeitsaufnahme des Kompressors ist, also:

$$(T_2 - T_1) = (T_3 - T_4) + \alpha(T_3^* - T_4^*), \tag{14}$$

wobei T_4 die Temperatur der den Rückkühler verlassenden Druckluft nach der Expansion, T_4^* dagegen die Temperatur der Netzdruckluft bezeichnen.

Für die Bestimmung des spezifischen Druckluftverbrauches wird hierbei der Faktor α genauso verwendet, als er schon beim Turboluftkühler mit Injektor definiert wurde.

Die Kenngrößen der in das geteilte Schneckengehäuse der Turbine gemäß Abb. 6 einströmenden Luft des Druckes p_3 kann eindeutig unter Berücksichtigung der Vorgänge im Kompressor ① und Rückkühler ② bestimmt werden [2]; [3], weshalb diese Frage hier unberücksichtigt bleibt. Der Druckwert der aus dem Druckluftnetz einströmenden Luft (3*) hängt dagegen von dem realisierten Drosselungsmaße vor dem Schneckengehäuse ab.

Die Temperatur ändert sich nicht mit der Drosselung, somit ist der Wert von T_3^* mit guter Näherung gleich der Luftraumtemperatur des tiefliegenden Bergwerkes.

Im Zusammenhang mit dem Wert p_3^* der Druckluft gelten die folgenden Überlegungen:

a) Der gedrosselte Druck der Netzdruckluft ($p_3^{*\prime} = 0{,}6$ MPa) vor der Turbine (p_3^*) ist immer gleich dem Druck p_3 der den Rückkühler ② verlassenden Druckluft ($p_3 = p_3^*$).

In diesem Fall dürfen beide Substanzen in einem gemeinsamen Schneckengehäuse expandieren, man braucht also kein getrenntes. In erster Näherung dürfen die Expansionswirkungsgrade (η_{ist}) beider Luftströme gleich sein. In diesem Fall wird die spezifische Kühlleistung ε infolge den zugenommenen Drosselverlusten äußerst gering. Diese energetischen Verhältnisse zeigt die Kurve ① der Abb. 8. Die Ausgangsdaten der Berechnungen sind mit denen der bei der energetischen Untersuchung der Ausführung mit Injektor angenommenen identisch. Die Faktoren β und ψ kommen hier selbstverständlich nicht vor, da diese nur Kenngrößen der Ausführung mit Injektor sind. Es wurden auch die energetischen Kenngrößen desjenigen Falles untersucht, in dem $p_3 = p_3^* = p_3^{*\prime}$ gilt, also der Gegendruck des auf der Erdoberfläche betriebenen und die Netzdruckluft liefernden Kompressors immer gleich dem Druck der den Rückkühler des Turboluftkühlers verlassenden ist. In diesem Fall entfallen die Drosselverluste, deshalb ist energetisch gesehen dieser Turboluftkühler am günstigsten. Diese Verhältnisse zeigt auch die Kurve ⑥ der Abb. 8.

b) Der andere Sonderfall tritt dann auf, wenn die Netzdruckluft ungedrosselt bleibt, und deren Druck unabhängig vom Druckwert p_3 ist. ($p_3^* = p_3^{*\prime} = \text{const} = 0{,}6$ MPa).

Durch den Einströmquerschnitt 3* des geteilten Schneckengehäuses gemäß Abb. 6 strömt die Luft mit unverändertem Netzdruck ein. ($p_3 \ll p_3^* = p_3^{*\prime}$) Energetisch ist das wegen den entfallenden Drosselverlusten günstig.

Die Kurve ⑤ der Abb. 8 zeigt den Fall bei der Bedingung, wonach die Wirkungsgrade des Hoch- und Niederdruckturbinenteiles einander gleich sind. ($\eta_{ist\,3} = \eta_{ist\,3*}$).

Aus einem Vergleich der Kurven ⑤ und ⑥ kann die Schlußfolgerung gezogen werden, wonach ohne Drosselverluste, bei gleichen Wirkungsgraden der beiden Turbinenteile (Hoch- und Niederdruckteil) die spezifische Kühlleistung ε im Grunde genommen vom Druck der Netzdruckluft unabhängig ist. Die unbedeutende Abweichung im Optimumbereich der Kurven ⑤ und ⑥ ergibt sich daraus, daß mit Zunahme des Netzdruckes die erforderliche Netzluftmenge abnimmt, aber auch die Temperatur der die Turbine verlassenden Netzluft sinkt. Hinsichtlich der Kühlleistung kompensieren sich beide Einflüsse nicht vollständig, woraus sich die keinesfalls wesentliche Abweichung der beiden Kurven herleiten läßt.

In der Wirklichkeit bleibt aber unter der Bedingung $p_3 \ll p_3^* = p_3^{*\prime}$ der Wirkungsgrad $\eta_{ist\,3*}$ des Hochdruck-Turbinenteils nicht konstant, sondern er nimmt wegen der unter Punkt *3* schon angegebenen Schaufelermüdungserscheinungen ab. Den Grund der Wirkungsgradabnahme zeigt Abb. 9. Das Arbeitsmedium des Druckwertes p_3^* verläßt das Leitrad notwendigerweise mit einer größeren Geschwindigkeit als das des Druckwertes p_3 ($c_3^* > c_3$) Dementsprechend tritt das Arbeitsmedium in die mit der gleichen Umfangsgeschwindigkeit u rotierenden Laufräder stoßbehaftet mit einer Relativgeschwindigkeit w (in Abb. 9 w_3^*) ein. Deshalb sinkt der Wirkungsgrad des Hochdruckturbinenteils. Die Stoßverluste wurden unter Anwendung der Literatur [10] berechnet. Der Luftenthalpieabfall nimmt auch zwischen des Laufradschaufeln

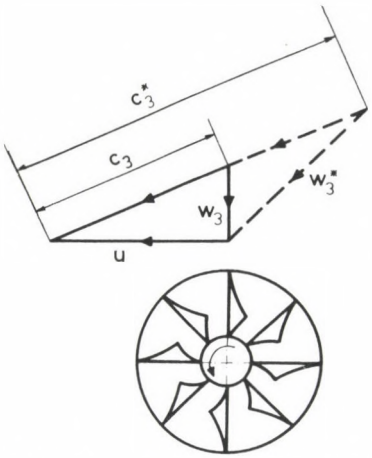

Abb. 9. Geschwindigkeitsdreiecke im Hoch- und Niederdruckturbinenteil

zu, da dort der Druckabfall kaum über den kritischen liegen darf. Eine Strahlablenkung der schräg abgeschnittenen Leitradschaufel verursacht keine Zunahme des Druckabfalles über den kritischen hinaus. Die zugenommene Enthalpieabnahme der Netzdruckluft ruft im Laufrad keinen optimalen Ausfluß hervor, weshalb auch der Wirkungsgrad des Hochdruck-Turbinenteils abnimmt.

Dier Wirkungsgrad des Niederdruck-Turbinenteils ist jetzt wiederum gleich mit dem in den vorigen Untersuchungen angenommenen ($\eta_{\text{ist}\,3}=0{,}78$), für den Wirkungsgrad des Hochdruck-Turbinenteils ergibt sich jedoch — nach unseren Untersuchungen — bei einem Arbeitssubstanzdruck von $p_3 \ll p_3^*=0{,}6$ MPa $=p_3^{*\prime}$ infolge von $\eta_{\text{ist}\,3^*}\approx 0{,}68$.

Bei teilweiser Drosselung ($p_3 < p_3^* < p_3^{*\prime}$) ergeben sich bessere Wirkungsgradwerte. Auf Grund unserer Analyse und Berechnung (deren Bekanntgabe weitaus die Grenzen dieses Beitrages überschreiten würden) ändert sich der Wert von $\eta_{\text{ist}\,3}^*$ bei einem konstanten Druck von $p_2=0{,}221$ MPa ($p_2/p_1=2{,}1$ also ein guter Mittelwert) gemäß der in Abb. 10 gezeichneten. Der Druck $p_2=\text{const}$ wurde so angenommen, daß dieser in der Umgebung des optimalen und energetisch am wichtigsten Druckverhältnisses p_2/p_1 des Turboluftkühlers liegen soll (Abb. 8).

Wie es aus Abb. 10 zu erkennen ist, nimmt der Wirkungsgrad des Hochdruck-Turbinenteils mit einer Zunahme von p_3^* zuerst in bedeutendem, dann aber in abnehmendem Maße ab. Das läßt sich dadurch erklären, daß die Absolutgeschwindigkeit c_3^* des das Leitrad verlassenden Arbeitsmediums mit steigendem Druckverhältnis desselben immer in kleinerem Maße bedeutend zunimmt, über dem kritischen Druckverhältnis hinaus jedoch (praktisch) einen konstanten Wert annimmt. Dementsprechend ändern sich auch die infolge der Richtungsänderung der Relativgeschwindigkeit w_3^* auftretenden Stoßverluste.

Die Kurve ⑦ der Abb. 8 zeigt den Fall, in dem $p_3^* = p_3^{*\prime} = 0{,}6$ MPa gilt, die Netzdruckluft also ohne Drosselung in die Turbine einströmt, aber der Wirkungsgrad des Hochdruck-Turbinenteils nur — entsprechend Abb. 10 — den Wert von $\eta_{ist\,3^*} = 0{,}68$ beträgt. Die Kurven ⑤ und ⑦ der Abb. 8 unterscheiden sich nur in den Wirkungsgradwerten des Hochdruck-Turbinenteiles.

Nach der bisher durchgeführten Analyse des injektorlosen Grubenturboluftkühlers strömt die Netzdruckluft mit einem Druck von $p_3^{*\prime}$ (Abb. 6) bei einer vollständig geöffneten Stellung des Drosselventils ⑥ mit einem Druck von $p_3^* = p_3^{*\prime}$ in die Turbine ein. In diesem Fall ruft nur der verminderte Wirkungsgrad des Hochdruck-Turbinenteils die Verluste hervor. Diese Verhältnisse stellt die Kurve ⑦ der Abb. 8 vor.

Wegen der Gefahr der Schaufelermüdung, bzw. eventueller Schaufelbrüche, soll die Luft des Druckes $p_3^{*\prime} = p_3^*$ nicht in die Turbine eingeleitet werden. Bei einem teilweisen Abschließen des Drosselventils ⑥ der Abb. 6 ($p_3^* < p_3^{*\prime}$) strömt die Luft in die Turbine mit einem vermindertem Druck ein. Die besonders großen Drosselverluste werden in bestimmtem Maße dadurch ausgeglichen, daß laut Abb. 10 eine Abnahme des Druckes p_3^* der in die Turbine einströmenden Luft den Expansionswirkungsgrad ($\eta_{ist\,3^*}$) der komprimierten Luft verbessert.

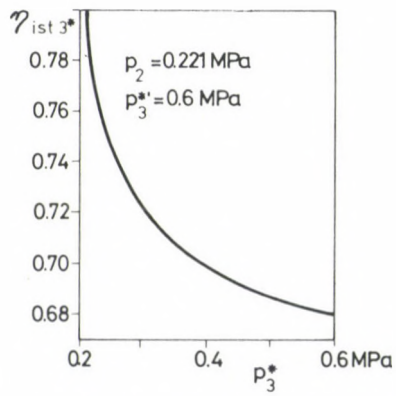

Abb. 10. Wirkungsgradverlauf ($\eta_{ist\,3^*}$) der Hochdruckturbine in Abhängigkeit von dem Druck (p_3^*) vor der Hochdruckturbine

Die Kurve ⑧ der Abb. 8 zeigt entspricht dem Fall, in dem $p_3^* = 0{,}4$ *MPa* ist, und dementsprechend ergibt sich gemäß Abb. 10 der Wert von $\eta_{ist\,3^*}$ zu 0,7. Es ist ersichtlich, daß die Drosselverluste ($p_3^* < p_3^{*\prime}$) wesentlich den Wert von ε herabsetzen, und nach unseren Berechnungen hat ε bei einer so bedeutenden, realen und erforderlichen Drosselung im Falle der Ausführungen mit und ohne Injektor praktisch den gleichen Wert. Bei der konkreten Ausführung des Turboluftkühlers ohne Injektor haben wir diese Lösung angewendet.

5. Die mit den ausgeführten Grubenturboluftkühlern erreichten praktischen Ergebnisse

5.1. Die Meßergebnisse des Grubenturboluftkühlers mit Injektor. Schlußfolgerungen

Die tatsächliche Ausführungsskizze des Grubenturboluftkühlers mit Injektor entsprach der in Abb. 5 gezeigten mit dem Unterschied, daß bei der praktischen Ausführung gemäß Abb. 11 ein Rückkühler ⑥ dazwischengeschaltet wurde, um den Betrieb des Grubenturboluftkühlers auch in schlagwettergefährdeter Umgebung ermöglichen zu können. Bei den vorzeitigen, ohne Verwendung des Rückkühlers

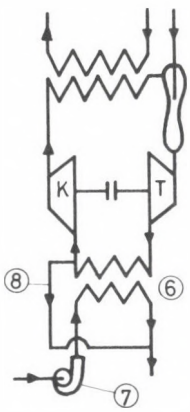

Abb. 11. Schaltskizze des Grubenturboluftkühlers für schlagwettergefährdete Umgebung

durchgeführten Messungen ergaben sich die Erfahrungen, daß die schwebenden Staubteilchen bei ihrem Aufprall am Turbinenlaufrad Funkenbildung hervorrufen, die in schlagwettergefährdeten Bergwerken gefährlich sein kann. Die in den Injektor eingeleitete Netzdruckluft hat das System durch das Funkenlöschrohrsystem ⑧ verlassen, wodurch dieser Turboluftkühler mit einem halbgeschlossenen Kreisprozeß betrieben wurde. Auf der „Warmseite" des Rückkühlers ⑥ wurde die Luft durch den druckluftangetriebenen Ventillator ⑦ in Strömung gebracht. Der Rückkühler, bzw. der halbgeschlossene Kreisprozeß wurde deshalb verwendet, da uns die Umleitung der gesamten, die Turbine verlassenden Luftmenge durch die Funkenlöschstrecke zu gewagt schien. Da der Rückkühler ⑥ und die Anzapfung ⑧ die thermischen und strömungstechnischen Verhältnisse des Turboluftkühlers in meßbarer Weise nicht beeinflussen, werden die Meßergebnisse an Hand der in Abb. 5 gezeigten Skizze angegeben.

Bei der Wiedergabe der Meßergebnisse beschränken wir uns auf die wichtigsten Ergebnisse, auf eine ausführliche Analyse der Messungen soll leider aus Platzgründen

verzichtet werden. Die relative Luftfeuchtigkeit war so niedrig, daß sie unberücksichtigt blieb.

Die wichtigsten gemessenen, bzw. eingestellten Werte waren die folgenden: $p_1 = p_0 = 0{,}1$ MPa; $T_0 = T_1 = 301$ K; $p_2 = 0{,}16$ MPa; $T_2 = 361$ K; $p_3 = 0{,}156$ MPa; $T_3 = 308$ K; $T'_3 = 306$ K; $p'_3 = 0{,}185$ MPa; $T_4 = 269{,}5$ K; $p_4 = 0{,}1$ MPa; $m^{*\prime}_3 = 0{,}29\ \text{kgs}^{-1}$ (Netzdruckluftmenge) $p^{*\prime}_3 = 0{,}53$ MPa; $T^{*\prime}_3 = 306$ K; $\dot{m}_0 = \dot{m}_3 = 0{,}45\ \text{kgs}^{-1}$ (die durch den eigenen Kompressor des Turboluftkühlers gelieferte Luftmenge).

Auf Grund der Meßergebnisse kann festgestellt werden:

1. Der gemessene Wert des Druckverlustfaktors des Turboluftkühler-Rückkühlers betrug $\sigma_{23} = 0{,}975$. Unter Berücksichtigung, daß bei dem realisierten System der Rückkühler ⑥ im Grunde genommen über einen Druckverlustfaktor gleicher Größe wie der Rückkühler ② verfügt, so übersteigt der gemessene Gesamt-Verlustfaktor den in der Berechnung angenommenen Wert von $\sigma = 0{,}93$ nicht.

2. Der isentropische Wirkungsgrad des Kompressors ergibt sich zu $\eta_{\text{isk}} = 0{,}72$. Dieser Wert liegt um 4% niedriger als der in den Berechnungen angenommene.

3. Der Turbinenwirkungsgrad ergab sich zu $\eta_{\text{ist}} = 0{,}74$, dieser Wert liegt ebenfalls um 4% niedriger als der geplante. Nach unseren Untersuchungen wurde weder der Kompressor noch die Turbine in dem optimalen Betriebszustand betrieben (Charaktersitikenproblem). Mit einer optimalen Betriebszustandseinstellung können diese Wirkungsgrade in die Nähe der geplanten gebracht werden.

4. Die vor der Turbine, bzw. nach dem Injektor berechneten und gemessenen Drücke und Temperaturen stimmen innerhalb ihren Fehlergrenzen überein, weshalb das in diesem Beitrag gezeigte Berechnungsverfahren für solche Injektoren anwendbar ist.

5. Die Kühlleistung des Grubenturboluftkühlers beträgt unter Beachtung des gesamten Temperaturunterschiedes $(T_1 - T_4)$ den Wert von

$$\dot{Q} = 23{,}31\ \text{kW}\,.$$

6. Der effektive Leistungsbedarf des die Netzdruckluft erzeugenden Kompressors (unter Annahme eines Kompressorwirkungsgrades von $\eta_{\text{eff}} = 0{,}7$) beträgt $P_{\text{eff}} = 76{,}2$ kW. Die effektive spezifische Kühlleistung des Grubenturboluftkühlers ergibt sich somit zu

$$\varepsilon_{\text{wirk}} = \frac{\dot{Q}}{P_{\text{eff}}} = 0{,}306\,.$$

7. Der berechnete Wert der effektiven spezifischen Kühlleistung ($\varepsilon_{\text{wirk}}$) (Abb. 8) lag in einem Bereich zwischen $0{,}35 \div 0{,}42$. In der Wirklichkeit ergaben sich die Wirkungsgrade der einzelnen Maschineneinheiten zu meßbär kleinere Werten als die angenommenen. Dieser Tatsache ist der realisierte niedrige Wert von $\varepsilon_{\text{wirk}}$ zuzu-

sprechen. Mit einer günstigen Einstellung der Kompressor- und Turbinenarbeitszustände (mit Steigerung ihrer Wirkungsgrade) kann die berechnete spezifische Kühlleistung relativ einfach erreicht werden.

5.2. Die Meßergebnisse des injektorlosen Turboluftkühlers mit geteiltem Schneckengehäuse

Die reale Ausführung des injektorlosen Grubenturboluftkühlers mit geteiltem Schneckengehäuse war mit der in Abb. 6 gezeigten identisch. Deshalb werden die Meßergebnisse mit Hilfe der in Abb. 6 verwendeten Bezeichnungen wiedergegeben. Die Versuchsmessungen wurden im Laboratorium der Thermo- und Strömungstechnischen Forschungsabteilung der Fabrik Ganz-Mávag durchgeführt. Wir erhielten die folgenden Meßdaten: $p_0 = p_1 = p_4 = 0{,}1$ MPa; $T_0 = T_1 = 297{,}5$ K; $p_2 = 0{,}168$ MPa; $T_2 = 364$ K; $p_3 = 0{,}166$ MPa; $T_3 = 294$ K; $p_3^{*\prime} = 0{,}6$ MPa; $T_3^{*\prime} = 296{,}8$ K; $p_0^* = 0{,}37$ MPa; $T_3^* = T_3^{*\prime} = 296{,}8$ K; $\dot{m}_3^{*\prime} = 0{,}27\ \mathrm{kgs}^{-1}$; $\dot{m}_0 = \dot{m}_3 = 0{,}2925\ \mathrm{kgs}^{-1}$; $T_4 = 263$ K. Der Verlustfaktor der Rückkühlers ② war praktisch kaum meßbar ($\sigma = 0{,}99$). Der Kompressorwirkungsgrad hatte den Wert von 0,715. Dieser lag niedriger als der bei unseren Berechnungen angenommene.

In der Turbine erfolgt die voneinander in bedeutendem Maße unabhängige Expansion zweier Medien. Jedoch ist die Expansion dieser Medien deshalb voneinander nicht vollständig unabhängig, da ihre Vermischung in bestimmtem Maße (max. 10%) schon während ihrer Expansion im Laufrad erfolgt.

Die Bestimmung der Expansionswirkungsgrade kann in Kenntnis der realen Expansionsendtemperaturen erfolgen. Mit Hilfe von Messungen kann nur die Temperatur T_4 des Gemisches ermittelt werden.

Um die unbekannten Temperaturen (die Endtemperaturen T_{4h} der Expansion bei hohem Druck, bzw. T_{4n} bei niedrigem Druck) bestimmen zu können, werden zwei, voneinander scheinbar unabhängige Gleichungen aufgestellt.

Die Energiegleichgewichtsgleichung des die Turbine verlassenden Gemisches lautet:

$$\dot{m}_3 T_{4n} + \dot{m}_3^* T_{4h} = (\dot{m}_3 + \dot{m}_3^*) T_4 \,. \tag{15}$$

Für die Energiegleichgewichtsgleichung des Kompressors und der Turbine kann geschrieben werden:

$$\dot{m}_3 (T_2 - T_0) = \dot{m}_3 (T_3 - T_{4n}) + \dot{m}_3^* (T_3^* - T_{4n}) \,. \tag{16}$$

Die Lösung der Gleichungen führt auf eine Identität, da ihr Informationsgehalt das gleiche ist. Da weitere Gleichungen nicht zur Verfügung stehen, können die Wirkungsgrade der beiden Expansionen *getrennt nicht berechnet werden.*

Der mittlere isentropische Wirkungsgrad der Turbine kann auf Grund folgender Formel ermittelt werden:

$$\eta_{ist} = \frac{\overline{\Delta T_{ist}}}{\bar{T}_3 - T_4}, \tag{17}$$

wobei $\overline{\Delta T_{ist}}$ den den Förderströmen entsprechenden mittleren isentropischen Temperaturabfall in der Turbine gemäß der Gleichung

$$\overline{\Delta T_{ist}} = \frac{\dot{m}_3 T_3 \left[1 - \left(\frac{p_4}{p_3}\right)^{\frac{\varkappa-1}{\varkappa}}\right] + \dot{m}_3^* T_3^* \left[1 - \left(\frac{p_4}{p_3^*}\right)^{\frac{\varkappa-1}{\varkappa}}\right]}{\dot{m}_3 + \dot{m}_3^*} \tag{18}$$

bedeutet. In Gl.17 bezeichnet $\bar{T}_3$ die mittlere, den Förderströmen entsprechende Anfangstemperatur der Expansion.

Der Turbinenwirkungsgrad ergibt sich somit zu $\bar{\eta}_{ist} = 0{,}479$. In diesem äußerst niedrigen Wirkungsgradwert spielen die in Abb. 9 gezeigten Stoßverluste eine wichtige Rolle, die infolge der Expansion unterschiedlicher Intensität zweier Luftströme entstehen. Diese Verluste rufen leider in der Wirklichkeit eine größere Wirkungsgradabnahme hervor, als in Abb. 10 gezeigt wurde. Da der schlechte Turbinenwirkungsgrad und die Drosselung der Netzdruckluft Drosselverluste verursachen, ergibt sich für die reale spezifische Kühlleistung ε_{wirk} des injektorlosen Grubenturboluftkühlers kein besserer Wert als der mit Injektor ausgerüsteten. Für die Kühlleistung erhält man laut der Definition von

$$\dot{Q} = (\dot{m}_3 + \dot{m}_3^*) c_p (T_0 - T_4)$$

einen Wert von $\dot{Q} = 19{,}4$ kW. Die effektive Leistungsaufnahme des netzseitigen Kompressors ergibt sich bei einem Druck von $p_3^{*\prime} = 0{,}6$ MPa zu $P_{eff} = 76{,}8$ kW. Der Wert $\varepsilon_{wirk} = 0{,}2526$ der realen spezifischen Kühlleistung liegt niedriger als der entsprechende Wert des mit Injektor ausgerüsteten.

Hätte die Netzdruckluft einen Druck von $p_3^{*\prime} = 0{,}37$ MPa, wodurch die Drosselverluste entfielen, $(p_3^* = p_3^{*\prime})$, so könnte der Wert von ε_{wirk} infolge der abnehmenden Leistungsaufnahme des netzseitigen Kompressors zunehmen. In diesem Fall erhält man die Werte von $P_{eff} = 52{,}1$ kW und $\varepsilon_{wirk} = 0{,}372$. Der wegen der Bedingung $p_3^* > p_3$ bestehende, und in der Turbine auftretende Stoß verursacht das Entstehen der Zusatzverluste, jedoch entfallen die Drosselverluste.

Die Kurve ⑧ der Abb. 8 zeigt diesen Fall. Die dort bestimmten höheren Werte von ε_{wirk} sind die Folgen des günstigeren Wirkungsgrades der Expansionsturbine.

Auf Grund eines Vergleiches der theoretischen und experimentellen Ergebnisse kann festgestellt werden, daß die Druckverluste und das Wärmeaustauschmaß (Temperaturstufe) die in unseren Berechnungen angenommenen Werte erreichen, bzw. diese überschreiten, jedoch bleiben die Kompressor- und Turbinenwirkungsgrade in sämtlichen Fällen unter demjenigen Wert, der zum Erreichen einer relativ günstigen effektiven (realen) spezifischen Kühlleistung benötigt wird.

Nach unseren theoretischen Untersuchungen [1]; [2]; [3]; [11] hängt die spezifische Kühlleistung der Turboluftkühler in entscheidendem Maße von den

Kompressions- und Expansionswirkungsgraden ab, da die Differenz der voneinander nicht bedeutend abweichenden Kompressor- und Turbinenarbeit $(W_k - W_t)$ durch die Wirkungsgrade, in speziellem Fall nahezu größenordnungsmäßig beeinflußt werden kann.

Für den optimalen Wert der spezifischen Kühlleistung der in diesem Beitrag analysierten Turboluftkühler mit dem untersuchten Kreisprozeß erhält man $\varepsilon_{wirk} = 0{,}4 \div 0{,}5$. Ein günstigerer Wert kann bei einem Druckluftnetz unter einem Druck von $0{,}5 \div 0{,}6$ MPa wegen den im Injektor (Abb. 7) bzw. in der zweiflutigen Turbine (Abb. 9) auftretenden Verlusten grundsätzlich nicht erreicht werden.

Bei gleichem Druckwert der Netzdruckluft und der durch eigenen Kompressor erzeugten Druckluft entfallen die Zusatzverluste, und der optimale (maximale) Wert der effektiven spezifischen Kühlleistung beträgt $\varepsilon_{wirk} \approx 0{,}75 \div 0{,}85$. Bei einem solchen Kreisprozeß kann ein günstiger Wert von ε_{wirk} beim heutigen Entwicklungsniveau der Strömungsmaschinen nicht erreicht werden

Zusammenfassung

Der Beitrag gibt die zusammenfassende Theorie der Turboluftkühler (Kältemaschinen mit Luftzyklus) an, und behandelt die theoretischen und praktischen Probleme der mit Netzdruckluft betriebenen Grubenturboluftkühler. Es wird die Möglichkeit untersucht, inwieweit die Turboauflader von Verbrennungsmotoren zu der praktischen Ausführung von Turboluftkühlern herangezogen werden kann. Der Beitrag begrenzt die Ausbildungsmöglichkeiten der mit Netzdruckluft großen Druckes betriebenen Grubenturboluftkühler, und gibt die mit ihnen erreichbaren optimalen Werte der spezifischen Kühlleistung an. Die mit zwei ausgeführten Grubenturboluftkühlern unterschiedlichen Kreisprozesses erreichten praktischen Ergebnisse werden analysiert, und es erfolgt ihr Vergleich mit den theoretisch berechneten Werten.

Schrifttum

1. Pásztor E.: Turbóléghűtők (Turboluftkühler). BME Tudományos Évkönyv (Wissenschaftliches Jahrbuch der Budapester Technischen Universität). 1960.
2. Пастор, Э.: Кондиционирование автобусов турбовозгушным охладителем *Periodica Polytechnica, Transportation Engineering.* (1976), **4,** No. 2
3. Pásztor, E.: Analyse des Arbeitsprozesses von Kältemaschinen mit Luftzyklus, und ihre Anwendungsmöglichkeiten. *Acta TechnHung.* **84** (1977), 221—239
4. Прохоров, В. И.: О применении воздушных холодилных машин в системах кондиционирования воздуха. *Холодильная техника* (1969), No 1
5. Coad, W. J.: Terminal Effectiveness of a Vapor Compression Cycle-Heating. *Piping, Air Conditioning* (1976), **48,** 34
6. Edwards, T. S., McDonald, A. T.: Rotor coder a new rotary vane open reversed Brayton cycle air conditioning and refrigeration system. *The 13th refrigeration congress.* Washington USA, 1972
7. Дубинский, М. Г.: Анализ реалных циклов воздушных холодильных машин для кондиционирования воздуха. *Холодильная техника* (1975), No 12
8. Прохоров, В. И. гр.: К определению энергетически целесообразных режимов работы систем кондиционирования воздуха с воздушными холодильными машинами. *Холодильная техника.* (1979), No 9
9. Hilbert, G. S.: Zur Praxis der kältetechnischen Ausrüstung von Klimaanlagen. *Gesund. Ing.* (1962), 83, No 12
10. Митрохин, В. Т.: Выбор параметров и расчет центростремительной турбины. Машиностроение 1966
11. Пастор, Э.: Анализ рабочего процесса воздушных турбохолодильных установок (ВТХУ) и их применение для наземного кондиционирования боздуха на самолетах. *Periodica Polytechnica. Transportation Engineering,* **9.** (1981), No 1

Acta Technica Academiae Scientiarum Hungaricae, 93 (3—4), pp. 237—259 (1981)

MESSVERFAHREN ZUR ERMITTLUNG DER ERDSCHLUSSKENNGRÖSSEN AUCH BEI NETZBETRIEBSFÜHRUNG

GY. DANYEK*

(Eingegangen am 14. Oktober 1980)

Measuring method for evaluating ground fault characteristics being applicable to computer controlled networks, too — The paper presents mathematical equations for a new measuring method based on voltages due to artificial unbalance. It was developed for evaluating residual fault and other characteristical currents in cable networks mainly, fitted with arc suppression coils. The method can also be applied to computer controlling. In the article instructions for choosing impedances making unbalance in practice and possibilities of realizing automatic measuring systems by means of devices available on market are published.

Einleitung

Exakte Erdschlußkenngrößen in gelöschten Netzen können nur vermittels künstlicher Erdschlüsse bestimmt werden. Es besteht aber in weit ausgedehnten Netzen beim Auftreten derartiger Fehler immer die Gefahr des kurzzeitigen Überganges vom Erdschluß zum Doppelschluß, so scheint es zweckmäßig solche Versuche möglichenfalls zu vermeiden.

Die Netzbetriebsführung mit Prozeßrechnern verbreitet sich schnell, wobei sich der Anspruch im fortgeschrittenen Stadium der Automatisierung immer öfter erhebt, damit die jeweiligen Erdschlußparameter auf Wunsch in Meldungsprotokollen erscheinen sollen. Die unterliegende Arbeit bezieht sich auf die Gleichungen eines Meßverfahrens, welches in dieser Form als neu genannt werden kann. Die mathematischen Zusammenhänge mit Verwendung entsprechender elektronischer Geräte sind geeignet die obigen Ansprüche auch in Netzbetriebsführung zu erfüllen.

1. Allgemeines

Der Erdschlußstromkreis ist ein Nullschwingungskreis, dessen Kenngrößen erst dann bestimmt werden können, wenn ein Nullstrom die in Serien oder parallel geschalteten Stromkreiselementen (L, R, C) durchfließt. So im ganz symmetrischen Zustand der Netze können die Erdschlußkenngrößen meßtechnisch nicht bestimmt werden. Kommt aber eine, den Normalbetrieb wesentlich nicht störende Unsymmetrie mit wohlbekannten Parametern zustande, so kann man, abhängig von der Auswertbarkeit der Spannungen und anderen praktischen Bedingungen zu einer relativ gut

* Dipl. Ing. Gy. Danyek, Forschunginstitut für Elektrische Energie, VEIKI. Budapest, Ungarn 1022, Bp. Törökvész u. 16/c. II. 1.

behandelbaren Methode gelangen. Eine bekannte Unsymmetrie kann auf zwei verschiedener Weise entstehen:

— mit Hilfe einer äußeren Energiequelle im Sternpunkt, bzw.
— vermittels einer bekannten Impedanz zwischen Leiter und Erde.

Es gibt nicht nur praktische, sondern auch prinzipielle Schwierigkeiten, wenn man eine äußere Stromquelle in den Sternpunkt eines Netzes mit in verschiedenen Abzweigen eingebauten mehreren Löschspulen einschaltet. So ist es zu empfehlen, auf diese Möglichkeit im weiteren zu verzichten.

Im Normalbetrieb — insbesondere mit größerem, nicht verdrilltem Freileitungsanteil — kann man immer mit einer Verlagerungsspannung zwischen Sternpunkt und Erde rechnen. Dies stammt einerseits aus den unsymmetrischen Leiter-Erde Impedanzen des Energieübertragungssystems (Kapazitäte und Ableitwiderstände), andererseits aus der unsymmetrischen Strombelastung der als symmetrisch angesehenen Drehstromquelle. Diese Verlagerungsspannung bei Rezonanzreglern für Löschspulen [1] kann als nützliche Information betrachtet werden, aber bei Methoden mit künstlicher Unsymmetrie meldet sie sich als ein Störsignal.

Dies gilt insbesondere dann, wenn ein bestimmter Kompensationsgrad zu erreichen ist, oder bei Meßverfahren, die die künstliche Unsymmetrie zur qualitativen Ermittlung der Netzkenngrößen benötigen. Die beim isolierten Sternpunkt auftretende sogenannte natürliche Unsymmetriespannung verändert sich mit der Zeit, ihre Größe beträgt 0,5 bis 1 Prozent der Betriebsspannung, so infolge dieser praktischen und meßtechnischen Schwierigkeiten ist es besser, die Meßmethoden auf eine „feste", wohlbekannte, unveränderliche Unsymmetrie zu bauen.

Die Gleichungen sind auf eine allgemeine Impedanz bzw. Admittanz bezogen, und enthalten auch die aus der natürlichen Unsymmetrie stammenden Strom- und Spannungskomponenten. Die Kenntnis der Komponenten ist beim Reststrom wichtig, da die Größe des Grundschwingungsreststromes wegen der obigen Unsymmetrie von dem fehlerbehafteten Leiter abhängt. Es werden zwei Varianten, die sogenannte Kreis- und die Matrixlösung diskutiert. Die allgemeinen mathematischen Zusammenhänge und ihre Herkünfte werden im Anhang vorgeführt.

Da in den Gleichungen viele Formelzeichen gebraucht werden, ist es zweckmäßig eine Erklärung zu geben.

2. Erläuterungen der Bezeichnungen

In der Arbeit für $\bar{Y}'$ und $\bar{Z}'$ wird der Oberbegriff Immittanz allgemeingültig gebraucht, abgesehen von Fällen, wo die Begriffe Impedanz, Reaktanz, Widerstand und Admittanz speziell genannt werden müssen.

Beziehen sich die Gleichungen auf Vektoren, so werden die gegebenen Formelzeichen durch einen Überstrich gekennzeichnet. Handelt es sich nur um die Größe eines Vektors, so wird der Strich weggelassen.

Hiermit sollte es bemerkt werden, daß die Gleichungen am meisten in mit kleinen Buchstaben bezeichneten relativen Größen ausgedrückt sind.

Die Bezugsgrößen sind wie folgt:

$\bar{U}_t$ — Leiter-Sternpunkt-Spannung (kurz genannt als Betreiberspannung) in der Bezugsphase des Drehstromnetzes, die sich in dieser Arbeit immer auf den durch die Immittanz $\bar{Y}'$ berührten Leiter bezieht.

$\bar{I} = \bar{Y}' \cdot \bar{U}_t$ — Strom, der die Immitanz $\bar{Y}'$ bei Spannung $\bar{U}_t$ durchfließt.

Die Anwendung der relativen Größen wird damit begründet, daß die Betreiberspannung $\bar{U}_t$ während der in verschiedenen Löschspulenstellungen durchgeführten Messungen sich verändert und dadurch die Meßgrössen bei der Auswertung nur in dieser Form ausgelegt werden können. Wo es aber möglich ist, dort werden die Originalgrößen verwendet.

Ströme (siehe Anhang)

$\bar{I}_r, \bar{I}_b, \bar{I}_w$ — Grundschwingungreststrom und dessen *B*lind- bzw. *W*irkkomponente
$\bar{I}_L, \bar{I}_{L0}$ — Löschspulenstrom bei Spannung $\bar{U}_r$, bzw. bei $\bar{U}_0$
$\bar{I}_c$ — kapazitiver Erdschlußstrom beim isolierten Sternpunkt
$\bar{I}_Y$ — der durch die Immittanz $\bar{Y}'$ fließende Strom

Spannungen (siehe Bild 10)

$\bar{U}_0$ — Spannung zwischen dem Sternpunkt und der Erde, kurz genannt als Sternpunkt- oder Nullspannung
$\bar{U}_Y$ — Spannung an der Immittanz Y'
$\bar{U}_{am}$ — Durchmesserzeiger des Kreises ③ für Spannung U_a die infolge der natürlichen Unsymmetrie auftritt
$\bar{U}'_Y$ — $\bar{U}_Y$, wenn $U_{am}=0$
$\bar{U}'_{am}$ — $\bar{U}_{am}$, wenn die Immittanz $\bar{Y}'$ eingeschaltet ist
$\bar{U}_m$ — Durchmesserzeiger des resultierenden Nullspannungskreises ①
$\bar{U}'_m$ — Durchmesserzeiger des Nullspannungskreises ② wenn $U_{am}=0$.

Indizes

R, S, T — Indizes für die Phasengrößen des Drehstromsystems
N, H — Indizes für den Kompensationsgrad (*N*iedrigere, *H*öhere)
l — Index für die Größen, die mit Faktor $l(u)$ verknüpft sind
s — Index für die symmetrischen Größen
a — Index für die unsymmetrischen Größen
x, y bzw. w, b — Indizes für die Real- und die Imaginärkomponenten
i — Index für die aktuale Löschspule, falls mehrere Spulen eingebaut sind

Bezeichnungen, die hier nicht aufgezählt sind, können nach Text und Bild erklärt werden.

3. Lineare Löschspulen im Netz mit geringer Unsymmetrie

Moderne Mittelspannungsnetze in Gebieten mit großer Energiedichte sind entscheidend mit Kabeln ausgerüstet. Da diese Kabel mit Nennspannung größer als 6 kV abgeschirmte Adern haben (H-Kabel), kann die geringe Unsymmetrie

vernachlässigt werden, und so werden die im Anhang abgeleiteten Gleichungen erhelblich vereinfacht. Diese Vereinfachung läßt sich in erster Linie bei der Kreislösung vorzeigen.

Ausgehend von Gl. A. 15 und angenommen, daß $\psi = \delta$ ist, d. h. es gibt praktisch keine Unsymmetrie ($\bar{U}_m = \bar{U}'_m$), ist nur $u'_m(U'_m)$ zu bestimmen, da δ schon bekannt ist, und ϑ nicht ausgelegt werden soll. Damit vereinfachen sich die Formel wie folgt:

$$i_{bs} = -\left[\frac{\tan(\alpha-\psi)}{u'_m} + \sin\psi\right] = i_b$$

$$i_{ws} = \frac{1}{u'_m} - \cos\psi = i_w \tag{1}$$

$$i_{ba} = i_{wa} = 0$$

Nach Bild 1 gilt

$$U'_m = \frac{U_0}{\cos(\alpha-\psi)}, \qquad \text{bzw.} \qquad u'_m = \frac{u_0}{\cos(\alpha-\psi)}, \tag{2}$$

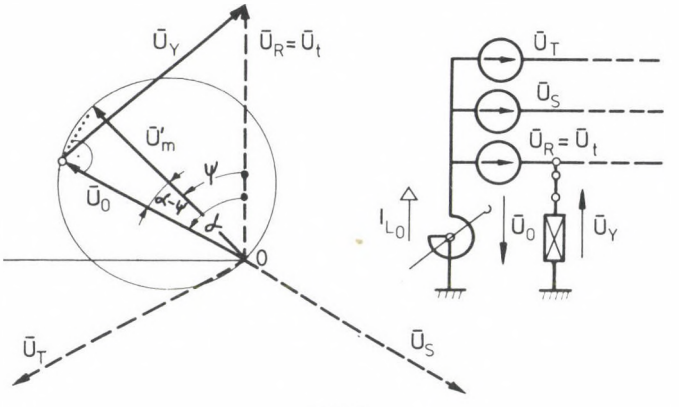

Bild 1

wodurch die Gl. 1 — mit Originalgrößen — umgeformt werden können.

$$I_b = I_{bs} = I \cdot i_{bs} = -U_t \cdot Y'\left[\frac{\sin(\alpha-\psi)}{u_0} + \sin\psi\right],$$

$$I_w = I_{ws} = I \cdot i_{ws} = U_t \cdot Y'\left[\frac{\cos(\alpha-\psi)}{u_0} - \cos\psi\right]. \tag{3}$$

Die Gleichung für den resultierenden Grundschwingungsreststrom — unter Verwendung auch des Cosinus-Satzes — vereinfacht sich zu (Siehe noch Bild 1)

$$I_r = I_{rs} = I \cdot \sqrt{i_{bs}^2 + i_{ws}^2} = U_t \cdot Y' \frac{U_Y}{U_0}. \tag{4}$$

Also, aufgrund von Gl. (4) *in einem Netz mit linearen Löschspulen und vernachlässigbarer Unsymmetrie ergibt sich der resultierende Grundschwingungsreststrom durch den Quotienten von zwei Spannungen.* Die Betreiberspannung U_t und die Immittanz Y' sind bekannt. In Kenntnis des Löschspulenstromes I_{L0} bei U_0 läßt sich der kapazitive Strom des Netzes wie folgt ausrechnen.

$$I_c = \frac{U_t}{U_0} \left\{ I_{L0} - I \left[\sin(\alpha - \psi) + \frac{U_0}{U_t} \sin \psi \right] \right\}. \tag{5}$$

α kann auf zwei verschiedener Weise bestimmt werden: — mit direkter Winkelmessung vom Zeiger $\bar{U}_t$, und — mit der Messung der Seiten des Zeigerdreiecks $\bar{U}_t - \bar{U}_0 - \bar{U}_Y$ (dies kann viel genauer gemacht werden, als die Winkelmessung), und danach mit Anwendung des Cosinus-Satzes

$$\alpha = \arccos \quad \frac{1}{2} \left[\frac{U_0}{U_t} + \frac{U_t}{U_0} - \frac{U_Y^2}{U_0 \cdot U_t} \right] \tag{6}$$

In der Praxis braucht man also *nur*

$$U_0;\ U_Y;\ U_t \quad \text{und} \quad I_{L0}$$

zu messen, aber erst dann, wenn alle Erdschlußkenngrößen zu ermitteln sind.

Es ist bekannt, daß in unterirdischen Netzen die Vermeidung der Doppelerdschlüßen von besonders hoher Bedeutung ist. Diese Lösungsvariante läßt sich deshalb in erster Linie in Bergbaunetzen ihre Vorteile hervorragen, da der resultierende Reststrom mit Gl. (4) sehr rasch und ohne Gefahr von Überströmen und Überspannungen bestimmt werden kann, wenn als Immittanz ein dem Netz gut angepaßte Widerstand benützt wird.

4. Nichtlineare Löschspulen im Netz mit geringer Unsymmetrie

Die mit Resonanzreglern einstellbaren modernen Tauchkernspulen haben am meisten lineare Spannung-Strom Kennlinien. In Netzen mit größerer Ausdehnung kann es wirtschaftlicher sein, Anzapflöschspulen mit weniger linearen $U-I$ Kurven außer der Speisestation eingebaut werden zu lassen. Aus Bild 2 ist ersichtlich, daß, wenn ein Arbeitspunkt bei 50- bis 60-prozentiger Spannung mit einer Gerade durch

Origo (gestrichelte Linie) auf die Nennspannung der Löschspule projiziert wird, ergeben sich zu jedem Arbeitspunkt (N, H) je zwei Stromwerte, I_L und I_{Ll}. Dies beweist, daß bei nichtlinearen Löschspulen die genauen Berechnungen genaue Kennlinien, bzw. Korrektionskurven $l(u_0)$ benötigen. Die vorgeschlagenen Korrektionskurven $l(u_0)$ können entsprechend der linken Seite von Bild 2 in Betracht gezogen werden. Der Faktor $l(u_0)$ knüpft eine Verbindung zwischen der induktiven Reaktanz X_{Ll} im von der jeweiligen Spulenspannung abhängigen Arbeitspunkt und der zur Nennspannung (U_n) gehörenden Reaktanz X_L an:

$$l(u_0) = \frac{X_L}{X_{Ll}} = \frac{\dfrac{U_n}{I_L}}{\dfrac{U_n}{I_{Ll}}} = \frac{I_{Ll}}{I_L}. \tag{7}$$

In Kenntnis von Faktor $l(u_0)$ können, unter Beachtung der auf den linearen symmetrischen Zustand bezogenen Gl. 3, die endgültigen Formel der gesuchten Kenngrößen beschrieben werden (siehe Bild 2).

$$\begin{aligned} I_c &= \sum^{i} [I_{L_i} \cdot l_i(u_0)] + I_{bs} \\ I_b &= I_c - \sum^{i} I_{L_i} \\ I_w &= I_{wl} \\ I_r &= \sqrt{I_b^2 + I_w^2} \end{aligned} \tag{8}$$

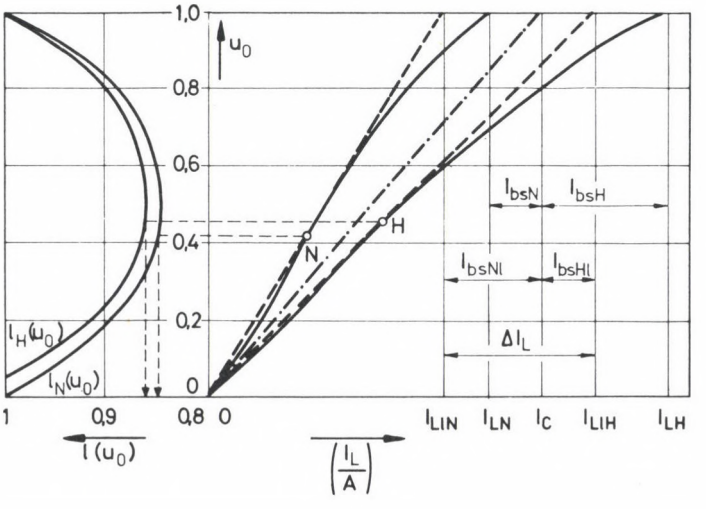

Bild 2

Hierbei sind

I_{L_i} — *im linearen Stromkreis* — induktiver Strom, gerechnet aus dem bei U_0 gemessenen Spulenstrom I_{L0} in einer Position der Löschspule: $I_L = I_{L0} \cdot U_t/U_0$

— *im nichtlinearen Stromkreis* — induktiver Strom, genommen aus der bekannten $U-I$ Kennlinien in einer Position der Löschspule

$l_i(u_0)$ — *im linearen Stromkreis:* 1

— *im nichtlinearen Stromkreis* — Korrektionsfaktor aus einer für Löschspule mit Index (*i*) maßgebenden Kurvengruppe in Abhängigkeit von der Spannung $u_0 = U_0/U_t$.

Mangels der nichtlinearen Löschspulenkennlinien oder der Korrektionskurven und in Kenntnis der induktiven Nennströme, empfehlt es sich die Messungen beim isolierten Sternpunkt durchzuführen. Gl. (3), Gl. (4) und sinngemäß auch Gl. (8) können, unter Beachtung der Tatsache, daß es sich hier um den Grenzfall der Erdschlußlöschung handelt, ohne weiteres angewendet werden. Da ist es aber zu beachten, daß die Impedanz, möglichenfalls der Widerstand relativ kleinohmig sein und ans Netz gut angepaßt werden muß.

5. Erdschlußkenngrößen in Netzen mit Unsymmetrie und nichtlinearen Löschspulen

Die Umsymmetrie kann den 50 Hz-Reststromwert beträchtlich beeinflussen. Dies läßt sich besonders dann vorzeigen, wenn die 50 Hz-Restströme in verschiedenen Phasen miteinander vergleicht werden. Abhängig von der tatsächlichen Größe der Unsymmetrie erhält man verschiedene Blind- und Wirkreststromkomponente — auch bei denselben örtlichen Messungen. Der Unterschied zwischen den Phasen erklärt sich dadurch, daß solange der Unsymmetriereststrom in einem Zeitintervall konstant ist, die Phasenlage der symmetrischen Reststromkomponenten dagegen von der Betreiberspannung $\bar{U}_t$ abhängt. Die Stromzeiger in Abhängigkeit von der Betreiberspannung sind im Bild 3 gezeigt. Üblicherweise liegt der Spannungszeiger $\bar{U}_t$ in der Realachse. Daher, abhängig von der jeweiligen Phasenspannung sollte eine Transformation mit einem Winkel von $\xi = 0; \pm 120°$ durchgeführt werden. Dies bedeutet aber praktisch, daß statt Transformation des Koordinatensystems der Unsymmetriereststromzeiger $\bar{I}_a$ mit dem obigen Winkel ξ, aber mit umgekehrtem Vorzeichen gedreht werden soll. Die Varianten sind dem Bild 3 zu entnehmen. Es zeigt sich, daß die beliebige Unsymmetriespannung auch negativen Wirkreststrom zustande bringen kann (siehe Bild 3c).

Wie es von obigen und aus Gl. (A.5)—(A.7) folgt, benötigt man in dem Abschnittstitel entsprechenden Falle wenigstens zwei (*N*iedrigere und *H*öhere) Löschspulenpositionen, um die vier Reststromkomponenten vermittels vier unabhängiger Beziehungen ermitteln zu können.

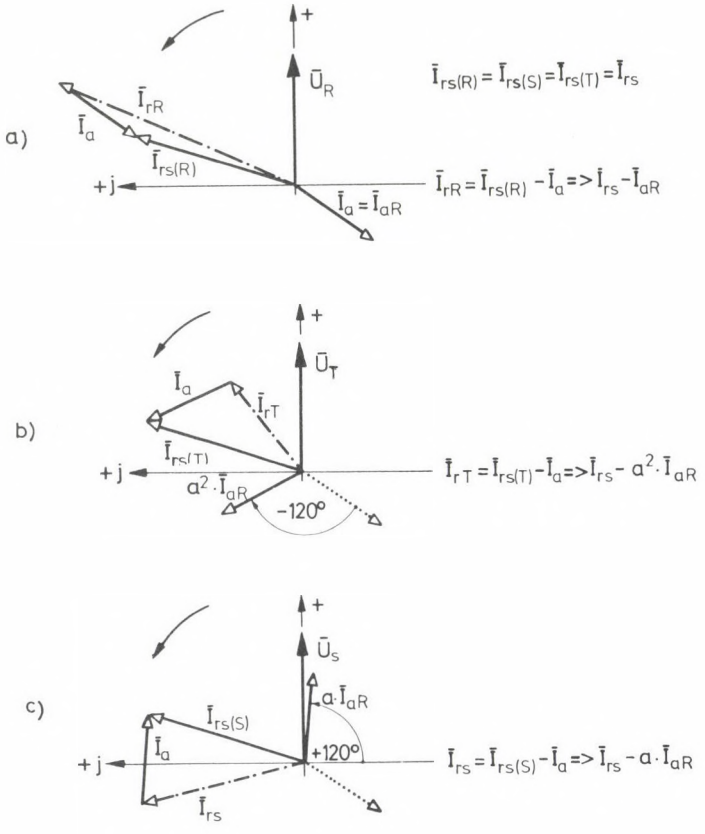

Bild 3

Diese sind in Gl. (A.14) zusammengefaßt, wo es aber zweckmäßiger scheint, sie in Matrixform zu benutzen:

$$\begin{bmatrix} 1 & 0 & -u_{xN} & u_{yN} \\ 0 & 1 & -u_{yN} & -u_{xN} \\ 1 & 0 & -u_{xH} & u_{yH} \\ 0 & 1 & -u_{yH} & -u_{xH} \end{bmatrix} \cdot \begin{bmatrix} i_w \\ i_{bN} \\ i_{ws} \\ i_{bsN} \end{bmatrix} =$$

$$= \begin{bmatrix} u_{xN} \cdot \cos\psi - u_{yN} \sin\psi \\ u_{yN} \cdot \cos\psi + u_{xN} \cdot \sin\psi \\ u_{xH} \cdot \cos\psi + u_{yH}(\Delta i_L - \sin\psi) \\ u_{yH} \cdot \cos\psi - u_{xH}(\Delta i_L - \sin\psi) + \Delta i_L \end{bmatrix} \tag{9}$$

Spannungen in relativen Größen rechnen sich wie folgt aus (Bild 4).

$$u_{xN} = \frac{U_{YN}}{U_{tN}} \cos \beta_N , \qquad u_{yN} = \frac{U_{YN}}{U_{tN}} \sin \beta_N ,$$
$$u_{xH} = \frac{U_{YH}}{U_{tH}} \cos \beta_H , \qquad u_{yH} = \frac{U_{YH}}{U_{tH}} \cdot \sin \beta_H . \tag{10}$$

β kann ebenso wie α im Abschnitt *3* bestimmt werden. Es empfehlt sich in der Praxis den Cosinus-Satz zu verwenden.

$$\beta_{N,H} = \arccos \frac{1}{2}\left[\frac{U_{YN,H}}{U_{tN,H}} + \frac{U_{tN,H}}{U_{YN,H}} - \frac{U^2_{0N,H}}{U_{YN,H} \cdot U_{tN,H}}\right] \tag{11}$$

$\Delta i_L = \Delta I_L / I$ kann nach Gl. (A. 13) berechnet werden. Matrixsystem nach Gl. (9) gibt die linearen, mit relativen Größen ausgedrückten Reststromkomponenten in Pos. *N* an. Die gesuchten Werte in Pos. *H* ergeben sich, wenn der symmetrische Blindreststrom i_{bsN} mit Δi_L vorzeichenrichtig erhöht wird, denn die übrigen Komponenten sind unverändert.

In Kenntnis der Kenngrößen in Pos. *N* nach Gl. (9) ÷ Gl. (11) erhält man den Blind- und Wirkreststrom in Originalgrößen — bei linearen Löschspulen — in Abhängigkeit von ξ (Die von ξ abhängigen Werte sind durch hochgestellten Stern gekennzeichnet).

$$I^*_{bN} = I_{bsN} - I^*_{baN} = I\{i_{bsN} - [(i_{bsN} - i_{bN}) \cos \xi + (i_{ws} - i_w) \sin \xi]\} ,$$
$$I^*_{wN} = I_{ws} - I^*_{wa} = I\{i_{ws} - [(i_{ws} - i_w) \cos \xi + (i_{bsN} - i_{bN}) \sin \xi]\} . \tag{12}$$

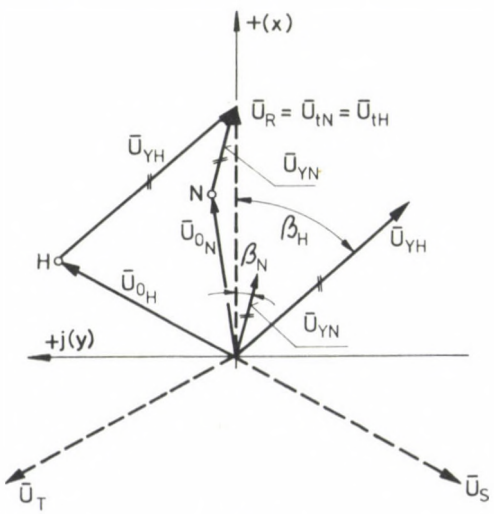

Bild 4

Lineare Werte in Pos. H sind im Sinne der oben gesagten:

$$I^*_{bH} = I^*_{bN} + \Delta i_L \cdot I\,; \qquad I^*_{wH} = I^*_{wN} \tag{13}$$

Da das Endziel die nichtlinearen Erdschlußkenngrößen zu erreichen ist, sollen die linearen Formeln ähnlich der Gl. (8) korrigiert werden. Ist das Netz mit einer Tauchkernspule in der Umspannstation und mit einigen Anzapflöschspulen irgendwo in den Abzweigen ausgerüstet, ergeben sich die endgültigen Formeln wie folgt:

$$\begin{aligned} I_c &= \sum^{i} [I_{LiN} \cdot l_{iN}(u_{0N})] + I_{bsN}\,, \\ I_{bN} &= I_c - \sum^{i} I_{LiN} - I^*_{baN}\,, \\ I_{wN} &= I^*_{wN}\,, \\ I_{bH} &= I_{bN} + \Delta i_L \cdot I\,, \\ I_{wH} &= I_{wN}\,, \end{aligned} \tag{14}$$

wobei I_{LiN} und $l_{iN}(u_{0N})$ können wie die ähnlichen Größen in Abschnitt *4* ausgelegt werden.

Es ist vermutlich auffallend, daß es sich hier um Nichtlinearität handelt und zur Aufgabelösung doch der Überlagerungssatz verwendet wird. Dies rechtfertigt sich damit, daß die Kennlinien der Anzapflöschspulen bis zu etwa 60 Prozent der Betreiberspannung U_t praktisch linear sind und so ist die Zerlegung der symmetrischen und unsymmetrischen Stromanteile in diesem Bereich noch möglich. Der unsymmetrische Stromanteil ist unabhängig von der Löschspule, der symmetrische kann dagegen — wie vorher gezeigt — mit der empirischen Funktion $l(u_0)$ korrigiert werden. Der 60-prozentigen Grenzwert trifft auch deswegen zu, da der Normalbetrieb mit größerer Unsymmetrie sowieso nicht gestört werden darf. Daher, um diese prozentuale Spannung nicht zu überschreiten, soll die Immittanz $\bar{Y}'$ in Netzen mit erheblicher natürlicher Unsymmetrie und nichtlinearen Löschspulen in einem streng gegebenen Bereich gehalten werden.

6. Impedanzen zur Verwirklichung

Da die Impedanzwerte am meisten ziemlich hochohmig sein müssen, können in der Praxis nur

— die kapazitive Impedanz und

— der Widerstand

berücksichtigt werden.

Der Normalbetrieb darf mit größerer Unsymmetrie nicht gestört werden, deshalbs muß der Zusammenhang zwischen der einschaltbaren Immittanz und der Spannung etwas näher untersucht werden.

Kapazitive Impedanzen

Da es sich nicht empfehlt, eine sogenannte „nackte" Kapazität an das Netz zu schalten, sollte man die kapazitive Impedanz aus einem Kondensator und einem damit in Serien geschalteten Widerstand gestalten.

Bringt man die Admittanz $\bar{Y}'$ auf die Form von

$$G' + jB'_c$$

und die natürliche Unsymmetrie kennzeichnende Admittanz auf

$$\bar{A} \sim jA\,,$$

ergibt sich dann näherungsweise der Maximalwert des Sternpunktspannung in relativen Größen ausgedrückt

$$u_m = \frac{\frac{1}{g} \cdot i'_c}{\frac{2}{g} \cdot i'_c \cdot \sqrt{i'_c\left(\frac{I_c}{I_K}\right)} + 4 \cdot i'_c\left(\frac{I_c}{I_K}\right) + 1} \approx \frac{i'_c}{g} \tag{15}$$

wobei $\left(\frac{I_c}{I_K}\right)$ — Quotient des kapazitiven Stromes im Netze und des dreiphasigen Kurzschlußstromes an der Sammelschiene

$g = \mathrm{G} \cdot \frac{U_t}{I_c}$ — Ableitung des Netzes in relativen Größen

$i'_c = \frac{B'_c}{\left(\frac{I_c}{U_t}\right)} \cong \frac{I}{I_c}$ — dem eingeschalteten Kondensator entsprechender Strom (Admittanz) in relativen Größen.

Um den Einschaltverlauf des Stromes durch Kondensator aperiodisch halten zu können, empfehlt es sich auch die Bedingung der Aperiodizität in Kauf zu nehmen:

$$\left(\frac{R'}{\mathrm{ohm}}\right) \geqq 55\left(\frac{U}{\mathrm{kV}}\right)^2 \cdot \sqrt{\frac{1}{\left(\frac{Q'_c}{\mathrm{kVAr}}\right)\left(\frac{S_k}{\mathrm{MVA}}\right)}}\,. \tag{16}$$

Hierbei

U — die Außenleiterspannung,

Q'_c — Blindleistung des eingeschalteten Kondensators mit einer Nennspannung von $1{,}5 \cdot U_t$,

S_k — Kurzschlußleistung der Sammelschiene.

Der Grenzfall der Aperiodizität wurde auch bei der Ableitung von Gl. (15) in Betracht gezogen und so ergab sich diese Näherungsformel.

Die Nennleistung von dem Kondensator auf die Spannung von $U_{nenn} = 1{,}5 \cdot U_t$ zu beziehen sind. Dies erklärt sich dadurch, daß U_Y viel größer als U_t sein kann (Siehe Bild 10), deshalb wird der Einfachheit und Sicherheit halber die genaue komplizierte Funktion von $|\bar{U}_Y|$ mit dem Wert $1{,}5 \cdot U_t$ majoriert. Die Annäherung hier und oben trifft auch deswegen zu, da die Werte g bzw. A insbesondere in einem Netz mit größerem Freileitungsanteil — gar nicht konstant sind, und so sollen die gesuchten Parameter in einem gegebenen Bereich gültig sein.

Auch von dieser Erwägung genügt es manchmal in der Praxis statt Gl. (15) einen Faustregel wie folgt zu verwenden:

$$i'_c \approx 0{,}5 \cdot g\,. \tag{17}$$

Rechnet man mit einem Ableitungswert nicht größer als 3%, wird die schon früher erwähnte 60-prozentige Sternpunktspannung meistens nicht überschritten.

Und noch etwas von der Nennleistung des Widerstandes. Der Strom, der den Widerstand durchfließt, ist durch den Kondensator begrenzt. Somit, unter Verwendung von Gl. (17) ($g = 5\%$) und von einem 2-fachen Sicherheitsfaktor läßt sich die Nennleistung des Widerstandes wie folgt ausrechnen:

$$\left(\frac{P'_R}{\mathrm{kW}}\right) = 1{,}25 \cdot 10^{-6} \left(\frac{I_c}{A}\right)^2 \cdot \left(\frac{R}{\mathrm{ohm}}\right) \tag{18}$$

Widerstände

Von den Transienten und den größten stationären Spannungen her zeigt sich die Verwendung von Widerstände statt Reaktanzen viel günstiger.

Es werden

$$\bar{Y}' = G' \qquad \text{und} \qquad \bar{A} = \pm A$$

gewählt. Die Sternpunktspannung in relativen Größen bildet sich

$$U_m = \frac{i'_R \pm a}{i'_R + g}\,, \tag{19}$$

wobei g und U_m schon bekannt sind, und

$a = A \cdot \dfrac{U_t}{I_c}$ — die natürliche Unsymmetrie kennzeichnende Admittanz in relativen Größen, bzw.

$i'_R = \dfrac{G'}{\left(\dfrac{I_c}{U_t}\right)} = \dfrac{1}{R'} \cdot \dfrac{U_t}{I_c}$ — dem eingeschalteten Widerstand entsprechender Strom (Leitfähigkeit), in relativen Größen.

Die Gl. (19) ist in Bild 5 dargestellt. In Kenntnis des Quotientes von U_t/I_c kann der Widerstandswert mit jener Berücksichtigung ausgewählt werden, daß u_m in einem Bereich von 40 bis 60% gehalten werden soll.

Im Diagramm sind drei, dem Grenzfall der natürlichen Unsymmetrie entsprechende Bereiche zu unterscheiden. Die Grenzkurven der Bereiche ergeben sich mit den

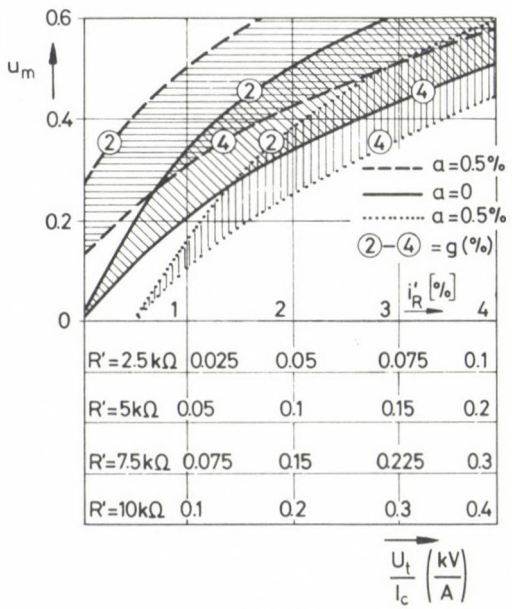

Bild 5

Ableitungswerten (g) von 2 bzw. 4%. Nach der Auswahl des Widerstandswertes ist die Nennleistung wie folgt auszurechnen:

$$\left(\frac{P'_R}{kW}\right) = \frac{\left(\frac{U_t^2}{kV^2}\right)}{\left(\frac{R}{k\,ohm}\right)}. \tag{20}$$

Obwohl die Gleichheit von $U_Y = U_t$ in der Praxis sozusagen nie vorkommt, sicherheitschalber ist die Leistung P'_R auch da majoriert.

Bei der Realisierung der Widerstände empfehlt es sich, sowohl die z. B. in Form von Spiralfedern aus Kanthal- oder CrNi-Draht herstellbaren Widerstandselementen, wie auch den Schalter unter Öl in einen Kessel einzubauen. Der Schalter soll unter günstigen wiederkehrenden Spannungsverhältnissen nur kleine Ströme ausschalten. Als Beweise für die Verwirklichkeit und die Anwendbarkeit der Ölwiderstände kann es

erwähnt werden, daß sie in Ungarn mit derartiger Konstruktion in 10, 20 und 35 kV Netzen, sogar zwecks Lockerung der 120 kV starr geerdeten Sternpunkte seit Jahrzehnten mit guten Erfahrungen im Betrieb sind. Ihr Typenkessel enthält eine Ölmenge, die z. B. bei einer Einschaltdauer von 10 Sekunden, unter einer Leistung von 400 kW, ohne äußere Wärmeabgabe nur mit etwa 7 K erwärmt wird. [2]

Um die eventuellen Überbeanspruchungen zu vermeiden, können die Widerstände mit einem thermischen Schutz ausgerüstet werden, der aber erst im Notfall den befugten Leistungschalter ausschalten wird.

7. Meßverfahren in der Praxis und bei Netzbetriebsführung

Bild 6 zeigt einen universalen elektronischen Kompensationsmesser, der so beim künstlichen Erdschluß, wie auch bei den Unsymmetriemethoden, anhand von einem programmierbaren, mit Magnetkarten ausgerüsteten Kleinrechner eine einmannige, einfache Ermittlungsmöglichkeit für Erdschlußkenngrößen zur Verfügung stellt. [3]

Bild 6

Entsprechend dem möglichen Blockschaltbild nach Bild 7, kann ein automatisches Meßsystem, begründet auf einen im Bezirkschaltdienst off-line betriebenen Kleinrechner, verwirklicht werden. Auf ein manuelles oder prozeßrechnergesteuertes Anlassen könnte sich das folgende automatische Zyklus durchführen lassen.

1. *Messung in Pos. N*
   1.1 Die Einstellung der Löschspule in Pos. N — mit Methode eines Resonanzreglers
   1.2 Einschalten des Schalters *S*
   1.3 Messung und Speicherung von U_0, U_t, U_Y und wenn es nötig ist, auch die der I_{LO}.
   1.4 Ausschalten des Schalters *S*.

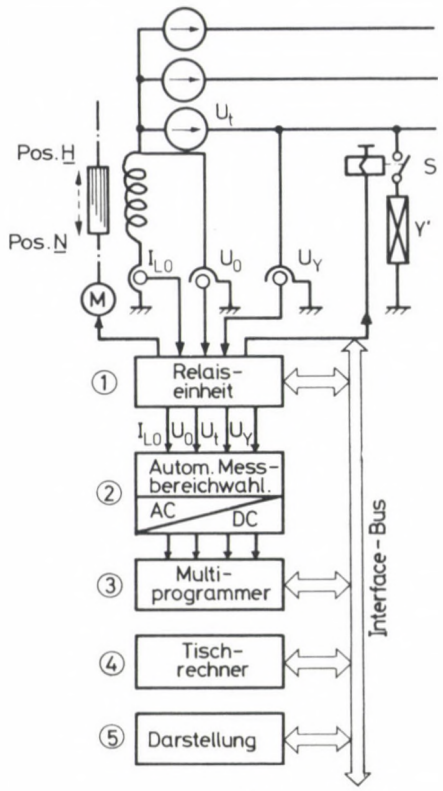

Bild 7

2. *Messung in Pos. H* (nur im Falle mit erheblicher natürlicher Unsymmetrie)
   2.1 Die Einstellung der Löschspule in Pos. H — wie oben
   2.2 Einschalten des Schalters *S*
   2.3 Messung und Speicherung von U_0, U_t, U_Y und wenn es nötig ist, auch die der I_{L0}
   2.4 Ausschalten des Schalters *S*

3. *Auswertung*
   3.1 Berechnung der gesuchten Werte aufgrund der Messungen und wenn es nötig ist, mit Verwendung der Korrektionsfunktionen.
   3.2 Darstellung der Ergebnisse durch Drucker oder Bildschirm.

Die Realisierung des automatischen Systems kann nur dann wirtschaftlich sein, wenn es bei einer tatsächlichen Netzbetriebsführung, z. B. in die Anlage einer Bezirkleitstelle eingebaut wird. Bild 7 zeigt eine mögliche Verwirklichung vermittels eines Interface-bus. Aus den dargestellten Einheiten muß nur die Einheit 2 speziell für diesen Zweck entwickelt werden. Die anderen stehen an der Netzleitstelle zur Verfügung bzw. können nach Katalog von großen Firmen beschaffen werden. [4]

8. Die Genauigkeit des Meßverfahrens

Das Verfahren beruht auf den Verhältnissen von Spannungen, so kann man sie „in sich selbst" für genau halten. Die resultierende Genauigkeit ist aber mit den untenstehenden Tatsachen eng verbunden:

— Wo die Arbeitspunkte in der Löschspulenkennlinie liegen
— Wie genau die Spannung $\bar{U}_0$ an im Netz ausgesetzen Löschspulen bekannt ist
— Wie genau man die $U-I$ Kennlinien oder die Korrektionsfunktionen der Löschspulen kennt
— Wie genau die Änderung des Widerstandswertes eingerechnet werden kann
— Zu welcher Genauigkeitsklasse die Meßwandler gehören
— Wie genau der Spannungsteiler im automatischen Meßbereichwähler realisiert wird. (Einheit 2)

Danksagung

Der Verfasser dankt Herrn Dipl.-Ing. Gy. Kakasi für den Einfall der Matrixlösungsmöglichkeit.

Kurzfassung

Ausgehend von Spannungen bei einer künstlichen Unsymmetrie wurden mathematische Beziehungen für eine neue Meßmethode behandelt, aufgrund deren die Erdschlußkenngrößen, in erster Linie für gelöschten Kabelnetze, auch in prozeßrechnergesteuerter Netzbetriebsführung bestimmt werden können. Dabei werden auch praktische Hinweise für verwendbare Impedanzen, bzw. Vorschläge für die Realisierung der automatischen Steuerung durch hauptsächlich im Handelsverkehr erhältliche Geräte bekannt gegeben.

Schrifttum

1. Rijanto, H.: Resonanzregler zur Einstellung von Petersenspulen im Netzbetrieb Konferenzsammelbuch: Sternpunkterdung in Mittelspannungsnetzen, *Ceske Budějovice* (1976)
2. Danyek, Gy.—György, D.—Valaska, L.: Schutz- und Automatiksystem vermittels Widerstand im Ölkessel Konferenzsammelbuch: Automatisierung und Steuerung, *Ceske Budějovice* (1978)
3. Danyek, Gy.: Universaler Kompensationsmesser Studienarbeit, VEIKI, 1979
4. Electronic Instruments and Systems Hewlett-Packard Katalog, 1980
5. Willheim, R.—Waters, M.: Neutral Grounding in High-Voltage Transmission. Elsevier Publishing Company, 1956
6. Komponenten in Drehstromnetzen DIN 13 321, Entwurf 1978. Aug.

Anhang

I. Grundsätzliches

Bei künstlicher Unsymmetrie mittels einer Immittanz $\bar{Y}'$ werden die folgenden Kenngrößen benötigt:

— Strom durch die Immittanz, $\bar{I}_Y$ und die darauf fallende Spannung, $\bar{U}_Y$
— Sternpunktspannung, $\bar{U}_0$ und
— Grundschwingungsreststrom $\bar{I}_r$, der aus dem Strom $\bar{I}_Y$ bei $\bar{Y}' \to \infty$ folgt.

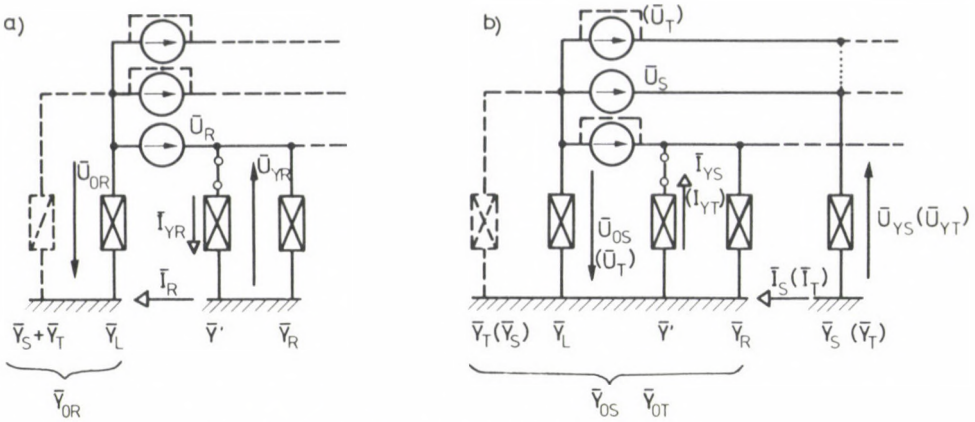

$\bar{I}_Y = \bar{I}_{YR} - \bar{I}_{YS} - \bar{I}_{YT}$ - Strom durch Impedanz $\frac{1}{\bar{Y}'}$

$\bar{U}_Y = \bar{U}_{YR} - \bar{U}_{0S} - \bar{U}_{0T}$ - Spannung auf Impedanz $\frac{1}{\bar{Y}'}$

$\bar{U}_0 = \bar{U}_{0R} - \bar{U}_{0S} - \bar{U}_{0T}$ - Sternpunkt - Erde Spannung

Bild 8

Die Gleichungen werden aufgrund von Bild 8 mit dem Überlagerungssatz aufgestellt. Bild 8. zeigt die Spannungen und Ströme, die durch jene Phasenspannung erzeugt werden, in der Phase die Immittanz eingeschaltet wird. Bild 8b stellt dagegen die Spannungen und Ströme dar, die durch die anderen Phasenspannungen zustande kommen. Abgesehen von den ausführlichen Ableitungen ergeben sich die Beziehungen:

Phase R

$$\bar{U}_{YR} = \bar{U}_t \frac{\bar{Y}_S + \bar{Y}_T + \bar{Y}_L}{\bar{Y} + \bar{Y}'},$$

$$\bar{I}_{YR} = \bar{U}_{YR} \cdot \bar{Y}', \tag{A.1}$$

$$\bar{U}_{0R} = \bar{U}_t \cdot \frac{\bar{Y}_R + \bar{Y}'}{\bar{Y} + \bar{Y}'};$$

Phase S

$$\bar{U}_{YS} = \bar{U}_t \cdot \frac{a^2[(\bar{Y} - \bar{Y}_S) + \bar{Y}']}{\bar{Y} + \bar{Y}'},$$

$$\bar{I}_{YS} = -\bar{U}_{0S} \cdot \bar{Y}', \tag{A.2}$$

$$\bar{U}_{0S} = \bar{U}_t \cdot \frac{a^2 \cdot \bar{Y}_S}{\bar{Y} + \bar{Y}'};$$

Phase T

$$\bar{U}_{YT}=\bar{U}_t\frac{a[(\bar{Y}-\bar{Y}_T)+\bar{Y}']}{\bar{Y}+\bar{Y}'};$$

$$\bar{I}_{YT}=\bar{U}_{0T}\cdot\bar{Y}'; \tag{A.3}$$

$$\bar{U}_{0T}=\bar{U}_t\frac{a\cdot\bar{Y}_T}{\bar{Y}+\bar{Y}'},$$

wobei

$$\bar{Y}=\bar{Y}_R+\bar{Y}_S+\bar{Y}_T+\bar{Y}_L; \qquad a=-0{,}5+j\frac{\sqrt{3}}{2};$$

$$a^2=-0{,}5-j\frac{\sqrt{3}}{2}$$

Unter Beachtung der Gleichungen in Bild 8, erhält man

$$\bar{I}_Y=\bar{U}_t\cdot\frac{\bar{Y}'}{\bar{Y}+\bar{Y}'}\cdot[\bar{Y}-\bar{A}]. \tag{A.4}$$

Die Spannung $\bar{U}_Y$ auf der Impedanz errechnet sich:

$$\bar{U}_Y=\frac{\bar{I}_Y}{\bar{Y}'}=\bar{U}_t\cdot\left[\frac{\bar{Y}}{\bar{Y}+\bar{Y}'}-\frac{\bar{A}}{\bar{Y}+\bar{Y}'}\right]=\bar{U}'_Y-\bar{U}_a \tag{A.5}$$

Hierbei vertritt

$$\bar{Y}=\bar{Y}_R+\bar{Y}_S+\bar{Y}_T+\bar{Y}_L$$

die sogenannte symmetrische, dagegen aber

$$\bar{A}=\bar{Y}_R+a^2\cdot\bar{Y}_S+a\cdot\bar{Y}_T$$

unter der Bedingung $\bar{Y}_R\neq\bar{Y}_S\neq\bar{Y}_T$, den unsymmetrischen Stromanteil. Die Sternpunktspannung ergibt sich aus der Formel

$$\bar{U}_0=\bar{U}_t\left[\frac{\bar{Y}'}{\bar{Y}+\bar{Y}'}+\frac{\bar{A}}{\bar{Y}+\bar{Y}'}\right]=U'_0+\bar{U}_a. \tag{A.6}$$

Die Zeiger nach A.4—A.6 sind in Bild 9 zu sehen. Unter der Bedingung $\bar{Y}'\to\infty$ gelangt man zu dem meistbekannten praktischen Fall der Parallelresonanz

$$\bar{I}_Y\to\bar{I}_r=\bar{U}_t[\bar{Y}-\bar{A}]. \tag{A.7}$$

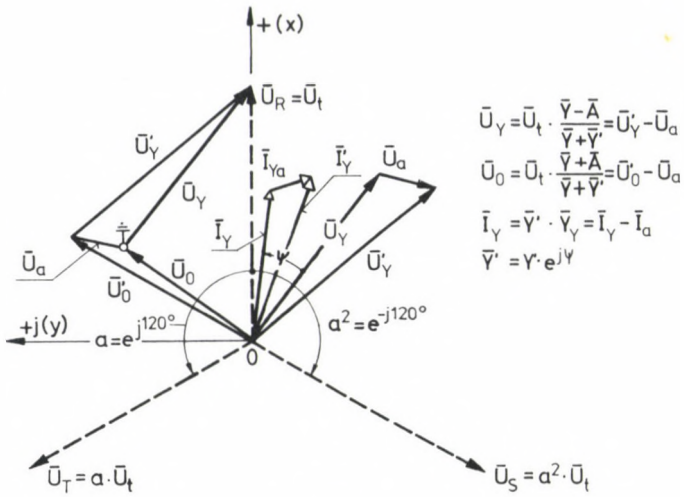

Bild 9

Der Reststromvektor $\bar{I}_r$ setzt sich also aus

— dem symmetrischen Stromvektor $\bar{I}_{rs} = \bar{U}_t \cdot \bar{Y}$, bzw.

— dem unsymmetrischen Stromvektor $\bar{I}_{ra} = \bar{U}_t \cdot \bar{A}$

zusammen.

II. Grundsätzliches für die Matrixlösung

Zu der Matrixlösung bildet man den Quotient der Gl. (A.7) und (A.4), woraus folgt

$$\bar{I}_r = \bar{I}_Y \cdot \frac{\bar{Y} + \bar{Y}'}{\bar{Y}} = \bar{U}_Y \cdot \bar{Y}' \frac{\bar{Y} + \bar{Y}'}{\bar{Y}'} = \bar{U}_Y \cdot (\bar{Y} + \bar{Y}') . \tag{A.8}$$

Werden die einzelnen Vektoren auf Komponenten zerlegt, ergibt sich

$$I_w + jI_b = (U_{Yx} + jU_{Yy})[(G + j\Delta B) + (G' + jB')] , \tag{A.9}$$

wobei

$$G = G_R + G_S + G_T + G_L ,$$

$$\Delta B = B_R + B_S + B_T - B_L ,$$

$$G' = Y' \cdot \cos\psi ,$$

$$B' = Y' \cdot \sin\psi .$$

Unter Verwendung von $I = U_t \cdot Y'$ wird Gl.(A.8) etwas umgeformt, nach Komponenten zerlegt und in relativen Größen ausgedrückt:

$$i_w - u_x \cdot i_{ws} + u_y \cdot i_{bs} = u_x \cdot \cos\psi - u_y \cdot \sin\psi\,,$$
$$i_b - u_y \cdot i_{ws} - u_x \cdot i_{bs} = u_y \cdot \cos\psi + u_x \cdot \sin\psi\,. \tag{A.10}$$

Sind die Bezugsgrößen für die Spannungen gleich U_t und für die Ströme gleich $I = U_t \cdot Y'$, so folgen die relativen Kenngrößen:

$$i_w = \frac{I_w}{I}; \qquad i_b = \frac{I_b}{I}, \qquad i_{bs} = \frac{\Delta B \cdot U_t}{I}; \qquad i_{ws} = \frac{G \cdot U_t}{I};$$

$$u_x = \frac{U_{Yx}}{U_t}; \qquad u_y = \frac{U_{Yy}}{U_t}.$$

In Gl. (A.10) befinden sich vier unbekannte Stromkomponenten, daher braucht man zwei weitere, von den obigen unabhängige Beziehungen. Wird die Löschspule in eine andere Position gestellt, z. B. in Richtung der größeren induktiven Ströme, werden praktisch nur der resultierende i_b und der symmetrische Blindreststrom i_{bs} geändert.

Nimmt man in einer Position N

$$i_{bN} \qquad \text{und} \qquad i_{bsN}$$

und in einer anderen Position H

$$i_{bH} \qquad \text{und} \qquad i_{bsH}$$

an, dann ergibt sich mit Verwendung von $i_{LH} = i_{LN} + \Delta i_L$ für die den zwei Arbeitspunkten gehörenden, symmetrischen Blindrestströme:

$$i_{bsH} = i_c - i_{LH} = i_c - (i_{LN} + \Delta i_L) = (i_c - i_{LN}) - \Delta i_L = i_{bsN} - \Delta i_L\,. \tag{A.11}$$

Dies gilt auch für die resultierenden Blindrestströme, da der unsymmetrischer Strom, bzw. seine Komponenten sich nicht verändern:

$$i_{bH} = i_{bN} - \Delta i_L \tag{A.12}$$

Bild 2 zeigt die Verhältnisse. Δi_L kann nach

$$\Delta i_L = \frac{I_{LH} \cdot l_H(u_{0H}) - I_{LN} \cdot l_N(u_{0N})}{U_t \cdot Y'} = \frac{\Delta I_{Ll}}{I} \tag{A.13}$$

berechnet werden. Wobei

I_{LH}, I_{LN} — induktive Ströme in Pos. H und N, die bei Spannung U_t auf der Löschspule sie durchfließt

u_{0H}, u_{0N} — Sternpunktspannung, bzw. Spannung an der Löschspule im Arbeitspunkt der Pos. H und N, bezogen auf Spannung U_t.

$l_H(u_{0H}); l_N(u_{0N})$ — Korrektionsfaktor in Pos. H und N bei nichtlinearen Löschspulen nach Bild 2.

In Kenntnis der den gesagten wird die für Pos. *N* bezogene Gl. (A.10) auch für Pos. *H* mit dem Unterschied aufgeschrieben, daß die Blindströme da laut Gl. (A.11) und (A.12) ersetzt werden. So ergibt sich für die unbekannten Kenngrößen i_w, i_{ws}, i_{bN} und i_{bsN} je eine Gleichung in Pos. *N*.

$$\begin{aligned}
i_w - u_{xN} \cdot i_{ws} + u_{yN} \cdot i_{bsN} &= u_{xN} \cdot \cos\psi - u_{yN} \cdot \sin\psi\,, \\
i_{bN} - u_{yN} \cdot i_{ws} - u_{xN} \cdot i_{bsN} &= u_{yN} \cdot \cos\psi + u_{xN} \cdot \sin\psi\,, \\
i_w - u_{xH} \cdot i_{ws} + u_{yH} \cdot i_{bsN} &= u_{xH} \cdot \cos\psi + u_{yH}(\Delta i_L - \sin\psi)\,, \\
i_{bN} - u_{yH} \cdot i_{ws} - u_{xH} \cdot i_{bsN} &= u_{yH} \cdot \cos\psi - u_{xH}(\Delta i_L - \sin\psi) + \Delta i_L\,.
\end{aligned} \tag{A.14}$$

III. Grundsätzliches für die Kreislösung

Die allgemeingültigen Gleichungen für die Kreislösung können aufgrund von Bild 10, mit Hilfe der Vektoralgebra und der Koordinatengeometrie abgeleitet werden. Wie es aber auch aus dem Bild hervorkommt, ist die Ableitung recht

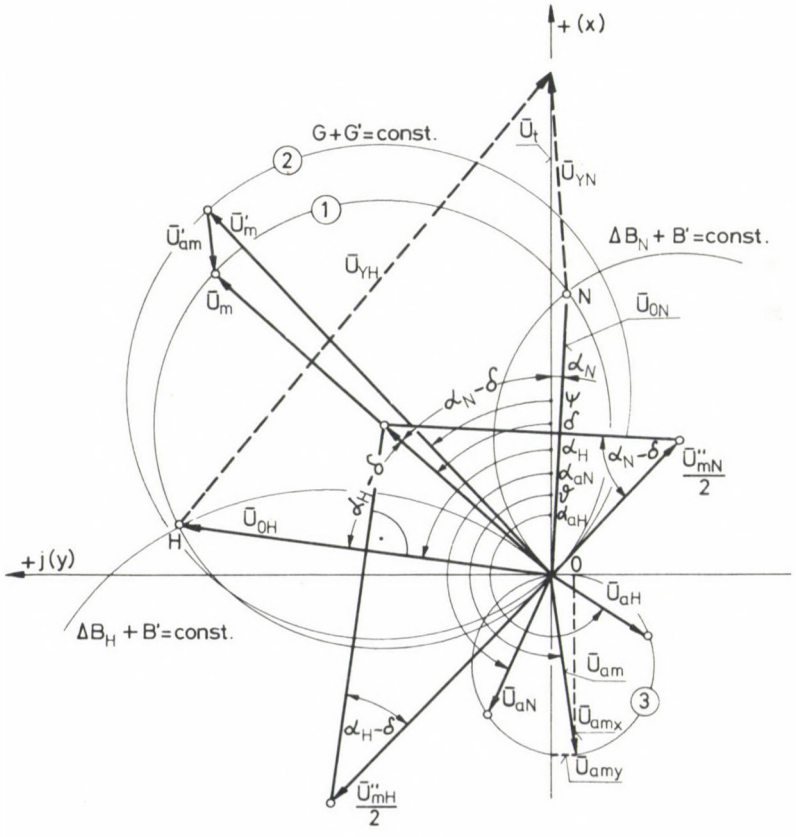

Bild 10

kompliziert, so können hier nur die Gedankenfolge und die Ergebnisse geschildert werden.

Diese Lösungsvariante beruht auf der Idee, daß die Endpunkte der Zeiger $\bar{U}_0$ bzw. $\bar{U}'_0$, und $\bar{U}_a$ sich entlang je einem Kreis durch das Origo bewegen, wobei die resultierende Leitfähigkeit $(G+G')$ konstant ist, und die Position der Löschspule fortwährend in die eine bzw. in die andere Richtung gestellt wird (Kreise ① ② ③). Mittels den Kreiskenngrößen, sowie den Durchmesserzeiger und den zu Pos. N und H gehörenden Sehnenzeiger $\bar{U}_{0H}$, $\bar{U}_{0N}$ können die allgemeingültigen Reststromkomponenten beschrieben werden:

$$
\begin{aligned}
i_{bs} &= \frac{I_{bs}}{I} = -\left[\frac{\tan(\alpha-\delta)}{u'_m} + \sin\psi\right], \\
i_{ws} &= \frac{I_{ws}}{I} = \left[\frac{1}{u'_m} - \cos\psi\right], \\
i_{ba} &= \frac{I_{ba}}{I} = u_{am_y}\left[\frac{1}{u'_m} - \cos\psi\right], \\
i_{wa} &= \frac{I_{wa}}{I} = u_{am_x}\left[\frac{1}{u'_m} - \cos\psi\right].
\end{aligned}
\tag{A.15}
$$

Hierbei

$$
u'_m = \frac{m - \dfrac{n}{\tan\vartheta}}{\sin(\alpha_N - \alpha_H)}
$$

$$
\tan\vartheta = \frac{\mathrm{n}}{\mathrm{m}},
$$

$$
\begin{aligned}
n &= -[u_H \cdot \cos\alpha_N - u_N \cdot \cos\alpha_H]; \qquad u_H = \frac{U_{0H}}{U_{tH}}, \\
m &= [u_H \sin\alpha_N - u_N \cdot \sin\alpha_H]; \qquad u_N = \frac{U_{0N}}{U_{tN}},
\end{aligned}
\tag{A.16}
$$

bzw.

$$
\begin{aligned}
u_{am_x} &= \frac{m_a}{\sin(\alpha_{aN} - \alpha_{aH})}, \\
u_{am_y} &= \frac{n_a}{\sin(\alpha_{aN} - \alpha_{aH})},
\end{aligned}
\tag{A.17}
$$

$$\tan \vartheta = \frac{n_a}{m_a},$$

$$n_a = -[u_{aH} \cdot \cos(\alpha_{aN}) - u_{aN} \cdot \cos(\alpha_{aH})]; \qquad u_{aH} = \frac{U_{0aH}}{U_{taH}},$$

$$m_a = [u_{aH} \cdot \sin(\alpha_{aN}) - u_{aN} \cdot \sin(\alpha_{aH})]; \qquad u_{aN} = \frac{U_{0aN}}{U_{taN}},$$

und

$$\begin{aligned} i_b &= i_{bs} - i_{ba}, \\ i_w &= i_{ws} - i_{wa}, \\ I &= U_t \cdot Y'. \end{aligned} \tag{A.18}$$

Die Formelzeichen können aufgrund von Bild 10 verstanden werden.

Acta Technica Academiae Scientiarum Hungaricae, 93 (3—4), pp. 261—286 (1981)

ADDENDA TO THE IGNITION AND COMBUSTION PROCESSES OF DIRECT INJECTION SUPERCHARGE MARINE DIESEL ENGINES

P. LOSONCI*

[Manuscript received: 5 Jan. 1982]

The present-day theories covering the mixture formation, ignition and combustion processes in the combustion spaces of the marine Diesel engines operating with undivided combustion chambers and multi-spray nozzles are rather complex. This article has attempted to partially resolve these complexities, emphasizing the heat radiation effect of the lighting flame, which plays an important role in the fast heating-up of the fuel particles, as well as the high-speed evaporation process, the so-called steam blast, which can be regarded as essential in the process of mixture formation and makes the mixture formation and combustion processes self-sustaining.

Introduction

The processes of mixture formation, ignition and combustion going on in the combustion chambers of Diesel engines are, unfortunately, not known in detail even today, so the planning of the injection systems of new engines is mainly based on experimental results. It is an undisputable fact, however, that the research work done and the experiments made in the last few decades led to a number of qualitatively new results in the fields of mixture formation and the processes of ignition and combustion. In spite of this, mixture formation, ignition and combustion still have aspects where the currently known results of research and the theories formulated need to be supplemented or amended. Such an aspect may be the self-sustaining quality of the combustion taking place in a direct injection Diesel engine, especially in the last phase of the combustion, when the oxygen concentration of the air in the combustion converges on the minimum and the unburnt fuel particles and vapours are losing their chances of obtaining free oxygen molecules.

The present paper aims at giving an overall view of the ignition and combustion properties of the combustion chambers of *low r.p.m.* direct injection *marine Diesel engines*, the related experimental observations, the results as well as the conclusions to be drawn from the experimental measurements.

1. Some ignition and combustion properties of direct injection combustion chambers with no orderly air-flow, with special reference to the low r.p.m.

As an introductory step, let us compare the actual parameters of a high r.p.m. Diesel engine of a fast-moving ship with those of another, low r.p.m. moderately fast ship. The comparison is illustrated in Table 1.

* P. Losonci. Otthon u. 37, H-1118 Budapest, Hungary

From the data of Table 1 it may be concluded that

— the combustion chambers of low r.p.m. Diesel engines are several times larger than those of high r.p.m. Diesel engines;

— the fuel quantity injected in a cycle is also several times greater;

— the fuel has to be forwarded to a much greater distance in the combustion chamber;

— a good mixture formation has to be implemented in a volume several times as big;

— the time available for burning the larger amount of injected fuel is several times longer;

— the geometrical injection time of the fuel is also several times longer.

Table 1

	revolution per minute r.p.m.	mean piston speed, m/sec	compression ratio,	combustion chamber volume, cm^3	cycle portion of fuel, cm^3	geometrical injection time, 10^{-3} sec	mean effective pressure, bars
1.	1800	12.6	12	455	0.36	1.4	9.0
2.	400	6.0	12	3200	2.5	11.25	10.7
The ratio values of the properties of number 1 and 2 engines:							
1/2	4.5	2.1	1	0.14	0.144	0.1244	0.84

The foregoing leave no doubt about the following:

a) The demand for the fuel to be injected to a greater distance necessitates the shaping of the fuel jet to have a larger degree of penetration. A fuel jet with a higher influx rate contains, on an average, larger fuel particles to a greater number. It is rather difficult to make the larger-size fuel droplets evaporate, ignite and burn smokelessly under favourable conditions. Even after their distribution the major particles are more likely to reach the colder combustion chamber walls, where they condense and cause loss.

b) In the case of direct injection low r.p.m. Diesel engines with no orderly air-flow a difficult problem is posed by the distribution and smokeless burning of the fuel droplets arriving to the cylinder, especially in the last phase of the injection, when the oxygen concentration of the combustion air converges to the minimum.

c) The evaporation, ignition and combustion procedures are favourably affected by the multiplication of available time.

d) The first fuel particles entering the cylinder evaporate and ignite under fairly good circumstances, owing to the amount of air available for combustion being incomparably greater, and having absorbed far more heat.

2. Investigations and experimental observations on marine Diesel engines

The chief characteristics of the engine put at our disposal for investigations and experiments:

Number of cylinders:	$z = 8$
Effective continuous rating:	$P_e = 736$ kW
Continuous revolution number:	$n = 400$ r.p.m.
Rating with one hour's overloading:	$P'_e = 810$ kW
R.p.m. with overloading:	$n' = 412$ r.p.m.
Specific fuel consumption:	$b_e = 231$ g/kW × h; +5.5% (170 g/HP × h; +5.5%)
Bore:	$D = 315$ mm
Stroke:	$S = 450$ mm
Total piston displacement:	$V_t = 281$ l
Compression ratio:	$\varepsilon = 10.8$
Break mean effective pressure:	$p_e = 8.0$ bars
Supercharge air pressure (overpressure):	$p_s = 0.4$ bar
Final combustion pressure:	$p_c = 53 + 2$ bars
Final compression pressure:	$p_{cp} = 36$ bars
Combustion chamber:	undivided and disc-shaped with a half-lens shaped trough in the light metal piston crown; direct injection; no regulated air-flow in the cylinder
Type of injection nozzle:	Bosch DLT 183 ($6 \times 0.4 \times 120°$)
Type of injection pump:	Bosch PF 1W 190; separate pump for each cylinder
Supercharging system:	pulsating, every two cylinders attached to a common pipe. If mounted on engine, one BBC VTR 320 type supercharger. No air cooling.
Number of valves:	one inlet and one exhaust valve.
Degree of valve overlap:	$\Delta\varphi = 150$ crankshaft degrees
Specific oil consumption:	$b_{ek} = 4.08$ g/kW × h; +10%
Mean piston speed:	$v_{pm} = 6$ m/sec

2.1. Observations made and conclusions drawn during engine operation mainly covering the ignition and burning of fuel

At the initial stage of the investigations the engine was observed in the course of its operation and the important components of the engine were studied in its uncleaned state.

The engine exhibited the following disorders:

— during continuous operation the engine smoked moderately, even under partial loading;

— as many carbon hillocks were deposited on the piston crown as were the number of bores on the injection nozzle (Fig. 1)

Fig. 1. Coke hillocks on the piston head

The conclusion arrived at after an analysis of the disorders described above was that investigations will have to be carried out to cover

— the combustion air ratios and

— the mixture formation and combustion phases of the engine.

The combustion air ratio (m_c) and the total air ratio (m_t) of the engine were studied in the case of the characteristics $P_e = 736$ kW and $n = 400$ r.p.m., relying on the measurements taken earlier.

These preliminary analyses gave

$m_t = 2.45$ for the total air ratio

and

$m_c = 1.75 - 1.8$ for the combustion air ratio

with approximative calculations.

Considering these numerical results, smoke coming from lack of combustion air was out of question.

2.2 *The investigations of the elements of the fuel injection system*

On the ground of the contents of item 2.1. combustion disorders were inferred. As the injection process influences combustion significantly, it seemed reasonable to reconsider the adjustment of the injection nozzle to the combustion chamber, its relation to the combustion itself.

Accordingly, several different types of nozzles were purchased and tested.

2.3. The new experimental injection nozzles and the measurement results

Eight kinds of nozzles having different geometrical characteristics from the original one were applied. The chief geometrical characteristics of these nozzle types are shown in Table 2.

Nozzle number 1 was part of the original engine.

Table 2. The geometrical characteristics of the experimental nozzles

Serial number	Nozzle type	Total cross section of bores		Arrangement of bores
		mm^2	percentage	
1.	6 × 0.4 × 120	0.756	100	symmetrically on a cone shell
2.	6 × 0.35 × 120	0.576	76	—do—
3.	7 × 0.35 × 120	0.6723	89	—do—
4.	8 × 0.35 × 120	0.767	101	—do—
5.	8 × 0.30 × 120	0.564	75	—do—
6.	9 × 0.30 × 120	0.634	84	—do—
7.	10 × 0.30 × 120	0.705	92	symmetrically alternating on two cone shells
8.	12 × 0.30 × 120	0.846	112	—do—
9.	12 × 0.25 × 120	0.588	78	—do—

The interpretation of the individual digits of the nozzles' characteristics:

— first digit — the number of bores
— second digit — the diameter of the bores in mms
— third digit — the bevel angle of injection (in angle degrees)

The results of the experiments made with the nozzles enumerated in Table 2 are shown in Fig. 2.

During the experiments with the nozzles the following values were kept constant:

— the initial fuel injection pressure,
— the preliminary injection angle and
— the geometry of injection.

Whilst the above parameters remained constant, the other characteristics of the injection naturally changed.

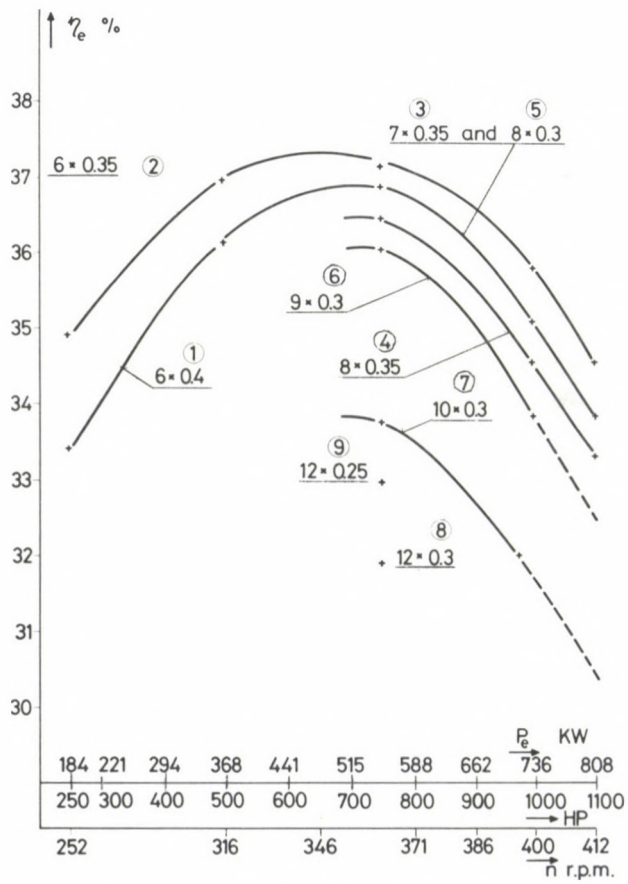

Fig. 2. The change in the effective efficiency of the engine in the course of the measurements taken with the original and experimental nozzles

2.4. Conclusions and suppositions derived from the experimental results

— Nozzle 2 presented the most optimal effective efficiency value. There was neither engine smoking, nor deposit of carbon hillocks on the piston crown throughout the whole range of operation. Hence, it can be stated that with medium-speed direct injection marine Diesel engines with no orderly air-flow, an optimal nozzle ensuring efficient, smokeless combustion can be selected;

— an overall change in the geometrical cross section of the nozzle exerted no clear-cut effect on the effective efficiency;

— an increase in the number of bores initially resulted in a moderate deterioration of the effective efficiency, and subsequently a very marked one. This leads to the assumption that a nozzle with an optimal number of bores can be chosen in order that optimal effective efficiency might be achieved;

— a decrease in the diameters of the bores improved the effective efficiency in the case of the second nozzle. However, when the decrease in the diameters went hand in hand with an increase in the number of bores, the effective efficiency showed an abrupt deterioration.

On the basis of the foregoing it can be stated that in the case of medium-speed, direct injection multi-spray nozzle supercharge marine Diesel engines with no orderly air-flow in the combustion chamber, it is needless to strive at distributing the fuel injected in the combustion chamber with maximum evenness, when the mixture formation takes place.

This conclusion is diametrically opposed to the classical approach to the mixture formation and combustion processes taking place in the combustion chamber of a Diesel engine.

2.5. Experiences gathered from nozzle experiments carried out with other engines

2.5.1. Experiences arrived at in the course of experiments with an M-50-F type mechanical supercharged direct-injection multipurpose Diesel engine:

The main characteristics of the engine:

Effective continuous rating:	$P_e = 736$ kW
Continuous revolution number:	$n = 1700$ r.p.m.
Performance in 1 hour's overload:	$P'_e = 808$ kW
Excess load revolution number:	$n' = 1800$ r.p.m.
Specific fuel consumption:	$b_e = 258$ g/kW × h
Number and arrangement of cylinders:	2×6 V
	$D = 180$ mm
	$S = 200$; 209.8 mm
	$V_t = 62.4$ l
	$\varepsilon = 12.2$

$p_e = 8.3$ bars
$p_s = 0.65$ bar (overpressure)
$p_c =$ unknown
$p_{cp} = 51$ bars

Type of combustion chamber: an undivided Hesselman combustion chamber with direct injection; no orderly air-flow.
Supercharging system: mechanical, no air cooling.
Number of valves: two suction and two exhaust valves
Main piston speed: $\sqrt{v_{pm}} = 12$ m/sec
Injection nozzle: $8 \times 0.35 \times 140°$
Degree of valve overlap: $\Delta\varphi = 100$ crankshaft degrees

The injection nozzle experiments made on this engine unambiguously pointed to the assertion that the most favourable results were associated with the $8 \times 0.35 \times 140°$ nozzle. With that, the engine apparently worked without smoking and the temperature of the exhaust gases was the lowest.

In that case the macro-mixture number was: [9]

$$\frac{V_c}{V_{\text{spray total}}} \cong 5.8 \qquad \frac{\text{compression volume}}{\text{total volume of fuel spray cones}}$$

Black spots of discolouration appeared on the piston crown, burnt unevenly and starting from the peak, following the direction of the eight nozzle sprays (Fig. 3).

It was to be noted that part of the fuel sprayed in becomes spread on the piston crown, evaporates and may get partly cracked, but all the same burns smokelessly. Having studied the geometrical positions of the sprays and the piston crown we observed that the fuel particles cannot directly reach the piston crown, if they follow the so-called "cold" injection path. From the discolouration on the piston crown it may be

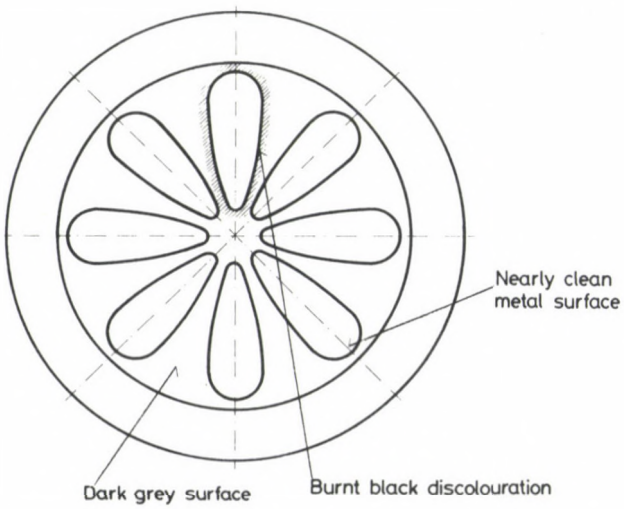

Fig. 3. A sketch of the discolouration on the piston head

concluded that the tinges are caused by the circumstance that the sprays expand to three or four times their original volume in an advanced phase of the injection, when the piston still stays in the vicinity of the upper dead point. So the paths of a certain proportion of the fuel particles travelling in the vicinity of the piston change so much that they become spread on the hot piston crown, evaporate and burn while causing the discolouration described above.

2.5.2. Experiences gathered from experiments with the 6LD 315 RNF type marine Diesel engine

A similar phenomenon was to be noted with the high-pressure supercharge unit of the engine family described in item 2. The main characteristics of this engine were the following (with only the differences being enumerated):

Type:	6 LD 315 RNF
Number of cylinders:	$z=6$
Specific fuel consumption:	$b_e=209$ g/kW × h
Total piston displacement:	$V_t=211$ l
Compression ratio:	$\varepsilon=12$
Mean effective pressure:	$p_e=10.7$ bars
Supercharge air pressure (overpressure):	$p_s=0.67$ bar
Final combustion pressure:	$p_c=88$ bars
Final compression pressure:	$p_{cp}=49$ bars
Type of combustion chamber:	undivided Hesselman with direct injection, with no regulated air-flow in the cylinder
Type of injection nozzle:	Bosch $6\times0.5\times120°$
Type of injection pump:	Bosch PF 1W 220, a separate pump for each cylinder
Supercharging system:	pulsating; two to three cylinders attached to a common exhaust pipe; a NAPIER MS/HP 204 type turbo supercharger mounted on engine. Air cooling: $\Delta t=40\,°C$
Number of valves:	two suction and two exhaust valves
Degree of valve overlap:	$\Delta\varphi=110$ crankshaft degrees.

With this engine the macro-mixture number [9] had the value:

$$\frac{V_c}{V_{\text{spray total}}} \cong 12$$

From now on the changes in the various physical characteristics will be dealt with, which were brought about in the case of the cylinder supercharge as well as the injected fuel.

3. Changes in the different physical characteristics of the cylinder supercharge and the injected fuel

In the course of injection and combustion a series of changes takes place in the physical characteristics of the cylinder supercharge and the fuel particles [1], [2].

Let us follow these changes with attention.

3.1. The change in the physical properties of the cylinder supercharge

The change in the average pressure of the supercharge can be measured and calculated and the change in its average temperature can be calculated with sufficient accuracy.

Reliable data concerning the high-pressure supercharge marine Diesel engine described under 2.5.2. are shown in Fig. 4 [5].

In the course of mixture formation the movements and changes occurring in the supercharge air should be considered:

— the irregular eddying movements that were created during the induction stroke and still extend at the time of the injection and combustion;

— a certain degree of local movement of the supercharge air owing to the injected fuel particles;

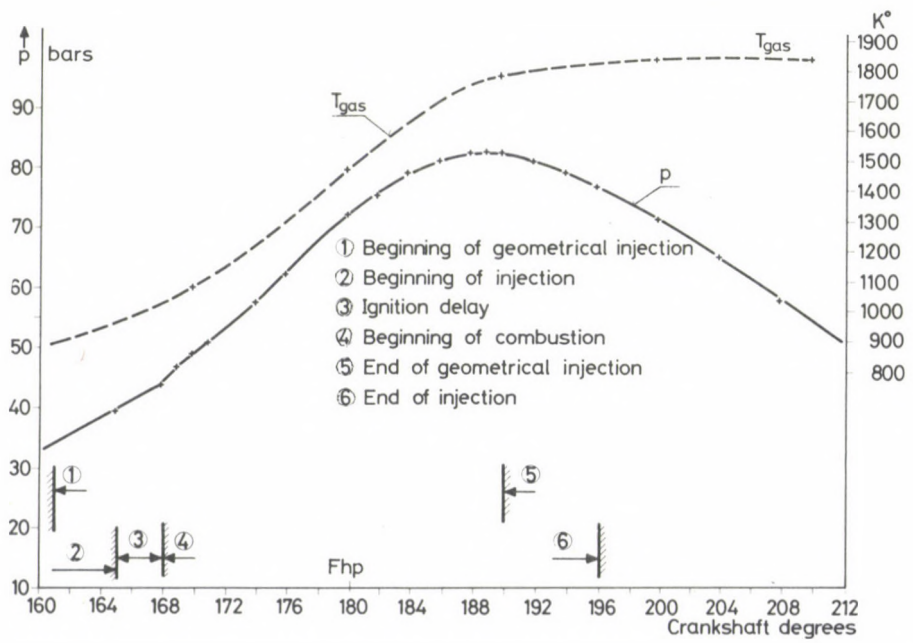

Fig. 4. The change of the supercharge pressure and temperature in the mixture formation and combustion phases of the engine

— the irregular internal currents (turbulence) formed at the moment of ignition and intensified during the lasting continuous combustion.

In connection with the changes of the above-mentioned characteristics it must be noted that in the cylinder space considerably greater local pressure, temperature and speed values may arise in the ignition and combustion centres and in their immediate vicinity for a short time, but subsequently, in the course of the combustion they will be levelled to the average.

— The oxygen concentration of the cylinder supercharge will decrease during the combustion and converge to the minimum.

— At the moment of the ignition the flare flame appears, which enables the fuel droplets to continue to absorb a considerable amount of heat through thermal radiation.

3.2. The changes occurring in the fuel particles

In the course of the injection the fuel droplets arriving at the cylinder space travel through a medium, in a different state, every moment. [1]

A study of Fig. 4 reveals that the fuel particle injected in the cylinder space crosses with an ever-increasing pressure (density) and temperature of the air and gases while travelling, and its velocity decreases significantly. Due to the rising pressure and temperature of the supercharge air the pressure and temperature of the fuel particle increases, too.

From the moment of ignition and combustion the pressure and temperature of the supercharge air soars upwards.

After achieving its highest value the pressure of the supercharged air falls abruptly, while its temperature keeps rising and then becomes steady at a nearly constant value. A significant drop comes only afterwards, which can be attributed to the decrease of the fuel quantity due to its burning and to the expansion of the supercharge air becoming more intensive. The abrupt fall of pressure also occurs in the fuel particle, while its temperature rises.

While travelling in the cylinder the fuel particle heats up and evaporates owing to its continuous and ever-increasing heat absorption.

The degree and regularity of the evaporation are considerably effected by the physical properties of the fuel in addition to heat absorption.

The following Tables have been inserted to illustrate the changes in the physical characteristics of the fuel ([11] partly calculated values).

The density of the gas oil moderately increases with the increase of the pressure and abruptly decreases with the increase of temperature.

The *specific heat of the gas oil* increases rapidly with the rising of the temperature (Table 4).

The *distillation temperature of the gas oil* abruptly increases with the rising of the pressure (Table 5).

Table 3

Temperature (C) \ Pressure (bars)	1	20	40	60
	The density of gas oil (kg/dm^3)			
20	0.830	0.832	0.835	0.841
200	0.695	0.700	0.704	0.718
300	0.600	0.629	0.641	0.653
400	0.455	0.547	0.559	0.577

Table 4

t; (C)	0	20	100	150	200	250	300	350	400	500	600	700	800
$c\frac{kJ}{kgK}$	1.88	1.97	2.26	2.47	2.72	2.93	3.14	3.35	3.56	3.98	4.40	4.81	5.23

Table 5

Distilled volume (%) \ Pressure (bars)	1	20	40	60
	Distillation temperature (C)			
first drop	160	322	378	427
10	200	390	440	475
30	233	410	485	530
50	265	455	530	585
70	300	500	570	630
90	348	560	660	740
boiling point of last component	375	595	700	800

The size and shape of the fuel particle undergoes a continual change, while the particle is travelling. Depending on the degree of evaporation, the size of the particle decreases, and depending on the extent of heating up, it increases. Its nearly spherical shape, which exists in the first few moments of injection, changes — the major particles divide as they move along.

On the surface of the particle a steam layer of changing thickness is formed depending on its shape due to evaporation. Let us now study the heat absorption relations of the particle in the combustion chamber with regard to the fact that the current heat absorption is being dwelt on through convection, and heat absorption through radiation, which takes place from the moment of the appearance of the flare flame, will be treated separately.

The amount of heat absorbed through radiation from the liner in the combustion chamber and that transmitted to it through radiation will be neglected.

3.3. The heat absorption conditions of the fuel particle

The fuel particle absorbs heat from its environment through convection and radiation and loses a certain amount owing to evaporation. The amount of heat used for warming up the fuel particle is:

$$Q_w = Q_c + Q_r - Q_e \qquad \text{(kJ)}$$

Until the moment of the appearance of the flare flame the fuel particle absorbs a notable amount of heat from the working medium through convection. The following well-known equation will be used as a starting point for the definition of the degree of heat absorption:

$$Q_c = \alpha_c \cdot A(t_g - t_p) \cdot \tau \qquad (1)$$

When defining the approximative values of absorption of radiated heat we used the following formula as our starting-point:

$$Q_r = \sigma \cdot \varepsilon_r \cdot A_p \left[\left(\frac{T_f}{100} \right)^4 - \left(\frac{T_p}{100} \right)^4 \right] \tau \qquad (2)$$

The designations are interpreted as follows: (6)

Q_w — the amount of heat used for warming up the fuel particle (kJ)
Q_c — the amount of heat absorbed by the fuel particle from the cylinder gas trough convection (kJ)
Q_r — the amount of heat absorbed by the particle through radiation heat exchange (kJ)
Q_e — the amount of heat abstracted from the fuel particle by evaporation (kJ)
α_c — convection heat transmission factor (kJ/m^{2}h K)
A^p — the heat absorption area of the fuel particle (m^2)
t_g — the average temperature of the gas (C)
t_p — the average temperature of the fuel particle (C)
τ — time (10^{-3} sec)
σ — heat radiation coefficient (21.3 kJ/m^{2}h(K)^4)
ε_f — the emission factor of the radiating flame, taking into account the formula

$$\varepsilon_f = \varepsilon_0 (1 - e^{-k \cdot p \cdot l}) \qquad [10]$$

ε_0 — the discolouration factor of the fuel particle (taken as 0.8)
T_f — the absolute temperature of the flare flame (K)
T_p — the absolute temperature of the fuel particle (K)
ρ_g — the density of the cylinder gas (kg/dm^3)
k = $k(m, \varphi)$ its value depends on the air ration (m) and on the angle of rotation of the crankshaft (φ) [10. Fig. 4]
p — pressure in the combustion chamber
l — medium length in the combustion according to the following formula;

$$l = \frac{3{,}6\ V}{A}, \quad \text{where}$$

V — the momentaly volume of the combustion chamber
A — the momentaly boundaly surface of the combustion chamber

3.3.1. Heat transmission through convection. The factors of equation (1) constantly change in the phase of injection in the following manner:

— *the average temperature of the particle* tends to rise on its way. As the droplet passes through micro-environments of various physical characteristics, this tendency prevails, but the increase of its temperature is realized with divergences in accordance with its travel through varying microenvironments;

— until the beginning of the evaporation process the change in the *average temperature* of the gas takes place by the law of polytropic compression. From this moment *till the appearance of the first ignition centre* the temperature rise follows a different pattern. Again, the average temperature of the gas changes differently from the moment of the ignition to the point when the maximum temperature is reached, and again differently until that stage of expansion, constituting the end of the combustion.

— *the average temperature of the particle* is directly dependent on the amount of heat absorbed and the amount lost during evaporation;

— the amount of heat absorbed from the gas through convection depends, among other things, on the area of the surface absorbing the heat, "A". Taking into consideration that the droplet starts evaporating from the moment it gets into the cylinder space as its temperature grows, the value of "A" increases to a smaller degree than could be expected as a consequence of the increase of volume due to the temperature rise of the droplet;

— *the surface of the droplet depends on its shape.* In the phase of the division of the major drops the size of the surface area undergoes a constant change. Also the proportion of the active and less active surfaces in heat absorption changes;

— when the flare flame appears, the surface of the droplet changes differently due to heat absorption from radiation, and still differently, if the surface of the droplet itself is in flames. In all probability a quasi-boiling arises on the surface of the droplet owing to a quick heating up of the layers near the surface. Evaporation from these layers may take place at such a high speed that the droplet falls apart, that is to say, it blasts. (Steam blast [9]).

— in the course of the *evaporation of the droplet* a steam blanket is formed on the surface, which acts against the absorption of the convection heat;

— the value of the α_c heat transmission factor changes while the fuel particle is travelling in the cylinder space as a function of time [1].

The major factors bringing about the change are:

— the measure-setting speed of the droplet,

— the measure-setting diameter and shape of the droplet,

— the thickness of the steam envelope,

— the density of the supercharge air and

— the burning of the surface of the particle.

With the above consideration the convection heat absorption of the fuel particle may be characterized with the following complicated function:

$$Q_c = Q_c(A; \alpha_c; t_p; t_g; \tau;) \tag{3}$$

The equation is made complicated by the facts that on the one hand A; α_c; t_p; t_g are partly functions of the time τ, and on the other, A; and t_p are also functions of Q_c and the specific heat, c, that is

$$A = A(Q_c; t_p; \tau; c;) \tag{4}$$

$$t_p = t_p(Q_c; \tau; \alpha_c;), \qquad \text{and} \tag{5}$$

$$\alpha_c = \alpha_c(A; \lambda; w; \rho_g; \delta_{se}; \tau;) \tag{6}$$

λ ..... is the heat conduction factor of air (gas)
w ..... is the changing relative speed of the fuel particle
δ_{se} ..... is the thickness of the steam envelope forming round the superficies of the fuel droplet
ρ_g ..... is the density of the cylinder supercharge.

Unfortunately, it should be noted that functions (3), (4), (5) and (6) are not known yet.

3.3.2. An analysis of heat transmission through radiation. The time passing between the beginning of the injection and the appearance of the first combustion centres and the flare flame is only a fraction of the total time of the injection and combustion [1]. With the appearance of the flare flame the fuel particles have another heat transmitting source at their disposal, the heat radiation of the flare flame.

Taking equation (2) into account the heat absorption of the fuel particle from radiation may be described with the following function:

$$Q_r = Q_r(A; T_p; \tau;) .$$

This equation is complicated by the circumstance that both A and T_p are functions of Q_r, and, in addition, T_p depends on the c specific heat of the particle. Specific heat, on the other hand, depends on the T_p value.

This continues to add to the elaborateness of the calculation method of the heating conditions of the particle. All in all, a joint consideration of the heat absorption of the fuel particle through convection and radiation leads to the observation that at the present level of our knowledge the intricate interdependence of the factors prevent us from accurately calculating the heating up of particles.

3.4. A comparison between heat absorption through convection and radiation

Heat absorption through convection and radiation, which have been discussed in items *3.3.1.* and *3.3.2.* separately, are simultaneously present in the most important phase of mixture formation and combustion, from the moment of the appearance of the flare flame to the end of the combustion, in an extremely perplexing interrelation.

Now let us examine the heating of fuel droplets with diameters of 10, 20 and 30 μ, with the following stipulations:

— the droplet remains spherical and is not enveloped in steam,

— the diameter of the droplet does not change with its mass, remaining constant,

— the change in the gas temperature will be considered,

— the change in specific heat will also be considered,

— the temperature of the cylinder supercharge will be considered as indicated in Fig. 4,

— the initial value of the temperature of the droplet will, in every case, be selected 150 C, and α_c heat transmission factor [1]; will be assigned the values

$$\alpha_{10} = 50.4 - 53.0 \text{ kJ/m}^2 \text{ h K}$$

$$\alpha_{20} = 25.2 - 26.3 \text{ kJ/m}^2 \text{ h K}$$

$$\alpha_{30} = 16.74 - 17.56 \text{ kJ/m}^2 \text{ h K}$$

whereas in the maximum temperature range it will have the following values: [1], [6]

$$\alpha_{10} = 74.7 \qquad -\text{do}-$$

$$\alpha_{20} = 37.3 \qquad -\text{do}-$$

$$\alpha_{30} = 24.9 \qquad -\text{do}-$$

— the growth of the α_c heat transmission factor coming from the increase of the density of the supercharge air will be neglected.

The heating will be examined at a period of $1.2 \cdot 10^{-3}$ seconds and the temperature of the flame will be selected 2500 degrees K on the basis of several measurement results. [7], [10]. The calculations were made with repeated approximations using medium temperature values and corresponding specific heat values.

The process of the calculation was the following: it was practicable to resort to a partial interval of $0.1 \cdot 10^{-3}$ seconds. Heat absorption through convection and radiation was simultaneously calculated. With the increase in the temperature of the supercharge air the increase of α_c was also taken into consideration. Knowing the initial temperature of the droplet, 150 degrees C, we determined the amount of convection

Table 6

Size of droplet	10μ	20μ	30μ
Evaporation time	$1 \cdot 10^{-3}$ sec	$3.3 \cdot 10^{-3}$ sec	$8 \cdot 10^{-3}$ sec

and radiation heat and then calculated the heating up of the droplet with an estimated specific heat value.

The calculation was corrected with the iterative method until the desired accuracy was achieved.

With two or a maximum of three such approximations a completely satisfactory degree of accuracy was obtained.

As the average temperature was known, the temperature of the fuel droplet at the end of the interval could easily be arrived at, which was, at the same time, an approximate value of the fuel droplet temperature at the beginning of the next interval.

The results of the approximate calculations are shown in Figures 5 and 6.

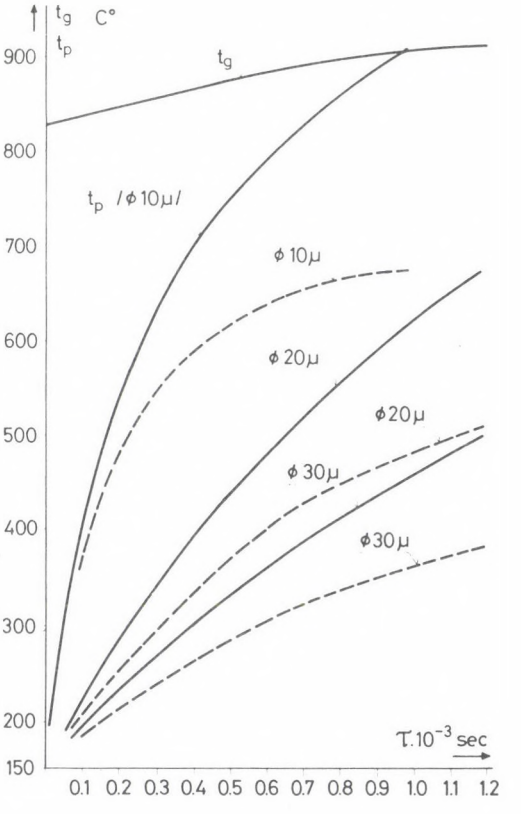

Fig. 5. The change in the average heating-up of the fuel particles with diameters of 10, 20 and 30 μ as a function of time, in a medium of air and combustion products having an increasing pressure and temperature. The temperature of the flame, $T_1 = 2500$ K. The curves in – – – – represent only the partial heating-up of the fuel droplet through convection

In Fig. 3 we have already demonstrated the theoretical fuel particle evaporation times obtained by approximative calculations using parameters, which were taken into account when dealing with the tendencies in heating up exposed in Fig. 5. [1].

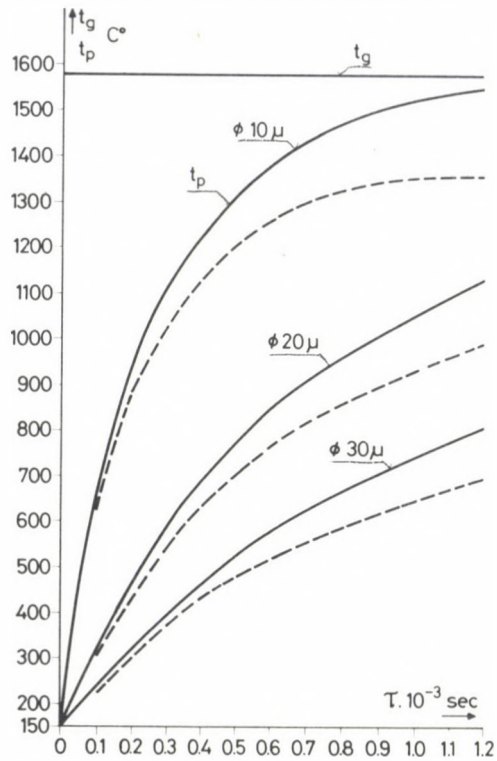

Fig. 6. The average heating-up of the fuel particles with diameters of 10—20 and 30 μ as a function of time, in a medium of air and combustion products with a decreasing pressure and permanent temperature. The temperature of the flame: $T_1 = 2500$ K. The curves in – – – – represent only the partial heating-up of the droplet through convection

4. The conclusions of the investigations

The heating up of the fuel particles with diameters of 20 μ or bigger, is significantly smaller at a given time than that of particles with diameters of 10 μ, because the surface — mass proportion of particles with a diameter of 10 μ is more favourable and their heat transmission factor, α_c is significantly larger because of the smaller diameter of the droplets [1]. In order to achieve a more perfect mixture formation it would be desirable to produce small droplets that evaporate fast, in the first phase of injection, and so the ignition delay could be reduced.

In the phases following the self-ignition of the fuel larger and larger size droplets should be aimed at owing to the rapid increase in the supercharge pressure. Their greater capability of penetration may guarantee the fuel particles getting to those partial volumes of the combustion chamber that are at a greater distance from the nozzle.

— From the moment of the appearance of the flare flame the heat absorption of the particles is considerably enlarged due to the heat radiation of the flare flame.

— The particles with diameters larger than 10 μ are divided after entering the combustion chamber.

The main reasons for the division are as follows:

— As a result of the changing pressures arising along the superficies of the particle injected at a great speed the particle becomes deformed. The quasi-spherical shape is not preserved persistently;

— The heating up of the particle takes place at an enormous speed;

— The Diesel oil consists of components having different boiling points.

Owing to very fast heat absorption the steam bubbles of the components with lower boiling points strive to leave the droplets at a great speed, in a manner of an explosion. They tear up the superficies of the droplet, thus promoting division. So the droplet can explode and burn completely in the blaze, if there is an ideal mixture formation.

Having investigated the average heating up of the fuel particle (Fig. 5) it may be concluded that the amount of heat absorbed from radiation from the moment of the appearance of the flare flame constitutes the following percentage of the total average heating-up:

for a particle with a diameter of

$D = 10\ \mu$	30.5%
$D = 20\ \mu$	31.2%
$D = 30\ \mu$	33.8%

In case the temperature of the supercharge air has achieved its highest value, a smaller percentage of the particle's average heating up is constituted by the heating up through radiation (Fig. 6).

In this case the heating up through radiation constitutes the following percentage of the total average heating up:

for particles with diameters of

$D = 10\ \mu$	13.5%
$D = 20\ \mu$	14.2%
$D = 30\ \mu$	16.7%

Let us next examine the average heating up of a particle with a diameter of 20 μ before the moment of the extinction of the flare flame, assuming that the fuel still follows the shape of droplets in this phase.

The approximative calculations were made under the conditions outlined in item *3*. The temperature of the gas was regarded as a constant value, as the decrease was negligible. Furthermore, on the basis of [7] and [1]

$$T_1 = 2500 \text{ K}$$

$$P_g = \text{decreasing}$$

while for α_c the following datum may be arrived at: [1]

$$\alpha_{20} = 28.1 \text{ kJ/m}^2\text{h K}$$

The results of the approximative calculations are shown in Fig. 7.

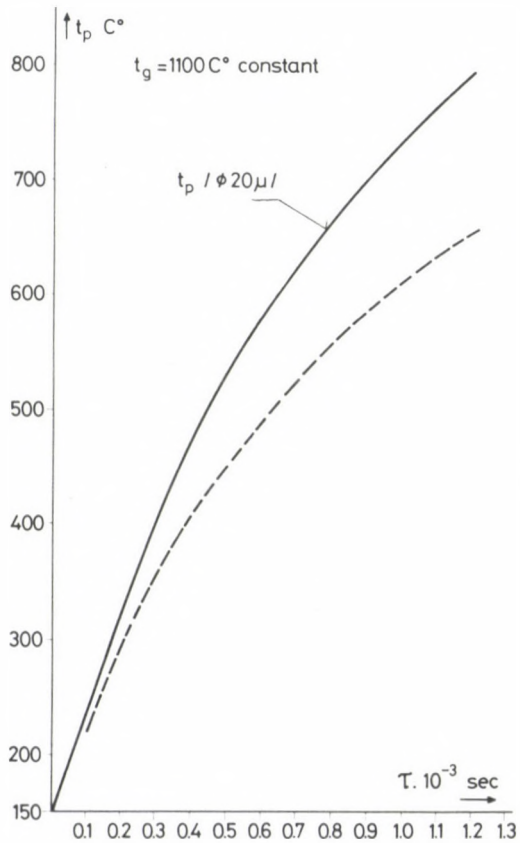

Fig. 7. The average heating-up of the fuel particles with diameters of 20 μ as a function of time, in a medium of air and combustion products having a decreasing pressure and nearly permanent temperature. The temperature of the flame is: $T_1 = 2500$ K. The curve in – – – – represents only the partial heating-up of the droplet through convection

From Fig. 7 it appears that in the last moments of the combustion, due to the flare flame, the average partial heating up of the particle through radiation constitutes 21.7% of the total average heating up of the particle in $1.2 \cdot 10^{-3}$ seconds. It is desirable to summarize the partial results of the calculations and include them in one figure.

On the ground of Figs 5,6 and 7 Fig. 8 may be compiled. Figure 8 shows the approximative percentage distribution of the average heating up of a particle with a diameter of 20 μ through convection and radiation from the moment of the appearance

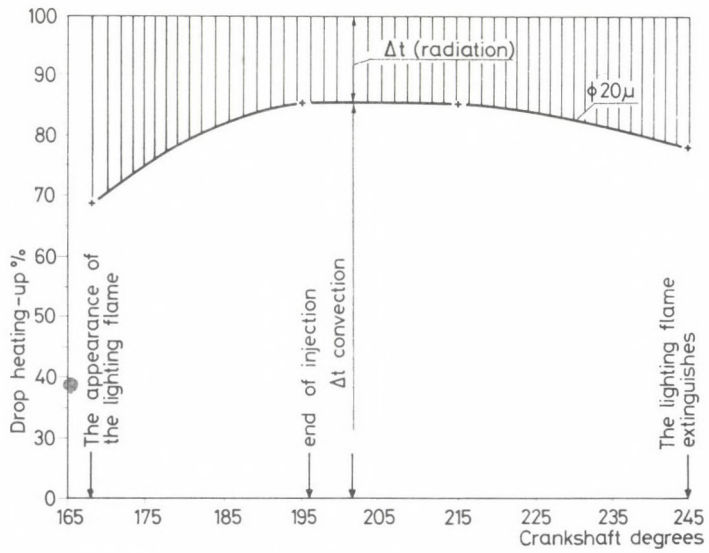

Fig. 8. The percentage distribution of the average partial heating-up of a fuel particle with a diameter of 20 μ through convection and radiation in phases II, III and IV of the mixture formation and combustion. Heating-up time: 1.2×10^{-3} sec

of the flare flame to the moment of its extinction. The flame extinction value expressed in crankshaft degrees belonging to the engine under item *2.5.2.* is based on estimation. [8]

From Fig. 8 it appears that with the mixture formation and combustion processes taking place in Diesel engines the heat radiation of the flare flame plays an important role in the phase of perfect combustion. The significance of heat radiation is especially important from the moment of the appearance of the flare flame till the moment when the highest temperature has been achieved and in the final phase of the combustion, when the combustion air ratio converges on the minimum.

Note: The ignition and heat radiation effect of the flare flame makes itself felt favourably also in the mixture formation and combustion processes taking place in the combustion chambers of the gas turbines and boilers. The ignition and radiation effect

continuously affect the fuel particle from its entry into the combustion chamber up to the combustion.

When making the approximative calculations several factors have been neglected. From among these the ratio $\Delta t_r/\Delta t_t$ is significantly increased by the following: in spite of an increase in the average temperature of the particle both the mass and the diameter of the particle were regarded as constant.

In case the mass of the particle is considered to be decreasing because of the evaporation and, in addition the increase of the diameter due to abrupt heating up is noted, the $\Delta t_r/\Delta t_t$ ratio will considerably increase and the heating up of the particle will take place at a great speed. This tendency can be explained by the circumstance that though α_c decreases to a greater proportion with the size of the particle growing than the proportion of increase of the heat-absorbing surface of the particle, the heat radiation conditions remain unchanged, the mass of the particle decreases, and so the average partial heating-up occurring due to the amount of heat absorbed by the particle from radiation will be relatively larger than in the cases demonstrated in the Figures.

5. Analysis of the heating-up and evaporation processes of the fuel particle

The development of highly efficient mixture formation and combustion processes in the combustion chambers of Diesel engines having no orderly airflow and are operating with multi-spray nozzles depends primarily on the intensity of the heating-up and evaporation processes of the fuel particles.

From the heating-up procedures discussed in item *3.4.* it appears that the average heating-up of the fuel particles of relatively smaller size and mass takes place at a very high speed, especially from the moment of the appearance of the flaring flame.

In the foregoing we have already dwelt with the high-speed evaporation of the fuel particles, the so-called steam combustion. Let us now discuss the causes underlying steam combustion.

The laws of heat transmission holding also within the fuel particle, the calculated average temperature of the droplet is only an assumed value. In reality a difference of temperatures arises between the inner and outer layers of the particle. The temperature of the outer layer increases at a much higher speed than the average temperature. In the 3rd and 4th phases of mixture formation and combustion, when the heating-up of the particle continues to take place at a high speed, the speed of evaporation is further increased by an abrupt decrease of the combustion chamber pressure, as the distillation temperature of the individual fractions decreases abruptly with the decrease of pressure.

A reference to the data of table 5 reveals that the lighter fractions of gas oil may start boiling within the droplet if the temperature of the droplet reaches the value 500 ÷ 550 C. According to the calculations, there is a real possibility for this. So it can be

assumed that in the slow-operation engines the state of boiling takes place in the droplets and if there is overheating, the droplet explodes. Such explosions have been observed in water drops earlier.

6. A simplified theory of the mixture formation and combustion processes in multi-spray Diesel engines

The theories worked out for the mixture formation and combustion processes going on in Diesel engines are rather complicated. Among other things this complexity comes from the following:

— we have no accurate knowledge of the behaviour of the liquid state, multi-component fuels at high pressure and high temperature space in the various phases of mixture formation and combustion, in case of a continually decreasing air ratio, with special reference to very high-speed heat absorption,

— we do not know the convection and heat exchange processes taking place in a small-size fuel particle in the course of injection,

— the attachment and interaction of the series of evaporation, ignition and combustion processes are not known, especially because among the subsequent fuel particles entering the combustion chamber there are not two, which evaporate, ignite and burn under the same circumstances,

— our knowledge is deficient concerning how heat transmission takes place through convection on the surface of the fuel droplet, when it has already taken fire.

Conflicting tendencies may turn up, e.g. in the experimental results of the author, namely that the efforts to make the macro-mixture more even and the micro-mixture of finer distribution lead to more intensive smoke and coke formation, when the macro-mixture number decreased gradually from 6 to 3. The total efficiency of the engine became seriously impaired.

The injection spray expansion described in *2.5.1.* is a clearly proven fact (Figs 3 and 9). In the case of a nozzle with a larger-than-optimum number of bores two neighbouring sprays got so near each other, owing to the expansion of the sprays in the course of mixture formation and combustion, that the flame fronts forming during the combustion caused mutual disturbance. This phenomenon led to a local enrichment of the mixture, the burning was not perfect in that environment, the engine smoked. This observation contradicts a classical approach to combustion, which strives at making the macromixture as fine as possible.

In order to eliminate some of the complexity extant in the multi-spray mixture formation and combustion theories, the author suggests a simplified theory of mixture formation and combustion, a "dynamic approach" to combustion, which may be worded as follows: in the course of the injection fuel particles of different size enter the combustion space. Among the droplets of divergent sizes there are some *with optimal circumstances for evaporation, ignition and burning.* Some of them have not such

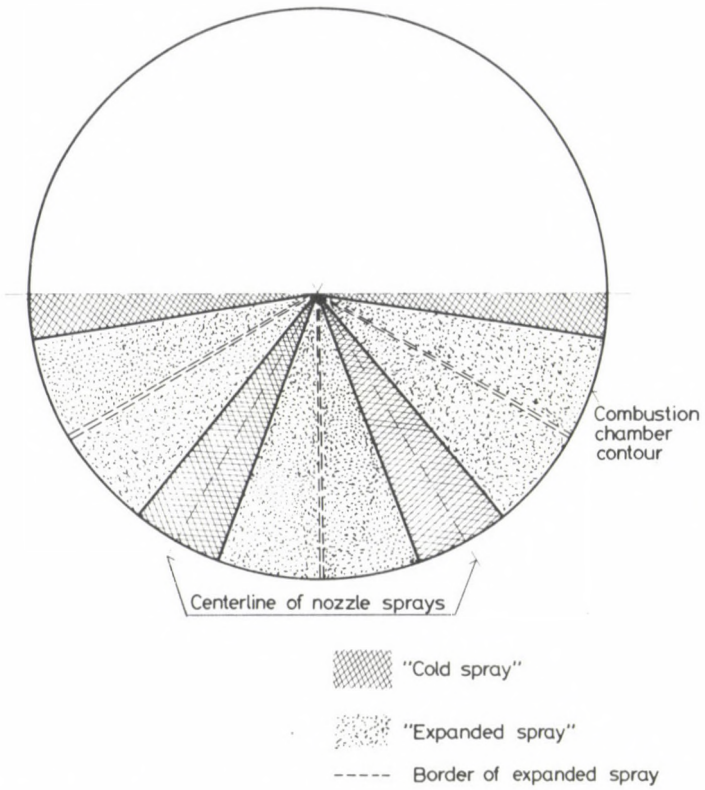

Fig. 9. The expansion of the injection nozzle sprays in case of smokeless, high-efficiency burning

favourable circumstances and others have definitely bad properties. The particles with bad qualities will transform into particles with favourable features during their division.

The particles with optimal features are characterized by having optimal evaporation, mixture formation, ignition and combustion qualities considering the given engine, combustion space and injection system, and the particles burn smokelessly, with a high efficiency. In all probability it may be stated that the sizes of the optimum-quality particles are different in the ignition delay phase (I), in the phase lasting from the moment of combustion, when the lighting flame appears, till the highest pressure of the circular process (II), in the phase lasting until the highest temperature of the circular process (III), and again different in the final stage of the combustion (IV)

Highly efficient, smokeless burning can only take place, when the injection nozzle produces mostly fuel particles of optimal size and in the course of mixture

formation and combustion the larger particles also transform into optimal or near-optimal ones due to division.

Let us review the details of the simplified theory in the various stages of mixture formation and combustion.

Phase I. Ignition delay. This phase is characterized by a relatively slow warming up of the fuel particles and the initial stage of their evaporation, when some of the lighter fractions will transform into steam state and the centres capable of ignition are formed. These centres are located in the outward part of the spray cone shell, in nearby volumes, where the air ratio is the most favourable for self-ignition.

In the phase of ignition delay the average warming up of the particle or the warming up of its outer layer takes place at a much lower speed than in the later phases of the process because of the lower temperature of the supercharge air.

In the phase of the ignition delay part of the lighter fuel vapour that had been emitted by the particles becomes detached from the particles still travelling at a greater speed, loses speed and becomes distributed in the environment due to diffusion. Another part constitutes the steam envelope formed round the particles. The mixing of the fuel vapours is promoted by the movement of air, which arose during the induction stroke and still exists.

The fuel particles with their size decreasing follow the so-called "cold path" and the vapours are mostly located in the volume of the injected spray and in its vicinity and reach the ignition temperature gradually.

In this phase it is desirable to produce as little particles as possible with a small capability of penetration in order to bring about fast evaporation in spite of the relatively small differences in temperature. The particles with a strong capability of penetration that retained the shape of droplets can reach the wall of the cylinder lining and may cause losses there.

Phase II. The stage from the beginning of the combustion to the highest pressure of the circular process. This phase is characterized by the self-ignition of the fuel vapours formed and the development and continuity of the combustion.

If the fuel vapours have reached the self-ignition temperature, they are very likely to ignite in the vicinity of the injected spray cone shell and their combustion is accompanied by detonation. It is mainly the fuel fractions with the lowest distillation temperatures that are to be found in the mixture that has developed until the moment of the ignition and self-ignition takes place by them. The reason for a combustion with detonation is volume self-ignition. The circumstance that the detonation does not develop further, as in the case of the Otto engine, where the conditions were not desirable, can be explained by the fact that the fuel quantity injected during the ignition delay is about one tenth of the total fuel quantity and even the injected fuel will only partly be transformed into steam.

After ignition the combustion will become continuous with the appearance of the lighting flame.

With the appearance of the flare flame a new element enters the process of mixture formation and combustion, due to the ignition and heat radiation effect of the flame.

In this phase of mixture formation and combustion the pressure of the supercharge air reaches its highest-ever value, and the temperature is approaching its highest value. The heating-up and evaporation of the newly formed droplets take place quickly. The average air ratio gradually decreases.

In this phase the production of the fuel particles with a higher capability of penetration is already desirable, primarily because in this way the fuel can arrive to the air layers located near the cylinder liner wall.

In the case of Diesel engines with no orderly air-flow the fuel is injected into a smaller part of the compression volume and an automatic process is needed for the combustion to take place in time, which maintains a high-quality mixture formation continuously at a large speed and extends the combustion to that combustion space volume, filled with the mixture.

The automatic mixture formation process is brought about by the high speed heating-up of the fuel particles partly by the expansion of the spray, partly by the circumstance that the evaporation of some of the droplets takes place in the form of an explosion, in steam blasts. This results in both the burning fuel vapour and the burning fuel particles getting into the volumes outside the geometrical injection spray cone shell.

The diffusion of the fuel vapours into the neighbouring volumes naturally continues, though their ignition hinders the diffusion to a certain degree.

In this phase the new fuel particles arriving at the combustion space are already received by a real blaze and their surfaces catch fire shortly after their entry. This phenomenon leads to an improvement in the quality of mixture formation and combustion. The burning of the surface creates a state of boiling together with the thermal effects of convection and radiation, which, joined by the aerodynamic forces, promotes steam blasts. The decrease of the average combustion air ratio and the continuous ignition and the combustion result in a reduction of the speed of combustion. A combustion accompanied by detonation cannot take place, because the volume of the mixed fuel vapours is limited.

Phase III. The stage ranging from the place of maximum pressure to the end of maximum temperature. This phase is characterized by an abrupt decrease in the pressure of the supercharge air, by the temperature of the supercharge air reaching its maximum and staying at approximately the same value until the end of the phase. The fuel injection is terminated.

The most favourable conditions of mixture formation and combustion are created in this phase. The explosion-like evaporation here takes place at a higher speed than earlier, which is backed up by a fuel-distillation temperature reduction, caused by an abrupt decrease of the pressure of the supercharge air.

An ever-increasing quantity of the injected fuel burns entailing a gradual decrease of the oxygen concentration. Thus, the conditions of mixture formation become rather difficult in the last part of the phase, but the explosion-like evaporation promotes the mixture formation taking place at a high efficiency. The carbon, coke and soot particles, which may have been formed in phases I, II, and III, still burn perfectly in this phase, if the injection nozzle is properly tuned.

Phase IV. The stage ranging from the maximum temperature until the extinction of the flame. This phase is characterized by

— a decrease in pressure and temperature

— the burning of the injected fuel is finished, the flame extinguishes

— the value of air ratio reaches its minimum.

At this stage of the combustion the explosion-like evaporation of the particles, which still retain their drop-like shape, continues as a consequence of the abrupt fall in pressure accompanied by only a moderate decrease of temperature, and this phenomenon automatically provides for a mixture formation with the mostly optimal fuel particles and a combustion with a nicely tuned injection nozzle without any soot and with a high efficiency.

The burning procedure described above can be demonstrated with the author's experimental results. So, for instance, the experiments with carburettors having different numbers of bores (6×0.35, 7×0.35, 8×0.35) pointed out that the mixture formation and efficiency deteriorated if the sprays met and their surface suitable for mixture formation decreased. In the case of properly selected carburettors the diameters of the bores ensure the necessary depth of penetration and droplet sizes, while the number of sprays should be chosen so as to ensure totally free surfaces for mixture formation.

If the spray travels longer, its expansion is larger and its cone angle increases. So in a combustion space with a larger diameter a carburettor with a smaller number of bores (6×0.35 or 6×0.5) gave an optimal result, while in a cylinder with a smaller diameter one with a larger number of bores (8×0.35) did.

Conclusions

The main factors guaranteeing a high efficiency of the mixture formation and combustion processes of the slow-operation Diesel engines working with multi-spray nozzles and having no regulated air-flow can be summarized as follows:

— the bore diameter of the carburettor ensures a proper depth of penetration and droplet diameter,

— the number of bores on the carburettor ensures the persistence of the free spray surface during the time of mixture formation, thus providing for the possibility of mixture formation on the total surfaces of the sprays,

— the effect of radiation heat brought about by the lighting flame, which
— results in the expansion of the spray,
— it overheats some of the fuel droplets and may cause steam blasts.

References

1. Sitkey, Gy.: Mixture Formation and Combustion Process in Diesel Engines. (In Hungarian). Akadémiai Kiadó, Budapest 1960
2. Löhner, K.: Brennkraftmaschine, VDI, 1963
3. Brodszky, D.: Supercharged Diesel Engines. (In Hungarian). Műszaki Könyvkiadó, Budapest 1970
4. Meurer, S.: Der Wendel in der Vorstellung vom Ablauf der Gemischbildung und Verbrennung im Dieselmotor, *MTZ*. Heft 4, 1966
5. Kalmár, I.: Some Results Obtained from Electronic Calculations of Working Processes, (In Hungarian), Budapest Technical University, scientific session. 1st volume, 1967
6. Sitkei, Gy.: Heat Transmission and Heat Loading in Internal Combustion Engines. Akadémiai Kiadó, Budapest 1962
7. Kalmár, I.: The Questions of the Simulation of Working Processes, *Műszaki Tudomány* 47, Akadémiai Kiadó, Budapest 1973
8. Aeplér, E.—Baturin, CN.: Optische Methode zur Untersuchung der Russkonzentration in Brennraum von Diesel-motoren Maschinenbautechnik 24/1975/3
9. Sitkei, Gy.: Flammenstrahlung in Diesel-motoren. *Archiwum Procesow Spalania*, **5.** (1974), Nr. 2
10. Maxwell, J. B.: DATA Book on Hydrocarbons. D. Van Nonstrand Co. Princeton, N. J. 1950
11. Pischinger, A.: Alte und neuere Verstellungen über die Gemischbildung im Diesel-motor. *Österreichische Ingenieur Zeitschrift* **10,** Heft 7

Acta Technica Academiae Scientiarum Hungaricae, 93 (3—4), pp. 289—310 (1981)

STATISTICAL EVALUATION OF CALCULATED AND MEASURED SETTLEMENTS

L. RÉTHÁTI*

[Manuscript received: 3 April, 1982]

In dimensioning of structures, the solutions based on the theory of probability come into the foreground more and more. This makes it necessary to work out, also in the field of geotechnics, an up-to-date investigation methodology for each type of the problems. Since significant economic interests are connected with the limitation of the settlements, this problem has a rather great importance. The paper tries to clear up the problems for the solution of which the new approach may furnish additional information.

Introduction

Field observations prove that the damages of buildings are never caused by the *failure of the soil* but by large or/and uneven settlements. The overwhelming part of the few constructions which suffered damages owing to failure of the soil, were silos (where a drastic decrease of the shear strength took place under the effect of sudden loading). According to present-day conception, by retaining the settlement under a given limiting value, the construction is protected against the failure of soil too. That is why a particular care should be taken on the reliability of the *prediction* for the settlements.

In working out the prognostic one has to start from the fact that both the load and the physical characteristics of the soil are random variables, i.e., beside the expected value of the settlement (or the settlement differences) also the values to be expected with different probabilities should be determined. With their knowledge the *technico-economical optimum* may be determined which, by making consistent the two aspects with each other, gives the best solution.

The *measurement of the settlements* permits to check the calculations and to forecast a possible dangerous situation but also allows a better recognition of the characteristics of soil. Thus, the statistical evaluation of the settlements measured may offer equally useful information both to the designer and the user.

1. Prediction of the settlements

1.1. Reliability of the mean settlement

Let us set out from the formula the most frequently used, according to which

$$s = \frac{B \cdot q \cdot f}{E_s},$$

wherein:

* Dr. Réthási L. 1092, Budapest, Ráday u. 43.

s = calculated settlement,
B = width of foundation,
q = contact pressure,
f = influence factor for the settlements,
E_s = modulus of compressibility of soil.

Let us assume that the settlement of the footing No. 1 to be seen in Fig. 1 ought to be predicted, and to E_s, with random spatial distribution, the values indicated in Table 1 have been measured. Accordingly, the statistical parameters of the *modulus of compression* are as follows:

$\bar{E}_s = 12.2 \cdot 10^3$ kN/m^2 (expected value);
$\sigma_E = 2.61 \cdot 10^3$ kN/m^2 (standard deviation);
$C_{vE} = 0.214$ (coefficient of variation);
$C_s = -0.008$ (coefficient of skewness);
$C_k = -0.83$ (kurtosis).

Table 1. Initial values for the numerical examples of sections 1.1 and 1.2

E_s (MN/m^2)	s (cm)	$\sqrt{s}$	ln s
14.2	3.845	1.961	1.3468
13.8	3.957	1.989	1.3755
16.3	3.350	1.830	1.2090
14.9	3.664	1.914	1.2986
9.5	5.747	2.397	1.7487
11.3	4.832	2.198	1.5753
12.4	4.403	2.098	1.4823
8.1	6.741	2.596	1.9082
9.9	5.515	2.348	1.7075
11.6	4.707	2.170	1.5491

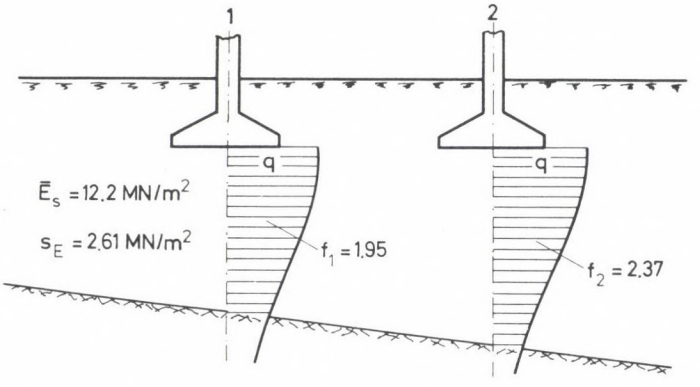

Fig. 1. Starting data of the numerical example of Chapter 1.1.

For distinguishing the settlement and standard deviation the latter is designated with σ, although it symbolizes an empirical deviation.

In the second column of Table 1 the settlements calculated to the ten E_s values are to be seen. Their statistical parameters are as follows:

$$\bar{s}=4.676 \text{ cm}, \qquad \sigma_s=1.065 \text{ cm},$$

$$C_{vs}=0.228, \qquad C_s=0.725 \qquad \text{and} \qquad C_k=-0.31.$$

Accordingly, the *coefficient of variation* hardly changed in comparison with C_{vE}, however, at the same time, the series *s is not at all symmetric*; the very same may be stated in connection with the $\sqrt{s}$ and ln *s*.

It may be proved (Rétháti, 1979) that the coefficient of skewness of the series formed from the reciprocals of the settlements is approximately zero, thus, according to the formula of the settlement, it differs from the distribution of E_s merely by a constant.

Hereafter, the *confidence interval* of the mean settlement might be calculated as follows. Since the number of the measurements is relatively small, ($n=10$), the Student distribution should be used. By selecting the probability level $\alpha=0.05$, $t_\alpha=1.833$, thus:

$$E_s=12.2+1.833\frac{2.61}{\sqrt{10}}=12.2\pm1.5 \text{ MN/m}^2$$

Accordingly, it can be stated with a 90 per cent probability that the settlement to be expected is not less than

$$100\frac{1.4\cdot200\cdot1.95}{13.7\cdot10^3}=4.0 \text{ cm},$$

and not deeper than

$$100\frac{1.4\cdot200\cdot1.95}{10.7\cdot10^3}=5.1 \text{ cm}$$

The confidence interval can be defined in cases where E_s *has no trend in the horizontal sense* and for the *average settlement* of an individual foundation body and for the reliability of it are wanted numeric data. This should be the way of proceeding in case, for example, where an aperture of elliptic cross section in a rigid foundation body for a pipe to be led through, ought to be determined.

1.2. Forecasting settlement differences

This problem might be solved in two different ways according to whether a single footing (a), or two separate ones are to be handled (b).

Case (a). Let us assume that the first eight values of the first column of Table 1 have been measured not at the environment of a single footing but at the axis of a strip

foundation at a spacing of d. Then the equation of the regression line defined to the s_i value will be

$$s = 0.346\ d + 3.01\,,$$

and the value of the correlation coefficient $r = 0.73$.

According to the above equation the settlement to be expected at point 1 is $s_1 = 3.36$ cm, at point 8, $s_8 = 5.78$ cm, thus, the expected value of the differential settlement will be $\Delta s = 2.42$ cm.

The standard deviation of the regression coefficient is

$$\sigma_a = \sqrt{\frac{\sigma_r^2}{(n-1)\sigma_d^2}} = \sqrt{\frac{0.792^2}{(10-1)2.45^2}} = 0.108\,.$$

considering that the σ_r residual standard deviation is

$$\sigma_r = \sigma_s \sqrt{1-r^2} = 1.159 \sqrt{1-0.73^2} = 0.792\,.$$

Accordingly, it may be stated with a 90 per cent probability that the regression coefficient (a) has not a larger value than

$$0.346 + 1.28 \cdot 0.108 = 0.484\,,$$

and Δs is not larger than

$$(8-1)\ 0.484 = 3.39 \text{ cm}\,.$$

Case (b). Let us assume that the subsoil under both footings to be seen in Fig. 1 is characterized by the values of ten E_s of random spatial distribution. In this case the expected value of the differential settlement is

$$\overline{\Delta s} = 100 \frac{q \cdot B}{E_s} (f_2 - f_1) = \frac{200 \cdot 1.4}{12.2 \cdot 10^3} (2.37 - 1.95) = 0.96 \text{ cm}\,.$$

The variance of the settlement of the foundation No. 1 (by neglecting the standard deviation of q and B):

$$\sigma_1^2 = \left(- \frac{qBf_1}{\bar{E}_s^2} \right)^2 \sigma_E^2 + \left(- \frac{qBf_1}{\bar{E}_s^2} \right) \frac{2qBf_1}{\bar{E}_s^3} C_{sE} \sigma_E^3 = 91.98 \cdot 10^{-6}\,,$$

therefore, $\sigma_1 = 0.00959$, i.e., 0.959 cm. By proceeding in a similar way, to the standard deviation of the footing No. 2 $\sigma_2 = 1.164$ cm has been obtained.

The difference Δs over which the probability of occurrence of a higher value is 10 per cent, is as follows:

$$\Delta s = (\overline{\Delta s} + t_\alpha \sqrt{\sigma_1^2 + \sigma_2^2}) 100 =$$

$$= (0.096 + 1.28 \sqrt{0.00959^2 + 0.01164^2} = 2.9 \text{ cm}\,.$$

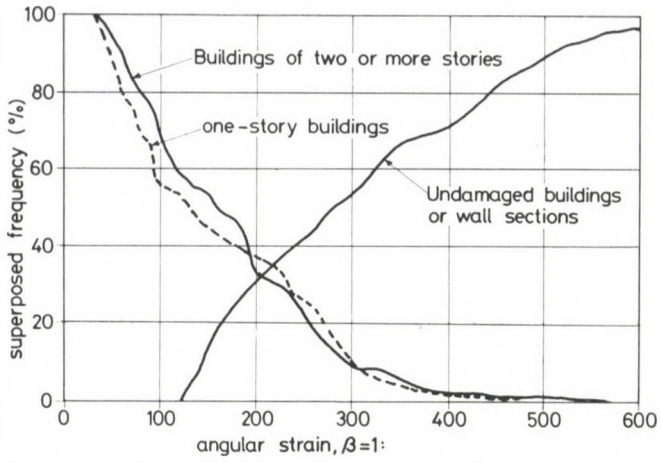

Fig. 2. Determination of the critical angular distortions with the aid of the empirical distribution functions of the angular distortions measured on intact and damaged buildings (walls) (Rétháti 1977)

In the designing practice it is usual to compare the calculated settlements with the limiting values of the settlement criterions. For the determination of the limiting values of *angular distortion* the investigation of several 100 buildings damaged in Hungary has been offered (Rétháti, 1977). Plotting the empirical distribution functions of the angular distortions measured on damaged and undamaged buildings (i.e., walls) (Fig. 2),the β associated with the intersection point of these functions can be considered the upper limit of the danger value.

1.3. Random components of motion in homogeneous soil

The settlement of isolated footings lying on homogeneous soil having identic· surface and loaded identically, are considered in the traditional (deterministic) method of dimensioning, as identic.

This assumption is very far removed from reality. The site observations show that differential settlements also develope in such cases and, in general, not only in an order of magnitude of a few mms but in cms, the causes of which are as follows:

— the fact of the "homogeneity" is declared on the basis of relatively few samples;

— the distribution of the payload, and frequently that of the deadload is of random character;

— the conditions developed during construction of the individual footings are not identical (one or another trench might be drenched or become loose, etc.);

— some of the footings may suffer unexpected local damages (as, for example, afflux of surface waters is not identical).

On the basis of information obtained from the literature on the subject, Leussink (1955) investigated buildings which, both in horizontal and vertical sense, have been situated on foundations standing on homogeneous soil, the foundations being within a

building of identical dimensions with the same value of contact pressure. He determined to each building the ratio

$$\alpha = \frac{s_{max} - s_{min}}{\bar{s}},$$

and then he classified these ratios into groups, according to whether the compressible layer is situated under or over a certain depth, which corresponds to the half width of the strip footing and to the lower value from $B/2$ and $L/4$ in case of an isolated footing. By establishing the empirical density functions of α he experienced that their mode is about $\alpha = 0.3$, i.e., $\alpha = 0.9$. This means that the settlement of the footings may differ from the expected value even by ± 15 per cent, i.e., by ± 45 per cent, which, however, are significant differences.

Also from Leussink's statistical data the significant conclusion may be drawn that *in case where the foundation system is settling, also differential settlements occur.* This means that the average depth of settlement should be limited, even in case of homogeneous soil, and not only owing to functional or other reasons (for example, joining of pipe conduits) but also for the protection of the construction against undesirable uneven movements. The *maximum tolerable* $\bar{s}$ might be calculated as follows (Réthái, 1968).

According to Skempton's and Macdonald's (1956) sophisticated statistical investigations, the *maximum permissible differential settlement* for footings standing on clay or sand, i.e., on soils of slow and quick consolidation respectively, is

$$\Delta s_{max} = 4.5 \text{ cm and } 3.2 \text{ cm},$$

respectively.

By equating these values with Leussink's values, the following equalities may be described:

$$4.5 = 0.9\bar{s}, \qquad \text{and} \qquad 3.2 = 0.9\bar{s}.$$

Accordingly, the average permissible settlements in case of clay and sand soil are $\bar{s} = 5$ cm and $\bar{s} = 3.5$ cm respectively. Similar results are obtained in case where one sets out from Skempton's and Macdonald's other criterion, namely, from that relating to the *maximum settlement* to be measured within the building. According to the authors, the permissible value of this is in case of clay 7.6 cm and of sand 5.1 cm; whereby the following equations are obtained:

$$7.6 = \bar{s} + 0.45\bar{s}, \qquad \text{and} \qquad 5.1 = \bar{s} + 0.45\bar{s}$$

respectively.

The values of $\bar{s}$ yielded by these equations (5.2 cm and 3.6 cm) are nearly the same as the $\bar{s}_{critical}$ determined above.

Resendiz and Herrera (1969) investigate the components of the movements carried out by a solitair footing subjected to uniformly distributed loading, for the case,

where the deformation characteristics of the soil *have no horizontal trend.* With the aid of their formulae the variances of the average settlement and the x and y-directed tiltings (θ_x and θ_y). (While the expected value of s is a finite value, the values of θ_x and θ_y are, as a matter of course, equal to zero.) The noteworthy basic idea of the procedure is, that to the occurrence of an event of zero expected value a *probability differing from zero is* coordinated. That is why the probability theory has a great significance in such cases because such problems *cannot be solved with the aid of deterministic methods.*

2. Evaluation of the measured settlements

The measurement of settlement also fosters the solution of a number of other problems beside those mentioned in the beginning of this paper: pointing out the local effects (for example, in case of a building construction near by), observation of new structures, technologies or foundation systems, determination of the rate of the settlement (for example, before the reconstruction of the building), etc. Four problems from among these will be discussed in a detailed way.

2.1. Extrapolation of the consolidation curve measured

The gradual reduction of safety requires the knowledge of the *final values* of the components of motion in many cases in order to take the necessary measures in due time.

The two methods described here, and especially the first one (Réthàti 1971), may, strictly speaking, be used only for the case of *unidimensional consolidation.*

By proceeding according to the *first* method, the final value of the settlement s_u should be esteemed on the basis of the measurements, then the quotients associated with the different moments t_i

$$\kappa_i = \frac{s_i}{s_u}.$$

are calculated.

From Fig. 3 the T_i time factors corresponding to the boundary conditions should be read, then the quotiens

$$\alpha_i = \frac{t_i}{T_i}$$

formed. The reliability of the settlement s_u may be characterized by the coefficient of variation of α_i, i.e., by the quotient $C_v = \sigma_\alpha / \bar{\alpha}$. In varying s_u those values ar considered to be the most probable, at which $C_v =$ minimum.

Assuming that the distribution of the vertical stresses corresponds to case 5 of Fig. 3 and $\xi = p_f / p_a = 2$, that is,

$$\kappa_i = \kappa_1 - \frac{\xi - 1}{\xi + 1}(\kappa_1 - \kappa_2) = \frac{2}{3}\kappa_1 + \frac{1}{3}\kappa_2.$$

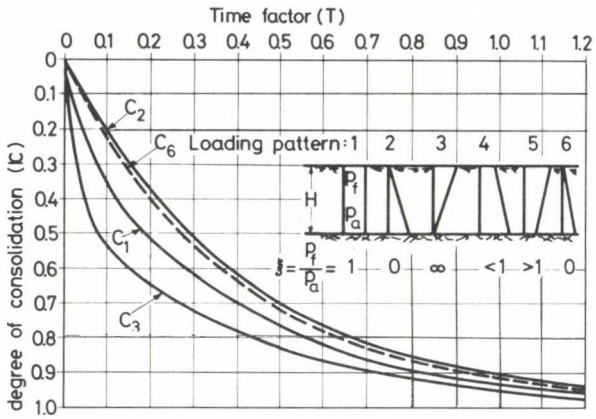

Fig. 3. Relationship between the time factor (T) and the degree of consolitadion (κ) in case of a unidimensional consolidation

Table 2. Determination of the final settlements (numerical example)

s_u (cm)	t_i (month): s_i (cm):	3 1.8	4.7 2.7	7.5 4.0	9.5 4.4	12 4.8	σ_α, σ_A	$C_{v\alpha}$, C_{vA}
6.0	$\alpha=$	24.0	21.4	17.6	18.6	19.0	2.58	0.128
6.6		27.3	25.4	22.1	22.4	23.5	2.20	0.091
6.8		27.3	26.1	22.1	23.8	25.5	2.05	0.082
7.0		30.0	27.6	24.2	24.7	26.7	2.34	0.088
7.2		31.6	27.7	25.0	26.8	28.2	2.42	0.087
6.0	$A=$	0.1189	0.1272	0.1465	0.1391	0.1341	0.0106	0.0799
6.8		0.1025	0.1076	0.1183	0.1096	0.1020	0.0066	0.0614
7.0		0.0991	0.1037	0.1130	0.1043	0.0965	0.0063	0.0611
7.2		0.0959	0.1000	0.1081	0.0994	0.0916	0.0061	0.0618

Let us assume further that the time series s_i measured at moments t_i (months) have passed since the beginning of the construction is as shown in Table 2. In the lines 3 to 7 of the same Table the α_i values are indicated as associated with $s_u = 6.6$ to 7.2 cm, their standard deviations and coefficients of variation. Accordingly, $s_u = 6.8$ cm may be considered as being the most probable value.

The *second method* is based on the fact that in the one dimensional case the second section of the curve may be approached by an exponential function. Thus, it may be rigthly expected, that the settlements can well be described with the expression

$$s = s_u(1 - e^{At}) .$$

Since neither this function can be linearized, one can proceed again in a way that one estimates again the value of s_u, whereafter, one calculates the A_i values belonging to the pairs of values t_i, s_i by the formula

$$A = -\frac{\ln(1 - s/s_u)}{t} .$$

Then, the corresponding coefficients of variation associated with the different s'_us, that settlement should be accepted at which C_v = minimum.

According to the data entered in the lines 8 to 11 of Table 2 the most probable value is $s_u = 7.0$ cm agreeing well with the value found by the first method.

With the knowledge of s_u and A, the settlement corresponding to an optional t_i or the time associated with the consolidation degree, κ might be determined. With their help also the reliability of the calculation might be characterized; thus, for example, in the case of the second method the measured settlements (s_m) and the calculated ones (s_c) constitute the following pairs of values:

Table 3.

s_m	1.80	2.70	4.00	4.40	4.80
s_c	1.86	2.68	3.76	4.36	4.96

Accordingly, the correlation coefficient is $r = 0.993$, and the residual standard deviation only $\sigma_r = 0.15$ cm.

2.2. Control of the calculation models

A great number of authors have dealt with the comparison of the calculated and measured values, weighing the reliability of the individual elements (limiting depth, etc.).

Several of the investigations were related to the settlement of buildings standing on *sand* where the deformation behaviour of the soil has been determined, in most cases, by using penetrometers.

Wu (1974) determined, from several data taken from the literature on the subject, the ratio of the calculated and measured settlements $\mu = s_c/s_m$, then, their distribution function. He considered the settlement to be identical with the ratio $s_c = q/q_c$, wherein q is the contact pressure and q_c may be calculated with the aid of the formula taking the shape

$$q_c = 0.36(N-3)\left(\frac{B+1}{2B}\right)^2,$$

recommended by Terzaghi and Peck (1948), and means the pressure causing a settlement of max. 1 inch. (The symbol N designates the number of blows needed to 30 cm penetration in performing the standard penetration test, B meaning the width of the footing in feet.)

On the basis of the distribution functions an estimation may be made for the probability, that the settlement does not surpass the *threshold value* preliminarily

defined. The curves also show that the formula has rather a conservative nature, involving about a threefold safety.

Schultze and Sherif (1973) took another step: they tried to find a new relationship having a more general value between N and s. They determined their formula with the aid of the methods of the mathematical statistics insofar as they,

a) calculated the values of the four constants from a multivariable correlation;

b) considered the fifth one — treating it as a *random number* — identical with the value giving r_{max};

c) characterized the *reliability* of the formula by a statistical parameter.

The eventual form of the formula is

$$s\,(\text{cm}) = \frac{p \cdot f}{1.71 N^{0,87} \sqrt{B}} \frac{1}{(1+0.4t/B)}$$

wherein:

p = one hundredth of a whole contact pressure in kN/m^2;
f = influence factor for the settlements;
B (cm) = width of footing;
t (cm) = depth of footing.

From Fig. 4 representing the ratio s_c/s_m it may be stated that the error in prediction is, in most cases, less than 40 per cent. (The value of the multiple correlation coefficient was 0.938!)

According to formula s linearly varying with p which means that the subgrade coefficient of the soil is not a function of the contact pressure.

In investigating the standard deviation one should endeavour to differentiate the values μ with respect to the physical or other characteristics. The evaluation of the settlement of 105 footings situated on loess soil (Egri—Rétháti 1959, 1960) gave a good example. The high value obtained for $\bar{\mu}$ (higher than 4.3), referring to the oedometric

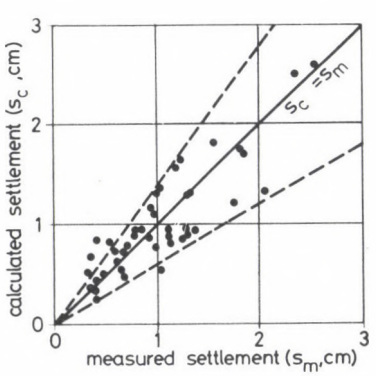

Fig. 4. Comparison of the settlements calculated from the standard penetration test and those actually measured (Schultze–Sherif 1973)

test, gave an unreal value to the loess and, at the same time it has been recognized that the highest values are associated with the footings of *large surfaces* (Fig. 5). This phenomenon shows, among others, that the *limiting value of the depth* (m_0) of the vertical stresses is the lower than that assumed, the larger the surface of the footing is. This fact has been convincingly justified by the investigations performed by Altes (1976)

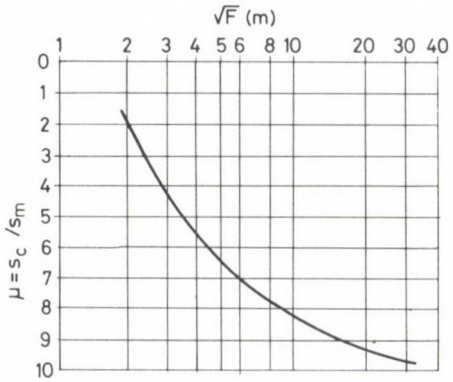

Fig. 5. Ratio of the settlement calculated on the basis of oedometric investigation of foundations supported by macroporous loess and the settlements measured in dependence on the square root of the contact area (Egri—Rétháti 1959, 1960)

who elaborated the results of 132 measurements. His empirical formula established by *multivariable correlation* written in the form was $m_0/B = f(p, F, E_s, B/L)$ where, besides the designations used so far, B and L and F are the shorter and the longer sides and the surface of the foundation body, respectively. (The multiple correlation coefficient was 0.82.)

From the diagrams plotted for the different F and E_s values (Fig. 6), the following may be stated:

a) the limiting value of the depth decreases with the increase of E_s;

b) the ratio m_o/B decreases with the increase of B;

c) the limiting depth defined by the condition $\sigma_z = 0.2z\gamma$ differs the more from the value calculated with the formula, the more prolate is the foundation body and the *larger* is its surface.

Schultze and Sievering (1977) compared *different methods of settlement calculations*, taking as a base the settlements of 148 buildings. The moduli of compressibility have been determined by static or dynamic soundings or by oedometric tests. The limiting value of the depth has been assumed to be identical with the width B in case of strip foundation and with the double of B in case of isolated foundation. The settlements were calculated using ten different methods. In the first three cases E_s = constant has been assumed and the influence factor for the settlement has been taken as the following combination of Fröhlich's concentration coefficient (ν) and of Poisson's ratio (μ): $\nu = 3$, $\mu = 0$; $\nu = 5$, $\mu = 0$; $\nu = 3$, $\mu = 0.3$. The three other cases

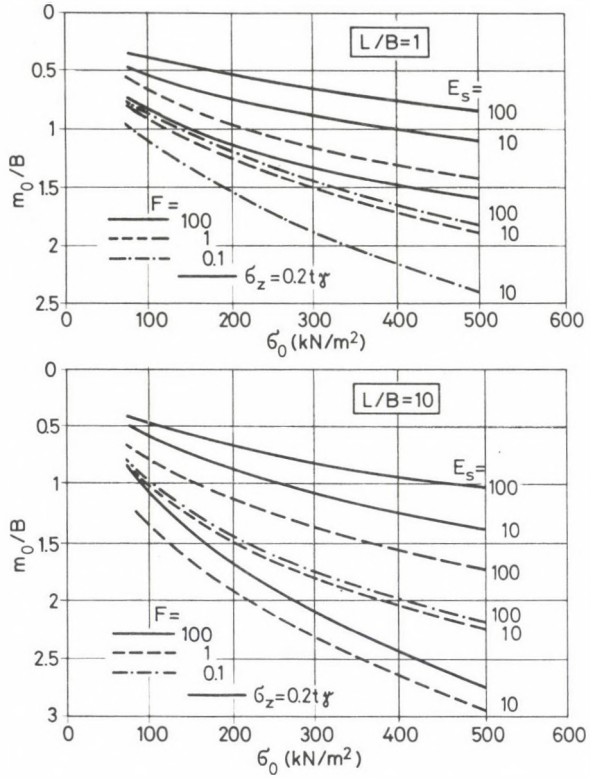

Fig. 6. The limiting depth (m_0) of the vertical stresses depending on the contact pressure (σ_0), the contact area (F, m^2) and the ration of edges L/B (Altes, 1976)

differ from the above ones, in that E_s has been assumed to be linearly variable with the depth. The formulae used to calculation 7 to 10 are as follows:

$$s = 3.5 \frac{pR_H}{E_s},$$

$$s = \frac{L \cdot B \cdot p}{E_s(L+B)},$$

$$s = 2.3 \frac{p}{2E_s(L-B)} \log \frac{2B+z}{2E_s+z} \frac{L}{B},$$

$$s = \frac{0.6pB}{E_s}.$$

The mean values of the μ ratios of the calculated and measured settlements determined for the different methods of calculation varied between 0.55 and 3.71 (Table

Table 4. The mean values, standard deviation and the variational coefficients relating to the proportion of the real (measured) settlements and the calculated settlements, determined by different methods

Sign of the method of calculation	for all kinds of foundations			for plate foundations			for block foundations		
	$\bar{\mu}$	σ_μ	C_v	$\bar{\mu}$	σ_μ	C_v	$\bar{\mu}$	σ_μ	C_v
1	1.82	1.43	0.79	1.99	1.54	0.78	1.51	0.79	0.52
2	2.16	1.66	0.77	2.28	1.78	0.78	2.07	1.05	0.51
3	1.49	1.15	0.77	1.60	1.24	0.78	1.31	0.69	0.52
4	1.41	1.12	0.79	1.56	1.21	0.77	1.05	0.52	0.50
5	1.63	1.27	0.78	1.78	1.37	0.77	1.36	0.66	0.49
6	1.13	0.89	0.78	1.24	0.96	0.77	0.89	0.44	0.50
7	3.71	3.37	0.91	4.30	3.64	0.85	2.05	1.05	0.51
8	1.70	1.45	0.85	1.92	1.58	0.82	1.06	0.49	0.46
9	0.55	0.49	0.90	0.64	0.53	0.82	0.35	0.16	0.46
10	2.02	1.75	0.87	2.31	1.90	0.82	1.27	0.59	0.46

4). Within each group, the values μ follow Poisson distribution, and in case of isolated foundations, a normal distribution. By separating the foundation bodies according to their types, the dispersion decreases. For the relationships

$$s_m = a + bs_c$$

established to the measured and calculated settlements, the correlation coefficient is $r = 0.81$ to 0.87, and since $a \sim 0$ to every method of calculation a *coefficient of correction* may be coordinated (see the Table).

2.3. Subsequent determination of the modulus of compression

The method of calculation should be selected by taking the *soil conditions* and the *method of measurement of the settlement* into account. This latter may be realized by a) continuous instrumental measurements or b) a single leveling of an originally horizontal structural part. In the following a few examples are shown to demonstrate the calculation methodology (Rétháti 1977, 1980, 1981).

a) Homogeneous stratification

In case where the *load and the surface of the foundations are identical*, one proceeds as follows. The mean settlement measured on 21 pillars of a hall was $\bar{s} = 27.0$ mm and the standard deviation $\sigma = 4.22$ mm. Therefore, the confidence limits for the settlement were (at a probability level of $\alpha = 0.05$)

$$s = 27 \pm 2.086 \frac{4.22}{\sqrt{20}} = 27 \pm 1.92 \text{ (mm)}$$

and for the modulus of compressibility:

$$\frac{F}{27+1.92} \leqq E_s \leqq \frac{F}{27-1.92},$$

wherein F is the area of the stress diagram. By replacing the numerical values into the above inequality, the following statement may be made: the probability that the value of E_s falls between 10.3 and 11.9 MN/m^2 is 95 per cent.

In case of foundations of different loadings and/or surfaces one may proceed according to one of the following two methods.

1. To each footing the values of E_s should be calculated, and their mean value *characterized by the standard deviation.*

2. A *correlation* should be established between F and s (see later).

b) One of the strata is of high compressibility

In this case, the settlement should be brought into relation with the stresses rising in the layer in question, and the deformation of the other layers are to be neglected. The run of the calculation depends on *how many equations* could be written down to E_s.

The strip foundations of the damaged building to be seen in Fig. 7, are 0.45 m wide and transfer a load of 146 kN/m. They are lying at the sections along cellars on sand and at other sections on turfary clay ($\bar{w}=53$ per cent, $w_p=38$ per cent). According to the leveling $\Delta s=2.7$ cm, and so accordingly,

$$E_s = \frac{F}{s} \cong \frac{F}{\Delta s} = \frac{0.0848}{0.027} = 3.14 \text{ MN/m}^2.$$

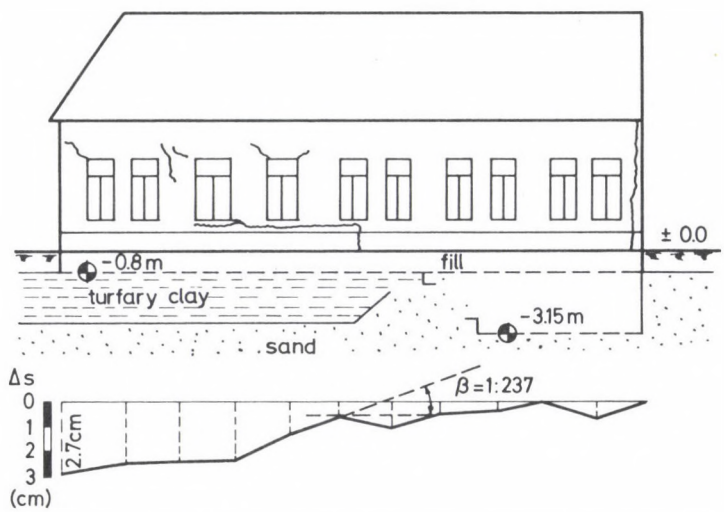

Fig. 7. Subsequent determination of the modulus of compression from the deformed line of footing in case of a single compressible layer

In Fig. 8 the schematic boring profiles around a building which suffered a significant settlement ($\Delta s = 15$ cm) are depicted. The abandoned bed of the Danube has been buried with fine grained sand in which peat veins have been located. With the aid of levelling of the footing one can coordinate to each bore profile a relative settlement

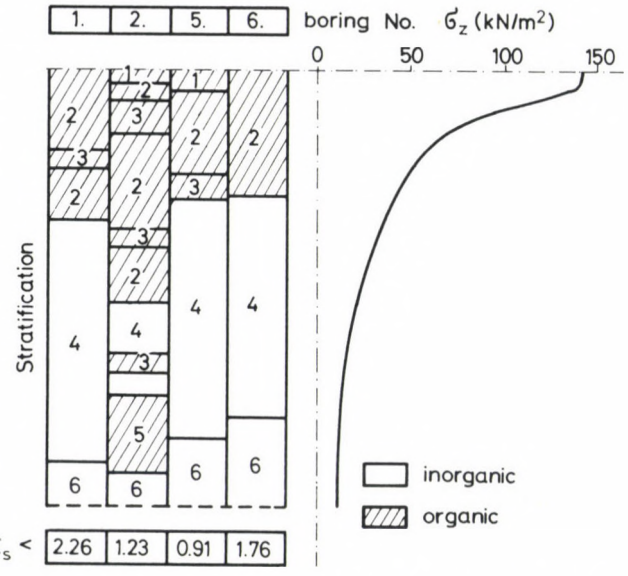

Fig. 8. Subsequent determination of E_s from the relative settlements with the knowledge of four bore profiles and Δs-values

Δs and to them, by summing up the areas of the stress diagrams associated with the organic layers, an F-value:

Table 5.

Boring	F (kN/mm)	Δs (mm)	$F/\Delta s$
1.	135.4	60	2.26
2.	184.1	150	1.23
3.	109.7	120	0.91
4.	105.6	60	1.67

The equation of the regression line obtained for the two variables is

$$\Delta s = 0.792\ F - 8.4 \qquad (r = 0.64)\,.$$

From the intercept, $(-8, 4)$ it can be stated with a probability of 90 per cent that it *does not significantly differ from zero*, wherefore $\Delta s \sim s$, i.e., the ratios $F/\Delta s$ may be considered

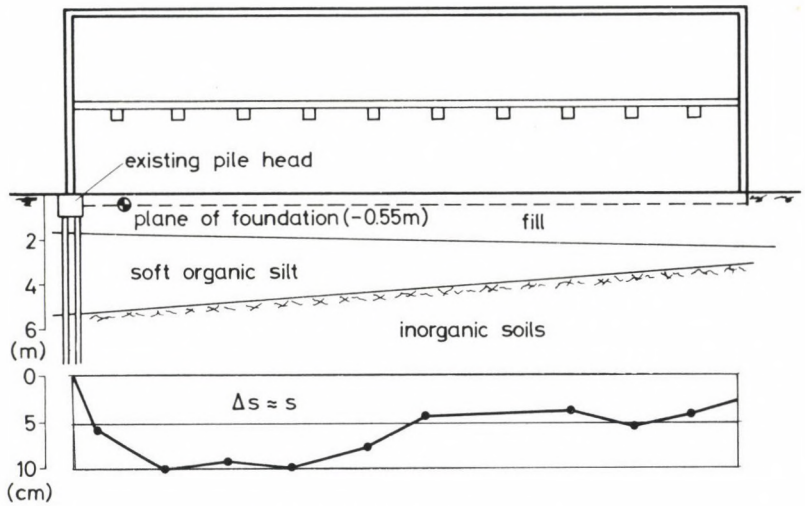

Fig. 9. Subsoil conditions under a hall and the relative settlements measured on the pillars

the E_s values of the organic layers. The average value and standard deviation obtained for the four borings are respectively:

$$\bar{E}_s = 1.54 \text{ MN/m}^2 \qquad \text{and} \qquad \sigma_E = 0.59 \text{ MN/m}^2.$$

The reciprocal of the slope of the regression line is 1.26, which is identical with the E_s defined with the aid of the method of least squares.

c) Two or more compressible layers

In this case we can look for answers to two questions:

— which layer had a decisive effect in producing settlements (damages)?

— what a modulus of compressibility characterizes these layers?

In selecting the calculation model *two examples* will be seen.

The band foundation supporting 12 pillars and the floor beams of a hall were broken off in about a year after construction and in the partition walls rather wide cracks presented themselves. The band foundation ($B = 0.50$ m, $q = 100$ kN/m^2) had been connected at one side to an old pile head, under the further sections of the foundation sandy brick bat fill of 1.2 to 1.8 m thickness is to be found, which lies on an organic clay layer of 0.8 to 3.8 m thickness (Fig. 9). The physical characteristics of the latter are: $w = 76$ per cent, $w_p = 42$ per cent, $I_{om} = 11$ per cent.

The relative settlements of the pillars, the thickness of the fill and organic clay layer as well as the areas of the corresponding parts of the stress diagram are represented in Table 6. The equality $\Delta s \approx s$ wants to express that the pile head supporting the pillar No. 1 is assumed to be immovable.

Table 6. Relative settlements of the pillars of a hall (Δs, mm), the thickness of the fill and the organic layer (v_1 and v_2, m) and the area of the sections of the stress diagram (F_1 and F_2, kN/mm)

Sign of the pillar	1	2	3	4	5	6	7	8	9	10
$\Delta s \approx s$	107	98	103	82	42	41	49	56	41	30
v_1	1.3	1.35	1.35	1.35	1.4	1.4	1.45	1.5	1.55	1.6
v_2	3.1	2.85	2.6	2.4	1.95	1.7	1.45	1.15	0.9	0.8
F_1	58.7	59.7	59.7	59.7	60.7	60.7	61.7	62.7	63.7	64.7
F_2	37.2	34.7	32.8	31.1	26.6	23.6	20.6	16.7	13.4	11.9

The behaviour of the two compressible layers may be investigated by *correlation calculation* where s is the dependent and F the independent variable. The equation of the regression line obtained for the fill is

$$s = -12.1\ F_1 + 806 \qquad (r = -0.80)\,.$$

The negative sign of the correlation coefficient (r) shows that the settlement difference is not generated by the deformation of the fill. (Δs and F change their values in an opposed sense!)

The equation of the regression line found for the *organic material* is

$$s = 2.85\ F_2 - 5.9\,,$$

and $r = 0.88$ which indicates a *very close connection.* (Let us consider that the heterogeneity of the layer, the restricted accuracy of the measurement, the marking of the bound of the layers all constitute sources of errors.) From the intercept ($b = -5.9$) it can be proved than this does not differ significantly from zero, thus, the assumption $\Delta s \approx s$ is real.

The connection v_2, s is also as close as the above one ($r = 0.90$) where v_2 is the thickness of the organic layer.

The *modulus of compressibility* of the organic layer may be calculated using three different methods.

1. *As an inverse of the slope*:

$$E_{s2} = 1/2.85 = 0.35\ \mathrm{MN/m^2}\,.$$

2. *As the average value* of the quotients $E_{s2} = F_2/\Delta s$ calculated separately for each pillar:

$$\overline{E_{s2}} = 0.40 \pm 0.112\ \mathrm{MN/m^2}\,.$$

3. *By analysing the standard deviation, namely, in the following way.* By definitely assuming the quotient of the moduli of compressibility of the two layers $\alpha = E_{s1}/E_{s2}$, at each measuring point a value of E_{s2} may be calculated. The mean of the 10 values ($\bar{E}_{s2}$)

and their standard deviation (σ_E) should be determined and a coefficient of variation

$$C_v = \frac{\sigma_E}{\bar{E}_{s2}}$$

to the given α should be coordinated. By varying the value of α, the parameters investigated take up the following values

Table 7. Mean values, dispersions and coefficients of variation of the ratios of settlements calculated with the aid of different methods and the actual (measured) ones

α	$\bar{E}_{s2}$	σ_E	C_v	E_{s1}
2	0.98	0.30	0.309	1.97
3	0.79	0.23	0.294	2.37
4	0.69	0.19	0.280	2.77
5	0.63	0.17	0.273	3.17
10	0.52	0.13	0.258	5.20
∞	0.41	0.11	0.265	∞

It is a justifiable assumption that the real value E_{s2} is approximated most closely by $\bar{E}_{s2}$ at which C_v = minimum. According to the Table this extreme value exists, and falls between $\alpha = 10$ and $\alpha \to \infty$. This means that

$$0.41 < E_s < 0.52 \qquad (\mathrm{MN/m^2}).$$

The *second example* contains such an instance where the building tilted as a stiff body.

In the second month subsequent to finishing the panel-mounting of a 10-story building it was discovered that the lift shaft was tilted to 12 cm in comparison to the vertical line. It was found by the borings made at the proximities of the four corners of the building, that under the *raft foundation* a *fill* of 0.15 to 1.35 m thickness existed with silt and a layer of sand, 2.5 to 3.0 thick under it (Fig. 10). The fill consists of fine sand, slack and rubble of very loose structure. The void ratio of the silt was $e = 0.80$ to 0.92 which also denotes loose layers.

From the *angles of inclination* determined for the edges of the building the relative settlements (Δs, mm) may be calculated. From the boring profiles the thicknesses v_1 and v_2 of the fill and silt respectively, as well as the partial areas F_1 and F_2 (kN/mm) of the diagram of the vertical stresses may be defined. The values coordinated may be summarized in the following table.

Table 8.

Borings	Δs	v_1	v_2	F_1	F_2
3.	0	1.35	0	224.1	0
4.	24.3	0.15	1.75	24.9	290.5
2.	87.9	0.30	2.85	49.8	473.1
1.	124.8	0.90	3.20	149.4	531.2

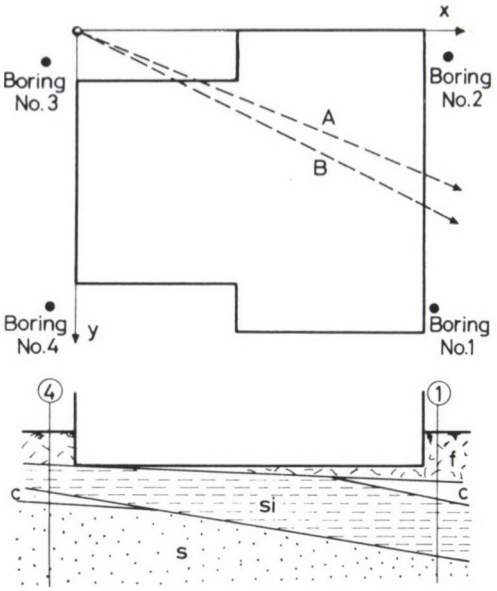

Fig. 10. Tilt direction of a panel building determined by a measuring instrument (*A*) and calculated from the thickness of the compressible layer (in the profile of stratification: *f* — fill, *c* — clay, *si* — silt, *s* — sand

The influence of the two loose layers on the development of the tilt may be determined by a *correlation calculation.* The equation of the regression line obtained for the fill is

$$\Delta s = -0.115\ F_1 + 72.2\,,$$

and the correlation coefficient $r = -0.19$. The negative sign cannot be defined from a physical point of view, consequently, the fill *did not play any part* in the development of the tilt.

The equation of the regression line for the *silt* is

$$\Delta s = 0.233\ F_2 - 13.0\,,$$

and the correlation coefficient $r = 0.93$. This extraordinarily high value unequivocally proves that the damaging degree of the tilt is the consequence of the *uneven thickness of the silt.*

Thereafter, the question arises whether the differences in the thicknesses of the silt can define with what accuracy the principal direction of the tilt. The investigation may be carried out with the aid of a *tervariable correlation.* In construing the horizontal coordinates x and y according to Fig. 10, the following equation will be obtained for the regression plane:

$$v_2 = 0.1169x + 0.0611y + 0.348\,.$$

If $v_2 = 0$, so

$$y = -1.915x - 5.704\,,$$

which is the equation of the line of intersection of the plane placed on the values v_2 and the plane x, y. The negative reciprocal of the slope of the straight line is $m' = 0.5223$, therefore, the angle of inclination of the plane v_2 is

$$\alpha = \arctan 0.5223 = 27.6^\circ\,.$$

Since, according to the surveys, the principal direction of the inclination subtends an angle 23.3° with the x-axis, it can be stated that the *change in the thickness of the layer defines very accurately the angle of inclination of the building.*

This example shows that the direction and degree of the tilt to be expected may be calculated with a good approximation even in the *designing phase.* The mathematical statistics not only give the expected value of these parameters but also the standard deviation, i.e., the *accuracy of the prediction.*

2.4. Geometric evaluation of the tilt

In case where the system of foundation or the superstructure is properly stiff, also the entity of the building behaves as a rigid body. However, if at the same time the load attacking the foundation is not centric or the stratification is not uniform, the deformation of the soil may cause the tilt of the building. (To this effect, according to Chapter *1* it is sufficient that the soil is "at random" heterogeneous.)

This type of movement — besides being from the point of view of appearance undesirable — might endanger the stability and functional utilization of the building. To form an opinion of this, one should know the geometric characteristics of the movement both for the *momentary* and *consolidated* state.

The settlements s_i determine a plane, the equation of which may be established with the aid of a tervariable correlation. The *principal direction of the tilt* is perpendicular to the line of intersection of the plane mentioned above and that defined by x, y. (The progress of calculation is identical with the procedure followed in connection with the numerical example of Chapter *2.3.*) The angle formed by the system of the straight lines parallel to the principal direction of the tilt is identical with the *angular displacement* of the vertical axis of the building. From the entire course of the movement one can obtain a comprehensive concept by plotting the angle of the direction of tilt formed by the axis x (or y) as well as the angular displacement of the vertical axis in the very same system of coordinates *in dependence on time.*

An example relating to a silo is represented in Fig. 11. It may be well observed that the silo under the effect of the *dead weight* tilted towards the machine tower, thereafter, simultaneously with the sudden application of the *payload,* in the opposite direction. A significant increase of the angle of inclination took place at the very same period.

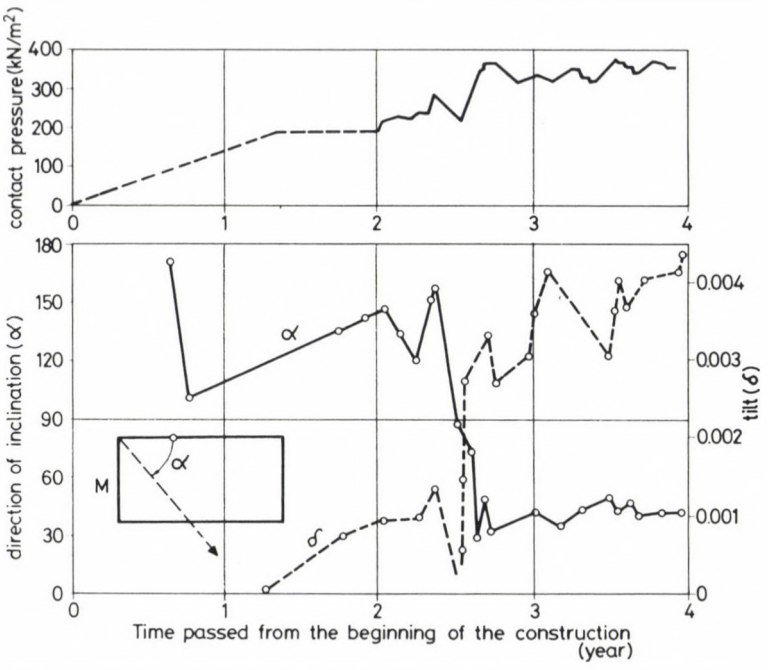

Fig. 11. Change in the tilt direction and angle of inclination depending on the nature and magnitude of the loading (*M* — place of the machine tower)

Since the correlation calculation also checks the degree of linearity it also gives information on the fact whether the building is tilted as a rigid body or not. The answer might be obtained for this question by the comparison of the residual standard deviation and the accuracy of the measurement.

References

1. Altes, J.: Die Grenztiefe bei Setzungsberechnungen — *Bauingenieur* (1976), No. 3
2. Egri, Gy.—Rétháti, L.: Statistical Elaboration of the Settlement Measurements of the Institute for Geodesy and Geotechnics — *Mélyépítéstudományi Szemle* (1959), No. 1–2*
3. Egri, Gy.—Rétháti, L.: Conclusions drawn from the measurements of settlements — *Mélyépítéstudományi Szemle* (1960), No. 6*
4. Leussink, H.: Über die Gleichmässigkeit von Bauwerksetzungen — *Vorträge der Baugrundtagung*, Hamburg (1954)
5. Resendiz, D.—Herrera, I.: A probabilistic Formulation of Settlement-controlled Design — *Proc. of the 7th Int. Conf. on Soil Mech. and Found. Eng.*, Vol. 2., Mexico (1969)
6. Rétháti, L.: Up-to-date Criterions of Settlements — *Mélyépítéstudományi Szemle* (1968), No. 8–9*
7. Rétháti, L.: Planning of Plane Foundations — *Manual of Foundation* (Editor Rózsa L.) Műszaki Könyvkiadó, Budapest 1971*

* In Hungarian

8. Rétháti, L.: *Soil caused Building Damages.* Akadémiai Kiadó, Budapest 1977*
9. Rétháti, L.: Symmetrizing of Data Sequences of Asymmetric Distribution by Raising to Power. *Alkalmazott Matematikai Lapok* (1979), No. 3–4*
10. Rétháti, L.: Subsequent Comparative Analysis of the Deformation of Soil Layers — *Mélyépítéstudományi Szemle* (1980), No. 9*
11. Rétháti, L.: Analyse der Kippung von Gebäuden — *Proc. of the Int. Conf. on Found. Eng.'81 Vysoke Tatry.* Dom techniky ČSVTS, Košice
12. Schultze, E.—Sherif, G.: Prediction of Settlements from Evaluated Observation for Sand — *Proc. of the 8th Int. Conf. on Soil Mech. and Found. Eng.*, Vol. **1.3.**, Moscow 1973
13. Schultze, E.—Sievering, W.: Statistical Evaluation of Settlement Observations — *Proc. of the 9th Int. Conf. on Soil Mech. and Found. Eng.*, Vol. **1.**, Tokyo 1977
14. Skempton, A. W.—Macdonald, D. H.: The Allowable Settlement of Buildings — *Proc. of the Institute Civil Engineering*, **5.** (1956)
15. Terzaghi, K.—Peck, R. B.: *Soil Mechanics in Engineering Practice* — John Wiley and Sons, New York 1948
16. Wu, T. H.: Uncertainty, Safety and Decision in Soil Engineering — *Proc. of the ASCE* (1974), *No. GT3*

Acta Technica Academiae Scientiarum Hungaricae, 93 (3—4), pp. 311—318 (1981)

UPPER LIMIT FOR THE DYNAMIC TENSILE STIFFNESS OF A BAR OF VARYING CROSS SECTION

I. ECSEDI*

Cand. of Techn. Sci

[Manuscript received: 19 September, 1981]

A linearly elastic bar of isotropic material and varying cross section is treated. The verification of the inequality relation relating to the dynamic tensile stiffness of a bar of varying cross section and nonhomogeneous material decisively takes place by making use of the minimum property of Rayleigh's quotient and the Schwarz-inequality.

Notation

The following significant symbols are used in this paper:

x, y, z	orthogonal coordinates,
$\rho = \rho(z)$	density,
$E = E(z)$	Young's modulus of elasticity,
t	time,
ω	angular frequency of load,
l	length of bar,
$A = A(z)$	cross sectional area of bar
$\bar{w} = \bar{w}(z, t)$	axial displacement
$w = w(z)$	amplitude of axial displacement,
R	dynamic tensile rigidity of bar,
$H = 1/R$	dynamic tensile "flexibility" of bar,
α_1	*minimum* angular eigenfrequency of bar carrying out longitudinal vibration,
$b = b(z), f = f(z)$	auxiliary functions.

Other symbols and variables are constructed by the text.

1. Introduction

Figure 1 represents a bar of varying cross section. The planes of the cross sections of the bar are parallel to the plane xy and the axis of the bar is the z-axis of the system of coordinates.

The end cross section of the bar defined by the coordinate $z = l$ is submitted to a load $\bar{F} = F \cos \omega t$ harmonically varying with the time (Fig. 1).

* Dr. I. Ecsedi, Vászonfehérítő u. 24. H-3531 Miskolc, Hungary

The function of two variables $\bar{w} = \bar{w}(z, t)$ describing the displacements of the cross sections of the bar may be brought into relationship with the following boundary-value problem ([1], [2]):

$$\rho A \frac{\partial^2 \bar{w}}{\partial t^2} = \frac{\partial}{\partial z}\left(AE \frac{\partial \bar{w}}{\partial z}\right) \qquad \begin{matrix} 0 < z < l, \\ 0 < t < \infty, \end{matrix} \tag{1.1}$$

$$\bar{w}(0, t) = 0 \qquad 0 < t < \infty, \tag{1.2}$$

$$\left[AE \frac{\partial \bar{w}}{\partial z}\right]_{z=l} = F \cos \omega t, \qquad 0 < t < \infty. \tag{1.3}$$

By conveniently selecting the starting conditions

$$\bar{w}(z, 0) \qquad \text{and} \qquad \left(\frac{\partial \bar{w}}{\partial t}\right)_{t=0}$$

may be attained by the solution of the boundary value problem defined by Eqs (1.1), (1.2), (1.3) and is

$$\bar{w}(z, t) = w(z) \cos \omega t. \tag{1.4}$$

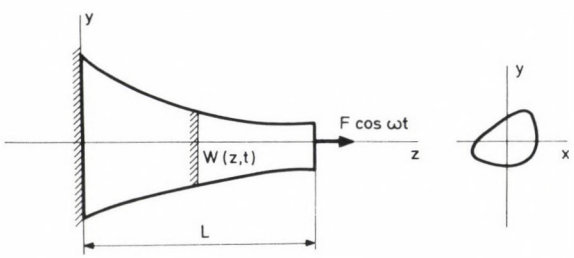

Fig. 1. Bar submitted to harmonic generating force

In connection with the angular frequency ω for the moment it is assumed that it does not agree with either of the angular eigenfrequencies α_i $(i = 1, 2, \ldots)$ associated with the free vibration of the bar represented in Fig. 1.

The solution of the form (1.4) describes the motion corresponding to the "steady state" condition associated with the harmonic generating force $\bar{F}$.

To the amplitude of displacement $w = w(z)$ $(0 \leqq z \leqq l)$, by replacing the solution of the form (1.4) into Eqs (1.), (1.2), (1.3) the following boundary value problem may be deduced:

$$\frac{\mathrm{d}}{\mathrm{d}z}\left(AE \frac{\mathrm{d}w}{\mathrm{d}z}\right) + \rho \omega^2 A w = 0, \qquad 0 < z < l, \tag{1.5}$$

$$w(0)=0\,, \tag{1.6}$$

$$\left[AE\frac{\mathrm{d}w}{\mathrm{d}z}\right]_{z=l} = F \tag{1.7}$$

Let us consider the function of one variable interpreted by the prescription

$$b(z) = \frac{w(z)}{F}\,. \tag{1.8}$$

This function may be determined by the solution of the boundary-value problem

$$\frac{\mathrm{d}}{\mathrm{d}z}\left(AE\frac{\mathrm{d}b}{\mathrm{d}z}\right) + \rho\omega^2 b = 0\,, \qquad 0<z<l\,, \tag{1.9}$$

$$b(0)=0\,, \tag{1.10}$$

$$\left(AE\frac{\mathrm{d}b}{\mathrm{d}z}\right)_{z=l} = 1\,. \tag{1.11}$$

From formula (1.8) it may be read that

$$F = \frac{1}{b(l)}\,w(l) \tag{1.12}$$

that is, the force amplitude F and the amplitude of the displacement $w(l)$ are proportionate to each other. The quantities defined by the prescription

$$R = \frac{1}{b(l)} = \frac{F}{w(l)} \tag{1.13}$$

is called *the dynamic tensile stiffness of the bar of variable cross section.*

The dynamic tensile "flexibility' is described by the formula

$$H = \frac{1}{R}\,. \tag{1.14}$$

From Eq. (1.14) it is easy to recognize that the value of R is the function of the material, length, form of the bar and that of the angular frequency ω, and it is also obvious that for the determination of the exact value of R, the boundary-value problem should be solved, defined by Eqs (1.9), (1.10), (1.11). However, the solution having a closed form of the ordinary differential equation (1.9) of variable coefficients, is very frequently unknown, wherefore, such inequality relationships which foster the estimate of the value of R have great significance.

The primary purpose of the present paper is the deduction of an inequality relationship with the application of which an *upper* limit might be determined for R, also without the knowledge of the solution of the boundary-value problem designated by Eqs (1.9), (1.10), (1.11).

In the following another formula will be deduced which is suitable for the calculation of the value $H = b(l)$.

On the basis of the Eq. (1.9) it might be written

$$b\frac{\mathrm{d}}{\mathrm{d}z}\left(AE\frac{\mathrm{d}b}{\mathrm{d}z}\right) + \omega^2\rho Ab^2 = \frac{\mathrm{d}}{\mathrm{d}z}\left(AEb\frac{\mathrm{d}b}{\mathrm{d}z}\right) -$$

$$- AE\left(\frac{\mathrm{d}b}{\mathrm{d}z}\right)^2 + \omega^2\rho Ab^2 = 0\,. \tag{1.15}$$

Integration of Eq. (15) yields

$$\int_0^l AE\left(\frac{\mathrm{d}b}{\mathrm{d}z}\right)^2 \mathrm{d}z - \omega^2 \int_0^l \rho Ab^2\,\mathrm{d}z = \left\{AEb\frac{\mathrm{d}b}{\mathrm{d}z}\right\}_{z=0}^{z=l}. \tag{1.16}$$

By combining Eq. (1.16), and formulae (1.14), (1.13) as well as boundary conditions (1.10), (1.11) the relationship

$$H = \int_0^l AE\left(\frac{\mathrm{d}b}{\mathrm{d}z}\right)^2 \mathrm{d}z - \omega^2 \int_0^l \rho Ab^2\,\mathrm{d}z \tag{1.17}$$

may be deduced.

By making use of the minimum-property of the Rayleigh-quotient it can be pointed out that H is positive, if

$$\omega^2 < \alpha_1^2\,.$$

As a consequence of the minimum-property of the Rayleigh-quotient the inequality

$$\alpha_1^2 \leqq \frac{\displaystyle\int_0^l AE\left(\frac{\mathrm{d}g}{\mathrm{d}z}\right)^2 \mathrm{d}z}{\displaystyle\int_0^l A\rho g^2\,\mathrm{d}z} \tag{1.18}$$

is valid for each of the functions of one variable, not being identically equal to zero,

satisfying the homogeneous boundary condition $g(0)=0$, and, which is continuous in the closed interval $0 \leqq z \leqq l$, and continuously differentiable by sections in the open interval $0<z<l$.

In the inequality relation (1.18) the sign of equality is only valid in case where $g=g(z)$ designates the eigenfunction of the bar associated with its minimum angular eigenfrequency α_1.

The immediate consequence of the inequality relation (1.18) is the inequality (1.19)

$$\int_0^l AE\left(\frac{\mathrm{d}g}{\mathrm{d}z}\right)^2 \mathrm{d}z - \omega^2 \int_0^l A\rho g^2 \,\mathrm{d}z > 0 \tag{1.19}$$

because $\omega^2 < \alpha_1^2$.

Consider $g=b(z)$. In this case, on the basis of (1.19) the following may be written

$$H = \int_0^l AE\left(\frac{\mathrm{d}b}{\mathrm{d}z}\right)^2 \mathrm{d}z - \omega^2 \int_0^l \rho A b^2 \,\mathrm{d}z > 0 \tag{1.20}$$

because

$$\left(AE\frac{\mathrm{d}b}{\mathrm{d}z}\right)_{z=l} \neq 0\,. \tag{1.21}$$

2. The upper limit

Theorem. We have $\omega^2 < \alpha_1^2$. Further let the function be $f=f(z)$ of one variable, satisfying the conditions

$$f(0)=0\,, \tag{2.1}$$

$$f(l)\neq 0\,, \tag{2.2}$$

continuous in the closed interval $0 \leqq z \leqq l$ and differentiable by sections in the open interval $0<z<l$. In this case it can be stated that the inequality relation

$$R \leqq \frac{\int_0^l AE\left(\frac{\mathrm{d}f}{\mathrm{d}z}\right)^2 \mathrm{d}z - \omega^2 \int_0^l \rho A f^2 \,\mathrm{d}z}{[f(l)]^2} \tag{2.3}$$

is valid.

Demonstration. Since

$$\int_0^l AE\left(\frac{\mathrm{d}g}{\mathrm{d}z}\right)^2 \mathrm{d}z - \omega^2 \int_0^l \rho A g^2 \,\mathrm{d}z > 0\,, \tag{2.4}$$

on the basis of the Schwarz-inequality may be written:

$$\left(\int_0^l AE\left(\frac{\mathrm{d}b}{\mathrm{d}z}\right)^2 \mathrm{d}z - \omega^2 \int_0^l \rho A b^2 \,\mathrm{d}z\right) \cdot \left(\int_0^l AE\left(\frac{\mathrm{d}f}{\mathrm{d}z}\right)^2 \mathrm{d}z - \omega^2 \int_0^l \rho A f^2 \,\mathrm{d}z\right) \geqq$$

$$\geqq \left\{\int_0^l AE \frac{\mathrm{d}b}{\mathrm{d}z}\frac{\mathrm{d}f}{\mathrm{d}z}\,\mathrm{d}z - \omega^2 \int_0^l \rho A b f \,\mathrm{d}z\right\}^2. \tag{2.5}$$

The integral entering on the right hand side of the Schwarz-inequality (2.5) should be transformed as follows:

$$\left\{\int_0^l AE \frac{\mathrm{d}b}{\mathrm{d}z}\frac{\mathrm{d}f}{\mathrm{d}z}\,\mathrm{d}z - \omega^2 \int_0^l \rho A b f \,\mathrm{d}z\right\}^2 = \left\{\left[f AE \frac{\mathrm{d}b}{\mathrm{d}z}\right]_{z=0}^{z=l} -\right.$$

$$\left. - \int_0^l \left[\frac{\mathrm{d}}{\mathrm{d}z}\left(AE\frac{\mathrm{d}b}{\mathrm{d}z}\right) + \omega^2 \rho A b\right] f \,\mathrm{d}z\right\}^2 = [f(l)]^2\,. \tag{2.6}$$

By combining the formula

$$R = \frac{1}{\displaystyle\int_0^l AE\left(\frac{\mathrm{d}b}{\mathrm{d}z}\right)^2 \mathrm{d}z - \omega^2 \int_0^l \rho A b^2 \,\mathrm{d}z} \tag{2.7}$$

and those (2.6) and (2.5) the inequality relation (2.3) is immediately obtained q.e.d.

3. Comments in connection with the dynamic tensile stiffness

3.1 The material, form and length of a bar having been given, the stiffness of it is only the function of the angular frequency ω of the loading, i.e.

$$R = R(\omega)^2 \tag{3.1}$$

The function $R = R(\omega)^2$ has a monoton property defined in the following theorem.

Theorem. Consider the inequality

$$\omega_1^2 < \omega_2^2 < \alpha_1^2 . \tag{3.2}$$

In this case it is stated that the inequality relation

$$R(\omega_1^2) \geqq R(\omega_1^2) \tag{3.3}$$

is valid.

Demonstration. The solution of the boundary-value problem defined by Eqs (1.9), (1.10), (1.11) should be designated by $b_i = b_i(z)$, if $\omega = \omega_i$. On the basis of the inequality relation (2.3) may be written as

$$R(\omega_2^2) \leqq \frac{\int_0^l AE\left(\frac{\mathrm{d}b_1}{\mathrm{d}z}\right)^2 \mathrm{d}z - \omega_2^2 \int \rho A b_1^2 \,\mathrm{d}z}{[b_1(l)]^2} . \tag{3.4}$$

The expression entering on the right-hand side of the inquality relation (3.4) is transformed as follows:

$$\frac{\int_0^l AE\left(\frac{\mathrm{d}b_1}{\mathrm{d}z}\right)^2 \mathrm{d}z - \omega_2^2 \int_0^l \rho A b_1^2 \,\mathrm{d}z}{[b_1(l)]^2} =$$

$$= \frac{\int_0^l AE\left(\frac{\mathrm{d}b_1}{\mathrm{d}z}\right)^2 \mathrm{d}z - \omega_1^2 \int_0^l \rho A b_1^2 \,\mathrm{d}z}{[b_1(l)]^2} - (\omega_2^2 - \omega_1^2) \frac{\int_0^l \rho A b_1^2 \,\mathrm{d}z}{[b_1(l)]^2} . \tag{3.5}$$

From Eq. (3.5) the following might be read:

$$\frac{\int_0^l AE\left(\frac{\mathrm{d}b_1}{\mathrm{d}z}\right)^2 \mathrm{d}z - \omega_2^2 \int_0^l \rho A b_1^2 \,\mathrm{d}z}{[b_1(l)]^2} \leqq$$

$$\leqq \frac{\int_0^l AE\left(\frac{\mathrm{d}b_1}{\mathrm{d}z}\right)^2 \mathrm{d}z - \omega_1^2 \int_0^l \rho A b_1^2 \,\mathrm{d}z}{[b_1(l)]^2} = R(\omega_1)^2 , \tag{3.6}$$

$$(\omega_1^2 < \omega_2^2) .$$

Combination of inequalities (3.4) and (3.6) resulted in the inequality relation (3.3) q.e.d.

3.2 Substitution of $\omega^2 = 0$ yields the static tensile stiffness S:

$$S = R(0). \tag{3.7}$$

Be $\omega^2 < \alpha_1^2$. In this case, on the basis of the inequality relation proved above, it may be written that

$$R(\omega^2) < S. \tag{3.8}$$

4. Some examples to the formation of the upper limit

4.1 The solution of the boundary-value problem (1.9), (1.10), (1.11) is, in case of $\omega^2 = 0$, the function

$$b(z) = \int_0^l \frac{\mathrm{d}\zeta}{A(\zeta)E(\zeta)}. \tag{4.1}$$

By elementary calculation we have

$$S = R(0) = \frac{1}{b(l)} = \frac{1}{\displaystyle\int_0^l \frac{\mathrm{d}\zeta}{A(\zeta)E(\zeta)}}. \tag{4.2}$$

Combination of the inequality relation (3.8) and formula (4.2) results in

$$R(\omega^2) \leqq \frac{1}{\displaystyle\int_0^l \frac{\mathrm{d}\zeta}{A(\zeta)E(\zeta)}}, \qquad (\omega^2 < \alpha^2). \tag{4.3}$$

4.2 By calculating with the function of the form

$$f(z) = z \tag{4.4}$$

one obtains an upper limit of rather simple structure for the value R:

$$R(\omega^2) \leqq \frac{1}{l^2}\left(\int_0^l AE\,\mathrm{d}z - \omega^2 \int_0^l \rho A z^2\,\mathrm{d}z\right). \tag{4.5}$$

References

1. Кин, Н. Тонг.: Теория механических Колебаний. Москва. Наука. 1963. смр. 219
2. Бабаков, И. М.: Теория колебаний. 2-е изд. Москва. Наука. 1965. стр. 233—253.

Acta Technica Academiae Scientiarum Hungaricae, 93 (3—4), pp. 319—330 (1981)

A SUBOPTIMAL SOLUTION FOR THE ALLOCATION OF CONTROLLERS IN DISTRIBUTION NETS

D. SINGER*

[Manuscript received: 2 March, 1982]

An algorithm is given for the suboptimal allocation of controllers based on graph theoretic considerations and on the theory of Kirchhoffian nets. A short description of the computer program followed by some considerations concerning the applicability of the method is presented.

1. Introduction

In the last decades, an augmented interest is directed to the problem of decentralized control of large electric, gas, water, etc. distribution nets. It is evident that for such systems dislocated on large area, the decentralized control with autonomous controllers is the most appropriate solution, avoiding central processing with long communication lines. As a typical example, Fig. 1 schematically shows the pressure control of a gas distribution net. The low pressure net is fed through pressure reduction valves (direct acting pressure controllers) from a higher pressure net.

The following questions can be asked:

— how good is the control of the net by a given number and location of controllers?

— how many controllers are needed to reach a prescribed control quality for the total net?

— how can the controllers be optimally allocated, if their numbers are given?

The solution of the first problem is relative straightforward and belongs methodically to the problem of network analysis. There are very effective programs able to analyse stationary nonlinear nets with several thousand branches, see e.g. [6], [7]. The problem of the optimal number of controllers is not free from economical considerations. Augmenting the number of controllers, generally augments the dimensions of the feeding (high potential) net and following this the needed investitions.

The problem together with that mentioned last, can be viewed as a set-covering problem and can be solved, if not otherwise, by direct enumeration [1], [4], [5]. Little information is available for effective methods to solve such large scale problems.

Our paper deals with the last problem, the optimal allocation of n decentralized controllers and is interested in solving the problem for large nets. The given solution is

* Computer and Automation Institute, Hungarian Academy of Sciences, 1502-Budapest, Kende u. 13—17 Hungary.

based on graph theoretical considerations and on some circumstances concerning real nets.

The considerations can be divided into two parts. In the first, a theoretic justification of the solution algorithm, especially for the simplifications made, are given. The second part gives a description of the algorithm.

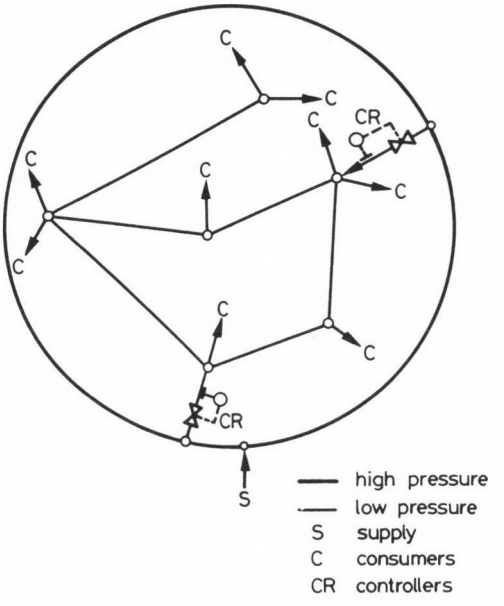

Fig. 1

2. The state equation and the quality index of the net control

In the first instance, a definition of the control quality of the net must be given.

Definition: The quality index Q of the net control is the mean square deviation of all load node potentials after disturbing the net simultaneously in all load nodes by unit changes of the load currents.

Remark: The nodes of the net are divided into load nodes, source nodes and control nodes. The last two are distinguished as we do not exclude the possibility of existing source nodes without control.

We assume that the controllers stabilizing the potentials in the source nodes work ideally. This means that the control deviations can be neglected and time processes are much more rapid than those of the uncontrolled system. The problem of expressing the control quality Q with the state equation of the net is, therefore, a stationary one.

The optimal allocation of the decentralized controllers can be stated as the unconstrained optimization problem

$$Q = \Delta \boldsymbol{e}^t \Delta \boldsymbol{e} \rightarrow \min \tag{1}$$

where $\Delta \boldsymbol{e}$ is the vector of the node potential changes in the case of unit current changes. Assuming that the changes $\Delta \boldsymbol{e}$ are small and the controllers work as assumed ideally, $\Delta \boldsymbol{e}$ depends only on the allocation of the controllers.

An ideal controller of the source potential can be considered as a constant branch source potential V located in a *virtual* branch of very low impedance connected between the control node and a basis node to which the node potential is related. (The virtual branch has a very low impedance to avoid variable pressure drops due flow changes.) The control scheme in Fig. 1 can be transformed, in this manner, to a pure Kirchhoffian network. Figure 2. In this substitution scheme the high potential net is reduced to the basis point B.

For the substitution scheme, the following equations are valid:

$$\begin{aligned} &\mathbf{A}\boldsymbol{i} = \mathbf{0}\,, \\ &\boldsymbol{v} = \mathbf{A}^t \boldsymbol{e} \\ &\boldsymbol{i} = \mathbf{G}(v)\boldsymbol{V} + \boldsymbol{I}' - \mathbf{G}(v)\boldsymbol{V} \end{aligned} \tag{2}$$

where $\boldsymbol{e} \in R^n$ is the vector of node potentials, $\boldsymbol{i}$, $\boldsymbol{v} \in R^b$ are the branch current and potential drop vectors, respectively. $\boldsymbol{I}'$ and $\boldsymbol{V} \in R^b$ are the branch source current and

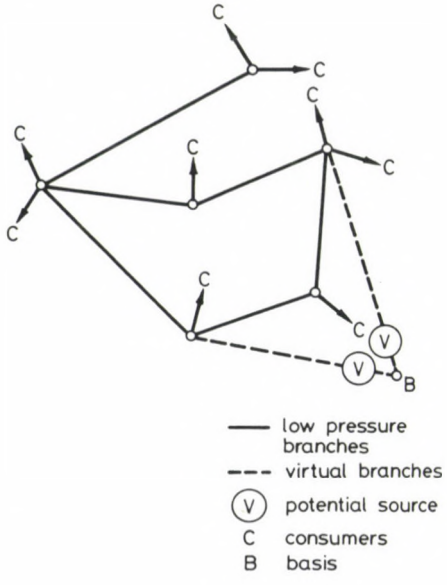

Fig. 2

branch source potential vectors, $\mathbf{G}(v) \in R^{b \times b}$, is the conductance matrix of the substitution scheme, $\mathbf{A} \in R^{n \times b}$ is its incidence matrix. The elements a_{ij} of $\mathbf{A}$ are

$$a_{ij} = \begin{cases} 1 & \text{if current } i_j \text{ emerges from the node with index } i \\ -1 & \text{if current } i_j \text{ enters node } i \\ 0 & \text{if current } i_j \text{ is not incident to node } i. \end{cases}$$

n is the number of nodes without the basis node, b the number of branches. If we denote with n' and b' the number of nodes and branches of the original net, the appropriate numbers for the substitution scheme are $n = n'$, $b = b' + r$, r is the number of the controllers.

The first of the equations (2) is the expression of Kirchhoff's current law. The second is the constitutive relation of all branches. The third expresses the relation between node and branch potentials. Equations (2) can be combined to relation [3]:

$$\boldsymbol{e} = -[\mathbf{A}\mathbf{G}(v)\mathbf{A}^t]^{-1}[\mathbf{A}\boldsymbol{I}' - \mathbf{A}\mathbf{G}(v)\boldsymbol{V}] \tag{3}$$

As can be easily verified

$$\mathbf{A}\boldsymbol{I}' = \boldsymbol{I}$$

where $\boldsymbol{I} \in R^b$ is the vector of node source currents. Therefore,

$$\boldsymbol{e} = -[\mathbf{A}\mathbf{G}(v)\mathbf{A}^t]^{-1}[\boldsymbol{I} - \mathbf{A}\mathbf{G}(v)\boldsymbol{V}] \tag{4}$$

The change of the node potentials by a small change of $\Delta\boldsymbol{I}$ is:

$$\Delta\boldsymbol{e} = -[\mathbf{A}\mathbf{G}(v)\mathbf{A}^t]^{-1}\Delta\boldsymbol{I} \tag{5}$$

According to (1) and (5), the quality index of the net control will be

$$Q = \Delta\boldsymbol{e}^t\Delta\boldsymbol{e} = \Delta\boldsymbol{I}^t[\mathbf{A}\mathbf{G}(v)\mathbf{A}^t]^{-1}\mathbf{A}\mathbf{G}(v)\mathbf{A}^t\Delta\boldsymbol{I} \tag{6}$$

Q can be decomposed into tree and into link components. Decomposing $\mathbf{A}$ and $\mathbf{G}(v)$ in the appropriate submatrices

$$\mathbf{A} = [\mathbf{A}_T\mathbf{A}_L]; \quad \mathbf{G} = \begin{bmatrix} \mathbf{G}_T & \mathbf{0} \\ \boldsymbol{0} & \mathbf{G}_L \end{bmatrix}$$

The indices T and L denote tree and link submatrices. Substituting this into (6), one gets

$$\begin{aligned} Q = \Delta\boldsymbol{I}^t\{[\mathbf{A}_T\mathbf{G}_T(v)\mathbf{A}_T^t + \mathbf{A}_L\mathbf{G}_L(v)\mathbf{A}_L^t]^{-1}\}^t \cdot \\ \cdot \{[\mathbf{A}_T\mathbf{G}_T(v)\mathbf{A}_T^t + \mathbf{A}_L\mathbf{G}_L(v)\mathbf{A}_L^t]^{-1}\Delta\boldsymbol{I}\} \end{aligned} \tag{7}$$

Now a simplification can be made: the terms in (7) with index L can be neglected by comparison with those with index T.

Proof: We operate instead of the matrices with their quadratic (Euclidian) norms and show that if

$$\text{norm}\,\{\mathbf{A}_T\} \gg \text{norm}\,\{\mathbf{A}_L\} \text{ and} \tag{a}$$

$$\text{norm}\,\{\mathbf{G}_T(v)\} > \text{norm}\,\{\mathbf{G}_L(v)\} \tag{b}$$

then

$$\text{norm}\,\{\mathbf{A}_T\mathbf{G}_T(v)\mathbf{A}_T^t\} \gg \text{norm}\,\{\mathbf{A}_L\mathbf{G}_L(v)\mathbf{A}_L^t\} \tag{c}$$

The first inequality holds because for the real distribution nets, the number of linearly independent loops is small, relative to that of the branches. The second inequality can always be assumed if one chooses as basis for the net calculations a *maximal tree*, also a tree with branches of maximal conductances G.

For any real matrices $\mathbf{M}$ and $\mathbf{N}$ we have:

$$\text{norm}\,\{\mathbf{MN}\} \leqq \text{norm}\,\{M\} \cdot \text{norm}\,\{N\}$$

Therefore, if (a) and (b) holds, (c) eo ipso holds and the terms with index L can be neglected in (7).

For further calculations of Q the simplified expression

$$Q = \boldsymbol{\Delta I}^t\{[\mathbf{A}_T\mathbf{G}_T(v)\mathbf{A}_T^t]^{-1}\}^t[\mathbf{A}_T\mathbf{G}_T(v)\mathbf{A}_T]^{-1}\boldsymbol{\Delta I} \tag{8}$$

will be used. Performing some simple transformations, one gets

$$Q = \boldsymbol{\Delta I}^t[(\mathbf{A}_T^{-1})^t\mathbf{G}_T^{-1}(v)\mathbf{A}_T^{-1}(\mathbf{A}_T^{-1})^t\mathbf{G}_T^{-1}(v)\mathbf{A}_T^{-1}]\boldsymbol{\Delta I} \tag{9}$$

which can easily be interpreted as (8).

3. The optimum allocation of the controllers

The optimum allocation of the controllers is characterized according to (1) by a minimum of the function (9). For smaller nets the minimum can be determined by direct enumeration. In these cases the number of possible controller locations are small.

Example: The 3 control alternatives of a simple net with constant conductances are shown in Fig. 3a–c. The tree branches with $G = 2$ and 3 are denoted with full lines, the single link with $G = 1$ with dashed line. The virtual branch with the chosen large value $G = 100$ and the potential source V substituting the controller is denoted with a dotted line. The quality indices Q of the single control alternatives calculated according to (9) are 2.140, 2.805, 0.384. The best, therefore, is the control alternative in Fig. 3c.

The direct enumeration method is naturally not appropriate to solve larger problems. The possible combination to allocate r controllers in a net with n nodes

increases as

$$\binom{n}{r} = \frac{n!}{r!(n-r)!}. \tag{10}$$

The method given in the following, does not need the direct evaluation of Q and satisfies with the determination of the *medians* of appropriate chosen regions of the net. First we investigate the simpler case of the net control, that with a single controller. We prove the following statement.

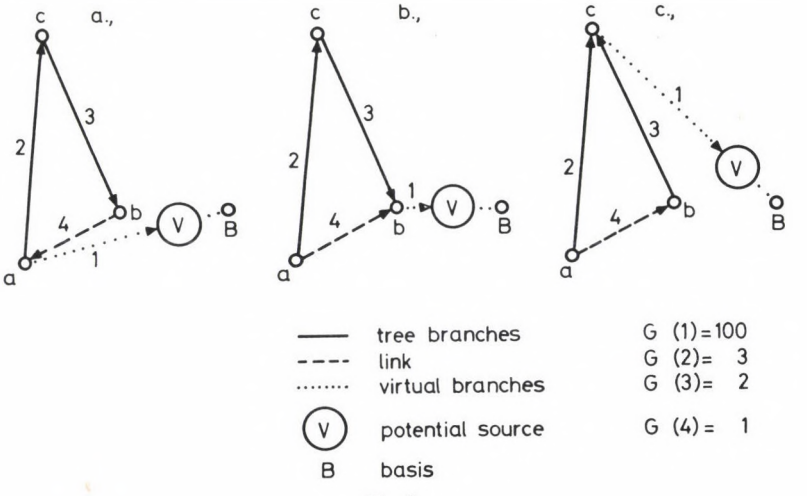

Fig. 3

Statement: for a net with a single control node function (9) has a minimum — if the control node is the *median* of the net.

Proof: Between the $\mathbf{A}_T$ matrix and the *node-to-basis* path matrix $\mathbf{B}_T$ the fundamental graph-theoric relation is valid [3]

$$\mathbf{A}_T^{-1} = \mathbf{B}_T^t. \tag{11}$$

The elements b_{ij} of $\mathbf{B}_T$ are:

$$b_{ij} = \begin{cases} 1 & \text{if branch } (i,j) \text{ is directed to the basis} \\ -1 & \text{if branch } (i,j) \text{ is directed away from the basis} \\ 0 & \text{if branch } (i,j) \text{ does not exist} \end{cases}$$

The rows of matrix $\mathbf{B}_T$ show which branch constitutes the node-to-basis paths for each node of the net. Using (10), the expression (9) of Q can be written:

$$Q = \boldsymbol{\Delta I}^t \mathbf{B}_T \mathbf{Z}(v)\, \mathbf{B}_T^t \mathbf{B}_T\, \mathbf{Z}(v) \mathbf{B}_T^t \boldsymbol{\Delta I} \tag{12}$$

where $\mathbf{Z}(v) = \mathbf{G}^{-1}(v)$ is the branch impedance matrix.

Because the branch directions for network calculations can be chosen freely, $\mathbf{B}_T$ can always be made positive definite. Similarly, the diagonal matrix $\mathbf{Z} \geqq 0$, and therefore

$$\mathbf{Z}\mathbf{B}^t \cdot \Delta \boldsymbol{I} = \boldsymbol{D}_i \,. \tag{13}$$

can be considered as the vector of the node-to-basis path weighted with the branch impedances. The matrix product $\Delta \boldsymbol{e}^t \mathbf{B}_T \mathbf{Z}$ is its transpose, $\boldsymbol{D}_i^t$, i is the serial number of the control alternative which we set equal to the node number of the control node.

It can be proved that $Q \to Q_{\min}$, if $\boldsymbol{D}_i^t \boldsymbol{D}_i \to \min$. $\mathbf{Z}$ is the same for all control alternatives. Therefore, if for two control alternatives $i = 1, 2$,

$$\mathbf{B}_T^t \mathbf{B}_T|_{i=1} \geqq \mathbf{B}_T^t \mathbf{B}_T|_{i=2} \tag{14}$$

holds, the same is true for

$$\boldsymbol{D}_1^t \boldsymbol{D}_1 \geqq \boldsymbol{D}_2^t \boldsymbol{D}_2 \tag{15}$$

and therefore

$$Q_1 \geqq Q_2 \tag{16}$$

Remark: The sign $\geqq$ is meant here in the quadratic norm sense.

$$\boldsymbol{D}_i^t \boldsymbol{D}_i \to \min \qquad \text{for} \quad i = i_{\text{opt}} \,.$$

One can now suggest that $\boldsymbol{D}_i^t \boldsymbol{D}_i$ will have a minimum if $i = i_{\text{opt}} = i_M$, thus if the control node is the *median* i_M of the net.

Definition. The median of a weighted graph is defined as a node i_M with the smallest possible weighted distance to all other nodes [2].

The minimum weighted distance between nodes i and j of the graph will be denoted by $d(i, j)$. The median is any node i_M, such, that

$$\begin{aligned} S(i) &= \sum_j d(i, j) \,, \\ S(i_M) &= \min_i \{S(i)\} \,. \end{aligned} \tag{17}$$

Because $S(i)$ is the sum of the elements of vector D and according to the foregoings, D_i is positive definite, minimizing $S(i)$ by setting $i = i_{\text{opt}} = i_M$, minimize also $\boldsymbol{D}_i^t \boldsymbol{D}_i$ Q.E.D. Locating the controller in the median of the net, the quality index Q will thus have a minimal value. The proved statement concerning the single controller case enables us to find a suboptimal solution for the multicontroller one.

Statement: For a multicontroller net a suboptimal allocation of the controllers can be found for $n \gg r$, allocating the controllers in the medians of the regions chosen in such a way that each region contains the nodes having minimal weighted distances to their own medians.

Proof: In the simple case of two regions 1 and 2, matrices **A** and **G** can be decomposed as follows:

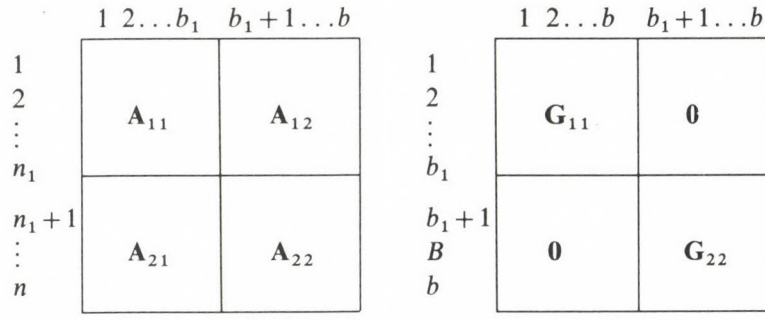

Nodes belonging to region 1 are signed from 1 to n_1, those of region 2 from n_1+1 to n. Branches located entirely in region 1 belong to the submatrix $\mathbf{A}_{11}$, that in region 2 to $\mathbf{A}_{22}$. Branches traversing the region borders belong to $\mathbf{A}_{12}$ and $\mathbf{A}_{21}$.

The norm $\{\mathbf{AG}\}$ can be considered as the measure of the inner "cohesion" of the net. Similarly norm $\{\mathbf{A}_{11}\mathbf{G}_{11}\}$ and norm $\{\mathbf{A}_{22}\mathbf{G}_{22}\}$ are the inner cohesions of regions 1 and 2. Further the sum [norm $\{\mathbf{A}_{12}\mathbf{G}_{22}\}$ + norm $\{\mathbf{A}_{21}\mathbf{G}_{11}\}$] can be considered as the measure for the mutual influence of regions 1 and 2.

The mutual influence between regions 1 and 2 is the more feeble the smaller the ratio ρ is.

$$\rho = \frac{\text{norm}\{\mathbf{A}_{12}\mathbf{G}_{22}\} + \text{norm}\{\mathbf{A}_{21}\mathbf{G}_{11}\}}{\text{norm}\{\mathbf{A}_{11}\mathbf{G}_{11}\} + \text{norm}\{\mathbf{A}_{22}\mathbf{G}_{22}\}} \tag{18}$$

This is the case if $\mathbf{A}_{12}$ and $\mathbf{A}_{21}$ has few elements $\neq 0$ and the appropriate elements of $\mathbf{G}_{11}$ and $\mathbf{G}_{22}$ are relatively small. In other words: if there are few interconnections between the regions and/or the interconnection lines are long, eventually of small diameters.

Equation (18) can be generalized for nets partitioned to more than two regions. To obtain relatively autonomous regions, the algorithm must thus assure small ρ values for the single regions making large the denominators of the $\rho - s$. The regions should be chosen so that the branches with large admittances should be inner-branches with end nodes, of minimal weighted distances to the regions weighted medians.

According to (18) the number of branches traversing the region borders must be relatively small. This is generally automatically fulfilled if the number of nodes *inside* the regions is large, relative to the control nodes, thus if $n \gg r$.

As a conclusion one can, therefore, state that by a fair partitioning of the net, a suboptimal solution of the multicontroller allocation problem can be found, based on the solution of the single controller allocation problem Q.E.D.

4. Solution procedure

The global scheme of the solution procedure for the suboptimal allocation of controllers based on the considerations in the foregoings can be seen in Fig. 4. It consists of the following modules:

1. Module for input operations
2. Calculation of the node potentials

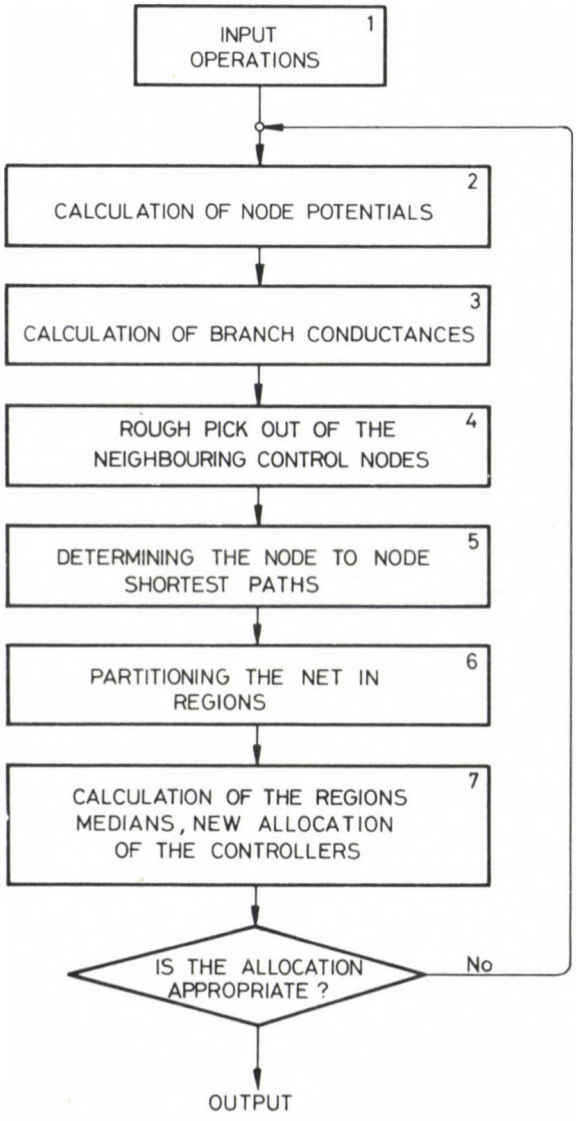

Fig. 4

3. Calculation of branch impedances
4. Rough pick-out of 5 neighbouring control nodes to each load node
5. Calculation of node-to-node weighted shortest paths
6. Partitioning the net in regions
7. Calculation of the medians.

It is not the aim of this paper to give an adequate description of the program scheme. Only some remarks of algorithmical nature to the single modules will be given.

The *input operation* (modul 1) uses the data handling software of the computer. The input file contains the following data:

— number of nodes n
— number of controlled nodes r
— branch identifiers: the serial numbers of the end nodes
— the length l, diameter d and eventually other constants of each branch
— the $n-r$ node load currents $\mathbf{I}$
— the r setting values $\boldsymbol{V}$ of controllers
— the r rough estimates for the location of controllers
— some constants belonging to the nodes (e.g., at water- or gas nets the n geodetical heights of the nodes.)

For the *evaluation of the node potentials* (modul 2), a highly efficient algorithm for the analysis of a large net is used [6], [7]. The algorithm starts by searching for the *minimal tree* of the net and after this the independent loops with minimal loop currents. Because under these circumstances the net's state is essentially determined with the state of the tree, using this as initial values for the Cross-Hardy iteration, the state of the whole net can be determined in relatively few iteration cycles.

The *calculation of impedances* (modul 3) is essential only for nonlinear nets. With the calculated values of node potentials the calculation of Z is straightforward. E.g., for a branch of a gas net

$$e_1 - e_2 = \Delta e = Ki^2; \qquad K = k\frac{l}{d^5}$$

e_1, e_2 are node pressures (potentials) on both ends, i the branch current, l, d are pipe lengths and diameter, resp., K and k are constants. According to the definition of Z

$$Z = \partial \Delta e / \partial i = 2Ki$$

Modules 4 and 5 perform preparing functions for decomposing the net in regions. Modul 5 calculates the *node-to-node shortest path* between a given node and 5 control nodes in its vicinity. It allocates the node in that control node region where the node-to-control node weighted distance is minimal. The region of a control node is thus formed from load nodes with minimal node-to-control node paths.

To reduce the calculation work, modul 4 performs a rough preselection of the 5 control nodes between which, that with the shortest path to the load node in question should be searched for by modul 5.

The node-to-node shortest paths are evaluated by the Dijkstra-algorithm serving the shortest paths from a starting node to all nodes of an *arborescence* [8].

Remark: The direct calculation of the shortest path with matrix **A**, according to (10) is for more time-consuming because the matrix inversion needs operations proportional to n^3 and the Dijkstra-algorithm is only proportional to n^2.

The algorithm finds the shortest path between the nodes s and t as follows: Supposing it is known that m nodes are the closest to the starting node s, the shortest paths to all of these nodes can be considered as known. (In our case shortest path means a path with a minimum of $\sum_j Z_j$.) Node s and these m nodes will be marked. The $(m+1)st$ closest node to s will be found in the following manner. For each unmarked node y, n distinct paths from s to y will be constructed, joining the shortest path from s to x with branch (x, y) *for all marked* nodes x. Selecting the shortest of these paths, the shortest path from s to y will be obtained. Starting with $m=0$ and repeating the process, the shortest path to the terminal node t can be found.

The *calculation of the medians* (modul 7) uses the foregoing path algorithm for determining the shortest path between the control nodes and all load nodes of the region in question. The medians are then calculated according to (17).

The optimal allocation of the controllers is multifold recursive. For finding the medians of the single regions, the region areas must be known. On the other hand, to determine the latters, the locations of the controllers are needed, which presume that the locations of the controllers are known. Beside this, the impedances for nonlinear nets are functions of the node potentials, which are known only after the determination of the controller locations. Further recursions are implicit in the single operation modules, so in those for the calculation of the node potentials and in the determination of node-to-node shortest paths.

According to these — as by other multifold recursive algorithms — the numerical stability strongly depends on the initial values. In our case the initial location of the controllers is the main factor influencing the numerical stability. A stability diminishing effect can have the ill-structuredness of the net and the growing number of controllers. On the other hand — except abnormal nets — where modul 2 for net analysis becames instabil, the one controller case is always stable.

As a final conclusion, one can state that the algorithm avoids the danger of "combinatorial explosion" inherent generally in the methods of discrete programming and can, therefore, be used for large nets with many controllers.

5. Final remarks

A doubt can arise concerning the premise of the given method. Really by the optimal allocation of controllers in the net, not only the quality index Q must be a minimum but also the values of the node potentials must be above a prescribed limit.

Instead of (1), the allocation is an optimization problem with constraints:

$$Q \rightarrow \min$$
$$\boldsymbol{e} \geqq \boldsymbol{e}_{\min} \tag{19}$$

What importance can be attached to the solution of the unconstrained task (1)?

Three cases can arise concerning the unconstrained problem: a) the solution satisfies automatically (19); b) the nodes for which the constraints for the potentials are not fulfilled are dispersed in the full area of the net; c) the nodes with lower potentials, as $e_{\min}$ are concentrated in one or more districts of the net.

In the first case all is in order. In case b) the described method is not applicable, but any other solution method is dubious, because the problem generally has no solution. From the technical standpoint it is evident that in an ill-dimensioned net the conditions for optimal control generally *cannot be* achieved by simple reallocation of the controllers, but the bottlenecks must also be removed. Case c) is a consequence of the insufficient local transport capacity of the nets' district in question.

A remedy can be achieved by the installation of further feeding points with pressure controllers. The method given here is an appropriate one for the optimal location of the new controllers.

References

1. Chen, W. K.: Applied Graph Theory. Graphs and Electrical Networks, North-Holland Publ. Co., Amsterdam 1976
2. Minieka, E.: Optimization Algorithms for Networks and Graphs. M. Dekker, New York 1978
3. Branin, F. H.: D–C and Transient Analysis of Networks Using a Digital Computer. *IRE Int. Conf. Rec.* (1962) 235–256
4. Christofides, N., S. Korman (1975): A Computation Survey of Methods for the Set Covering Problem. *Management Science*, **21,** 591–599
5. Grosz, M. (1977): Designing with Integer Programming etc. *Acta Techn. Hung.*, **85,** (1977), 123–134
6. Singer, D.—J. Elek: Software-Fragen der Analyse. Projektierung und Steuerung von Gasnetzen. *Acta Techn. Hung.*, **87,** (1978), 375–390
7. Singer, D.—Bognár, G.—Borossay, J.—Elek, J.: A Database Aided Simulator for Large Distribution Nets. *Int. J. Syst. Sci.* **12,** pp. 1261–1271
8. Dijkstra, E. W. (1959): A Note on Two Problems in Connection with Graphs. *Numer. Math.*, **1,** (1959), 269–271

Acta Technica Academiae Scientiarum Hungaricae, 93 (3—4), pp. 331—345 (1981)

LOWER AND UPPER BOUNDS FOR THE TORSIONAL STIFFNESS OF A BAR OF CIRCULAR CROSS SECTION OF VARIABLE DIAMETER STRENGTHENED BY A THIN SHELL AT ITS PERIMETER

I. ECSEDI*

Cand. of Techn. Sci.

[Manuscript received: 19 September, 1981]

The paper deals with a bar of circular cross section of variable diameter, strengthened by a thin shell at its perimeter, made from linearly elastic material. The proofs of the bounds of the numerical value of the torsional stiffness to be determined by making use of Michell's theory may be deduced by the application of the well-known theorems of mathematical analysis. The application of the bounds proved are demonstrated by examples.

Notation

The symbols of major significance used in this paper are as follows:

r, φ, z	cylinder coordinates,
$\mathbf{e}_r, \mathbf{e}_\varphi, \mathbf{e}_z$	unit vectors,
$\mathbf{u}=\mathbf{u}(r,\varphi,z)=\mathbf{u}(r,\varphi,z)\mathbf{e}_r+$ $+v(r,\varphi,z)\mathbf{e}_\varphi+w(r,\varphi,z)\mathbf{e}_z$	displacement vector,
$\sigma_r, \sigma_\varphi, \sigma_z$	normal stresses,
$\tau_{r\varphi}, \tau_{rz}, \tau_{\varphi z}$	shear stresses,
G, Γ	shear moduli of elasticity,
$\psi=\psi(r,z)=v(r,z)/r$	rotation,
$\nabla=\frac{\partial}{\partial r}\mathbf{e}_r+\frac{\partial}{\partial z}\mathbf{e}_z$	Hamilton's differential operator,
$\Phi=\Phi(r,z)$	stress function,
$\cdot$	designation of scalar multiplication,
$\times$	designation of vectorial multiplication,
T	inplane region rz defined by the meridian section of bar,
$\partial T=\partial T_1+\partial T_2+\partial T_3+\partial T_4$	bordering curve of region T,
s	arc coordinate interpreted on curve ∂T,
$\mathbf{t}=t_r\mathbf{e}_r+t_z\mathbf{e}_z$	tangent unit vector
$\mathbf{n}=n_r\mathbf{e}_r+n_z\mathbf{e}_z$	normal unit vector,
$\partial/\partial n$	derivative marked with number in the direction $\mathbf{n}$,
$h=h(s)$	thickness of layer,
S	torsional stiffness,
$H=1/S$	
M	moment of torsion,
$r=R(z), 0\leqq z\leqq l$	equation of bordering curve ∂T_2,
$F=F(r,z)$	Auxiliary function,

* Dr. István Ecsedi, Vászonfehérítő ú. 24. H-3531 Miskolc, Hungary.

$\mathbf{b}=\mathbf{b}(r,z)=b_r(r,z)\mathbf{e}_r+b(r,z)\mathbf{e}_z$	inplane vector field,
$B=B(r,z)$	auxiliary function,
l	length of bar.

The other values and variables are defined in the text of the paper.

1. Introduction

In this paper the problem of the torsion of a bar of circular cross section of variable diameter strengthened at its perimeter by a thin shell, made of a linearly elastic material is dealt with (Fig. 1).

The solution of the problems of torsion of an elastic material strengthened by a thin shell at its perimeter had been given by O. C. Zienkiewicz and B. Schimming by generalizing the results of Michell-theory ([1], [3]).

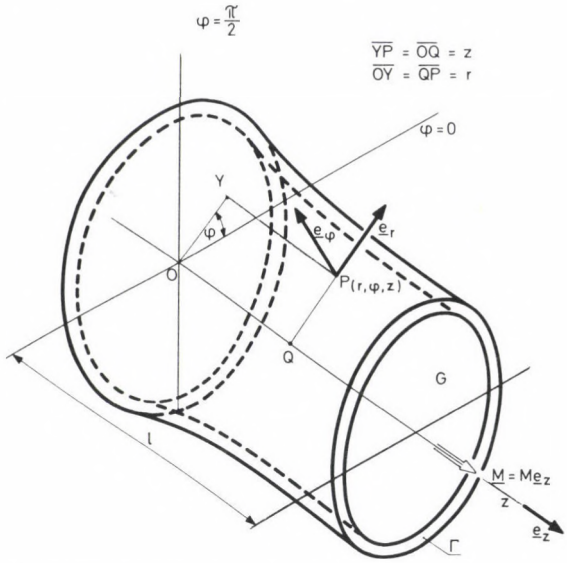

Fig. 1. Bar of circular cross section with varying diameter strengthened at its perimeter by an elastic shell

According to the theory in question the displacement vector

$$\mathbf{u}=\mathbf{u}(r,\varphi,z)=u(r,\varphi,z)\mathbf{e}_r+v(r,\varphi,z)\mathbf{e}_\varphi+w(r,\varphi,z)\mathbf{e}_z$$

may be expressed in the form:

$$\mathbf{u}=v(r,z)\mathbf{e}_\varphi\,. \tag{1.1}$$

By making use of the geometric equations and the general Hooke's law, from Eq. (1.1) one obtains the relationships:

$$\sigma_r = \sigma_\varphi = \sigma_z = \tau_{rz} = 0\,, \tag{1.2}$$

$$\tau_{r\varphi} = \tau_{r\varphi}(r, z)\,, \qquad \tau_{z\varphi} = \tau_{z\varphi}(r, z)\,. \tag{1.3), (1.4}$$

The present paper investigates the specific problem of the torsion of a bar of circular cross section with variable diameter strengthened at its perimeter by an elastic thin shell, which is the case where the cross section defined by the coordinate $z=0$ is steadily fixed and the cross section defined by $z=l$ carries out a rotation of an angle ϑ around the z-axis at unloaded state of the superficies of the bar. The meridian cross section of the bar at a meridian plane, chosen at will at an angle φ, is represented in Fig. 2.

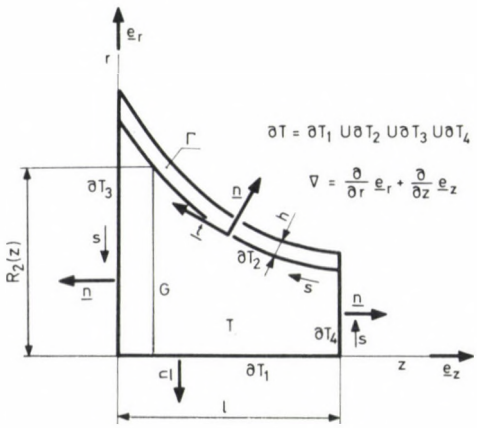

Fig. 2. A meridian cross section of the bar

By making use of Michell-theory as well as O. C. Zienkiewicz's and B. Schimming's results and taking into account the geometric boundary conditions of the extreme cross sections and the unloaded state of the superficies of the bar, the problem of torsion given above may be brought into relationship with the following boundary value problem ([2], [3]):

$$\nabla \cdot \left(\frac{1}{r^2} \nabla \Phi \right) = 0 \qquad (r, z) \in T\,, \tag{1.5}$$

$$\Phi = 0 \qquad (r, z) \in \partial T_1\,, \tag{1.6}$$

$$\frac{\partial \Phi}{\partial n} = 0 \qquad (r, z) \in \partial T_3 + \partial T_4\,, \tag{1.7}$$

$$\Phi + \frac{\Gamma h}{G} \frac{\partial \Phi}{\partial n} = \frac{1}{2\pi} \qquad (r, z) \in \partial T_2\,. \tag{1.8}$$

The modulus of shear elasticity of the material of the bar is designed with G, and that of the shell of revolution of a thickness h is denoted with Γ.

With the knowledge of the stress function $\Phi = \Phi(r, z)$, at point P of the bar of elastic material the induced shear stresses $\tau_{r\varphi}$ and $\tau_{z\varphi}$ may be calculated with formulae

$$\tau_{r\varphi} = -\frac{M}{r^2}\frac{\partial \Phi}{\partial z}, \tag{1.9}$$

$$\tau_{z\varphi} = \frac{M}{r^2}\frac{\partial \Phi}{\partial r}. \tag{1.10}$$

The shear stress $\tau_{s\varphi}$ having been generated at point Q of the thin shell layer of thickness h might be determined by using formula [2].

$$\tau_{s\varphi} = \frac{MG}{R^2 \Gamma h}\left(\Phi - \frac{1}{2\pi}\right). \tag{1.11}$$

In Eqs (1.9), (1.10) and (1.11) the symbol M means the moment of torsion attacking the extreme cross sections of the bar (Fig. 1). From the familiar relationships ([1], [2])

$$\frac{\partial \psi}{\partial r} = \frac{1}{rG}\tau_{r\varphi} = -\frac{M}{r^3 G}\frac{\partial \Phi}{\partial z}, \tag{1.12}$$

$$\frac{\partial \psi}{\partial z} = \frac{1}{rG}\tau_{z\varphi} = \frac{M}{r^3 G}\frac{\partial \Phi}{\partial r} \tag{1.13}$$

wherein

$$\psi(r, z) = \frac{v(r, z)}{r} \tag{1.14}$$

one finds by elementary calculation

$$\psi(r, z) - \psi(r_0, z_0) = -M \int_{P_0}^{P} \frac{1}{Gr^3}\frac{\partial \psi}{\partial n}\,\mathrm{d}s. \tag{1.15}$$

The curve $\widehat{P_0 P}$ is represented in Fig. 3.

The application of formula (1.15) to the boundary curve ∂T_2 yields the following equation:

$$\vartheta = M \int_{\partial T_2} \frac{1}{Gr^3}\frac{\partial \Phi}{\partial n}\,\mathrm{d}s. \tag{1.16}$$

The quantity defined by the prescription

$$S = \frac{M}{\vartheta} \tag{1.17}$$

is called the torsional stiffness of the bar of circular cross section of variable diameter strengthened at its perimeter by a thin shell.

Determination of S is carried out with the help of the formula

$$S = \frac{1}{\frac{1}{G}\int\limits_{\partial T_2} \frac{1}{r^3}\frac{\partial \Phi}{\partial n}\,\mathrm{d}s}. \tag{1.18}$$

For simplification, the *flexibility coefficient*

$$H = \frac{1}{S} \tag{1.19}$$

may be conveniently introduced.

The main purpose of the present paper is the deduction of the lower and upper bounds for the torsional stiffness defined by formula (1.17).

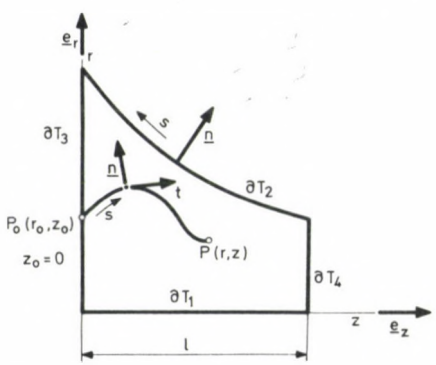

Fig. 3. Representation of the curve $\widehat{P_0P}$

For the determination of the exact value the boundary value problems designated by Eqs (1.5), (1.6), (1.7), (1.8) should be solved. However, the solution in a closed form of the boundary value problem prescribed by Eqs (1.5), (1.6), (1.7), (1.8), also including the production in the form of a series of the function of solution, is known only for very particular instances [2]. Therefore, such methods and principles are of great significance with whose application without the knowledge of the function of

solution $\Phi = \Phi(r, z)$, for the numerical value of the torsional stiffness lower and upper bounds might be established.

Prior to the deduction of the inequalities serving to establish the said bounds a few formulae are to be presented in connection with the coefficient H. Combination of Eqs (1.18) and (1.19) results in the relationship

$$H = \frac{1}{G} \int_{\partial T_2} \frac{1}{r^3} \frac{\partial \Phi}{\partial n} \, \mathrm{d}s \tag{1.20}$$

and the use of Eq. (1.8) allows to deduce from Eq. (1.20) the following formula

$$H = \frac{1}{2\pi\Gamma} \int_{\partial T_2} \frac{\mathrm{d}s}{hr^3} - \frac{1}{\Gamma} \int_{\partial T_2} \frac{\Phi}{r^3 h} \, \mathrm{d}s \,. \tag{1.21}$$

Considering Eq. (1.5) it can be written

$$\nabla \cdot \left(\Phi \frac{1}{r^3} \nabla \Phi \right) - \frac{1}{r^3} |\nabla \Phi|^2 = \Phi \nabla \cdot \left(\frac{1}{r^3} \nabla \Phi \right) = 0 \,. \tag{1.22}$$

Integration of Eq. (1.22) and application of the Gauss-theorem on integral transformation yields

$$\int_{\partial T_2} \frac{1}{r^3} \Phi \frac{\partial \Phi}{\partial n} \, \mathrm{d}s = \int_T \frac{1}{r^3} |\nabla \Phi|^2 \, \mathrm{d}T \tag{1.23}$$

because

$$\int_{\partial T_1 + \partial T_3 + \partial T_4} \frac{1}{r^3} \Phi \frac{\partial \Phi}{\partial n} \, \mathrm{d}s = 0 \,. \tag{1.24}$$

From Eq. (1.23) by elementary transformation and making allowance for the boundary condition (1.8) the following equation may be deduced:

$$\frac{1}{G} \int_T \frac{1}{r^3} |\nabla \Phi|^2 \, \mathrm{d}T = \frac{1}{2\pi G} \int_{\partial T_2} \frac{1}{r^3} \frac{\partial \Phi}{\partial n} \, \mathrm{d}s - \int_{\partial T_2} \frac{\Gamma h}{G^2} \frac{1}{r^3} \left(\frac{\partial \Phi}{\partial n} \right)^2 \mathrm{d}s \,. \tag{1.25}$$

In order to find the value of the coefficient H, the formula (1.20) and Eq. (1.25) should be combined, which results in the formula

$$H = \frac{2\pi}{G} \left(\int_T \frac{1}{r^3} |\nabla \Phi|^2 \, \mathrm{d}T + \int_{\partial T_2} \frac{\Gamma h}{G} \frac{1}{r^3} \left(\frac{\partial \Phi}{\partial n} \right)^2 \mathrm{d}s \right). \tag{1.26}$$

From formula (1.26) by making use of Eq. (1.8) the relation

$$H=2\pi\left(\frac{1}{G}\int_T\frac{1}{r^3}|\nabla\Phi|^2\,\mathrm{d}T+\frac{1}{\Gamma}\int_{\partial T_2}\frac{1}{r^3h}\left(\frac{1}{2\pi}-\Phi\right)^2\mathrm{d}s\right) \tag{1.27}$$

may be deduced.

From formulae (1.26) and (1.27) it may be gathered also that $H=1/G$ can never be negative.

The formulae expressing the bounds should only be put down for the quantity $H=1/S$.

2. Upper bound

Theorem. With any function $F=F(r,z)$ continuously differentiable in the region $T+\partial T$ vanishing on the curve ∂T_1, the inequality

$$H\leqq 2\pi\left\{\frac{1}{G}\int_T\frac{1}{r^3}|\nabla\Phi|^2\,\mathrm{d}T+\frac{1}{\Gamma}\int_{\partial T_2}\frac{1}{hr^3}\left(\frac{1}{2\pi}-F\right)^2\mathrm{d}s\right\} \tag{2.1}$$

is true.

Demonstration. Consider the two-variable function $L=L(r,z)$ defined by the prescription:

$$L(r,z)=F(r,z)-\Phi(r,z)\,. \tag{2.2}$$

With elementary calculation we have:

$$2\pi\left\{\frac{1}{G}\int_T\frac{1}{r^3}|\nabla F|^2\,\mathrm{d}T+\frac{1}{\Gamma}\int_{\partial T_2}\frac{1}{hr^3}\left(\frac{1}{2\pi}-F\right)^2\mathrm{d}s\right\}=$$

$$=2\pi\left\{\frac{1}{G}\int_T\frac{1}{r^3}|\nabla\Phi|^2\,\mathrm{d}T+\frac{1}{\Gamma}\int_{\partial T_2}\frac{1}{hr^3}\left(\frac{1}{2\pi}-\Phi\right)^2\mathrm{d}s+\right.$$

$$+\frac{1}{G}\int_T\frac{1}{r^3}|\nabla L|^2\,\mathrm{d}T+\frac{1}{\Gamma}\int_{\partial T_2}\frac{1}{hr^3}L^2\,\mathrm{d}s+\frac{2}{G}\int_T\nabla\Phi\cdot\nabla L\,\mathrm{d}T-$$

$$\left.-\frac{2}{\Gamma}\int_{\partial T_2}\frac{1}{hr^3}\left(\frac{1}{2\pi}-\Phi\right)L\,\mathrm{d}s\right\}=H+2\pi\left(\frac{1}{G}\int_T\frac{1}{r^3}|\nabla L|^2\,\mathrm{d}T+\right.$$

$$\left.+\frac{1}{\Gamma}\int_{\partial T_2}\frac{1}{hr^3}L^2\,\mathrm{d}s\right). \tag{2.3}$$

In considering Eq. (2.3) the formula (1.27) and the equation

$$\frac{1}{G}\int_T \frac{1}{r^3}\nabla\Phi\cdot\nabla L\,\mathrm{d}T - \frac{1}{\Gamma}\int_{\partial T_2}\frac{1}{r^3 h}\left(\frac{1}{2\pi}-\Phi\right)L\,\mathrm{d}s =$$

$$= \frac{1}{G}\int_T \nabla\left(L\frac{1}{r^3}\nabla\Phi\right)\mathrm{d}T - \frac{1}{G}\int_T L\nabla\cdot\left(\frac{1}{r^3}\nabla\Phi\right)\mathrm{d}T -$$

$$- \frac{1}{\Gamma}\int_{\partial T_2}\frac{1}{r^3 h}\left(\frac{1}{2\pi}-\Phi\right)L\,\mathrm{d}s =$$

$$= \frac{1}{G}\int_{\partial T} L\frac{1}{r^3}\frac{\partial\Phi}{\partial n}\,\mathrm{d}s - \frac{1}{\Gamma}\int_{\partial T_2}\left(\frac{1}{2\pi}-\Phi\right)\frac{L}{r^3 h}\,\mathrm{d}s =$$

$$= \int_{\partial T_2}\frac{L}{r^3}\left[\frac{1}{G}\frac{\partial\Phi}{\partial n} - \frac{1}{\Gamma h}\left(\frac{1}{2\pi}-\Phi\right)\right]\mathrm{d}s = 0 \tag{2.4}$$

deduced by simultaneous application of the Gaussian integral transformation curve and the theorem of derivation of the product function, have been used. In deducing equation (2.4) also Eqs (1.5), (1.7), (1.8) have been applied as well as the equation

$$L(o, z) = F(o, z) - \Phi(o, z) = 0\,; \qquad 0 \leqq z \leqq l \tag{2.5}$$

ensuing from the condition prescribed for the function $F = F(r, z)$

$$F(r, z) = 0\,; \qquad (r, z) \in \partial T_1\,. \tag{2.6}$$

From Eq. (2.3) and from the evident inequality

$$\frac{1}{G}\int_T \frac{1}{r^3}|\nabla L|^2\,\mathrm{d}T + \frac{1}{\Gamma}\int_{\partial T_2}\frac{L^2}{hr^3}\,\mathrm{d}s \geqq 0 \tag{2.7}$$

the validity of the inequality immediately follows (2.1).

3. Sharpening of the upper bound (2.1)

Let us apply the inequality relation (2.1) to the function

$$\hat{F}(r, z) = pF(r, z) \tag{3.1}$$

wherein p is an arbitrary real parameter. By elementary calculation the following result may be deduced

$$H \leqq p^2 \left\{ \frac{2\pi}{G} \int_T \frac{1}{r^3} |\nabla F|^2 \, \mathrm{d}T + \frac{2\pi}{\Gamma} \int_{\partial T_2} \frac{1}{r^3 h} F^2 \, \mathrm{d}s \right\} -$$

$$- p \frac{4\pi}{\Gamma} \int_{\partial T_2} \frac{F}{2r^3 h\pi} \, \mathrm{d}s + \frac{1}{2\pi\Gamma} \int_{\partial T_2} \frac{\mathrm{d}s}{hr^3} . \tag{3.2}$$

The right-hand side of inequality (3.2), in case of a given $F = F(r, z)$ function is a second-order integer rational function of the variable p which, by a convenient selection of the variable p might be brought to a minimum. Taking the value of the minimum in question into account, the following upper bound may be established, assuming that F is not identically equal to zero in the region $T + \partial T$:

$$H \leqq \frac{1}{2\pi} \left\{ \frac{1}{\Gamma} \int_{\partial T_2} \frac{\mathrm{d}s}{r^3 h} - \frac{\left(\int_{\partial T_2} \frac{F}{\Gamma r^3 h} \, \mathrm{d}s \right)^2}{\int_T \frac{|\nabla F|^2}{G r^3} \, \mathrm{d}T + \int_{\partial T_2} \frac{F^2}{\Gamma r^3 h} \, \mathrm{d}s} \right\} . \tag{3.3}$$

From the inequality relation (3.3) also the upper bound might be recognized which has the following simple structure

$$H \leqq \frac{1}{2\pi\Gamma} \int \frac{\mathrm{d}s}{r^3 h} . \tag{3.4}$$

4. The lower bound

4.1 *Theorem.* The formula

$$\mathbf{b} = \mathbf{b}(r, z) = b_r(r, z)\mathbf{e}_r + b_z(r, z)\mathbf{e}_z$$

should represent a plane vector field rz which is not identically equal to zero and satisfies the equations

$$\nabla \cdot \left(\frac{1}{r^3} \mathbf{b} \right) = 0 \qquad (r, z) \in T , \tag{4.1}$$

$$\mathbf{b} \cdot \mathbf{n} = 0 \qquad (r, z) \in \partial T_3 + \partial T_4 . \tag{4.2}$$

It is stated that in this case the inequality relation

$$H \geqq \frac{1}{2\pi G} \frac{\left(\int\limits_{\partial T_2} \frac{\mathbf{b} \cdot \mathbf{n}}{r^3} \, \mathrm{d}s \right)^2}{\int\limits_T \frac{1}{r^3} \mathbf{b}^2 \, \mathrm{d}T + \int\limits_{\partial T_2} \frac{\Gamma h}{r^3 G} (\mathbf{b} \cdot \mathbf{n})^2 \, ds} \tag{4.3}$$

houlds true.

Demonstration. The basis of verification of the inequality (4.3) is the Schwarz-inequality relation

$$E(\boldsymbol{\alpha}) E(\boldsymbol{\beta}) \geqq \{E(\boldsymbol{\alpha}, \boldsymbol{\beta})\}^2 \tag{4.4}$$

wherein

$$E(\boldsymbol{\alpha}, \boldsymbol{\beta}) = \int\limits_T \frac{1}{r^3} \boldsymbol{\alpha} \cdot \boldsymbol{\beta} \, \mathrm{d}T + \int\limits_{\partial T_2} \frac{\Gamma h}{G} \frac{1}{r^3} (\boldsymbol{\alpha} \cdot \mathbf{n}) (\boldsymbol{\beta} \cdot \mathbf{n}) \, \mathrm{d}s \,, \tag{4.5}$$

$$E(\boldsymbol{\alpha}) = E(\boldsymbol{\alpha}, \boldsymbol{\alpha}) \qquad E(\boldsymbol{\beta}) = E(\boldsymbol{\beta}, \boldsymbol{\beta}) \,. \tag{4.6), (4.7}$$

In the integrals (4.5), (4.6), (4.7)

$$\boldsymbol{\alpha} = \boldsymbol{\alpha}(r, z) = \alpha_r(r, z) \mathbf{e}_r + \alpha_z(r, z) \mathbf{e}_z$$

and

$$\boldsymbol{\beta} = \boldsymbol{\beta}(r, z) = \beta_r(r, z) \mathbf{e}_r + \beta_z(r, z) \mathbf{e}_z$$

represent plane vector fields in respect to which the integrals in question exist and are of finite values.

In the inequality relation (4.4) let us have

$$\boldsymbol{\alpha} = \nabla \Phi \,, \qquad \beta = \mathbf{b} \,. \tag{4.8), (4.9}$$

By making use of the formula (1.26) it could easily be pointed out that

$$E(\nabla \Phi) = \frac{G}{2\pi} H \,. \tag{4.10}$$

Combination of Eqs (4.4) and (4.10) as well as Eqs (4.8), (4.9) yields

$$\frac{G}{2\pi} H E(\mathbf{b}) \geqq \left\{ \int\limits_T \frac{1}{r^3} \nabla \Phi \cdot \mathbf{b} \, \mathrm{d}T + \int\limits_{\partial T_2} \frac{G}{\Gamma h r^3} \frac{\partial \Phi}{\partial n} (\mathbf{b} \cdot \mathbf{n}) \, \mathrm{d}s \right\}. \tag{4.11}$$

By application of Eqs (1.6), (1.8), (4.1), (4.4) and by making use of the theorem of the derivation of the product function and the Gaussian theorem of integral trans-

formation, the integral, entering at the right-hand side of Eq. (4.11) might be transformed as follows

$$\int_T \frac{1}{r^3} \nabla\Phi \cdot \mathbf{b}\, dT + \int_{\partial T_2} \frac{G}{\Gamma h r^3} \frac{\partial \Phi}{\partial n} (\mathbf{b} \cdot \mathbf{n})\, ds = \int_T \nabla \cdot \left(\Phi \frac{1}{r^3} \mathbf{b} \right) dT -$$

$$- \int_T \nabla \cdot \left(\frac{1}{r^3} \mathbf{b} \right) dT + \int_{\partial T_2} \frac{G}{\Gamma h} \frac{1}{r^3} \frac{\partial \Phi}{\partial n} (\mathbf{b} \cdot \mathbf{n})\, ds =$$

$$= \int_{\partial T_2} \frac{\mathbf{b} \cdot \mathbf{n}}{r^3} \left[\Phi + \frac{G}{\Gamma h} \frac{\partial \Phi}{\partial n} \right] ds = \frac{1}{2\pi} \int_{\partial T_2} \frac{\mathbf{b} \cdot \mathbf{n}}{r^3}\, ds . \tag{4.12}$$

By combining the formulae (4.11) an (4.12), in the case where one makes allowance for the relation

$$E(\mathbf{b}) = \int_T \frac{1}{r^3} \mathbf{b}^2\, dT + \int_{\partial T_2} \frac{G}{\Gamma h r^3} (\mathbf{b} \cdot \mathbf{n})^2\, ds \tag{4.13}$$

the inequality relation (4.3) to be proved, is directly obtained.

4.2 *Theorem.* Be $B = B(r, z)$ in the closed region $T + \partial T$ at least once, while in the region T at least twice continuously differentiable, such a not identically constant function of two variables which at the segments ∂T_3 and ∂T_4 of the boundary curve is of constant value, that is, satisfies the boundary conditions

$$B(r, o) = B_3 \qquad o \leqq r \leqq R(o), \tag{4.14}$$

$$B(r, l) = B_4 \qquad o \leqq r \leqq R(l). \tag{4.15}$$

It is stated that in this case the inequality relation

$$H \geqq \frac{1}{2\pi G} \frac{(B_3 - B_4)^2}{\displaystyle\int_T r^3 |\nabla B|^2\, dT + \int_{\partial T_2} \frac{\Gamma h}{G} r^3 \left(\frac{\partial B}{\partial s} \right)^2 ds} \tag{4.16}$$

holds true.

Demonstration. Consider in the inequality relation (4.3) the vector $\mathbf{b} = \mathbf{b}(r, z)$ interpreted by the prescription

$$\mathbf{b} = r^3\, \nabla B \times \mathbf{e}_\varphi . \tag{4.17}$$

By elementary calculation it may be pointed out that the vector **b** of the above form, assuming continuously differentiable function $B=B(r, z)$, identically satisfies differential equation (4.1).

In conformity with Eq. (4.2)

$$\mathbf{n}\cdot\mathbf{b}=r^3(\nabla B\times\mathbf{e}_\varphi)\cdot\mathbf{n}=r^3\nabla B\cdot\mathbf{t}=r^3\frac{\partial B}{\partial s}=0 \qquad (r, z)\in\partial T_3 \tag{4.18}$$

that is,

$$B(r, z)=B_3=\text{const.}; \qquad (r, z)\in\partial T_3\,. \tag{4.19}$$

With a similar calculation it may be pointed out that also the prescription relating to the segment ∂T_4 of the boundary curve associated with vector **b** is satisfied in the case where

$$B(r, z)=B_4=\text{const.}; \qquad (r, z)\in\partial T_4\,. \tag{4.20}$$

With an elementary calculation it may be proved that

$$\int_{\partial T_2}\frac{\mathbf{b}\cdot\mathbf{n}}{r^3}\,\mathrm{d}s=\int_{\partial T_2}\frac{\partial B}{\partial s}\,\mathrm{d}s=B_3-B_4\,, \tag{4.21}$$

$$\int_T\frac{1}{r^3}\mathbf{b}^2\,\mathrm{d}T+\int_{\partial T_2}\frac{G}{\Gamma hr^3}(\mathbf{b}\cdot\mathbf{n})^2\,\mathrm{d}s=\int_T r^3|\nabla B|^2\,\mathrm{d}T+$$

$$+\int_{\partial T_2}\frac{G}{\Gamma h}r^3\left(\frac{\partial B}{\partial s}\right)^2\mathrm{d}s\,. \tag{4.22}$$

Together with the above results, by combining them with inequality (4.3), the inequality (4.16) has been directly obtained, q.e.d.

5. Examples for establishing bounds

5.1. From the inequality relation (2.1), by making use of the function

$$F(r, z)=\frac{1}{2\pi}\left\{\frac{r}{R(z)}\right\}^4 \tag{5.1}$$

the following upper limit may be deduced for H

$$H \leqq \frac{2}{G\pi} \int_0^l \left\{ 1 + \frac{2}{3} (R'(z))^2 \right\} \frac{\mathrm{d}z}{[R(z)]^4} . \tag{5.2}$$

It is to be noted that the function $F = F(r, z)$ given by formula (5.1) satisfies, besides the boundary condition

$$F(o, z) = 0 \qquad o \leqq z \leqq l \tag{5.3}$$

also the condition

$$F(r, z) = \frac{1}{2\pi} \qquad (r, z) \in \partial T_2 \tag{5.4}$$

and thus, the integral related to the boundary curve ∂T_2 entering in the right-hand side of the inequality relation, will be equal to zero.

5.2 Application of the inequality relation (3.3) to the function

$$F(r, z) = r^4 \qquad (r, z) \in T + \partial T \tag{5.5}$$

results in the following upper limit:

$$H \leqq \frac{1}{2\pi} \left(\frac{1}{\Gamma} \int_0^l \frac{\sqrt{1 + [R'(\zeta)]^2}}{h(\zeta)[R(\zeta)]^3} \right) \mathrm{d}\zeta - \frac{\left(\frac{1}{\Gamma} \int_0^l \frac{R(\zeta)}{h(\zeta)} \sqrt{1 + [R'(\zeta)]^2}\, \mathrm{d}\zeta \right)^2}{\int_0^l \left(\frac{4}{G} + \frac{1}{\Gamma} \frac{R(\zeta)}{h(\zeta)} \sqrt{1 + [R'(\zeta)]^2} \right) [R(\zeta)]^4 \, \mathrm{d}\zeta} . \tag{5.6}$$

5.3 In the inequality relation (4.16) be

$$B(r, z) = z \qquad (r, z) \in T + \partial T. \tag{5.7}$$

One obtains immediately that

$$B_3 = 0 , \qquad B_4 = l . \tag{5.8), (5.9)}$$

In this case an elementary calculation yields

$$H \geqq \frac{1}{G\pi} \frac{l^2}{\int_0^l \left\{ \frac{1}{2} + \frac{2\Gamma}{G} \frac{h(\zeta)}{R(\zeta)} \frac{1}{\sqrt{1 + [R'(\zeta)]^2}} \right\} [R(\zeta)]^4 \, \mathrm{d}\zeta} . \tag{5.10}$$

5.4 In the inequality relation (4.16) be

$$B(r, z) = f(z) \qquad (r, z) \in T + \partial T \tag{5.11}$$

wherein $f = f(z)$ fulfils the following boundary conditions

$$f(o) = 0\,, \qquad f(l) = 1\,. \tag{5.12), (5.13}$$

A lengthy but elementary calculation gives the bound

$$H \geqq \frac{1}{G\pi C} \tag{5.14}$$

wherein

$$C = \int_0^l [f'(\zeta)]^2 \left(\frac{1}{2} + \frac{2\Gamma}{G}\,\frac{h(\zeta)}{R(\zeta)}\,\frac{1}{\sqrt{1 + [R'(\zeta)]^2}}\right)[R(\zeta)]^4\,\mathrm{d}\zeta\,. \tag{5.15}$$

By making use of the known results of the variation calculus may point out that the bound (5.14) is the sharpest in the case where

$$f(z) = \frac{\displaystyle\int_0^z \frac{\mathrm{d}\zeta}{\left(\frac{1}{2} + \frac{2\Gamma}{G}\,\frac{h(\zeta)}{R(\zeta)}\,\frac{1}{\sqrt{1 + [R'(\zeta)]^2}}\right)[R(\zeta)]^4}}{\displaystyle\int_0^l \frac{\mathrm{d}\zeta}{\left(\frac{1}{2} + \frac{2\Gamma}{G}\,\frac{h(\zeta)}{R(\zeta)}\,\frac{1}{\sqrt{1 + [R'(\zeta)]^2}}\right)[R(\zeta)]^4}}\,. \tag{5.16}$$

On the basis of the bound produced by the above function the result might be written as

$$H \geqq \frac{1}{G\pi} \int_0^l \frac{\mathrm{d}\zeta}{\left(\frac{1}{2} + \frac{2\Gamma}{G}\,\frac{h(\zeta)}{R(\zeta)}\,\frac{1}{\sqrt{1 + [R'(\zeta)]^2}}\right)[R(\zeta)]^4}\,. \tag{5.17}$$

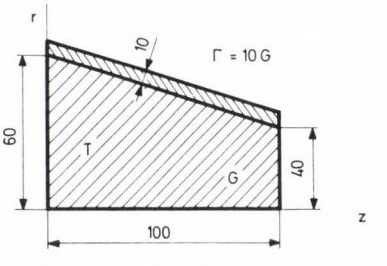

Fig. 4. A cone-shaped bar strengthened at its perimeter by a thin shell

5.5 For the torsional stiffness S of the solid of revolution having the meridian curve represented in Fig. 4 (a cone-shaped axis), by applying formulae (5.6) and (5.17), the result

$$5.68 \cdot 10^{-5}\,\mathrm{mm}^{-3} < HG < 6.02 \cdot 10^{-5}\,\mathrm{mm}^{-3}$$

may be derived, assuming that $\Gamma = 10G$.

6. A complementary note

The case $h=0$ has been investigated by E. Reissner. He deduced the lower and upper bounds by the application of the minimum theorems associated with the functions of the potential energy and the complementary energy for the torsional stiffness of a bar with a cross section having a variable diameter. E. Reissner did not establish the formulae expressing the relationship between the stress function and the torsional stiffness, wherefore his study does not contain, for example, the formula

$$H = \frac{2\pi}{G} \int_T \frac{1}{r^3} |\nabla \Phi|^2 \, \mathrm{d}T \tag{6.1}$$

relating to the bar of solid cross section having a variable diameter, derivable from the formula (1.26) by the substitution $h=0$.

References

1. Timoshenko, S. P.—Goodier, I. N.: Theory of Elasticity. 3rd Ed. 341–349. McGraw Hill, New York 1970
2. Арутюнян, Н. Х.—Адрамян, Б. Л.: Кручение упругих тел, физматгиз, Москва 1963. стр 448—486
3. Zienkiewitz, N. H.—Schimming, B.: Torsion of Non-Homogeneous Bars with Axial Symmetry. *Int. Journ. of Mechanical Sciences* **4** (1962), 15–23
4. Reissner, E.: On Bounds for the Torsional Stiffness of Shafts of Varying Circular Cross Section. *Journal of Elasticity* **8** (1978), 211–219

Acta Technica Academiae Scientiarum Hungaricae, 93 (3—4), pp. 347—366 (1981)

DUAL VARIATIONAL PRINCIPLES IN LINEAR MICROPOLAR ELASTOSTATICS

GY. SZEIDL*

[Manuscript received: 24 September, 1980]

In the paper the total system of dual equations of linear micropolar elasticity for three dimensional problems is presented. The functional of the free variational problem — being equivalent to the system of dual equations is composed by the use of the complementary energy functional. The dual functionals which are valid with subsidiary conditions are part cases of the functional of free variational problem. Using the stationary from variations of dual functionals with respect to stress functions follows the compatibility of strains.

1. Introduction, preliminaries

The composition of dual variational principles of linear elasticity were made by several authors [1–7]. Varying the total complementary energy functional — which is a basic dual functional — the first was Southwell, R. V. who applied stress functions for the determination of statically admissible stress fields. By this he arrived at the so-called Southwell's paradox which states, that an arbitrary stress field can be expressed in terms of three — three Maxwell's and Morera's stress functions, however to the existence of the six Saint-Venant compatibility field equations — which are Euler equations following from the principle of minimum complementary energy — six stress functions are needed. Further dual functionals are proposed by Tonti, E. [2], Oden, J. T.—Reddy, J. N. [3] and Abovskij, N. P.—Andrejev, N. P.—Deruga, A. P. [4]. The latest authors take into consideration all six independent components of the stress function tensor to be nonzero and vary them, to make sure the existence of all the six Saint-Venant compatibility field equation (escaping in this way Southwell's paradox). On one side Kozák, I. proved [5], that to the single-valuedness of the displacement field the three suitably chosen Saint-Venant compatibility boundary conditions are sufficient and necessary, and on other hand he gave a solution for Southwell's paradox [6] proving by formal calculations, that the existence of the three compatibility field equations and compatibility boundary conditions are followed from the principle of minimum complementary energy in such a situation as well when — composing the statically admissible stresses — from the six independent components of the stress function tensor the three suitably chosen components are zero [8], and the other three components are varied. In the next paper of Kozák, I. the dual functionals — introduced in [2, 3, 4] — were further clarified, by the application of such a kind of stress function tensor which had only three suitably chosen nonzero coordinates and the state of the boundary was examined, particularly from the point of the compatibility boundary conditions.

* Dr. Gy. Szeidl, Derkovits u. 54. 3529 Miskolc, Hungary

1.2. Composing the dual variational principles of linear micropolar elastostatics there are several questions which have to be answered on the base of the previously introduced problems:

a) it should be examined how many components of the stress function tensors have to be different from zero when composing statically admissible stress fields with the help of stress function tensors;
b) the independent necessary and sufficient conditions for single valued displacements (with the exception of a rigid body motion) should be determined;
c) what kind of Euler equations and boundary conditions are followed from the principle of total complementary energy as basic dual variational principle, if the statically admissible stress fields are expressed in terms of stress functions should be examined;
d) for the determination of further dual variational principles the dual equation system of linear micropolar elastostatics should be composed;
e) and last, further there should be composed the dual variational principles, which can be taken as the generalization of the dual variational principles of [2, 3, 4, 7] for micropolar cases.

The answers to the first three questions are given in the paper of Kozák, I. and the author [9]. First the present paper shortly summarizes the maint points of [9] for the solution of problems $\underline{d}$ and $\underline{e}$.

1.3. Let the volume region and the surface of the body be denoted by V and S. The region V is assumed to be single connected and the surface S is composed of a finite number of smooth parts.

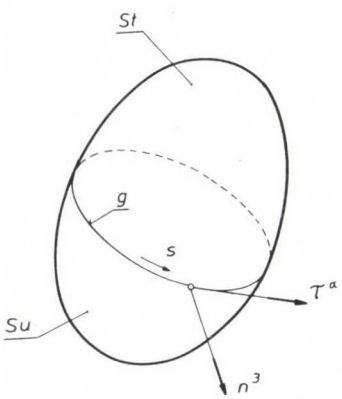

We apply the usual notations in the arbitrary, body oriented curvilinear coordinate system (x^1, x^2, x^3): values of the latin indices can be 1, 2, 3; the summation convention for dummy index pairs are valid, the covariant differentiation is denoted by an index after semicolon; g^{kl}, g_{pq} are the metric tensors; ε^{klm}, ε_{pqr} are the permutation tensors, n_k is the unit outward normal of surface S.

Let u_k be the displacement field and φ^a be the rotation field (together displacements). We denote the components of the asymmetric strain tensor, torsion tensor (together strains), force stress tensor and couple stress tensor (together stresses), by γ_{kl}, $\kappa_a^{\cdot b}$, t^{kl} and $\mu_{\cdot b}^{a}$, respectively.

Let x denote the totality of point coordinates.

Let the body be homogeneous, centro-symmetric and loaded by body forces b^l and body couples c_b.

On the base of Tonti's work [16] Oden and Reddy's paper [3] makes a difference, due to the configuration variable between primal and dual form of the boundary value problems of mathematical physics. In the linear classical elastostatics the configuration variable of the primal boundary value problem is the displacement field, the intermediate variable of first kind is the strain field, the intermediate variable of second kind is the stress field. The configuration variable of the dual boundary value problem is the stress function tensor, the intermediate variable of first kind is the stress field, and the intermediate variable of the second kind is the strain field. To the primal boundary value problem the primal variational principles and functionals (Hu-Washizu principle, Hellinger—Reissner principle, Lagrange principle and their functionals) can be placed. To the dual boundary value problem can be placed the dual variational principles and their functionals [3, 7].

The primal equation system of the linear micropolar elastostatics can be written in an analogous manner of a classical case by the displacement fields u_k, φ^a as configuration variables, by the strain fields γ_{kl}, $\mu_a^{\cdot b}$ as intermediate variables of first kind and by the stress fields t^{kl}, $\mu_{\cdot b}^{a}$ as intermediate variables of second kind:

kinematic equations

$$u_{l;k} + \varepsilon_{lks}\varphi^s = \gamma_{kl} \qquad x \in V \qquad (1.1)_1$$

$$\varphi^a_{\cdot;b} = \kappa_b^{\cdot a} \qquad (1.1)_2$$

displacement boundary conditions

$$u_k = \hat{u}_k\,, \qquad \varphi^a = \hat{\varphi}^a \qquad x \in S_u \qquad (1.2)_{1,2}$$

constitutive equations (Hooke's law)

$$\underset{-1}{a}{}^{klpq}\gamma_{pq} = t^{kl} \qquad x \in V \qquad (1.3)_1$$

$$\underset{-1}{c}{}^{abpq}\kappa_{pq} = \mu^{ab} \qquad (1.3)_2$$

stress boundary conditions

$$n_n t^{kl} = \hat{t}^l\,, \qquad n_a \mu_{\cdot b}^{a} = \hat{\mu}_b \qquad x \in S_t \qquad (1.4)_{1,2}$$

equilibrium equations

$$t^{kl}_{\cdot\cdot;k} + b^l = 0 \qquad x \in V \qquad (1.5)_1$$

$$\mu^{a}_{\cdot b;a} + \varepsilon_{bpq}t^{pq} + c_b = 0 \qquad (1.5)_2$$

where $\underset{-1}{a}^{klpq}$, $\underset{-1}{c}^{abpq}$ are the tensors of elastic coefficients, $\hat{u}^k$ and $\hat{\varphi}^a$ are prescribed diplacements on the part S_u of the boundary, $\hat{t}^l$ and $\hat{\mu}_b$ are prescribed tractions on the part S_t of the boundary. $S_u \cup S_t = S$, $S_u \cap S_t = 0$ and g is the common curve of the parts S_u and S_t of the boundary. In extreme cases $S_u = 0$ or $S_t = 0$.

The primal variational principles concerning the primal equation system of the linear micropolar elastostatics (1.1)–(1.5) are the generalizations* of the principles of Hu-Washizu, Hellinger—Reissner and Lagrange for the micropolar case [10], [11].

1.4. The stress fields $t^{kl}(x)$, $\mu^a_{.b}(x)$ are called equilibrated (statically admissible) if they satisfy the equilibrium equations (1.5) (and the stress boundary conditions (1.4)). Equilibrated (statically admissible) stress fields can be composed of stress function tensors [12], [13], [14]. By taking Günther's solution to be complete, Schaefer, H. and Carlson, D. E. at the same time proved, but independently from each others, that any solution of the equilibrium equations (1.5) can be constructed by the suitably smooth but arbitrary stress function tensors $h^l_y(x)$, $f_{yb}(x)$:

$$t^{kl} = \varepsilon^{kmy} h^l_{y:;m} + \mathring{t}^{kl} \qquad x \in V \qquad (1.6)_1$$

$$\mu^a_{.b} = \varepsilon^{apy}(f_{yb;p} + \varepsilon_{bpl} h^l_y) + \mathring{\mu}^a_{.b} \qquad x \in V \qquad (1.6)_2$$

where $\mathring{t}^{kl}$ and $\mathring{\mu}^a_{.b}$ are the particular solutions of the equilibrium equations (1.5). They can be composed from the vector fields $p^l(x)$, $q_b(x)$ which satisfy the conditions (1.8) according to the following:

$$\mathring{t}^{kl} = p^l_{.;m} g^{mk}, \qquad x \in V \qquad (1.7)_1$$

$$\mathring{\mu}^a_{.b} = g^{am}(\varepsilon_{mby} p^y + q_{b;m}) \qquad (1.7)_2$$

$$g^{mn} p^l_{.;mn} = -b^l, \qquad g^{mn} q_{b;mn} = -c_b \qquad x \in V. \qquad (1.8)_{1,2}$$

Re-inserting into (1.5), it can be controlled, that the stress fields $t^{kl}(x)$, $\mu^a_{.b}(x)$ are equilibrated.

In the following the particular solutions $\mathring{t}^{kl}$, $\mathring{\mu}^a_{.b}$ are assumed to be known.

It can be shown [9], that three of the nine stress functions h^l_y and similarly, three of the nine stress functions f_{yb} — denoted by the index pairs AB or KL: f_{AB} and h^L_K — can be chosen to be zero.** The index pairs AB and KL cannot be arbitrary. Their values have to be chosen in such a way, that the solvability of the equations

$$r^L_{.;K} = \beta^L_{.K}(x) \qquad x \in V \qquad (1.9)_1$$

$$w_{B;A} + \varepsilon_{RAs} r^s = \alpha_{BA}(x) \qquad x \in V \qquad (1.9)_2$$

* Paper [10] introduces and systemizes the primal variational principles of linear micropolar elastostatics with rather general boundary conditions. Further, it introduces the weak (generalized) solution of the primal boundary value problem and prooves its existence and unicity.

** The starting point is, that to the stress function tensors

$$h^l_y = r^l_{.;y}(x), \qquad f_{yb} = w_{b;y}(x) + \varepsilon_{bys} r^s(x) \qquad x \in V$$

— which are composed of the sufficiently smooth vector fields $r^l(x)$, $w_b(x)$ — belong identically zero stress fields.

are to be assured in the case of arbitrary functions $\beta^L_{.K}(x)$ and $\alpha_{BA}(x)$ for the vector fields $r^l(x)$ and $w_b(x)$. In this way it is enough to consider only the six-six stress functions h^T_S and f_{XY} which are characterized by their index pairs ST and XY together with the index pairs KL and AB give all the possible values of the index pairs of yb and yl.

According to the above the structures of the stress function tensors f_{yb}, h^l_y are assumed to have only six-six independent components different from zero. The non-zero and the zero components in the (x_1, x_2, x_3) coordinate-system are further denoted in the above mentioned manner.

1.5. The equations and calculations on the body surface can be better understood by the introduction of a suitable surface coordinate system [5, 9].

Let (ξ^1, ξ^2, ξ^3) be a surface oriented coordinate system on the boundary surface ($x^k = x^k(\xi^1, \xi^2)$, ξ^1 and ξ^2 are surface parameters) and on its immediate neighbourhood V_S, where ξ^3 is the algebraic distance along the outward normal, and on S let $\xi^3 = 0$. Totality of the coordinates ξ^k is denoted by (ξ). The values of the Greek indices can be 1, 2.

The transformed form of a vector or tensor is denoted by an underline in the introduced coordinate system. It is clear, that $\underline{n}_3 = 1$ and $\underline{n}_\alpha = 0$.

Between the components $\underline{C}^k_{.l}$, $C^p_{.q}$ of second-order tensor $\mathbf{C}$ the next transformation formulas are valid:

$$\underline{C}^k_{.l} = C^p_{.q}\sigma^{.k}_{p}\tau^{.q}_{l} \tag{1.10}_1$$

$$C^p_{.q} = \underline{C}^k_{.l}\tau^{.p}_{k}\sigma^{.l}_{q} \tag{1.10}_2$$

$$\det \tau^{.k}_{e} \neq 0\,, \qquad \sigma^{.k}_{p}\tau^{.l}_{k} = \delta^{.l}_{p} \tag{1.10}_{3,4}$$

For the components of the stress function tensors the following formulas can be written:

$$\underline{h}^{.l}_{\eta} = h^{.T}_{S}\tau^{.S}_{\eta}\sigma^{.l}_{T} \tag{1.11}_1$$

$$\underline{h}^{.l}_{3} = h^{.T}_{S}\tau^{.S}_{3}\sigma^{.l}_{T} \tag{1.11}_2$$

$$\underline{f}_{\eta b} = f_{XY}\tau^{.X}_{\eta}\tau^{.Y}_{b} \tag{1.11}_3$$

$$\underline{f}_{3b} = f_{XY}\tau^{.X}_{3}\tau^{.Y}_{b}\,. \tag{1.11}_4$$

The paper assumes, that the transformations $(1.11)_1$ and $(1.11)_3$ between the stress functions h^T_S, $\underline{h}^{.l}_{\eta}$ and f_{XY}, $\underline{f}_{\eta b}$ are possible in a one-to-one manner. In this case six independent, not identically zero stress functions $\underline{h}^{.l}_{\eta}$ are ordered to the six independent, not identically zero stress functions h^T_S and vice versa. A similar statement is valid for the stress functions f_{XY} and $\underline{f}_{\eta b}$.

The stress functions $h^{.l}_{3}$ and f_{3b} are not present in the equations concerning the body boundary surface.

In the paper, generally, the introduced coordinate system (ξ) is applied for the equations on the surface of the body.

1.6. The strain fields $\gamma_{kl}(x)$, $\kappa_a^{\cdot b}(x)$ are called {compatible} [kinematically admissible] if the differential equations

$$\gamma_{kl}(x) = u_{l;k} + \varepsilon_{lks}\varphi^s \qquad x \in V \qquad (1.12)_1$$

$$\kappa_a^{\cdot b}(x) = \varphi^a_{\cdot;b} \qquad x \in V \qquad (1.12)_2$$

have solutions for the displacement fields u_k and φ^a [and the solution satisfies the kinematic boundary conditions (1.2)].

With the knowledge of the {compatible} [kinematically admissible] strain fields, the displacement fields can be formulated by the Cezaro's formula [11].

Let the incompatibility tensors be denoted by e^{yb} and $d^y_{\cdot l}$:

$$e^{yb}(x) = \varepsilon^{ypa}\kappa_{a\cdot;p}^{\cdot b} \qquad x \in V \qquad (1.13)_1$$

$$d^y_{\cdot l}(x) = \varepsilon^{ymk}(\gamma_{kl;m} + \varepsilon_{kls}\kappa_m^{\cdot s}) \qquad x \in V. \qquad (1.13)_2$$

The independent, necessary and sufficient conditions of the compatibility of the strain fields $\gamma_{kl}(x)$ and $\kappa_{ab}(x)$ were given in the paper [9]. Accordingly, the six-six compatibility field equations and compatibility boundary conditions concerning the strain fields should be valid:

compatibility field equations:

$$e^{XY}(x) = 0\,, \qquad d^S_{\cdot T}(x) = 0 \qquad x \in V \qquad (1.14)_{1,2}$$

compatibility boundary conditions:

$$n_y e^{yb}(x) = 0\,, \qquad n_y d^y_l(x) = 0 \qquad x \in S \qquad (1.15)_{1,2}$$

In the equations (1.11) the index pairs XY, ST should be chosen in the same way as has been shown in paragraph *1.4.* concerning the non zero coordinates f_{XY}, h_S^T of the stress function tensors f_{yb}, h_y^l.

Let us note, that to the compatibility of the strain fields as in the classical case — the existence of one part of the compatibility equations $e^{yb} = 0$, $d^y_{\cdot l} = 0$ and the compatibility boundary conditions are enough. In this situation the other compatibility equations

$$e^{AB}(x) = 0\,, \qquad d^K_{\cdot L}(x) = 0 \qquad x \in V \qquad (1.16)_{1,2}$$

are also valid

2. Dual equation system of linear micropolar elastostatics

2.1. Configuration variable of dual equation system of linear classical elastostatics is the stress function tensor field, the intermediate variable of first kind is the stress field, the intermediate variable of second kind is the strain field. [2, 3, 7].

The total dual equation system also including the correct boundary conditions was determined by Kozák, I. principally in such a way that in the case of stress

formulation of the boundary value problems of classical elastostatics the stress fields were written in the usual manner [1, 2, 3] with the help of stress function tensor, also taking note of the change of zero and non zero components of stress function tensor and correct forms of the boundary conditions as well. Composing the dual boundary value problem of linear micropolar elastostatics the present paper principally follows the same order of ideas.

2.2. Field equations and boundary conditions of micropolar elastostatics written for stress fields are the following:

compatibility field equations

$$e^{XY}(x)=\varepsilon^{Xpa}\kappa^{\cdot Y}_{a\cdot;p}=0\,, \qquad x\in V \tag{2.1}_1$$

$$d^{S}_{\cdot T}(x)=\varepsilon^{Smk}(\gamma_{kT;m}+\varepsilon_{kTs}\kappa^{\cdot s}_{m})=0 \qquad x\in V\,; \tag{2.1}_2$$

compatibility boundary conditions

$$\underline{n}_y\underline{e}^{yb}(\xi)=\underline{e}^{3b}=\underline{\varepsilon}^{3\pi\alpha}\underline{\varkappa}^{\cdot b}_{\alpha\cdot;\pi}=0\,, \qquad \xi\in S \tag{2.2}_1$$

$$\underline{n}_y\underline{d}^{y}_{\cdot l}(\xi)=\underline{d}^{3}_{\cdot l}=\varepsilon^{3\nu\chi}(\underline{\gamma}_{\chi l;\nu}+\underline{\varepsilon}_{\chi ls}\underline{\kappa}^{\cdot s}_{\nu})=0\,, \qquad \xi\in S \tag{2.2}_2$$

displacement boundary conditions

$$\underline{u}_k=\hat{\underline{u}}_k\,, \qquad \underline{\varphi}^{\lambda}=\hat{\underline{\varphi}}^{\lambda} \qquad \xi\in S_u \tag{2.3}_{1,2}$$

Hooke's law

$$\gamma_{kl}=a_{klpq}t^{pq}\,, \qquad \kappa_{ab}=c_{abpq}\mu^{pq} \qquad x\in V \tag{2.4}_{1,2}$$

stress boundary conditions

$$\underline{n}_k\underline{t}^{kl}=\hat{\underline{t}}^{l}\,, \qquad \underline{n}_a\underline{\mu}^{a}_{\cdot b}=\hat{\underline{\mu}}_b \qquad \xi\in S_t \tag{2.5}_{1,2}$$

equilibrium equations

$$\begin{aligned} &t^{kl}_{\cdot\cdot;k}+b^{l}=0\,, \\ &\mu^{a}_{\cdot b;a}+\varepsilon_{bpq}t^{pq}+c_b=0\,. \end{aligned} \qquad x\in V \tag{2.6}_{1,2}$$

The dual equation system can be obtained from the above equations making use of two further ideas and equation (1.6).

I. In the case of the existence of the equations

$$\underline{\gamma}_{\chi l}-\hat{\underline{\mu}}_{l;\chi}-\underline{\varepsilon}_{l\chi s}\hat{\underline{\varphi}}s=0 \qquad \xi\in S_u \tag{2.7}_1$$

$$\underline{\varkappa}^{b}_{\alpha}-\hat{\underline{\varphi}}^{b}_{\cdot;\alpha}=0 \qquad \xi\in S_u \tag{2.7}_2$$

the compatibility boundary conditions (2.2) are valid on boundary S_u, and — by the Cezaro's formula* [9, 11] — the displacement field, which satisfy the displacement boundary conditions, can be composed.

It is to be noted that to the existence of kinematically admissible strain fields $\gamma_{kl}(x)$, $\kappa^{b}_{a}(x)$ — taking into account the above — the validity of (2.1) in V, (2.2) on S_t and (2.7) on S_u are necessary.

* Formulas, shown in [11] are valid in a rectilinear coordinate system.

II. Let us change the not identically zero stress function tensors $\underset{\eta}{\hat{h}}^{l}(\xi)$, $\underset{\eta b}{\hat{f}}(\xi)$ $\xi \in S_t$ in such a way, that the equations

$$\underset{}{\hat{t}}^{l} - \underset{}{\mathring{t}}^{l} = \underset{}{\varepsilon}^{3\nu\eta} \underset{\eta.;\nu}{\hat{h}}^{l} \qquad \xi \in S_t \qquad (2.8)_1$$

$$\underset{b}{\hat{\mu}} - \underset{b}{\mathring{\mu}} = \underset{}{\varepsilon}^{3\pi\eta} (\underset{\eta b;\pi}{\hat{f}} + \underset{}{\varepsilon}_{b\pi l} \underset{\eta}{\hat{h}}^{l}) \qquad \xi \in S_t \qquad (2.8)_2$$

where

$$\underset{}{\mathring{t}}^{l} = \underset{}{\mathring{t}}^{3l}, \qquad \underset{b}{\mathring{\mu}} = \underset{.b}{\mathring{\mu}}^{3} \qquad \xi \in S \qquad (2.9)$$

become valid. Let us assume that the stress function tensors $\underset{\eta}{\hat{h}}^{l}(\xi)$, $\underset{\eta b}{\hat{f}}(\xi)$ are known. In this case the equations

$$\underset{}{\varepsilon}^{3\nu\eta} (\underset{\eta}{h}^{l} - \underset{\eta}{\hat{h}}^{l})_{;\nu} = 0 \qquad \xi \in S_t \qquad (2.10)_1$$

$$\underset{}{\varepsilon}^{3\pi\eta} [\underset{\eta b;\pi}{f} - \underset{\eta b;\pi}{\hat{f}} + \underset{}{\varepsilon}_{b\pi l} (\underset{\eta}{h}^{l} - \underset{\eta}{\hat{h}}^{l})] = 0 \qquad \xi \in S_t \qquad (2.10)_2$$

are equivalent to the stress boundary conditions $(2.5)_{1,2}$, if the stress fields $\underset{}{t}^{kl}(\xi)$, $\underset{.b}{\mu}^{a}(\xi)$ are obtained with the help of formulas (1.6).

2.3. The field equations and boundary conditions of linear micropolar elastostatics are obtained from the equations (2.1)–(2.6) by the equation (1.6) and the ideas of I and II:

field equations

$$\varepsilon^{kmy} \mathrm{h}^{l}_{y.;m} = t^{kl} - \mathring{t}^{kl} \qquad x \in V \qquad (2.11)_1$$

$$\varepsilon^{apy} (f_{yb;p} + \varepsilon_{bpl} h^{l}_{y.}) = \mu^{a}_{.b} - \mathring{\mu}^{a}_{.b} \qquad x \in V \qquad (2.11)_2$$

$$a_{klpq} t^{pq} = \gamma_{kl} \qquad x \in V \qquad (2.12)_1$$

$$c_{abpq} \mu^{pq} = \kappa_{ab} \qquad x \in V \qquad (2.12)_2$$

$$e^{XY} = \varepsilon^{Xpa} \kappa^{.Y}_{a.;p} = 0 \qquad x \in V \qquad (2.13)_1$$

$$d^{S}_{.T} = \varepsilon^{Smk} (\gamma_{kT;m} + \varepsilon_{kTs} \kappa^{.s}_{m.}) = 0 \qquad x \in V \qquad (2.13)_2$$

boundary conditions

$$\underset{\chi l}{\gamma} - \underset{l;\chi}{\hat{u}} - \underset{l\chi s}{\varepsilon} \underset{}{\hat{\varphi}}^{s} = 0 \qquad \xi \in S_u \qquad (2.14)_1$$

$$\underset{\alpha}{\varkappa}^{b} - \underset{.;\alpha}{\hat{\varphi}}^{b} = 0 \qquad \xi \in S_u \qquad (2.14)_2$$

$$\underset{}{\varepsilon}^{3\pi\alpha} \underset{\alpha.;\pi}{\varkappa}^{b} = 0 \qquad \xi \in S_t \qquad (2.15)_1$$

$$\underset{}{\varepsilon}^{3\nu\chi} (\underset{\chi l;\nu}{\gamma} + \underset{\chi ls}{\varepsilon} \underset{\nu}{\varkappa}^{.s}) = 0 \qquad \xi \in S_t \qquad (2.15)_2$$

$$\underset{}{\varepsilon}^{3\nu\eta} (\underset{\eta.;\nu}{h}^{l} - \underset{\eta.;\nu}{\hat{h}}^{l}) = 0 \qquad \xi \in S_t \qquad (2.16)_1$$

$$\underset{}{\varepsilon}^{3\pi\eta} [\underset{\eta b;\pi}{f} - \underset{\eta b;\pi}{\hat{f}} + \underset{}{\varepsilon}_{b\pi l} (\underset{\eta}{h}^{l} - \underset{\eta}{\hat{h}}^{l})] = 0 \qquad \xi \in S_t \qquad (2.16)_2$$

condition of continuity along the curve g (Fig. 1)

$$\tau^{\alpha} (\underset{\alpha}{\varkappa}^{b} - \underset{.;\alpha}{\hat{\varphi}}^{b}) = 0 \qquad \xi \in g \qquad (2.17)_1$$

$$\underset{}{\tau}^{\chi} (\underset{\chi l}{\gamma} - \underset{l;\chi}{\hat{u}} - \underset{l\chi s}{\varepsilon} \underset{}{\hat{\varphi}}^{s}) = 0 \qquad \xi \in g \qquad (2.17)_2$$

where $\underline{\tau}^{\alpha}$ is the tangent unit of the curve g. We remark that the equations (2.17) include the self evident condition that the fields γ_{kl}, $\kappa_a^{\cdot b}$ change continuously throughout the curve.

Let us take into account that equations $(2.8)_{1,2}$ are formally equivalent to the compatibility boundary conditions. That is why the boundary conditions

$$\underline{h}_{\eta}^{\cdot l} - \hat{\underline{h}}_{\eta}^{\cdot l} = 0 \qquad \xi \in S_t \tag{2.18}_1$$

$$\underline{f}_{\eta b} - \hat{\underline{f}}_{\eta b} = 0 \qquad \xi \in S_t \tag{2.18}_2$$

can be prescribed instead of $(2.16)_{1,2}$. Owing to the above, either the equation system (2.11)–(2.17) or the equation system (2.11)–(2.15), (2.17)–(2.18) can be taken as the dual equation system.

The configuration variables of dual equation system are the stress function tensor fields $h_y^{\cdot l}$, f_{yb}, the intermediate variables of first kind are the stress fields t^{kl}, $\mu_{\cdot b}^{a}$ and the intermediate variables of second kind are the strain fields γ_{kl}, $\kappa_a^{\cdot b}$.

3. Dual variational principles of linear micropolar elastostatics

3.1. The basic dual variational principle of linear micropolar elastostatics is the minimum complementary energy principle. The total complementary energy function

$$K = \frac{1}{2}\int_V (\gamma_{kl} t^{kl} + \kappa_a^{\cdot b}\mu_{\cdot b}^{a})\,\mathrm{d}V - \int_{S_u} (n_k t^{kl}\hat{u}^l + n_a \mu_{\cdot b}^{a}\hat{\varphi}^b)\,\mathrm{d}S \tag{3.1}$$

is a functional on the statically admissible stress fields $t^{kl}(x)$, $\mu_{\cdot b}^{a}(x)$, because the values of γ_{kl}, $\kappa_a^{\cdot b}$ are obtained from the statically admissible stress fields with the help of constitutive law (2.12). Owing to the total complementary energy minimum principle the above functional has at the exact solution — that is, if the statically admissible strain fields being obtained from the statically admissible stress fields are also at the same time kinematically admissible — a strict minimum.

The first dual functional belongs to the dual equation system (2.11)–(2.17) or (2.11)–(2.15), (2.17)–(2.18) can be obtained from (3.1), that the statically admissible stress fields are expressed in terms of stress functions on the base of (2.11):

$$K = \frac{1}{2}\int_V (\gamma_{kl} t^{kl} + \kappa_a^{\cdot b}\mu_{\cdot b}^{a})\,\mathrm{d}V - \int_{S_u} \{(\underline{\varepsilon}^{3\gamma\eta}\underline{h}_{\eta;\gamma}^{\cdot l} + \underline{\overset{\circ}{t}}^{l})\underline{\hat{u}}_l +$$

$$+ [\underline{\varepsilon}^{3\pi\eta}(\underline{f}_{\eta b;\pi} + \underline{\varepsilon}_{b\pi l}\underline{h}_{\eta}^{\cdot l}) + \underline{\mathring{\mu}}_b]\underline{\hat{\varphi}}^b\}\,\mathrm{d}S\,. \tag{3.2}$$

Further for the time being we can concentrate on the equation system (2.11)–(2.17).

In this case the field equations (2.11), (2.12) as subsidiary conditions, and the equations (2.16) as boundary conditions belong to the functional (3.2).

Kozák, I. and the author proved [9], that from the stationarity condition of the functional (3.2) as Euler equations — taking into consideration that the one components of the stress function tensors are identically zero — follow the field equations $(2.13)_{1,2}$ and — as natural boundary conditions — the boundary conditions (2.14), (2.15), and further the equations of continuity (2.17) exists, too. In other words, from the stationarity of the functional (3.2) we obtain the kinematical admissability of strain fields $\gamma_{kl}(x)$, $\kappa_a^{\cdot b}(x)$.

3.2. Free variational problem without subsidiary conditions can be obtained by the method of Lagrange multipliers be denoted by

$$\overset{(t)}{\lambda}{}^{kl},\ \overset{(\mu)}{\lambda}{}^{a}_{\cdot b},\ \overset{(\gamma)}{\lambda}{}_{kl},\ \overset{(\kappa)}{\lambda}{}^{\cdot b}_{a},$$

$$\overset{(u)}{\underline{\lambda}}{}_{l},\ \overset{(\varphi)}{\underline{\lambda}}{}^{\cdot}.$$

which are at this moment unknowns yet. With them and with the use of equations of subsidiary conditions (2.11), (2.12) and (2.16) the next functional can be built up from (3.2):

$$\tilde{J}_4(\gamma_{kl}, \kappa_a^{\cdot b}, t^{kl}, \mu^a_{\cdot b}, h^{\cdot l}_{y}, f_{yb}, \underline{\hat{h}}^{\cdot l}_{\eta}, \underline{\hat{f}}_{\eta b}, \overset{(\gamma)}{\lambda}{}_{kl}, \overset{(\kappa)}{\lambda}{}^{\cdot b}_{a},$$

$$\overset{(t)}{\lambda}{}^{kl}, \overset{(\mu)}{\lambda}{}^{a}_{\cdot b}, \overset{(u)}{\underline{\lambda}}{}^{l}, \overset{(\varphi)}{\underline{\lambda}}{}^{b}) = \tilde{J}_4^{V1} + \tilde{J}_4^{V2} + \tilde{J}_4^{U} + \tilde{J}_4^{T} \tag{3.3}_1$$

where

$$\tilde{J}_4^{V1} = \frac{1}{2}\int_V (t^{kl}\gamma_{kl} + \mu^a_{\cdot b}\kappa_a^{\cdot b})\,\mathrm{d}V + \frac{1}{2}\int_V [\overset{(t)}{\lambda}{}^{kl}(a_{klpq}t^{pq} - \gamma_{kl}) +$$

$$+ \overset{(\mu)}{\lambda}{}^{ab}(c_{abpq}\mu^{pq} - \kappa_{ab})]\,\mathrm{d}V \tag{3.3}_2$$

$$\tilde{J}_4^{V2} = -\int_V \{\overset{(\gamma)}{\lambda}{}_{kl}(t^{kl} - \mathring{t}^{kl} - \varepsilon^{kmy}h^{\cdot l}_{y;m}) + \overset{(\kappa)}{\lambda}{}^{\cdot b}_{a}[\mu^a_{\cdot b} - \mathring{\mu}^a_{\cdot b} - \varepsilon^{apy}(f_{yb;p} + \varepsilon_{bps}h^{\cdot s}_{y})]\}\,\mathrm{d}V \tag{3.3}_3$$

$$\tilde{J}_4^{U} = -\int_{S_u} \{(\underline{\varepsilon}^{3\nu\eta}\underline{h}^{\cdot l}_{\eta\cdot;\nu} + \mathring{\underline{t}}^{l})\hat{\underline{u}}_l + [\underline{\varepsilon}^{3\pi\eta}(\underline{f}_{\eta b;\pi} + \varepsilon_{b\pi s}\underline{h}^{s}_{\eta}) + \underline{\mathring{\mu}}_b]\hat{\underline{\varphi}}^{b}\}\,\mathrm{d}S \tag{3.3}_4$$

$$\tilde{J}_4^{T} = \int_{S_t} \{\underline{\varepsilon}^{3\nu\eta}(\underline{h}^{\cdot l}_{\eta\cdot;\nu} - \underline{\hat{h}}^{\cdot l}_{\eta\cdot;\nu})\overset{(u)}{\underline{\lambda}}{}_{l} + \underline{\varepsilon}^{3\pi\eta}[\underline{f}_{\eta b;\pi} - \underline{\hat{f}}_{\eta b;\pi} + \underline{\varepsilon}_{b\pi s}(\underline{h}^{s}_{\eta} - \underline{\hat{h}}^{s}_{\eta})]\overset{(\varphi)}{\underline{\lambda}}{}^{b}\}\,\mathrm{d}S\,. \tag{3.3}_5$$

The functional $\tilde{J}_4$ can be transformed by using (6.2), (6.3), (6.4) and reordering into the following form

$$\tilde{J}_4 = \tilde{J}_4^{V1} + \tilde{J}_4^{V21} + \tilde{J}_4^{V22} + \tilde{J}_4^{T1} + \tilde{J}_4^{U1} + \tilde{J}_4^{G1} + \tilde{J}_4^{T2} + \tilde{J}_4^{G2} \tag{3.4}_1$$

Here

$$\tilde{J}_4^{V21} = -\int_V [\overset{(\gamma)}{\lambda}_{kl}(t^{kl} - \mathring{t}^{kl}) + \overset{(\kappa)}{\lambda}_a^{\cdot b}(\mu_{\cdot b}^a - \mathring{\mu}_{\cdot b}^a)]\, \mathrm{d}V \tag{3.4}_2$$

$$\tilde{J}_4^{V22} = \int_V [\varepsilon^{ypa} \overset{(\kappa)}{\lambda}_{a.;p}^{\cdot b} f_{yb} + \varepsilon^{ymk}(\overset{(\gamma)}{\lambda}_{kl;m} + \varepsilon_{kls} \overset{(\kappa)}{\lambda}_m^{\cdot s}) h_y^{\cdot l}]\, \mathrm{d}V \tag{3.4}_3$$

$$\tilde{J}_4^{T1} = -\int_{S_t} [\underline{\varepsilon}^{3\chi\eta}(\overset{(\gamma)}{\underline{\lambda}}_{\chi l} + \overset{(u)}{\underline{\lambda}}_{l;\chi} + \underline{\varepsilon}_{l\chi s} \overset{(\varphi)}{\underline{\lambda}}^s) \underline{h}_\eta^{\cdot l} + + \underline{\varepsilon}^{3\alpha\eta}(\overset{(\kappa)}{\underline{\lambda}}_\alpha^{\cdot b} + \overset{(\varphi)}{\underline{\lambda}}_{\cdot;\alpha}^b)\, \underline{f}_{\eta b}]\, \mathrm{d}S \tag{3.4}_4$$

$$\tilde{J}_4^{U1} = -\int_{S_u} [\underline{\varepsilon}^{3\chi\eta}(\overset{(\gamma)}{\underline{\lambda}}_{\chi l} - \hat{\underline{u}}_{l;\chi} - \underline{\varepsilon}_{l\chi s} \hat{\underline{\varphi}}^s) \underline{h}_\eta^{\cdot l} + + \underline{\varepsilon}^{3\alpha\eta}(\overset{(\kappa)}{\underline{\lambda}}_\alpha^{\cdot b} - \hat{\underline{\varphi}}_{\cdot;\alpha}^b)\, \underline{f}_{\eta b} + \mathring{\underline{t}}^l \hat{\underline{u}}_l + \mathring{\underline{\mu}}_b \hat{\underline{\varphi}}^b]\, \mathrm{d}S \tag{3.4}_5$$

$$\tilde{J}_4^{G1} = \oint_g [(\overset{(u)}{\underline{\lambda}}_l + \hat{\underline{\mu}}_l) \underline{h}_\eta^{\cdot l} \underline{\tau}^\eta + (\overset{(\varphi)}{\underline{\lambda}}^b + \hat{\underline{\varphi}}^b) \underline{f}_{\eta b} \underline{\tau}^\eta]\, \mathrm{d}s \tag{3.4}_6$$

$$\tilde{J}_4^{T2} = \int_{S_t} [\underline{\varepsilon}^{3\chi\eta}(\overset{(u)}{\underline{\lambda}}_{l;\chi} + \underline{\varepsilon}_{l\chi s} \overset{(\varphi)}{\underline{\lambda}}^s) \hat{\underline{h}}_\eta^{\cdot l} + + \underline{\varepsilon}^{3\alpha\eta} \overset{(\varphi)}{\underline{\lambda}}_{\cdot;\alpha}^b\, \hat{\underline{f}}_{\eta b}]\, \mathrm{d}S \tag{3.4}_7$$

$$\tilde{J}_4^{G2} = \oint_g (\overset{(u)}{\underline{\lambda}}_l \hat{\underline{h}}_\eta^{\cdot l} \underline{\tau}^\eta + \overset{(\varphi)}{\underline{\lambda}}^b \hat{\underline{f}}_{\eta b} \underline{\tau}^\eta)\, \mathrm{d}s\,. \tag{3.4}_8$$

3.3. For the determination of the unknown Lagrangian multipliers let us compose the variation of the functional $\tilde{J}_4$ with respect to the strain fields γ_{kl} and $\kappa_a^{\cdot b}$, the stress fields t^{kl} and $\mu_{\cdot b}^a$ and the stress function tensors $h_y^{\cdot l}$, f_{yb}, $\underline{h}_\eta^{\cdot l}$, $\underline{f}_{\eta b}$ (variations with respect to the multipliers by making use of stationarity, give the subsidiary conditions) and let us apply the condition of stationarity.

It should be taken into account, that

— the stress function tensors have only six-six not identically zero coordinates which can be varied;

— the variations of the stress functions $\underline{h}_\eta^{\cdot l}$, $\underline{f}_{\eta b}$ according to the transformation formulas $(2.11)_1$, $(2.12)_1$ can be expressed with the variations of the six-six not identically zero components of the $h_y^{\cdot l}$, f_{yb} in a one-to-one manner (taking this fact the $\underline{h}_\eta^{\cdot l}$ and $\underline{f}_{\eta b}$ are varied freely on S_t);

— the stress functions $\hat{\underline{h}}_\eta^{\cdot l}$, $\hat{\underline{f}}_{\eta b}$ — though not freely — but can be varied on S_t.

This last should explained particularly.
The paper assumes, that

$$\delta \overset{\circ}{t}{}^{kl} = 0\,, \qquad \delta \overset{\circ}{\mu}{}^{a}_{.b} = 0\,. \tag{3.5}$$

Because the variation of the prescribed tractions on S_t are necessarily zero, the equations

$$\underset{\varepsilon}{}^{3\nu\eta}\delta \underset{\eta.;\nu}{\hat{h}}{}^{.l} = 0 \qquad \xi \in S_t \tag{3.6}_1$$

$$\underset{\varepsilon}{}^{3\pi\eta}(\delta \underset{\eta b;\pi}{\hat{f}} + \underset{b\pi l}{\varepsilon}\delta \underset{\eta}{\hat{h}}{}^{.l}) = 0 \qquad \xi \in S_t \tag{3.6}_2$$

which were obtained by the variation of the stress boundary conditions $(2.8)_{1,2}$ are valid. Let $\hat{r}^l$, $\hat{w}_b$ be arbitrary vector fields on S_t. It can easily be controlled, that the equations $(3.6)_{1,2}$ are always valid, if

$$\delta \underset{\eta}{\hat{h}}{}^{.l} = \delta \underset{.;\eta}{\hat{r}}{}^{l} \qquad \xi \in S_t \tag{3.7}_1$$

$$\delta \underset{\eta b}{\hat{f}} = \delta \underset{b;\eta}{\hat{w}} + \underset{b\eta l}{\varepsilon}\delta \underset{.}{\hat{r}}{}^{l} \qquad \xi \in S_t \tag{3.7}$$

The suitable variations of the functional $\tilde{J}_4$ can already be composed.*
From the conditions of stationarity

$$\delta_{t,\mu}\tilde{J}_4 = \delta_{t,\mu}\tilde{J}_4^{V1} + \delta_{t,\mu}\tilde{J}_4^{V21} = 0 \tag{3.8}_1$$

$$\delta_{\gamma,\kappa}\tilde{J}_4 = \delta_{\gamma,\kappa}\tilde{J}_4^{V1} = 0 \tag{3.8}_2$$

$$\delta_{h,f}\tilde{J}_4 = \delta_{h,f}\tilde{J}_4^{T1} + \delta_{h,f}\tilde{J}_4^{U1} + \delta_{h,f}\tilde{J}_4^{G1} = 0 \tag{3.8}_3$$

and by making use of the above-mentioned ideas and the formulas $(3.3)_2$, $(3.4)_{2,\ldots 5}$, because of the fact, that the variations are arbitrary the following equations and boundary conditions can be obtained:

$$\frac{1}{2}\gamma_{kl} + \frac{1}{2}\overset{(t)}{\lambda}{}^{pq}a_{pqkl} - \overset{(\gamma)}{\lambda}_{kl} = 0$$

$$\frac{1}{2}\kappa_a^{.b} + \frac{1}{2}\overset{(\mu)}{\lambda}{}^{pq}c_{pqa}^{\cdot\cdot\cdot b} - \overset{(\kappa)}{\lambda}{}_a^{.b} = 0 \qquad x \in V \tag{3.9}_{1,2}$$

$$t^{kl} - \overset{(t)}{\lambda}{}^{kl} = 0\,, \quad \mu^a_{.b} - \overset{(\mu)}{\lambda}{}^a_{.b} = 0 \qquad x \in V \tag{3.9}_{3,4}$$

$$\varepsilon^{Xpa}\overset{(\kappa)}{\lambda}{}^{.Y}_{a.;p} = 0$$

$$\varepsilon^{Smk}(\overset{(\gamma)}{\lambda}_{kT;m} + \varepsilon_{kTs}\overset{(\kappa)}{\lambda}{}^{.s}_{m}) = 0 \qquad x \in V \tag{3.10}_{1,2}$$

* The indices beside δ, at the bottom right corner show the variable by which the variation was formed.

$$\overset{(\gamma)}{\underline{\lambda}}_{\chi l} + \overset{(u)}{\underline{\lambda}}_{l;\chi} + \underline{\varepsilon}_{l\chi s}\overset{(\varphi)}{\underline{\lambda}}^{s} = 0$$

$$\overset{(\kappa)}{\underline{\lambda}}_{\alpha}^{\cdot b} + \overset{(\varphi)}{\underline{\lambda}}_{\cdot;\alpha}^{b} = 0 \qquad \xi \in S_t \qquad (3.10)_{3,4}$$

$$\overset{(\gamma)}{\underline{\lambda}}_{\chi l} - \hat{\underline{u}}_{l;\chi} - \underline{\varepsilon}_{l\chi s}\hat{\underline{\varphi}}^{s} = 0$$

$$\overset{(\kappa)}{\underline{\lambda}}_{\alpha}^{\cdot b} - \hat{\underline{\varphi}}_{\cdot;\alpha}^{b} = 0 \qquad \xi \in S_u \qquad (3.10)_{5,6}$$

$$\overset{(u)}{\underline{\lambda}}_{l} + \hat{\underline{u}}_{l} = 0 \qquad \overset{(\varphi)}{\underline{\lambda}}^{b} + \hat{\underline{\varphi}}^{b} = 0 \qquad \xi \in g \qquad (3.10)_{7,8}$$

By using the identities of (6.5) and (6.6) it can be seen, that

$$\delta_{\hat{h},\hat{f}}\bar{J}_4 = \delta_{\hat{h},\hat{f}}\bar{J}_4^{T2} + \delta_{\hat{h},\hat{f}}\bar{J}_4^{G2} \equiv 0\,. \qquad (3.11)$$

Since the above equation is an identity by the variations of $\underline{\hat{h}}_{\eta}^{\cdot l}$ and $\underline{\hat{f}}_{\eta b}$ we do not get any further equations.

From the equations (3.9), (3.10) and the subsidiary conditions (2.11), (2.12), (2.16) — taking also into account that the vector fields $\overset{(u)}{\underline{\lambda}}_{l}$ and $\overset{(\varphi)}{\underline{\lambda}}^{b}$ $\xi \in S_t$ being obtained on the base of the equations $(3.10)_{3,4}$ and $(3.10)_{7,8}$ by the Cesaro's formula give the real solutions $\underline{u}_l$, $\underline{\varphi}^b$ — we get the following results on the Lagrangian multipliers:

$$\overset{(t)}{\lambda}^{kl} = t^{kl}\,, \qquad \overset{(\mu)}{\lambda}_{\cdot b}^{a} = \mu_{\cdot b}^{a} \qquad x \in V \qquad (3.12)_1$$

$$\overset{(\gamma)}{\lambda}_{kl} = \gamma_{kl}\,, \qquad \overset{(\kappa)}{\lambda}_{a}^{\cdot b} = \kappa_{a}^{\cdot b} \qquad x \in V \qquad (3.12)_2$$

$$\overset{(u)}{\underline{\lambda}}_{l} = -\underline{u}_l \qquad \overset{(\varphi)}{\underline{\lambda}}^{b} = -\underline{\varphi}^{b} \qquad \xi \in S_t \qquad (3.12)_3$$

3.4. On the base of formulas (3.12) the Lagrangian multipliers can be ignored from the equation (3.3). After resubstitution of the multipliers we obtain the functional $\overset{*}{J}_4$ of a variational principle which is equivalent with the equation system (2.11)–(2.17):

$$\overset{*}{J}_4 = \overset{*}{J}_4(\gamma_{kl}, \kappa_{a}^{\cdot b}, t^{kl}, \mu_{a}^{\cdot b}, h_{y}^{\cdot l}, f_{yb}, \underline{\hat{h}}_{\eta}^{\cdot l}, \underline{\hat{f}}_{\eta b}, \underline{u}_l, \underline{\varphi}^{b}) =$$
$$= \overset{*}{J}_4^{V} + \overset{*}{J}_4^{V'} + \overset{*}{J}_4^{U} + \overset{*}{J}_4^{T} \qquad (3.13)_1$$

where

$$\overset{*}{J}_4^{V} = \frac{1}{2}\int_V (\gamma_{kl}t^{kl} + \kappa_{a}^{\cdot b}\mu_{\cdot b}^{a})\,\mathrm{d}V +$$

$$+ \frac{1}{2}\int_V [t^{kl}(a_{klpq}t^{pq} - \gamma_{kl}) + \mu^{ab}(c_{abpq}\mu^{pq} - \kappa_{ab})]\,\mathrm{d}V \qquad (3.13)_2$$

$$\overset{*}{J}_4^{V'} = -\int_V \{\gamma_{kl}(t^{kl} - \mathring{t}^{kl} - \varepsilon^{kmy} h^{l}_{y.;m}) +$$

$$+ \kappa^{.b}_{a}[\mu^{a}_{.b} - \mathring{\mu}^{a}_{.b} + \varepsilon^{apy}(f_{yb;p} + \varepsilon_{bps}{}^{h.s}_{y})]\} \, \mathrm{d}V \qquad (3.13)_3$$

$$\overset{*}{J}_4^{U} = \mathring{J}_4^{U} \qquad (3.13)_4$$

$$\overset{*}{J}_4^{T} = -\int_{S_t} \{\underset{\sim}{\varepsilon}^{3\nu\eta}(\underset{\sim}{h}^{l}_{\eta.;\nu} - \underset{\sim}{\hat{h}}^{l}_{\eta.;\nu})\underset{\sim}{u}_l +$$

$$+ \underset{\sim}{\varepsilon}^{3\pi\eta}[\underset{\sim}{f}_{\eta b;\pi} - \underset{\sim}{\hat{f}}_{\eta b;\pi} + \underset{\sim}{\varepsilon}_{b\pi s}(\underset{\sim}{h}^{s}_{\eta} - \underset{\sim}{\hat{h}}^{s}_{\eta})]\underset{\sim}{\varphi}^{b}\} \, \mathrm{d}S \, . \qquad (3.13)_5$$

From the condition of stationarity $\delta \overset{*}{J}_4 = 0$ follows the validity of the dual equation system (2.11)–(2.17). For proof the chain of ideas by which the equation (3.9), (3.10) was obtained should be repeated. Not seeing the transformations particularly we only briefly show what kind of equations and boundary conditions are followed from the variations of the functional $\overset{*}{J}_4$ with respect to the different variables.

The equations

$$\delta_{t,\mu} \overset{*}{J}_4 = 0, \qquad \delta_{\gamma,\kappa} \overset{*}{J}_4 = 0 \qquad (3.14)_1$$

made sure of the existence of $(2.11)_{1,2}$ and $(2.12)_{1,2}$.

From the equation

$$\delta_{h,f} \overset{*}{J}_4 = 0 \qquad (3.14)_2$$

follow $(2.13)_{1,2}$, $(2.14)_{1,2}$ and further

$$\underset{\sim}{\lambda}_{\chi l} - \underset{\sim}{u}_{l;\chi} - \varepsilon_{l\chi s}\underset{\sim}{\varphi}^{s} = 0 \, , \qquad \underset{\sim}{\varkappa}^{.b}_{\alpha} - \underset{\sim}{\varphi}^{b}_{.;\alpha} = 0 \qquad \xi \in S_t \qquad \text{(a)}$$

$$\underset{\sim}{u}_l = \underset{\sim}{\hat{u}}_l \, , \qquad \underset{\sim}{\varphi}^{b} = \underset{\sim}{\hat{\varphi}}^{b} \qquad \xi \in g \qquad \text{(b)}$$

In the case of the existence of the latest equations the compatibility boundary conditions $(2.15)_{1,2}$ are also valid and $(2.17)_{1,2}$ is also true.

The real displacement field $\underset{\sim}{u}_l$, $\underset{\sim}{\varphi}^{b}$ can be determined by the Cesaro's formula [9, 11].

From the equation

$$\delta_{u,\varphi} \overset{*}{J}_4 = 0 \qquad (3.14)_3$$

we obtain $(2.16)_{1,2}$, while the equation

$$\delta_{\hat{h},\hat{f}} \overset{*}{J} \equiv 0 \qquad (3.14)_4$$

is an identity, and does not give further equations.

3.5. If we consider equations (2.11)–(2.15), (2.17)–(2.18) as the dual equation system, then — for the composition of the equivalent variational problem — we should take the field equations (2.11), (2.12) and further the boundary condition* (2.18) and the condition of continuity

$$\underset{\sim}{\tau}^{\eta}(\underset{\sim}{h}^{l}_{\eta} - \underset{\sim}{\hat{h}}^{l}_{\eta}) = 0 \, , \qquad \underset{\sim}{\tau}^{\eta}(\underset{\sim}{f}_{\eta b} - \underset{\sim}{\hat{f}}_{\eta b}) = 0 \qquad \xi \in g \qquad (3.15)$$

* The suitable form:

$$\underset{\sim}{\varepsilon}^{3\chi\eta}(\underset{\sim}{h}^{l}_{\eta} - \underset{\sim}{\hat{h}}^{l}_{\eta}) = 0 \, , \qquad \underset{\sim}{\varepsilon}^{3\chi\eta}(\underset{\sim}{f}_{\eta b} - \underset{\sim}{\hat{f}}_{\eta b}) = 0 \, .$$

as joining subsidiary conditions to the functional (3.2). To obtain free variational problem it is also possible by using the Lagrangian multipliers method. Not showing the formal transformations, at last we obtain the functional of the free variational problem

$$J_4 = J_4(\gamma_{kl}, \kappa_a^{\cdot b}, t^{kl}, \mu^a_{\cdot b}, h_y^{\cdot l}, f_{yb}, \underline{\hat{h}}_\eta^{\cdot l}, \underline{\hat{f}}_{\eta b}) =$$

$$= J_4^V + J_4^{V'} + J_4^U + J_4^T + J_4^G \tag{3.16}_1$$

where

$$J_4^V = \overset{*}{J}{}_4^V \qquad J_4^{V'} = \overset{*}{J}{}_4^{V'} \tag{3.16}_{2,3}$$

$$J_4^U = \overset{*}{J}{}_4^U = \tilde{J}_4^U \tag{3.16}_4$$

and

$$J_4^T = \int_{S_t} [\underline{\varepsilon}^{3\chi\eta}(\underline{h}_\eta^{\cdot l} - \underline{\hat{h}}_\eta^{\cdot l})\,\underline{\lambda}_{l\chi} + \underline{\varepsilon}^{3\alpha\eta}(\underline{f}_{\eta b} - \underline{\hat{f}}_{\eta b})\underline{\varkappa}^b_{\cdot\alpha}]\,\mathrm{d}S \tag{3.16}_5$$

$$J_4^G = -\oint_g [\underline{\hat{u}}_l(\underline{h}_\eta^{\cdot l} - \underline{\hat{h}}_\eta^{\cdot l})\underline{\tau}^\eta + \underline{\hat{\varphi}}^b(\underline{f}_{\eta b} - \underline{\hat{f}}_{\eta b})\tau^\eta]\,\mathrm{d}s \tag{3.16}_6$$

Remark: Such kinds of functionals can also be constructed which ascertain the existence of — beside the equations (2.11)–(2.15) and (2.17)–(2.18) — the equation (2.8), too.

By using the formulas (6.2), (6.3) and (6.4) the functional J_4 can be transformed into the following forms:

$$J_4 = J_4(\gamma_{kl}, \kappa_a^{\cdot b}, t^{kl}, \mu^a_{\cdot b}, h_y^{\cdot l}, f_{yb}, \underline{\hat{h}}_\eta^{\cdot l}, \underline{\hat{f}}_{\eta b}) =$$

$$= J_4^{V1} + J_4^{V1'} + J_4^{U1} + J_4^{T1} + J_4^{G1} \tag{3.17}_1$$

where

$$J_4^{V1} = J_4^V \tag{3.17}_2$$

$$J_4^{V1'} = -\int_V [\gamma_{kl}(t^{kl} - \mathring{t}^{kl}) + \kappa_a^{\cdot b}(\mu^a_{\cdot b} - \mathring{\mu}^a_{\cdot b})]\,\mathrm{d}V +$$

$$+ \int_V [\varepsilon^{ypa}\kappa^{\cdot b}_{a\cdot;p} f_{yb} + \varepsilon^{ymk}(\gamma_{kl;m} + \varepsilon_{kls}\kappa_m^{\cdot s})h_y^{\cdot l}]\,\mathrm{d}V \tag{3.17}_3$$

$$J_4^{U1} = -\int_{S_u} [\underline{\varepsilon}^{3\chi\eta}(\underline{\gamma}_{\chi l} - \underline{\hat{u}}_{l;\chi} - \underline{\varepsilon}_{l\chi s}\underline{\hat{\varphi}}^s)\underline{h}_\eta^{\cdot l} +$$

$$+ \underline{\varepsilon}^{3\alpha\eta}(\underline{\varkappa}_\alpha^{\cdot b} - \underline{\hat{\varphi}}^b_{\cdot;\alpha})\underline{f}_{\eta b}]\,\mathrm{d}S \tag{3.17}_4$$

$$J_4^{T1} = \int_{S_t} (\underline{\varepsilon}^{3\chi\eta}\underline{\gamma}_{\chi l}\underline{\hat{h}}_\eta^{\cdot l} + \underline{\varepsilon}^{3\alpha\eta}\underline{\varkappa}_\alpha^{\cdot b}\underline{\hat{f}}_{\eta b})\,\mathrm{d}S \tag{3.17}_5$$

$$J_4^{G1} = \oint_g (\underline{\hat{u}}_l\underline{\hat{h}}_\eta^{\cdot l}\underline{\tau}^\eta + \underline{\hat{\varphi}}^b\underline{\hat{f}}_{\eta b}\underline{\tau}^\eta)\,\mathrm{d}s\,. \tag{3.17}_6$$

If the variations of the functional J_4 are composed with respect to its different variables, then — from the condition of stationarity, since the variations are arbitrary — the existence of the dual equation system (2.11)–(2.15), (2.17)–(2.18) follows. Really, from the equations

$$\delta_{\gamma,\kappa} J_4 = \delta_{\gamma,\kappa} J_4^{V'} + \delta_{\gamma,\kappa} J_4^{T} = 0 \tag{3.18}_1$$

$$\delta_{t,\mu} J_4 = \delta_{t,\mu} J_4^{V} + \delta_{t,\mu} J_4^{V'} = 0 \tag{3.18}_2$$

$$\delta_{h,f} J_4 = \delta_{h,f} J_4^{V1'} + \delta_{h,f} J_4^{U1} = 0 \tag{3.18}_3$$

$$\delta_{\hat{h},\hat{f}} J_4 = \delta_{\hat{h},\hat{f}} J_4^{T1} + \delta_{\hat{h},\hat{f}} J_4^{G1} = 0 \tag{3.18}_4$$

we can put in order the field equations and boundary conditions (2.11), (2.18), (2.12), (2.13), (2.14), (2.15), if we take into account the statements concerning the structure of the stress function tensors and — in the case of $(3.18)_4$ — (3.7), (6.7), (6.8).

Further, the functionals of variational problems with subsidiary conditions are composed which can be obtained from the functional J_4.

3.6. It is possible to prescribe the existence of a material law as a subsidiary condition. In this case we get from J_4 the following functional

$$J_3 = J_3(\gamma_{kl}, \kappa_a^{\cdot b}, h_y^{\cdot l}, f_{yb}, \underset{\eta}{\hat{h}}{}^{\cdot l}, \underset{\eta}{\hat{f}}{}_{b}) = \\ = J_3^V + J_3^U + J_3^T + J_3^G \tag{3.19}_1$$

where

$$J_3^V = -\frac{1}{2}\int_V (\gamma_{kl} \underset{-1}{a}{}^{klpq} \gamma_{pq} + \kappa_{ab} \underset{-1}{c}{}^{abpq} \kappa_{pq})\, \mathrm{d}V + \int_V \{\gamma_{kl}(\overset{\circ}{t}{}^{kl} + \varepsilon^{kmy} h_{y;m}^{\cdot l}) + \\ + \kappa_a^{\cdot b}[\overset{\circ}{\mu}{}_{\cdot b}^{a} + \varepsilon^{apy}(f_{yb,p} + \varepsilon_{bps}{}^{p} h_y^{\cdot s})]\}\, \mathrm{d}V \tag{3.19}_2$$

and

$$J_3^U = J_4^U, \qquad J_3^S = J_4^S, \qquad J_3^G = J_4^G, \tag{3.19}_3$$

or

$$J_3 = J_3'(t^{kl}, \mu_{\cdot b}^{a}, h_y^{\cdot l}, f_{yb}, \underset{\eta}{\hat{h}}{}^{\cdot l}, \underset{\eta}{\hat{f}}{}_{b}) = \ldots \tag{3.19}_4$$

The equation $\delta J_3 = 0$ as a variational principle ascertain the existence of all the equations of the dual equations system (2.11)–(2.15), (2.17)–(2.18), except the constitutive law (2.12).

3.7. If the stress boundary condition is prescribed as a subsidiary condition, then the following functional is obtained:

$$J_2 = J_2(\gamma_{kl}, \kappa_a^{\cdot b}, t^{kl}, \mu_{\cdot b}^{a}, h_y^{\cdot l}, f_{yb}) = J_2^V + J_2^U \tag{3.10}_1$$

where

$$J_2^V = J_4^V + J_4^{V'}, \qquad J_2^U = J_4^U \tag{3.20}_{2,3,4}$$

The equation $\delta J_2 = 0$ as a variational principle assure the existence of all the equations of the dual equation system (2.11)–(2.15), (2.17)–(2.18) except the stress boundary condition (2.18). To prove this the transformations should be done as was previously. But it has to be taken in consideration that the stress function tensors $h_y^{.l}$ and f_{yb} can be varied also on S_t, and their variations can be constructed by the vektor fields $\hat{\underline{r}}^l$, $\hat{\underline{w}}_b$ according to (3.7). The transformations (6.7), (6.8) should also be used.

3.8. If the equation (2.11) is prescribed as a subsidiary condition, then — after applicable transformation — the next functional can be written as

$$J_1 = J_1(\gamma_{kl}, \kappa_a^{.b}, h_y^{.l}, f_{yb}, \hat{\underline{h}}_\eta^{.l}, \hat{\underline{f}}_{\eta b}) =$$
$$= J_1^V + J_1^U + J_1^T + J_1^G \qquad (3.21)_1$$

where

$$J_1^V = \frac{1}{2}\int_V (\gamma_{kl} t^{kl} + \kappa_a^{.b} \mu_{.b}^a)\, \mathrm{d}V + \frac{1}{2}\int_V [\gamma_{kl}(t^{kl} - \underset{-1}{a}{}^{klpq}\gamma_{pq}) +$$
$$+ \kappa_{ab}(\mu^{ab} - \underset{-1}{c}{}^{abpq}\kappa_{pq})]\, \mathrm{d}V \qquad (3.21)_2$$

and

$$J_1^U = J_4^U, \qquad J_1^T = J_4^T, \qquad J_1^G = J_4^G. \qquad (3.21)_{3,4,5}$$

At present the equation $\delta J_1 = 0$ ascertains — as a variational principle — the existence of the dual equation system (2.11)–(2.15), (2.17), (2.18), without the equation (2.11).

3.9. Three further functionals can be constructed, if the existence of any two of the subsidiary conditions (2.11), (2.12) and (2.18) are prescribed.

They are not presented here.

If the independent quantities in (3.16) satisfy all the three above-mentioned subsidiary conditions, then — from (3.16) — the form (3.2) of the total complementary energy function is followed.

3.10. If the values of the incompatibility tensors $e^{yb}(x)$, $d_{.l}^y(x)$ are prescribed on the body volume, then the following integral should be added to J_4, J_3, J_2, J_1 and to the above-mentioned three functionals.

$$\int_V (e^{yb} f_{yb} + d_{.l}^y h_y^{.l})\, \mathrm{d}V$$

From the functionals won in this way J_4, J_3 and K are analogous with the functionals L, M and K of paper [7] in a micropolar case.

3.11. From the functional $\overset{*}{J}_4$ the functional $\overset{*}{J}_3$, $\overset{*}{J}_2$ can be constructed in an order which are analogous with J_3, J_1. The connections $J_1 = \overset{*}{J}_1$ are also valid.

4. Summary

4.1. The paper determines the total dual equation system of micropolar elastostatics (all the field equations and boundary conditions) in the case of three dimensional problems.

4.2. The paper defines the dual functionals $\overset{*}{J}_4$ and J_4 of free variational problems which are equivalent with the dual equation systems (2.11)–(2.17) and (2.11)–(2.15), (2.17), (2.18), and further it determines the total system of dual functionals which are valid, besides different subsidiary conditions. Using the stationarity from the variations of dual functionals with respect to stress function tensors follows the compatibility of strain fields.

5. Acknowledgement

The author wishes to thank Professor I. KOZÁK (Head of Department of Mechanics, Miskolc) for his criticism and ádvises.

6. Appendix

6.1. In the appendix several long formal transformations are shown: Denotations are generally used, as has been shown in the previous text.

6.2. For the transformation of surface integrals the Stokes' theorem is also needed. In the case shown in Figure 1. let $C_a(\xi^1, \xi^2)$ be a suitably smooth vector field on the total surface S.

Then the Stokes' theorem is the following:

$$\int_{S_t} \underset{\sim}{\varepsilon}^{3\alpha\eta} \underset{\sim}{C}_{\alpha;\eta} \, \mathrm{d}S = - \oint_g \underset{\sim}{C}_\alpha \underset{\sim}{\tau}^\alpha \, \mathrm{d}s \tag{6.1}_1$$

$$\int_{S_u} \underset{\sim}{h}^{3\alpha\eta} \underset{\sim}{C}_{\alpha;\eta} \, \mathrm{d}S = \oint_g \underset{\sim}{C}_\alpha \underset{\sim}{\tau}^\alpha \, \mathrm{d}s \, . \tag{6.1}_2$$

Here s is an arc length measured in the direction of $\underset{\sim}{\tau}^\alpha$, $\underset{\sim}{\tau}^\alpha$ is the unit tangent of curve g.

6.3. The validity of the following equation can be proved by partial integration:

$$\begin{aligned} &\int_V [\overset{(\gamma)}{\lambda}_{kl} \varepsilon^{kmy} h^{.l}_{y.;m} + \overset{(\kappa)}{\lambda}{}^{.b}_{a} \varepsilon^{apy} (f_{yb;p} + \varepsilon_{bps} h^{.s}_{y})] \, \mathrm{d}V = \\ &= \int_V [\varepsilon^{ymk} (\overset{(\gamma)}{\lambda}_{kl;m} + \varepsilon_{kls} \overset{(\kappa)}{\lambda}{}^{.s}_{m}) h^{.l}_{y} + \varepsilon^{ypa} \overset{(\kappa)}{\lambda}{}^{.b}_{a.;p} f_{yb}] \, \mathrm{d}V - \\ &- \int_S (\underset{\sim}{\varepsilon}^{3\chi\eta} \overset{(\gamma)}{\underset{\sim}{\lambda}}_{\chi l} \underset{\sim}{h}^{.l}_{\eta} + \underset{\sim}{\varepsilon}^{3\alpha\eta} \overset{(\kappa)}{\underset{\sim}{\lambda}}{}^{.b}_{\alpha} \underset{\sim}{f}_{\eta b}) \, \mathrm{d}S \, . \end{aligned} \tag{6.2}$$

6.4. The following two equations can also be checked by partial integrations:

$$\int_{S_t} \{\underline{\varepsilon}^{3\nu\eta}(\underline{h}^{.l}_{\eta;\nu} - \underline{\hat{h}}^{.l}_{\eta;\nu})\overset{(u)}{\underline{\lambda}}{}^{l} + \underline{\varepsilon}^{3\pi\eta}[\underline{f}_{\eta b;\pi} - \underline{\hat{f}}_{\eta b;\pi} + \underline{\varepsilon}_{b\pi s}(\underline{h}^{.l}_{\eta} - \underline{\hat{h}}^{.l}_{\eta})]\overset{(\varphi)}{\underline{\lambda}}{}^{b}\} \, \mathrm{d}S =$$

$$= -\int_{S_t} [\underline{\varepsilon}^{3\chi\eta}(\underline{h}^{.l}_{\eta} - \underline{\hat{h}}^{.l}_{\eta})(\overset{(u)}{\underline{\lambda}}{}_{l;\chi} + \underline{\varepsilon}_{l\chi s}\overset{(\varphi)}{\underline{\lambda}}{}^{s}) + \underline{\varepsilon}^{3\alpha\eta}(\underline{f}_{\eta b} - \underline{\hat{f}}_{\eta b})\overset{(\varphi)}{\underline{\lambda}}{}^{b}_{.;\alpha}] \, \mathrm{d}S +$$

$$+ \oint_g [\overset{(u)}{\underline{\lambda}}{}^{l}(\underline{h}^{.l}_{\eta} - \underline{\hat{h}}^{.l}_{\eta})\underline{\tau}^{\eta} + \overset{(\varphi)}{\underline{\lambda}}{}^{b}(\underline{f}_{\eta b} - \underline{\hat{f}}_{\eta b})\underline{\tau}^{\eta}] \, \mathrm{d}s \,, \tag{6.3}$$

$$\int_{S_u} [\underline{\varepsilon}^{3\nu\eta}\underline{h}^{.l}_{\eta.;\nu}\underline{\hat{u}}_l + \underline{\varepsilon}^{3\pi\eta}(\underline{h}_{\eta b;\pi} + \underline{\varepsilon}_{b\pi s}\underline{h}^{.s}_{\eta})\underline{\hat{\varphi}}^{b}] \, \mathrm{d}S =$$

$$= -\int_{S_u} [\underline{\varepsilon}^{3\chi\eta}\underline{h}^{.l}_{\eta}(\underline{\hat{u}}_{l;\chi} + \underline{\varepsilon}_{l\chi s}\underline{\hat{\varphi}}^{s}) + \underline{\varepsilon}^{3\alpha\eta}\underline{f}_{\eta b}\underline{\hat{\varphi}}^{b}_{.;\alpha}] \, \mathrm{d}S -$$

$$- \oint_g (\underline{\hat{u}}_l\underline{h}^{.l}_{\eta}\underline{\tau}^{\eta} + \underline{\hat{\varphi}}^{b}\underline{f}_{\eta b}\underline{\tau}^{\eta}) \, \mathrm{d}s \,. \tag{6.4}$$

6.5. By the partial integration — which was made by ignoring the derivatives of the vector fields $\delta\underline{r}^{l}$ and $\delta\underline{w}_{y}$ — it can be shown that the next two integrals are identically zero:

$$I_1 = \int_{S_t} [\underline{\varepsilon}^{3\chi\eta}(\overset{(u)}{\underline{\lambda}}{}_{l;\chi} + \underline{\varepsilon}_{l\chi s}\overset{(\varphi)}{\underline{\lambda}}{}^{s})\delta\underline{\hat{r}}^{l}_{.;\eta} + \underline{\varepsilon}^{3\alpha\eta}\underline{\varepsilon}_{b\eta l}\delta\underline{\hat{r}}^{l}\overset{(\varphi)}{\underline{\lambda}}{}^{b}_{.;\alpha}] \, \mathrm{d}S -$$

$$- \oint_g (\overset{(u)}{\underline{\lambda}}{}_{l}\delta\underline{\hat{r}}^{l}_{.;\eta}\underline{\tau}^{\eta} + \overset{(\varphi)}{\underline{\lambda}}{}^{b}\underline{\varepsilon}_{b\eta l}\delta\underline{\hat{r}}^{l}\underline{\tau}^{\eta}) \, \mathrm{d}s \equiv 0 \tag{6.5}$$

$$I_2 = \int_{S_t} \underline{\varepsilon}^{3\alpha\eta}\delta\underline{\hat{w}}_{b;\eta}\overset{(\varphi)}{\underline{\lambda}}{}^{b}_{.;\alpha} \, \mathrm{d}S - \oint_g \overset{(\varphi)}{\underline{\lambda}}\delta\underline{\hat{w}}_{b;\eta}\underline{\tau}^{\eta} \, \mathrm{d}s \equiv 0 \tag{6.6}$$

6.6. The validity of the equations

$$-\int_{S_t} (\underline{\varepsilon}^{3\chi\eta}\underline{\gamma}_{\chi l}\delta\underline{\hat{r}}^{l}_{.;\eta} + \underline{\varepsilon}^{3\alpha\eta}\underline{\varepsilon}_{b\eta l}\underline{\varkappa}^{.b}_{\alpha}\delta\underline{\hat{r}}^{l}) \, \mathrm{d}S +$$

$$+ \oint_g (\underline{\hat{u}}_l\delta\underline{r}^{l}_{.;\eta}\underline{\tau}^{\eta} + \underline{\hat{\varphi}}^{b}\underline{\varepsilon}_{b\eta l}\delta\underline{\hat{r}}^{l}\underline{\tau}^{\eta}) \, \mathrm{d}s =$$

$$= -\int_{S_t} \underline{\varepsilon}^{3\nu\chi}(\underline{\gamma}_{\chi l;\nu} + \underline{\varepsilon}_{\chi ls}\underline{\varkappa}^{.s}_{\nu})\delta\underline{\hat{r}}^{l} \, \mathrm{d}S +$$

$$+ \oint_g (\underline{\gamma}_{\eta l} - \underline{\hat{u}}_{l;\eta} - \underline{\varepsilon}_{l\eta b}\underline{\hat{\varphi}}^{b})\underline{\tau}^{\eta}\delta\underline{\hat{r}}^{l} \, \mathrm{d}s \,, \tag{6.7}$$

and

$$-\int_{S_t} \underset{\sim}{\varepsilon}^{3\alpha\eta} \underset{\sim}{\varkappa}_{\alpha}^{\cdot b} \delta \underset{\sim}{\hat{w}}_{b;\eta} \, \mathrm{d}S + \oint_g \underset{\sim}{\hat{\varphi}}^b \delta \underset{\sim}{w}_{b;\eta} \underset{\sim}{\tau}^{\eta} \, \mathrm{d}s =$$

$$= -\int_{S_t} \underset{\sim}{\varepsilon}^{3\pi\alpha} \underset{\sim}{\varkappa}_{\alpha;\pi}^{\cdot b} \delta \underset{\sim}{\hat{w}}_b \, \mathrm{d}S + \oint_g (\underset{\sim}{\varkappa}_{\alpha}^{\cdot b} - \underset{\sim}{\hat{\varphi}}_{\cdot;\alpha}^{b}) \underset{\sim}{\tau}^{\alpha} \delta \underset{\sim}{\hat{w}}_b \, \mathrm{d}s \tag{6.8}$$

can also be seen by the transformations — which was made so as to ignore the derivatives of the vector fields $\underset{\sim}{r}^l$ and $\underset{\sim}{w}_b$ — and by the use of formula $(6.1)_1$.

References

1. Southwell, R. V.: Castigliano's Principle of Minimum Strain Energy and the Conditions of Compatibility for Strain, S. Timoshenko 60th Anniversary Volume, The Mac Millan Co., 1938
2. Tonti, E.: Variational Principles in Elastostatics, *Meccanica*, **2** (1976), 201–208
3. Oden, J. T.—Reddy, J. N.: On Dual Complementary Variational Principles in Mathematical Physics, *Int. J. Engng. Sci.*, **12** (1974), 1–29
4. Абовский, Н. П.—Андреев, Н. П.—Деруга, А. П.: Вариационные принципы теории упругости и теории оболочек, Москва, Наука, 1978
5. Kozák, I.: Notes on the Field Equations with Stresses and on the Boundary Conditions in the Linearized Theory of Elastostatics, *Acta Techn. Hung.*, **90** (3–4) (1980), 221–245
6. Kozák, I.: Determination of Compatibility Boundary Conditions in Linear Elastostatics with the Aid of the Principle of Minimum Complementary Energy, *Publ. Techn. Univ. Heavy Industry, Miskolc, Ser. D. Natural Sciences*, **34** (1980), 83–98
7. Kozák, I.: Contributions and Remarks to the Variational Principles of Linear Elastostatics in Terms of Stress Functions, To be published in *Acta Techn. Hung.*
8. Finzi, B.: Integrazione delle equazioni indefinite della meccanica dei sistemi continui. *Rend. Lincei*, Ser. 6., Vol. **19.** (1934), 578–584; 620–623
9. Kozák, I.—Szeidl, Gy.: The Field Equation and the Boundary Conditions with Force Stresses and Couple Stresses in the Linearized Theory of Micropolar Elastostatics, *Acta Techn. Hung.*, 91 (1–2) (1980), 57–80
10. Hlavácek, I.—Hlavácek, M.: On the Existence and Uniqueness of Solution and some Variational Principles in Linear Theories of Elasticity with Couple Stresses, I. *Aplikace Matematiky* **14** (1969), 387–410
11. Nowacki, W.: Theory of Micropolar Elasticity, Springler-Vlg. Wien–New York, Udine 1970
12. Günther, W.: Zur Statik und Kinematik des Cosseratschen Kontinuums, *Abh. Braunschweig Wiss. Ges.*, **10** (1958), 195–213
13. Carlson, D. E.: On Günther's Stress Functions for Couple Stresses. *Quart. Appl. Math.* **25** (1967), 139–146
14. Schaefer, H.: Die Spannungsfunktionen eines Kontinuums mit Momentenspannungen I. und II. *Bulletin de l'Académie Polonaise des Sciences*, Série des sciences techniques, Vol. XV. (1967), 63–67; 69–73
15. Courant, R.—Hilbert, D.: Methods of Mathematical Physics, Interscience publishers, 1953, p. 216–222
16. Tonti, E.: A Mathematical Model for Physical Theories I, II. *Rendiconti Accademia Nazionale dei Lincei*, **52** (1972), 175–181; 351–356

Acta Technica Academiae Scientiarum Hungaricae, 93 (3—4), pp. 367—374 (1981)

THE THERMAL PHENOMENA IN THE DRAWING DIE

A. T. NAGY*

[Manuscript received: December 14, 1979]

For wire drawing at high temperatures or at high speed it is very important to know the temperature conditions developing in the drawing die, because the temperature of the wire must be kept within given temperature limits.

During wire drawing heat is generated by the deformation work and by the friction work. Also the heat conduction due to the difference between the temperature of the die and of the wire must be considered. The amount of this depends on the temperature of the wire surface and the friction heat also arises here, so for thicker wires there may develop important temperature differences between the surface and the inside of the wire.

Exact determination of the temperature conditions is an extraordinarily complicated task. The approximation used here gives good results for rapid drawing of thick wires, provided that reduction is relatively small. Considering that the drawing speads in industrial use are not small even now and that a further increase of these speeds is to be expected, our results get nearer and nearer to reality.

Introduction

For its practical importance the plastic phenomena in the drawing die are an object of investigations since about 100 years [1–15]. The theory has already been worked out in so much detail that in university lecture notes it is one of the examples for the theory of plasticity [16].

The thermal phenomena connected with wire drawing can be neglected in certain cases. This is so when the wire drawing is done at room temperature with not too large a speed. This is possible with a material where the brittle-plastic transition temperature is below room temperature.

The deformation work and the friction work are transformed into heat to a great extent. At higher deformation speeds that can go with considerable temperature rise. At the drawing of "brittle" materials (where the brittle-plastic transition occurs above room temperature) the wire must be warmed up beforehand. During passage through the drawing channel the wire must not cool down below the brittle-plastic transition temperature. Similarly an excessive heating-up is nuisible because of structural change, oxidation. The wire leaving the die must not be too warm, because under the action of the drawing force the deformation might continue outside the die. This "after-elongation" is very nuisible.

In the above cases obviously the temperature conditions in the die are of decisive importance.

* A. T. Nagy MTA Műszaki Fizikai Kutató Intézet. Fóti út 56, H-1047 Budapest, Hungary

The thermal phenomena for the drawing die as a whole can be dealt with very simply in first approximation.

During the drawing of wire of length L a great part of the deformation work Q_a (its fraction α) is transformed into heat:

$$Q_{\text{forming}} = \alpha\varepsilon\sigma\bar{a}^2\pi L \tag{1}$$

where σ – deformation stress
ε – deformation
$\bar{a}$ – a mean radius

With good approximation

$$\varepsilon = 2\frac{\mathrm{d}a}{\bar{a}}$$

where da is the difference between the original radius and the radius after drawing.

It is assumed that the whole of the friction work is transferred into heat:

$$Q_{\text{friction}} = \mu\sigma 2\bar{a}\pi l L \tag{2}$$

where μ – the coefficient of friction
l – length of drawing die.

The ratio of the two quantities is

$$\frac{Q_{\text{deformation}}}{Q_{\text{friction}}} = \frac{\alpha\varepsilon\bar{a}}{2\mu l} \tag{3}$$

and depends on the diameter of the wire inasmuch the quantities $\varepsilon, \mu, \bar{a}, l$ vary. With the wires of smaller diameter the invested work of friction increases not for physical, but for technological reasons.

If the heat quantities (1) and (2) are divided by the thermal capacity $\bar{a}^2\pi LK/\kappa$ of the wire

(where K – the coefficient of heat conduction
κ – the diffusivity, $\kappa = K/c\rho$
with ρ the density of the material
c – the specific heat of the material

that temperature rise is obtained which would have arisen if the heat quantities $Q_{\text{deformation}}$ and Q_{friction} would have been distributed uniformly over the whole cross section of the wire length L.

But this quantity of heat does not remain in the wire: part of it is carried away by the die. The heat carried away during the time Δt is

$$Q_{\text{transmission}} = \Lambda\Delta T \cdot 2\bar{a}\pi l\Delta t \tag{4}$$

where Λ is the heat transmission coefficient of the lubricant being between the wire and the die:
$\Lambda = K_{\text{lubricant}}/d$, where
$K_{\text{lubricant}}$ — the thermal conductivity of the lubricant
d — the thickness of the lubricant

Calculation of the heat distribution

The wire being in the drawing die is sectioned by planes normal to its axis (Fig. 1) and the heat phenomena mentionned in the introduction are examined for sections of length Δx.

The following assumptions are made:

i) The die is a good heat conductor, therefore its temperature is uniform along the whole drawing hole. For a diamond drawing die this is a real assumption, because the

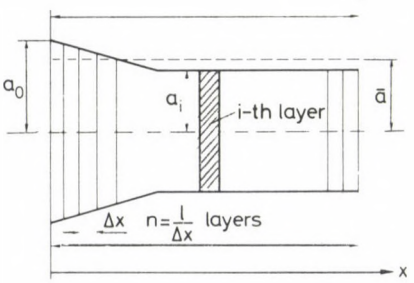

Fig. 1

thermal conductivity of the diamond is about $10\times$ that of metals. On the other hand this is not an essential restriction, because the temperature changing along the drawing channel — if it is known from somewhere — can be taken into account without any difficulty.

ii) The axial heat transmission is neglected (the heat conduction coefficient is imagined to be zero). Because of the good thermal conductivity of metals this is the most serious approximation. But the more the wire drawing is rapid, the more this approximation becomes real.

Figure 2 shows that distance $\sqrt{\kappa l/v}$ related to the length l of the drawing die (v — the speed of wire drawing) to which extends the effect of heat during the time $\Delta t = l/v$ (i.e. while the piece of wire stays in the die). On the y axis therefore is the expression

$$\frac{\sqrt{\kappa \frac{l}{v}}}{l} = \sqrt{\frac{\kappa}{lv}}$$

On the x-axis the product of the die length and the speed of wire drawing is shown; l being proportionate to the diameter of the wire, one can state that in the case of rapid drawing of a thick wire its speed may be much greater than the speed of thermal conduction, i.e. in axial direction the temperature conditions are determined by the heat quantities transported by the displacement of the wire and not by the heat conduction.

But even in the case that this statement is true for the whole of the drawing die, probably it is not true for a section of length Δx. But this does not mean that the wire section within the die must not be divided into too many parts. Namely, if in the surroundings of a section the heat gradient is constant (this is so more probable the smaller are the sections), on the piece of wire in question flows in so more heat from one side as flows out on the other boundary surface and so the axial heat conduction does not influence the temperature conditions.

But for sections of length x of the drawing channel for which

$$\sqrt{\kappa \frac{x}{v}} \approx x, \quad \text{i.e.} \quad x \approx \frac{\kappa}{v} \tag{5}$$

the non-linear sections of the calculated temperature distributions strongly smooth out.

iii) It is assumed that the reduction is relatively small so that the individual layers can be characterized well by a mean radius $\bar{a}$ and that the layer thickness Δx is constant. Considering that the diameter reduction is around 10% this neglection probably does not influence much the results.

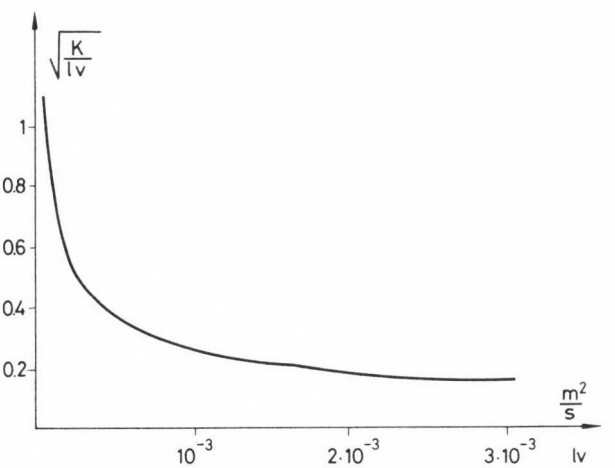

Fig. 2

In the calculations it is assumed that the deformation heat arises uniformly in the whole volume, while the frictional heat arises only at the surface. The conduction phenomena between the wire and the die also influence only the temperature of the wire surface. The heat flowing from the inside of the wire towards the surface (or vice versa) is considered as well.

For designing the radial heat flow in the wire the results published in literature are used [17]. Accordingly, if across the surface of a cylinder of infinite length (the

temperature of which is everywhere T_0 at the time $t=0$) the heat that flows through in F_0 per unit surface and per unit time, the heat distribution as a function of time and location will be:

$$T(r,t)=T_0+\frac{2F_0\kappa}{Ka}t\left\{1+\frac{a^2}{2\kappa t}\left(\frac{r^2}{2a^2}-\frac{1}{4}-\right.\right.$$

$$\left.\left.-\sum_{n=1}^{\infty}e^{-\frac{\kappa\alpha_n^2 t}{a^2}}\cdot\frac{2J_0(r\alpha_n/a)}{\alpha_n^2 J_0(\alpha_n)}\right)\right\} \tag{6}$$

where a — the radius of the cylinder
α_n — the roots of the Bessel function of first order $J_1(\alpha)=0$
$J_0(x)$ the Bessel function of zero order

(The cylinder must be assumed to be of infinite length in order to be able not to consider the axial heat conduction.)

In the present case the difference between the heat $\mu\sigma v$ generated by friction per unit surface and per second and the heat $\Lambda(T_{\text{wire}}-T_{\text{die}})$ carried away by the die flows towards the inside of the wire, i.e.

$$F_0=\mu\sigma v-\Lambda(T_{\text{wire}}-T_{\text{die}}) \tag{7}$$

where T_{wire} — the temperature of the wire surface
T_{die} — the temperature of the drawing die

The temperature of the i-th layer is determined by the principle of superposition:

a) The temperature increase of the incoming wire due to the deformation undergone until the i-the layer is determined.

b) The value of F_0 is calculated for the first layer: $F=\mu\sigma v-\Lambda(T_{\text{wire in}}-T_{\text{die}})$ and it is calculated which would be the temperature distribution if F_0 were constant for the time $t=x/v$, i.e. until the examined layer comes into the i-th position.

c) The values of F_0 for the second layer (because the temperature of the wire surface has risen to T_1) is modified by a value $\Lambda(T_{\text{wire in}}-T_1)$. This correction is imagined to be constant for the time $(x-\Delta x)/v$.

d) In the third layer the inflowing (or outflowing) heat is again modified, which modification is related to the time interval $(x-2\Delta x)/y$, and so one, until the $(i-1)$th layer, where the correction $\Lambda(T_{i-1}-T_{i-2})$ is used considering the time $\Delta x/v$.

The heat distribution of the i-th layer is given by the sum of the above partial results (the mean radius is designated by $\bar{a}$):

$$T_i(r,t)=T_{\text{wire in}}+2\alpha\frac{\kappa}{K}\sigma\frac{a_0-a_i}{\bar{a}}+$$

$$+\frac{2\kappa[\mu\sigma v-\Lambda(T_{\text{wire in}}-T_{\text{die}})]}{K\bar{a}}i\Delta tA+$$

$$+\frac{2\kappa\Delta t}{K\bar{a}}\sum_{s=1}^{i-1}\Lambda(T_{i-s-1}-T_{i-s})sB \tag{8}$$

where the T values with index on the right side signify the surface temperature of the wire in the layer designated by the indice ($T_0 = T_{\text{wireentering}}$), furthermore

$$A = 1 + \frac{\bar{a}^2}{2\kappa i \Delta t}\left(\frac{r^2}{2\bar{a}^2} - \frac{1}{4} - \sum_{n=1}^{\infty} \exp\left(-\frac{\kappa \alpha_n^2 i \Delta t}{\bar{a}^2}\right) \cdot \frac{2J_0(r\alpha_n/\bar{a})}{\alpha_n^2 J_0(\alpha_n)}\right)$$

$$B = 1 + \frac{\bar{a}^2}{2\kappa s \Delta t}\left(\frac{r^2}{2\bar{a}^2} - \frac{1}{4} - \sum_{n=1}^{\infty} \exp\left(-\frac{\kappa \alpha_n^2 s \Delta t}{\bar{a}^2}\right) \cdot \frac{2J_0(r\alpha_n/\bar{a})}{\alpha_n^2 J_0(\alpha_n)}\right)$$

where $\Delta t = \Delta x / v$.

In applying the above formula the infinite series of the Bessel functions have been approximated by its first 5 members.

Results

As an example some calculated temperature distributions are shown. The data of the drawing die are: half cone angle of the shaping cone 7°, entering wire 770 μm dia., leaving wire 700 μm dia., length of the calibrating cylinder 350 μm. The whole drawing die has been divided into 63 parts, so $\Delta x = 10$ μm.

For the calculations the material constants measured at several hundreds of °C of the tungsten were used [18]. They were

thermal conductivity	$K = 120$ W/m°c
diffusivity	$\kappa = 4.2 \cdot 10^{-5}$ m^2/s.

In the drawing of tungsten wires graphite suspension is used as a lubricant, thus the thermal conductivity of graphite [18] was considered. The thickness of the lubricant was taken as $d = 1$ μm. With these the heat transfer coefficient is $\Lambda = 1.7 \cdot 10^6$ W/m^2 °C. (Here the thermal resistance at the surface wire-lubricant and lubricant-drawing die were neglected. The Λ value used can still be real, if the thickness of the lubricant is smaller than the 1 μm mentioned. Anyhow it is a fact that in formula (8) the heat transmission coefficient Λ is the most uncertain parameter.) The deformation stress has been estimated to be $\sigma = 1.5 \cdot 10^9$ Pa [19], the value of α has been assumed to be 0.9.

Formula (8) shows that the temperature change $T_i(r, t) - T_{\text{wire, in}}$ depends only on the difference $T_{\text{wire, in}} - T_{\text{die}}$. This difference has been assumed to be 300 °C.

The results are shown in Fig. 3. The set of curves marked A in the upper part of the Figure shows the effect of the variation of the coefficient of friction. The three uppermost curves (marked 1 . . . 3) represent the temperature of the axis of the wire during advancing through the drawing die. The drawing speed is $v = 1$ m/s. The coefficients of friction were, counted downwards, $\mu = 0.20, 0.10, 0.00$.

The diffusion path calculated from formula (5) was 42 μm. The points being at 10 μm distance from each other, the calculated temperature profile can be judged real

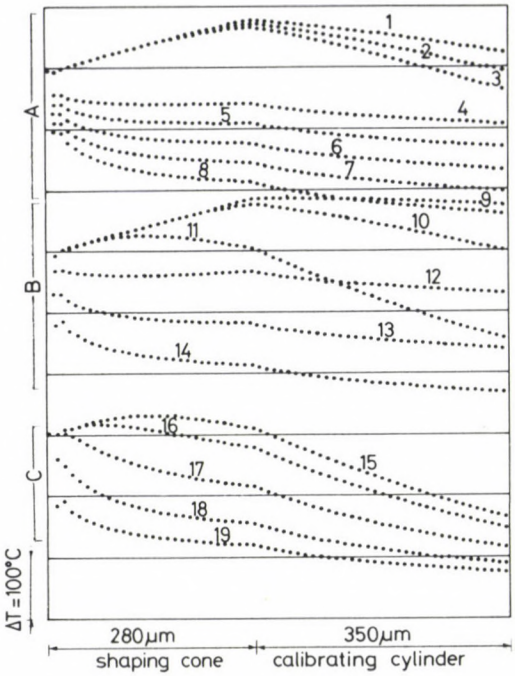

Fig. 3

as whole, at most the breaking point at the junction of the shaping cone and the calibrating cylinder is rounded off in reality.

The calculated curves 4...8 show the surface temperature of the wire for different coefficients of friction. The values of the coefficient of friction were — counted downwards — 0.20, 0.15, 0.10, 0.05, 0.00.

The set of curves in the central part of Fig. 3 — marked by *B* — shows the effect of the drawing speed at a coefficient of friction $\mu = 0.10$. The curves 9...11 show the temperature in the case of drawing speeds $v = 2$, 1 and 1.5 m/s, while curves 12...14 show the surface temperatures of the wire for the same speeds.

For one case the temperature distribution was determined for the whole wire cross section (Fig. 3 lower part, set of curves *C*.) Here was $v = 0.5$ m/s, $\mu = 0.10$, the values $r/\bar{a}$ were for the curves 15...19: 0.0, 0.4, 0.7, 0.8, 0.9, 1.0.

References

1. Smith, O.: J. Franklin Inst. **122** (1886), 321., **123** (1887), 232
2. Musiol, K.: *Kingler's Polytech. J.* **315** (1900), 428., 442
3. Lewis, K. B.: *Blast Furnace Steel Plant* **3** (1915), 1031

4. Sachs, G.: *Trans. Faraday Soc.* **24** (1928), 84
5. Siebel, E.: *Werkstattstechnik und Maschinenbau* **40** (1950), 373
6. Hoffmann, O.—Sachs, G.: Introduction to the Theory of Plasticity, McGraw-Hill, 1953
7. Thomsen, E. G.—Yang, C. T.—Kobayashi, S.: Mechanics of Plastic Deformation in Metal Processing, The MacMillan Company, N. Y. 1965
8. Sachs, G.—Van Horn, K. R.: Practical Metallurgy, American Society for Metals, 1940
9. Körber, F.—Eichinger, A.: *Mitt. K. W. Inst. Eisenforschung* **22** (1940), 57
10. Siebel, E.: *Stahl und Eisen* **66/67** (1947), 171
11. Davis, E. A.—Dokos, S. J.: *Trans. ASME, J. Appl. Mech.* **66** (1944) A-193
12. Whitton, P. W.: *J. Inst. Metals* **86** (1958), 417
13. Yang, C. T.: *Trans. ASME*, Series B, J. Eng. Ind. **83** (1961), 523
14. Avitzur, B.: *Journal of Engineering for Industry* **89** (1963) febr.
15. Avitzur, B.: *Journal of Engineering for Industry* **305** (1964) nov.
16. Gillemot, L.—Ziaja, Gy.: Fémek képlékeny alakítása. Tankönyvkiadó, Budapest, 1977
17. Carslaw, H. S.—Jaeger, J. C.: Conduction of Heat in Solids, Oxford, Clarendon Press, 1959, p. 203
18. Landolt—Börnstein: Zahlenwerte und Funktionen, 4. Band. Technik, 4. Teil: Wärmetechnik, Springer Verlag, 1967
19. Rieck, G. D.: Tungsten and its Compounds, Pergamon Press, 1967

Acta Technica Academiae Scientiarum Hungaricae, 93 (3—4), pp. 375—382 (1981)

NONLINEAR ANALYSIS OF CABLE-BEAM STRUCTURES

J. PIETRZAK*

[Manuscript received: June 12, 1982]

The paper concerns static analysis of cable-beam structures, the displacements of which are large enough to affect normal force distribution. Besides geometrical nonlinearity, analysis presented takes into account physical nonlinearity of cable elements. Analysis is based on energy approach and numerical minimization method is used for search of minimum point of total potential energy. Numerical example is enclosed.

1. Introduction

Cable-beam structures, two examples of which are shown in Fig. 1, have found wide application in constructing of large span roofs, suspension pipe-lines and bridges. A variety of methods have been proposed for static analysis of these structures, e.g. [1–9]. Most of the methods takes into account only geometrical nonlinearity of the cable system. In the present paper method of analysis is described which enables additionally to account for physical nonlinearity of cable elements. The method is based on the theorem of minimum value of total potential energy and makes use of numerical minimization technique for search of minimum point in node displacements space. It has been shown in many works that this approach is an efficient method of nonlinear analysis of discrete structures, e.g. [7–11].

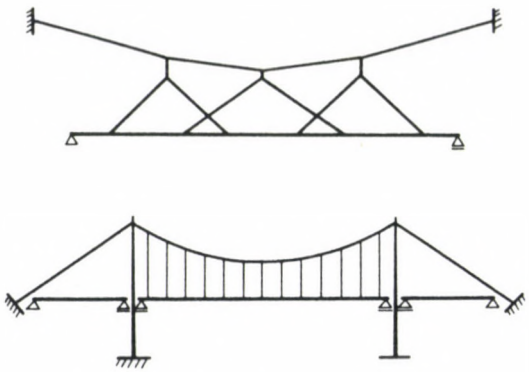

Fig. 1

* Dr. Jacek Pietrzak, Institute of Technology and Building Structures. Technical University of Poznań. Poznań, Poland

2. Formulation of problem

Cable-beam structure considered in the paper is assumed to fulfil the following assumptions:

— cable elements are straight and able to carry only tensile forces,

— girder of the structure is simply supported on its ends and restrained, at intermediate equally spaced points, with cable system,

— there are no initial stresses nor deformation of the structure,

— external loads are applied exclusively in nodes of the structure,

— external loading does not cause exceeding of allowable stress in any point of the structure nor slacking of cable elements,

— behaviour of girder is geometrically and physically linear,

— cable system exhibits geometrical and physical nonlinearity; stress-strain relationship of cable element material is following:

(i) for $0 \leqq \varepsilon \leqq \varepsilon_1$ (see Fig. 2)

$$\sigma = E(\varepsilon + K\varepsilon^N) \tag{1}$$

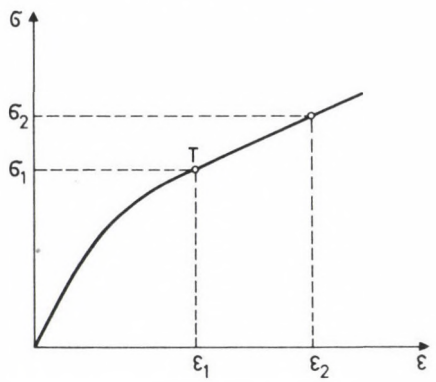

Fig. 2

(an alternate form of Ramberg-Osgood formula, proposed in [12])

(ii) for $\varepsilon_1 \leqq \varepsilon \leqq \varepsilon_2$

$$\sigma = \sigma_1 + E(1 + KN\varepsilon_1^{N-1})(\varepsilon - \varepsilon_1) \tag{2}$$

(straight line tangent at point $T(\varepsilon_1 \sigma_1)$ to the curve given by Eq. (1)).

Symbols E, K and N used in Eqs (1) and (2) mean, respectively,

$$E = \sigma_A/\varepsilon_A\,, \tag{3}$$

$$K = (\sigma_c - E\varepsilon_c)/E\varepsilon_c^N\,, \tag{4}$$

$$N = \left(\ln \frac{\sigma_c - E\varepsilon_c}{\sigma_B - E\varepsilon_B}\right) \Big/ \left(\ln \frac{\varepsilon_c}{\varepsilon_B}\right), \tag{5}$$

where $\sigma_A, \varepsilon_A, \sigma_B, \varepsilon_B$ and σ_c, ε_c are coordinates of points A, B and C selected of the results of tensile test of the cable in a manner which ensures good fitting of the curve $\sigma(\varepsilon)$ to experimental data (Fig. 3).

Value of strain interval boundary ε_1 is chosen in such a way that condition of tangency of the straight line (2) to the curve (1)

$$\left(\frac{\mathrm{d}\sigma}{\mathrm{d}\varepsilon}\right)_{\varepsilon=\varepsilon_1} = \frac{\sigma_D - \sigma_1}{\varepsilon_D - \varepsilon_1}$$

is satisfied. Symbols σ_D and ε_D used above denote coordinates of a point D obtained in tensile test.

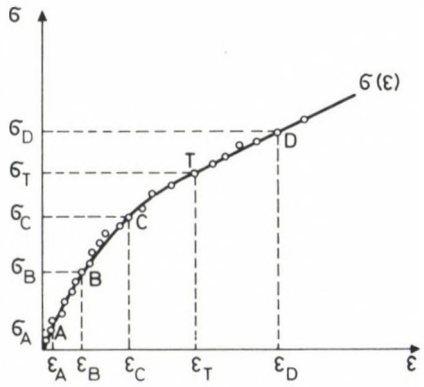

Fig. 3

The aim of static analysis of the cable-beam structure considered herein, subjected to the action of external forces $\mathbf{F}=\{F_{1x}F_{1y}\ \ldots\ F_{Jx}F_{Jy}\}$ is to find:

— node displacement matrix $\mathbf{x}=\{x_{1x}x_{1y}\ \ldots\ x_{Jx}x_{Jy}\}$,

— normal force matrix $\mathbf{P}=\{P_1P_2\ \ldots\ P_{G+R+1}\}$,

— girder shear force matrix $\mathbf{S}=\{S_1S_2\ \ldots\ S_{R+1}\}$,

— and girder bending moment matrix $\mathbf{M}=\{M_1M_2\ \ldots\ M_R\}$.

Subscripts J, R, G used in the above matrices denote, respectively, number of nodes undergoing displacements, number of intermediate cable supports of the girder, and number of cable segments, see Fig. 4.

In accordance with the theorem of minimum value of total potential energy, calculation of node displacement vector $\mathbf{x}$ is equivalent to finding minimum point $\mathbf{x}$ of the total potential energy $\pi(\mathbf{x})$. For the stiffened cable structure considered in the paper total potential energy is given by

$$\pi(\mathbf{x}) = U_c(\mathbf{x}) + U_b(\mathbf{x}) - \mathbf{F}^t\mathbf{x} \tag{6}$$

where $U_c(\mathbf{x})$ = strain energy of the cable system,

$U_b(\mathbf{x})$ = strain energy of the girder,

t = transposition symbol.

Energy $U_c(\mathbf{x})$ is a sum $\sum_{g=R+2}^{G+R+1} U_{cg}$ of energies

$$U_{cg}=\int_V \left(\int_0^{\varepsilon_{(g)}} \sigma(\varepsilon)\,\mathrm{d}\varepsilon\right)\mathrm{d}V \tag{7}$$

stored in all cable elements. Substituting (1) and (2) into (7) we obtain following formulas for U_{cg}:

(i) for $0 \leqq \varepsilon_{(g)} \leqq \varepsilon_1$

$$U_{cg}=EA_gL_g\left(\frac{\varepsilon_{(g)}^2}{2}+\frac{K}{N+1}\varepsilon_{(g)}^{N+1}\right); \tag{8}$$

(ii) for $\varepsilon_1 < \varepsilon_{(g)} \leqq \varepsilon_2$

$$U_{cg}=A_gL_g\left[E\left(\frac{\varepsilon_1^2}{2}+\frac{K}{N+1}\varepsilon_1^{N+1}\right)+(\varepsilon_{(g)}-\varepsilon_1)\sigma_1+\frac{t_1}{2}(\varepsilon_{(g)}-\varepsilon_1)^2\right] \tag{9}$$

where A_g = cross sectional area of element g,

L_g = length of element g,

$$t_1=\left(\frac{\mathrm{d}\sigma}{\mathrm{d}\varepsilon}\right)_{\varepsilon=\varepsilon_1}$$

$$\varepsilon_{(g)}=\varepsilon_{(g)}(\mathbf{x})=\left\{1+\frac{1}{L_g^2}\left[2(X_{px}-X_{rx})+(x_{px}-x_{rx})\right](x_{px}-x_{rx})+\right.$$
$$\left.+\frac{1}{L_g^2}\left[2(X_{py}-X_{ry})+(x_{py}-x_{ry})\right](x_{py}-x_{ry})\right\}^{\frac{1}{2}}-1\,. \tag{10}$$

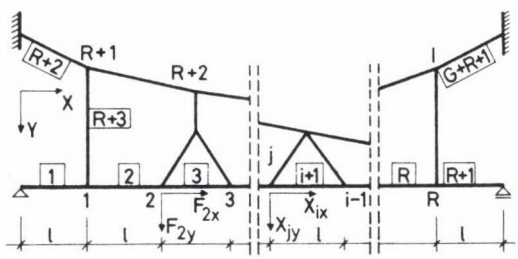

Fig. 4

In Eq. (10) $X_{px}, X_{py}, X_{rx}, X_{ry}$ denote coordinates of nodes p and r in undeflected position of the structure, measured with respect to global system of axes (x, y). Lower case $x's$, namely x_{px}, x_{py}, x_{rx} and x_{ry} used in Eq. (10), denote components of displacements of the nodes p and r.

Strain energy of the girder, $U_b(\mathbf{x})$, is given by

$$U_b(\mathbf{x}) = \frac{1}{2} E_b I \sum_{g=1}^{R+1} A_g \varepsilon_{(g)}^2 + \frac{l}{6E_b I} \sum_{j=1}^{R+1} (M_{j-1}^2 + M_j^2 + M_{j-1} M_j) \tag{11}$$

where E_b = modulus of elasticity of girder material,

l = length of girder segment (for $g = 1, \ldots, R+1 \quad L_g = l$),

I = second moment of area of girder,

M_j = value of bending moment at point j of the girder.

For $j = 0$ and $j = R+1$ $M_j = 0$, while for $j = 1, 2, \ldots, R$ values of bending moments are given by three moments equation:

$$\begin{bmatrix} M_1 \\ M_2 \\ \cdots \\ M_j \\ \cdots \\ M_R \end{bmatrix} = \frac{6E_b I}{l^2} \begin{bmatrix} 4 & 1 & & & & & & & & \\ 1 & 4 & 1 & & & & & & & \\ \cdots & \cdots & \cdots & \cdots & \cdots & \cdots & \cdots & \cdots & \cdots & \\ & & & & 1 & 4 & 1 & & & \\ \cdots & \cdots & \cdots & \cdots & \cdots & \cdots & \cdots & \cdots & \cdots & \\ & & & & & & & 1 & 4 & \end{bmatrix}^{-1}$$

$$\begin{bmatrix} 2x_{1y} - x_{2y} \\ -x_{1y} + 2x_{2y} - x_{3y} \\ \cdots \\ -x_{j-1,y} + 2x_{j,y} - x_{j+1,y} \\ \cdots \\ -x_{R+1,y} + 2x_{Ry} \end{bmatrix} \tag{12}$$

Gradient $\nabla\pi(\mathbf{x})$ of the total potential energy of the structure is of the form

$$\nabla\pi(\mathbf{x}) = \begin{bmatrix} \dfrac{\partial(U_0 + U_b)}{\partial x_{1x}} - F_{1x} \\ \cdots \\ \dfrac{\partial(U_c + U_b)}{\partial x_{jx}} - F_{jx} \\ \dfrac{\partial(U_c + U_b)}{\partial x_{jy}} - F_{jy} \\ \cdots \\ \dfrac{\partial(U_c + U_b)}{\partial x_{Jy}} - F_{Jy} \end{bmatrix}$$

where

$$\frac{\partial(U_c+U_b)}{\partial x_{jx}}=\sum_{g_{jn}}\left\{-\frac{\sigma_g A_g[(X_{nx}-X_{jx})+(x_{nx}-x_{jx})]}{L_g(1+\varepsilon_{(g)})}\right\}$$

$$\frac{\partial(U_c+U_b)}{\partial x_{jy}}=\sum_{g_{jn}}\left\{-\frac{\sigma_g A_g[(X_{ny}-X_{jy})+(x_{ny}-x_{jy})]}{L_g(1+\varepsilon_{(g)})}\right\}+a_j\,.$$

Symbol $\sum_{g_{jn}}$ used above denotes summation that is confined to elements $j-n$ incident with node j, and a_j is given by

$$a_j=\begin{cases}\dfrac{M_{j-1}-2M_j+M_{j+1}}{1} & \text{for} \quad 1\leqq j\leqq R\\[2ex] 0 & \text{for} \quad R+1\leqq j\leqq J\end{cases}$$

3. Solution of the problem

Minimum point **x** of total potential energy can be found with the use of any numerical minimization method. It is suggested herein to use Huang's reverse algorithm [13] which proved to be an efficient method in analyses of nonlinear discrete structures [10, 11]. The main advantage of Huang's reverse algorithm is avoidance of necessity of precise minimization in one-dimensional searches.

Having found node displacements one can calculate readily, from Eq. (10), axial strains $\varepsilon_{(g)}$ of elements of the structure, then normal stresses $\sigma_{(g)}$ (from Eqs (1) and (2)), and elements P_g of the normal force matrix **P**. The bending moment matrix, **M**, is given by Eq. (12). Making use of the matrix **M**, the shear force matrix **Q** can be obtained straightforwardly.

4. Numerical example

The method described in the paper, with Huang's reverse algorithm used as numerical minimization technique, has been implemented into computer programme. The programme has been used for calculation of the cable-beam structure shown in Fig. 5. Physical law adopted for cable elements of the structure is of the form:

$$\begin{aligned}&\text{for} \quad 0\leqq\varepsilon\leqq 0.01377\\ &\qquad \sigma=14.820(\varepsilon-145\,\varepsilon^{2.4}) \qquad [\mathrm{kN/cm^2}]\\ &\text{for} \quad 0.01377<\varepsilon\leqq 0.02\\ &\qquad \sigma=2028.103\,\varepsilon+102.751 \qquad [\mathrm{kN/cm^2}]\end{aligned}$$

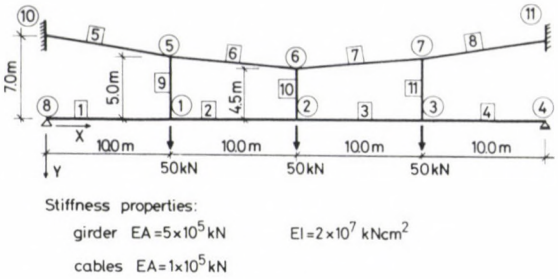

Fig. 5

Some numerical results obtained for the structure considered are presented in column 2 of Table 1.

For comparative purpose the structure shown in Fig. 5 has also been calculated for the case of physical linearity of cables ($E = \text{const.} = 14.800\ \text{kN/cm}^2$). Selected numerical results obtained are quoted in column 3 of Table 1.

Table 1

		Physically & geometrically nonlinear structure	Physically linear, geometrically nonlinear structure
Vertical	x_{1y}	27.91	26.55
displacements	x_{2y}	49.33	47.51
x_{iy}	x_{3y}	27.86	26.30
of nodes	x_{5y}	27.65	26.29
[cm]	x_{6y}	49.14	47.30
	x_{7y}	27.61	26.25
Normal	P_5	337.75	339.84
forces	P_6	329.94	332.08
P_1	P_7	330.01	32.14
[kN]	P_9	51.66	51.68
Bending	M_1	−146.19	−168.25
moments	M_2	1361.56	1343.68
M_1	M_3	−149.10	−170.92
[kN/cm]			

References

1. Saafan, S. A.: Theoretical Analysis of Suspension Bridges. *J. Str. Div. Proc. ASCE*, **92,** (1966), 1–11
2. Pugsley, A. G.: The Theory of Suspension Bridges. Arnold 1968
3. Jennings, A.—Mairs, J. E.: Static Analysis of Suspension Bridges. *J. Str. Div. Proc. ASCE*, **98,** (1972), 2433–2454

4. Van der Woude: Analysis of Suspension Bridges Using Energy Principles. *The Structural Engineer.* Vol. **54,** (1976), 121–131
5. Buchholdt, H. A.—McMillan, B. R.: Iterative Methods for the Solution of Pretensioned Cable Structures and Pin-jointed Assemblies Having Significant Geometrical Displacements. *IASS Pacific Symposium,* Tokyo and Kyoto, Japan (1971), 303–316
6. Rakowski, J.: Statics and Dynamics of Cable-grid System. (in Polish). *Archiwum Inżynierii Ladowej.* **27,** Z. 3, (1980) 577–589
7. Buchholdt, H. A.: Deformation of Prestressed Cable Nets. *Acta Polytechnica Scandinavica.* Ci **38,** (1966)
8. Murray, T. M.—Willems, N.: Analysis of Inelastic Suspension Structures. *J. Str. Div. Proc. ASCE,* **97,** (1971) 2791–2806
9. Contro, R.—Maier, G.—Zavelani, A.: Inelastic Analysis of Suspension Structures by Nonlinear Programming. *Computer Methods in Appl. Mech. and Engng.* No 5. (1975) 127–143
10. Pietrzak, J.: Matrix Formulation of Static Analysis of Cable Structures. *Int. J. Computers & Structures.* **9,** (1978), 39–42
11. Pietrzak, J.: Analysis of Geometrically and Physically Nonlinear Trusses. *Costruzioni metalliche.* No 5, (1979), 251–254
12. Rao, G. V.—Krishna Murty, A. V.: An Alternate Form of the Ramberg Osgood Formula for Matrix Displacement Analysis. *Nucl. Engng & Design.* **17,** (1971), 297–308
13. Huang, H. Y.: Method of Dual Matrices for Function Minimization. *JOTA,* No 5, (1974), 519–537

Acta Technica Academiae Scientiarum Hungaricae, 93 (3—4), pp. 383—389 (1981)

A COMMENT ON THE TORSION STIFFNESS OF THIN-WALLED PRISMATIC BARS OF CLOSED PROFILE

I. ECSEDI*
Cand. of Technic. Sci

(Manuscript received: July 1, 1981)

This paper deals with Saint-Venant's torsion problem of thin-walled prismatic bars of linearly elastic, anisotropic (orthotropic) but homogeneous material and closed profile, and investigates the question how the torsional stiffness changes in case where the anisotropy (orthotropy) is turned-off in comparison with the profile of the bar.

1. Introduction

Figure 1 represents a thin-walled prismatic bar of closed profile and variable wall thickness submitted to torsion. The material of the bar is homogenic, anisotropic and linearly elastic. The anisotropy is introduced by formulae (2.1) and (2.2). The centre line of the profile is the simple closed curve ∂A_k. By measuring half of the wall thickness h to the normal n of the centre line at both sides of this latter, the inside and outside contour lines ∂A_1 and ∂A_0 of the cross section are obtained.

The cross section of the bar is the doubly connected "ring-shaped" surface A in the plane xy.

The equation of the centre line (Fig. 2) is as follows:

$$\mathbf{R} = x(s)\mathbf{e}_x + y(s)\mathbf{e}_y \tag{1.1}$$

wherein s designates the arc coordinate measured along the centre line. The tangent unit vector of the centre line is described by the equation

$$\mathbf{t} = \frac{\mathrm{d}\mathbf{R}}{\mathrm{d}s} = \frac{\mathrm{d}x}{\mathrm{d}s}\mathbf{e}_x + \frac{\mathrm{d}y}{\mathrm{d}s}\mathbf{e}_y\,, \tag{1.2}$$

$\mathbf{e}_x$ and $\mathbf{e}_y$ being the unit vectors.

The assumptions of Saint-Venant's theory of torsion relating to the thin-walled prismatic bars of closed cross section are applied [1]. Accordingly, the shear-stress vector $\boldsymbol{\tau}_z$ generated at point P of the plane of the cross section takes the form (Fig. 2)

$$\boldsymbol{\tau}_z = \tau_{sz}\mathbf{t}\,, \tag{1.3}$$

* Dr. I. Ecsedi, Vászonfehérítő u. 24 H-3531, Miskolc, Hungary

in which

$$\tau_{sz} = \vartheta \frac{C}{h(s)}. \tag{1.4}$$

In Eq. (1.4)

ϑ = angle of relative torsion

C = constant to be defined on basis of compatibility conditions.

It can easily be pointed out that

$$\mathbf{F} = \int_A \tau_z \, dA = \mathbf{0}, \tag{1.5}$$

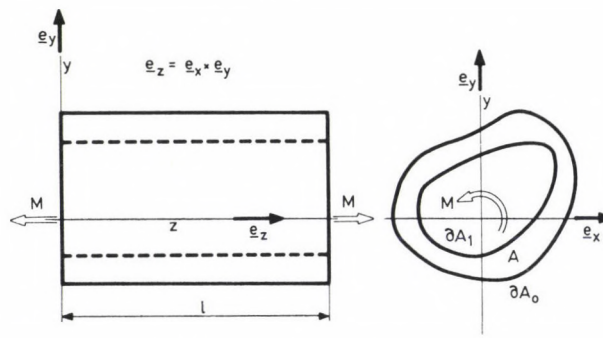

Fig. 1. Prismatic bar submitted to torsion

i.e.,the cross section is not attacked by shear force in case where the assumptions mentioned above have been adopted. This is true, indeed, because

$$\mathbf{F} = \int_A \tau_z \, dA = C\vartheta \int_{\partial A_k} \mathbf{t} \, ds = C \int_{\partial A_k} d\mathbf{R} = \mathbf{0}. \tag{1.6}$$

The relationship between the moment of torsion M and the angle of relative torsion ϑ is obtained by the detailed development of the equation

$$M = \mathbf{e}_z \cdot \left(\int_{\partial A_k} \mathbf{R} \times \tau h \, ds \right). \tag{1.7}$$

In Eq. (1.7) the the signs "·" and "×" designate the scalar and vectorial product, respectively, of both vectors; further

$$\mathbf{e}_z = \mathbf{e}_x \times \mathbf{e}_y .$$

Carrying out some elementary transformations on Eq. (1.7) yields the formula

$$M = C\vartheta [\mathbf{e}_z \cdot (\int_{A_k} \mathbf{R} \times d\mathbf{R})] = 2C\vartheta A_k . \tag{1.8}$$

A_k here means the surface inside the curve ∂A_k.

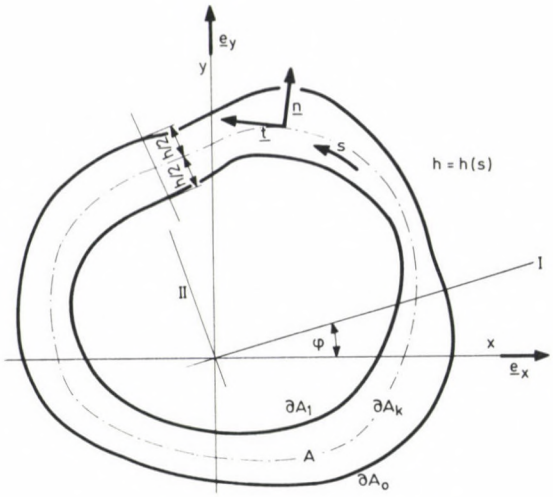

Fig. 2. Thin-walled closed profile

The torsional stiffness of the cross section is defined by the equation [1]

$$S = \frac{M}{\vartheta} = 2CA_k . \tag{1.9}$$

The intention of this paper is to investigate the relationship between the torsional stiffness of the cross section S and the principal directions of elasticity.

2. Relationship between the torsional stiffness and the principal directions of elasticity

One of the principal direction of elasticity of the homogeneous orthotropic, lineary elastic material is parallel to the z-axis. By applying Hooke's law we can put down

$$\gamma_{xz} = a_{11}\tau_{xz} + a_{12}\tau_{yz} \tag{2.1}$$

and

$$\gamma_{yz} = a_{21}\tau_{xz} + a_{22}\tau_{yz} . \tag{2.2}$$

In Eqs (2.1) and (2.2)

γ_{xz}, γ_{yz} = specific changes in angles,
τ_{xz}, τ_{yz} = shear stresses,
$a_{11}, a_{12} = a_{21}, a_{22}$ = material data.

The angle formed by the x-axis and by the principal direction of elasticity denoted by the sign | in the plane xy is φ (Fig. 2); the shearing moduli associated with the principal directions are G_1, G_2 $(G_2 > G_1)$.

The relation between the material data $a_{11}, a_{12}=a_{21}, a_{22}$ and shearing moduli G_1, G_2 are expressed by the relationship [2]:

$$a_{11}=\frac{\cos^2\varphi}{G_1}+\frac{\sin^2\varphi}{G_2}, \tag{2.3}$$

$$a_{22}=\frac{\sin^2\varphi}{G_1}+\frac{\cos^2\varphi}{G_2}, \tag{2.4}$$

$$a_{12}=a_{21}=\left(\frac{1}{G_1}-\frac{1}{G_2}\right)\sin\varphi\cos\varphi\,. \tag{2.5}$$

Warping of the cross section is described by the function $w=\vartheta\Phi(x, y)$. By applying the geometric equations, one can write the following relationships:

$$\gamma_{zx}=\vartheta\left(\frac{\partial\Phi}{\partial x}-y\right), \qquad \tau_{yz}=\vartheta\left(\frac{\partial\Phi}{\partial y}+x\right). \tag{2.6) (2.7}$$

Combining Eqs (2.1), (2.2), (2.6), (2.7) result in Eqs (2.8), (2.9)

$$\vartheta\left(\frac{\partial\Phi}{\partial x}-y\right)=a_{11}\tau_{xz}+a_{12}\tau_{yz}\,, \tag{2.8}$$

$$\vartheta\left(\frac{\partial\Phi}{\partial y}+x\right)=a_{21}\tau_{xz}+a_{22}\tau_{yz}\,. \tag{2.9}$$

Replacing the equations

$$\tau_{xz}=\boldsymbol{\tau}_z\cdot\mathbf{e}_x=\vartheta\frac{C}{h}\frac{\mathrm{d}x}{\mathrm{d}s}, \tag{2.10}$$

$$\tau_{yz}=\boldsymbol{\tau}_z\cdot\mathbf{e}_y=\vartheta\frac{C}{h}\frac{\mathrm{d}y}{\mathrm{d}s} \tag{2.11}$$

into Eqs (2.8), (2.9), yields

$$\frac{\partial\Phi}{\partial y}-y=\frac{C}{h}\left(a_{11}\frac{\mathrm{d}x}{\mathrm{d}s}+a_{12}\frac{\mathrm{d}y}{\mathrm{d}s}\right), \tag{2.12}$$

$$\frac{\partial\Phi}{\partial y}+x=\frac{C}{h}\left(a_{21}\frac{\mathrm{d}x}{\mathrm{d}s}+a_{22}\frac{\mathrm{d}y}{\mathrm{d}s}\right). \tag{2.13}$$

By integrating Eqs (2.12), (2.13) we obtain

$$\int_{\partial A_k}\left(\frac{\partial\Phi}{\partial x}\mathrm{d}x+\frac{\partial\Phi}{\partial y}\mathrm{d}y\right)+\int_{\partial T_k}(x\,\mathrm{d}y-y\,\mathrm{d}x)=$$

$$=C\int_{\partial T_k}\frac{1}{h}\left[a_{11}\left(\frac{\mathrm{d}x}{\mathrm{d}s}\right)^2+2a_{12}\frac{\mathrm{d}x}{\mathrm{d}s}\frac{\mathrm{d}y}{\mathrm{d}s}+a_{22}\left(\frac{\mathrm{d}y}{\mathrm{d}s}\right)^2\right]\mathrm{d}s\,. \tag{2.14}$$

From Eq. (2.14), by making use of

$$\int_{\partial A_k} \left(\frac{\partial \Phi}{\partial x} \mathrm{d}x + \frac{\partial \Phi}{\partial y} \mathrm{d}y \right) = 0 \tag{2.15}$$

and

$$\int_{\partial A_k} (x \, \mathrm{d}y - y \, \mathrm{d}x) = 2A_k \tag{2.16}$$

one obtains

$$C = \frac{2A_k}{\int_{\partial A_k} \frac{1}{h} \left[a_{11} \left(\frac{\mathrm{d}x}{\mathrm{d}s} \right) + 2a_{12} \frac{\mathrm{d}x}{\mathrm{d}s} \frac{\mathrm{d}y}{\mathrm{d}s} + a_{22} \left(\frac{\mathrm{d}y}{\mathrm{d}s} \right)^2 \right] \mathrm{d}s}. \tag{2.17}$$

Combining Eq. (1.9 with (2.17) for the torsional stiffness S yields the following result:

$$S = \frac{4A_k^2}{\int_{\partial A_k} \frac{1}{h} \left[a_{11} \left(\frac{\mathrm{d}x}{\mathrm{d}y} \right)^2 + 2a_{12} \frac{\mathrm{d}x}{\mathrm{d}s} \frac{\mathrm{d}y}{\mathrm{d}s} + a_{22} \left(\frac{\mathrm{d}y}{\mathrm{d}s} \right)^2 \right] \mathrm{d}s}. \tag{2.18}$$

In case of homogeneous isotropy the formula (2.18) takes the form

$$S = G \frac{4A_k^2}{\int \frac{\mathrm{d}s}{h}} \qquad (G_1 = G_2), \tag{2.19}$$

which is nothing but the well-known Bredt formula [3].

3. Determination of the highest and lowest values of S

For analysing the functional connection $S = S(\varphi)$ it is sufficient to investigate the function

$$f(\varphi) = \int_{\partial A_k} \frac{1}{h} \left[a_{11} \left(\frac{\mathrm{d}x}{\mathrm{d}s} \right)^2 + 2a_{12} \frac{\mathrm{d}x}{\mathrm{d}s} \frac{\mathrm{d}y}{\mathrm{d}s} + a_{22} \left(\frac{\mathrm{d}y}{\mathrm{d}s} \right)^2 \right] \mathrm{d}s \tag{3.1}$$

because

$$S = \frac{4A_k^2}{f(\varphi)}. \tag{3.2}$$

With a short calculation it may be pointed out that

$$f(\varphi) = g_{11} \cos^2 \varphi + 2g_{12} \cos \varphi \sin \varphi + g_{22} \sin^2 . \varphi , \tag{3.3}$$

wherein

$$g_{11}=\frac{1}{G_1}\int\limits_{\partial A_k}\frac{1}{h}\left(\frac{\mathrm{d}x}{\mathrm{d}s}\right)^2\mathrm{d}s+\frac{1}{G_2}\int\limits_{\partial A_k}\frac{1}{h}\left(\frac{\mathrm{d}y}{\mathrm{d}s}\right)^2\mathrm{d}s\,, \tag{3.4}$$

$$g_{22}=\frac{1}{G_1}\int\limits_{\partial A_k}\frac{1}{h}\left(\frac{\mathrm{d}y}{\mathrm{d}s}\right)^2\mathrm{d}s+\frac{1}{G_2}\int\limits_{\partial A_k}\frac{1}{h}\left(\frac{\mathrm{d}x}{\mathrm{d}s}\right)^2\mathrm{d}s\,, \tag{3.5}$$

$$g_{12}=g_{21}=\left(\frac{1}{G_1}-\frac{1}{G_2}\right)\int\limits_{\partial A_k}\frac{1}{h}\frac{\mathrm{d}x}{\mathrm{d}s}\frac{\mathrm{d}y}{\mathrm{d}s}\mathrm{d}s\,. \tag{3.6}$$

From those described above it is clear that the determination of the loci of the extreme values and the highest and lowest values of $f(\varphi)$ is equivalent with that of the principal directions and principal values of the symmetric, second order tensor

$$g=\begin{bmatrix} g_{11} & g_{12} \\ g_{21} & g_{22} \end{bmatrix}. \tag{3.7}$$

On the definiteness of the quadratic form

$$Q(u,v)=a_{11}u^2+2a_{12}uv+a_{22}v^2 \tag{3.8}$$

ensues that the eigenvalues of g_1 and g_2 of the matrix (3.7) are positive ($g_1 \geqq g_2 > 0$).

By a suitable placement of the elastic material — by the selection $\varphi=\hat{\varphi}$ (Fig. 2) — one can attain that the torsional stiffness of the bar takes the value

$$S_{\max}=\frac{4A_k^2}{g_2} \tag{3.9}$$

It is to be noted that

$$\min f(\varphi)=f(\hat{\varphi})=g_2\,. \tag{3.10}$$

The minimum value of the torsional stiffness might be found by making use of the formula

$$S_{\min}=\frac{4A_k^2}{g_1}\,, \tag{3.11}$$

in which case

$$\max f(\varphi)=f\left(\hat{\varphi}+\frac{\pi}{2}\right)=g_1\,. \tag{3.12}$$

4. Example

Figure 3 represents a closed profile with a triangular centre line.

In order to throw additional light on the question, the units of measure will not be indicated in treating the numerical example. Be

$$G_1 = 1/200, \qquad G_2 = 1/50 .$$

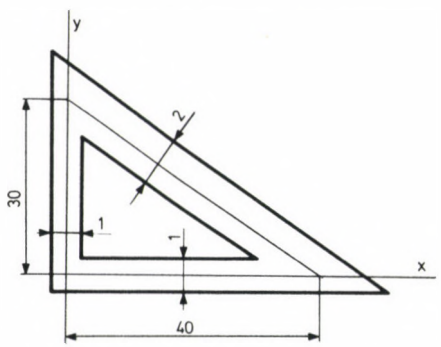

Fig. 3. Thin-walled closed profile with triangular centre line

By elementary calculation one obtains the following numerical values:

$$g_{11} = 13\,150, \qquad g_{22} = 10\,600,$$

$$g_{12} = -1\,800, \qquad A_k = 600 .$$

For the eigenvalues of the matrix **g** the following results are found

$$g_1 = 14\,080, \qquad g_2 = 9\,655,$$

and the angle $\hat{\varphi}$ is

$$\hat{\varphi} = 2.43 \text{ rad} .$$

Applying the formula (3.9) results in the maximum value of the torsional stiffness

$$S_{\max} = 1445.2 ,$$

and the minimum value is obtained by using formula (3.11):

$$S_{\min} = 1030 .$$

References

1. Арутюнян, Н. Х.—Абрамян, Б. Л.: Кручение упругих тел. Гос. изд. физ—мат. литературы, Москва, 1963
2. Саркисян, В. С.: Некоторые задачи математической теории упругости анизотропного тела. Изд. Ереванского Университета. Ереван. 1976, pp. 55–85
3. See for example: Szabó I.: Einführung in die technische Mechanik. 2. Auflage, formula (15.94). Springer Verlag, Berlin 1956

Acta Technica Academiae Scientiarum Hungaricae, 93 (3—4), pp. 391—394 (1981)

BOOK REVIEWS

P. CSONKA: *Shell Structures* Publishing House of the Hungarian Academy of Sciences, Budapest 1981, 1040 pp., 840 figures, 145 tables

This book is a compilation of the membrane theory of shells and of manual and minicomputer analysis methods for solving membrane shell problems. In this quality it is world-wide outstanding or even unique both by the profusion of its contents and by the extreme clearness of its style. It is concerned with almost the complete scope of the international literature and latest achievements in this subject. The Author presents a great deal of his mature research results from recent decades, including quite novel solutions. This book is especially valuable for its clear, surveyable composition, the didactically efficient train of thought. It is a helpful manual, since chapters on different shell forms refer exclusively to chapters on theoretical fundamentals, are relatively independent and understandable in themselves. Expediently selected examples of realized shell structures are highly valuable for the structural practice.

The rich material of this book is likely to offer a versatile tool to specialists. The designing architect will find almost the complete spectrum of shell forms possible in structural practice. At the same time it is a real treasury of numerical mathematics, offering a wide, ingenious choice of efficient approximate analysis methods requiring no digital computer. Last but not least, this book helps forming the way of thinking of its readers by the mode of treating its subject, by its simplicity relying on the comprehensive knowledge of its subject.

These characteristics — beyond its actual subject — rank the book by Prof. Dr. Pál Csonka among the best works in the Hungarian technical literature.

This decent, carefully got-up book — irrespective of language limitations — is likely to raise international interest. An English version would contribute to the fame of Hungarian engineers and technical books.

Dr. J. Peredy

G. FRANZ (Schriftleiter) *Beton-Kalender 1980* Taschenbuch für Beton-, Stahlbeton- und Spannbetonbau sowie die verwandten Fächer, Verlag von Wilhelm Ernst u. Sohn, Berlin—München—Düsseldorf 1980, 69. Jahrgang, I. Band, 1200 S., II. Band 1014 S.

Im Laufe der enormen Entwicklung der technischen Wissenschaften ist es keine geringe Leistung ein Taschenbuch herauszugeben, das das ganze Gebiet einer Fachwissenschaft umfaßt und trotz des beschränkten Rahmens das ganze von der Praxis beanspruchte Wissensmateral auf dem jüngsten wissenschaftlichen Niveau darstellt. Der allbekannte Schriftleiter des Beton-Kalenders Prof. G. Franz und das von ihm geleitete vorzügliche Verfasserensemble hat diese Aufgabe meisterhaft gelöst: dem Betonfach ein Werk zur Verfügung gestellt, das die wissenschaftlichen und praktischen Ansprüche der Fachleute des Entwerfens, der Ausführung und des Forschens in jeder Hinsicht weitgehend erfüllen kann.

Das in zwei Bänden erschienene Taschenbuch berichtet ausführlich unter anderen über die materiellen Eigenschaften des Betons (Prof. J. Bonzel), über die in der Baupraxis verwendeten Stahlmateriale und Produkte (D. Bertram), über die aktuellen Probleme der Festigkeitslehre (Prof. N. Dimitrov), über die Statik der Stabkonstruktionen und zugleich über die Berechnung von Stahltragwerken (H. Ahrens, Prof. D. Duddeck), über die Bemessung der Stahlbetonbauteile mit besonderem Bezug auf die Probleme der Bemessung für Biegung mit Längskraft, Schub, Torsion un Knicksicherheit (Prof. E. Gasser, Prof. K. Kordina, Prof. U. Quast) und über die Bemessung von Spannbetonbauteilen (Prof. H. Kupfer). Auf mehr als 500 Seiten werden die in der BRD gültigen Baubestimmungen und deren Erläuterungen bekanntgegeben (H. Goffin), weiterhin werden die neuesten Stahlbetonbestimmungen der USA in deutscher Sprache mitgeteilt (W. Hof), wodurch die Möglichkeit zu einem interessanten Vergleich zwischen der Auffassung der deutschen und amerikanischen Fachkreise geboten wird.

Infolge des nützlichen Inhalts der neuesten Ausgabe des Beton-Kalenders kann wie auch bei den vorigen Ausgaben auf eine günstige Aufnahme nicht nur auf dem deutschen Sprachgebiet, sondern auch weit über dessen Grenzen gerechnet werden.

Dr. P. Csonka

B. BEKE: *The Process of Fine Grinding* Publishing House of the Hungarian Academy of Sciences, Budapest 1981, 150 pp.

There are no reliable statistics on the world's energy consumption but most estimations ascribe 5% to grinding and milling. Both of these operations occur in several industrial fields such as in cement industry, silicate industry, mineral preparation, chemical industry and metallurgy where grinding and milling technologies are of decisive importance. Grinding and fine grinding are rather high energy consumers, so that examination of these processes from the aspect of physical, physico-chemical and mechanical laws is a safe guide to developing prospective energy-saving grinding technologies.

Several outstanding publications have been issued on grinding and milling systems and their operation. As mentioned in the introduction, however, little has been said about the materials to be ground, or the inherent physical and physico-chemical changes, although these operations are expected to produce these changes, or to avoid some changes to save useless energy expenditure.

This book comprises twenty chapters.

Processes of grinding and fine grinding have been concerned with in Chapters 1, 2, 3, 4, 5, 6, 7, 8, 10, 11, 16 and 17; several of them rely on the scientific research work of the Author, such as those on grinding kinetics, grindability of materials, grindability of material mixes, power demand and efficiency, cyclic grinding, practical methods of fine grinding, and extrafine grinding. From among a number of recent scientific results, special stress is laid on the recognition of constant n in the Rosin-Rammler function to be a material grindability index termed evenness coefficient. This recognition is confirmed by several test results of his own or found in publications. The evenness coefficient value is decisive for the grinding kinetics, for the agglomeration due to overenergizing; last but not least — according to Eqs (8.2) and (8.3) — for the energy consumption.

Between chapters on grinding and on fine grinding processes, previous to that on cyclic grinding, latest approach to grading and grading indices has been presented in Chapter 9.

Four chapters, i.e. Chapters 12, 13, 14 and 15 have been concerned with mechanics of drum mills, ring mills and cross-beater mills, and the involved processes from the aspect of grind characteristics. Processes in the grading equipment are discussed in Chapter 18.

Chapter 19 with the heading »Fulfilment of Technology Requirements« is a recapitulation of the Author's rich experience in grinding cements and cement raw materials.

The final Chapter 20 forecasts the development trend of grinding with a view to capacity increase, reduction of investment costs, energy saving, rising quality requirements as well as introduction of computerized process control.

This work, recapitulation of the hitherto activity of Prof. Beke, includes 137 references, each of them has been processed from the aspect of the goal mentioned in the introduction. Integration of references and own scientific results — partly relying on the former — is equivalent to set new bases to this scientific domain.

This book will be of use for scientific research workers, highly qualified specialists and university students. Its systematic study offers a raised professional standard and a motivation to research.

Dr. Sz. Pethő

K. WALZ (Redakteur): *Betontechnische Berichte 1978 und 1979* Beton-Verlag GmbH, Düsseldorf

Die zwei Bände enthalten in Form von Jahresbüchern die vom Forschungsinstitut der Zementindustrie, Düsseldorf, auf dem Gebiet der Betontechnologie erzielten und in der Bundesrepublik Deutschland erscheinenden Fachzeitschrift BETON veröffentlichten Forschungsergebnisse. Das Jahrbuch 1978. ist der 19., das Jahrbuch 1979. der 20. Band dieser Serie.

Die in diesen Bänden enthaltenen Studien befassen sich mit einzelnen, im Rahmen spezialer Themen allgemeinen Interesses vorgenommenen neueren Forschungen und deren praktisch verwendbaren Ergebnissen. Die Jahrbücher können Betontechnologen als wertvolle und nützliche Handbücher dienen. Sie können auch in den ungarischen betontechnologischen Forschungen und in deren Fortentwicklung gut gebraucht werden und erleichtern die fachliterarische Erschließung dieses Themenkreises.

Der Band 1978. umfaßt acht Studien. Die erste enthält die vom Institut verfaßten, provisorischen

Richtlinien bezüglich der Bodenverfestigung mit Zement im Wasserbau, vornehmlich der Stabilisierung von Anschüttungen, von Erd- und Steindämmen.

Die Studie von G. Wischers behandelt die Zusammenhänge zwischen Spannung und Formänderung bei druckbeanspruchten Betonkörpern, den eingeführten Energiebedarf, ferner die, auf diese ausgeübte Wirkung der Menge der eingebrachten Stahl- und Glasfasern.

Die Autoren der dritten Studie sind J. Dahms und K. Rendchen. Sie befassen sich mit dem Einfluß verschieden großer in Laboratorien gebräuchlicher Betonmischmaschinen auf die Eigenschaften des Frischbetons und auf die des erhärteten Betons. Hierbei wurde festgestellt, daß die mit verschiedenen großen Betonmischern und unterschiedlicher Mischungsdauer angefertigten Betonmischungen im Wesen einander gleich sind und die Größe des Mischers sowie die Mischungsdauer die Gleichmäßigkeit des Betons nicht beeinflußen. Dies ist eine wertvolle Feststellung.

U. Neck befaßt sich in der vierten Abhandlung mit der Feuerbeständigkeit des Betons und arbeitet einen Entwurf zur Eingliederung der erzielten Ergebnisse in DIN 4102. aus.

S. Sprung befaßt sich in seiner Studie mit den Bedingungen, die beim Bau von, der Entsalzung großer Mengen Meerwassers dienenden Betonbassins zu berücksichtigen sind. Das Thema ist für die ungarischen Fachkreise wenig interessant.

K. Rendchen gibt in seiner Abhandlung die auf das SI-System umgearbeiteten, in der Bauindustrie und in der Betontechnologie gebräuchlichen Maßeinheiten an. Diesbezüglich sind mehrere ungarische Veröffentlichungen bekannt.

J. Bonzel und J. Dahms haben zwecks genauerer Bestimmung des Wasserbedarfes eines Betons gegebener Plastizität Versuche unternommen und liefern auf Grund der Versuchsergebnisse genauere Richtzahlen, als die bisher bekannten.

Die letzte Studie befaßt sich mit der Luftelektrizität der Räume eines Gebäudes und faßt die Ergebnisse jener Versuche zusammen, die zwecks Feststellung der Abhängigkeit der Luftelektrizität vom Baustoff des Gebäudes vorgenommen wurden. Es wurde festgestellt, daß die Luftelektrizität geschlossener Räume von der abschirmenden Wirkung des Baustoffes der raumumschließenden Konstruktion unabhängig, doch abhängig von den geometrischen Daten und von der, mit elektrischen Geräten vorgenommenen menschlichen Arbeit ist.

Die Jahresausgabe 1979. enthält nur fünf Aufsätze. Die Verfasser des ersten sind W. Manns und K. Zeus. Sie befassen sich mit der Wirkung die Zusatzstoffe auf die Schwundrisse des Betons ausüben. Die günstige oder ungünstige Wirkung dieser Zusatzstoffe ist eindwandfrei nachweisbar. Abbindeverzögerer wirken sich im allgemeinen ungünstig aus, indem sie das Entstehen von Schwundrissen fördern.

J. Dahms berichtet über die technischen Kennwerte von, mit Stahl-, Kunststoff- und Glaseinlagen verstärktem Beton, die er im Versuchswege ermittelt hat. Es sind zahlreiche ungarische Forschungsergebnisse dieser Art bekannt.

H. Weigler behandelt die von den internationalen Verbänden (ISO, RILEM, CEB) ausgearbeiteten und veröffentlichten betontechnologischen Richtlinien und weist auf die in diesen enthaltenen, von den DIN-Vorschriften abweichenden Vorschläge hin.

K. Walz behandelt in seinem Aufsatz die von ACI Committee 201. veröffentlichten Richtlinien, welche die Herstellung von dauerhaften, verschiedenen Einwirkungen widerstehenden Betonen zum Gegenstand haben.

Die letzte Studie haben J. Bonzel und U. Neck verfaßt. Sie befaßt sich vornehmlich mit der Beseitigung der gesundheitsschädlichen Wirkungen der industriellen Abfälle, insbesondere des Schlammes, durch Zugabe von Zement. Die Versuchsergebnisse zeugen für die Brauchbarkeit der Methode.

Dr. T. Gyengő

G. FRANZ (Schriftleiter) *Beton-Kalender 1982, Jahrgang 71.* Taschenbuch für Beton-, Stahlbeton- und Spannbetonbau sowie die verwandten Fächer. Verlag von Wilhelm Ernst u. Sohn, Berlin—München 1982, I. Bd.: 1228 S., II. Bd.: 1015 S.

Dieses Werk gibt seit Jahrzehnten traditionsmässig von Jahr zu Jahr eine wertvolle Zusammenfassung der neuesten theoretischen resp. praktischen Kenntnisse des Beton-, Stahlbeton- und Spannbetonfaches. Sein gelehrter Verfasser, Prof. Dr.-Ing. Dr.-Ing. E. h. Gotthard Franz, emeritierter Professor der Technischen Universität Karlsruhe, wählte mit besonderer Sorge und mit der Mitwirkung der Besten seines Fachgebietes den bearbeitenden Stoff und seine Verfasser. Sein Ziel war eine entsprechende Information von den gegenwärtigen Kenntnissen des Betonfaches, besonders von den jüngsten Forschungsergebnissen zu bieten um auch damit den wirtschaftlichen Entwurf und die sparsame Bemessung der Tragwerke zu fördern.

In den 21 Kapiteln des ersten Bandes werden die besonderen Eigenschaften der verschiedenen Bau-

stoffe und die nötigen Kenntnisse zum Konstruktionsentwurf behandelt. Von dem äußerst vielseitigen Wissensmaterial bedeuten für den Entwurfsingenieur eine besondere Hilfe die von Prof. F. Czerny zusammengestellten Tafeln welche alle nötigen statischen Daten der verschiedenartig gelagerten Rechteckplatten von verschiedenen Seitenverhältnissen erhalten, wobei, außer dem Fall der gleichmäßigen Vollbelastung, auch der Fall der Dreieckvollbelastung ausführlich behandelt wird. Ein weiterer sehr ausführlich behandelter Abschnitt ist das von Prof. H. Duddeck und Prof. H. Ahrens verfaßte Kapitel über die Statik der Stabtragwerke, das einen ausgezeichneten Überblick der verschiedenen genauen und annähernden Rechnungsverfahren bietet. Sein reiches Tafelmaterial bedeutet eine wertvolle Hilfe zur Berechnung der Rahmentragwerke. Bemerkenswert ist auch die Zusammenfassung der Festigkeitslehre von Prof. N. Dimitrov, sowie das Kapitel von Prof. Grasser, das sich auf die Bemessung der Stahlbeton-Konstruktionselemente bezieht.

Der zweite Band des Werkes befaßt sich vorwiegend mit praktischen Fragen. Das äußerst ausführliche Kapitel von H. Goffin teilt alle gegenwärtig in der BRD gültigen Bestimmungen mit, die sich auf das Entwerfen und auf die Ausführung der Beton-, Stahlbeton- und Spannbetonbauten beziehen. Nachher wird von Prof. H. Paschen über Verfahren im Bauen mit Betonfertigteilen berichtet, wo die Vor-, resp. Nachteile dieser Methoden eingehend dargestellt werden. W. Klöckner und seine Mitarbeiter behandeln die verschiedenen Gründungsmethoden mit besonderer Rücksicht auf die im Laufe der Ausführung entstehenden Probleme. Zuletzt werden die Fragen des Abdichtens der Bauwerke erörtert, wobei besonders auf die Isolation des Grundwassers eingegangen wird.

Zusammenfassend kann festgestellt werden, dass der neueste, 71. Jahrgang des Beton-Kalenders — den vorangehangenen Jahrgängen ähnlich — für die Fachleute im Beton-, Stahlbeton- und Spannbetonbau ein wertvolles, unentbehrliches Nachschlagewerk bedeutet, das nicht nur im Verlagsland, sondern auch weit über seine Grenzen auf allgemeines Interesse rechnen kann.

Dr. P. Csonka

ACTA PHYSICA

ACADEMIAE SCIENTIARUM HUNGARICAE

EDITOR-IN-CHIEF

I. KOVÁCS

VOLUME 52 CONTENTS NUMBER 2

Papers in English. Published in two volumes (4 issues each) annually.
Subscription rate per vol ume: $40.00

AKADÉMIAI KIADÓ

Publishing House of the Hungarian Academy of Sciences

Budapest

Distributed by KULTURA, Hungarian Foreign Trading Co., P.O.B. 149, H-1389 Budapest

ACTA OECONOMICA

Periodical of the Hungarian Academy of Sciences

Founded 1966

Editor: T. Földi

Acta Oeconomica publishes articles mainly on Hungary's economic development, economic policy and on some issues of economic management system and planning, on economic reforms and on mathematics applied in economics. Extra space is devoted to issues dealing with recent phenomena of world economy, East-West trade, socialist integration (place of Hungary in the international division of labour) and finally with developing countries. The journal contains reviews as well.

Papers mainly in English, some articles in German or Russian
Published in two volumes per year of 4 issues each
Subscription rate: $40.00 per volume

AKADÉMIAI KIADÓ
Publishing House
of the Hungarian Academy of Sciences
Budapest

Distributors:
KULTURA
Hungarian Foreign Trading Co.
P.O.B. 149
H-1389 Budapest

Printed in Hungary
Akadémiai Kiadó és Nyomda, Budapest

The *Acta Technica* publish papers on technical subjects in English, French, German and Russian.

The *Acta Technica* appear in parts of varying size, making up one volume.

Manuscripts should be addressed to

Acta Technica
H-1051 Budapest
Münnich Ferenc u. 7
Hungary

Correspondence with the editors and publishers should be sent to the same address,

Subscription rate: $ 36.00 a volume.

Orders may be placed with "Kultura" Foreign Trading Company (H-1389 Budapest 62. P. O. B. 149. Account No. 218-10990) or its representatives abroad.

Les *Acta Technica* paraissent en français, allemand, anglais et russe et publient des travaux du domaine des sciences techniques.

Les *Acta Technica* sont publiés sous forme de fascicules qui seront réunis en volumes.

On est prié d'envoyer les manuscrits destinés à la rédaction à l'adresse suivante:

Acta Technica
H-1051 Budapest
Münnich Ferenc u. 7.
Hongrie

Toute correspondance doit être envoyée à cette même adresse.

Le prix de l'abonnement: $ 36.00 par volume.

On peut s'abonner à l'Entreprise du Commerce Extérieur «Kultura» (H-1389) Budapest 62, P. O. B. 149. Compte courant No. 218-10990) ou chez représentants à l'étranger.

«*Acta Technica*» публикуют трактаты из области технических наук на русском немещном, английском и французском языках.

«*Acta Technica*» выходят отдельными выпусками разного объема. Несколько вы пусков составляют один том.

Предназначенные для публикации рускописи следует направлять по адресу:

Acta Technica
H-1051 Budapest,
Münnich Ferenc u. 7.
Венгрия

По этому же адресу направлять всякую корреспонденцию для редакции и администрации.

Подписная цена — $ 36.00 за том. Заказы принимает предприятие по внешней торговле «Kultura» (H-1389 Budapest 62, P. O. B. 149 Текущий счет № 218-10990) или его заграничные представительства и уполномоченные.

Periodicals of the Hungarian Academy of Sciences are obtainable at the following addresses:

AUSTRALIA
C.B.D. LIBRARY AND SUBSCRIPTION SERVICE
Box 4886, G.P.O., *Sydney N.S.W. 2001*
COSMOS BOOKSHOP, 145 Ackland Street
St. Kilda (Melbourne), Victoria 3182

AUSTRIA
GLOBUS, Höchstädtplatz 3, *1206 Wien XX*

BELGIUM
OFFICE INTERNATIONAL DE LIBRAIRIE
30 Avenue Marnix, *1050 Bruxelles*
LIBRAIRIE DU MONDE ENTIER
162 rue du Midi, *1000 Bruxelles*

BULGARIA
HEMUS, Bulvar Ruszki 6, *Sofia*

CANADA
PANNONIA BOOKS, P.O. Box 1017
Postal Station "B", *Toronto, Ontario M5T 2T8*

CHINA
CNPICOR, Periodical Department, P.O. Box 50
Peking

CZECHOSLOVAKIA
MAD'ARSKÁ KULTURA, Národní třida 22
115 66 Praha
PNS DOVOZ TISKU, Vinohradská 46, *Praha 2*
PNS DOVOZ TLAČE, *Bratislava 2*

DENMARK
EJNAR MUNKSGAARD, Norregade 6
1165 Copenhagen K

FEDERAL REPUBLIC OF GERMANY
KUNST UND WISSEN ERICH BIEBER
Postfach 46, *7000 Stuttgart 1*

FINLAND
AKATEEMINEN KIRJAKAUPPA, P.O. Box 128
SF-00101 Helsinki 10

FRANCE
DAWSON-FRANCE S. A., B. P. 40, *91121 Palaiseau*
EUROPÉRIODIQUES S. A., 31 Avenue de Versailles, *78170 La Celle St. Cloud*
OFFICE INTERNATIONAL DE DOCUMENTATION ET LIBRAIRIE, 48 rue Gay-Lussac
75240 Paris Cedex 05

GERMAN DEMOCRATIC REPUBLIC
HAUS DER UNGARISCHEN KULTUR
Karl Liebknecht-Straße 9, *DDR-102 Berlin*
DEUTSCHE POST ZEITUNGSVERTRIEBSAMT
Sraße der Pariser Kommüne 3–4, *DDR-104 Berlin*

GREAT BRITAIN
BLACKWELL'S PERIODICALS DIVISION
Hythe Bridge Street, *Oxford OX1 2ET*
BUMPUS, HALDANE AND MAXWELL LTD.
Cowper Works, *Olney, Bucks MK46 4BN*
COLLET'S HOLDINGS LTD., Denington Estate
Wellingborough, Northants NN8 2QT
WM. DAWSON AND SONS LTD., Cannon House
Folkstone, Kent CT19 5EE
H. K. LEWIS AND CO., 136 Gower Street
London WC1E 6BS

GREECE
KOSTARAKIS BROTHERS INTERNATIONAL BOOKSELLERS, 2 Hippokratous Street, *Athens-143*

HOLLAND
MEULENHOFF-BRUNA B.V., Beulingstraat 2,
Amsterdam
MARTINUS NIJHOFF B.V.
Lange Voorhout 9–11, *Den Haag*
SWETS SUBSCRIPTION SERVICE
347b Heereweg, *Lisse*

INDIA
ALLIED PUBLISHING PRIVATE LTD., 13/14
Asaf Ali Road, *New Delhi 110001*
150 B-6 Mount Road, *Madras 600002*
INTERNATIONAL BOOK HOUSE PVT. LTD.
Madame Cama Road, *Bombay 400039*
THE STATE TRADING CORPORATION OF INDIA LTD., Books Import Division, Chandralok
36 Janpath, *New Delhi 110001*

ITALY
INTERSCIENTIA, Via Mazzé 28, *10149 Torino*
LIBRERIA COMMISSIONARIA SANSONI, Via Lamarmora 45, *50121 Firenze*
SANTO VANASIA, Via M. Macchi 58
20124 Milano
D. E. A., Via Lima 28, *00198 Roma*

JAPAN
KINOKUNIYA BOOK-STORE CO. LTD.
17-7 Shinjuku 3 chome, Shinjuku-ku, *Tokyo 160-91*
MARUZEN COMPANY LTD., Book Department, P.O. Box 5050 Tokyo International, *Tokyo 100-31*
NAUKA LTD. IMPORT DEPARTMENT
2-30-19 Minami Ikebukuro, Toshima-ku, *Tokyo 171*

KOREA
CHULPANMUL, *Phenjan*

NORWAY
TANUM-TIDSKRIFT-SENTRALEN A.S., Karl Johansgatan 41–43, *1000 Oslo*

POLAND
WĘGIERSKI INSTYTUT KULTURY, Marszałkowska 80, *00-517 Warszawa*
CKP I W, ul. Towarowa 28, *00-958 Warszawa*

ROUMANIA
D. E. P., *Bucureşti*
ILEXIM, Calea Grivitei 64–66, *Bucureşti*

SOVIET UNION
SOJUZPECHAT — IMPORT, *Moscow*
and the post offices in each town
MEZHDUNARODNAYA KNIGA, *Moscow G-200*

SPAIN
DIAZ DE SANTOS, Lagasca 95, *Madrid 6*

SWEDEN
ALMQVIST AND WIKSELL, Gamla Brogatan 26
101 20 Stockholm
GUMPERTS UNIVERSITETSBOKHANDEL AB
Box 346, *401 25 Göteborg 1*

SWITZERLAND
KARGER LIBRI AG, Petersgraben 31, *4011 Basel*

USA
EBSCO SUBSCRIPTION SERVICES
P.O. Box 1943, *Birmingham, Alabama 35201*
F. W. FAXON COMPANY, INC.
15 Southwest Park, *Westwood Mass. 02090*
THE MOORE-COTTRELL SUBSCRIPTION AGENCIES, *North Cohocton, N. Y. 14868*
READ-MORE PUBLICATIONS, INC.
140 Cedar Street, *New York, N. Y. 10006*
STECHERT-MACMILLAN, INC.
7250 Westfield Avenue, *Pennsauken N. J. 08110*

YUGOSLAVIA
JUGOSLOVENSKA KNJIGA, Terazije 27, *Beograd*
FORUM, Vojvode Mišića 1, *21000 Novi Sad*

HU ISSN 0001—7035

Index: 26.025